ATDL-76/14



# Environmental Research Laboratories

Air Resources
Atmospheric Turbulence and Diffusion Laboratory

Oak Ridge, Tennessee

September 1976

# 1975 ANNUAL REPORT



U. S. Department of Commerce
National Oceanic and Atmospheric Administration

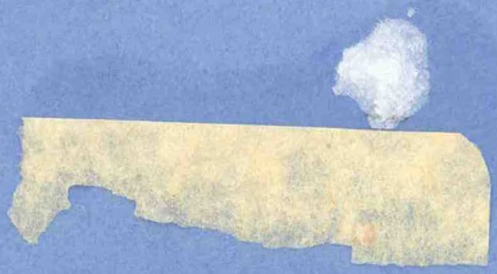

## NOTICE



Available from the National Technical Information Service, U. S. Department of Commerce, Springfield, Virginia 22161

Price: Paper Copy $13.75 (domestic)
$16.25 (foreign)
Microfiche $2.25 (domestic)
$3.75 (foreign)

## Foreword

The following is a compilation of research contributions from the National Oceanic and Atmospheric Administration Air Resources Atmospheric Turbulence and Diffusion Laboratory for the calendar year 1975. It was prepared by the Technical Information Center, U. S. Energy Research and Development Administration, Oak Ridge, Tennessee. Subsequent volumes will be issued on an annual basis. The research reported in this document was performed under an agreement between the U. S. Energy Research and Development Administration and the National Oceanic and Atmospheric Administration.

F. A. Gifford
Director
Atmospheric Turbulence
and Diffusion Laboratory

CONTENTS

# Summary of Activities and Plans FY 1976 - 1977

Air Resources
Atmospheric Turbulence and Diffusion Laboratory
National Oceanic and Atmospheric Administration
Oak Ridge, Tennessee
July 1976

Rayford P. Hosker, Jr.
and
Ruth A. Green

## I. Preface.

### A. Scope.

The Atmospheric Turbulence and Diffusion Laboratory (ATDL) in Oak Ridge, Tennessee, is operated for the Energy Research and Development Administration (ERDA) by the National Oceanic and Atmospheric Administration's (NOAA) Air Resources Laboratories, a group of research units generally concerned with problems of environmental pollution and its control. Major funding is from ERDA's Division of Biomedical and Environmental Research. ATDL works closely with various divisions of Oak Ridge National Laboratory (ORNL) on environmental projects of joint interest, and also functions as a meteorological consultant and advisor to that laboratory.

The ATDL is organized to perform research studies on atmospheric diffusion, transport, and removal of pollutants, including heat, and moisture with most emphasis on scales up to regional size (up to $\sim$ 200 km). Current research programs include air transport studies, especially for the eastern Tennessee region; air pollution studies, including the meteorological effects of cooling towers and energy centers; research on plume and wake behavior, including effects of buoyancy, active thermal convection, and removal processes; extension of atmospheric transport, diffusion, and effluent removal models to special situations such as over-water and over-forest flows; and study of the role of forest structure on the energy balance and on diffusion.

### B. FY 1976 Highlights.

Air parcel trajectories over the eastern Tennessee River Valley region were computed using data obtained during ATDL's ETTEX experiment of 1974, and also with extrapolated surface data, and the results were compared. The ORNL-ATDL air transport model was used to assess sulfur transport from large point sources, lead deposition near highways, and radon concentrations from mine tailings. Eddy diffusivity parameterizations of turbulent atmospheric mixing were conducted with the one-dimensional planetary boundary layer model. Work was begun on the solution of potential flow over complex terrain by both finite difference and finite element techniques.

A one-dimensional cooling tower plume and cloud growth model was developed and tested against field data. Models of drift deposition from cooling towers were compared. Coal combustion assessment studies were begun in collaboration with ORNL. Possible effects of moisture flux on atmospheric stability were studied using Bowen ratio estimates from field data. A prototype of an autopilot-equipped drone aircraft to study the mixing layer was constructed.

A Monte Carlo diffusion technique was developed, using ETTEX data to estimate the required velocity fluctuation cross-products. A model for plume rise terminated by convective turbulence was derived. Asymptotic forms for plume dispersion coefficients were suggested, and turbulent diffusion typing schemes were reviewed. A wind tunnel for small-scale studies in a simulated atmospheric surface layer and a water flow table were procured.

A summary of the distribution of solar radiation in a deciduous forest was completed. Instrumentation of a new forest meteorology field site was begun. New instruments including analog computation circuitry for measurements of momentum, heat, and moisture fluxes were designed and/or purchased.

A research-grade solar radiation monitoring station was designed and the requisite instruments purchased; this station will contribute to the NOAA-wide observing network.

C. FY 1977 Highlights

Verification of ATDL's mesoscale trajectory model will continue. This model will be used to examine the emissions from TVA fossil-fuel steam plants located in the eastern Tennessee region. A model for regional-scale sulfate transport including both chemical and physical removal mechanisms will be developed. A two-dimensional model of potential flow over sinusoidal terrain by both finite difference and finite element methods will be completed and generalized to three dimensions. The stable planetary boundary layer will be studied using a higher-order-closure numerical model. Physical modeling of mesoscale flows will begin in the water channel.

A model for multiple plume merger, rise, and cumulus cloud formation will be developed and compared to field data from TVA's Paradise cooling towers. The possibility of vorticity enhancement and concentration because of heat released from energy parks will be studied, possibly with a modification of Deardorff's subgrid turbulence modeling scheme. The instrumented drone airplane will be constructed, tested, and used to obtain mixing layer data.

ETTEX relative diffusion results will be compared to the Monte Carlo predictions. Expressions for plume dispersion coefficients will be tested. Wind tunnel tests on several near-obstacle flow phenomena will be conducted at EPA's facility in Triangle Park, N.C., and in the ATDL wind tunnel.

Instrumentation of the new forest site will continue; studies of turbulent fluxes will begin at the site and at the pine plantation. Data for energy budgeting and for characterizing forest structure will be taken at the new site.

The solar radiation monitoring station will begin routine operation, gathering data between wavelengths of 0.285 μm and 50 μm.

## II. Fy 1976 Accomplishments - ATDL.

### A. Air Transport Studies.

Data collected during the Eastern Tennessee Trajectory Experiment (ETTEX) were analyzed and reported. Using these data, air parcel trajectory calculations have been made and compared with similar calculations using estimated winds obtained from vertically adjusted surface wind observations. Results indicate that trajectory calculations using surface winds are unreliable both in unstable atmospheric conditions (Pasquill-Gifford classes A and B), and in stable conditions (classes E and F) if significant terrain features exist.

The ATDL-ORNL joint effort to improve the Air Transport Model (ATM) continued. The ATM is part of a comprehenisve program to follow the pathways and assess the environmental insult of trace contaminants in the atmosphere. An updated version of the model was published. In addition to previous validation for sulfur emanating from continuous point sources, the line source segment was used for estimating lead (Pb) deposition from a highway, while the area source section was employed to predict concentrations of radon from mine tailings. The results of the lead simulation studies showed that lead emissions behave very little differently from gaseous emissions, permitting considerable simplification of a potentially complex problem.

The ATDL one-dimensional planetary boundary layer (PBL) model has been used to investigate the parameterization of turbulent mixing in the atmosphere. Results indicate that eddy coefficients which are defined using local wind shear and stability tend to propogate surface-generated disturbances upward many times slower than in the real atmosphere, so that the

upper regions of the simulated PBL are in effect cut off from the surface region. On the other hand, eddy coefficients which are defined only near the surface, and then extended upward by extrapolation, tend to propagate disturbances upward nearly instantaneously, so that the simulated PBL lacks the natural phase lag of the real atmosphere. In the real atmosphere, the dynamics of the upper PBL are connected with those of the surface layer by a convective time scale, which must be somehow simulated if a model is to be successful. It appears at this time that gradient transport ("k") theory will not provide a correct simulation in this respect.

Work on a potential flow model for the eastern Tennessee River Valley regional wind field was begun. Both finite difference and the newer finite element computational techniques are being used; the two solutions will be compared. The initial model is of two-dimensional potential flow over sinusoidally corrugated terrain, for which an exact analytic solution is available to validate the numerical results. The model will then be extended to a simple three-dimensional case and further tested.

B. Atmospheric Pollution.

A one-dimensional model of cooling tower plume and cloud growth was refined and tested with a set of recent measurements at the John E. Amos power plant in West Virginia. Agreement between observed and predicted plume rise and visible plume length was obtained. The same model was used to establish a climatology of visible plume lengths, plume rise, and cloud growth. Several types of cooling towers were used as input to this model, ranging from single natural draft towers to multiple banks of towers typical of a power park. For the power parks, plumes at times rose to the tropopause and cumulus clouds developed.

The ATDL model for drift deposition from cooling towers was applied to the Paducah, Kentucky, gaseous diffusion plant and to a frictional natural draft cooling tower being used by ORNL as a basis for comparisons of models.

Joint ATDL-ORNL coal combustion studies continued. TVA data from a meteorological tower at Bull Run Steam Plant were used for determination of meteorological conditions during aerosol sampling periods. Windrose data and stability conditions were provided to the Environmental Sciences Division of ORNL for work on the environmental fate of emissions from coal combustion plants.

Mean humidity and temperature profiles collected on the pine plantation's forest tower were used to estimate the effect of Bowen ratio on atmospheric stability. Similar estimates were made with the Project Prairie Grass data. The results indicate that the effect can be quite large over forested areas only during transitions from stable to unstable conditions or vice versa, as in early morning or late afternoon, but is not very significant at any time over the much dryer environs of the Prairie Grass experiments.

A prototype radio-controlled drone airplane intended for vertical and horizontal atmospheric soundings was constructed using commercial components. An onboard electrostatic autopilot is provided to aid vehicle stabilization at large distances from the ground-based pilot. The prototype has a 1.2m wingspan and is powered by a $3.3cm^3$ displacement engine of roughly 0.3 hp output; it is uninstrumented and is intended to be a training aid and autopilot test vehicle. The instrumented airplane will have 2.5m wingspan, and be powered by a $10cm^3$ engine of about 1 hp output. It will carry fast-response temperature, humidity, and acceleration sensors, as well as a pressure altimeter. Information will be telemetered to the ground for decoding and recording. Tracking will be by double optical theodolites. Surveys will be made of horizontal inhomogeneities in the boundary layer over terrain discontinuities (water to field, field to forest), and of vertical structure and temporal development of the mixing layer.

C. Plume and Wake Behavior

Analyses of the convective diffusion and buoyant lift-off field experiments were completed. Analysis of $SO_2$ ground concentrations monitored by TVA were begun to determine which plume rise models best account for the trends with wind speed. Field experiments on lift-off of an initially wake-entrained buoyant plume were terminated in early winter. They will be resumed only after wind tunnel tests can be performed to permit parameter estimations under more controlled conditions than those obtainable in the field.

A Monte Carlo diffusion technique was developed, in which the fluctuations in lagged velocity cross products are accounted for. The ETTEX tetroon observations were used to estimate the fluctuations of the velocity cross-products.

A model for plume rise terminated by the action of convective turbulence was developed and presented at the American Meteorology Society's Workshop on Meteorology and Environmental Assessment.

To assist in deposition estimates in the mesoscale region and beyond, a scale height approach to concentration and deposition modeling was formulated and published.

Theoretical studies were made of asymptotic equations for diffusion coefficients. New information on turbulence in the convective and stable boundary layers was utilized. Comparisons with available field measurements were begun. A review of turbulent diffusion typing schemes was completed.

A low speed, open return-type wind tunnel was purchased under an ERDA-EPA agreement for cooling tower research. The tunnel is roughly 14m long, with a 1m x 1m x 6m long test section. An additional 3m long test section module may be added later. Flow speeds range between 1m/sec or less and 22m/sec or more, with turbulence intensities less than 0.5%. The tunnel will be used, with proper atmospheric boundary layer simulation, for studies of flow around cooling towers, including reingestion and mutual interference phenomena, for systematic studies of flow around obstacles in general, and for anemometer calibrations. Funds for a 30.5m x 9.1m x 4.5m high steel building to house the wind tunnel, a darkroom, and model storage space have been provided by ERDA. A recirculating water flow table 1.2m x 6m x 14cm deep was procured from surplus property lists, and will be installed in the same building to extend the range of possible fluid test conditions. Equipment for flow measurements and for visualization experiments was purchased.

D. Forest Meteorology.

A monograph summarizing ATDL research on the space and time distribution of solar radiation within a deciduous forest was completed. Greatest amounts of solar radiation penetrate the forest in the early spring, just before leaf expansion begins. Because of the lower than maximum solar elevation present at this time, optical paths through the forest are long and the woody forest biomass effects a significant attenuation of the incident solar radiation. As a result, less than 50 percent of the radiation incident upon the forest penetrates the leafless overstory canopy in the early spring. In winter, amounts are drastically lower because of the

minimal solar elevations around the winter solstice. In summer, amounts of radiation penetrating the forest are even lower despite maximal solar elevations, because of the expansion of leaves.

Further investigation was made of the effects of solar beam geometry--forest phenology intersections upon the penetration of solar radiation into a deciduous forest. It was shown that, despite the great attentuation of beam radiation by forest biomass throughout the year, the beam radiation component dominates the radiation budget within the forest at all times. Further analyses of these data are continuing.

Installation of equipment at the new Walker Branch Watershed (WBW) deciduous forest study site continued. Meteorological support was provided for ORNL Environmental Sciences Division personnel studying sulfur transport from power plants to this site. Instrumentation for the measurement of the vertical variation in solar radiation budget, and wet/dry deposition samplers of the type designed by ERDA's Health and Safety Laboratory were constructed and installed in and above the canopy of oak-hickory forest on WBW. Construction of leaf wetness sensors was begun. Analog computation circuitry for continuous elevation of momentum, heat, and moisture fluxes has been designed and is being constructed at ORNL.

Calibration drift problems with existing pine plantation hygrographs led to extensive testing of several other humidity probe types in a controlled chamber. A "Brady array" probe exhibited considerable hysteresis, making it unuseable. A plastic film capacitance-type probe, however, was found to be accurate, linear, repeatable, and fast-responding over a wide range of relative humidities and ambient temperatures. A number of these probes are being installed at both the pine plantation and Walker Branch sites. A new data-logging system to replace the presently-used sequential-scanning strip chart recorder has been ordered for the pine plantation to facilitate data collection and reduction.

In view of the increased importance of solar energy in the current and projected ORNL energy research and development program, it was decided to upgrade the present solar radiation measurement program in Oak Ridge. The establishment of a research quality solar radiation monitoring station to be operated as a cooperating station to the NOAA network was begun.

Solar radiation measuring instruments have been selected and purchased. Site location and instrument mounting arrangement has been determined. Conceptual design of a data logger has been finalized and components have been ordered.

## III. FY 1977 Goals - ATDL.

### A. Air Transport Studies.

Work will continue on the verification of the ATDL mesoscale model by comparing air parcel trajectories observed in the ETTEX experiment with similar trajectories determined from the model predictions.

Using this trajectory model, an examination of the effluent emissions from the various TVA steam plants in the Tennessee Valley region will be made. Aerosol and gaseous removal processes, with particular emphasis on the largely neglected rainout phenomena, will be included. In particular, a model for regional sulfate transport will be developed. Several chemical transformation and removal mechanisms will be considered. Results will be compared to TVA and EPA data.

The two-dimensional model of potential flow over sinusoidally corrugated terrain will be completed. The model will be generalized to three dimensions and again encoded for both finite difference and finite element solutions. Testing for a simple case such as flow near a hemisphere on a ground-plane will begin. Eventually the model will be extended to the complicated surface topography of the eastern Tennessee River Valley; verification will be done using the ETTEX data.

The structure of the stably-stratified planetary boundary layer will be studied with a higher-order-closure numerical model.

Preliminary work on the physical modeling of mesoscale flows using the ATDL water channel will begin. This will be a long term project whose aim is to determine the kinematic effect of gross topographic features on the mesoscale flows. Results will be compared to the numerical models and to the ETTEX data.

B. Atmospheric Pollution

A comprehensive state-of-the-art literature survey will be conducted of available mathematical and numerical prediction models for merging of vapor plumes and cloud growth. A model for multiple plume rise and cumulus cloud formation will then be developed, for use in the study of meteorological effects of power parks. Lumley's second-order turbulence closure model will be adopted and used in this study.

Several years of observations at the TVA Paradise cooling towers will be used to develop a climatology of visible plume length and plume rise, for comparison with the predictions of the ATDL vapor plume and cloud growth model. Time-lapse movies of cooling tower plumes at the Oak Ridge gaseous diffusion plant and the Rancho Seco power plant will be studied to estimate the magnitudes of secondary velocities.

A major danger of heat release from the proposed energy parks is the possibility of concentration of vorticity. Deardorff's subgrid scale turbulence modeling approach will be considered for application to this study. This is part of a long term step-by-step program which involves exploration of model applicability, resolution, computing time and memory requirements, adaption and modifications of the program code, and plume simulation in several simple flows before the complex questions on vorticity concentration and severe storm triggering because of the heat release from the energy parks can be answered by modeling.

The instrumented drone airplane will be constructed and tested extensively. Atmospheric boundary layer surveys will be conducted over the large open field at the pine plantation site. Data on mixing layer growth will be compared to several existing theoretical results.

C. Plume and Wake Behavior.

Relative diffusion observations obtained during the ETTEX program will be compared with predictions of the ATDL Monte Carlo diffusion technique. Equations for diffusion coefficients based on theory and tested against field data will be developed.

The sections on flow near obstacles and on plume rise for inclusion in Meteorology and Power Production will be completed, and Plume Rise will be revised.

Wind tunnel tests will be carried out at the EPA Fluid Modeling Facility in Research Triangle, N.C. Experiments will include the lift-off of a buoyant wake, diffusion and downwash around a few simple building shapes, and the behavior of buoyant plumes close to the source, including interactions with flow around buildings.

The ATDL wind tunnel and water flow table will be installed in a steel building located behind the existing ATDL complex. After extensive checkout of the tunnel, flow modification devices will be devised and installed to simulate the mean and turbulent velocity profiles of the neutral atmospheric surface layer. Visualizations of flow around cooling towers and clusters of cooling towers will begin. Diffusion and downwash studies close to simple obstacles will be conducted to complement the research done at the EPA facility.

D. Forest Meteorology.

Installation of equipment at the Walker Branch Watershed deciduous forest site will continue. The walkup tower installed late in FY 1976 will be instrumented to provide information of the profiles of temperature, humidity, wind speeds, and wind direction. Electronic integrators for high speed turbulence data are being designed and built for this study by the Instrumentation and Control Division, ORNL. These integrators will allow measurement and recording of turbulence variables that cannot now be handled by virtue of data acquisition limitations. With the completion of these integrators, studies of the turbulence characteristics within and above this forest will be initiated.

As the other towers for the WBW site are erected, installation of equipment for studies of the forest energy budget will be completed as well. Data collection for such energy budget and partitioning studies will begin, as well as studies for the characterization of forest structure and forest physiology.

Fast-response probes and signal conditioning equipment for heat and momentum fluxes will be constructed and placed in use at Walker Branch and at the pine plantation. Improved estimates of Bowen ratio effect on the stability length, L, will be made using data from the new pine plantation sensors. A climatology of the mean conditions within and above the pine plantation canopy will be compiled for comparison with the open-field conditions prevailing over the same time period.

Solar monitoring instrumentation will be calibrated and installed. Routine collection and archiving of data will begin. The incoming solar radiation spectrum will be separated into four wave bands; ultra violet (.285-.385μm), visible (.385-.700μm), near infra-red (.700-2.85μm), and far infra-red (2.85-50μm). Additionally, the diffuse and direct components of the global radiation will be determined.

## IV. Laboratory Staff.

During FY 1976 the ATDL staff totaled approximately 20. Of this number, ten were professional scientists and seven were technical and administrative personnel. Several part-time workers, mostly students, account for the remainder. No overall increase in staff is planned for FY 1977, but it is expected that two professional positions will be filled that were delayed during FY 1976. The staff is frequently augmented by visiting scientists from abroad. Several have come via International Atomic Energy Agency-National Research Council Fellowships, to work on problems of nuclear meteorology. Others have been assigned here to work on basic problems of atmospheric diffusion through various programs, such as Oak Ridge Associated Universities (ORAU) faculty research fellowships. Also much use of university students at various levels is made, including part-time undergraduate workers, summer fellowship students, "co-op" students, and part-time graduate students. University students in these various capacities supplied approximately three person-years in FY 1976, a substantial fraction ($\sim$15%) of the ATDL total.

When the ATDL wind tunnel installation is completed, now anticipated for the middle of FY 1977, employment of an additional two to three graduate students to collect, reduce, and analyze data is planned. The test programs should be suitable for master's theses in several departments at the University of Tennessee or at other universities.

Publications in FY1976

Hanna, S. R. and F. A. Gifford: "Meteorological Effects of Energy Dissipation." Published in Bulletin of AMS, Vol. 56,, No. 10, 1975, pp 1069-1076.

Gifford, F. A.: "A Review of Turbulent Diffusion Typing Schemes." Published in Nuclear Safety, Vol. 17-1, Jan.-Feb. 1976, pp 68-86.

Hanna, S. R.: "Modeling Smog Along the Los Angeles-Palm Springs Trajectory." To be published in Advances in Envir. Sci. and Tech.

Gifford, F. A.: Atmospheric Dispersion Models for Environmental Pollution Applications. Presented at AMS Workshop on Meteorology and Environmental Assessment, Boston, Mass., September 29-October 3, 1975, and published in Proceedings "Lectures on Air Pollution and Environmental Impact Analyses," pp 35-58.

Hanna, S. R.: Urban Diffusion Problems. Presented at AMS Workshop on Meteorology and Environmental Assessment, Boston, Mass., September 29-October 3, 1975, and published in Proceedings "Lectures on Air Pollution and Environmental Impact Analyses," pp 209-227.

Gifford, F. A. and S. R. Hanna: "Part III. Dispersion of Sulfur Dioxide Emissions from Area Sources." Published in Power Generation Monitoring and Control, pp. 71-81.

Culkowski, W. M.: Standard Deviation of Wind Direction as a Function of Time: Three Hours to Five Hundred Seventy-Six Hours. ATDL Cont. #75/11, July, 1975.

Hosker, R. P.: Comparison of Two Plume Depletion Estimation Techniques: The ADPIC Method vs. The Gaussian Model. ATDL Cont. #75/12, August, 1975.

Hutchison, B. and D. Matt: "Beam Enrichment of Diffuse Radiation in a Deciduous Forest." Accepted for publication in Ag. Met.

Briggs, G. A.: Plume Rise Predictions. Presented at AMS Workshop on Meteorology and Environmental Assessment, Boston, Mass., September 29-October 3, 1975, and published in Proceedings "Lectures on Air Pollution and Environmental Impact Analyses," pp 59-111.

D'Arruda, J. J. and S. R. Hanna: Asymptotic Solutions of a Simple Urban Dispersion Model for Chemical Pollutants, ATDL Cont. #75/16, September, 1975.

Hutchison, Boyd A. and D. R. Matt: "The Distribution of Solar Radiation Within a Deciduous Forest." Submitted for publication in Ecological Monographs, October 1975.

Baes, C. F., J. T. Holdeman, and W. M. Culkowski: Chemistry of Sulfur in the Atmosphere. ATDL Cont. File No. 75/19, October 1959.

Gifford, F. A., and S. R. Hanna: Discussion of paper by Goumans and Clarenburg "A Simple Model to Calculate the $SO_2$-Concentrations in Urban Regions." Published in Atmospheric Environment, Vol. 10, No. 7, 1976, pp 564.

Hanna, S. R., "A Comparison of Observed and Predicted Cooling Tower Plume Rise and Visible Plume Length." To be published in Atmospheric Environment, November 1975.

Ulriksen, Pablo: "A Note on Diffusion from Some Simple Extended Sources Treated as a Collection of Gaussian Point Sources." ATDL Cont. File No. 75/22.

Culkowski, Walter M.: "Scale Height Approximations for Deposition Estimates at Extended Distances." ATDL Cont. File No. 76/1.

Culkowski, W. M. and M. R. Patterson: A Comprehensive Atmospheric Transport and Diffusion Model. Published as ORNL/NSF/EATC-17. ATDL Cont. File No. 76/2.

Hanna, S. R.: Local and Global Transport and Dispersion of Airborne Effluents. Proceedings "Controlling Airborne Effluents from Fuel Cycle Plants," Topical Meeting by the ANS-AIChE, Sun Valley, Idaho, August 5-6, 1976.

Hutchison, Boyd A. and D. R. Matt: Forest Meteorology Research Within the Oak Ridge Site, Eastern Deciduous Forest Biome, USIBP. ATDL Cont. File No. 76/4.

Hutchison, Boyd A. and D. R. Matt: Effects of Sky Brightness Distrubiton Upon Diffuse Radiation Within a Deciduous Forest. Submitted for publication in Agricultural Meteorology. April 1976.

Baes, C. F., J. T. Holdeman, and Walter M. Culkowski: SULCAL - A Model of Sulfur Chemistry in a Plume. Published as ORNL Report: ORNL/NSF/EATC-21.

Hutchison, Boyd A. and D. R. Matt: The Annual Cycle of Deciduous Forest Radiation Regimes. Submitted to Ecology for publication. May 1976.

Nappo, Carmen J., Jr.: The Simulation of Atmospheric Transport Using Observed and Estimated Winds. Published in the Proceedings of the Third Symposium on Atmospheric Turbulence, Diffusion and Air Quality, October, 1976, Raleigh, N.C.

Gifford, F. A.: Relative Atmospheric Diffusion Observations. ATDL Contribution File No. 76/10.

Gifford, F. A., Rayford P. Hosker, Jr., and Steven R. Hanna: First Annual Report on Weather Modification Effects of Cooling Towers. Submitted for publication in Annual Reports to EPA.

Hanna, Steven R.: Comments on "Observations of an Industrial Cumulus." Submitted for publication in JAM.

Rao, K. S., I. Thomson and B. A. Egan: Regional Transport Model of Atmospheric Sulfates. Presented at the 69th Annual Meeting of the Air Pollution Control Association, Portland, Oregon, June 27 - July 1, 1976.

[Reprinted from BULLETIN OF THE AMERICAN METEOROLOGICAL SOCIETY, Vol. 56, No. 10, October 1975, pp. 1069–1076]
Printed in U. S. A.

# meteorological effects of energy dissipation at large power parks

Steven R. Hanna
and Franklin A. Gifford
Atmospheric Turbulence and Diffusion Laboratory
National Oceanic and Atmospheric Administration
Oak Ridge, Tennessee 37830

## Abstract

Large (10 000 to 50 000 MW) power parks are being studied as one means of satisfying the nation's demand for energy. The dissipation of waste energy from these installations may result in significant meteorological effects. It is shown that the rate of atmospheric dissipation of the waste energy from these power parks is approximately equal to the atmospheric dissipation of energy by geophysical phenomena such as thunderstorms, volcanoes, and large bushfires. Cumulus clouds and whirlwinds often result from these energy releases. There is a possibility that natural vorticity will be concentrated by large power parks. A theory of multiple plume rise is used to estimate the enhancement of plume rise from multiple cooling towers.

Calculations of plume rise, ground level fog intensity, and drift deposition due to emissions from cooling towers at a hypothetical 40 000 MW nuclear power park are made. The plume rise from 50 towers is estimated to be more than 110% of that from a single tower if the tower spacing is less than about 300 m. At locations within 100 km of the cooling towers, excess fog will occur about one or two percent of the time. The vapor plume will be appreciably longer than those from present installations; for instance it should be clearly visible from earth satellites most of the time. Since there are no power parks of this magnitude yet in existence, there are no measurements to test these calculations. The conclusions are highly tentative and indicate that much more research is required on this subject.

## 1. Introduction

The maximum amount of electric power currently generated at a single thermal power station site is about 3000 MW. Many environmental impact statements have been written concerning the atmospheric effects of heat dissipation at such sites. On the basis of these calculations and a few observation programs presented at the Symposium "Cooling Tower Environment—1974," it can be concluded that the atmospheric effects of current heat dissipation rates are not serious problems, provided that efforts are made to design the facility such that downwash is eliminated, drift is minimized, and plume rise is maximized. Fog formation and drift deposition are generally localized and have little effect beyond the plant boundaries. Clouds are sometimes observed to form due to heat and moisture from cooling towers, but no significant changes in rainfall in the areas of study have been detected.

However, several sites are being studied by power utility companies and government agencies as potential "power parks" or energy centers. Two of these sites are on the Mississippi River north of Baton Rouge and on the Columbia River on the Hanford reservation. Such fossil or nuclear powered plants could generate 10 000 to 50 000 MW of useable power on a land area on the order of 5 to 100 km$^2$. Assuming 33% efficiency, there might be as much as 100 000 MW of waste energy dissipated to the atmosphere, probably through some type of cooling towers. This dissipation rate represents an increase of between one and two orders of magnitude of the energy release over that from the largest currently operating power plants. The meteorological effects of such a power input to the atmosphere are uncertain. In this report, comparisons with natural energy processes and calculations of diffusion are used to make a rough estimate of some possible impacts of the proposed power parks. Calculations refer primarily to wet, natural draft towers, but effects of other types of cooling mechanisms are also considered.

## 2. Comparison of power center with natural energy processes

If evaporative cooling towers are used at a power center, then about 80% of the dissipated heat will be in the form of latent heat, which would be released to the atmosphere only when the water vapor condenses. The other 20% of the dissipated heat is sensible or convective heat, which is immediately available to the environment. If cooling towers are deployed on an area of, say, 100 km$^2$, the total heat output per unit area at a heat dissipation rate of 100 000 MW would be $10^3$ W/m$^2$. This figure is, by the way of comparison, three times greater than the average flux per unit area of solar energy (340 W/m$^2$) at the outer edge of the earth's atmosphere. It is about 20% of the vertical flux per unit area of energy in a thunderstorm as estimated by Hanna and Swisher (1971). The total rate of energy released by the cooling towers is nearly equal to the total rate of energy release in a thunderstorm. However, it is a factor of about 30 less than the rate of energy release by a squall line or a severe Great Lakes snow squall (2.5 cm of precipitation in 6 h over $10^5$ km$^2$). It appears that power parks will be on the same energy intensity scale as mesoscale natural processes, possibly

larger than a single thunderstorm cell but probably smaller than a squall line.

It is clear in any case that a heat release of the planned magnitude has the potential for generating a thunderstorm at times and can be expected to act as a thunderstorm "triggering" mechanism, especially in areas where thunderstorm activity is naturally frequent. Also, the plumes from the power center can alter natural weather phenomena by acting somewhat like a hill or small mountain, producing a barrier to air flow and causing abrupt local lifting of air and so increasing thunderstorm frequency and precipitation amount in its neighborhood (Stern and Malkus, 1953). It should be understood that this effect is not primarily dependent on the moisture addition by the cooling towers. It is the combined effects of moisture addition and buoyant lifting which augment natural precipitation phenomena. The particular phenomena that occur will of course depend on meteorological conditions. For example, in a dry, windy, stable atmosphere, no large clouds will be initiated. But on days when the atmosphere is conditionally unstable and conducive to large cloud development, the preferred location for cloud and thunderstorm development will in all likelihood be over the power center.

Since there are no existing power facilities of this size, we do not know for certain from experience what the meteorological effects will be. Some indication can be gained from the behavior of plumes from existing large power plants with cooling towers, but the proposed scale-up is still an order of magnitude or greater. The only comparable stationary heat sources of this magnitude are large fires and certain geophysical phenomena. Bourne (1964), and Thorarinsson and Vonnegut (1964) describe meteorological phenomena that accompanied the Surtsey volcano, which released an estimated 100 000 MW of heat continuously to the atmosphere from an area less than 1 km$^2$. This energy was released in the form of sensible (convective) heat and was accompanied by the release of many small ash particles. A permanent cloud extending to heights of 5 to 9 km, visible 115 km away, formed over the volcano. Waterspouts formed below the bent-over plume from this volcano. This indicates that the indraft at the cloud base, caused by the rising, buoyant cloud, acted to concentrate local atmospheric vorticity. A more detailed discussion of vorticity concentration is given in Section 4.

## 3. Comparison of power center with man-made heat sources

In the previous section, natural energy inputs such as thunderstorms and volcanoes were discussed. There are also some man-made heat sources, such as controlled bushfires and rocket firings, that have approximately the same magnitude of energy release as the proposed power park. Taylor *et al.* (1973) describe their observations of a large, controlled bushfire on an area of 50 km$^2$ in Australia. The maximum heat output, obtained for 15 min, was estimated as 200 000 MW. The average heat output over a 6 h period was about 100 000 MW. A cumulus cloud reaching to a height of 6 km formed over about one-tenth of the area of the fire. Some convergence of winds into the fire area was observed. Taylor *et al.* (1973) analyzed other smaller fires (50 000–100 000 MW) in Australia and found that a large cumulus cloud usually forms over these fires. They do not report any precipitation or thunder from the clouds, but emphasize the similarity of changes in meteorological conditions associated with fires to those associated with severe thunderstorms and tornadoes. It is possible that cloud condensation nuclei injected into the atmosphere by the brush fires also influenced the development of clouds.

The similarity between severe storms and wildfires was also noted by Taylor and Williams (1968), who analyzed a wildfire (The Hellgate, Va., fire) which occurred in the warm sector of an extratropical cyclone system. Atmospheric conditions were favorable to the formation of severe storms. Whirlwinds were observed during this fire.

Morris (1968) reports that the static firing of a Saturn V booster rocket produced 148 000 MW of power over a period of 150 s. It was concluded that ". . . when meteorological conditions in the lower atmosphere allow for cumulus growth through appreciable depths, a Saturn V booster captive firing will initiate convection. . . ." A cumulus cloud of depth 3.8 km, with a central toroid which revolved cyclonically, was observed on a day when natural convection caused many natural cumulus clouds and rain showers. Much carbon was produced by the firing, which may have contributed to the cloud formation. While the power of the Saturn V firing is approximately equal to the power from an energy center, the two phenomena have different time and length scales.

In another example of man-made heat generation, Dessens (1964) operated 100 oil burners in an area of 3200 m$^2$ in order to artificially induce cumulus convection. The total heat release of 700 MW generated cumulus clouds as well as dust devils near the burners. Davies (1959) reports on the results of an accidental oil fire which occurred in Long Beach. Energy was released at a rate of 10 000 MW (Briggs, 1969) for a few days, producing a black plume which rose to a height of 4000 m. The area of the source is not reported and it is not known whether whirlwinds were produced.

It may be useful to comment on the differences between the possible meteorological effects of the heat release from the power center and the well known "urban heat island" effects discussed by Peterson (1969), including their known role in altering downwind rainfall amounts (e.g. Huff and Changnon, 1972). Although the total heat output from the center will compare with that of a large city, the heat output per unit area is one or two orders of magnitude greater. Whereas a large city's heat creates the so-called "urban heat island," a

TABLE 1. Energy characteristics of natural and man-made sources.

| Source | Area | Time duration | Total power | Observations |
|---|---|---|---|---|
| Surtsey volcano (Bourne, 1964) | 1 km² | Several months | 100 000 MW | Continuous cloud water spouts |
| Australian bushfire (Taylor *et al.*, 1973) | 50 km² | Several hours | 100 000 MW | Cumulus cloud convergence |
| Booster rocket test (Morris, 1968) | 300 m² | 150 seconds | 148 000 MW | Cumulus cloud |
| Oil burners (Dessens, 1964) | 3.2 km² | Several hours | 700 MW | Cumulus cloud dust devils |
| Oil fires (Davies, 1959) | — | Day | 10 000 MW | Large plume |
| Large city (Peterson, 1969) | $10^3$ km² | Continuous | 100 000 MW | Effects on climate |
| Thunderstorm (Hanna and Swisher, 1971) | 10 km² | Hour | 50 000 MW | 2 cm $h^{-1}$ rain |
| Power park | 5 to 100 km² | Continuous | 100 000 MW | — |

small (a few degrees) thermal "bump" on the lowest few hundred meters of the planetary boundary layer of the atmosphere, the heat plume from the power center is capable of penetrating the boundary layer and may rise to great elevations in the troposphere (Koenig and Bhumralkar, 1974).

The observations of volcanoes, and comparisons with energy processes in thunderstorms and squall lines in Section 2, and studies of brushfires and other man-made heat sources in Section 3 are summarized in Table 1. These studies suggest that the proposed energy center may cause the development of large clouds, and may sometimes trigger thunderstorm and whirlwind activity in the area. It may also increase precipitation in naturally occurring widespread rain systems of the frontal type. These changes would be difficult to detect because of the area variability of natural rainfall.

## 4. Vorticity concentration by large power sources

Vortices are often associated with large intense energy sources. Dust devils, waterspouts, and tornadoes can be caused by natural convective forces. Waterspouts were observed near the Surtsey volcano. Whirlwinds caused by fire bombing in World War II are described by Landsberg (1947) and Rotty (1975). Fire whirlwinds are often observed over fires in the turbulent lee wakes of mountain ridges in the Pacific Northwest (see Graham, 1955). It has already been mentioned that the cloud from the Saturn V rocket was reported to circulate cyclonically and that the firing of oil burners caused the formation of dust devils.

Briggs (1975) has suggested a criterion to determine whether a given buoyant source with access to large scale natural vorticity will concentrate the vorticity into a waterspout or other strong vortex. If the ratio of the tangential component of the horizontal velocity of the environmental air, $V_\infty$, to the characteristic vertical speed of the buoyant source, $V_B$, is less than 0.15, buoyancy is dominant and there is no significant vortex. When $V_\infty/V_B$ is greater than 0.9, there is no concentration of vorticity by the vertical motions and the whole flow swirls. At values of $V_\infty/V_B$ between 0.15 and 0.9 it is possible for vorticity to be concentrated. Briggs estimates that the characteristic vertical speed of the buoyant source, $V_B$, equals $(F/R)^{1/3}$, where $R$(m) is the radius of the buoyant source and $F(m^4/s^3)$ is the buoyancy flux from the source (total heat release in watts divided by $\rho\pi c_p T/g$). To convert heat fluxes from MW to $m^4/s^3$, multiply by 8.8.

To estimate the tangential velocity of natural convection in the mixing layer, $V_\infty$, Briggs used results of a numerical experiment by Deardorff (1972). Briggs states that "The maximum possible value of $V_\infty$ is about 0.8 $(Hz_i)^{1/3}$, where $z_i$ is the height of the mixing layer (usually of the order of 1 km) and $H$ equals $g\,H_0/(c_p\rho T)$, where $H_0$ is the average sensible heat flux at the ground." On a scale equal to $z_i$, the maximum value of $V_\infty$ is about 1.7 m/s for a strongly convective day ($H = 10^{-2}$ $m^2/s^3$ and $z_i = 10^3$ m). On smaller scales, $V_\infty \simeq 6(Hz_i)^{1/3}(R/z_i)$. The vorticity concentration criterion is applied to several types of sources in Table 2.

From this table it is seen that the plumes from the Saturn V rocket ($V_\infty/V_B = 0.0025$) and the single cooling tower ($V_\infty/V_B = 0.06$) are too dominated by buoyancy to permit vortex formation. On the other hand, vorticity is not usually concentrated by natural convection ($V_\infty/V_B = 1$). When vorticity is concentrated by natural convection, it is typically at scales small compared to $z_i$ (e.g., dust devils), for on these scales $V_\infty/V_B$ is smaller. At small $R$, $V_\infty/V_B = (R/z_i)^{2/3}$ for natural convection. It is expected that vorticity will be concentrated in the oil burner experiment ($V_\infty/V_B = 0.44$). Since the ratio $V_\infty/V_B$ equals 0.12 for Australian bushfires, it is possible for vorticity to be concentrated on occasion.

For clusters of 20 natural draft cooling towers, with effective radii of 500 m and 5000 m, the ratios $V_\infty/V_B$ are 0.33 and 0.71, respectively, and we can predict that concentration of vorticity will occur. If dry cooling towers were used, the sensible heat flux would increase by a factor of five, and the ratios $V_\infty/V_B$ would decrease to 0.19 and 0.41, figures which are still well within the range of vorticity concentration.

TABLE 2. Calculation of the vorticity concentration parameter for several sources.

| Source | Source environment: Radius $R$(m) | Buoyancy flux $F$ ($m^4/s^3$) | Heat flux $H\left(\frac{m^2}{s^2}\right)$ | Mixing height $z_i$(m) | $V_B\left(\frac{m}{s}\right)$ | $V_\infty\left(\frac{m}{s}\right)$ | $V_\infty/V_B$ |
|---|---|---|---|---|---|---|---|
| Single cooling tower sensible heat | 25 | 3500 | $10^{-2}$ | $10^3$ | 5.2 | 0.32 | 0.06 |
| Cluster of 20 cooling towers sensible heat | 500 | 70 000 | $10^{-2}$ | $10^3$ | 5.2 | 1.7 | 0.33 |
| | 5000 | 70 000 | $10^{-2}$ | $10^3$ | 2.4 | 1.7 | 0.71 |
| Strong natural convection | 500 | 2500 | $10^{-2}$ | $10^3$ | 1.7 | 1.7 | 1.0 |
| Oil burners | 125 | 6000 | $10^{-2}$ | $10^3$ | 3.6 | 1.6 | 0.44 |
| Saturn V | 10 | 1 300 000 | $10^{-2}$ | $10^3$ | 51.0 | 0.13 | 0.0025 |
| Australian bushfires | $10^3$ | 900 000 | $10^{-2}$ | $10^3$ | 13.8 | 1.7 | 0.12 |

Observations agree with most of the predictions of this table. Whirlwinds were observed during the oil burner experiment and during some bushfires. Concentration of vorticity is not observed at single cooling towers. The Saturn V cloud did experience a cyclonic circulation, but did not induce whirlwinds or waterspouts. Dust devils and tornadoes are only occasionally observed during strong natural convection. The Surtsey volcano is not included in this table because it induced waterspouts by a different process from that implied in the criterion derived above. The strong inflow to the bottom of the volcano plume caused surface convergence under the bentover plume. Natural vorticity created by the air flowing around the volcano (vortex shedding) was concentrated by this convergence. Similarly, whirlwinds associated with the wildfires to the lee of mountain ranges in the Pacific Northwest derive their vorticity from the strong wind shears near the mountain top. In these cases, we are not sure how to estimate the environmental speed $V_\infty$.

## 5. Problems of calculating cloud formation and plume merging for multiple plumes

As Huff (1972) points out, atmospheric scientists do not yet have adequate information to provide good quantitative answers to the question of cloud and precipitation augmentation by cooling towers. A few simple models of cumulus cloud growth have been applied to cooling tower plumes (e.g. Hanna, 1971; EG&G, 1971; McVehil and Heikes, 1974). These models use Kessler *et al.*'s (1964) parameterizations of cloud microphysics, which were developed using observations from natural clouds. There is the possibility that the droplet size distributions are different in cooling tower plumes, due to the source characteristics of drift (water drops splashed from the tower), and therefore Kessler's approximations may not be appropriate in this case. No comprehensive observation program has yet been conducted to verify these cloud microphysics models for cooling tower plumes. Some aircraft measurements of cloud droplet spectra and total liquid water flux are being made in cooling tower plumes by meteorology groups at Penn State University and Battelle Pacific Northwest Laboratory. Lacking detailed information on the cloud microphysics of cooling tower plumes, estimates of cooling tower plume phenomena must necessarily be somewhat speculative.

Cloud formation by wet and dry cooling towers with equal total heat outputs was analyzed using Hanna's (1971) model. It was found that, during given environmental conditions, if a cloud developed over the wet tower, it would usually develop over the dry tower also. By the time both plumes reach cloud level, most of their volume flux is due to entrained environmental air. The plume acts as a carrier for environmental air, raising it to the natural lifting-condensation level.

In a power park there would be many large cooling tower plumes. If they merge, the possibility of cloud formation increases. Briggs (1975) developed an enhancement factor, $E_N$, for bent over plumes, which gives the factor by which the plume rise, $\Delta h$, from a single source should be multiplied to give the plume rise from $N$ sources.

$$E_N = \left|\frac{N+S}{1+S}\right|^{\frac{1}{3}} \quad \text{where} \quad S = 6\left|\frac{(N-1)\Delta x}{N^{\frac{1}{3}}\Delta h}\right|^{\frac{3}{2}}. \quad (1)$$

The symbol $\Delta x$ represents the spacing between adjacent sources. If this formula is applied to clusters of sources, then $(N-1)\Delta x$ should be replaced by the maximum diameter of the clusters. This technique was tested with data from multiple smoke stacks, with $N$ as great as nine, but has not yet been tested with data from cooling towers. It is possible to calculate the spacing $\Delta x$ necessary to keep the enhancement factor $E_N$ below a certain value, say 1.1. When $E_N$ equals 1.1, the plume rise of the aggregate is 10% greater than the plume rise from a single tower. For example, if the plume rise from a single tower, $\Delta h$, equals 500 m and the number of sources, $N$, equals 50, then, according to this technique, the spacing, $\Delta x$, must be at least 320 m to insure that $E_N$ is less than 1.1.

There are advantages and disadvantages to increasing the tower spacing. An advantage is that the chances of cloud and rainstorm generation are less if the plumes do not merge. A disadvantage is that the chances of high ground level concentrations of fog, drift, and cooling water chemical additives are increased if the plumes do not merge but stay closer to the ground.

A mathematical cloud growth model for multiple plumes must account for interactions between the

plumes and the environmental air. Recent models by Arakawa and Schubert (1974) and Hill (1974) are first steps towards the development of a comprehensive natural cloud growth model. The main stumbling block in the development of such a model has been the problem of computational instability in the computer models of multiple clouds. As these models are developed, it will be possible to apply them to cooling tower plumes to explain the convergence fields beneath the cloud layer and the moisture changes in the environmental air due to the cooling tower energy input.

## 6. Fog possibility

It is of great interest whether fog will occur at the ground downwind of cooling towers. To estimate this effect the Gaussian plume dispersion model can be applied to annual average meteorological conditions (Gifford, 1968; Hanna, 1974). The vertical plume distribution is assumed to be Gaussian with standard deviation $\sigma_z$(m) given by:

$$\sigma_z = 0.056\ x/(1 + 0.0015x)^{0.5}\ \text{m} \qquad (2)$$

which is valid for "D stability" or nearly neutral conditions (Briggs, 1973). Following the references, the horizontal distribution is assumed to be governed by the wind direction distribution. The water concentration, $X$ (g/m$^3$ or g/kg), is then given by the formula:

$$X = (2.0\ Q/U\ \sigma_z x)\ \exp\ (-h_e^2/2\sigma_z^2) \qquad (3)$$

where $Q$(g/s), $U$(m/s), and $h_e$(m) are source strength, wind speed, and effective plume height, respectively. Estimates of $\sigma_z$ have been validated only out to distances of about 20 km. However, in this analysis we will use the formula out to distances of 100 km, in order to make some rough estimates of water concentration at great distances. To determine average annual concentrations, the concentration calculated in a given wind direction is weighted by the frequency with which the wind blows in that direction.

As an example of these calculations, source strength, $Q$, is assumed to equal $4 \times 10^7$ g/s of water, or 80 000 MW heat dissipation (assuming that 2000 MW of heat dissipation is roughly equal to $10^6$ g/s of water evaporation). The magnitude of water flux can be seen by considering that it is the equivalent of about 12 cm/yr of water evaporated over an area of $10^4$ km$^2$. Effective plume height is assumed here to be 100 m, but can be more accurately calculated using Hanna's (1972) formulas for plume rise from a single cooling tower. This figure is probably on the low side of the range of possible plume heights, but will be used because it yields conservative estimates of ground level water concentrations. As shown by equation (3), ground level concentrations can be greatly reduced by increasing the effective plume height, $h_e$. This can be accomplished by placing the cooling towers as close together as possible, so that their plumes combine. But it was mentioned in the previous section that if the plumes combine the possibility of large cloud development is enhanced. There is a paradox that certain atmospheric effects are enhanced no matter how the towers are spaced. Further study is necessary to determine which of these atmospheric effects is more tolerable.

An alternative model, simpler than the Gaussian plume model, is provided by the well-mixed piece-of-pie model: in this, water is assumed to be mixed uniformly within a sector of angular width 22.5° and within the vertical depth, $Z$. The formula for the concentration, $X$, is

$$X = \frac{Q}{UZ(2\pi x/16)}. \qquad (4)$$

The results of both (3) and (4) are given in Table 3. For the purposes of illustration it is assumed that the average wind speed is 3.7 m/s, and that the plumes from all of the towers merge by a distance of 10 km from the site. The mixing depth, $Z$, is assumed to be 300 m.

The results of the two plume models agree within a factor of two, indicating that they are not particularly sensitive to the form of model chosen.

These figures must be compared with the saturation deficit $\Delta m$ (g water vapor/kg air), defined as the difference between the saturation mixing ratio and the actual mixing ratio. If the concentration, $X$, of excess water is greater than the saturation deficit, $\Delta m$, then fog forms. We will assume, for the sake of illustrating the point, that the probability distribution of saturation deficits measured at Oak Ridge, Tennessee, and reported by Hanna and Perry (1973) is the same as that of this hypothetical site. Thus the probability that the saturation deficit is less than 0.5, 1, 2, and 4 g/kg is 21, 32, 49, and 66%, respectively. Based on the results of the Gaussian plume model, we can predict that fog due to the cooling towers will occur downwind, at the ground under the plume about 66, 32, and 21% of the time at distances of 20, 50, and 100 km from the site. If winds are equally probable from all directions, then on an annual basis fog due to the cooling towers will occur at any given spot about 4, 2, and 1% of the time at distances of 20, 50, and 100 km, respectively. Since the average occurrence of rain is about 10%, and of light and dense fog is 6% and 2%, respectively, then the cooling towers are predicted to cause a significant increase in fog concentrations at these distances.

If the cooling towers were spaced at least 1 km apart, their plumes would not merge until 5 or 10 km downwind. Close to the towers, the source strength, $Q$, would thus be that of a single tower, about $10^6$ g/s, and ground level excess water concentrations would be 0.30, 1.0, and 0.70 at distances of 1, 2, and 5 km from the towers.

TABLE 3. Ground level concentrations of excess water from cooling towers, assuming $Q = 4 \times 10^7$ g/s. $U = 3.7$ m/s, and neutral stability.

| Distance downwind | $x$(km) | 10 | 20 | 50 | 100 |
|---|---|---|---|---|---|
| Gaussian plume | $X$(g/kg or g/m$^3$) | 13 | 4.9 | 1.1 | 0.42 |
| Well-mixed pie | $X$(g/kg or g/m$^3$) | 7.9 | 4.0 | 1.6 | 0.79 |

Annual increases in fog at any given location for this configuration would be of the order of 2%.

These calculations assume, in keeping with all current models of water dispersion from cooling towers, that water is thermodynamically inert which, of course, it is not. When the water vapor condenses, latent heat is released, and this contributes to the plume dynamics in a way that must necessarily affect plume growth, merging, height of rise, fogging, and so on. Natural cloud physics processes operate and should be included in any more detailed model of fog occurrence.

In the case of the low-level, mechanical draft (wet) cooling towers, plume aerodynamic downwash to the ground within a few tens of meters of the banks of towers can be expected to occur frequently. Based on Oak Ridge experience (Hanna, 1975), this can be expected to occur approximately 30% of the time. This would result in a fairly dense fog at ground level within several hundred meters downwind of the tower banks, and it would be well on this account to consider the location of these with respect to highways. These plumes will ordinarily rise at still greater downwind distances owing to buoyancy, but subsequently will diffuse downward to the surface again, just as in the case of natural draft towers. However, the added contribution to the effective plume height, $h_e$, due to the initial tower height will not in this case be available. Although we have not made calculations for this case, it is clear that plume saturation, i.e., fogging, will occur sooner (i.e., closer to the source) and more frequently, for mechanical draft towers.

## 7. Drift deposition

It is assumed that about $5 \times 10^3$ g/s of circulating water would be sprayed as drift from wet cooling towers at the site considered in the last section. According to Shofner *et al.* (1975), typical drop diameter of the drift water from modern cooling towers is about 100 $\mu$m. We do not know what the concentration of chemical impurities will be in the drift water. To calculate drift deposition accurately, drop evaporation and plume kinetics must be accounted for, using techniques proposed by Laskowski (1975) or Hanna (1974). Here we will make only a crude calculation since the exact chemical makeup is not known.

The settling speed of water drops with diameters of 100 $\mu$m is about 0.27 m/s. Consequently, it will take the drops about 750 s to fall to the ground from a plume height of 200 m. If the wind is blowing at an average speed of 3.7 m/s, the drops will strike the ground about 2780 m from the towers. If it is then assumed that the drops are deposited uniformly on a ring around the site, with inner radius 2000 m and outer radius 4000 m, then the deposition rate of water, $\omega$(g/m$^2$s) equals

$$\omega = \frac{5 \times 10^3 \text{ g/s}}{\pi[(4000 \text{ m})^2 - (2000 \text{ m})^2]} = 1.3 \times 10^{-4} \text{ g/m}^2 \text{ or } 2.1 \times 10^7 \text{ g/acre yr.} \quad (5)$$

This figure is the equivalent of a rainfall rate of 0.4 cm/yr. The deposition rate of chemicals that are present in the circulating water would equal the deposition rate of water times the mass concentration of the chemicals in the water. For example if the cooling water were sea water with a salt (NaCl) concentration of 30 000 ppm, the deposition rate of salt would be $3.9 \times 10^{-6}$ g/m$^2$ s or $6.3 \times 10^5$ g/acre yr.

## 8. Summary

By comparison with the energy production of natural atmospheric processes, the generation of waste heat at a 10 000 to 50 000 MW power park ranks between thunderstorms and squall lines on the energy intensity scale. Certain geophysical phenomena have produced energy at rates on the order of that for the proposed power centers. These have caused cumulus clouds to form to heights of more than 5 km in the atmosphere, accompanied by local inflow of air at the surface, by intense vortices, and sometimes by thunderstorm phenomena.

A criterion for determing whether natural vorticity will be concentrated by a buoyant source is applied to the natural and man-made heat sources discussed in this paper. The predictions of this criterion are shown to be generally correct for sources such as bushfires, oil fires, and natural convection. The criterion predicts vortices to be formed around power parks.

Using an empirical method for estimating multiple plume rise, it is predicted that the plume rise from an aggregate of cooling towers will be 10% or more greater than the rise from a single tower if the towers are spaced closer than 300 m.

A condensed plume is predicted to occur about 20% of the time at distances of 100 km from natural draft towers dissipating about 80 000 MW of waste heat, for a power park location in the southeast U.S. At a given location within 100 km of such towers, excess ground fog due to the towers would occur about 2% of the time. Drift deposition of water would average about 0.4 cm/yr at distances from 2 to 4 km from the towers. Naturally occurring precipitation phenomena would be augmented.

The preceding numerical estimates are all tentative and approximate, and they should be verified in the future using more complete theories and data. There is, however, no reason to doubt their general level of accuracy, even though the precise values are in some question.

## 9. Suggestion for future research

Almost all of the problems related to the meteorological effects of large power centers are currently marked by inadequate theories and the absence of observations. The following research programs are urgently needed in support of any more detailed consideration of the meteorological effects of a power center.

1) A theory of the merging of separate convective elements should be developed.

2) Models of multiple cloud growth and their interaction with the environment should be studied and applied to the power park problem.

3) Mathematical models of cloud growth due to large, continuous, latent and sensible heat plumes from fixed sources should be devised and studied. These phenomena should be measured in the atmosphere and the model calculations tested with the observations.

4) Models combining both thermodynamical (buoyancy and latent heat) effects and passive diffusion of cooling tower plumes should be developed and tested.

5) Physical modeling in a wind or water tunnel of aerodynamic (downwash) effects of various cooling tower configurations is needed. (Groups of towers may act as a collective barrier to air flow.)

6) A more detailed drift deposition model is needed, which should account for the initial distribution of drift drops across the plume.

7) Scavenging of pollutants (including radioactive species) by cooling tower plume water drops needs to be studied.

8) A modeling effort, mathematical or in a suitable wind tunnel, or preferably both, should be made to study the possible role of the contemplated waste heat releases from energy centers in organizing and concentrating local atmospheric convection and vorticity. There is a particular need for more measurement programs to accompany all these theoretical and design studies, because the values of many controlling parameters must be determined.

*Acknowledgments:* This research was performed under an agreement between the U.S. Atomic Energy Commission and the National Oceanic and Atmospheric Administration. The authors thank I. Spiewak and R. Bryan of the Oak Ridge National Laboratory for many helpful discussions regarding the power plant concept, and G. Briggs of this office for his guidance in the problems of vorticity concentration and plume merging.

## References

Arakawa, A., and W. Schubert, 1974: Interaction of a cumulus cloud ensemble with the large-scale environment, Part I. *J. Atmos. Sci.,* **31,** 674–701.

Bourne, A. G., 1964: Birth of an island. *Discovery,* **25,** 16–19.

Briggs, G. A., 1969: *Plume Rise.* AEC Critical Review Series, USAEC-TID-24635, available from Springfield, Va., National Technical Information Service (NTIS), vi + 81 pp.

——, 1973: Diffusion estimation for small emissions. Available as ATDL Report No. 79, ATDL, P.O. Box E, Oak Ridge, Tenn. 37830, 59 pp.

——, 1975: Plume rise from multiple sources. In *Cooling Tower Environment—1974.* Springfield, Va., NTIS, pp. 161–179.

*Cooling Tower Environment—1974:* Symposium proceedings, CONF-74032, available from Springfield, Va., NTIS, 638 pp.

Davies, R. W., 1959: Large scale diffusion from an oil fire. In *Advances in Geophysics,* **6,** F. N. Frenkiel and P. A. Sheppard (Eds.), New York, Academic Press, Inc., pp. 413–415.

Deardorff, J. W., 1972: Numerical investigation of neutral and unstable planetary boundary layers. *J. Atmos. Sci.,* **29,** 91–115.

Dessens, J., 1964: Man made thunderstorms. *Discovery,* **25,** 40–44.

Edgerton, Germeshausen, and Grier, Inc., 1971: Potential environmental modifications produced by large envaporative cooling towers. Prepared by EG&G, Inc., Boulder, Colo. under Cont. No. 16130 DNH 01/71 from the Water Quality Office, EPA, available from Supt. of Documents, U.S. Govt. Printing Office, Washington, 77 pp.

Gifford, F. A., 1968: An outline of theories of diffusion in the lower layers of the atmosphere. In *Meteorology and Atomic Energy—1968.* D. H. Slade (Ed.), USAEC Report TID-24190, available from Springfield, Va., NTIS, pp. 65–116.

Graham, H. E., 1955: Fire whirlwinds. *Bull. Amer. Meteor. Soc.,* **36,** 99–103.

Hanna, S. R., 1971: Meteorological effects of cooling tower plumes. Presented at Cooling Tower Inst. Meeting, available as Report 48, ATDL, P.O. Box E, Oak Ridge, Tenn. 37830, 15 pp.

——, 1972: Rise and condensation of large cooling tower plumes. *J. Appl. Meteor.,* **11,** 793–799.

——, 1974: Fog and drift deposition from evaporative cooling towers. *Nuclear Safety,* **15,** 190–196.

——, 1975: Meteorological effects of the mechanical draft cooling towers of the Oak Ridge Gaseous Diffusion Plant. In *Cooling Tower Environment—1974.* Springfield, Va., NTIS, pp. 291–306.

——, and S. G. Perry, 1973: Meteorological effects of the cooling towers at the Oak Ridge Gaseous Diffusion Plant, Part I. ATDL Report No. 86, ATDL, P.O. Box E, Oak Ridge, Tenn. 37830, 40 pp.

——, and S. D. Swisher, 1971: Meteorological effects of the heat and moisture produced by man. *Nuclear Safety,* **12,** 114–122.

Hill, G. E., 1974: Factors controlling the size and spacing of cumulus clouds as revealed by numerical experiments. *J. Atmos. Sci.,* **31,** 646–673.

Huff, F. A., 1972: Potential augmentation of precipitation from cooling tower effluents. *Bull. Amer. Meteor. Soc.,* **53,** 639–644.

——, and S. A. Changnon, Jr., 1972: Climatological assessment of urban effects on precipitation at St. Louis. *J. Appl. Meteor.,* **11,** 825–843.

Kessler, E., P. J. Feteris, E. A. Newberg, and G. Wickham, 1962–1964: Relationship between tropical precipitation and kinematic cloud models. Prog. Repts. 1–5, The Travelers Research Center, Inc., Hartford, Conn., Cont. DA-36-039-SC89099 (Available from DDC, Cameron Station, Alexandria, Va., as AD 286 737, AD 296 036, AD 402 766, AD 424 993, AD 437 817).

Koenig, L. R., and C. M. Bhumralkar, 1974: On possible undesirable atmospheric effects of heat rejection from large electric power centers. Report No. R-1628-RC, Santa Monica, Calif., Rand, 40 pp.

Landsberg, H., 1947: Fires storms resulting from bombing conflagrations. *Bull. Amer. Meteor. Soc.,* **28,** 72.

Laskowski, S., 1975: A mathematical transport model for salt distribution from a salt water-natural draft cooling tower. In *Cooling Tower Environment—1974*. Springfield, Va., NTIS, pp. 591–613.

McVehil, G., and K. Heikes, 1974. Cooling tower plume modeling and drift measurement. Prepared by Ball Bros. Res. Corp., Boulder, Colo., iv + 125 pp.

Morris, D. G., 1968: Initiation of convective clouds due to static firing of the Saturn V first stage. *Bull. Amer. Meteor. Soc.*, **49**, 1054–1058.

Peterson, J., 1969: The climate of cities: A survey of recent literature. U.S. Dept. of Health, Educ., and Welfare, Pub. Health Ser., Raleigh, N.C.

Rotty, R. M., 1975: Waste heat disposal from nuclear power plants. NOAA Tech. Memo ERL-ARL 47.

Shofner, F., T. Carlson, and R. Webb, 1975: Measurement and interpretation of drift particle data. In *Cooling Tower Environment—1974*. Springfield, Va., NTIS, pp. 427–451.

Stern, M. E., and J. S. Malkus, 1953: The flow of a stable atmosphere over a heated island. *Bull. Amer. Meteor. Soc.*, **10**, 105–120.

Taylor, D. F., and D. T. Williams, 1968: Severe storm features of a wildfire. *Agric. Meteor.*, **5**, 311–318.

Taylor, R. J., S. T. Evans, N. K. King, E. T. Stephens, D. R. Packham, and R. G. Vines, 1973: Convective activity above a large scale brushfire. *J. Appl. Meteor.*, **12**, 1144–1150.

Thorarinsson, S., and B. Vonnegut, 1964: Whirlwinds produced by the eruption of Surtsey Volcano. *Bull. Amer. Meteor. Soc.*, **45**, 440–444.

# Consequences of Effluent Release

**Edited by R. L. Shoup**

# Turbulent Diffusion-Typing Schemes: A Review

By F. A. Gifford*

**Abstract:** *Recent environmental concerns have greatly increased the need for turbulent typing schemes in atmospheric diffusion calculations. The standard methods by Brookhaven National Laboratory, Pasquill, the Tennessee Valley Authority, and others are reviewed, and differences, inconsistencies, and modifications to the basic schemes are discussed. Various exceptional flows occur to which existing turbulence typing schemes should not be applied directly: diffusion in near-calm, very stable conditions; diffusion over cities, water bodies, and irregular terrain; and diffusion in building wakes and near highways. Possible modifications to typing schemes in these cases are discussed. In all such exceptional cases, many more observational data are needed before reliable diffusion estimates can be made.*

Pollutants are released from various sources near the earth's surface, and the resulting ground-level air concentration patterns have to be estimated. This information is needed for a wide variety of air-pollution analyses and forecasts required by various provisions of the National Environmental Policy Act (NEPA), as well as for facility siting and design and many other industrial and social planning purposes. For instance, average values of pollutant concentrations must be calculated over periods ranging from an hour or less to a year in order to satisfy various current legal requirements for environmental control.

*Franklin A. Gifford is Director of the Atmospheric Turbulence and Diffusion Laboratory of the National Oceanic and Atmospheric Administration, Oak Ridge, Tenn. He received the B.S. degree in meteorology from New York University in 1947 and the M.S. and Ph.D. degrees from Penn State University in 1954 and 1955, respectively. He spent 5 years with Northwest Airlines (1945–1950) and 16 years with the U. S. Weather Bureau (1950–1966) before assuming his present position in 1966. He has been a member of the Advisory Committee on Reactor Safeguards from 1958 to 1969 and a consultant to the Committee since 1969.

NUCLEAR SAFETY, Vol. 17, No. 1, January–February 1976

Air concentration patterns are controlled by atmospheric diffusion, a process that depends on the state of the atmospheric turbulence at any location and time; however, atmospheric turbulence is difficult and expensive to measure directly. Consequently it is useful to be able to describe the boundary-layer turbulence in terms of routine measurements of the mean values* of meteorological quantities and their vertical gradients, principally the average temperature, the horizontal wind, and the vertical gradients of wind and temperature. The theory of the relation between these quantities and the turbulence has been worked out in considerable detail for the lower part of the boundary layer and is, by and large, quite successful. Detailed summaries were given in a recent workshop on micrometeorology[1] and in a review by Panofsky.[2] However, the relation between the quantities and atmospheric diffusion is much less well understood. Therefore it has been found necessary to develop empirically based, more-or-less qualitative, turbulence typing schemes in order to handle practical atmospheric diffusion problems.

Probably the most widely used typing system is based on the scheme proposed by Pasquill.[3] A closely related method, the Brookhaven National Laboratory (BNL) turbulence types, is also in fairly widespread use. The recent surge of activity in the area of air-pollution analysis, in the wake of NEPA and such court cases as the Sierra Club ruling on environmental nondegradation, has highlighted the need for such turbulence typing systems. By emphasizing the often considerable social and economic issues that ride on diffusion calculations, the current need has led to a

*Averaged over a time period of the order of 30 to 60 min.

ATDL Contribution File No. 75/2

large number of applied studies involving various developments and modifications of the original typing schemes. These have not always been entirely in agreement, either with one another or with the original intent. It seems useful to try to sort out much of this material with the object of bringing out interrelations and emphasizing, if only qualitatively, the straightforward physical reasoning that underlies all these typing schemes.

## TURBULENCE TYPING SCHEMES

### BNL Turbulence Types

An early attempt to categorize turbulence was made by Giblett,[4] who was concerned with the dimensions of eddies as they affected the mooring and ground handling of large airships. He distinguished categories of atmospheric turbulence based on the character of the wind as measured continuously by a sensitive recorder (Dines anemograph) and the accompanying vertical temperature gradients. This system consisted of four types, ranging from type I (unstable, gusty, cumulonimbus clouds present) to type IV (strong temperature inversion; anemograph trace shows practically no turbulence).

The BNL turbulence typing scheme, as originally presented by Smith,[5] is quite similar to Giblett's four-category scheme. The BNL scheme has been refined, developed, and summarized in a series of papers.[6-10] The types are based on the range of fluctuations of the (horizontal) wind-direction trace as recorded by a Bendix–Friez aerovane located at the 108-m level of the BNL tower. It was found desirable to expand the original four-category scheme, and the BNL types now have the following definitions:[9]

A. Fluctuations (peak to peak) of the horizontal wind direction exceeding 90°

$B_2$. Fluctuations ranging from 40 to 90°.

$B_1$. Fluctuations similar to A and $B_2$ but confined to 15 and 45° limits.

C. Fluctuations greater than 15° distinguished by the unbroken solid core of the trace.

D. The trace approximates a line; short-term fluctuations do not exceed 15°.

(Fluctuations are recorded over a 1-hr period.)

This system was applied to the analysis of extensive air concentration data in the form of measurements of the dispersion of oil-fog plumes from a source 108 m high. The BNL types were related to the observed horizontal standard deviations of the plume concentration distribution. Values of the vertical plume standard deviations $\sigma_z$ were calculated on the assumption of a Gaussian form for the concentration distribution. As in Sutton's[11] diffusion theory, the power laws for vertical and horizontal spread as a function of downwind distance, $\sigma_z(x)$ and $\sigma_y(x)$, were assumed to have equal indices. These results are summarized in Table 1, and curves of $\sigma_y$ and $\sigma_z$ vs. downwind distance $x$ are reproduced in Fig. 1.

The BNL scheme provides for categorizing turbulence by means of reasonably simple measurements and relating the categories to atmospheric dispersion estimates derived from data. Note that the categories are site specific, applying strictly to conditions equivalent to those found at BNL. The diffusion data are for a nonbuoyant plume released at 108 m, and the wind speeds and trace characteristics refer to that height. All measurements refer to average values over a period of the order of 1 hr (wind averaged over 1 hr; concentrations averaged over 30 to 90 min).

### Pasquill's Turbulence Types

Pasquill[3] proposed a simple scheme of turbulence typing that has been widely applied. Information on this scheme has been included in earlier papers by

**Table 1 Properties of the BNL Turbulence Types**

| Type | Seasonal frequency, % | $\Delta T/\Delta z$ per 123 m, °C | Average wind speed at 108 m, m/sec | $\sigma_y$, m | $\sigma_z$, m | $n$ | $C_y$ | $C_z$ | Average wind speed at 9 m, m/sec |
|---|---|---|---|---|---|---|---|---|---|
| A | 1 | −1.25 ± 7* | 1.8 ± 1.1* | | | | | | |
| $B_2$ | 3 | −1.6 ± 0.5 | 3.8 ± 1.8 | $0.40x^{0.91}$ | $0.41x^{0.91}$ | 0.19 | 0.56 | 0.58 | 2.5 |
| $B_1$ | 42 | −1.2 ± 0.65 | 7.0 ± 3.1 | $0.36x^{0.86}$ | $0.33x^{0.86}$ | 0.28 | 0.50 | 0.46 | 3.4 |
| C | 14 | −0.64 ± 0.52 | 10.4 ± 3.1 | $0.32x^{0.78}$ | $0.22x^{0.78}$ | 0.45 | 0.45 | 0.32 | 4.7 |
| D | 40 | +2.0 ± 2.6 | 6.4 ± 2.6 | $0.31x^{0.71}$ | $0.06x^{0.71}$ | 0.58 | 0.44 | 0.05 | 1.9 |

*Standard deviation.

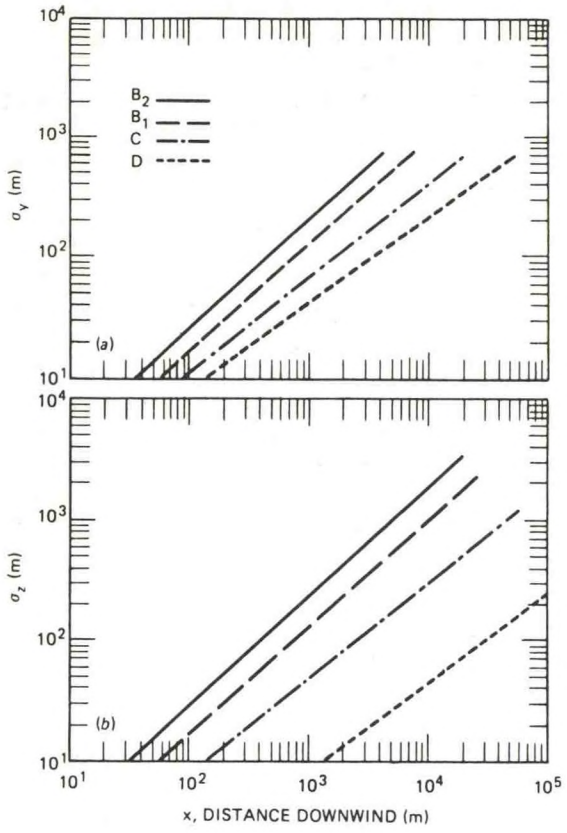


**Fig. 1 Curves of $\sigma_y$ and $\sigma_z$ for BNL turbulence types from Singer and Smith.[9] Letters refer to BNL stability types in Table 1.**

Meade [12,13] that were based on a still earlier unpublished note by Pasquill. Pasquill presented information on the lateral spreading $\theta$ and the vertical spreading $h$ of diffusing plumes in the form of a graph for the latter and a table for the former as functions of six atmospheric stability classes designated A to F. These were arranged so that class A corresponds to extremely unstable conditions and class F to stable conditions. The quantities $h$ and $\theta$ mark the 10% points of the plume concentration distribution relative to its mean centerline value. The applicable stability category is chosen by reference to a table relating these to observed wind speed, cloud cover, and isolation conditions (Table 2). These weather elements are widely observed routinely all over the world.

Gifford[14] described this turbulence typing scheme in a review article based on the earlier presentations of Pasquill's $h$ and $\theta$ values by Meade and converted the plume spreading data into families of curves of the standard deviations, $\sigma_y$ and $\sigma_z$, of the plume concentration distribution (Fig. 2).* This was done partly because the standard deviation is a very commonly used statistic and partly to emphasize that the method could readily be used with the Gaussian plume formula. A plume formula of this type had been used as a convenient interpolation formula for diffusion data by Cramer,[15] Hay and Pasquill,[16] and others. Pasquill's typing scheme has almost always been used and quoted in the form of these or similar graphs of $\sigma_y$ and $\sigma_z$ which, for this reason, are frequently called the Pasquill–Gifford (PG) curves. Although grateful for the association, the writer would like to reemphasize that the idea behind this useful scheme is attributed to Pasquill.

Turner[17,18] introduced a version of Pasquill's scheme in which the incoming solar radiation is classified in terms of elevation angle and cloud amount and height. The procedure is objective and involves meteorological quantities (i.e., cloud cover and height and solar angle) that are known for most locations. Thus it is well adapted to air-pollution studies and has been widely used.

Turner expressed his $\sigma_y$ and $\sigma_z$ curves as functions of travel time, $t = x/u$, rather than downwind distance $x$. Curves were labeled numerically: 1 for extreme instability, 4 for neutral conditions, to 7 for extreme stability, etc. Turner pointed out that curves for classes 1 to 5 are essentially identical to PG curves A to E. It seems clear that Turner intended this correspondence and that his use of numbers rather than letters to designate the stability types was fortuitous. However, Golder,[20] who studied large amounts of micrometeorological and diffusion data, including the Kerang (Australia), Round Hill (Mass.), O'Neill (Nebr.), Hanford (Wash.), and Cape Kennedy (Fla.) data sets, calculated both Pasquill and Turner classes and found some differences. Golder concluded that the best conversion is provided by A to 1, B to 2, C to 3, D to 4, E to 6, and F to 7.

Klug[21] developed a typing scheme very similar to Pasquill's. It differs primarily in that Table 2 is

*The curves of $h$ published by Pasquill[3] were slightly modified as compared with the earlier versions, those presented by Meade,[12,13] and in the earlier note by Pasquill. The $\sigma_z$ curves of Fig. 2 are based on the later $h$ curves and consequently differ slightly from those in Gifford,[14] which were necessarily based on the earlier version. The principal difference is that the A and B curves of Fig. 2 bend upward less rapidly for $x$ greater than about 200 m. This is in accord with theoretical results on the free-convection limit of boundary-layer turbulence, which affects the A and B categories and, as will be seen, is closer to recently proposed interpolation formulas by Briggs.[19]

**Table 2 Meteorological Conditions Defining Pasquill Turbulence Types**

A: Extremely unstable conditions
B: Moderately unstable conditions
C: Slightly unstable conditions
D: Neutral conditions*
E: Slightly stable conditions
F: Moderately stable conditions

| Surface wind speed, m/sec | Daytime insolation | | | Nighttime conditions | |
|---|---|---|---|---|---|
| | Strong | Moderate | Slight | Thin overcast or ≥4/8 cloudiness† | ≤3/8 cloudiness |
| <2 | A | A–B | B | | |
| 2 | A–B | B | C | E | F |
| 4 | B | B–C | C | D | E |
| 6 | C | C–D | D | D | D |
| >6 | C | D | D | D | D |

*Applicable to heavy overcast day or night.

†The degree of cloudiness is defined as that fraction of the sky above the local apparent horizon that is covered by clouds.

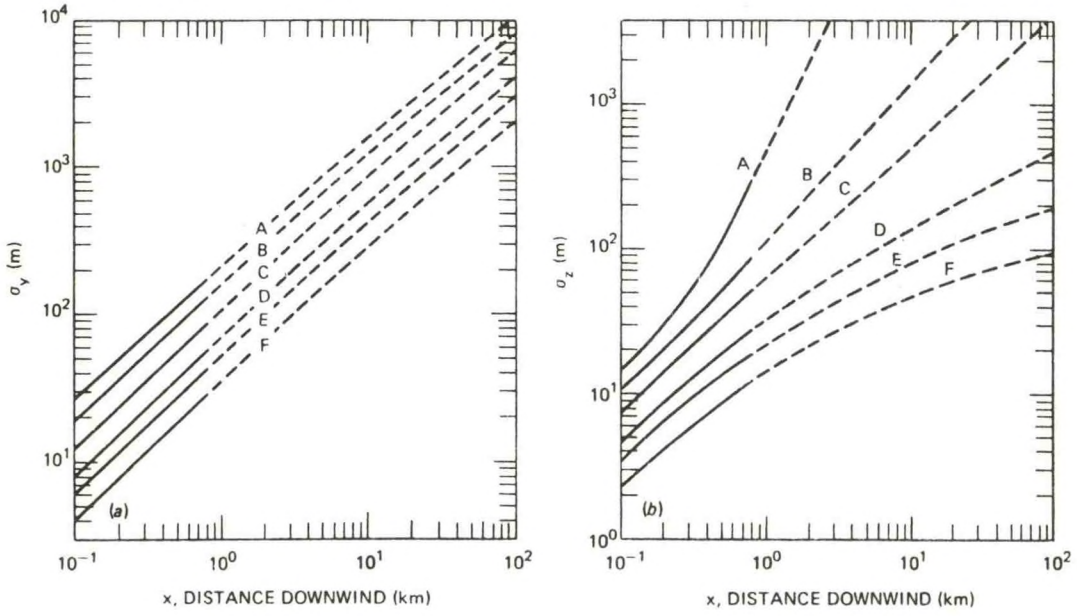


**Fig. 2 Curves of $\sigma_y$ and $\sigma_z$ for Pasquill's turbulence types based on Pasquill.[3] See also Gifford,[76] Slade,[30] and Turner.[36]**

replaced by a more detailed set of rules relating cloudiness, wind speed, time of day, and season.

Pasquill's types, which were subjectively chosen, appear to be approximately linearly related to turbulence intensity, which is a desirable property. Luna and Church[22] showed that the total change in median turbulence intensity (at Augusta, Ga.) as the category changes from A through F is equal to about an order of magnitude and occurs approximately linearly. However, attempts to relate the types to various objective stability criteria (such as lapse rate and bulk Richardson number) have been characterized by considerable scatter.

### Use of Measurements of Wind-Direction Standard Deviation

Cramer[15,23] suggested a method of classifying turbulence for the purpose of diffusion estimation based on the standard deviation of the wind measured by bidirectional wind vanes. By correlating observations of $\sigma_A$ and $\sigma_E$, the azimuth and elevation angle standard deviations, for a range of stabilities with

simultaneously measured horizontal plume spreading data, he set up a table of correspondences between $\sigma_A$ and $\sigma_E$ values and the plume standard deviations using a four-category system (Table 3).*

Cramer's system was based on the Round Hill and Prairie Grass experimental data. Studies of these and later experimental diffusion data, summarized by Islitzer and Slade,[24] generally supported the kind of values proposed by Cramer (e.g., the summaries of Idaho Falls data by Islitzer[25] and of Hanford data by Fuquay et al.).[26] These were also similar to the experimental values presented by Hay and Pasquill.[16] On the basis of these and related studies, Islitzer and Slade[24] proposed correspondences between $\sigma_A$ values and the PG curves. These are summarized in Table 4, together with the conversions to the Turner and the BNL types.

It seemed that, at least in principle, plume standard deviations could be estimated by measuring either the lapse rate $-\Delta_T/\Delta z$ or the standard deviation of the horizontal wind direction $\sigma_A$ as well as mean wind speed. For this reason relations among the Pasquill types, lapse rates, and $\sigma_A$ values have frequently been adopted as standards [e.g., U. S. Nuclear Regulatory Commission (NRC) Regulatory Guide 1.21].[31] This method is satisfactory at any particular site; see, for example, the study by Vogt and Geiss[32] of dispersion at Jülich. However, the relation of turbulence type to lapse rate has generally proved to be too variable from site to site to be very useful, for reasons given below.

### TVA Experience

Carpenter et al.[33] summarized 20 years of Tennessee Valley Authority (TVA) experience with the measurement of concentration patterns and related values of meteorological parameters. The emissions in this case were all in the form of buoyant plumes from tall stacks. Stack heights ranged from about 75 to 250 m, and the effective stack height (i.e., the stack height plus buoyant plume rise) was rarely less than twice that figure. TVA used a six-category typing scheme, ranging from neutral to strong inversion, based on lapse rate. The resulting families of $\sigma$ curves are reproduced in Fig. 3, together with the lapse-rate values measured at plume height, to which they apply. Further details of the TVA approach can be found in Islitzer and Slade.[24] It should be noted that the TVA plume samples refer to an effective averaging time of about 2 to 5 min, which is somewhat shorter than that for the other schemes.

Table 3 Cramer's Turbulence Classes

| Stability description | $\sigma_A$, deg | $\sigma_E$, deg |
|---|---|---|
| Extremely unstable | 30 | 10 |
| Near neutral (rough surface; trees, buildings) | 15 | 5 |
| Near neutral (very smooth grass) | 6 | 2 |
| Extremely stable | 3 | 1 |

Table 4 Relations Among Turbulence Typing Methods

| Stability description | Pasquill | Turner* | BNL† | $\sigma_A$, deg‡ |
|---|---|---|---|---|
| Very stable | A | 1 | $B_2$ | 25 |
| Moderately unstable | B | 2 | $B_1$ | 20 |
| Slightly unstable | C | 3 | $B_1$ | 15 |
| Neutral | D | 4 | C | 10 |
| Moderately stable | E | 6 | | 5 |
| Very stable | F | 7 | D | 2.5 |

*Golder.[20]
†Philadelphia Electric Company.[29]
‡Slade.[30]

## MODIFICATIONS OF THE BASIC SCHEMES

The preceding section is a brief, essentially historical, account of the major turbulence typing systems now in use. Because they reflect different diffusion-data bases and, to a certain extent, were at least originally addressed to different applied problems, these schemes might be expected to differ from each other, and they do. Comparison of Figs. 1 to 3 reveals major disagreements; the curves do not have the same shape. The PG curves of $\sigma_z$ have larger values and more sharply increasing upward curvature with distance for unstable conditions and conversely for stable conditions, although the difference is in that case less pronounced. PG curves of $\sigma_y$ are slightly steeper than the BNL curves for all stability conditions but more so for stable. These differences have been discussed by several workers; see, for example, Strom.[34] The TVA

*It was pointed out by Holland[27] and verified by Markee[28] that there is a simple convenient rule of thumb relating the wind-direction standard deviation for a sample of the order of an hour and the range of wind-direction fluctuations over the period; namely, $\sigma_A \simeq (A_{max} - A_{min})/6$, where $A$ is measured in degrees. Thus $\sigma_A$ can easily be found directly from the trace of $A(t)$, i.e., the chart record of a wind vane, by inspection.

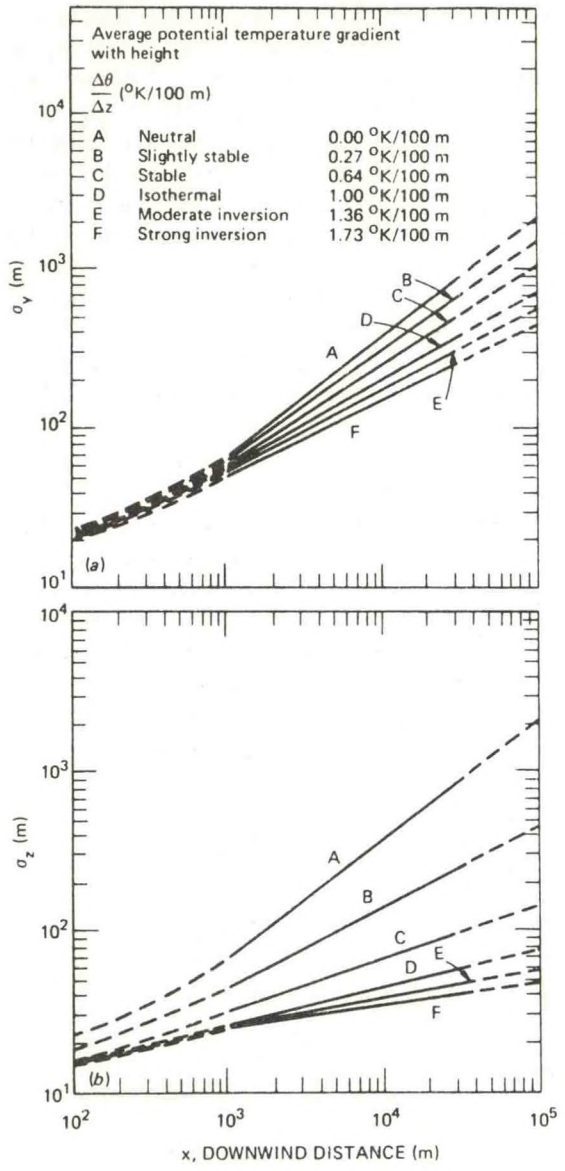


**Fig. 3 Curves of $\sigma_y$ and $\sigma_z$ for TVA data from Carpenter et al.[33] Average potential temperature gradients with height refer to plume height.**

curves differ from both the BNL and the PG curves. Not only are the shapes of the TVA curves rather different, particularly for shorter distances, but also the range of atmospheric stability conditions encountered for these elevated plumes is much narrower and includes no unstable conditions at plume height. This is in contrast to the wide range of near-surface-level stability conditions encountered for releases near the ground.

### Briggs's Interpolation Formulas

This situation has been discussed and resolved to the extent possible by Briggs.[19] The diffusion-data bases for the various typing systems have the following characteristics. The PG curves were developed primarily with the aid of diffusion measurements made to a distance of 800 m using a passive (i.e., nonbuoyant) tracer gas that was released near the surface. The BNL curves also reflected nonbuoyant-plume-dispersion data but from an elevated (108-m) source. Ground concentration values were obtained out to several kilometers, but only rarely were measurements made within 800 m of the source. On the other hand, TVA data reflected still greater *effective* heights, from 150 to 600 m or more, and downwind distances of up to tens of kilometers. Moreover, the rate of spreading of plumes from sources of this type primarily reflects buoyancy and entrainment effects on plume behavior rather than ambient atmospheric turbulence properties to considerable distances downwind, of the order of 5 to 10 source heights. According to Briggs,[35] the diffusion of a plume from such a source is quite different from that of passive diffusion from a ground-level source (i.e., the PG curves).

This led Briggs to propose a series of interpolation formulas for $\sigma$ curves that would have the following properties: they would agree with PG curves given by Gifford,[14] Slade,[30] and Turner[36] in the range $100\ \text{m} < x < 10{,}000$ m, except that the curves of $\sigma_z$ for A and B stability would approximate the very unstable and unstable curves recommended by Smith[37] in the American Society of Mechanical Engineers (ASME) guide for $\sigma_z > 100$ m. The $\sigma$ curves in the ASME guide reflect primarily BNL experience. Other than at small distances, where the TVA curves display strong plume-buoyancy effects, the TVA and BNL curves agree reasonably well with one another and, except for A and B conditions as noted, with the PG curves at about 10 km. Beyond that distance, TVA curves are less steeply inclined. Briggs's recommendations apply up to 10 km and could perhaps be extended to 20 or 30 km, although he does not recommend this. Few plume-dispersion values have been reported for distances beyond 10 km. Differences among the various sets of curves probably reflect the uncertainty of the data fairly well. However, as pointed out recently by Draxler,[38] there are systematic differences in $\sigma_y$ and $\sigma_z$ values computed from the various sets of diffusion data related to release height. Briggs's recommended interpolation formulas are summarized in Table 5 and shown in Fig. 4. These are intended primarily for use in

**Table 5 Formulas Recommended by Briggs[19] for $\sigma_y(x)$ and $\sigma_z(x)$; $10^2 < x < 10^4$ m, Open-Country Conditions**

| Pasquill type | $\sigma_y$, m | $\sigma_z$, m |
|---|---|---|
| A | $0.22x(1 + 0.0001x)^{-1/2}$ | $0.20x$ |
| B | $0.16x(1 + 0.0001x)^{-1/2}$ | $0.12x$ |
| C | $0.11x(1 + 0.0001x)^{-1/2}$ | $0.08x(1 + 0.0002x)^{-1/2}$ |
| D | $0.08x(1 + 0.0001x)^{-1/2}$ | $0.06x(1 + 0.0015x)^{-1/2}$ |
| E | $0.06x(1 + 0.0001x)^{-1/2}$ | $0.03x(1 + 0.0003x)^{-1}$ |
| F | $0.04x(1 + 0.0001x)^{-1/2}$ | $0.016x(1 + 0.0003x)^{-1}$ |

calculating ground-level concentrations, in particular the maximum values of these quantities for plumes from elevated stack sources. Consequently these values reflect diffusion data for a higher source at greater downwind distances.

### Use of Power-Law Interpolation Formulas

Many authors have proposed power-law formulas for the type $\sigma_y = ax^b$, $\sigma_z = cx^d$ for use in diffusion formulas. The parameters of these expressions have been tabulated in terms of each of the standard typing schemes by various authors. Values of $a$, $b$, $c$, and $d$ have been given for Pasquill's turbulence types by Tadmor and Gur,[39] Fuquay et al.,[40] Martin and Tickvart,[41] and Eimutis and Konicek.[42] The BNL curves have been approximated as power laws by Singer and Smith,[9] Smith,[37] and Islitzer and Slade.[24] Values of power-law parameters for Cramer's scheme are contained in his paper and in the summary by Islitzer and Slade.[24] In addition, values of the Sutton[11] stability parameter $n$ and diffusion coefficients $C_y$ and $C_z$, based on data comparisons, have been given by Yanskey et al.,[43] as well as in Table 1 and in several of the foregoing references. In Sutton's work, $n$ defines the exponent of a power law for $\sigma$ values. Finally, TVA power-law interpolation formulas have been given by Montgomery et al.[44]

A general limitation of all these results is that no single power law can fit diffusion data over all downwind distance ranges. This point was first made clear by Barad and Haugen[45] and is obvious from Figs. 1 to 3. Moreover, a single power exponent for both horizontal and vertical spreading, as in Table 1, is now known to be inadequate. The elevated-source diffusion observations of $\sigma_z$ reported by Högström[46]

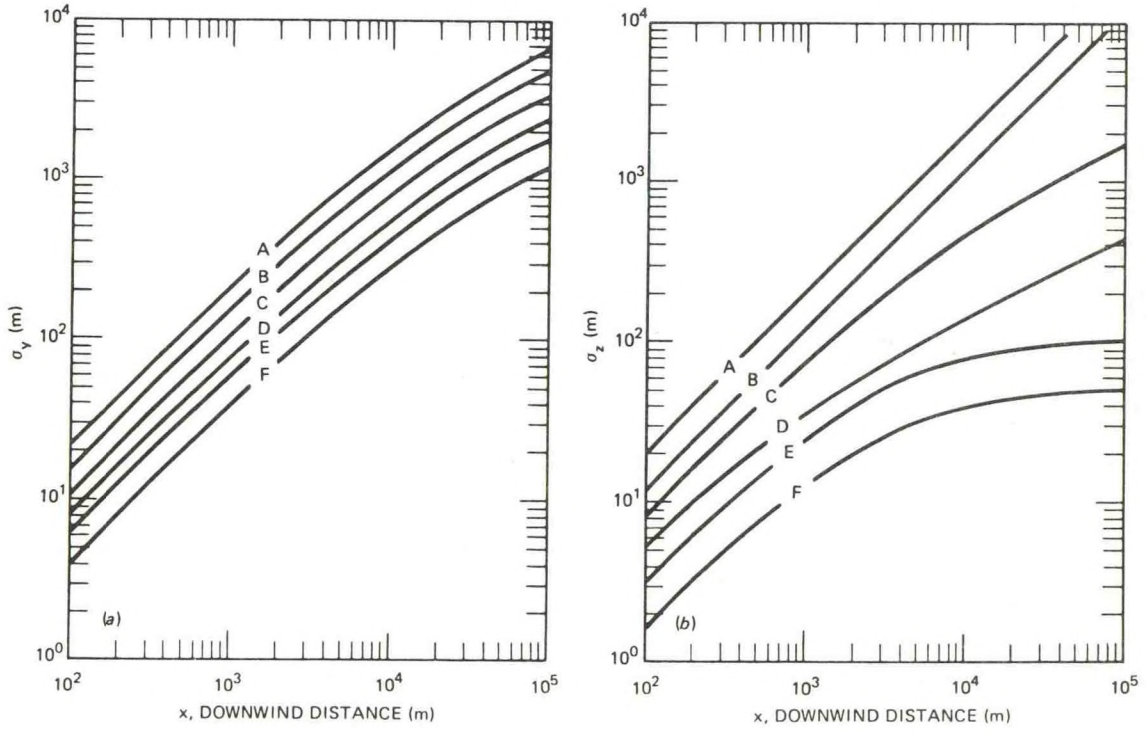


**Fig. 4 Curves of $\sigma_y$ and $\sigma_z$ based on interpolation formulas by Briggs[19] for flow over open country (see Table 5); from Hosker.[55]**

and discussed by Pasquill[47] show that $\sigma_y$ varies as distance to a power in the neighborhood of 0.85, as compared with about 0.55 for $\sigma_z$, in neutral conditions. Briggs's equations (Table 5) are the simplest interpolation formulas that give reasonable approximations to the various diffusion types over the range $100 < x < 10^4$ m. The use of simple power laws in diffusion equations has some purely mathematical advantages, and, for some people, this seems to outweigh the problem of the limited distance over which they apply. For this reason, such power laws will probably always be used to some extent. As long as the distance range is suitably restricted, this practice is acceptable, although Briggs's formulas are preferable.

On the other hand, interpolated values of the parameters in power-law formulas for $\sigma_y$ and $\sigma_z$ have been quoted to three and occasionally four significant figures in some of the papers referred to above. This gives a quite false impression of the degree of precision involved. Studies such as those by Luna and Church[22] and Golder[20] indicate that estimates of $\sigma$ values by these turbulence typing methods have considerable scatter. Pasquill[48] concludes that estimates of pollution concentration based on typing methods may be accurate to within 20% for long-term averages, given good quality emissions and meteorological data, but may exceed a factor of 2 for short-term values.

### Relation of Empirical Stability Categories to Boundary-Layer Turbulence Criteria

From studies by Luna and Church,[22,49] Golder,[20] and others, it is known that qualitative stability categories like those of Pasquill correspond generally to direct measurements of boundary-layer turbulence intensity but that there is considerable scatter. Lapse rate has also proved to be an uncertain discriminator, partly because material dispersing from surface sources experiences a much wider range of lapse-rate conditions compared with those experienced by elevated emissions. The lapse rates corresponding to the data of Fig. 2 reflect surface-level emissions, whereas those shown in Fig. 3 are based on elevated emissions and are measured at plume height. But variations in surface roughness and thermal properties (soil type and moisture content) from site to site, not specifically allowed for in the simple typing schemes originally proposed, should also have an effect, particularly on the vertical dispersion. This situation has led various workers to examine relations between stability types and theoretical criteria, or indices, of boundary-layer turbulence that specifically account for these factors.

Islitzer[25] gave Richardson numbers for the Pasquill types ranging from −0.26 for type A to 0.046 for type F. The values were calculated from micrometeorological profile data measured on a 45-m mast at the National Reactor Testing Station (now the Idaho National Engineering Laboratory) in Idaho Falls. The Richardson number (Ri) is defined by

$$\mathrm{Ri} = \frac{g}{T}\frac{\partial\theta/\partial z}{(\partial u/\partial z)^2} \qquad (1)$$

where $g$ = gravitational acceleration
$T$ = absolute temperature
$\theta$ = potential temperature
$\partial\theta/\partial z$ = minus the vertical gradient of potential temperature lapse rate
$\partial u/\partial z$ = wind shear

Thus the Richardson number contains information of the required kind; however, it varies with height in the steady-state boundary layer. A more useful index of the state of the boundary-layer turbulence is the Monin–Obukhov length

$$L = -(u_*^3 c_p \rho T)/kgH \qquad (2)$$

where $c_p$ = specific heat at constant pressure
$\rho$ = density
$k$ = von Karman's constant
$H$ = vertical heat flux
$u_*$ = friction velocity as determined from the surface shear stress $u_* = (\tau/\rho)^{1/2}$

As a rule, all these parameters can be assumed to be constants or to vary only slowly in a steady-state boundary layer. Therefore it seems likely that $L$ should bear a convenient relation to turbulence types.

Gifford[50] estimated order-of-magnitude relations between stability classes and $L$ ranging from $\pm 10^3$ m for near neutral conditions to +10 m for very stable and −10 m for very unstable conditions. These values were chosen arbitrarily, based on qualitative indications provided by studies of boundary-layer wind profiles in conditions of varying stability. Pasquill and Smith,[51] guided by detailed atmospheric diffusion experiments with accompanying micrometeorological profile data, provided more refined estimates, specifically tailored to the Pasquill stability categories, for the case of flow over a fairly smooth surface (short grass, $z_0$ = 1 cm). These are summarized in Table 6.

Golder,[20] using the five detailed micrometeorological data sets referred to previously, calculated $L$ values and Pasquill stability classes to derive the relation shown in Fig. 5. He also gives nomograms relating Ri to

**Table 6 Relations Between Pasquill Type and Turbulence Criteria Ri and $L$ for Flow over Short Grass, $z_0$ = 1 cm, According to Pasquill and Smith[51]**

| Pasquill type | Ri (at 2 m) | $L$, m |
|---|---|---|
| A | −1.0 – −0.7 | −2 – −3 |
| B | −0.5 – −0.4 | −4 – −5 |
| C | −0.17 – −0.13 | −12 – −15 |
| D | 0 | ∞ |
| E | 0.03 – 0.05 | 35 – 75 |
| F | 0.05 – 0.11 | 8 – 35 |

$z/z_0$ and to the more easily measured bulk Richardson number $B$ (Lettau and Davidson[52]), which he defines as follows:

$$B = \frac{g}{T}\frac{\partial\theta/\partial z}{u^2}z^2 \qquad (3)$$

Since Ri is analytically related to $L$, Eq. 3 and Fig. 5 provide the means for determining Pasquill's categories over various surfaces, given values of meteorological quantities usually available. The required measurements are made, by regulation, at all nuclear power-reactor sites. In principle, this method should provide stability class estimates exhibiting less scatter than the lapse-rate method because it accounts for variations in thermal and mechanical turbulence parameters from site to site.

### Diffusion Categories for Great Distances

The foregoing schemes for classifying turbulent diffusion are all specifically restricted to distances up to 10 km or several tens of kilometers at most because the experimental data base of these essentially qualitative and empirical schemes is very scanty for downwind distances beyond a few kilometers. However, this restriction has not always been observed in applications. Nonetheless, many urgent environmental problems require consideration of diffusion at great distances from sources.

Diffusion beyond a few kilometers from a source, even in the relatively straightforward case of open country that is assumed in typing schemes, is complicated by a number of effects that are not particu-

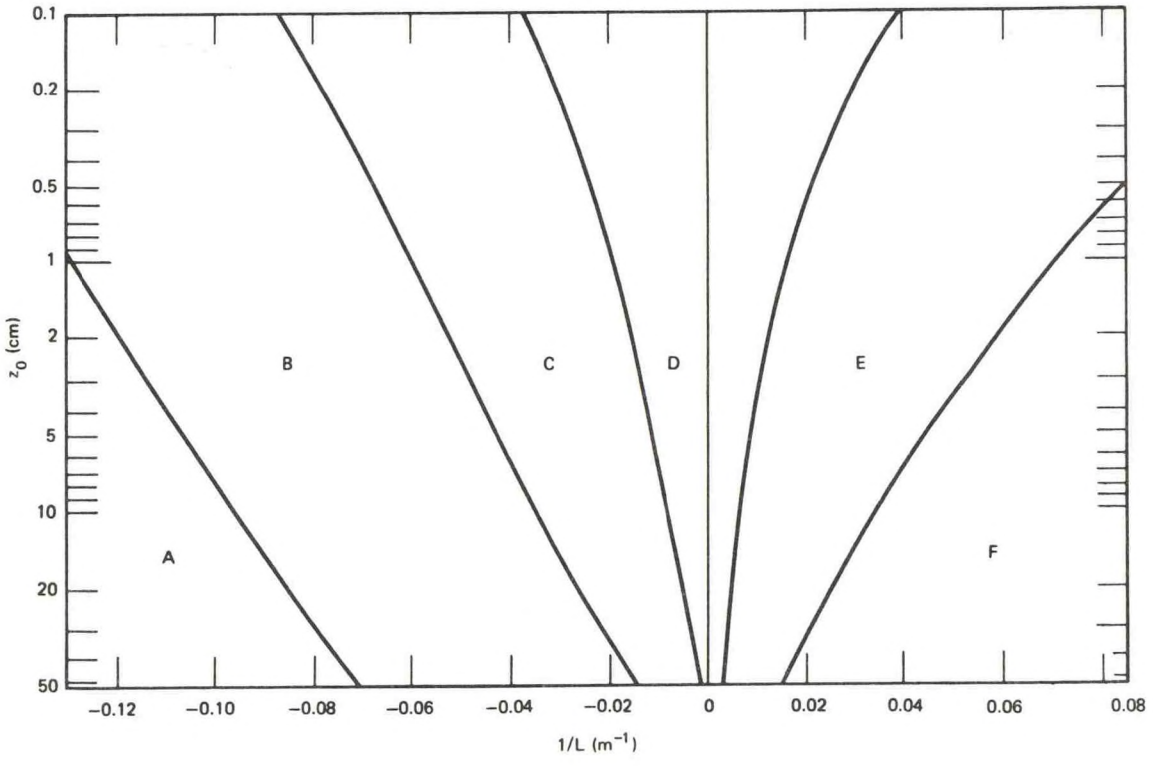


**Fig. 5 Curves by Golder[20] showing Pasquill's turbulence types as a function of the Monin–Obukhov stability length and the aerodynamic roughness length.**

larly important at short distances. The underlying surface type may change, introducing changes in roughness and thermal conditions. Vertical diffusion ultimately extends through the entire boundary layer, which is usually surmounted by a stable layer. This limits $\sigma_z$ to the so-called "mixing depth" (see, e.g., Holzworth[53]). Use of the mixing depth as a limit of $\sigma_z$ is recommended in nearly all typing schemes. As travel time (downwind distance) increases, diurnal changes in governing such parameters as stability become important.

Considering these problems, Smith[54] (see also Pasquill[47]) enlarged on Pasquill's original scheme as follows. He obtained numerical solutions to the diffusion equation for downwind distances up to 100 km, using wind-speed and diffusivity values based on actual experience over a range of stability conditions. He then used these results to define $\sigma_z$ values based on (1) the stability of the lower layers, as ordinarily determined in Pasquill's method, and (2) the overall stability of the planetary boundary layer. Provision is also made to introduce the "typical" roughness length over the plume path, the incoming solar radiation, the upward heat flux, the mixing depth, and the variation of stability along the path. The method is not yet complete (curves for $\sigma_y$ have not yet been published), but it will ultimately provide a way to extend the basic typing scheme to distances up to 100 km. Curves of $\sigma_z$ computed by Hosker[55] according to Smith's procedure are shown in Fig. 6.

## DIFFUSION CATEGORIES FOR EXCEPTIONAL FLOWS

Various flows occur in the planetary boundary layer which, from the viewpoint of the standard turbulence categories, must be considered exceptional despite their practical importance in applications. Estimates of spread based on Pasquill's categories are intended to be applied in specifically limited situations only: $u > 2$ m/sec, nonbuoyant plumes, and flow over open country. This is because boundary-layer turbulence is conceived, for the purpose of turbulence typing, as consisting of a mechanical component created by frictional wind shear at the surface and a thermal component arising from vertical boundary-layer heat flux. Their relative importance in any particular situation determines the turbulence type; e.g., type A is low mechanical and high thermal content, type D is all mechanical, etc. However, flows exist for which the turbulence is not generated, solely

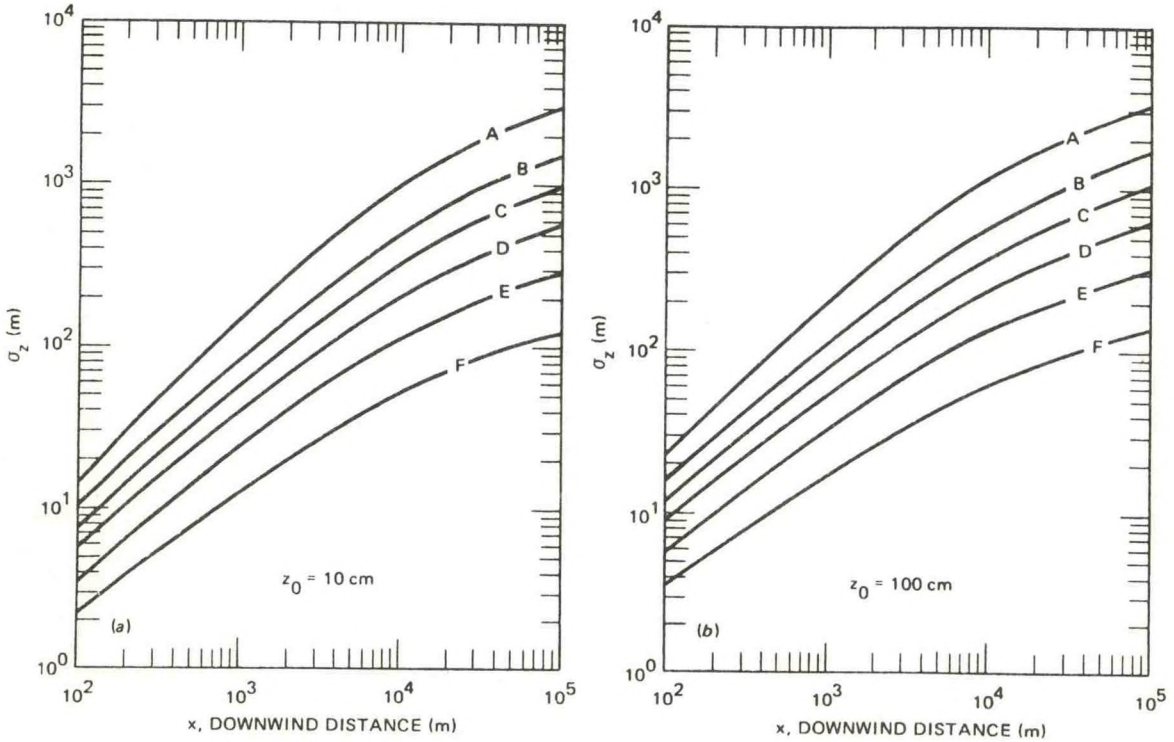


Fig. 6 Curves of $\sigma_z$ ($z_0$ = 10 cm) and $\sigma_z$ ($z_0$ = 100 cm) based on Smith's method;[54] after Hosker.[55]

by these two mechanisms, e.g., flows over cities, flows over large bodies of water, flows with buoyancy, wake flows (flows behind obstacles), and very light-wind, stable flows (calm, clear nights). These all clearly lie outside the limits of Pasquill's basic system and were specifically excluded by him. Attempts have nevertheless been made to apply PG curves to diffusion estimates in these situations, a Procrustean approach which understandably always fails. This is not the fault of the typing system, of course, but of the application. In some cases, reasonable modifications can be suggested, as will be described below, and in other cases this is not yet possible. In all these exceptional cases, much more research is needed.

### Diffusion Categories in Near-Calm, Very Stable Conditions

Beattie[56] determined the frequency of occurrence of Pasquill classes at eight British meteorological stations, and results for others were reported by Bryant.[57] Others have since repeated this exercise at various locations. The results are similar, as a rule, although there is some variation with locality. Categories A and B provide around 10%, C and D around 60%, and E about 10%; category F applies in the remaining 20% of the time, at least at the British stations.

However, included in the latter 20% are a number of near-calm situations typically occurring on clear nights with frost or heavy dew. Such conditions were specifically excluded by Pasquill from the original categories because the diffusing plume could be expected to be very variable with "little definable travel." Since these conditions occurred some 5 to 8% of the time in Beattie's study, they have considerable practical importance. Beattie assigned them the designation G without proposing any $\sigma$ curves.

On the not unreasonable assumption that actual diffusion under category G conditions would be less than that under F conditions, users have arbitrarily assigned diffusion values; see, for instance, NRC Regulatory Guide 1.21 (Ref. 31), which indicates that category G diffusion has been assumed to be appreciably slower than category F. Atmospheric diffusion experiments reported by Sagendorf[58] suggest that under category G conditions the plume is subject to a good deal of irregular horizontal "meander," or swinging. The applicable value of $\sigma_A$, instead of being the small value indicated in Regulatory Guide 1.70, was found to be greater than 8° and at times equaled 20° or more. When averaged over 1 hr, the resulting concentration values at a point are much lower than was at first assumed under these conditions. Nickola, Clark, and Ludwick,[59] on the basis of results of two low-wind (1.5 m/sec) diffusion experiments in which the tracer was released for 30 min from a point quite near the ground, came to similar conclusions. In the test run under stable conditions, varying between types E and G, the averaged concentration values corresponded approximately to category C. In the test run under unstable conditions, varying between types A and D, the average concentration values were found to be a factor of 2 below category A values.

A review of several sets of diffusion data for such light-wind, stable conditions by Van der Hoven[60] indicates that the effective $\sigma$ values can correspond to anything between categories A and F. This supports Pasquill's original assertion that diffusion under these conditions will be very irregular and indefinite. In dealing with these conditions at any site, it will clearly be necessary as a minimum to have measurements or estimates of $\sigma_A$, as well as the usual quantities required to define the turbulence type.

### Diffusion over Cities

Diffusion over cities is enhanced, compared with that over open country, not only because the surface roughness is greatly increased but also because of the great heat capacity of the cities. Thus both mechanical and thermal turbulence are increased. The net increase in turbulence intensity is evidently about 40%, as compared with open country, according to Bowne, Ball, and Anderson.[61] This study and other material on atmospheric transport and dispersion over cities were summarized by Gifford.[62]

Estimates of turbulence types of urban diffusion have been based on the series of observations of diffusion over St. Louis reported by McElroy and Pooler.[63] On the basis of these data, Pasquill[64] compared diffusion types in open country and over a city (Table 7). Johnson et al.[65] analyzed additional urban tracer experiments and presented revised estimates of $\sigma_z$. Considering these data and analyses, Briggs[19] proposed the urban $\sigma_y$ and $\sigma_z$ curves shown in Fig. 7 and described in Table 8. These are based on Figs. 9 and 10 of the paper by McElroy and Pooler.[63] The $\sigma_z$ curves are in essential agreement with those of Johnson et al.

### Diffusion over Water

Flow over bodies of water has long been known to be characterized by greatly reduced turbulence in-

**Table 7 Vertical Diffusion $\sigma_z$ over St. Louis Compared with Diffusion over Open Country[63,64]**

| Downwind distance, km | Location | Ratio of $\sigma_z$ to value in neutral conditions for stability categories | | | |
|---|---|---|---|---|---|
| | | B | C | D | E–F |
| 1 | City* | 4.5 | 2.7 | 1.7 | 0.7 |
| | City† | 4.0 | 2.4 | 1.5 | 0.6 |
| | Open country | 3.2 | 1.9 | 1.0 | 0.5 |
| 10 | City* | 9 | 3.4 | 1.0 | 0.3 |
| | City† | 11 | 4.1 | 1.2 | 0.4 |
| | Open country | 6 | 2.4 | 1.0 | 0.3 |

*Using McElroy and Pooler's curve for $B = \pm 0.01$ in their Fig. 2.

†Using data for bulk Richardson number $B = \pm 0.01$ in evening conditions only.

**Table 8 Formulas Recommended by Briggs[19] for $\sigma_y(x)$ and $\sigma_z(x)$; $10^2 \leqslant x \leqslant 10^4$ m, Open-Country Conditions**

| Pasquill type | $\sigma_y$, m | $\sigma_z$, m |
|---|---|---|
| A–B | $0.32x(1 + 0.0004x)^{-1/2}$ | $0.24x(1 + 0.001x)^{1/2}$ |
| C | $0.22x(1 + 0.0004x)^{-1/2}$ | $0.20x$ |
| D | $0.16x(1 + 0.0004x)^{-1/2}$ | $0.14x(1 + 0.0003x)^{-1/2}$ |
| E–F | $0.11x(1 + 0.0004x)^{-1/2}$ | $0.08x(1 + 0.0015x)^{-1/2}$ |

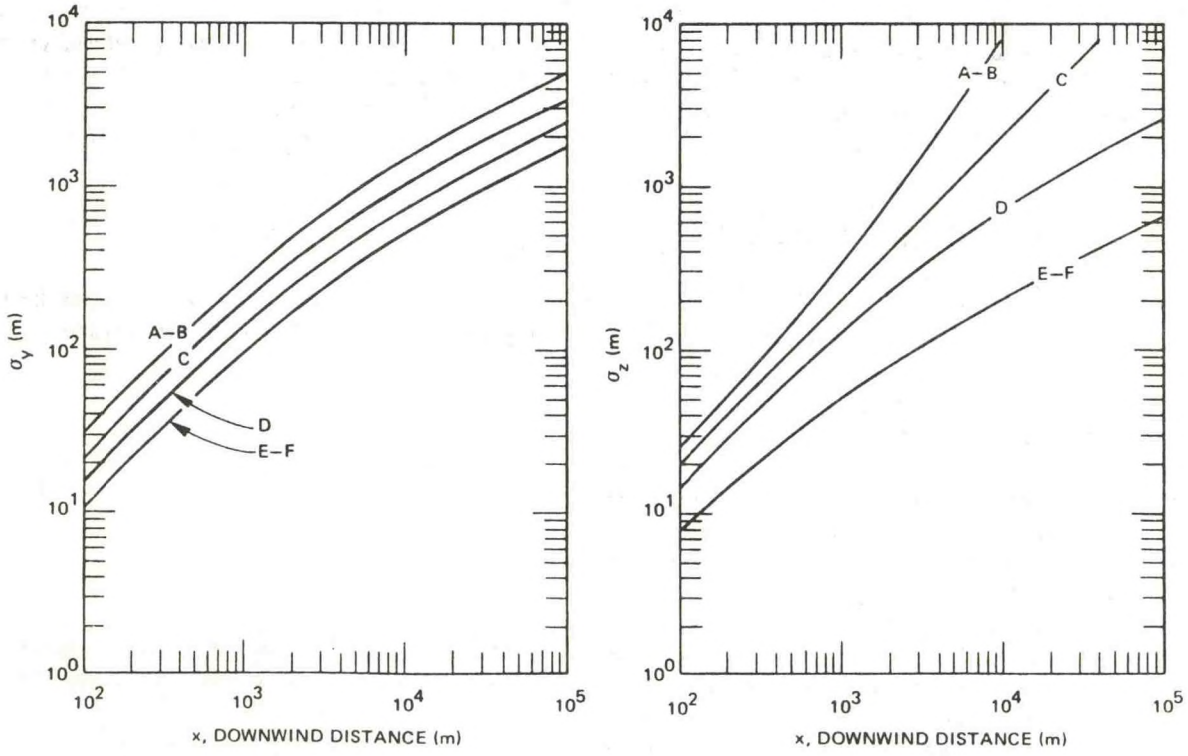


Fig. 7 Curves of $\sigma_y$ and $\sigma_z$ based on interpolation formulas by Briggs[19] for flow over urban areas (see Table 10); from Hosker.[55]

tensity[66] and a correspondingly decreased diffusion rate.[67] According to Kitaigorodskii,[68] in order to describe the neutral boundary-layer wind profile over a water surface, account has to be taken of the fact that the waves are in motion relative to the air. Consequently they do not act as ordinary, land-surface, fixed roughness elements except in the initial stages of wave development.

In engineering terms the roughness length $z_0$, which serves to characterize the wind profile and turbulence, depends on an "equivalent sand roughness" of the sea surface, $h_s$, which is in turn a function of the stage of wave development. The exact form of this dependence is determined by the Reynolds number of the surface,[68] which may be either aerodynamically "smooth," or "fully rough" (see Schlichting[69]). A simple expression characterizing $h_s$ is not available. In order to evaluate the surface Reynolds number and to compute $z_0$ from $h_s$, Kitaigorodskii[68] considers the flow over individual waves of all possible phase velocities and determines $h_s$ as a function of $S(\omega)$, the frequency spectrum of the waves, and the root-mean-square rms wave height $\sigma$.

The wave frequency $\omega$ and the phase velocity $c$ are related, for deep-water gravity waves, by $c = g/\omega$.[70] The frequency spectrum will typically have a peak at some frequency $\omega_0$ corresponding to a phase speed $c_0$. Using the experimentally and theoretically supported assumption that only "steep" waves (i.e., those with $\omega > \omega_0$) can contribute to the drag, Kitaigorodskii[68] finds

$$h_s \simeq \begin{cases} \sigma & \text{if } \omega_0 u_*/g \gg 1 \\ \sigma e^{-kg/\omega_0 u_*} & \text{if } \omega_0 u_*/g \sim 0 \\ 0.38 u_*^2/g & \text{if } \omega_0 u_*/g \ll 1 \end{cases} \qquad (4)$$

These equations may be interpreted as follows. When $\omega_0 u_*/g = u_*/c_0 \gg 1$, so that $u_*$ is much greater than the phase speeds of all the waves that contribute to the drag, the waves all behave as immobile roughness elements, and so the equivalent sand roughness of the sea surface is approximately equal to the rms value of the wave heights. This corresponds to the very early stages of wave development. At the other extreme, where $\omega_0 u_*/g \equiv u_*/c_0 \ll 1$, $h_s$ is independent of the state of wave development and is determined only by the aerodynamic quantity $u_*$. For these fully developed waves, note that $h_s$ is quite small; if $u_* =$ 50 cm/sec, a fairly large but realistic value, $h_s$ is less than 1 cm. For the intermediate stages of wave development, corresponding to usually observed situations, $\omega_0 u_*/g \equiv u_*/c_0 \simeq 0.01$ to 1.0, and $h_s$ depends on the wave spectrum parameters $\sigma$ and $\omega_0$ as well as on $u_*$. Hence $h_s$ can be expected to vary with such factors as fetch and duration of the wind. In these cases of intermediate wave development, $h_s$ can be much smaller than the rms wave height. Therefore it seems quite possible that, even for large waves on a rough sea, the surface may not be fully rough in the usual aerodynamic sense. This may be the reason why diffusion observations over the sea, such as those reported recently by Raynor et al.,[71] show little spreading and marked departure from the standard PG curves.

The effect of mechanical roughness can be introduced into the marine boundary layer as outlined above, although the details are somewhat complex as compared with the situation over land. Another major difference arises from the intense evaporation of water that takes place from the sea surface most of the time. Density stratification over water is controlled by the heat flux, as over land, but also depends on the water-vapor flux. (The water-vapor flux may well exert an important degree of control on the turbulence type over heavily vegetated land as well. This point deserves more consideration than it has received.) If fluctuations of virtual temperature are considered, rather than those of temperature as ordinarily defined (Lumley and Panofsky,[72] p. 95), the vapor flux can be taken into account. This leads (see, for example, Monin[73]) to a redefinition of the stability parameters Ri and $L$ for overwater flows, as follows:

$$\mathrm{Ri}_w = Rf\,(1 + m/B_0) \qquad (5)$$

where $m = 0.61 c_p \theta/\bar{\ell}$, $\bar{\ell}$ being the latent heat of vaporization (for $\theta \sim 300°\mathrm{K}$, $m \simeq 0.075$) and

$$L_w = L\,(1 + m/B_0)^{-1} \qquad (6)$$

where $L_w$ is the Monin–Obukhov length over water, $Rf$ is the usual flux form of Richardson number, and $B_0$ is the Bowen ratio:

$$B_0 = (c_p/\bar{\ell})\,(\theta_a - \theta_w)/(e_a - e_w) \qquad (7)$$

where $e$ is specific humidity. Over the ocean, $|B_0|$ usually range between $\frac{1}{4}$ and $\frac{1}{20}$, so that the term $m/B_0$ is quite significant.[74,75]

The above presents at least a general framework for including the complexities present in flows over water in the determination of the characteristics of turbulent diffusion. Pasquill's turbulence types could, in prin-

ciple at least, be determined for overwater flows by calculating the appropriate roughness and stability length and then referring to nomograms of Golder[20] or Smith.[54]

### Diffusion in the Lee of Flow Obstacles

Most sources of airborne contaminants are located on or near buildings or other structures, such as cooling towers. Isolated tall stacks, which, when properly designed, do as a practical matter approximate the point source assumed in diffusion theory, are the exception rather than the rule among pollutant sources. Thus it is curious and disturbing to find that so little is known about the properties of diffusion in the wakes that exist in the atmosphere downwind of such structures.

A wake is a region of low-speed flow that extends downwind from a flow obstacle. Within the wake the flow is turbulent, having properties at first strongly conditioned by the size and shape of the obstacle. The lowered wind speed in the wake creates shear at the boundary, and the resulting fine-scale turbulence entrains air from the ambient atmospheric flow into the wake, gradually expanding it, reducing the velocity deficit, and ultimately dissipating the wake. Thus dilution downwind of a source like a roof vent or a building leak is strongly influenced by the building nearby and then farther downwind comes to be dominated by atmospheric diffusion in the ordinary sense.

For this reason an early proposal was to combine the building and atmospheric effects into the following expression for the downwind concentration $X$:

$$X/Q = [(\pi\sigma_y\sigma_z + cA)u]^{-1} \qquad (8)$$

where $Q$ is the source strength, $A$ is the area of the building cross section normal to the flow, and $c$ represents the fraction of $A$ over which the plume is dispersed. Gifford[76] suggested that $\frac{1}{2} < c < 2$. These limits were proposed on purely intuitive grounds but have been widely quoted. Halitsky's[77] detailed wind-tunnel studies of the near-wake region and Barry's[78] summary of both atmospheric and wind-tunnel tests in general give support for $c$ values near $\frac{1}{2}$, and this value has moreover been assigned on grounds of conservatism. This simple scheme permits wake effects to be combined with turbulence types in a logical way, but in practice it has two defects.

The first problem relates to wake diffusion under low-wind-speed, stable ambient turbulence conditions, mainly type G but also types E and F to some extent. Under these conditions the plume from a release in a building wake, although it may spread slowly by diffusion, undergoes erratic larger scale horizontal meanders owing to flow fluctuations not accounted for in the usual typing schemes. The result is that hourly averaged concentration values much lower than Eq. 8 would indicate are experienced. Halitsky and Woodard[79] give an example of wake concentration measurements at one site in an effort to resolve this question. These observations show that, under stable, light-wind conditions, wake plumes do meander horizontally. A firm general plume model for these conditions which correctly combines the wake effect, the ambient turbulence type, and the ensuing plume meander has yet to be formulated and tested, but the common assumption of very slow dispersion in category C conditions, together with the building effect of Eq. 8, is certainly quite conservative.

The second problem occurs in higher wind-speed, less stable conditions (types B through D) when wakes are steadier. Wind-tunnel studies by Meroney and Symes[80] and Meroney and Yang[81] indicate that building wakes persist much farther downstream in neutral and stable conditions than Eq. 8 would indicate. In their tests the wake persists as an entity and grows slowly by the entrainment process to downwind distances greater than 30 times the building height.

The decrease in axial ground-level concentration in wake plumes is therefore small, varying with distance to the power $-0.6$ to $-0.7$, according to Meroney and Yang,[81] and its effect on ambient stability variation is slight. This contrasts with the usual open-country PG curves, which imply concentration variation with distance to the power $-1.5$ or so with a strong stability dependence. However, before a suitable interpolation formula can be made between these two cases, more research on wake behavior needs to be done. Meroney's wind-tunnel work needs to be extended to various building shapes and arrays and to downwind distances adequate to define the end of the far-wake region, where ambient diffusion begins to dominate the flow. Also, parallel atmospheric experiments greatly extending those begun by Dickson et al.[82] should be carried out. Until this work is done, it should be realized that formulas like Eq. 8 or the equivalent curves recently presented by Bowne[83] may somewhat underpredict concentration values at large downwind distances in well-developed wake plumes. On the other hand, at small distances under stable conditions, when the wake is poorly developed, the meandering effect results in lower concentration values than Eq. 8 would indicate.

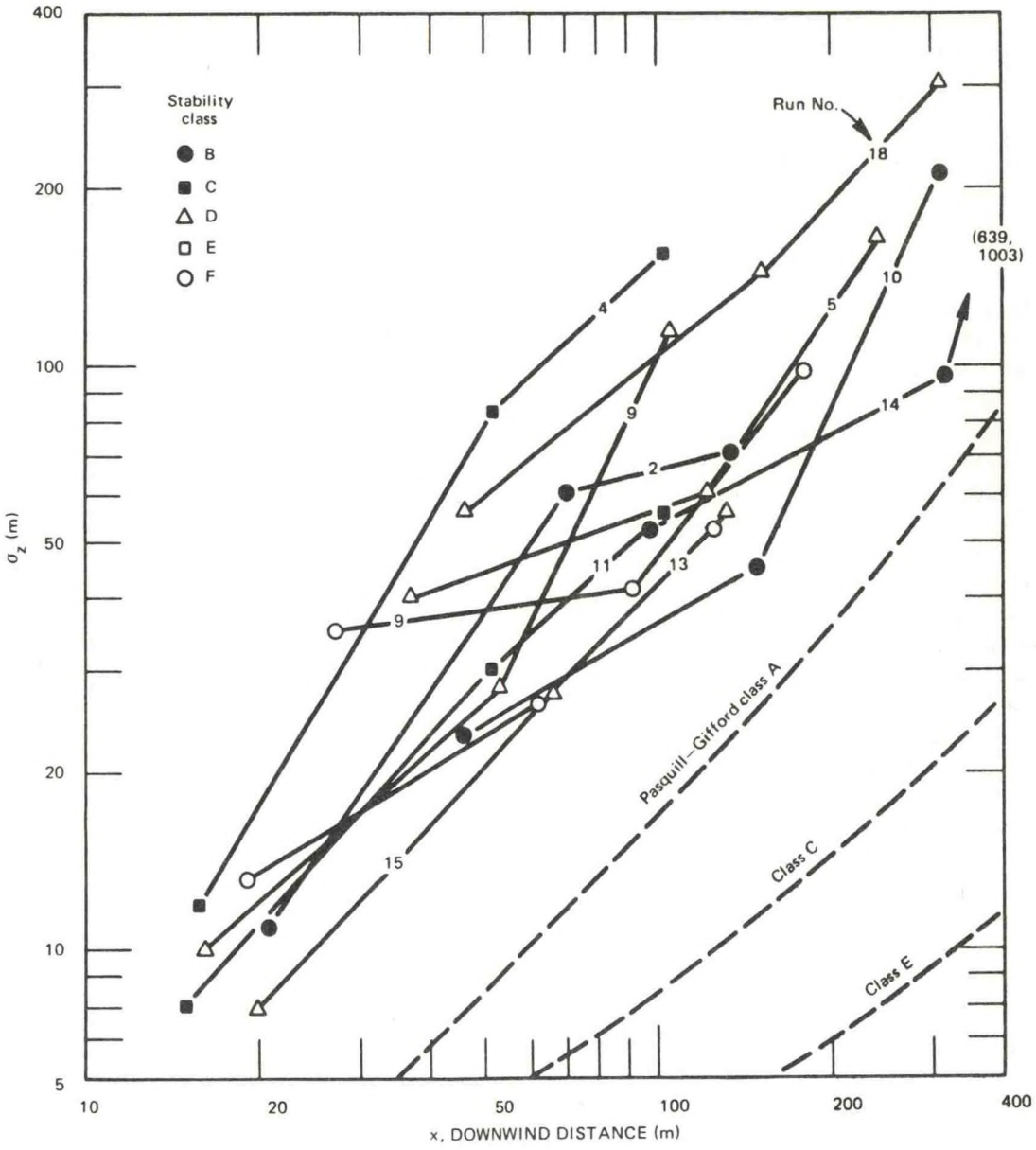


Fig. 8 Johnson's[8,5] comparison of vertical diffusion based on observations of concentrations perpendicular to a highway vs. distance from the highway for various stability categories. Conventional PG curves are indicated for comparison.

### Diffusion near Highways

The wakes generated by vehicles are even less understood than the wakes behind buildings. Dabbert, Cagliostro, and Meisel[84] conducted a literature survey and concluded that there is very little definite information on vehicle-wake properties. Several studies[85,86] have recently been reported on diffusion near roadways. Not surprisingly, it has been found that concentrations measured near highways do not conform to the standard PG curves. Johnson's comparison of curves of $\sigma_z$ vs. downwind distance (from a highway), inferred from concentration data, is reproduced in Fig. 8. The figure shows that there is little if any organization of the data by stability classes and the vertical diffusion is considerably enhanced over the usual PG curves. This should certainly be interpreted as a wake effect, although of a more complicated kind, involving penetration and interaction of successive vehicle wakes.

The strength and the distance from the highway to which this complex effect dominates diffusion and beyond which presumably the ordinary PG curves, suitably adjusted for initial wake diffusion, will then apply will be determined by extension of the above and related studies, such as those summarized by Ludwig et al.[87]

### Diffusion in Irregular and Rugged Terrain

As previously mentioned, Pasquill's typing scheme is designed only to account for mechanically and thermally generated boundary-layer turbulence. Flows in rugged terrain have irregular, often turbulent, features that originate otherwise than with boundary-layer turbulence and heat transfer [e.g., drainage (katabatic) winds, vortices shed from terrain obstacles, channeling effects, and flow separations of various kinds]. None of these features were contemplated in the original typing systems, and so departures under such conditions can and do occur.

Methods of calculating diffusion over hills and terrain obstacles, based on the assumption of potential flow of the mean motion, have been discussed by Stümke[88-90] and Berlyand.[91,92] As to diffusion categories under such flow conditions, several papers at the American Meteorological Society Symposium on Atmospheric Diffusion and Air Pollution, Santa Barbara, Calif., Sept. 9–13, 1974, touched on this topic. Start, Dickson, and Hicks[93] reported results of a series of diffusion measurements conducted in a deep, steep-walled canyon system in southern Utah. They found that diffusion rates are systematically greater within these deep canyons, implying departures from the usual Pasquill categories. These departures resulted in lower concentrations, compared with those calculated from the usual PG curves. The differences ranged from a factor of 1.4 in category B conditions to 4 in weak lapse to near-neutral conditions to 15 in category F conditions. The authors state that most of the phenomena mentioned earlier (i.e., greatly enhanced roughness, density flows, wake flows, and channeling effects) were probably operating. Similar results were reported by Hovind, Spangler, and Anderson.[94] Start et al. believe that their results represent a fairly extreme example of the terrain effect on diffusion categories and speculate that less-rugged terrain should lead to departures intermediate between these results and the open-country values. More experimental work clearly is needed.

## SUMMARY AND CONCLUSIONS

Recent environmental concerns have greatly increased the need to calculate air concentrations downwind from pollutant sources of various kinds. Because concentration depends on diffusion and hence on atmospheric turbulence, which is difficult and expensive to measure, qualitative turbulence typing schemes have been devised. These attempt to relate certain average properties of the planetary boundary layer (including wind speed, stability, insolation, surface roughness, and heat flux) to atmospheric diffusion.

The most widely used of several turbulence typing schemes is that proposed by Pasquill[3] for diffusion from low-level, nonbuoyant sources over open country. Its relation to other typing schemes is shown in Table 4. Modifications of Pasquill's scheme have been proposed to account for elevated and buoyant sources (Table 5), theoretical boundary-layer stability criteria (Table 6 and Fig. 5), and diffusion at great distances downwind (10 to 100 km).

There are various boundary-layer flows that can be classed as exceptional, in that they involve sources of turbulence (and hence diffusion) additional to the mechanical friction and thermal buoyancy that are the basic mechanisms in Pasquill's original scheme. The turbulence categories have been extended in attempts to account for (1) diffusion in near-calm, very stable conditions; (2) diffusion over cities; (3) diffusion over water; (4) diffusion in the lee of flow obstacles (wakes); (5) diffusion near highways; and (6) diffusion in irregular and rugged terrain. Available guidelines on these exceptional cases, summarized previously, should be used whenever applications require them; however,

not all details have been worked out. More research and, in particular, more careful experimental studies are needed to resolve several important problem areas.

## ACKNOWLEDGMENTS

The writer wishes to thank R. P. Hosker for clarifying the role of water waves as aerodynamic roughness elements and for many helpful suggestions. S. D. Swisher supplied preliminary reference material which materially aided the preparation of this review. This work was done under an agreement between the U. S. Energy Research and Development Administration and the National Oceanic and Atmospheric Administration.

## REFERENCES

1. D. A. Haugen (Ed.), *Workshop on Micrometeorology*, American Meteorological Society, 1973.
2. H. Panofsky, The Atmospheric Boundary Layer Below 150 Meters, *Annu. Rev. Fluid Mech.*, **6**: 147 (1974).
3. F. Pasquill, The Estimation of the Dispersion of Windborne Material, *Meteorol. Mag.*, **90**: 33-49 (1961).
4. M. A. Giblett, The Structure of Wind over Level Country, *Meteorological Office Geophysical Memoirs No. 54*, **6(4)**, Her Majesty's Stationery Office, London, 1932.
5. M. E. Smith, The Forecasting of Micrometeorological Variables, *Meteorol. Monogr.*, No. 4: 50-55 (1951).
6. M. E. Smith, The Variation of Effluent Concentrations from an Elevated Point Source, *Arch. Ind. Health*, **14**: 56-68 (1956).
7. M. E. Smith et al., The Variation of Effluent Concentrations During Temperature Inversions, *J. Air Pollut. Control Ass.*, 7: 194-197 (1957).
8. I. A. Singer and M. E. Smith, Relation of Gustiness to Other Meteorological Parameters, *J. Meteorol.*, **10**: 121-126 (1953).
9. I. A. Singer and M. E. Smith, Atmospheric Dispersion at Brookhaven National Laboratory, *Int. J. Air Water Pollut.*, **10**: 125-135 (1966).
10. I. A. Singer, J. A. Frizzola, and M. E. Smith, A Simplified Method of Estimating Atmospheric Diffusion Parameters, *J. Air Pollut. Control Ass.*, **16**: 594-596 (1966).
11. O. G. Sutton, A Theory of Eddy Diffusion in the Atmosphere, *Proc. Roy. Soc. London, Ser. A*, **135**: 143 (1932).
12. P. J. Meade, The Effects of Meteorological Factors on the Dispersion of Airborne Material, in *Proceedings of the Sixth International Electronic and Nuclear Congress, Rome, July 1959*, Vol. 2, pp. 106-130, Comitato Nazionale per le Ricerche Nucleari, Rome, 1959.
13. P. J. Meade, Meteorological Aspects of the Peaceful Uses of Atomic Energy, Technical Note 33, Part 1, Meteorological Aspects of the Safety and Location of Reactor Plants, WMO No. 97, TP. 41, World Meteorological Organization, Geneva, Switzerland, 1960.
14. F. A. Gifford, Jr., Use of Routine Meteorological Observations for Estimating Atmospheric Dispersion, *Nucl. Safety*, 2(4): 47-57 (June 1961).
15. H. E. Cramer, Engineering Estimates of Atmospheric Dispersion Capacity, paper presented at the annual meeting of the American Industrial Hygiene Association, Chicago, Ill., Apr. 30, 1959.
16. J. S. Hay and F. Pasquill, Diffusion from a Fixed Source at a Height of a Few Hundred Feet in the Atmosphere, *J. Fluid Mech.*, 2: 299-310 (1957).
17. D. B. Turner, Relationships Between 24-Hour Mean Air Quality Measurements and Meteorological Factors in Nashville, Tenn., *J. Air Pollut. Control Ass.*, **11**: 483-489 (1961).
18. D. B. Turner, A Diffusion Model for an Urban Area, *J. Appl. Meteorol.*, 3(1): 83-91 (1964).
19. G. A. Briggs, Diffusion Estimation for Small Emissions, in Environmental Research Laboratories, Air Resources Atmosphere Turbulence and Diffusion Laboratory 1973 Annual Report, USAEC Report ATDL-106, National Oceanic and Atmospheric Administration, December 1974.
20. D. Golder, Relations Among Stability Parameters in the Surface Layer, *Boundary-Layer Meteor.*, 3: 47-58 (1972).
21. W. Klug, Ein Verfabren zur Bestimmung der Ausbreitungsbedingungen aus synoptischen Beobachtungen (in German), *Staub*, 29(4): 143-147 (1969).
22. R. E. Luna and H. W. Church, A Comparison of Turbulence Intensity and Stability Ratio Measurements to Pasquill Turbulence Types, in *Conference on Air Pollution Meteorology*, American Meteorological Society, Apr. 5–9, 1971,, Raleigh, N. C., available from the American Meteorological Society, Boston, Mass.; also, USAEC Report SC-DC-70-5443, Sandia Laboratories, 1970.
23. H. E. Cramer, A Practical Method for Estimating the Dispersal of Atmospheric Contaminants, in *Proceedings of the First National Conference on Applied Meteorology*, Section C, pp. 33-55, American Meteorological Society, Hartford, Conn., October 1957.
24. N. Islitzer and D. H. Slade, Diffusion and Transport Experiments, in Meteorology and Atomic Energy—1968, USAEC Report TID-24190, pp. 117-118, Environmental Science Services Administration, 1968.
25. N. F. Islitzer, Program Review and Summary of Recent Accomplishments at NRTS, in Conference on AEC Meteorological Activities, May 19–22, 1964, USAEC Report BNL-914, pp. 57-64, Brookhaven National Laboratory, 1965.
26. J. J. Fuquay, C. L. Simpson, and T. W. Hinds, Estimates of Ground-Level Air Exposures Resulting from Protracted Emissions from 70-Meter Stacks at Hanford, *J. Appl. Meteorol.*, 3(6): 761-770 (1964); also, USAEC Report HW-80204, 1964.
27. U. S. Weather Bureau, A Meteorological Survey of the Oak Ridge Area: Final Report Covering the Period 1948–1952, USAEC Report ORO-99, 1953.
28. E. H. Markee, On the Relationships of Range to Standard Deviation of Wind Fluctuations, *Mon. Weather Rev.*, 91(2): 83-87 (1963).
29. Final Safety Analysis Report, Peach Bottom Atomic Power Station, Units 2 and 3, Vol. 1, Section 2 (Table 2.3.10), Philadelphia Electric Company, Philadelphia, Pa., 1970.
30. Meteorology and Atomic Energy—1968, D. H. Slade

(Ed.), USAEC Report TID-24190, Environmental Science Services Administration, 1968.

31. U. S. Nuclear Regulatory Commission, *Measuring, Evaluating, and Reporting Radioactivity in Solid Wastes and Releases of Radioactive Materials in Liquid and Gaseous Effluents from Light-Water-Cooled Nuclear Power Plants,* Regulatory Guide 1.21, 1974.
32. K. J. Vogt and H. Geiss, Tracer Experiments on the Dispersion of Plumes over Terrain of Major Surface Roughness, paper presented at the First Asian Regional Congress on Radiation Protection, Bombay, India, Dec. 15–20, 1974, Publication No. 1131, Atomic Research Center, Julich, October 1974.
33. S. B. Carpenter et al., Principal Plume Dispersion Models: TVA Power Plants, *J. Air Pollut. Control Ass.,* **21**: 491-495 (1971).
34. G. H. Strom, Atmospheric Diffusion of Stack Effluents, in *Air Pollution,* 2nd ed., A. C. Stern (Ed.), Vol. I, pp. 227-274, Academic Press, Inc., New York, 1968.
35. G. A. Briggs, *Plume Rise,* AEC Critical Review Series, USAEC Report TID-25075, 1969.
36. D. B. Turner, Workbook of Atmospheric Dispersion Estimates, U. S. Public Health Service, Publication 999-AP-26, Robert A. Taft Sanitary Engineering Center, Cincinnati, Ohio, 1967.
37. M. E. Smith (Ed.), *Recommended Guide for the Prediction of the Dispersion of Airborne Effluents,* 1st ed., American Society of Mechanical Engineers, New York, May 1968.
38. R. R. Draxler, Determination of Atmospheric Diffusion Parameters, to be published in *Atmospheric Environment.*
39. J. Tadmor and Y. Gur, Analytical Expressions for the Vertical and Lateral Dispersion Coefficients in Atmospheric Diffusion, *Atmos. Environ.,* **3**: 688-689 (1969).
40. J. J. Fuquay, C. L. Simpson, and W. T. Hinds, Prediction of Environmental Exposures from Sources near the Ground, Based on Hanford Experimental Data, USAEC Report HW-81746, pp. 1.1-1.19, Hanford Atomic Products Operation, 1964.
41. D. O. Martin and J. A. Tickvart, A General Atmospheric Diffusion Model for Estimating the Effects on Air Quality of One or More Sources, paper presented at the 61st Annual Meeting of the Air Pollution Control Association, 1968.
42. E. C. Eimutis and M. G. Konicek, Derivations of Continuous Functions for the Lateral and Vertical Atmospheric Dispersion Coefficients, *Atmos. Environ.,* **6**: 859-863 (1972).
43. G. R. Yanskey, E. H. Markee, Jr., and A. P. Richter, Climatography of the National Reactor Testing Station, USAEC Report IDO-12048, 1966.
44. T. L. Montgomery et al., A Simplified Technique Used to Evaluate Atmospheric Dispersion of Emissions from Large Power Plants, *J. Air. Poll. Control Ass.,* **23**: 395 (1973).
45. M. L. Barad and D. A. Haugen, A Preliminary Evaluation of Sutton's Hypothesis for Diffusion from a Continuous Point Source, *J. Meteorol.,* **16**: 12-20 (1959).
46. U. Högström, An Experimental Study on Atmospheric Diffusion, *Tellus,* **16**(2): 205-251 (1964).
47. F. Pasquill, *Atmospheric Diffusion,* 2d ed., Halsted Press, New York, 1974.
48. F. Pasquill, The Basis and Limitations of Pollution from Meteorological Data, presented at the Nordic Symposium on Urban Air Pollution Modelling, Vedbaek, Denmark, Oct. 3–5, 1973, U. K. Meteorology Office, Report Met. 0.14, T.D.N. 37.
49. R. E. Luna and H. W. Church, A Comparison of Turbulence Intensity and Stability Ratio Measurements to Pasquill Stability Classes, *J. Appl. Meteorol.,* **11**(4): 663-669 (1972).
50. F. Gifford, Diffusion in the Diabatic Surface Layer, *J. Geophys. Res.,* 67(8): 3207-3212 (1962).
51. F. Pasquill and F. B. Smith, The Physical and Meteorological Basis for the Estimation of the Dispersion of Windborne Material, in *Proceedings of the Second International Clean Air Congress,* Washington, D. C., 1970, H. M. Englund and W. T. Beery (Eds.), pp. 1067-1072, Academic Press Inc., New York, 1971.
52. H. H. Lettau and B. Davidson (Eds.), *Exploring the Atmosphere's First Mile,* Pergamon Press, Inc., New York, 1957.
53. George C. Holzworth, Mixing Heights, Wind Speeds, and Potential for Urban Air Pollution Throughout the Contiguous United States, Report AP-101, U. S. Office of Air Programs, 1972.
54. F. B. Smith, A Scheme for Estimating the Vertical Dispersion of a Plume from a Source near Ground Level, in Proceedings of the Third Meeting of the Expert Panel on Air Pollution Modeling, NATO-CCHS Report 14, North Atlantic Treaty Organization, Brussels, 1972.
55. R. P. Hosker, Estimates of Dry Deposition and Plume Depletion over Forests and Grassland, *Physical Behavior of Radioactive Contaminants in the Atmosphere,* Symposium Proceedings, Vienna, 1973, pp. 291-308, International Atomic Energy Agency, Vienna, 1974 (STI/PUB/354).
56. J. R. Beattie, An Assessment of Environmental Hazard from Fission Product Releases, British Report AHSB(S)R-64, 1961.
57. P. M. Bryant, Methods of Estimation of the Dispersion of Windborne Material and Data To Assist in Their Application, British Report AHSB(RP)R-42, 1964.
58. J. Sagendorf, Diffusion Under Low Wind Speed and Inversion Conditions, NOAA, Environmental Research Laboratories, Air Resources Laboratory, Technical Memorandum 52, 1975.
59. P. W. Nickola, G. H. Clark, and J. D. Ludwick, Frequency Distribution of Atmospheric Tracer Concentration During Periods of Low Winds, in Pacific Northwest Laboratory Annual Report for 1974 to the USAEC Division of Biomedical and Environmental Research, USAEC Report BNWL-1950, Part 3, pp. 51-55, 1974.
60. I. Van der Hoven, A Survey of Field Measurements of Atmospheric Diffusion Under Low Wind Speed, Inversions Conditions, to be published in *Nuclear Safety,* 17(2).
61. N. E. Bowne, J. T. Ball, and G. E. Anderson, Some Measurements of the Atmospheric Boundary Layer in an Urban Complex, Report TRC-7237-295 (AD-842951L), Travelers Research Center, 1968.
62. F. A. Gifford, Jr., Atmospheric Transport and Dispersion over Cities, *Nucl. Safety,* **13**(5): 391-402 (September–October 1972).
63. J. L. McElroy and F. Pooler, St. Louis Dispersion Study, U. S. Public Health Service, National Air Pollution Control Administration, Report AP-53, 1968.
64. F. Pasquill, Prediction of Diffusion over an Urban

Area—Current Practice and Future Prospects, in Proceedings of a Symposium on Multiple-Source Urban Diffusion Models, Chapel Hill, N. C., 1969, U. S. Air Pollution Control Office, Publication AP-86, pp. 3.1-3.26, 1970.

65. W. B. Johnson et al., Field Study for Initial Evaluation of an Urban Diffusion Model for Carbon Monoxide, Stanford Research Institute Report, SRI Project 8563, June 1971.
66. D. H. Slade, Atmospheric Diffusion over Chesapeake Bay, *Mon. Weather Rev.*, **90**: 217-224 (1962).
67. I. Van der Hoven, Atmospheric Transport and Diffusion at Coastal Sites, *Nucl. Safety*, **8**(5): 490-499 (September–October 1967).
68. S. A. Kitaigorodskii, *The Physics of Air–Sea Interaction.* (Translated from Russian and published by Israel Program for Scientific Translations, Ltd., Jerusalem, 1970, and available as TT72-50062.)
69. H. Schlichting, *Boundary Layer Theory*, 4th ed., pp. 607-613, McGraw-Hill Book Company, Inc., New York, 1960.
70. J. J. Stoker, *Water Waves*, Interscience Publishers, New York, 1957.
71. G. S. Raynor et al., A Research Program on Atmospheric Diffusion from an Oceanic Site, in *Symposium on Atmospheric Diffusion and Air Pollution*, American Meteorological Society, Santa Barbara, Calif., Sept. 9–13, 1974, pp. 289-295, available from the American Meteorological Society, Boston, Mass.
72. J. L. Lumley and H. A. Panofsky, *The Structure of Atmospheric Turbulence*, Interscience Publishers, New York, 1964.
73. A. S. Monin, The Atmospheric Boundary Layer, *Annu. Rev. Fluid Mech.*, **2**: 225-250 (1970).
74. N. Thompson, Turbulence Measurements over the Sea by a Tethered-Balloon Technique, *Quart. J. Roy. Meteorol. Soc.*, **98**: 745-762 (1972).
75. J. Warner, Spectra of the Temperature and Humidity Fluctuations in the Marine Boundary Layer, *Quart. J. Roy. Meteorol. Soc.*, **99**: 82-88 (1973).
76. F. A. Gifford, Jr., Atmospheric Dispersion Calculations Using the Generalized Gaussian Plume Model, *Nucl. Safety*, **2**(2): 56-59 (December 1960).
77. J. Halitsky, Gas Diffusion near Buildings, in Meteorology and Atomic Energy—1968, D. H. Slade (Ed.), USAEC Report TID-24190, pp. 221-252, Environmental Science Services Administration, 1968.
78. P. J. Barry, Estimation of Downwind Concentration of Airborne Effluents Discharged in the Neighborhood of Buildings, Canadian Report AECL-4043, July 1964.
79. J. Halitsky and K. Woodard, Atmospheric Diffusion Experiments at a Nuclear Plant Site Under Light Wind Inversion Conditions, in *Symposium on Atmospheric Diffusion and Air Pollution*, American Meteorological Society, Santa Barbara, Calif., Sept. 9–13, 1974, pp. 172-179, available from the American Meteorological Society, Boston, Mass.
80. R. N. Meroney and C. R. Symes, Entrainment of Stack Gases by Buildings of Rounded Geometry, in *Conference on Air Pollution Meteorology*, American Meteorological Society, Apr. 5–9, 1971, Raleigh, N. C., pp. 132-135; also, USAEC Report COO-2053-5, 1970.
81. R. N. Meroney and B. T. Yang, Gaseous Plume Diffusion About Isolated Structures of Simple Geometry, in *Proceedings of the Second International Clean Air Congress*, H. M. Englund and W. T. Beery (Eds.), pp. 1022-1029, Academic Press Inc., New York, 1971; also, USAEC Report COO-2053-1, 1970.
82. C. R. Dickson, G. E. Start, and E. H. Markee, Aerodynamics Effects of the EBR-II Containment Vessel Complex on Effluent Concentration, Canadian Report AECL-2787, 1967.
83. N. E. Bowne, Diffusion Rates, *J. Air Pollut. Control Ass.*, **24**: 832-835 (1974).
84. W. F. Dabbert, D. C. Cagliostro, and W. S. Meisel, Analyses, Experimental Studies, and Evaluations of Control Measures for Air Flows and Air Quality on and near Highways, Quarterly Progress Report 2, Stanford Research Institute, Jan. 25, 1974.
85. W. B. Johnson, Field Study of Near-Roadway Diffusion Using a Fluorescent Dye Tracer, in *Symposium on Atmospheric Diffusion and Air Pollution*, American Meteorological Society, Santa Barbara, Calif., Sept. 9–13, 1974, pp. 261-266, available from the American Meteorological Society, Boston, Mass.
86. J. F. Clarke and K. F. Zeller, Tracer Study of Dispersion from a Highway, in *Symposium on Atmospheric Diffusion and Air Pollution*, American Meteorological Society, Santa Barbara, Calif., Sept. 9–13, 1974, available from the American Meteorological Society, Boston, Mass.
87. F. L. Ludwig et al., Air Quality Impact Study for Proposed Highway Widening near Ojai, Stanford Research Institute Report, SRI Project 2852, 1975.
88. H. Stümke, Correction of the Chimney Height Due to an Influence of the Terrain (in German), *Staub*, **24**(12): 525-528 (1964); translated in USAEC Report ORNL-tr-997, Oak Ridge National Laboratory.
89. H. Stümke, Investigation on the Turbulent Dispersion of Stack Gases over Uneven Terrain (in German), *Staub*, **26**(3): 97-104 (1966).
90. H. Stümke, Dispersion of Stack Gases over a Plain with a Long Valley of Basin-Shaped Valley Perpendicular to the Wind Field (in English), *Staub*, **33**(8): 312-316; 336-340 (1973).
91. M. E. Berlyand, Atmospheric Diffusion Investigation in the USSR, in Dispersion and Forecasting of Air Pollution, Technical Note 121, World Meteorological Organization, Geneva, Switzerland, 1972.
92. M. E. Berlyand, Investigations of Atmospheric Diffusion Providing a Meteorological Basis for Air Pollution Control, *Atmos. Environ.*, **6**: 379-388 (1972).
93. G. E. Start, C. R. Dickson, and N. R. Ricks, Effluent Dilutions over Mountainous Terrain and Within Mountain Canyons, in *Symposium on Atmospheric Diffusion and Air Pollution*, American Meteorological Society, Santa Barbara, Calif., Sept. 9–13, 1974, pp. 226-232, available from the American Meteorological Society, Boston, Mass.
94. E. Hovind, T. C. Spangler, and A. J. Anderson, The Influence of Rough Mountainous Terrain upon Plume Dispersion from an Elevated Source, in *Symposium on Atmospheric Diffusion and Air Pollution*, American Meteorological Society, Santa Barbara, Calif., Sept. 9–13, 1974, pp. 214-217, available from the American Meteorological Society, Boston, Mass.

**Environmental Research Laboratories**

**Air Resources**
**Atmospheric Turbulence and Diffusion Laboratory**

**Oak Ridge, Tennessee**

FEBRUARY 1975

# PHOTOGRAPHIC ASSESSMENT OF DECIDUOUS FOREST RADIATION REGIMES

Boyd A. Hutchison

U. S. DEPARTMENT OF COMMERCE
NATIONAL OCEANIC AND ATMOSPHERIC ADMINISTRATION

ATDL Contribution File No. 75/3

ABSTRACT

PHOTOGRAPHIC ASSESSMENT OF DECIDUOUS

FOREST RADIATION REGIMES

Boyd Allan Hutchison

Yale University
1975

A model of forest radiation is proposed that assumes that radiation in the forest is composed of a spatially non-varying diffuse component upon which is superimposed a spatially varying direct beam component. Structural parameters required to drive this model are obtained from measurements made on hemispherical canopy photographs. Predictions calculated using this model and measurement approach are compared to observed data collected in the forest on clear, partly cloudy, and overcast days. Agreement between prediction and observation is generally poor. This assessment technique overestimates the penetrating, transmitted, and down-reflected diffuse radiation in the forest on all days and underestimates the transmitted and down-reflected direct beam radiation on clear to partly cloudy days. The predicted space distributions of direct beam radiation extend to higher flux densities than are observed and the predicted distributions are bimodal. Only at the 16 meter level around midday is there any evidence of bimodality in the observed data. Lack of agreement between prediction and observation is attributed to photo exposure problems and deficiencies in the model. Methods of minimizing the problem arising from photo exposure and modifications of the model are suggested and further tests of this assessment technique are proposed.

# PHOTOGRAPHIC ASSESSMENT OF DECIDUOUS FOREST RADIATION REGIMES

A Dissertation

Presented to the Faculty of the Graduate School

of

Yale University

in Candidacy for the Degree of

Doctor of Philosophy

by

Boyd Allan Hutchison

June, 1975

Acknowledgements

Research supported by the U. S. Atomic Energy Commission (Division of Biomedical and Environmental Research) and by the Eastern Deciduous Forest Biome, U. S. International Biological Program, funded by the National Science Foundation under Interagency Agreement AG-199, BMS69-01147 A09 with the U. S. Atomic Energy Commission, Oak Ridge National Laboratory. Special thanks are due Dr. D. R. Matt for his help in translating my ideas into mathematical form and for computer programming assistance.

Table of Contents

List of Tables

List of Figures

## Introduction

The physical structure of the primary producer component of an ecosystem has apparently evolved in such a manner that the efficiency of the photosynthetic fixation of solar energy received is maximized within the constraints imposed by physiologic characteristics, temperature and moisture conditions, nutrient availability, and intra- and inter-specific interactions (e.g. Horn, 1971). This maximization of energy fixation is achieved through adjustment of canopy depth and closure, leaf distribution and orientation, and the cellular geometry of the leaves (Salisbury, 1949; Warren Wilson, 1960; Anderson, 1964c; Gay, Knoerr, and Braaten, 1971; and Horn, 1971). Canopy depth and closure along with leaf distribution, orientation, and inclination, and the optical characteristics of the leaves affect primary production through their control of the penetration of solar radiation into the vegetative stand and of the absorption of this radiation by leaves. Because of these controls, the relationships between the geometry of the photo-synthesizing surfaces of an ecosystem and the distribution of solar radiation within that ecosystem have far reaching consequences in terms of ecosystem structure and function.

As part of the Analysis of Ecosystems portion of the United States International Biological Program effort within the Eastern Deciduous Forest Biome, I am studying the distribution of solar radiation within a deciduous forest and the relationships between this distribution and the structure of the forest ecosystem. The specific objectives of this study are:

1. to determine the distribution of direct beam, diffuse, and total solar radiation in space and in time.

2. to relate these distributions to the structure of this forest.

3. to develop means of assessing forest structure from measurements of structural parameters recorded upon hemispherical canopy photographs.

While a number of models exist that predict mean radiation conditions within vegetation from incident radiation data and structural characteristics, the information required by these models regarding structural geometry is difficult to obtain in forests (e.g. Monsi and Saeki, 1953). Most of these models were originally devised for agricultural crops where canopy geometry is somewhat more simple and much more easily measured than in forests. Furthermore, nearly all of these models predict mean radiation within vegetation, a parameter somewhat less than satisfactory owing to the nonnormality of flux density frequency distributions there induced by the presence of direct beam radiation (Ramaan, 1911; Gay, Kœrr, and Braaten, 1971; Miller and Norman, 1971a).

For these reasons, I am approaching the problem of relating radiation in the forest to forest structure as stated in the objectives above. First, distributions of flux densities are predicted rather than mean quantities and second, these distributions are predicted from forest structure measurements that can be made using methods and equipment available to agronomists, ecologists, and foresters working in remote field sites with limited time and manpower. Thus the photographic method seems to be a logical technique to use. While the hemispherical lens camera required for this assessment is rather expensive, once purchased it can be used in many locations nearly simultaneously. The cost of film and processing is minimal and the time required for taking the photographs and analyzing them is reasonable.

Following the pioneering efforts of Evans and Coombe (1959), Anderson (1964a) and Madgwick and Brumfield (1969) in using hemispherical canopy photographs to assess forest structure, I propose a model that predicts mean diffuse radiant flux densities plus the distribution of direct beam flux densities within a deciduous forest composed primarily of Liriodendron tulipifera (tulip poplar). This prediction is based upon records of incident direct beam and diffuse radiation incident upon the top of the canopy and from the vertical and horizontal distributions of canopy gaps and gap sizes as measured from canopy photographs.

This model is validated by comparing predicted distributions with distributions measured within this forest during the 1972 growing season under overcast and clear sky conditions.

## Past Work

The penetration of solar radiation into vegetative stands has received considerable attention in the past and continues to intrigue agronomists, ecologists, foresters, micrometeorologists and others. G. C. Evans (1966) attributes this continuing popularity to two factors. First, solar radiation influences organisms in myriad ways and as these effects have been discovered, the need to define the radiation climates of the habitats of these organisms in order to understand their functioning has become apparent. For green plants, radiation effects are of three basic types: 1) the photosynthetic effect whereby a portion of the incident radiation in the spectral band 0.38 to 0.71 microns is converted to energy in chemical form; 2) the thermal effect whereby absorbed incident radiation is converted to heat energy and then

partitioned to radiative heat losses, convective heat losses, latent heat losses through transpiration, or heat storage in plant biomass which results in a warming of plant parts; and 3) the photomorphogenic effects of radiation upon plant growth and development (Ross, 1968). In nonphotosynthesizing organisms, heating effects (heat storage) and photoperiodic effects predominate. Because of these effects, the understanding of the structure and function of organisms or of systems of organisms implies an understanding of radiation distributions within ecosystems.

The second factor involved in the continuing interest in the radiation climates of plant stands according to Evans (1966) is that the relationships between radiation distributions and the physical geometry and the optical characteristics of the vegetation are quite complex. Hence the problem of defining these relationships remains challenging.

During the mid-seventeenth century, van Helmont showed that Aristotle's pronouncement that plants obtained total nourishment from the soil to be incomplete at best (Spoehr, 1926). Van Helmont performed a carefully controlled experiment of growing a willow of known weight at the time of planting in soil also of known weight. After five years, the willow was reweighed and was found to have increased its weight thirty-fold. The weight of the soil, however, had changed imperceptibly. Thus, van Helmont concluded that the increase in the weight of the willow had its origins elsewhere than in the soil. Some 200 years later, Priestley discovered that green plants could "purify" air that had been "contaminated" by occupation by mice (Spoehr, 1926). Ingen-Housz further showed that only the green parts of plants could

purify such air and, significantly, that this purification was accomplished only in the presence of sunlight (Spoehr, 1926). A few years later, de Saussure experimentally demonstrated that the carbon content of plants had its origins in the carbon dioxide of the atmosphere and surmised that sunlight was necessary for the transformation of $CO_2$ to carbohydrate since he could find no evidence of carbon fixation in the absence of light (Spoehr, 1926). Finally in the 1840's, Julius Mayer conclusively demonstrated that the energy content of carbohydrate is indeed derived from solar energy (Spoehr, 1926).

As this series of discoveries led to a crude understanding of the process of photosynthesis, the discovery of other photochemical effects of solar radiation led to development of crude means of measuring "light." Such techniques, while of limited accuracy, allowed early botanists to begin to quantify the radiation climates of plant communities. As a result, a considerable body of literature existed early in this century regarding the problem of light in vegetation. Von Sachs (1887) considered the problems of interpretation of light measurements in his plant physiology lectures (Anderson, 1964c). In 1907, Weisner's The Light Enjoyment of Plants was published in which he summarized the results of studies of light distribution in plant stands. He considered the problems of sunflecks and of the effect of plant geometry upon light penetration. He also showed that the "relativ lichtgenuss," defined as the fraction of diffuse light in the open that reaches a point within a plant stand, remains fairly constant over time but cautioned that similar plant communities at different latitudes or in different climates will possess different "relativ lichtgenuss" factors.

With the discovery of photoelectric effects, photocells were soon developed which made reliable and inexpensive light measuring instruments available to field scientists for the first time. The use of this kind of sensor became so widespread that a system of photometric units evolved. This system of units has greatly confused the issue of radiation in vegetation because photocells have variable sensitivity over the solar spectrum. Most photocells are designed to duplicate the sensitivity of the human eye thereby eliminating solar radiation of wavelengths beyond around 0.7 microns. Because of this, confusion has arisen since photometric units are convertible to energy units only if the spectral composition of the light being measured is known (Anderson, 1946c). Despite this limitation many early workers were well aware of the problems engendered by the spectral selectivity of their instruments and interpreted their results accordingly (e.g. Atkins, Poole, and Stanbury, 1937).

The development of pyranometers utilizing thermopiles as the sensing units provided spectrally nonselective instruments which can be calibrated to yield measures of radiant flux densities in units of energy. A major disadvantage of such instrumentation continues to be its high cost.

A surprising number of extensive reviews of the problem of radiation in plant communities can be found. Following the early summaries of von Sachs (1887) and Weisner (1907), Shirley (1935, 1945) surveyed the ecologic aspects of radiation climates quite thoroughly. The various editions of Geiger's The Climate Near The Ground (1927, 1950, 1957, 1965) contain summaries of studies of radiation in vegetation conducted mostly in Germany. Roussel (1953) and later, Chartier (1966)

present extensive reviews of research in this area with emphasis upon research conducted in France. Tranquillini (1960) has also surveyed the literature regarding radiation climates of plant stands. Undoubtedly the most thorough and critical review of radiation in plant communities is that by Anderson (1964c) in which she considers the light relations of plant stands and their problems of measurement in great depth. Reifsnyder and Lull (1965) have considered the energy relations of forests in great detail while D. H. Miller (1965) has published an exhaustive review of literature regarding the heat and water budget of the earth's surface in which he considers the problem of the penetration of radiation into forests. Miller's fluency in reading the Russian language makes this review especially valuable as he cites Russian scientific literature extensively.

As noted above, Weisner (1907) recognized that in order to obtain any sort of reasonably constant ratio between radiation within and without vegetation, direct beam radiation (sunfleck) must be eliminated from measurements. Since the time of Weisner, a considerable debate has raged over the importance of sunflecks to the radiation climate of plant stands. Shirley (1945) concludes that sunflecks are not of great ecologic significance to plants growing in the shade of other vegetation. Similarly, Atkins, Poole, and Stanbury (1937) state that illumination within forests depends only upon sky brightness. However, Evans (1956) disputes these views citing his measurements of illumination within a Nigerian rain forest that showed that the bulk of the light reaching the undergrowth was in the form of sunflecks. Gay, Knoerr, and Braaten (1971) estimate, by a rather tenuous process, that at least half of the radiant energy reaching the floor of the pine plantation

studied was direct beam radiation.[1] Similarly, Reifsnyder, Furnival, and Horowitz (1971/72) found that direct beam radiation accounted for 21 and 53 percent of the radiation reaching the floors of deciduous and conifer forests, respectively. In some measurements made in the deciduous forest under consideration here, I found similar results at the forest floor. With the forest fully leafed and under nearly cloud-free skies, nearly half of the energy measured at the forest floor was in the form of penetrating direct beam radiation, i.e., sunflecks (Hutchison, 1971). The conclusion that direct beam radiation is of significance to the photosynthetic production of shaded vegetation is further supported by the theoretical considerations of radiation in vegetative stands by Monteith (1965), Ross and Nilson (1968), and Ross and Tooming (1968).

The flux density of direct beam radiation in plant stands is highly variable. One needs only to reflect upon the ever-changing pattern of sunfleck and shade on the forest floor to realize this. On the other hand, the flux density of diffuse radiation is much less variable as is qualitatively indicated by the uniformity of illumination in forests on cloudy days. Because of these differences in

---

[1]Gay, Knoerr, and Braaten (1971) measured total radiation reaching the floor of a loblolly pine plantation on clear days. They estimated the diffuse radiation by drawing a smooth curve through the minimum values of total radiation observed assuming that these minimum values represented diffuse radiation only. Since their data were collected on clear days, there must have been some contribution to this minimum value from down-reflected direct beam radiation. Reifsynder, Furnival, and Horowitz (1971/72) estimate that in a red pine plantation, such reflected direct beam amounts to some 14 percent of the total. However, this fact would only serve to make Gay, Knoerr, and Braaten's (1971) method of estimating direct beam radiation a conservative one. Hence their conclusion remains valid.

variability, attempts to define the radiation climates of vegetative stands by a single constant factor expressing the radiation within the stand as a fraction of that received outside are doomed to failure. When diffuse radiation only is considered however, then relatively constant factors such as the "lichtgenuss" of Weisner (1907) or the "daylight factor" of Atkins, Poole, and Stanbury (1937) can indeed be derived. Because of this, many early workers took great pains to exclude direct beam radiation from their measurements in order to obtain reproducible results. Anderson (1964c) has shown however that the relative amounts of diffuse radiation penetrating plant communities differs between clear and cloudy sky conditions. Thus it appears impossible to truly describe the radiation climate of plant stands by single numbers.

The reasons for the differences between the extremely variable penetration of direct beam and the more uniform penetration of diffuse radiation into plant stands lie in differences in the physical characteristics of the vegetation governing the penetration of these two components (Anderson, 1964b). The penetration of direct beam radiation to any point in a plant stand depends only upon the intensity of the direct beam radiation impinging upon the top of the stand and upon the number, and the size and height distributions of canopy gaps along the apparent solar path as viewed from the point in question (Anderson, 1964c; Anderson and Denmead, 1969; Horn, 1971; Miller and Norman, 1971b; Reifsnyder, Furnival, and Horowitz, 1971/72). The penetration of diffuse radiation depends upon the distribution of sky brightness, upon the size and space distribution of canopy gaps in the hemisphere of space above the point in question, as well as upon the

inclination, orientation, and optical characteristics of leaves and other biomass making up the stand (Verhagen, Wilson, and Britten, 1963; Anderson, 1964b,c; Anderson and Denmead, 1969; Horn, 1971).

The number and size of gaps along the apparent solar path is highly variable in most plant stands and this induces great spatial variation in the penetration of direct beam radiation. As the solar disk appears to move across the sky, this spatial variation constantly changes; thus temporal variation is induced as well. With diffuse radiation however, the factors involved in its penetration are much less variable both in space and in time. The zenith is generally the brightest portion of the sky under a range of sky conditions when the area of sky near the solar disk is excluded from consideration (Anderson, 1964a,b,c). Furthermore, most plant stands have minimal closure directly overhead thereby allowing maximal penetration of diffuse skylight from the brightest portion of the sky (Anderson, 1964a,b,c; Horn, 1971). Although this diffuse radiation from the sky is enriched as it penetrates into a stand by down reflected direct beam radiation, such enrichment seems to be directionally random owing to the distribution of biomass and hence large increases in variability are not induced (Reifsynder, Furnival, and Horowitz, 1971/72).

Because of these differences in the manners of penetration and in the variabilities of the two radiation components, both direct beam and diffuse radiation must be measured in order to assess the radiation climate of a plant stand. Since their variabilities differ however, the same sampling scheme for both radiative components will not produce comparable accuracy in the results. For example, Reifsynder, Furnival, and Horowitz (1971/72) found that 412 and 18 sensors would be required

to obtain instantaneous space averages of direct beam flux densities having standard errors of the mean of 10 millilangleys or less in a red pine plantation and in a deciduous forest, respectively. To obtain this same level of accuracy for measurements of diffuse radiation, only two replications would be required in either stand. Gatherum (1961) found that 2620 observations made with a photocell would be needed to obtain reliability within ten percent of the mean at the 99 percent level of probability for total radiation in the upland oak forest in which he worked.

Most past studies of radiation in forests have dealt only with radiation reaching the forest floor. However the distribution of radiation varies vertically as well as horizontally and temporally. Since much past work dealing with radiation in forests was designed to yield information regarding the light requirements of forest tree regeneration, this vertical variation was not of concern. Such variation is of especial importance to primary productivity assessments in forest ecosystems however, since most of the photosynthetic production of a forest occurs in the overstory canopy. Trapp (1938) found a curvilinear relationship between radiation and height in a mature red beech forest as shown in Figure 1. As is evident from Figure 1, the height distribution of radiation differs between clear and cloudy days. Baumgartner (1955) reports similar curves for radiation attenuation in both young beech stands and young pine stands. P. C. Miller (1969) has reported that under certain conditions, the vertical profile of radiation in gaps between trees will show an increase above incident near the top of the canopy. Below that level, the usual exponential decay type curve results. He found that this

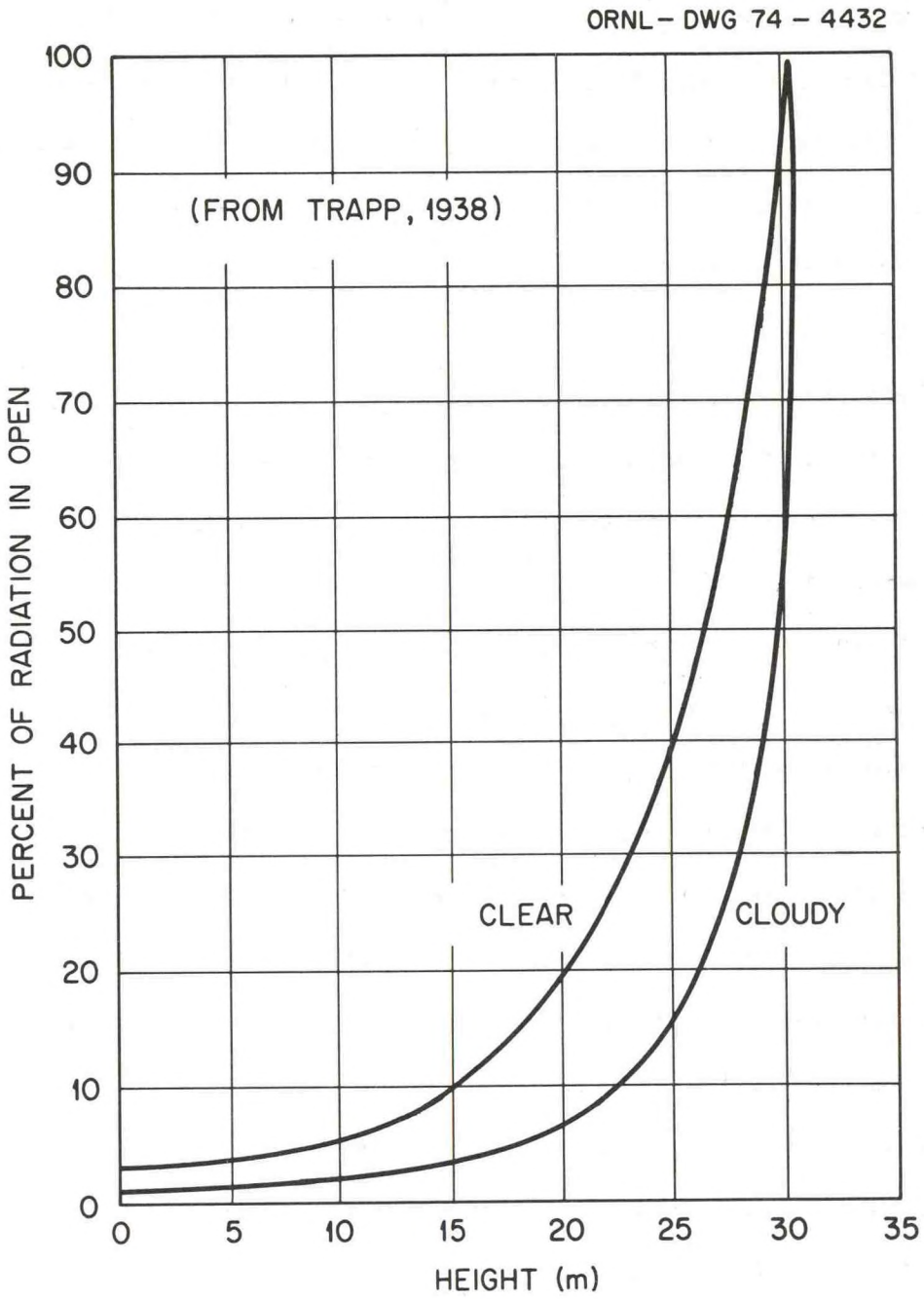


Figure 1: Vertical Distribution of Radiation in a Red Beech Forest.

enrichment occurs where direct solar beam intensity is high and where the proportion of diffuse skylight in the total is low and attributes the phenomenon to downward reflection from leaves in the topmost canopy layers.

A further problem beyond those engendered by the extreme variability of direct beam radiation in space and in time in assessing the radiation climate within a plant community is that of assessing this climate in biologically meaningful terms. As early as 1911, Ramaan recognized that the determination of mean radiation within plant stands was biologically less than satisfactory owing to the nonnormal frequency distribution of radiant flux densities found there. Carter (1934) realized that his reported results were probably in error because of this but he was unable to resolve the problem further. Impens, Lemeur, and Moermans (1970) report bimodal distributions of net radiation flux densities in the upper portions of a bean canopy (Figure 2). Lower in the canopy, unimodal distributions are found that are skewed to higher flux density values (Figure 2). Data that I collected in a Liriodendron forest yield similar results. Between the projecting tips of the trees, above canopy closure, bimodal frequency distributions of direct beam flux densities are found while at levels lower in the canopy, skewed, unimodal distributions are present (Hutchison, 1971). Modal flux densities decrease with depth in the forest as would be expected. Skewed, unimodal distributions of radiant flux densities are reported by Ovington and Madgwick (1955) on the floors of both oak and spruce forests, by Evans (1956) for sunfleck areas in a Nigerian rain forest, by Nageli (1940) in a deciduous forest, and by Roussel (1953) in a conifer forest. Kornher and Rodskjer's

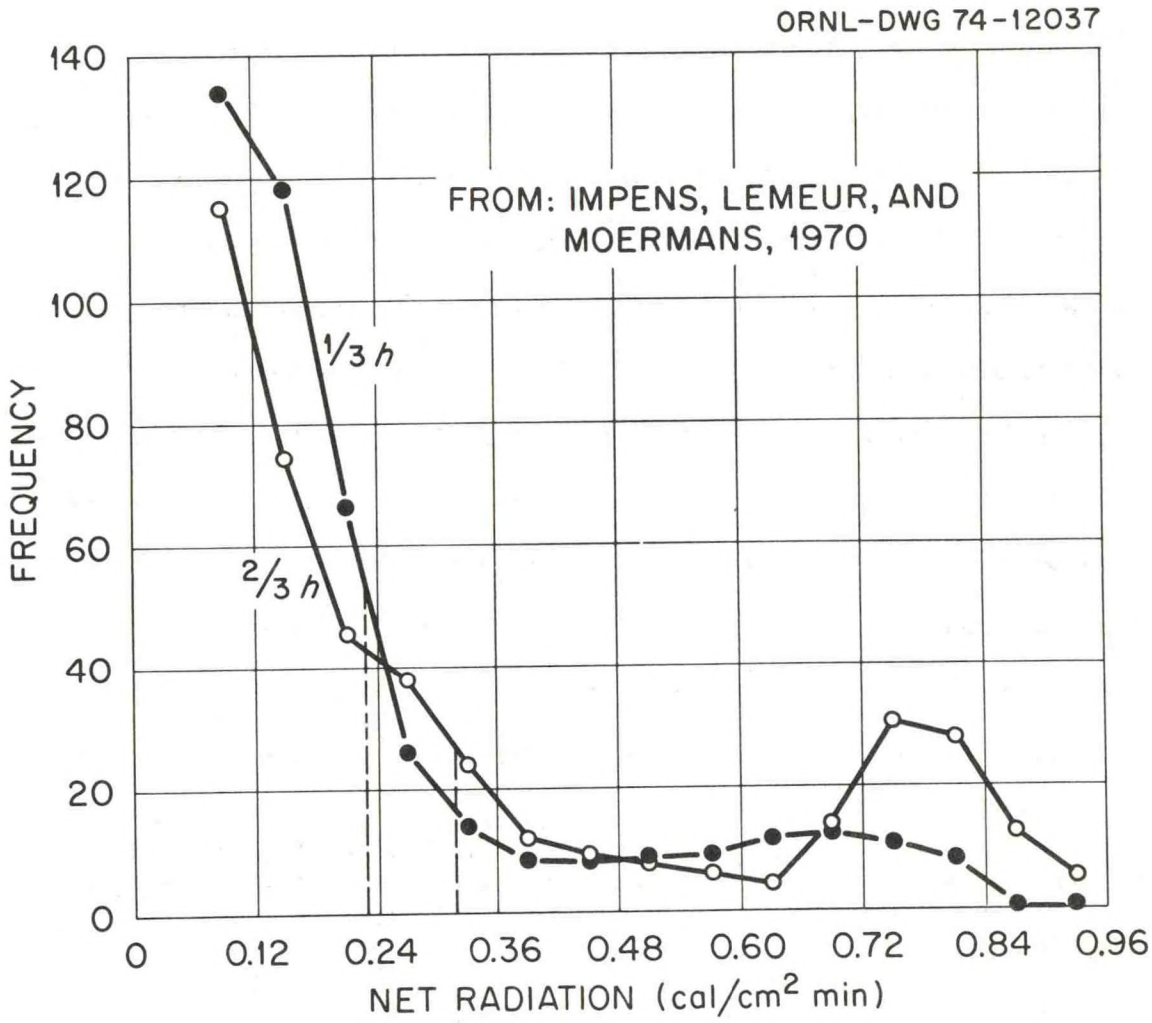


Figure 2: Frequency Distribution of Net Radiation in a Bean Canopy for a One-Hour Period Around Solar Noon. (h = height of canopy)

(1967) results from studies of radiation in a stand of oats also show skewed, unimodal time distribution of radiant flux densities at 5 and 15 cm elevations above the ground. In their theoretical approach, Ross and Nilson (1968) predict asymmetrical distributions of flux densities when direct beam radiation is included in consideration. In the absence of direct beam radiation, their model predicts symmetrical distributions. Alekseev (1963) concludes that measures of skewness and kurtosis of the flux density distributions are needed beyond the commonly cited mean and standard error of the mean in order to correctly characterize the radiation climates of forests. The biologic interpretation of these statistical parameters is not clear however.

According to Ross (1968), the radiation regime of any plant stand is a function of four factors:

1. the spectral composition and direction distribution of incident solar radiation and of sky radiation.

2. the optical properties of the floor of the stand.

3. the optical properties of the various plant parts making up the stand.

4. the geometric structure of the stand.

The first two factors represent boundary conditions while the latter two are properties of the stand. There have been a number of attempts to relate the radiation regime within plant communities to these factors but few have considered all four simultaneously.

Such attempts may be classified either empirical or theoretical but in reality, many of the theoretical relationships derived depend upon empirically determined coefficients (e.g. Czarnowski and Slomka,

1959; Newton and Blackman, 1969; Federer, 1971/72). Strictly theoretical approaches to this problem have been of two general types; the geometric approach where vegetation is idealized as an array of geometric solids or the mathematical approach which considers the vegetative layer as a turbid medium (Ross and Nilson, 1968).

Shul'gin (1961) treats the problem of radiation in forests as a purely geometric one. He calculates the degree of shading effected by hemispheres in north-south rows for various solar elevations. While this approach is trigonometrically simple, it becomes intractable for other shaped solids and for other spatial arrangements of the solids. Jahnke and Lawrence (1965) model forests as a geometric array of cones (with apexes upward) having various height-base diameter ratios and conclude that the more steeply the sides of the cones are inclined, the greater the radiation that can be intercepted. Unfortunately they fail to normalize their calculations by the surface area of the cone. Hence this conclusion only reflects that as cone heights increase (with base diameters remaining constant), so also does cone surface area and the greater the surface exposed, the greater the interception of radiation. Brown and Pandolfo (1969) treat the problem of radiation interception by vegetation or other obstacles using a triangular array of right solid cyclinders as their geometric model. Here again, deviations from right cylinders or the triangular array lead to conditions difficult to characterize by trigonometric formulae. Combining the geometric and turbid media approaches, Federer (1971/72) models a winter deciduous forest by assuming that the crown space is a uniformly absorbing turbid medium while the trunk space constitutes a random array of right cylinders. It appears that the purely

geometric approach for characterizing radiation climates of vegetation is of very limited usefulness because of the difficulties involved in extending the approach to the complex geometries of natural vegetation.

The characteristic exponential decay type curve of radiation attenuation in vegetation as reported by Trapp (1938) led Monsi and Saeki (1953) to characterize radiation in vegetation using a negative exponential equation variously known as Beer's, Bourguer's, Lambert's, or a combination of these name's law. While such equations explain the attenuation of diffuse radiation in homogeneous turbid media precisely, their extension to radiation attenuation in vegetation requires a considerable number simplifying assumptions regarding the geometrical and optical characteristics of the vegetation as well as of the incident radiation. The use of this approach in vegetation requires that the stand be capable of characterization as follows:

1. the stand is completely homogeneous and of constant optical density.

2. the stand is such that all radiation is perfectly diffuse at any depth.

3. the reflection coefficient is constant with depth.

4. the absorption coefficient is constant and independent of depth.

5. the stand is of infinite width and breadth having a finite depth.

Since these assumptions are not met in vegetation and because the models requiring these assumptions in general predict only mean radiative conditions, Monteith (1965) and Verhagen and Wilson (1969) conclude that this approach cannot be used to predict primary

productivities of plant communities. Nevertheless, the approach is widely used.

Monsi and Saeki (1953) expressed the modified Beer's, Bourguer's, Lambert's law for vegetation as

$$I = I_o e^{-KF}$$

where I = average radiation at a given level in the stand, $I_o$ = average incident radiation, K = the extinction coefficient, and F = the total leaf area index above the level in the stand in question. Monsi and Saeki (1953) tested this model in a variety of plant communities and concluded that the agreement between theory and observation was quite acceptable. Both they and later Kasanaga and Monsi (1954) used this model to predict diffuse radiative conditions only; they excluded direct beam radiation from consideration. Despite this exclusion, their predictions along with later ones by Davidson and Philip (1958) of photosynthetic production of plant communities were in good agreement with observed values.

De Wit (1959) modified the Monsi and Saeki approach to allow consideration of both diffuse and direct beam radiation thus eliminating one of the more inaccurate assumptions required. About this same time, Warren Wilson (1959, 1960) extended the theory of inclined point-quadrat measurements to explain the penetration of radiation into vegetation. As Anderson (1966) showed later, the independent derivation of Warren Wilson is essentially identical to Monsi and Saeki's (1953) approach assuming the equivalency of leaf area per unit ground area and per unit stand volume.

The agreement between theory and observation was further improved

by modifications of the Monsi and Saeki (1953) approach by Saeki (1960) and by Verhagen, Wilson, and Britten (1963) which corrected the model for that radiation transmitted through leaves. Working in corn, Allen, Yocum, and Lemon (1962) found that while radiation attenuation in corn stands is more closely related to cumulative leaf area indexes, the relationships between radiation attenuation and crop height (a more easily measured parameter) was satisfactory for predicting productivity. Later Yocum, Allen, and Lemon (1964) further modified Monsi and Saeki's (1953) approach substituting the product of radiation-path length and the concentration of absorbing material for leaf area index (F) in the original equation. Thus changing path lengths with apparent solar movement can be accounted for in their version of the model.

In the original work on this approach, Monsi and Saeki (1953) concluded that the extinction coefficient (K), for any given plant community, was a constant, characteristic parameter of that community. Isobe (1962) found that this coefficient is not constant but is actually a function of solar angle and of leaf inclination angle for all but horizontal leaves. Thus Isobe (1962) independently explained on a theoretical basis, the difference in productivities between wild sea beets with prostrate leaves and cultivated beets with inclined leaves as observed by Watson and Witts (1959). As elucidated by Verhagen, Wilson, and Britten (1963), if the upper leaves of a plant stand are steeply inclined with respect to incident radiation, they will intercept less radiation than if perpendicularly inclined to incident radiation. Since radiation is rarely a limiting factor to photosynthesis in the upper regions of plant canopies and, in general, exceeds the light saturation levels of the leaves, this positioning of

leaves in no way reduces productivity. In fact, the productivity of the stand is increased since the steeply inclined upper leaves reflect radiation downward into the canopy thus increasing radiation amounts reaching lower canopy levels. At these levels, radiation is often a limiting factor of photosynthesis and hence this enrichment results in increased productivity. In this way then, a plant stand may regulate the radiation regime within itself to maximize productivity. This occurs when a closed stand receives relatively uniform illumination throughout and the lowest leaves receive sufficient radiation to allow their photosynthetic production to equal their energy consumption through respiration (Warren Wilson, 1960). The non-constancy of the extinction coefficient (K) is further supported by the theoretical considerations of Warren Wilson (1960), Anderson (1966), and Loomis, Williams, and Duncan (1967) as well as by the experimental studies of Newton and Blackman (1969).

Cowan (1968, 1971) further modified the Monsi and Saeki (1953) approach by incorporating crown depth into the model thus simulating by a different approach, the modification proposed by Yocum, Allen, and Lemon (1964). Anderson (1966) showed that the Monsi and Saeki (1953) model explained direct beam penetration in its unintegrated form and used both the integrated and unintegrated forms to estimate average radiation conditions in plant stands.

In their independent but equivalent approach to that of Monsi and Saeki (1953), Warren Wilson (1960) and Reeve (appendix to Warren Wilson, 1960) used the ratio of the projected leaf area in the direction of the solar beam to actual leaf area as the negative exponent thereby eliminating the extinction coefficient (K), from the equations for

direct beam and diffuse radiation penetration. Loomis, Williams, and Duncan (1961) and Duncan, Loomis, Williams, and Hanau (1967) have further modified Warren Wilson's approach by correcting the path length through the canopy.

Monteith (1965) has criticized the exponential model approach as noted earlier, because it yields mean radiation conditions only. Since photosynthetic rates are nonlinear functions of radiant intensities, the use of mean radiation can introduce errors into productivity calculations. Ideally, the time distribution of radiant intensities is required. With Monteith's (1965) binomial expansion model, such distributions can be predicted. Monteith (1965) assumes that the radiant intensities of sunflecks are constant and his model predicts the proportion of any level covered by sunflecks. In addition, his model also predicts the proportion of the area that is once shaded, i.e., that area receiving radiation that has been transmitted through one layer of leaves. While this model is quite simplistic, it recognizes that sunfleck areas receive much greater amounts of radiation than either once shaded or shaded areas and predicts radiation distributions accordingly. Curiously, this approach has received little further attention since being proposed in 1965.

Ross and Nilson (1968), utilizing a theory of the propagation of radiation in stellar atmospheres, have developed yet another exponential model of radiation attenuation in vegetation which assumes that radiation attenuation is controlled by three parameters rather than two as in the Monsi and Saeki (1953) model. These parameters are the optical thickness of the vegetation, which is essentially equivalent to Monsi and Saeki's (1953) extinction coefficient, the leaf area of the

vegetation, and a scattering coefficient. Equations are developed for the penetration of diffuse radiation and for the scattering of direct beam and of diffuse radiation.

Anderson (1969a) has compared the Monsi and Saeki theory with the Ross and Nilson (1968) theory and has shown that for both horizontal and vertical leaves, the two models are identical. For randomly inclined leaves, she shows that the Ross and Nilson (1968) approach better agrees with observed data. She points out however, that foliage is rarely randomly distributed and that scattering by leaves is not strictly isotropic; thus, the Ross and Nilson (1968) approach is lacking.

In his further work in this area, Nilson (1971) has proceeded from Warren Wilson's (1960) inclined point-quadrat approach. He develops probability expressions of canopy gap distribution for random, regular, or clumped foliage dispersions. For randomly dispersed foliage, a negative exponential or Poisson model is derived while for regularly dispersed foliage, a positive binomial model results. In the case of clumped foliage, a Markov model is derived which takes into account the nonstatistically independent distribution of foliage in most plant stands. However, this last model requires three additional characterizing parameters whose physical meanings are as yet unknown.

The theoretical approaches thus far discussed have dealt with one or two distinct problems — the relationship between the structural geometry of vegetation and the radiation climate within that vegetation and also, in Nilson's (1971) recent publication, the anisotropy of radiation reflected from leaves. Further problems remain.

Despite Monteith's (1965) attempt to characterize the radiation climate of vegetation stands on the basis of mean sunfleck and mean shade intensities, the actual distribution of intensities would be much more meaningful and preferable. Norman (1971), Norman, Miller, and Tanner (1971), and Miller and Norman (1971a,b) have developed a theory which predicts gap-size distributions for a canopy of flat, horizontal, randomly dispersed leaves from measurements of the proportion of horizontal transects through such a canopy falling in sunfleck areas. Using this predicted gap-size distribution and from consideration of penumbral effects produced because of the finite size of the solar disk, the flux density distribution of direct beam radiation can be calculated.

The problem of spectral changes in the penetrating radiation induced by the vegetation has been cited by a number of workers in the field but as yet there appears to be no model available that take such effects into account. From their extensive observation of spectral quality of radiation in plant stands, Loomis, Williams, and Duncan (1967) conclude that the spectral modification of radiation within vegetation is small compared to the modification (reduction) of intensity.

A final problem noted by Anderson (1967b) is that of relating predicted or measured radiant flux densities, whether mean or frequency distributions, on horizontal surfaces to the actual inclined surfaces of the leaves. Anderson (1969b) points out that while differences in diffuse intensities received by horizontal and inclined surfaces are small, the differences in direct beam radiation received can be very large. Anderson and Denmead (1969) have extended the Monsi and Saeki

(1953) theory to predict direct beam illumination of inclined leaves by integrating the equation over the range of leaf inclinations present. For diffuse radiation, the luminance of an overcast sky proposed by Moon and Spencer (1942) is integrated over the hemisphere of sky and the penetration of radiation from this overcast sky is assumed to follow the negative exponential decay theory of Monsi and Saeki (1953).

In general, these models have been applied to grain or other crop canopies where the determination of the structural parameters required by the models, while tedious, is somewhat less difficult than in forests. Owing to the difficulties involved in assessing forest structure, most investigators working in forests have understandably sought other characterizing parameters that are more easily measured than leaf area indexes or leaf inclinations and orientations. Most early investigators simply described the forest qualitatively as to species composition (e.g. Carter, 1934). Salisbury (1916) used the time elapsed since coppicing as a means of comparing light conditions in different oak-hornbeam stands while Shirley (1945) used the age of forest stands as the normalizing factor. In mixed oak forests, Gatherum (1961) was able to relate the variation in radiation received on the forest floor to the proportion of dominant trees removed by harvesting. Wellner (1948), working in western white pine stands, used basal area as a characterizing parameter and further stratified the stands on the basis of the ratio of numbers of small-crowned species to large-crowned species. Jackson and Harper (1955) and Shoemaker (1968) used basal area as the parameter governing radiation penetration

in shortleaf pine forests while Roussel (1953) used the number of stems per unit area.

Brecheen (1951); D. H. Miller (1959); Fairbairn (1961); Akulova, Khazanov, Tsel'Niker, and Shishov (1964); Vezina and Pech (1964); and Khazanov and Tsel'Niker (1968) have all used some measure of crown closure as a means of comparing radiation in different stands. In D. H. Miller's (1959) analysis, the degree of scatter in plots of percent radiation in the stand over crown closure led him to conclude that some measure of crown depth is also needed to obtain more definitive relationships.

The leaf area index alone proved an inadequate characterizing parameter in Rauner and Rudnev's (1962) attempt to relate radiation to forest structure. In a deciduous stand and a coniferous stand having equal leaf area indexes, nearly one and one-half times the radiation reaching the floor of the conifer stand reached the floor of the deciduous stand. Thus, in stands of different species composition, further characterization beyond leaf area such as the Monsi and Saeki extinction coefficient, K, is needed to predict radiation climates.

Obviously canopy structure is of primary importance in governing the penetration of radiation into the canopy. Therefore the elucidation and determination of suitable structural parameters is necessary for both theoretical and empirical predictive techniques. While simple measures such as stem density or basal area may suffice for the prediction of radiation in stands of similar species composition, better characterizing parameters are needed for the prediction of radiation in stands composed of different species. The utility of photography as a means of assessing canopy structure was recognized some time ago but

because of the distortion produced in the reduction of the three-dimensional canopy to a two-dimensional image on the photographic plate, few quantitative data were obtained. A number of investigators have derived crown closure data from such photos (Brecheen, 1951; Berger, 1953; and Brown, 1958). Berger (1953) went so far as to consider the closure along the apparent solar path separately from the vertical closure. The most extensive photographic analysis of forest canopies appears to be that made by Evans in a Nigerian rain forest in 1948 (Evans and Coombe, 1959). Using a plate camera, Evans photographed the canopy at a series of azimuth and elevation angles. Following processing of the plates, he fitted the photos together into a hollow hemisphere for analysis. Later, Coombe performed similar analyses upon photos that he made of a woodland canopy near Cambridge, England. While the time and labor involved in such a technique must have rivaled that required for direct measurement, the utility of the technique was demonstrated.

Later, it was discovered that Robin Hill (1924) had designed a camera for use in studies of clouds capable of reducing objects in the hemisphere of space above the camera to a single photographic image. Moreover, the design of the lens was such that the image produced was an equidistant projection of the hemisphere of space. That is, a given radial increment on the photo represents the same angular distance no matter where the radial increment is selected on the photo. Thus this camera is ideally suited for use in the photographic assessment of canopy structure.

Anderson (1964a), building upon the rather imprecise "lichtgenuss" concept of Weisner (1907) and the "daylight factor" of Atkins, Poole,

and Stanbury (1937), has outlined methods for computing what she terms the "diffuse" and "direct beam site factors" for any forest from hemispherical photographs of that canopy. While the diffuse site factor is closely related to canopy closure in principle, Anderson's (1964a) method factors in the sky brightness distribution as well. Although she chose only to use the standard overcast sky distribution as proposed by Moon and Spencer (1942), the technique can be applied to any sky brightness distribution desired.

Crown closure as generally defined yields little information regarding the penetration of direct beam radiation. Following Evans and Coombe (1959), Anderson (1964a) constructed solar path diagrams which were superimposed over the canopy photos. By assessing the degree of closure along the apparent solar path on any desired date, the direct beam site factor for that date can be computed. Comparison of data collected in the forest and predicted from computed site factors showed good agreement. Since the photographic film has a spectral sensitivity similar to that of photocells, this method is essentially a photometric technique as pointed out by Anderson (1964a). Hence the photographic method will underestimate in comparison to radiometric observations owing to the nonsensitivity of photographic films to the near-infrared radiation contained in the solar spectrum. This problem could probably be eliminated by computing site factors for visible and near-infrared radiation from photos made with regular and infrared film.

Madgwick and Brumfield (1960) have considered this approach further and point out that Anderson's method of assessing crown closure is somewhat subjective and therefore susceptible to observer bias. They

test the use of a photodensiometric technique that ensures that the data reduced from photos to be used in the calculation of diffuse and direct beam site factors is reproducible. In comparing diffuse site factors in the same stand for clear and cloudy days, they found little difference. Unfortunately, they have not attempted to validate their predictions by comparison with field measurement of solar radiation.

## A Model of Forest Radiation

The total solar radiation reaching any point on the earth's surface devoid of vegetation or of other obstruction represents the sum of a diffuse component that originates through scattering phenomena in the earth's atmosphere and a direct beam component penetrating the earth's atmosphere as a collimated beam from the sun. Within a forest, radiation is made up of these same two components. However, the ratio of diffuse to direct beam radiation as well as the absolute amounts of radiation reaching a point in a forest are considerably modified by the absorption, transmission, and reflection of the penetrating radiation components by the forest biomass.

As noted in the review of literature, the diffuse radiation reaching any level in a forest stand is quite uniform in space and time. The structure and optical characteristics of forest vegetation is such that gross changes in incident diffuse radiation are smoothed considerably within the stand. Hence I assume that the diffuse radiation at any level within a forest is actually a spatially nonvarying background radiation that can be characterized over a reasonable length of time (one to two hours) as a mean quantity for that level in the forest.

The direct beam radiation penetrating to a given level in the forest however fluctuates widely over a range of flux densities from zero to that incident above the forest. Because of the asymmetry of the frequency distribution of direct beam flux densities, the actual distribution of flux densities is needed rather than the space mean for many purposes. For this reason, I assume that the direct beam radiation reaching any level in a forest is a spatially and temporally varying quantity that can be characterized meaningfully by the space distribution of its flux densities.

Thus the total radiation reaching level z in a horizontally homogeneous forest at time $\tau$ is assumed in this model to be made up of the spatially non-varying (horizontal space) diffuse radiation upon which is superimposed the widely fluctuating direct beam radiation. This can be written as:

$$I_{z,\tau} = d_{z,\tau} + \frac{\int D_{z,\tau}(\xi)\, d\xi}{A_z}$$

where $I_{z,\tau}$ ≡ space mean total radiation flux density at level z at time $\tau$, $d_{z,\tau}$ ≡ diffuse radiation at level z at time $\tau$, $D_{z,\tau}(\xi)$ ≡ space distribution function of direct beam radiant flux densities reaching level z at time $\tau$, $\xi$ ≡ direct beam flux density, and $A_z$ ≡ area of level z. The variation in vertical space and in time is accounted for in this model by considering discrete levels in the forest and discrete time periods.

The background diffuse radiation is actually the sum of diffuse radiative components arising from a number of optical phenomena including the penetration of diffuse sky radiation through canopy openings, radiation transmitted through one or more leaves, and

radiation reflected downward from one or more leaves to the level in question. Although radiation that is down-reflected to a level may originate from above or below that level, the amount of radiation from below that is down-reflected is small because of the multiple reflections involved (Gay and Knoerr, 1970). Hence I assume here that this source of radiation is negligible and write:

$$d_{z,\tau} = p_{z,\tau} + t_{z,\tau} + r_{z,\tau} + T_{z,\tau} + R_{z,\tau}$$

where $d_{z,\tau}$ ≡ diffuse radiation reaching level z at time $\tau$, $p_{z,\tau}$ ≡ diffuse sky radiation penetrating canopy gaps to level z at time $\tau$, $t_{z,\tau}$ ≡ diffuse sky radiation transmitted through one or more leaves to level z at time $\tau$, $r_{z,\tau}$ ≡ diffuse sky radiation reflected from one or more leaves to level z at time $\tau$, $T_{z,\tau}$ ≡ direct beam radiation transmitted through one or more leaves to level z at time $\tau$, and $R_{z,\tau}$ ≡ direct beam radiation reflected from one or more leaves to level z at time $\tau$. Note that I consider transmitted and reflected direct beam radiation to reach level z in the forest as directionally isotropic, i.e., diffuse, radiation. This is done despite Anderson's (1969a) conclusion that these quantities are directionally anisotropic because while not strictly isotropic, the quantities cannot be isolated in the field as anything resembling the collimated beam of direct solar radiation. Owing to the cellular geometry and optical characteristics of leaves, the transmitted direct beam radiation is considerably diffused by its passage through the leaf tissues. Similarly, for all but high angles of incidence, leaves act more as Lambertian reflectors than specular reflectors thereby diffusing the reflected beam radiation as well. Therefore, for purposes of this model, these two quantities will be assumed to be perfectly diffuse.

The portion of the diffuse radiation at level z in a forest at time $\tau$ that is the result of skylight penetrating canopy gaps ($p_{z,\tau}$) is a function of the total amount of sky radiation incident upon the top of the stand, the amount and spatial distribution of canopy gaps, and the distribution of brightness over the hemisphere of sky. That is:

$$p_{z,\tau} = d_{o,\tau} \iint G_z(\phi,\theta)\ B_\tau\ (\phi,\theta)\ d\phi\ d\theta$$

where $d_{o,\tau} \equiv$ diffuse sky radiation incident upon the forest at time $\tau$, $G_z(\phi,\theta) \equiv$ space distribution of canopy gaps in hemisphere of space above level z expressed as a proportion of the total hemisphere, $B_\tau(\phi,\theta) \equiv$ space distribution of sky brightness expressed as a proportion of the total amount of diffuse radiation produced by the hemisphere of sky at time $\tau$, $\phi \equiv$ azimuth angle, and $\theta \equiv$ elevation angle. Since I am considering the radiation regime in a fully developed canopy for purposes of this study, I can assume that $G_z(\phi,\theta)$ is not a function of time. For vegetation with rapidly expanding leaves as in a deciduous forest in the spring or for vegetation in areas having persistent, gusty winds, this assumption would be invalid. The sky brightness distribution is a function of time because for all but completely overcast skies, the sky brightness distribution changes as the sun appears to move across the sky.

Since I assume that transmitted and reflected radiation is perfectly diffused by these two processes, the amount of radiation transmitted or reflected is a function only of the incident radiation, the number of leaves through or from which radiation is transmitted or reflected in reaching level z, and the degree of crown closure in the hemisphere of space above level z which determines the potential

transmission or reflection. Thus:

$$t_{z,\tau} \equiv d_{o,\tau} \iint E^{n_z(\phi,\theta)} \left[1 - G_z(\phi,\theta)\right] d\phi \, d\theta$$

where $t_{z,}$ ≡ diffuse radiation transmitted to level z at time $\tau$, E ≡ average transmissivity of leaves over entire solar spectrum and $n_z(\phi,\theta)$ ≡ space distribution of number of leaves through which radiation is transmitted to reach level z.

Similarly, the diffuse radiation reflected to level z at time $\tau$ may be expressed as:

$$r_{z,\tau} = d_{o,\tau} \iint f_z(\phi,\theta) \, C^{n_z(\phi,\theta)} \left[1 - G_z(\phi,\theta)\right] d\phi \, d\theta$$

where $f_{z,\tau}(\phi,\theta)$ ≡ the space distribution of the proportion of the total radiation reflected that is reflected downward into the stand to level z and C ≡ average reflectivity of leaves over the entire solar spectrum.

For the transmitted and reflected direct beam contributions to the diffuse radiation reaching level z at the time $\tau$:

$$T_{z,\tau} = D_{o,\tau} \iint E^{n_z(\phi,\theta)} \left[1 - G_z(\phi,\theta)\right] d\phi \, d\theta$$

and $$R_{z,\tau} = D_{o,\tau} \iint f_{z,\tau}(\phi,\theta) \, C^{n_z(\phi,\theta)} \left[1 - G_z(\phi,\theta)\right] d\phi \, d\theta$$

where $D_{o,\tau}$ ≡ direct beam radiation incident upon the canopy at time $\tau$.

I have retained the proportional distribution of canopy occlusions in the entire hemisphere of space above the level z because all irradiated leaves above level z and visible from that level will contribute transmitted and reflected radiation to the diffuse radiation received at that level.

The detail included in this model for $d_{z,\tau}$ is somewhat greater than that considered by most past workers. However, owing to recent experimental study of radiation in forests, it appears that this detail is necessary to fully explain the radiation climate of forests. For example, in their study of space and time variations in radiation reaching forest floors, Reifsynder, Furnival, and Horowitz (1971/72) attempted to separate the reflected and transmitted direct beam radiation from the total amount of diffuse radiation observed by computing the ratio of radiation received at the forest floor to that incident upon the stand on completely overcast days. This ratio was then multiplied by the diffuse radiation observed on clear days. The product then, was an estimate of the sum of the penetrating diffuse, transmitted diffuse, and down-reflected diffuse. Subtracting this estimate from the measured values of diffuse radiation on clear days yielded the further estimate of the transmitted plus down-reflected direct beam radiation. In the Connecticut deciduous stand in which they worked, the estimated contribution of transmitted and reflected direct beam to the total diffuse received at the forest floor for the two hour period centered on solar noon was greater than twice the average direct beam radiation penetrating the canopy and reaching the forest floor as sunflecks. Thus, the contribution of transmitted and reflected direct beam seems to be highly significant.

Horn (1971) has shown by simple geometric analysis that the shadow cast by a circular obstruction to the sun's rays such as a leaf extends to a distance 108 times the diameter of the obstruction beyond the obstruction. Utilizing the same geometric considerations, it can be shown that full direct beam flux density will penetrate a circular

hole in an opaque surface to a distance beyond the surface of 108 times the diameter of the hole. Beyond this distance, the penumbra produced at the edge of the hole or gap because of the finite size of the solar disk, overlap and the direct beam radiation is reduced. In essence then, as Miller and Norman (1971b) have developed, a canopy gap acts as a pin-hole camera and the sunfleck produced upon a surface such as the forest floor is simply the pin-hole image of the sun projected onto that surface. Figure 3 illustrates these relationships for the simplest case of the sun at the zenith, directly above the canopy gap. As is evident from this figure, the sunfleck size is a function only of the gap size and the height of the gap above the surface in question.

If equal brightness of all portions of the solar disk is assumed, then the fraction of direct beam radiation incident upon the canopy that is received at any point within the sunfleck is simply the fractional area of the solar disk visible from that point (Miller and Norman, 1971b). Thus the space distribution of direct beam flux densities in a sunfleck is also a function only of gap size and gap height. Summing over all sunflecks and multiplying by the fractional area occupied by sunflecks then yields the space distribution of direct beam flux densities for a given level. That is:

$$D_{z,\tau}(\xi) = D_{o,\tau}\, \psi_{z,\tau}(\nu/\delta,\ h)\, P_{z,\tau}$$

where $D_{z,\tau}(\xi)$ ≡ horizontal space distribution of direct beam flux density ($\xi$) at level z at time $\tau$, $D_{o,\tau}$ ≡ direct beam flux density incident upon the forest at time $\tau$, $\psi_{z,\tau}(\nu/\delta,\ h)$ ≡ size and height distributions of gaps in the canopy above level z corresponding to the

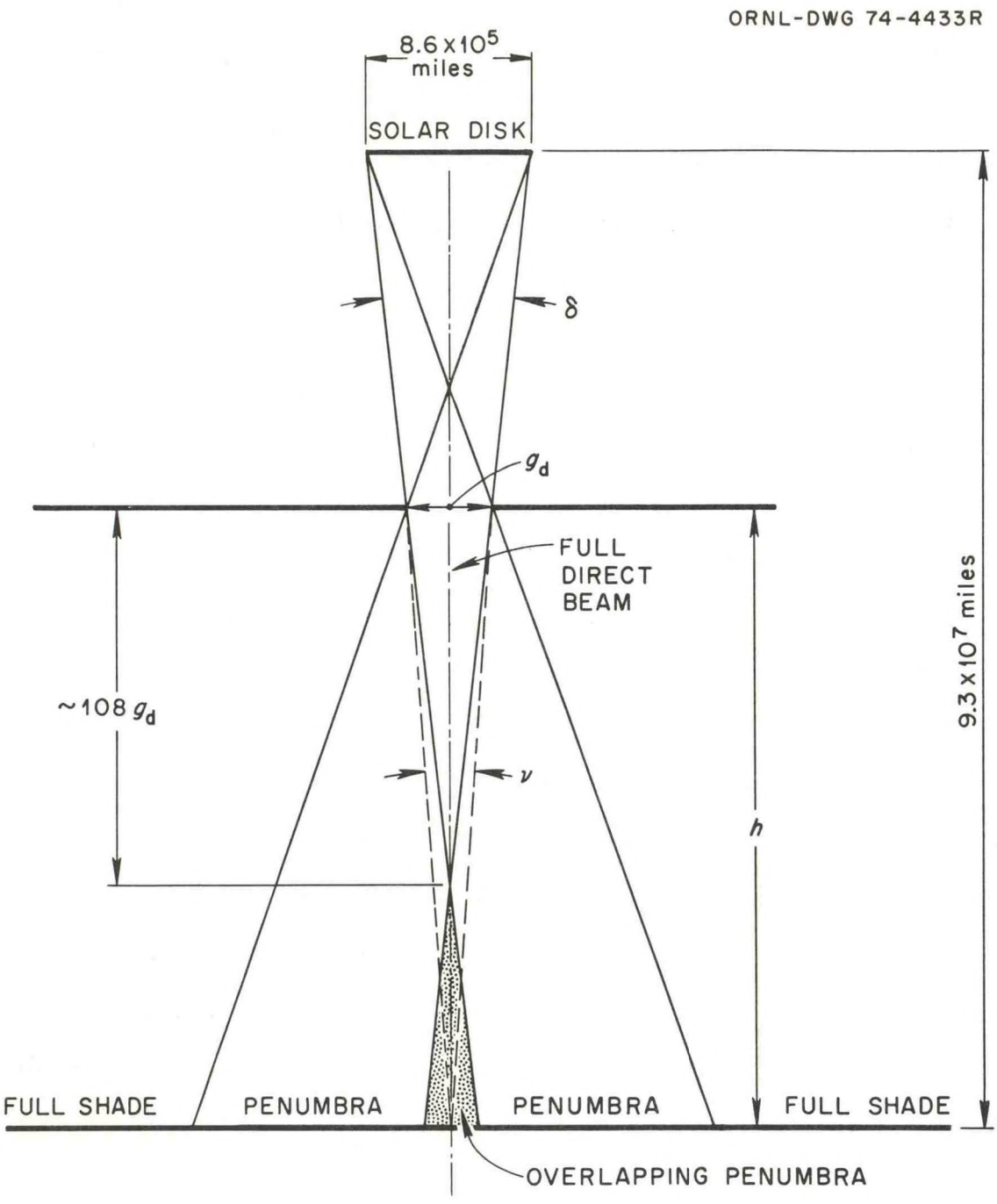


Figure 3: Sunfleck Geometry Where $\delta$ = Solid Angle Subtended by Solar Disk, $\nu$ = Solid Angle Subtended by Canopy Gap, $g_d$ = Gap Diameter (= $2h \tan \nu/2$), and h = Height of Gap Above Surface.

sun's position at time $\tau$, and $P_{z,\tau} \equiv$ fractional area of level z in sunfleck at time $\tau$. The solid angle subtended by the canopy gap, $\nu$, is normalized by the solid angle subtended by the solar disk, $\delta$, since it is the fractional area of the solar disk visible through the gap that determines the direct beam flux density received at any point within a sunfleck. This fractional area is governed by the ratio of the solid angle subtended by the gap to that subtended by the solar disk.

The parameters required to drive this model thus include the incident diffuse and direct beam flux densities above the forest at any time $\tau$ under consideration ($d_{o,\tau}$, $D_{o,\tau}$); the space distribution of canopy gaps above any level z under consideration $[G_z(\phi,\theta)]$; the sky brightness distribution for each time of consideration $[B_\tau(\phi,\theta)]$; the size and height distributions of canopy gaps above each level for each time $[\psi_{z,\tau}(\nu/\delta, h)]$; the space distribution of the number of leaves through which radiation is transmitted or from which radiation is reflected $[n_z(\phi,\theta)]$; and the space distribution of the fraction of the total radiation reflected that is reflected downward to level z, $[f_{z,\tau}(\phi,\theta)]$. Techniques of estimating these parameters from measurements made on hemispherical canopy photographs as well as modifications and simplifications of the model required to allow its use in this study are described in detail in the methods section of this paper.

## Methods

### Measurement of Solar Radiation:

Radiant flux densities above and within the cesium tagged tulip poplar forest at Oak Ridge, Tennessee (this forest is described in

detail by Sollins, Edwards, and Harris, in press) were measured using an array of Lintronic Dome Solarimeters. These sensors are a commercially available modification of a field solarimeter designed by Monteith (1959). The solarimeters are sensitive to radiation in the spectral band from 0.3 to 3 microns, this band width accounting for about 98 percent of the solar energy reaching the earth's surface (Fritz, 1958).

Horizontal space variation in the amount of total radiation received in the forest was assessed through replication of measurements in horizontal space. Vertical variation of this quantity was similarly assessed by replicating the horizontal solarimeter arrays at three levels within the forest. All sensors were randomly situated in horizontal space with 12 replications on the forest floor, 12 at three meters above the floor, and 11 replications at 16 meters elevation. The elevated sensors were mounted on the tops of telescoping television antenna masts, extended to the desired height.

Incoming diffuse radiation was also measured at each of these levels using the same kind of solarimeters as for total but equipped with shadow bands as designed by Horowitz (1969). Following Reifsnyder, Furnival, and Horowitz (1971/72), the measurements of diffuse radiation were replicated twice on the forest floor and at three meters. Only one measurement of diffuse radiation was possible at 16 meters because of instrument limitations.

Incident total radiation and diffuse radiation at the top of the forest canopy were measured using one open and one shaded solarimeter at 32 meters elevation, some one to two meters above the tops of the tallest trees.

All sensors were periodically recalibrated against an Eppley Precision Pyranometer. Owing to the nonlinear response of the Lintronic sensors, nonlinear calibration functions were empirically determined for each sensor which are used to convert the millivolt output of each sensor to flux densities in units of millilangleys per minute (Matt and Hutchison, 1974).

Output signals from the sensors were fed into a Novatronics digital data acquisition system. The signals were scanned at periodic intervals (10 minutes on workdays, 30 minute intervals on weekends because of limited tape capacity), converted to digital form and recorded on punch paper tape. Paper tapes were read and the data are converted to engineering units, edited, summarized, and rewritten on magnetic tapes.

Summarized data written on magnetic tape are filed in the Eastern Deciduous Forest Biome IBP Information Center and are available to interested scientists for further analysis. Raw data, also written on magnetic tape, are available from this author, ATDL, NOAA, P. O. Box E, Oak Ridge, Tennessee 37830.

Site Description:

The forest in which solar radiation distributions are being studied is located on the Atomic Energy Commission's Oak Ridge Reservation. The stand is situated some ten kilometers south of the town of Oak Ridge. The forest is growing within a moist limestone sink and is vegetatively similar to other cove hardwood stands in the Appalachian region. Because of the mesic nature of the site however, the forest is atypical of the predominating oak-hickory forests of this region.

Both the density and the species diversity of this stand is considerably higher than that of the oak-hickory forest of the more xeric hillsides surrounding the sink. The general appearance of this forest is shown in Figures 4 and 5.

The overstory of this forest is nearly pure tulip poplar (Liriodendron tulipifera) although numerous other species are present in very small numbers including red maple (Acer rubrum), shortleaf pine (Pinus echinata), ash (Fraxinus americana), white oak (Quercus alba), red oak (Quercus rubrum), several species of hickories (Carya spp.), black locust (Robinia pseudoacacia), black gum (Nyssa sylvatica), and sourwood (Oxydendron aboreum). This overstory extends from about 16 to 32 meters above the forest floor. A rather indefinite secondary understory canopy is present in this stand at a height of 3 to 12 meters. This understory canopy is primarily composed of redbud (Cercis canadensis), flowering dogwood (Cornus florida), and species of hickories with significant numbers of ash, sourwood, oak, maple, and tulip poplar saplings. Secondary species in the understory include slippery elm (Ulmus rubra), ironwood (Carpinus caroliniana), walnut (Juglans nigra), hawthorn (Crataegus spp.), mulberry (Morus rubra), sassafras (Sassafras albidum), hop hornbeam (Ostrya virginiana), and red cedar (Juniperus virginiana).

The pertinent mensurational data for this stand are summarized in Table 1 along with the Shannon-Weaver diversity indexes for the canopy levels. As shown in this table, the overall basal area of this forest is around 28 $m^2$ $hectare^{-1}$ while the total stem density exceeds 5500 stems $hectare^{-1}$. The total leaf area index for this forest under fully developed canopy conditions has been determined to be 6 $m^2 m^{-2}$

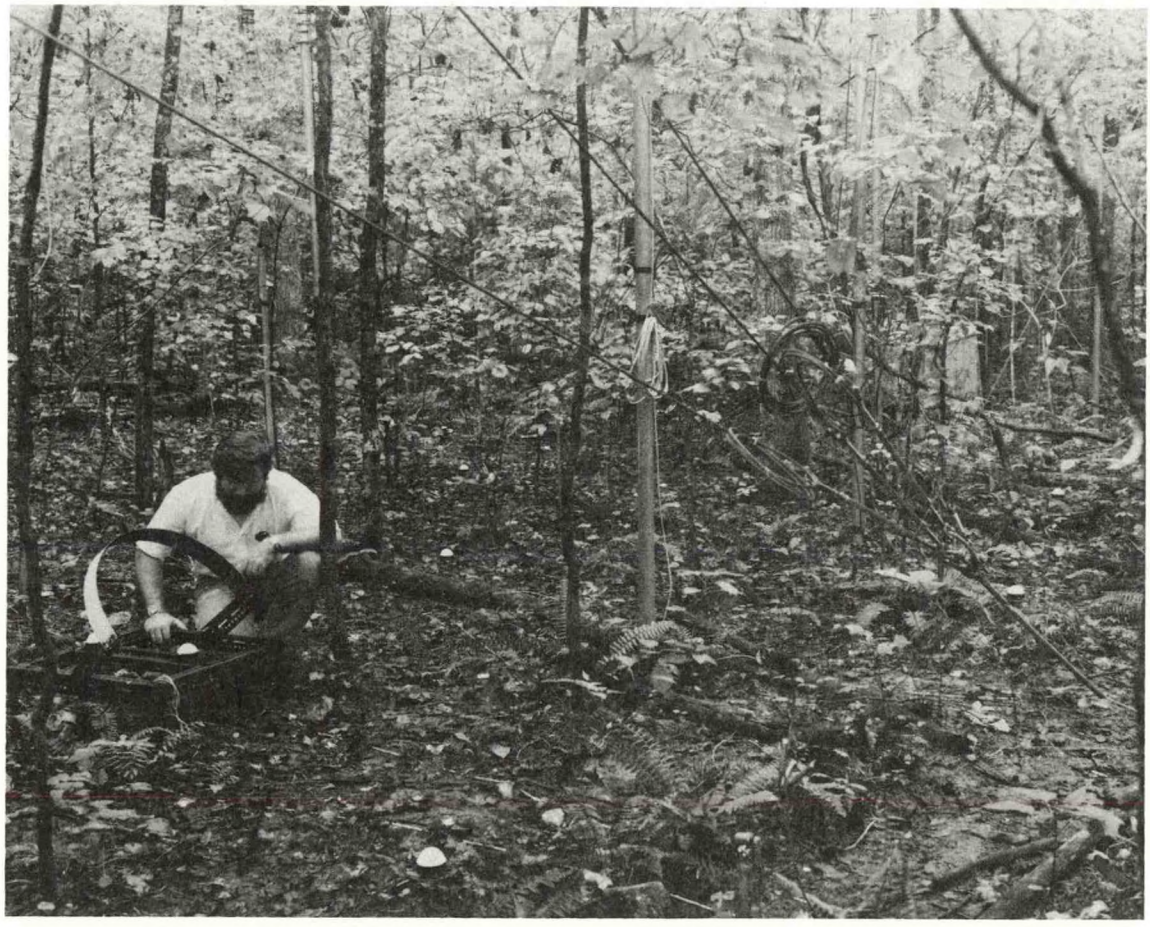

Figure 4: General View of Floor of Liriodendron Forest in Summer Showing Deployment of Sensors on Ground.

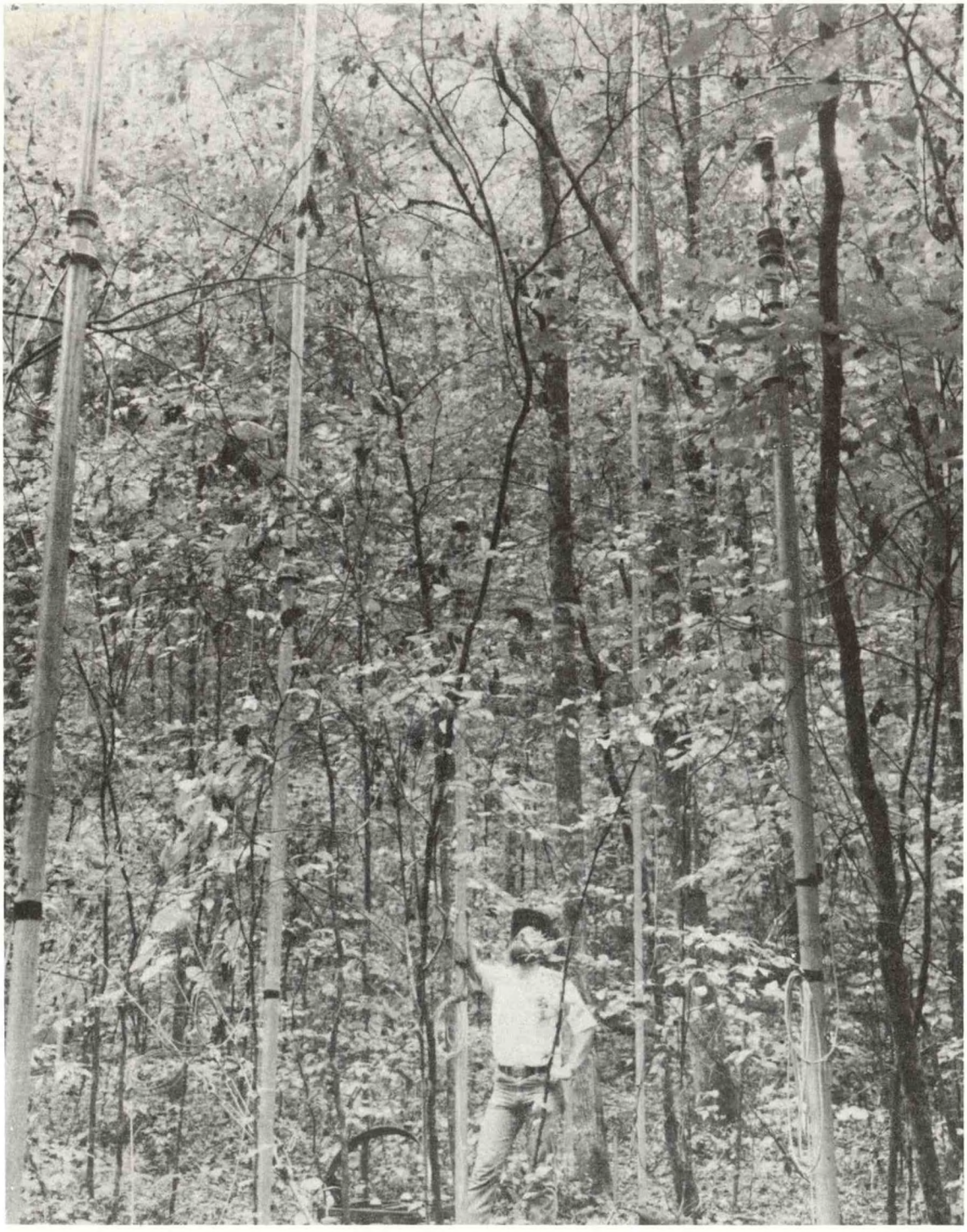

Figure 5: General View of Liriodendron Forest in Summer Showing Telescoping Masts Used to Elevate Solarimeters to 3 and 16 Meter Levels.

Table 1: Mensurational Data and Diversity of the Cesium Tagged Liriodendron Forest at the Oak Ridge Site*

| Canopy Level | Height (meters) | Average DBH (cm) | Basal Area ($m^2$ $hectare^{-1}$) | Density (stems $hectare^{-1}$) | Species Diversity Index |
|---|---|---|---|---|---|
| Upper | 16-30 | 23.8 | 24.0 | 518.1 | 1.11 |
| Mid | 10-15 | 8.6 | 1.7 | 286.9 | 1.42 |
| Forest floor | 1.5-9 | 2.3 | 3.0 | 4766.9 | 1.78 |
| Overall | 1.5-30 | - | 28.7 | 5571.9 | 2.06 |

*From Hutchison and Matt, 1973.

by Dinger, Richardson, and McConathy (1972). The overall Shannon-Weaver species diversity index for the stand is around two. A map of the study area showing locations of all trees and solarimeters is shown in Figure 6.

Photographic Assessment of Forest Structure:

Canopy photography. Canopy photographs were taken using the hemispherical field of view camera designed originally by Hill (1924) and now manufactured commercially by Beck, Ltd. of England. As noted earlier, the lens of this camera produces an image which is an equidistant projection of the objects included in the hemispherical field of view.

Since the forest canopy is not spatially homogeneous, replicate photographs were taken in order to characterize the variation in the space distribution of canopy gap proportion and in the space distribution of canopy gap sizes. To replicate, photos were taken from each point where an open sensor was situated. Thus ten replicate photos were obtained at the 16 meter level, ten from the 3 meter level, and 12 from the forest floor. Figures 7, 8, and 9 show representative canopy photographs from the 16, 3, and 0 meter levels, respectively.

Once the photos were obtained, the negatives were developed and enlarged to a standard size (10.2 cm radius) by a custom photo processing lab. Enlarged prints were made on high contrast paper to minimize the halo effect around canopy gaps that is produced by the lens of the Hill-type camera. (This halo effect was further reduced by obtaining photos only during periods of uniformly overcast sky conditions.)

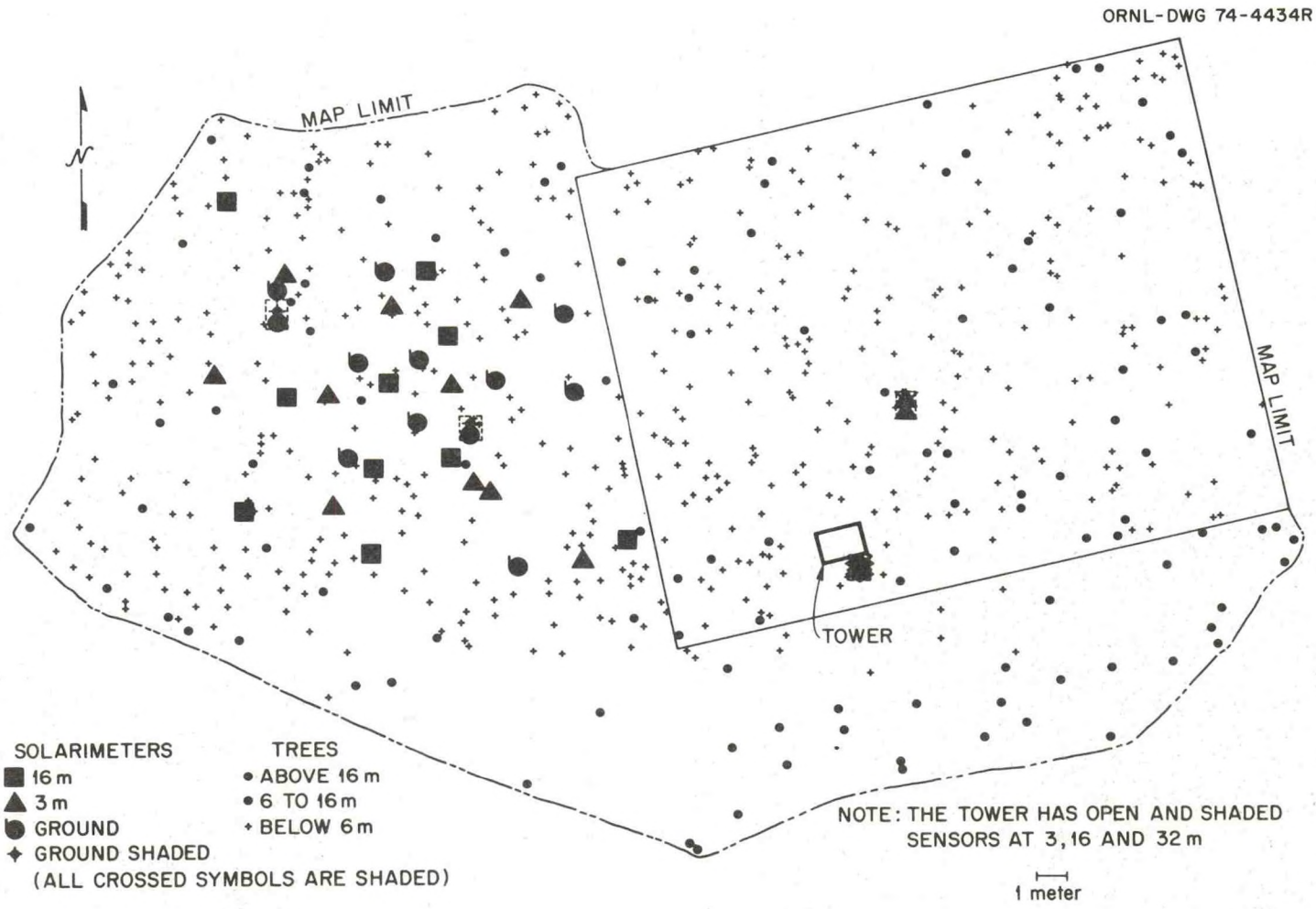


Figure 6: Map of Liriodendron Forest Study Site. (From Hutchison and Matt, 1972)

Figure 7: Hemispherical Canopy Photo Obtained at the 16 Meter Level in the Forest.

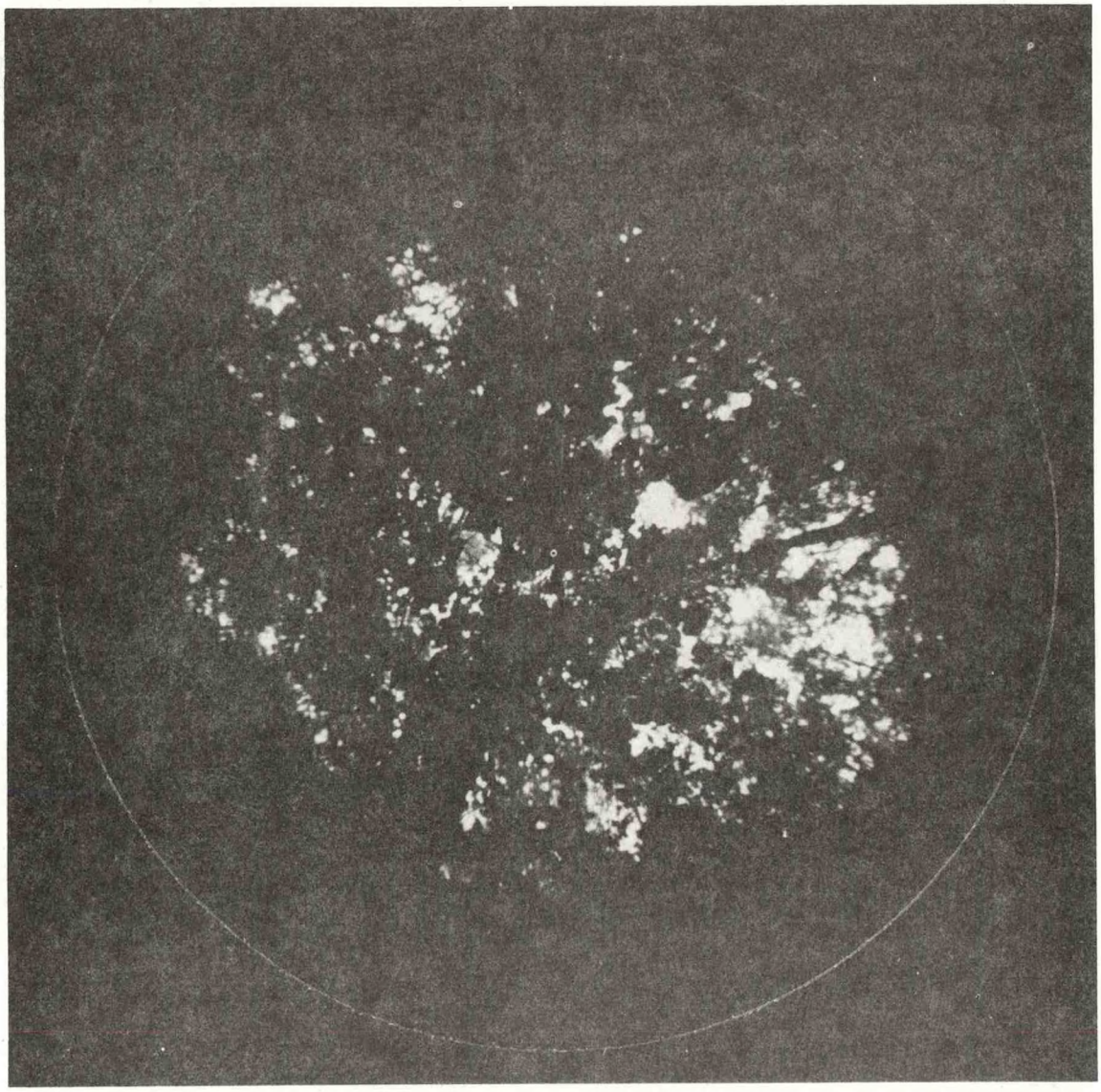

Figure 8: Hemispherical Canopy Photo Obtained at the 3 Meter Level in the Forest.

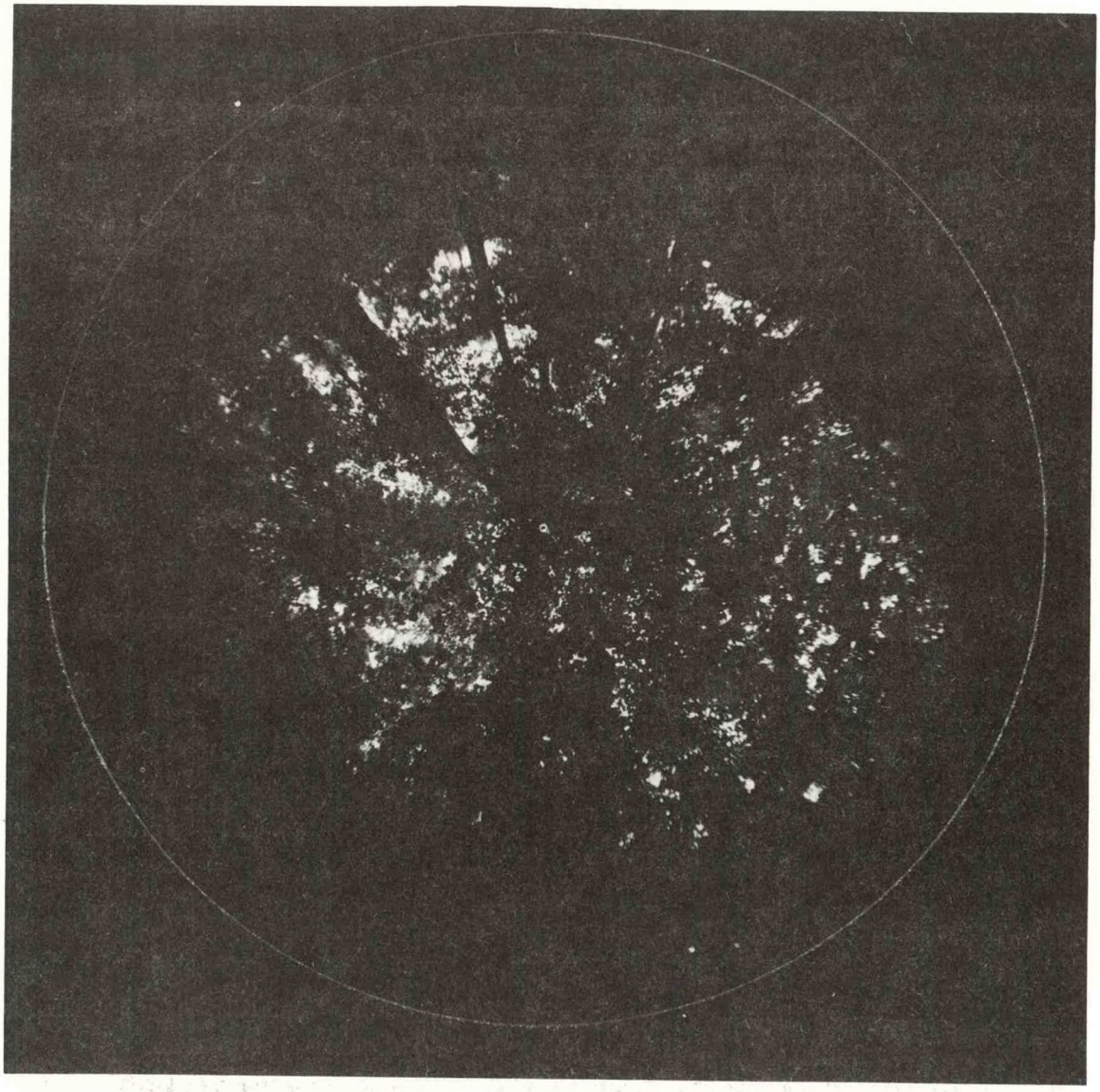

Figure 9: Hemispherical Canopy Photo Obtained from the Forest Floor.

Some difficulty was experienced in obtaining uniform exposure of the photographs, especially those at the 16 meter level since the camera was attached to the top of a telescoping mast and then raised to 16 meter elevation. The shutter was then tripped by a long air shutter release. Because of this, it was impossible to get a true exposure reading for the field of view of the camera at that level. Thus, differences in contrast are apparent on the photo negatives. Again, this effect was minimized during processing by having the photo lab technician produce prints of as uniform contrast as possible through ocular comparison of print density during the developing phase of the processing sequence.

Modifications of forest radiation model for use with photograph data. As noted above I have hypothesized that the radiation reaching any level in a horizontally homogeneous forest at any given time is comprised of a spatially nonvarying diffuse component plus a spatially varying direct beam component. This is written as:

$$I_{z,\tau} = d_{z,\tau} + \frac{\int D_{z,\tau}(\xi)d\xi}{A_z}$$

where $I_{z,\tau} \equiv$ the average total radiation received at level z at time $\tau$, $d_{z,\tau} \equiv$ the background diffuse radiation, $D_{z,\tau}(\xi) \equiv$ the space distribution of direct beam flux densities ($\xi$), and $A_z \equiv$ area of level z. Furthermore:

$$d_{z,\tau} = p_{z,\tau} + t_{z,\tau} + r_{z,\tau} + T_{z,\tau} + R_{z,\tau}$$

where $p_{z,\tau} \equiv$ the contribution to background diffuse radiation at level z at time $\tau$ from diffuse sky radiation which penetrates to level z via canopy openings, $t_{z,\tau}$ and $T_{z,\tau}$ are transmitted components, and $r_{z,\tau}$

and $R_{z,\tau}$ are down-reflected components with lower and upper case letters signifying diffuse and direct beam transmission (or down-reflection), respectively. These components are written:

$$p_{z,\tau} = d_{o,\tau} \iint G_z(\phi,\theta)\ B(\phi,\theta)\ d\phi\ d\theta$$

$$t_{z,\tau} = d_{o,\tau} \iint E^{n_z(\phi,\theta)} \left[1 - G_z(\phi,\theta)\right] d\phi\ d\theta$$

$$r_{z,\tau} = d_{o,\tau} \iint f_z(\phi,\theta)\ C^{n_z(\phi,\theta)} \left[1 - G_z(\phi,\theta)\right] d\phi\ d\theta$$

$$T_{z,\tau} = D_{o,\tau} \iint E^{n_z(\phi,\theta)} \left[1 - G_z(\phi,\theta)\right] d\phi\ d\theta$$

and

$$R_{z,\tau} = D_{o,\tau} \iint f_z(\phi,\theta)\ C^{n_z(\phi,\theta)} \left[1 - G_z(\phi,\theta)\right] d\phi\ d\theta$$

where $d_{o,\tau}$ ≡ the incident diffuse radiation at time $\tau$, $G_z(\phi,\theta)$ ≡ the distribution of degree of canopy opening, $\phi$ ≡ azimuth angle, $\theta$ ≡ elevation angle, E ≡ average transmissivity of leaves over solar spectrum, $n_z(\phi,\theta)$ ≡ distribution of number of leaves through which radiation is transmitted or from which radiation is reflected, $f_z(\phi,\theta)$ ≡ distribution of fraction of reflected radiation that is reflected downward to level z, C ≡ average leaf reflectivity over solar spectrum, $D_{o,\tau}$ ≡ incident direct beam radiation.

The space distribution of direct beam flux densities $D_{z,\tau}(\xi)$ is written as:

$$D_{z,\tau}(\xi) = D_{o,\tau}\psi_{z,\tau}(\nu/\delta,\ h)\ P_{z,\tau}$$

where $\psi_{z,\tau}(\nu/\delta,\ h)$ ≡ the normalized size and height distributions of canopy gaps above level z for the solar position at time $\tau$ and $P_{z,\tau}$ ≡ the fractional area of level z in sunfleck at time $\tau$.

Obviously no real forest is truly homogeneous in horizontal space. Thus the model as outlined here cannot be expected to predict realistic radiation regimes for real-world forests from a point measurement of canopy structure. As noted above, the nonhomogeneity of the tulip poplar forest that I am studying is accounted for through spatial replication of measurements. Similarly, the nonhomogeneity of canopy structure is assessed for predictive purposes through measurements on replicated canopy photographs. The radiation model is then driven by space mean structural parameters rather than point measurements of these parameters.

Furthermore, this model assumes that, for any instant of time, the average total radiation per unit area of a level is the sum of a spatially nonvarying diffuse background radiation and a spatially varying direct beam component that is averaged over space to yield units of energy x area$^{-1}$ x time$^{-1}$. However, both components of this total radiation amount vary with time. Hence, the model is used for discrete time periods in order to characterize the temporal variation in radiation throughout the day. For this purpose, the day is divided into segments, each of about two-hours duration, and the mid-period time taken as an instant of time that is representative of the entire two-hour period. Since the solar path is symmetric about solar noon, the day can also be folded upon solar noon yielding a half-solar-day equivalent to either morning or afternoon. Thus the time periods of interest are sunrise to 0700 hours (which is equivalent to 1700 hours of sunset), 0700 to 0900 hours (≡ 1500 to 1700 hours), 0900 to 1100 hours (≡ 1300 to 1500 hours), and 1100 hours to solar noon (≡ solar noon to 1300 hours) where all times are solar times. The mid-period

times used in all further calculations then are 0600 (≡ 1800), 0800 (≡ 1600), 1000 (≡ 1400) hours, and solar noon.

Because of seasonal changes in earth-sun geometry, there is a further temporal variation in radiation climate on the scale of a year. Since I am primarily interested in the relationship among forest canopy structure, forest radiation climate, and forest primary productivity, I shall consider only the summer forest in full-leaf. The forest in which I am working attains full-leaf on about 1 June in most years while leaf-fall begins about 24 September (personal communication, F. G. Taylor). During the interim, leaf senescence apparently balances the additional flushes of leaves that are produced by the tulip poplar trees throughout the summer because no change in leaf area index is evident during this time period (Dinger, Richardson, and McConathy, 1972). For this reason, I assume that $G_z(\phi,\theta)$, the distribution of canopy opening above a level z, is not a function of time.

The sky brightness distribution of a clear sky is however a function of solar position as will be shown below and solar position is a function of time of day and year. Hence this source of variability must be considered. Since the day-to-day changes in solar paths across the sky are symmetric about the two solstices, since the day-to-day changes in solar paths across the sky are minimal about the solstices, and since I am concerned with the radiation climate of a fully leafed forest, the summer solstice is chosen as the year date of interest for this study. As the solar elevations change only slightly from day to day around this solstice and since the forest is

in full leaf for an extended period before and after the solstice, the radiation conditions in the forest on the summer solstice should be representative of a significant portion of the growing season.

Bonhomme and Chartier (1972) have pointed out that the distribution of biomass in most forest canopies is not a function of solar position and from this fact, they conclude that forest foliage is distributed isotropically with respect to azimuth. This conclusion is supported by unpublished leaf distribution data that I collected from three tulip poplar trees harvested in 1971 from the AEC-Oak Ridge reservation. No significant differences were found among leaf biomass from the four major crown quadrants in either the top, middle, or lower one-third of the crown. Hence I make the further assumption that the leaves in the tulip poplar forest under study are distributed independently of azimuth and the forest radiation model is simplified accordingly:

$$I_{z,\tau} = d_{z,\tau} + \frac{\int D_{z,\tau}(\xi)d\xi}{A_z}$$

where

$$d_{z,\tau} = p_{z,\tau} + t_{z,\tau} + r_{z,\tau} + T_{z,\tau} + R_{z,\tau}$$

and

$$p_{z,\tau} = d_{o,\tau} \int G_z(\theta)\, B_\tau(\theta)d\theta$$

$$t_{z,\tau} = d_{o,\tau} \int E^{n_z(\theta)} \left[1 - G_z(\theta)\right]d\theta$$

$$r_{z,\tau} = d_{o,\tau} \int f_z(\theta)\, C^{n_z(\theta)} \left[1 - G_z(\theta)\right]d\theta$$

$$T_{z,\tau} = D_{o,\tau} \int E^{n_z(\theta)} \left[1 - G_z(\theta)\right]d\theta$$

and

$$R_{z,\tau} = D_{o,\tau} \int f_z(\theta)\ C^{n_z(\theta)}\ [1 - G_z(\theta)]d\theta\ .$$

Finally,

$$D_{z,\tau}(\xi) = D_{z,\tau}\psi_{z,\tau}(\nu/\delta,\ h)P_{z,\tau}\ .$$

The techniques used to assess the integral products, distributions of gap sizes and heights and proportional area in sunfleck for the four specified times on the summer solstice are further described below.

Photographic assessment of the diffuse component of forest radiation regimes. That protion of the diffuse radiation at a level that originates in diffuse skylight that penetrates canopy openings is written as:

$$p_{z,\tau} = d_{o,\tau} \int G_z(\theta)\ B_\tau(\theta)\ d\theta\ .$$

The incident diffuse radiation, $d_{o,\tau}$, is measured above the forest canopy with a solarimeter surrounded by a shadow-band adjusted such that the sensor is shielded from the direct rays of the sun as described in the methods of measurement of solar radiation section. The degree of canopy opening $G_z(\theta)$, can be measured on canopy photos leaving $B_\tau(\theta)$, the sky brightness distribution which must either be measured at the times of interest or specified in some other manner. For my purposes, empirically derived sky brightness distributions reported in the literature are used.

The limiting cases of sky brightness are completely overcast and completely cloud-free skies. Between these extremes, the distributions of sky brightness are exceedingly complex functions of amount of cloud cover, position of clouds relative to position of the sun,

and optical density of the cloud cover. In this study I consider only the limiting cases of completely overcast or clear skies.

For the case of an overcast sky, the equation for the brightness distribution of a "standard overcast sky" as proposed by Moon and Spencer (1942) is used. That is:

$$B_{\tau}(\theta) = 1/3\ B_{\gamma,\tau}(1 + 2\ \sin\theta)$$

where $B_{\tau}(\theta) \equiv$ the distribution of sky brightness in a uniformly overcast sky, $B_{\gamma,\tau} \equiv$ the brightness of the sky at the zenith at time $\tau$, and $\theta \equiv$ elevation angle. The technique used to derive the integral product of the degree of canopy opening and sky brightness, $\int G_z(\theta)\ B_{\tau}(\theta)d\theta$, from canopy photograph measurements is that formulated by Anderson (1964a). Integrating the standard overcast sky brightness equation given above with respect to a horizontal surface yields

$$2/3 \int_{o}^{\theta} (\sin\theta + 2\ \sin^2\theta)\ \cos\ \theta\ d\theta = 1/3\ \sin^2\theta + 4/9\ \sin^3\theta\ .$$

From this expression, the angular widths of annuli of sky contributing equal illuminance to a horizontal surface is determined. Table 2 gives the angular heights of 20 such annuli calculated by Anderson (1964a) along with the radial equivalent of these heights for an equidistant projection.

Plotting these radii to the scale of the photographs used for this study (radius = 10.2 cm) and dividing the 20 annuli radially into 50 segments yields Figure 10. Each segment of this grid then delineates an area of a standard overcast sky that contributes one-thousandth of the total diffuse radiation received by a horizontal

Table 2: Annular Radii for Construction of a Standard Overcast Sky Brightness Diagram*

| Angular Height (degrees) | Percent of Maximum Radius |
|---|---|
| 90.0 | 0.0 |
| 78.1 | 12.3 |
| 73.0 | 18.9 |
| 69.0 | 23.3 |
| 64.9 | 27.9 |
| 62.0 | 31.2 |
| 59.6 | 33.8 |
| 56.8 | 36.9 |
| 54.2 | 39.8 |
| 51.9 | 42.3 |
| 49.2 | 45.3 |
| 46.7 | 48.1 |
| 43.8 | 51.3 |
| 41.8 | 53.6 |
| 37.8 | 58.0 |
| 34.6 | 61.6 |
| 30.8 | 65.8 |
| 26.3 | 70.8 |
| 20.5 | 77.2 |
| 15.0 | 85.3 |
| 0.0 | 100.0 |

*From Anderson, 1964a.

ORNL - DWG 74 - 4436

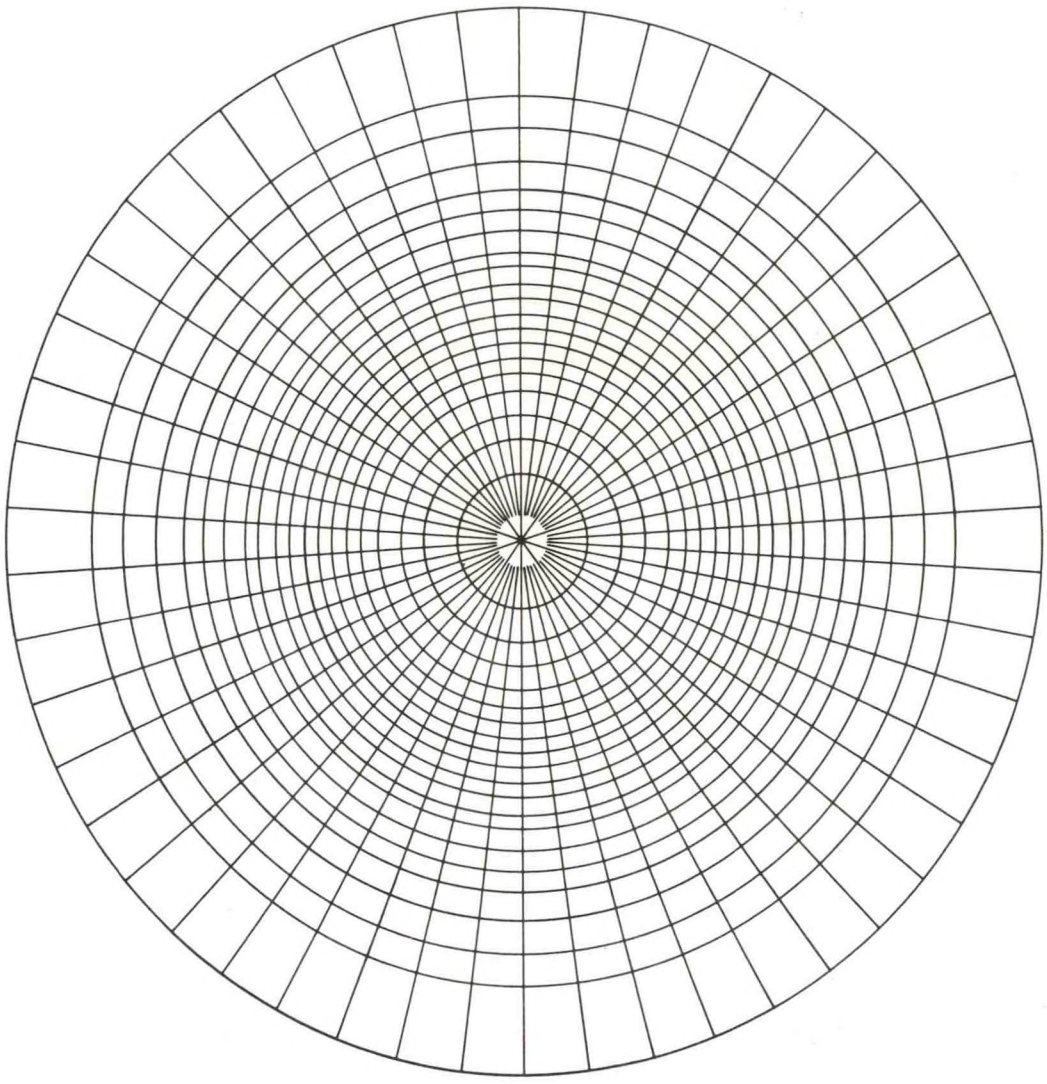

Figure 10. Standard Overcast Sky Brightness Distribution. (From Anderson, 1964a)

surface from the entire hemisphere of sky. (Some radial divisions in the center circle have been deleted in Figure 10 for clarity.)

Superimposing this grid onto a canopy photograph, the degree of opening in each segment is occularly estimated as falling into one of five opening classes, 0, 25, 50, 75, or 100 percent open, and recorded. After all segments are estimated, the number of segments in each class are multiplied by the fractional opening indicated by that class and these products are summed over all classes to obtain an estimate of $\int G_z(\theta)\ B_\tau(\theta)d\theta$ for the point in level z from which the photo was taken. Repeating this procedure for all replicate photos from each level and averaging over that level then yields a space average of $\int G_z(\theta)\ B_\tau(\theta)d\theta$ which is, using Anderson's terminology, the diffuse site factor for that level (under an overcast sky). An estimate of the amount of diffuse radiation penetrating canopy openings to that level is then calculated by multiplying this space average diffuse site factor $\left[\int G_z(\theta)\ B_\tau(\theta)d\theta\right]$ times the incident diffuse radiation upon the canopy ($d_{o,\tau}$) at time $\tau$.

For the case of clear-skies, the brightness distribution proposed by Pokrowski (1929) is used. That is:

$$B_\tau(\phi,\theta) \equiv B(\Delta,\theta) = L\left(1 - e^{-\rho\ \mathrm{cosec}\ \theta}\right)\frac{1 + \cos^2\Delta}{1 - \cos\ \Delta}$$

where $B(\Delta,\theta) \equiv$ the clear sky brightness at an angular elevation $\theta$ above the horizon and at an angular distance $\Delta$ from the sun, $L \equiv$ the sky brightness at the two points on the horizon that are 90 degrees from the sun, and $\rho \equiv$ a scattering coefficient. According to Walsh (1961), the best estimate of $\rho$ is 0.32 and this value is used in the calculation of all clear sky brightness distribution in this study.

As indicated, the brightness distribution of a clear sky is a function of time only by virtue of the changing solar position in the sky over time.

As developed above, the times of interest are 0600, 0800, 1000 hours, and solar noon on the summer solstice and for these times the solar elevations, at the latitude of Oak Ridge, are 15, 37.5, 60, and 73.5 degrees, respectively. Assuming a value of L of one, the sky brightness $B(\Delta,\theta)$ is calculated for five degree intervals of azimuth and angular elevation for each of these four solar elevations. Normalizing this computed brightness distribution by the maximum brightness value encountered in the five-degree grid outside the solar disk itself then yields the brightness distribution over the hemisphere of sky relative to the brightest portion of the sky. This grid is then plotted to the scale of the photographs used in this study and the normalized brightness values encountered at each point of intersection in the grid are noted. Contour lines of equal brightness are drawn in for preselected brightness class intervals which serve to delineate the areas of sky falling into normalized brightness classes. The four resultant sky brightness diagrams are shown in Figures 11, 12, 13, and 14.

Using a polar planimeter, the area of each brightness class on each diagram is determined and expressed as a fraction of the total area of the diagram. This fractional area is denoted as $X_{i,\beta}$ where i is the brightness class and $\beta$ is the solar elevation. Multiplying this fractional area by the relative brightness of the area, $B_{i,\beta}$, yields $X_{i,\beta}\ B_{i,\beta}$, the amount of diffuse radiation incident upon a horizontal surface originating in the area of sky corresponding to the $i^{\underline{th}}$

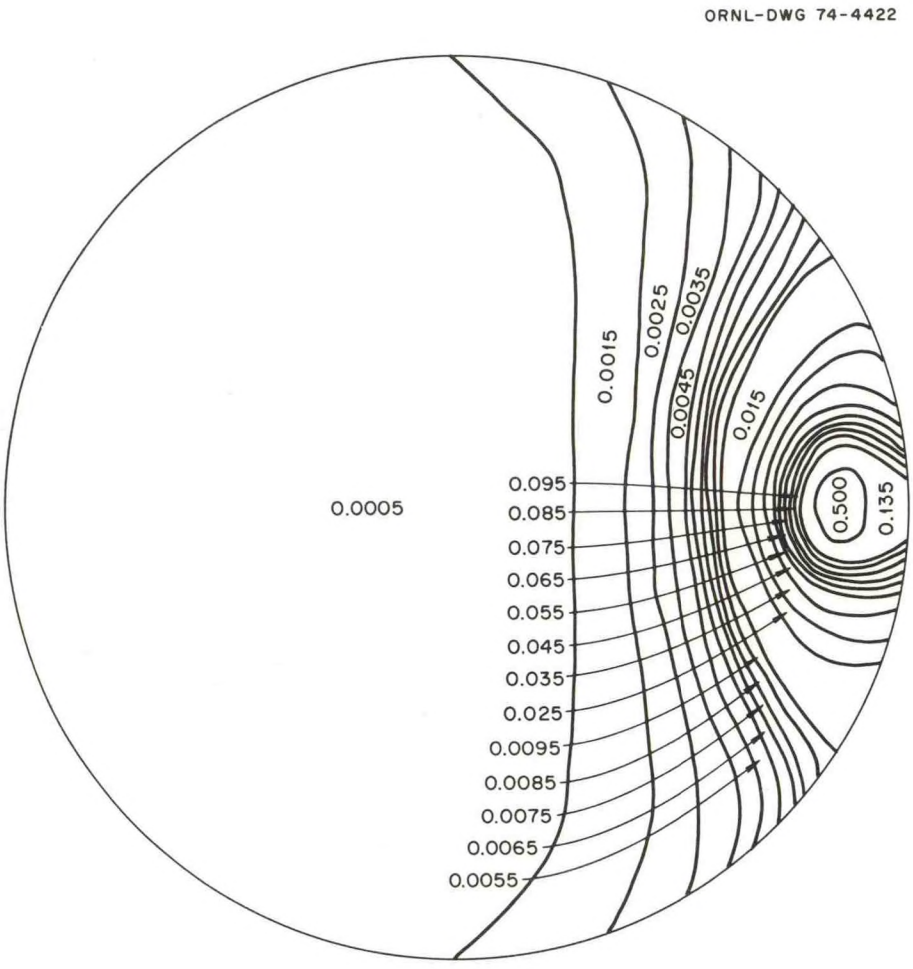


Figure 11: Clear Sky Brightness Distribution for Solar Elevation of 15.0 Degrees According to Pokrowski's (1929) Equation.

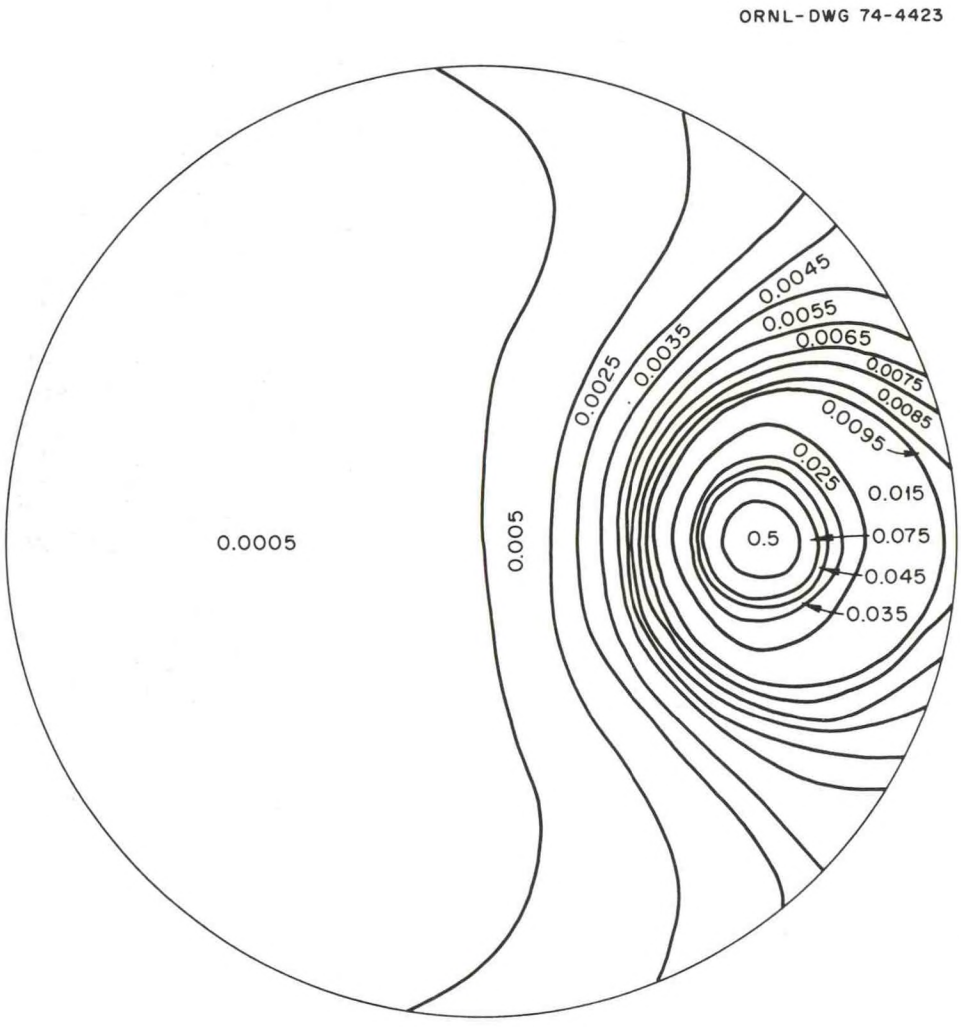


Figure 12: Clear Sky Brightness Distribution for Solar Elevation of 37.5 Degrees According to Pokrowski's (1929) Equation.

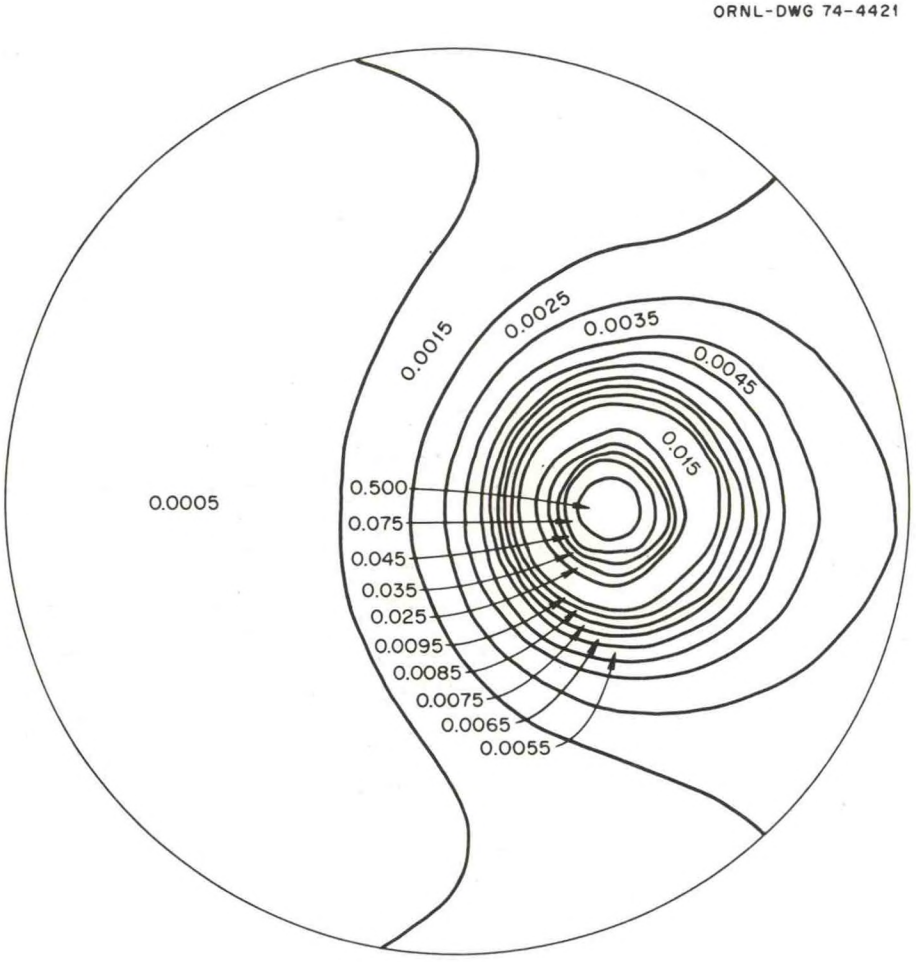


Figure 13: Clear Sky Brightness Distribution for Solar Elevation of 60.0 Degrees According to Pokrowski's (1929) Equation.

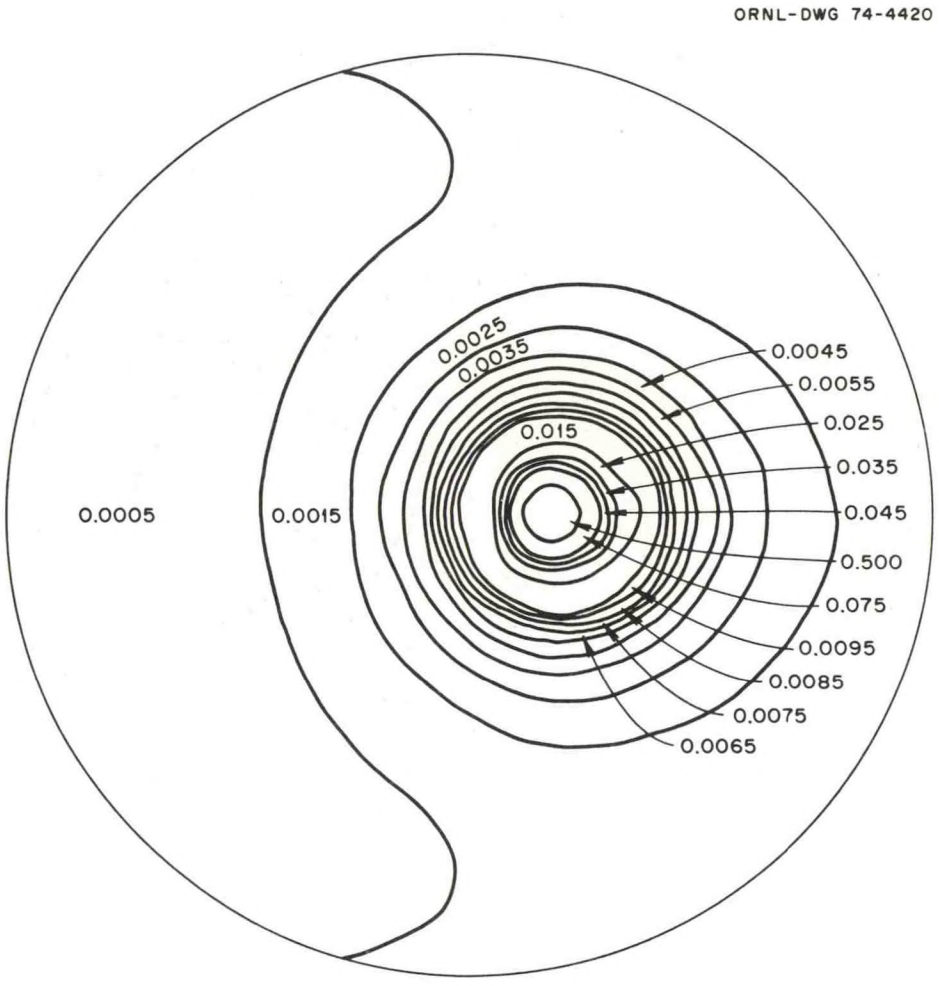


Figure 14: Clear Sky Brightness Distribution for Solar Elevation of 73.5 Degrees from Pokrowski's (1929) Equation.

brightness class expressed as a fraction of that contributed by the brightest class. Since the sum of these products for all brightness classes at a given solar elevation, $\sum_i (X_{i,\beta}\ B_{i,\beta})$, is equivalent to the total amount of diffuse radiation emitted by the hemisphere of sky, the relative contributions of each of the i brightness classes can be normalized by this sum to obtain the fraction of the total illuminance received by a horizontal surface originating from the $i^{\underline{th}}$ brightness class. That is:

$$\frac{X_{i,\beta}\ B_{i,\beta}}{\sum_i (X_{i,\beta}\ B_{i,\beta})} = \text{fractional illuminance of surface from } i^{\underline{th}} \text{ class.}$$

Thus $\sum_i \left[ \frac{X_{i,\beta}\ B_{i,\beta}}{\sum_i (X_{i,\beta}\ B_{i,\beta})} \right] = 1$ .

Since I have assumed azimuthal isotropy of forest structure, the azimuthal distribution of sky brightness can be ignored in the determination of the distribution of canopy closure so long as the results are weighted by the relative areas determined as described above. Hence I rotate the relative brightness classes on each clear sky brightness distribution diagram through 360 degrees yielding a series of concentric annuli. Combining the annuli from all four diagrams for ease of analysis yields Figure 15, the composite clear sky brightness diagram which consists of 55 annuli. Table 3 shows the annuli comprising each brightness class for each of the four solar elevations under consideration. These annuli are divided into radial segments as for the overcast sky case for ease of estimation of the degree of opening in each annulus.

Superimposing a transparent overlay corresponding to Figure 15 over a canopy photo, the fractional amount of opening of each radial

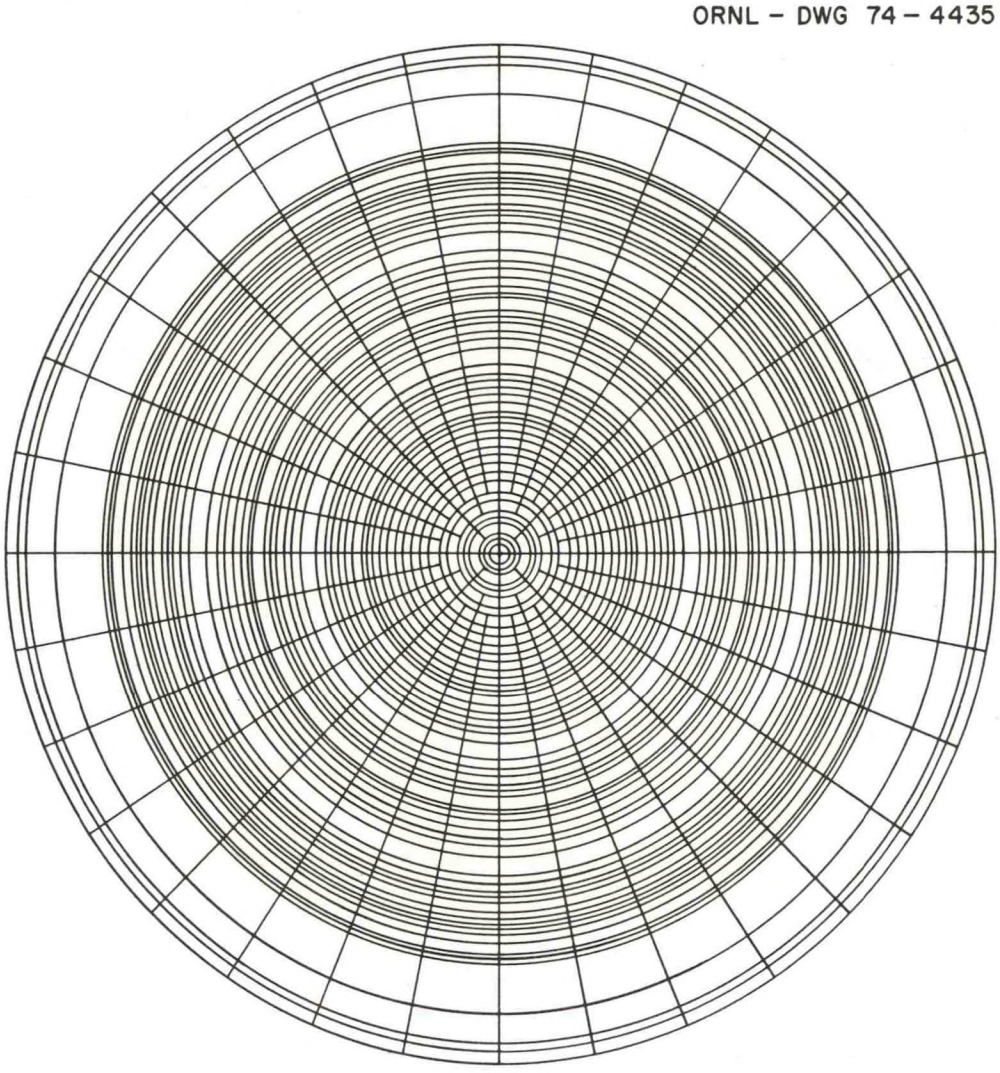


Figure 15: Composite Clear Sky Brightness Distribution.

Table 3: Composite Clear Sky Diagram Annuli Comprising Brightness Classes for Four Solar Elevations

| Brightness Class | Relative Brightness | Solar Elevation | | | |
|---|---|---|---|---|---|
| | | 15.0 | 37.5 | 60.0 | 73.5 |
| 1 | 0.0005 | 1-55 | 1-55 | 1-39 | 1-27 |
| 2 | 0.0015 | 1-39 | 1-54 | 1-48 | 1-39 |
| 3 | 0.0025 | 1-31 | 1-45 | 1-53 | 7-43 |
| 4 | 0.0035 | 1-28 | 1-42 | 3-55 | 17-46 |
| 5 | 0.0045 | 1-26 | 1-39 | 6-54 | 21-48 |
| 6 | 0.0055 | 1-24 | 1-36 | 12-51 | 22-49 |
| 7 | 0.0065 | 1-22 | 1-35 | 14-49 | 27-50 |
| 8 | 0.0075 | 1-21 | 1-34 | 17-48 | 28-51 |
| 9 | 0.0085 | 1-20 | 1-33 | 18-48 | 29-52 |
| 10 | 0.0095 | 1-19 | 1-32 | 19-47 | 30-53 |
| 11 | 0.0150 | 1-18 | 2-31 | 20-46 | 31-55 |
| 12 | 0.0250 | 1-17 | 5-30 | 25-44 | 32-52 |
| 13 | 0.0350 | 1-15 | 8-27 | 26-42 | 36-51 |
| 14 | 0.0450 | 1-13 | 10-26 | 27-41 | 37-50 |
| 15 | 0.0550 | 1-12 | --- | --- | --- |
| 16 | 0.0650 | 1-11 | --- | --- | --- |
| 17 | 0.0750 | 1-10 | 13-25 | 29-39 | 39-49 |
| 18 | 0.0850 | 1-9 | --- | --- | --- |
| 19 | 0.0950 | 1-8 | --- | --- | --- |
| 20 | 0.1350 | 1-7 | --- | --- | --- |
| 21 | 0.5000 | 4-5 | 15-23 | 31-38 | 43-47 |

segment is estimated and tallied as described above for the overcast sky case. Letting $N_{j,k}$ represent the number of segments in opening class j in annulus k and $G_j$ represent the fractional opening indicated by the $j^{\underline{th}}$ class, then

$$\frac{\sum_j N_{j,k} G_j}{N_k} = \text{fractional opening of annulus k.}$$

If $X_{i,k}$ is the area of annulus k expressed as a fraction of the total area of those annuli comprising the $i^{\underline{th}}$ brightness class, then

$$\left(\frac{\sum_j N_{j,k} G_j}{N_k}\right) X_{i,k} = \text{area of openings in annulus k as fraction of}$$

total area of the annuli contained in the $i^{\underline{th}}$ brightness class.

This fractional opening per annulus is then averaged over all photos at a given level to obtain the average degree of opening for each annulus at each level. Since the degree of opening in each annulus is expressed as a fraction of the total area of the $i^{\underline{th}}$ brightness class, these fractional areas are additive and can be summed over the appropriate annuli to obtain estimates of the degree of canopy opening in areas equivalent to the various areas of different sky brightness. That is

$$\sum_{k=\ell}^{m} \left(\frac{\sum_j N_{j,k} G_j}{N_k}\right) X_{i,k} = \text{fractional opening in the m-}\ell\text{ annuli}$$

comprising the $i^{\underline{th}}$ brightness class for solar elevation $\beta$ or

$$\sum_{k=\ell}^{m} \left(\frac{\sum_j N_{j,k} G_j}{N_k}\right) X_{i,k} = F_{i,\beta} .$$

Then the product of this fractional opening of the canopy corresponding to the $i^{\underline{th}}$ brightness class for a given solar elevation and the

fractional illuminance contributed by this $i^{\underline{th}}$ brightness class represents the portion of the diffuse radiation received by an unobscured horizontal surface from brightness class i that penetrates the canopy to the level in question. That is

$$\sum_i \left[ \frac{X_{i,\beta} \; B_{i,\beta}}{\sum_i (X_{i,\beta} \; B_{i,\beta})} \cdot F_{i,\beta} \right] = \int G_z \; (\theta) \; B_z(\theta) \; d \; \theta$$

and $p_{z,t}$ (clear sky case) =

$$\sum_i \left[ \frac{X_{i,\beta} \; B_{i,\beta}}{\sum_i (X_{i,\beta} \; B_{i,\beta})} \cdot F_{i,\beta} \right] \cdot d_{o,\tau} \; .$$

For the transmitted and down-reflected components of the diffuse radiation background at any level, the model as proposed above must be modified since it is impossible to obtain the space distribution of numbers of leaves through which radiation is transmitted or from which radiation is reflected $n_z(\theta)$, or the fraction of reflected radiation that is actually reflected downward to a given level, $f_z(\theta)$ from canopy photograph measurements. The equations for the transmitted and down-reflected radiation were developed previously as:

$$t_{z,\tau} = d_{o,\tau} \int E^{n_z(\theta)} \left[1 - G_z(\theta)\right] d \; \theta$$

$$r_{z,\tau} = d_{o,\tau} \int f_z(\theta) \; C^{n_z(\theta)} \left[1 - G_z(\theta)\right] d \; \theta$$

$$T_{z,\tau} = D_{o,\tau} \int E^{n_z(\theta)} \left[1 - G_z(\theta)\right] d \; \theta$$

and

$$R_{z,\tau} = D_{o,\tau} \int f_z(\theta) \; C^{n_z(\theta)} \left[1 - G_z(\theta)\right] d \; \theta \; .$$

Average values of the transmissivity (diathermancy) and of the reflectivity of tulip poplar leaves over the solar spectrum were not found in

any of the literature cited here. Thus I use the average value of leaf transmissivity (E) of 0.10 as cited by Geiger (1965) and the value 0.25 for the average hardwood leaf reflectivity (C) as derived by D. H. Miller (1955) in the calculation of these quantities.

Although $n_z(\theta)$, the space distribution of numbers of leaves involved in the transmission or reflection of radiation above level z cannot be measured directly from canopy photos, the relative photo density must be an index of this variable since photo density is a function of the amount of radiation received by each point on the photographic plate. Furthermore, the amount of radiation transmitted or reflected is shown to vary exponentially with the number of leaves involved and hence, if $n_z(\theta)$ is greater than three, the amount of radiation contributed to level z is negligible. Thus I consider $n_z(\theta)$ to have four possible values, 0, 1, 2, or 3 or more leaves. As before, I consider five values of $G_z(\theta)$, except that in this instance, it is the degree of crown closure that is needed rather than degree of opening. Thus the classes of $[1 - G_z(\theta)]$ used here are 0, 25, 50, 75, or 100 percent closed. With these two sets of values, I derive the matrices shown in Tables 4 and 5 for the possible products of $E^{n_z(\theta)}$ and $[1 - G_z(\theta)]$ and for $C^{n_z(\theta)}$ and $[1 - G_z(\theta)]$, respectively.

While $n_z$ is postulated to be a function of elevation angle, the amounts of radiation transmitted or down-reflected should not be functions of sky brightness distribution. Thus the integral product of $E^{n_z}$ or $C^{n_z}$ times $(1 - G_z)$ is determined using yet another overlay (see Figure 6) rather than either the standard overcast sky or the clear sky brightness distribution overlays. As shown on Figure 16, the overlay used to estimate $\int E^{n_z(\theta)} [1 - G_z(\theta)] \, d\theta$ and

Table 4: Values of $E^{n_z}[1 - G_z]$ for E = 0.10

| | $(1 - G_z)$ | | | | |
|---|---|---|---|---|---|
| $n_z$ | 0% | 25% | 50% | 75% | 100% |
| 0 | 0 | - | - | - | - |
| 1 | - | 0.02 | 0.05 | 0.08 | 0.10 |
| 2 | - | 0 (<0.01) | 0 (<0.01) | 0.01 | 0.01 |
| 3 | - | 0 (<0.01) | 0 (<0.01) | 0 (<0.01) | 0 (<0.01) |

Table 5: Values of $C^{n_z}(1 - G_z)$ for C = 0.25

| | $(1 - G_z)$ | | | | |
|---|---|---|---|---|---|
| $n_z$ | 0% | 25% | 50% | 75% | 100% |
| 0 | 0 | - | - | - | - |
| 1 | - | 0.06 | 0.12 | 0.19 | 0.25 |
| 2 | - | 0.02 | 0.03 | 0.04 | 0.06 |
| 3 | - | 0 (<0.01) | 0.01 | 0.02 | 0.02 |

ORNL- DWG 74-4430

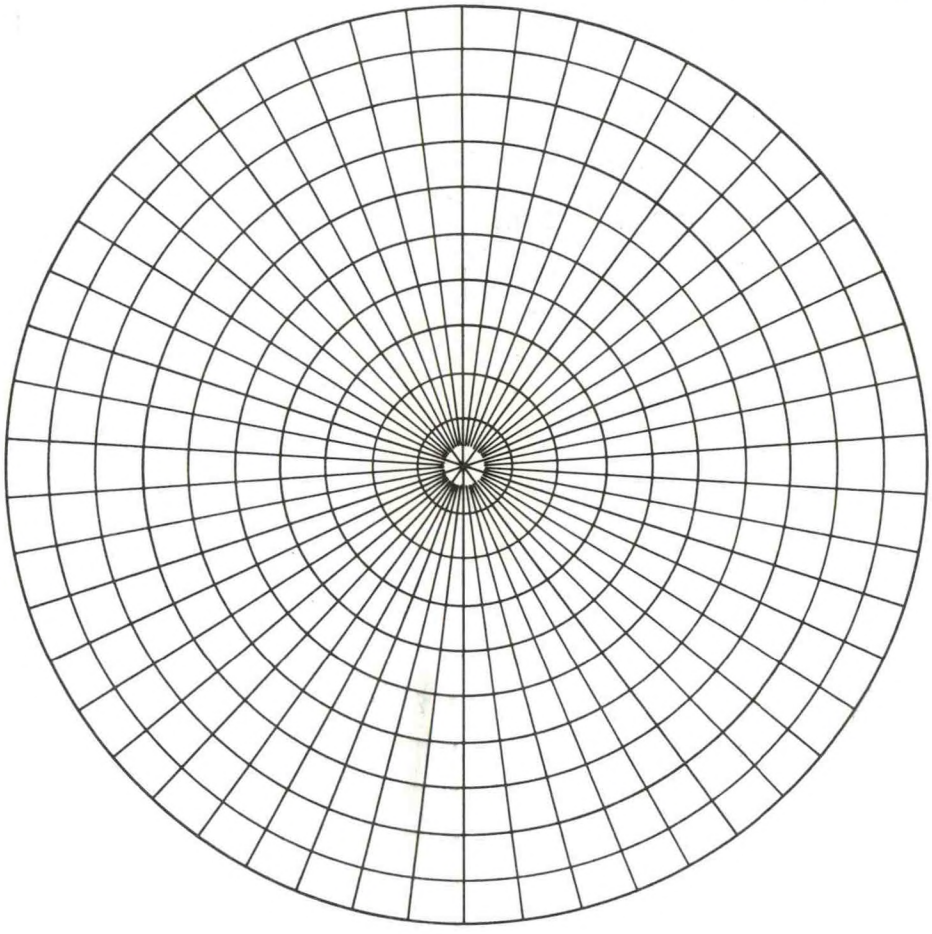

Figure 16: Overlay Grid for Determination of $E^{n_z(\theta)}\left[1 - G_z(\theta)\right]$ or $C^{n_z(\theta)}\left[1 - G_z(\theta)\right]$.

$\int C^{n_z(\theta)} [1 - G_z(\theta)] d\theta$ consists of ten annuli of equal radial width divided radially into 50 segments each. In essence then, the hemisphere of space is simply divided into regular annular segments for the determination of these integral products as functions of angular elevation.

I am unable to derive any technique for the estimation of the function of reflected radiation that is reflected downward, $f_z(\theta)$. In reality, this quantity will vary with angles of leaf inclination and will therefore differ for diffuse and direct beam radiation. The inclination of leaves is not detectable on canopy photographs however and for this reason I consider $f_z(\theta)$ as an adjustable parameter that is assumed constant for all angular elevations and all levels. As a first approximation, I assume that $f = 0.5$. That is, one-half of all radiation reflected in the forest is reflected downward. Since I assume that this parameter is constant, I move it outside the integral yielding the equations:

$$r_{z,\tau} = d_{o,\tau} f \int C^{n_z(\theta)} [1 - G_z(\theta)] d\theta$$

and

$$R_{z,\tau} = D_{o,\tau} f \int C^{n_z(\theta)} [1 - G_z(\theta)] d\theta .$$

This then serves to make the integral products contained in the equations for $t_{z,\tau}$, $T_{z,\tau}$, $r_{z,\tau}$, and $R_{z,\tau}$ of identical form.

Superimposing the overlay corresponding to Figure 16 over a photo, the degree of greyness along with the degree of closure is assessed in each segment of the overlay and the corresponding values of $E^{n_z} (1 - G_z)$ and $C^{n_z} (1 - G_z)$ recorded from Table 4 and Table 5, respectively. The

estimation of $n_z$ from greyness is done simply by setting $n_z$ for white areas equal to zero, for light grey areas, $n_z$ equal to one, for darker areas where individual leaves are still discernible, $n_z$ equals two, and for the darkest areas where no canopy structure is visible, $n_z$ is set equal to three.

As before, the products of $E^{n_z}$ $(1 - G_z)$ are summed over all classes in each annulus to obtain a fractional transmission or reflection quantity for the area of canopy corresponding to that annulus. Averaging these quantities for each annulus over all photos at each level yields the space average fraction of radiation incident upon the forest that is transmitted or reflected by the foliage in each annulus. Summing these space averaged fractions over all annuli then produces estimates of the fractions of incident radiation that is transmitted and reflected by the entire forest canopy, that is, the integral products

$$\int E^{n_z(\theta)} \left[1 - G_z(\theta)\right] d\theta$$

and

$$\int C^{n_z(\theta)} \left[1 - G_z(\theta)\right] d\theta .$$

Photographic assessment of space distribution of direct beam radiation. I have written the space distribution of direct beam flux densities at level z at a time $\tau$ as:

$$D_{z,\tau}(\xi) = D_{o,\tau}\, \psi_{z,\tau}\, (\nu/\delta,\ h) P_{z,\tau}$$

where $D_{o,\tau} \equiv$ the incident direct beam radiation at time $\tau$, $\psi_{z,\tau}(\nu/\delta,\ h) \equiv$ the size and height distribution of canopy gaps where the gap size

(solid angle subtended) is normalized by the size of the solar disk ($\delta$), h $\equiv$ gap height above level z, and $P_{z,\tau} \equiv$ the fractional area of level z in sunfleck at time $\tau$.

Photo overlays are constructed with annuli corresponding to the elevation of the sun at the four preselected times of interest plus and minus the elevation angle equivalent to about 20 minutes of time. Using an Elograph Coordinate Sensor interfaced with a Wang Programmable Desk Calculator, the diameters of all canopy gaps falling within these four annuli on all photos at all levels are calculated and recorded. The Elograph Coordinate Sensor measures the x and y coordinates of any point. That is, using appropriate memories of the Wang calculator, the coordinates of diametrically opposite points of a canopy gap are read and stored and gap diameter ($O_d$) calculated according to the equation

$$O_d = \sqrt{(x_2 - x_1)^2 + (y_2 - y_1)^2} \quad .$$

Irregular gaps are broken down into component circles and diameters for these circles recorded. In general, small gaps seem to be roughly circular but become increasingly irregular, especially at the edges, with increasing size. I consider large gaps as large circles with portions of smaller circular gaps comprising their edges. Because of this, the full direct beam sunfleck area produced by such gaps will be somewhat overestimated and the sunfleck penumbral area somewhat underestimated by this measurement technique. Once all gap sizes within the desired annuli are recorded, the gap size distribution for each level is derived using a 0.02 cm class interval.

Along with the size distribution of gaps above each level, the

distribution of gap heights is needed to derive the space distribution of direct beam flux densities. Such height distributions are not determinable from canopy photographs. Hence an approximation must be used. It can be shown that the degree of canopy closure above any point is a function of the total area of biomass above that point and the inclination of that biomass. As a first approximation I assume that leaves are the only components of total biomass significantly affecting crown closure and that the inclination of these leaves is constant in horizontal and vertical space. Therefore, crown closure is considered a function only of leaf biomass and the vertical distribution of crown closure serves as an index of the vertical distribution of leaf biomass. Since canopy gaps are formed by spaces between leaves, it seems likely that the vertical distribution of canopy opening will closely parallel this vertical distribution of leaf biomass and of its index, crown closure.

The vertical distribution of crown closure is determined from canopy photographs by estimating the degree of closure in an area centered on the zenith of each photo at each level. Areas about the zenith are selected so as to minimize errors arising because of increasing visual path lengths from a level to the tree-tops as elevation angles depart from vertical. Considering the top of the forest to be 33 meters above the forest floor, a circular area subtending 45 degrees of arc centered at 16 meters is calculated. Then the equivalent arc angles for this area as seen from 3 and 0 meters are computed and then three areas are drawn on overlays to the scale of the canopy photos. Superimposing the appropriate overlay over photos from the three levels, the degree of canopy opening in these

zenith areas is estimated and averaged over all photos from a given level yielding an average zenith crown closure for each of the levels.

For an opening to exist above a level requires a corresponding opening above all higher levels in the forest. Thus the average opening visible from a level when expressed as a fraction of the average opening above the next higher level represents the degree of openness of the forest stratum between those two levels and by subtracting this fractional opening per stratum from one, I obtain an estimate of the degree of crown closure in each of the forest canopy strata of interest. Assuming a linear distribution of crown closure within strata, these derived crown closures are plotted according to mid-stratum heights and the plot is then used as an index to gap height distribution (see Figure 17). That is, the percent canopy closure in all strata above any level is summed and the percent closure of each stratum above that level is then expressed as a percent of the sum of all closures. This fraction then represents the fraction of gaps occurring at the corresponding stratum midpoint and by subtracting the height of the level in question from the height of the strata midpoints, the fractional distribution of canopy gaps with height above each level is derived.

This approximation is applied across the entire gap size distribution for any level. Thus, the assumption that gap size is not a function of height is implicit in the technique.

Combining these size and height distributions, matrices are produced showing the fraction of the total number of gaps observed in each size-height category from each level. Using the mid-diameter of each 0.02 cm gap diameter class and the gap heights indicated in the

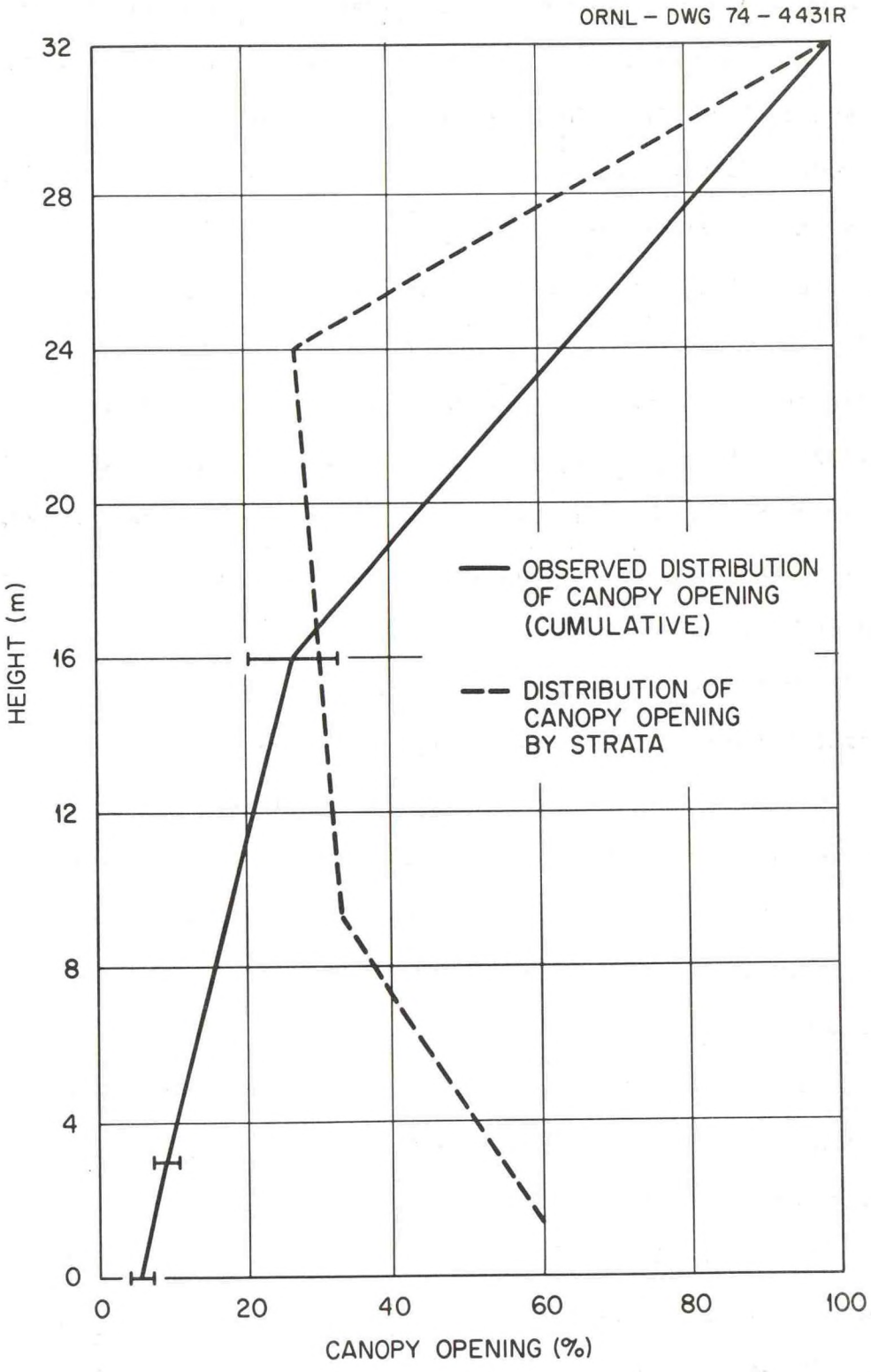


Figure 17: Vertical Distribution of Canopy Opening.

matrices, various dimensions of the sunflecks produced as direct beam radiation penetrates these midclass gap diameters at the various heights can be calculated. Figures 18 and 19 show the geometric relationships involved for the cases where $\nu \geq \delta$ and $\nu < \delta$, respectively, with the sun at an angular elevation $\beta$.

Since I have assumed in drawing these figures that the plane of any gap is normal to the rays of the sun, the gap edges are at different heights. Thus the sunflecks produced by those tilted circular gaps are ellipses. From Figures 18 and 19, the lengths of the major and minor axes of and elliptical sunfleck are given by:

$S_d \equiv$ sunfleck major axis $= h(1-\tan \nu/2 \cot \beta) [\tan (90-\beta + \nu/2) - \tan (90-\beta-\delta/2)] + h(1 + \tan \nu/2 \cot \beta) [\tan (90-\beta + \delta/2) - \tan (90-\beta-\nu/2)]$

and $s_d \equiv$ sunfleck minor axis $= 2h(\tan \nu/2 + \tan \delta/2)$. Similarly, the major and minor axes of the central portion of the sunfleck are given by:

$C_d \equiv$ center major axis $= h(1-\tan \nu/2 \cot \beta) [\tan (90-\beta + \nu/2) - \tan (90-\beta-\delta/2)] + h(1 + \tan \nu/2 \cot \beta) [\tan (90-\beta + \delta/2) - \tan (90-\beta-\nu/2)]$

and $c_d \equiv$ center minor axis $= 2h(\tan \nu/2 - \tan \delta/2)$ where $h \equiv$ gap height, $\nu \equiv$ solid angle subtended by the canopy opening, and $\delta \equiv$ solid angle subtended by the solar disk ($0^o$ 32' of arc). By this formulation, $C_d$ and $c_d$ may be either positive or negative depending upon whether or not the gap solid angle exceeds that subtended by the solar disk. If $C_d$ (and $c_d$) is positive, the sunfleck center receives full incident direct beam radiation. If $C_d$ is negative, the central area is covered by overlapping penumbra and the intensity of direct beam radiation

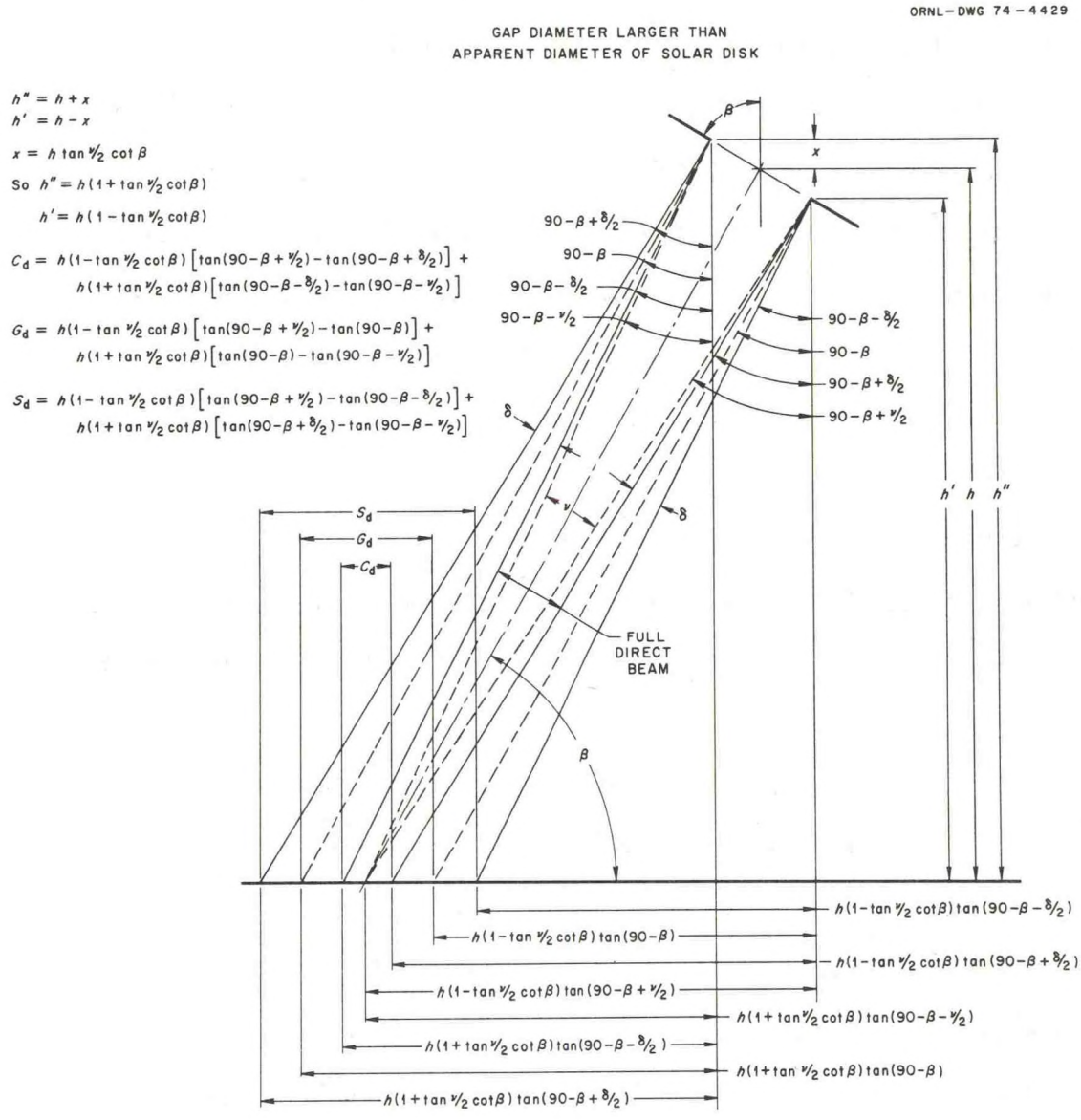


Figure 18: Sunfleck Geometry Where the Apparent Gap Diameter Exceeds the Apparent Diameter of the Solar Disk.

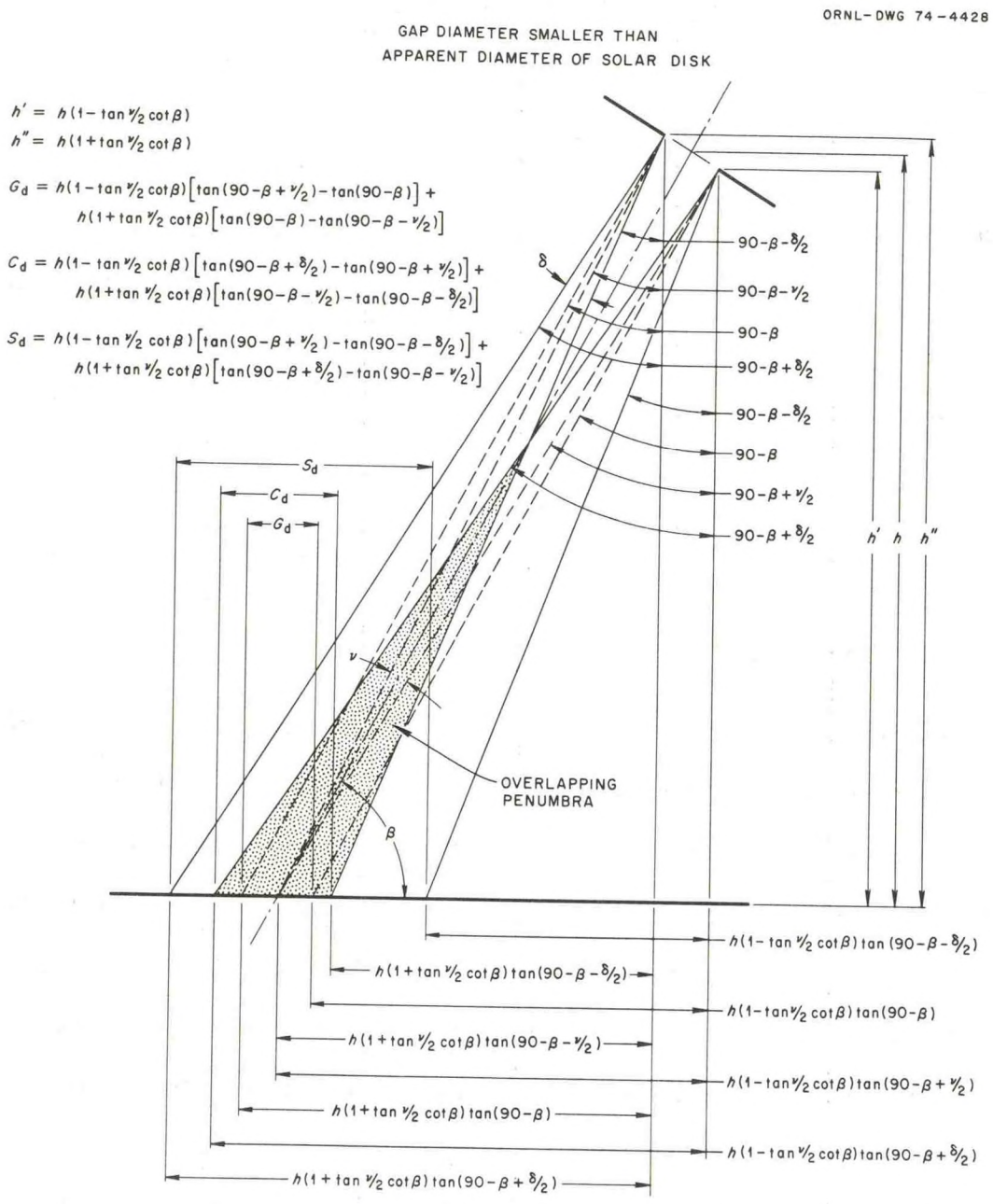


Figure 19: Sunfleck Geometry Where the Apparent Gap Diameter Is Less Than That of the Solar Disk.

received is equal to the fraction of the area of the solar disk that is visible through the gap. That is,

$$D_{s,\tau} = \frac{\pi\ (h \tan \nu/2)^2}{\pi\ (h \tan \delta/2)^2} \cdot D_{o,\tau}$$

which simplifies to:

$$D_{s,\tau} = D_{o,\tau} \frac{\tan^2 \nu/2}{\tan^2 \delta/2}$$

where $D_{s,\tau} \equiv$ direct beam flux density received per unit area of penumbral overlap in sunfleck s at time $\tau$. Since both $\nu/2$ and $\delta/2$ are small:

$$\tan \nu/2 = \nu/2$$

and

$$\tan \delta/2 = \delta/2 \ .$$

Therefore:

$$D_{s,\tau} = D_{o,\tau}\ \nu^2/\delta^2 \ .$$

In the equations derived for sunfleck major axis, $S_d$, and central area major axis, $C_d$, the quantity $(1 \pm \tan \nu/2 \cot \beta)$ is a factor which corrects h for the distance that the gap edges are above or below the height of the gap center. In actuality, for the largest gap encountered (20 degrees arc), for $\beta$, = $15^o$ where cot $\beta$ is maximum, and for the largest h (24 meters), this correction amounts to less than $\pm$ 5 percent and could therefore be deleted from the equations for actual calculations if desired.

Although the direct beam flux densities in the central area of the sunfleck as well as the area of this central portion can easily be computed, the calculation of the distribution of direct beam flux densities across the penumbra surrounding this central area is a bit more complex. This is because we must calculate the fraction of the

total area of the solar disk contained in the segment of the solar disk visible from any point in this penumbral area. For this calculation, Miller and Norman (1971b) have derived the expression

$$T_{pen}(U) = 1 + (U\sqrt{1-U^2} - \cos^{-1} U)/\pi$$

where $T_{pen}(U)$ = fractional area of the segment of solar disk visible when the fraction of the sun's angular radius visible is U. Plotting this expression over U yields Figure 20. As is evident on Figure 20, this expression deviates only slightly from a straight line. Thus, I approximate this expression for purposes of this study with the linear expression:

$$T_{pen}(U) = U$$

and so:

$$D_{z,\tau,r} = D_{o,\tau} \cdot U_r$$

where $D_{z,\tau,r} \equiv$ the direct beam flux density at a point r units from the sunfleck center and $U_r$ is the fraction of the sun's angular radius visible from that point. This expression is plotted in Figure 21. It can be further shown that

$$U_r = w_r/w_t$$

where $w_r/w_t \equiv$ the fractional width of penumbra with $w_r \equiv$ the distance from the inside edge of the penumbra to point r and $w_t \equiv$ the total penumbra width. Thus the direct beam intensity at any point in the penumbra is simply the fractional penumbral width times the incident direct beam radiant flux density.

Using this approximation then, the direct beam flux density distribution across any sunfleck can be computed. Figures 22 and 23 show

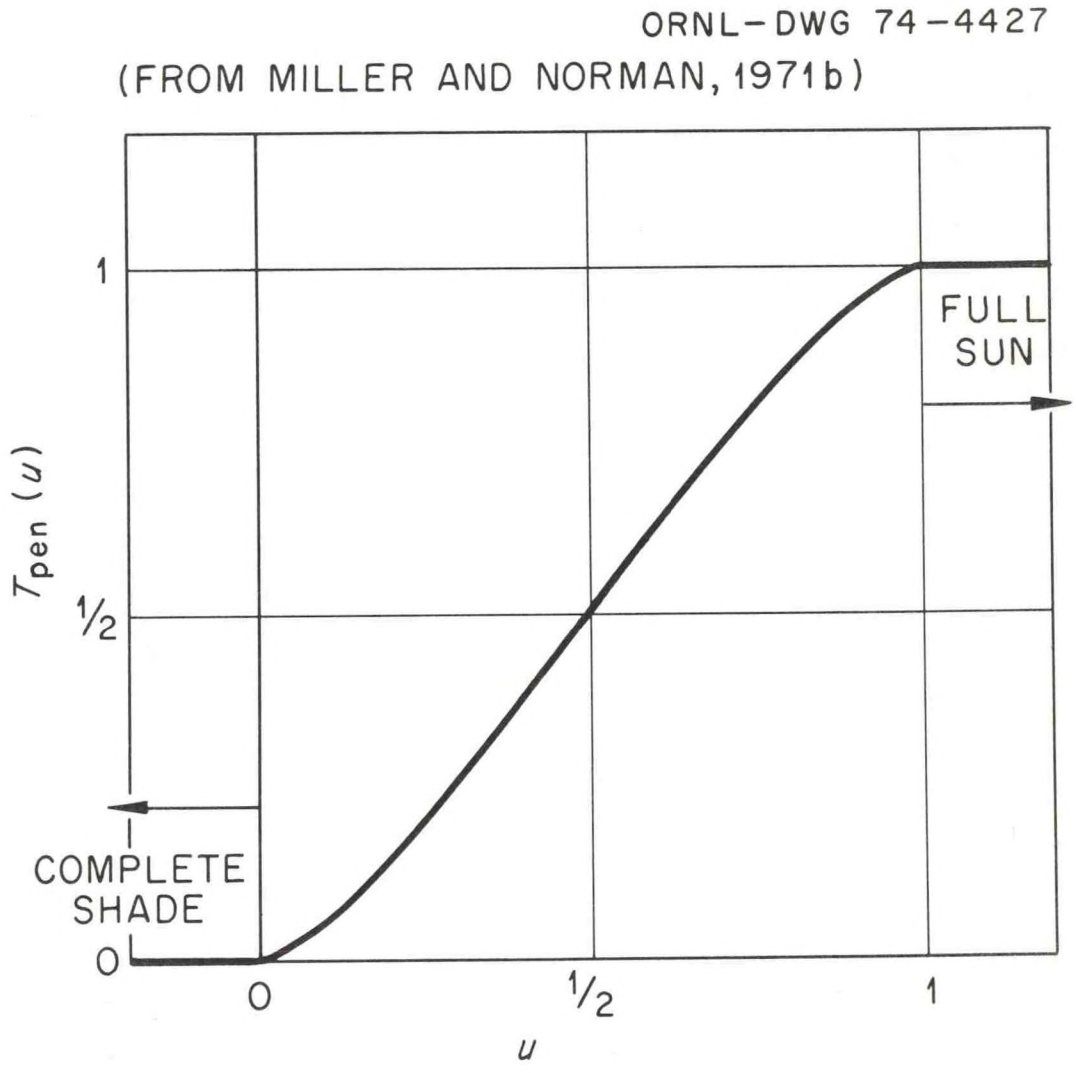


Figure 20: Distribution of Direct Beam Flux Density in Penumbra.

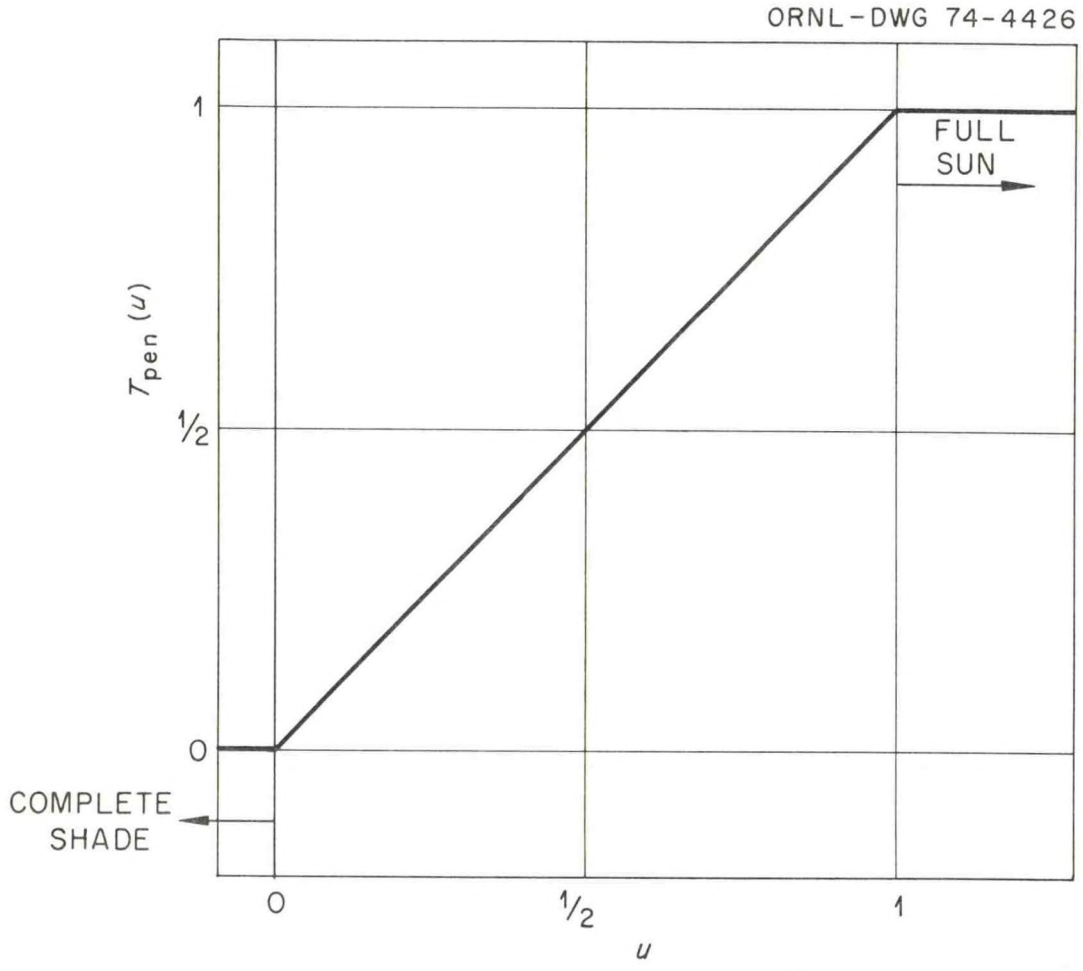


Figure 21: Linear Approximation of Distribution of Direct Beam Flux Density in Penumbra.

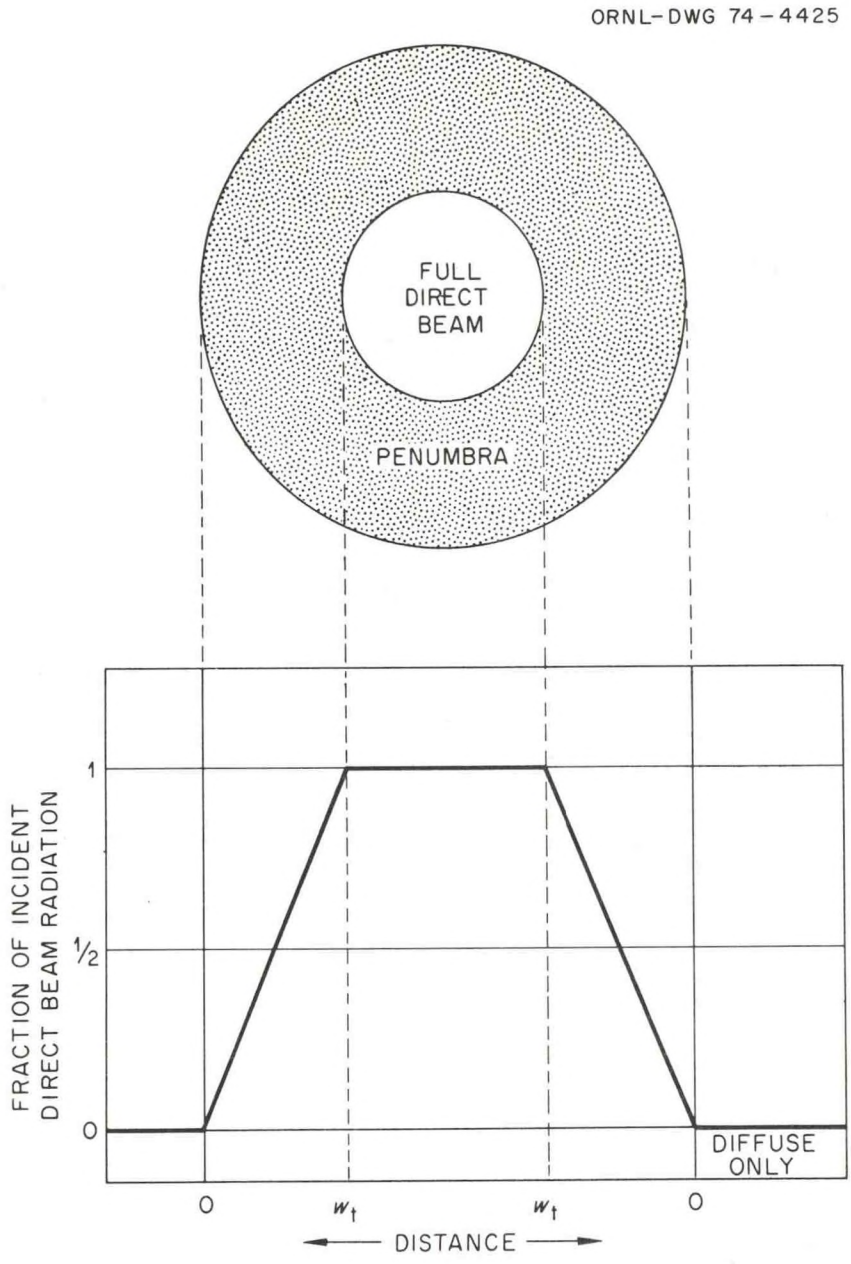


Figure 22: Distribution of Direct Beam Flux Density Across Sunfleck Where Apparent Gap Diameter Exceeds Apparent Diameter of Solar Disk.

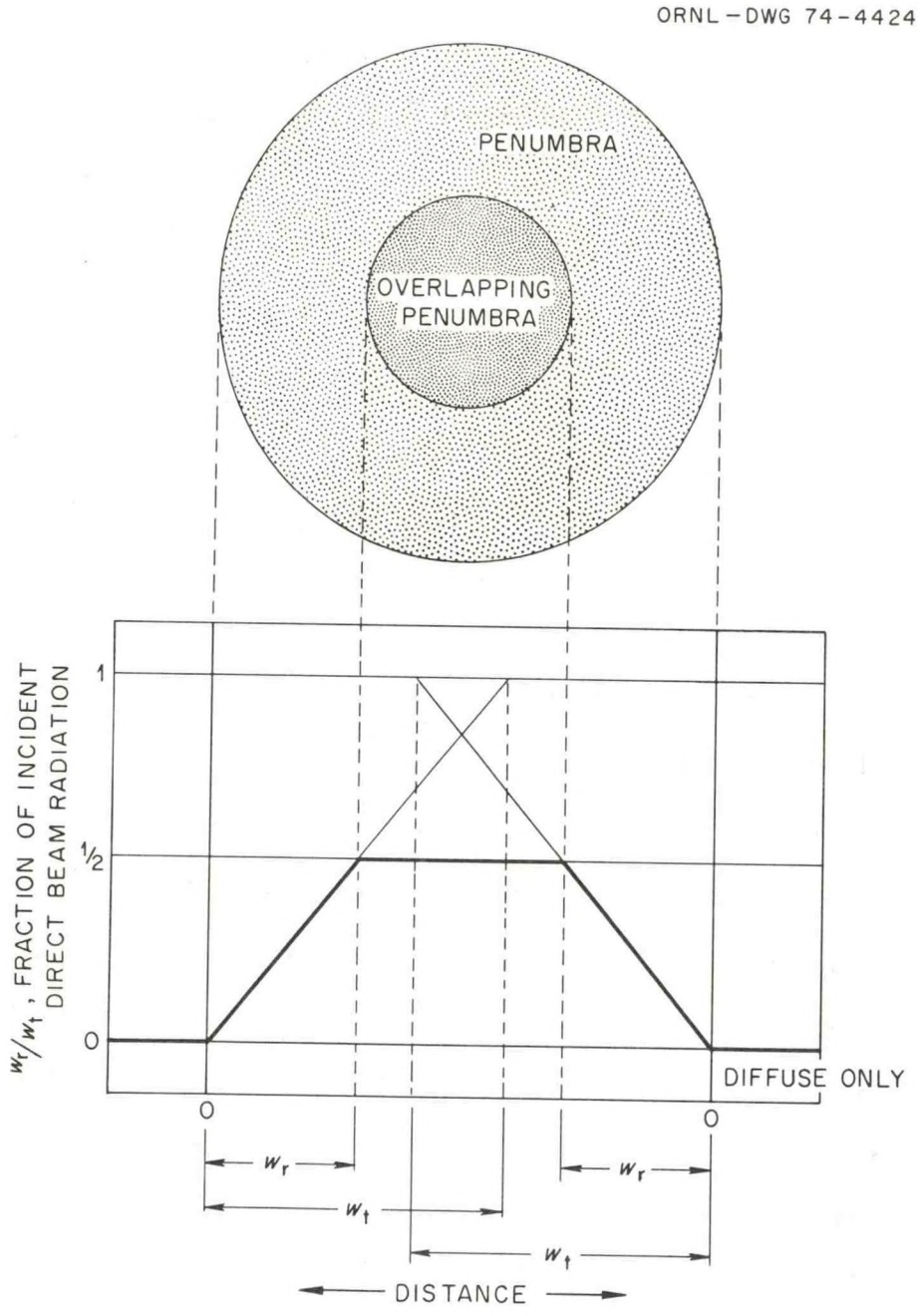


Figure 23: Distribution of Direct Beam Flux Density Across Sunfleck Where Apparent Gap Diameter Is Less Than Apparent Diameter of Solar Disk.

the space distribution of direct beam radiation across sunflecks where $\nu > \delta$ and $\nu < \delta$, respectively. To obtain the actual space distribution of direct beam flux densities for any level at any time then, the annular areas contained in flux density classes of multiples of 0.1 $D_{o,\tau}$ are calculated for the midclass gap major axis of each 0.02 cm gap major axis class for each height and the areas in each 0.1 $D_{o,\tau}$ class summed over all gaps present above a level. This yields the space distribution of direct beam flux densities within the sunflecks present at that level.

To convert this space distribution to an expression for the entire area rather than just area in sunfleck, I multiply the distribution obtained by the fractional area of a level in sunfleck at any given time.

If the sun were a point source of radiation, the fraction of area at any level in sunfleck at any time would simply be the average degree of canopy opening between each point at a level and the sun. Since the sun is not a point source however, each sunfleck is surrounded by penumbra. Terming the edge of a sunfleck produced by a point source sun, the geometric sunfleck edge, one-half of the penumbra in the finite-sized-sun sunfleck lies outside this geometric edge and one-half inside this edge. From Figures 18 and 19, the geometric sunfleck major axis is given by:

$$G_d = h\,(1 - \tan \nu/2 \cot \beta)\,[\tan (90 - \beta + \nu/2) - \tan (90 - \beta)] + h\,(1 + \tan \nu/2 \cot \beta)\,[\tan (90 - \beta) - \tan (90 - \beta - \nu/2)] .$$

The minor axis of the geometric sunfleck is:

$$g_d = 2h \tan \nu/2 .$$

The area of penumbra outside the geometric edges of all sunflecks at any level is then:

$$A_p = \sum_s \pi \left[S_{d,s}\, s_{d,s} - G_{d,s}\, g_{d,s}\right]$$

where $A_p \equiv$ total penumbral area outside the geometric sunfleck edges, $S_{d,s}$ and $s_{d,s} \equiv$ the major and minor axes of sunfleck s, respectively, and $G_{d,s}$ and $g_{d,s} \equiv$ the geometric major and minor axes of sunfleck s, respectively.

If $P_{z,\tau} \equiv$ the fraction of area at level z in sunfleck at time $\tau$, $G_{z,\tau} \equiv$ the fractional canopy opening between level z and the sun, $A_{\sigma,z,\tau} \equiv$ the total sunfleck area produced by gaps of the midclass sizes times the total number of gaps in each corresponding class above level z at time $\tau$, and $A_{g,z,\tau} \equiv$ the total geometric sunfleck areas as produced by a point source sun by these same gaps above level z at time $\tau$, the proportionality

$$P_{z,\tau}/G_{z,\tau} = A_{\sigma,z,\tau}/A_{g,z,\tau}$$

holds. From this:

$$P_{z,\tau} = (A_{\sigma,z,\tau}/A_{g,z,\tau})\, G_{z,\tau}$$

and thus, the fractional area in sunfleck at level z at time $\tau$ is corrected for the penumbral area outside the geometric sunfleck area. Hence, the space distribution of direct beam flux density at level z at time $\tau$ is given by:

$$D_{z,\tau}(\xi) = D_{o,\tau}\psi\,(\nu/\delta,\ h)\, P_{z,\tau}\ .$$

Diffuse Component:

Table 6 shows the diffuse site factors for standard overcast sky conditions derived as described above.

Table 6: Standard Overcast Sky Diffuse Site Factors (Percent)

| Elevation | Diffuse Site Factor |
|---|---|
| 0 m | 5.8 |
| 3 m | 6.4 |
| 16 m | 19.2 |

For clear sky conditions, the corresponding diffuse site factors are given in Table 7.

Table 7: Clear Sky Diffuse Site Factors (Percent) by Two-Hour Periods in the Solar Half-Day

| | Period | | | | |
|---|---|---|---|---|---|
| Elevation | 1 | 2 | 3 | 4 | Daily Mean |
| 0 m | 0.7 | 5.1 | 6.8 | 6.9 | 4.6 |
| 3 m | 0.5 | 5.0 | 7.1 | 8.5 | 4.8 |
| 16 m | 1.6 | 9.1 | 18.3 | 25.3 | 11.9 |
| | Sunrise-0700<br>1700 - Sunset | 0700-0900<br>1500-1700 | 0900-1100<br>1300-1500 | 1100-1300 | |
| | Hours Included | | | | |

As is evident from these two tables, differences between diffuse site factors at 0 and 3 meter elevations are slight. Indeed, for the clear sky case during periods 1 and 2, higher diffuse site factors are predicted for 0 meters than for the 3 meter level (Table 7). This is clearly impossible and appears to be the effect of two sources of error.

Despite the precautions taken to minimize the halos which form around the images of canopy openings, examination of the canopy photographs used in these analyses indicate that halos are present on many photographs. The halos seem to be most pronounced around the smaller openings and apparently disappear with larger gap sizes. Since the halos make gap images larger than they really are and since higher proportions of smaller gaps are encountered at lower levels in the forest, the result of these halos is an overestimation of the degree of canopy opening which increases with depth in the forest.

Another source of error lies in the exposure differences between photographs. As noted above, I tried to obtain prints of uniform density through use of standard exposure in the field and through ocular comparison of print densities during developing. Nevertheless, the 3 meter photos turned out generally more underexposed than the 0 meter photos. Because of this, the halo effect is less pronounced on the 3 meter photos. Hence the diffuse site factors of Tables 6 and 7 for the 0 and 3 meter levels are high relative to the 16 meter site factors by virtue of the overestimation of canopy opening resulting from halos around gap images. The 3 meter site factor is, furthermore, low relative to that at 0 meters because of the consistently more underexposed photos obtained at the 3 meter level.

Other errors that may be present include sampling error and observer bias. Because the photos from each level were replicated at least ten times in horizontal space, the errors arising from the method of sampling should be minimal. The technique of photo analysis used to derive diffuse site factors has been shown by Madgwick and Brumfield (1969) to be somewhat subjective and hence represents another source of error. However all photo measurements used in this study were made by myself and the same technique was used on photos from all levels. Because of the replicated random sampling and the use of consistent analytical technique, there seems to be no obvious reason to expect that either sampling error or observer bias are significantly involved in the lack of significant differences between the 0 and 3 meter diffuse site factors.

Madgwick and Brumfield (1969) have also concluded that little difference exists between diffuse site factors for the forest floor calculated using the standard overcast sky brightness distribution of Moon and Spencer (1942) and the clear sky brightness distribution of Pokrowski (1929). As shown in Tables 6 and 7, the differences in diffuse site factors at 0 meters between clear and overcast skies are small and on the order of 10 percent. However, at 16 meters, the difference is much greater and amounts to some 30 percent. Thus the differences become more pronounced with increasing height in the forest and the overcast sky approximation should become an increasingly poor predictor of the penetration of diffuse radiation from clear skies at higher levels in the forest.

Another limitation of the standard overcast sky approach is evident from examination of period mean penetration rates observed in

the forest on a clear and a cloudy day in June of 1972 (Figures 24 and 25). As shown on these figures, the curve of mean penetration rates over time at the 16 meter level are distinctly curvilinear on both clear and cloudy days. Since the standard overcast sky approach yields a diffuse site factor that is constant over time of day, it seems unlikely that this approach can predict radiation climates of forest canopies even on overcast days.

Table 8 shows the estimates of the transmission and down-reflection factors, i.e.,

$$\int_{E}^{n_z(\theta)} \left[1 - G_z(\theta)\right] d\theta \text{ and } f \int_{C}^{n_z(\theta)} \left[1 - G_z(\theta)\right] d\theta ,$$

calculated according to the technique described in the methods section of this paper.

Table 8: Transmission and Down-Reflection Factors (Percent)

| Elevation | Transmission | Down-Reflection | Total |
|---|---|---|---|
| 0 m | 0.2 | 1.2 | 1.4 |
| 3 m | 0.2 | 1.2 | 1.4 |
| 16 m | 0.3 | 1.3 | 1.6 |

As with the diffuse site factors, differences between the 0 and 3 meter levels are negligible. Even at 16 meters there is only a very slight increase over the values computed for the two lower levels. Again, limitations of the photographic approach appear to be involved along with limitations of the basic model.

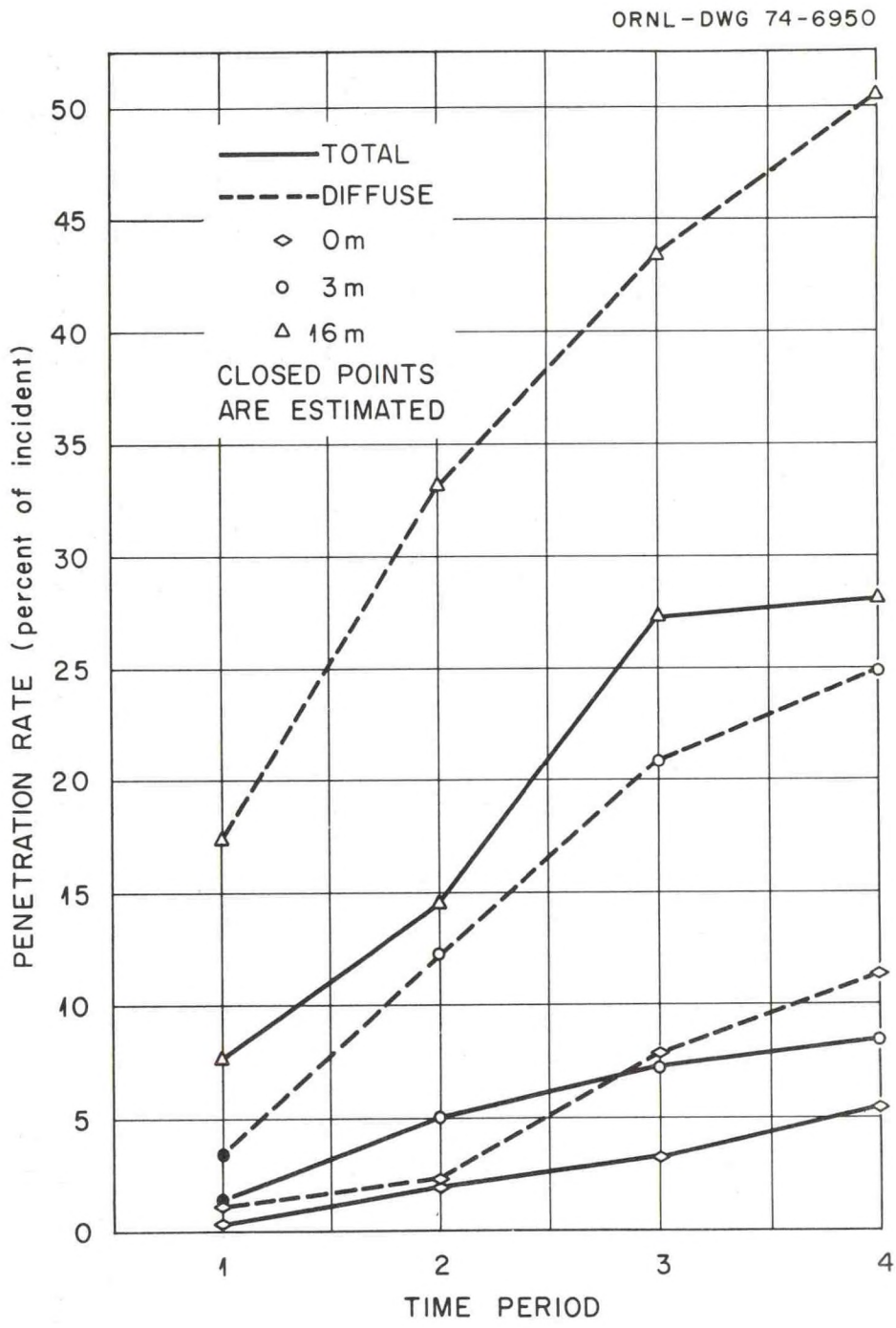


Figure 24: Clear Day Penetration Rates (June 8, 1972).

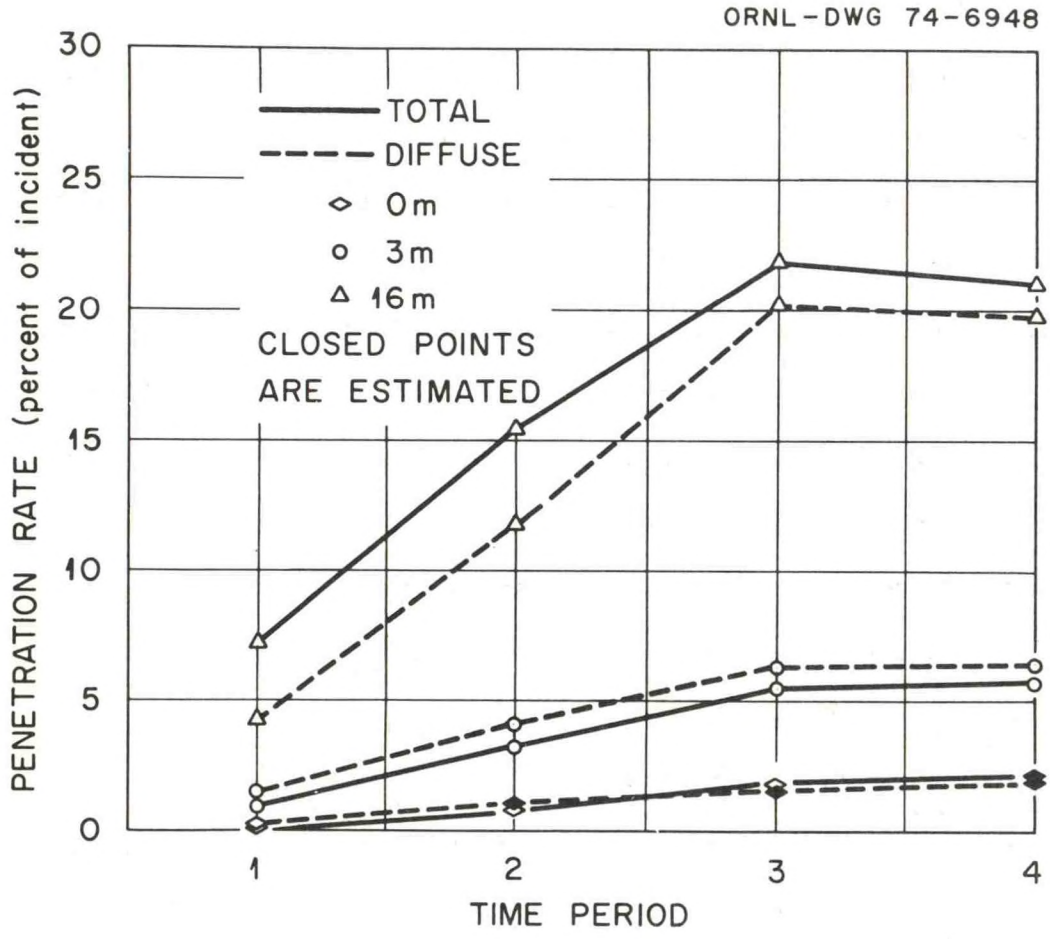


Figure 25: Overcast Day Penetration Rates (June 16, 1972).

Because of the degree of contrast between foliage and overcast sky, I found it impossible to obtain canopy photographs containing sufficient canopy detail to estimate with any confidence the number of leaves through which or from which radiation is transmitted or reflected without serious halo effects. On the other hand, photos having no discernible halo effect are so underexposed that no canopy detail is visible. Hence the single set of photos used for this study does not produce realistic results according to the model proposed. A future test of this approach should be made to determine whether more realistic results could be obtained using two sets of photographs, one set sufficiently and uniformly underexposed to eliminate halos and the other exposed for maximum canopy detail. In this way, the problem arising from the limited contrast latitude of photographic films and papers might be circumvented.

For purposes of validation of these assessment techniques, two clear, one partly-cloudy, and three overcast days in June of 1972 were selected for which radiation data were collected above and within the tulip poplar forest. The time plots of incident total and diffuse radiation for each of these six days are shown on Figures 26 through 31. Although the record for June 8 and 26 is incomplete, the folding of the day upon solar noon and the construction of a composite day consisting of four periods allows comparison of predicted values with observed. Data from complete periods only were used in the calculation of period means. The period means of total and diffuse radiation above and within the forest are plotted over periods in Figures 32 through 37 for these same six days.

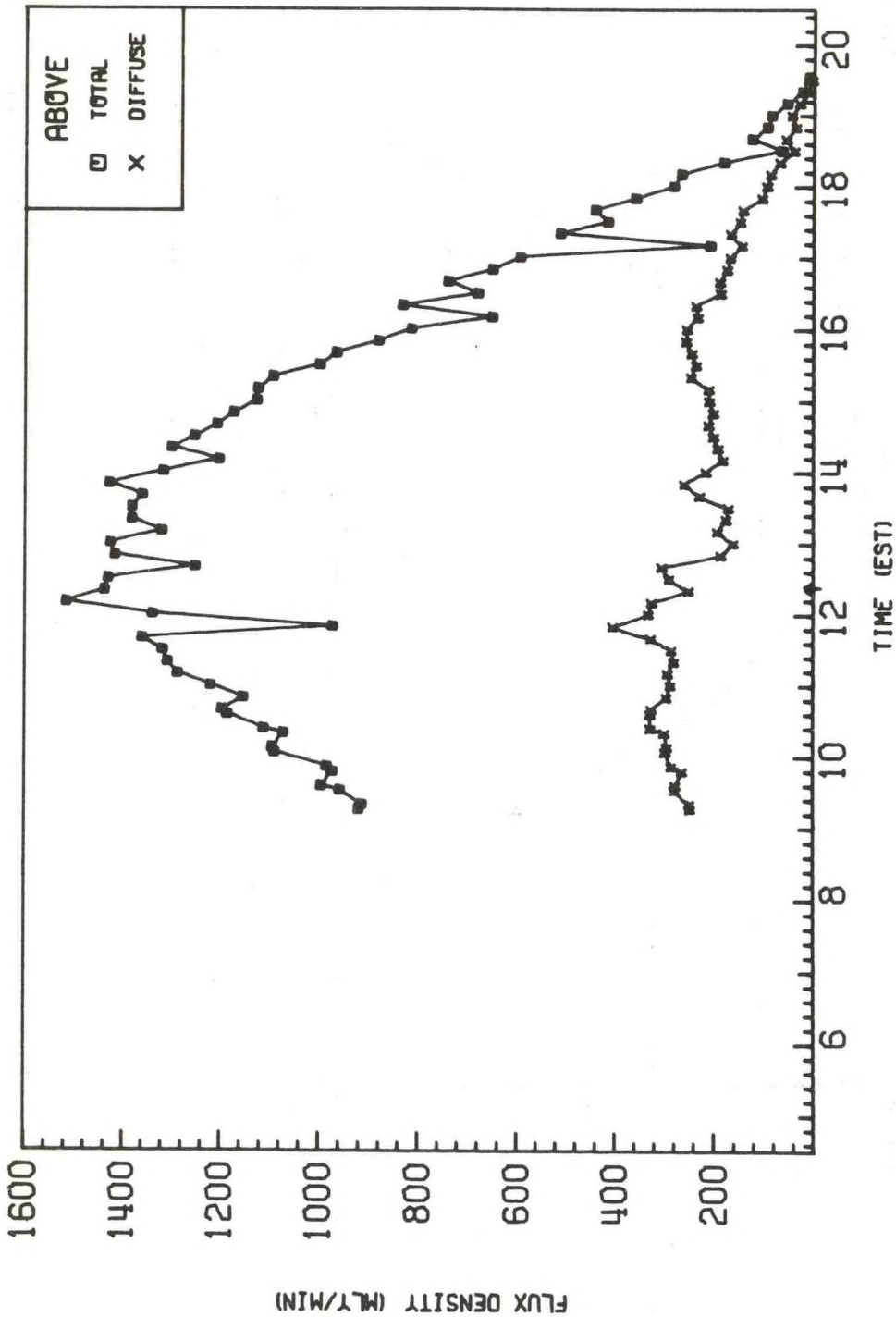


Figure 26: Clear Day Radiation Incident on Forest (June 8, 1972).

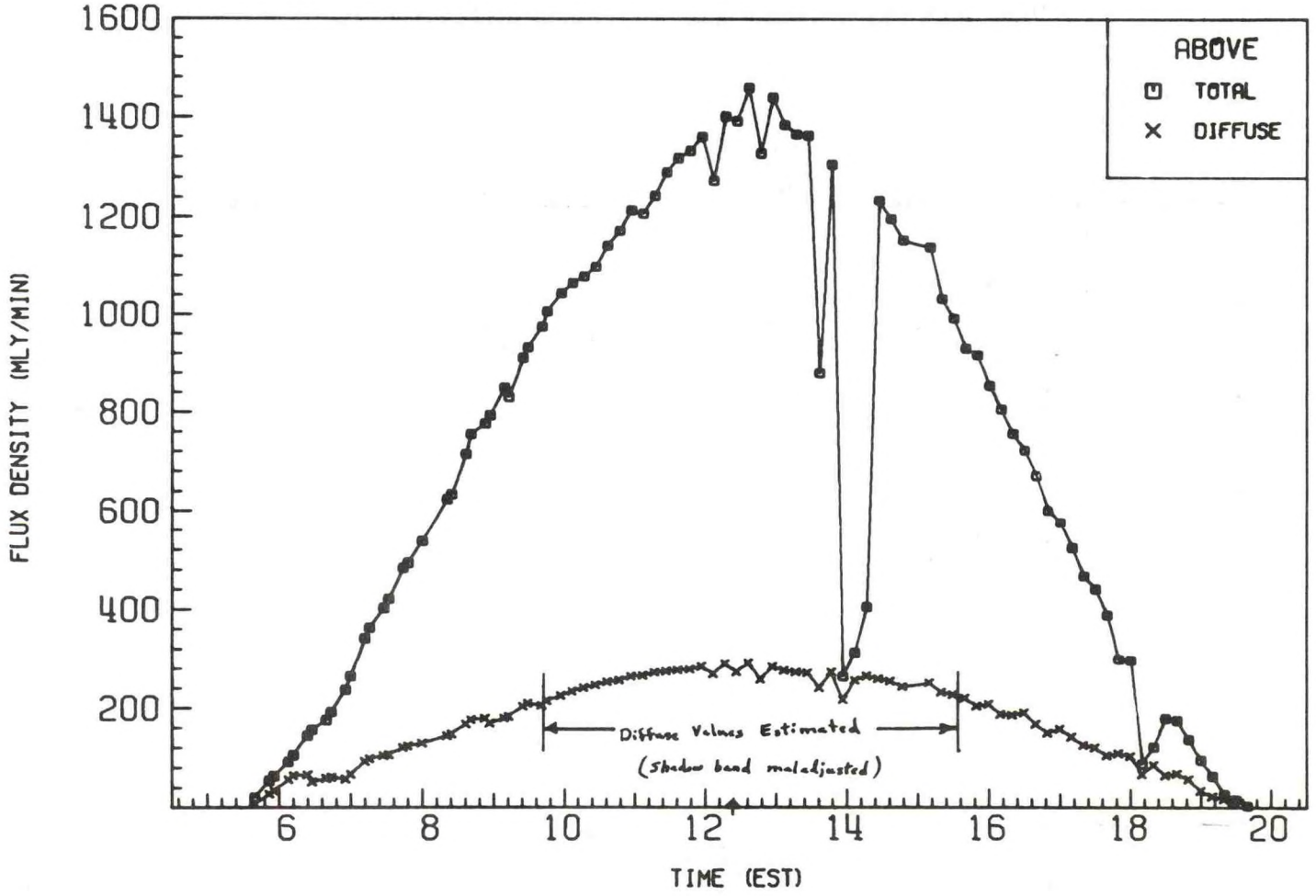


Figure 27: Clear Day Radiation Incident Upon Forest (June 14, 1972).

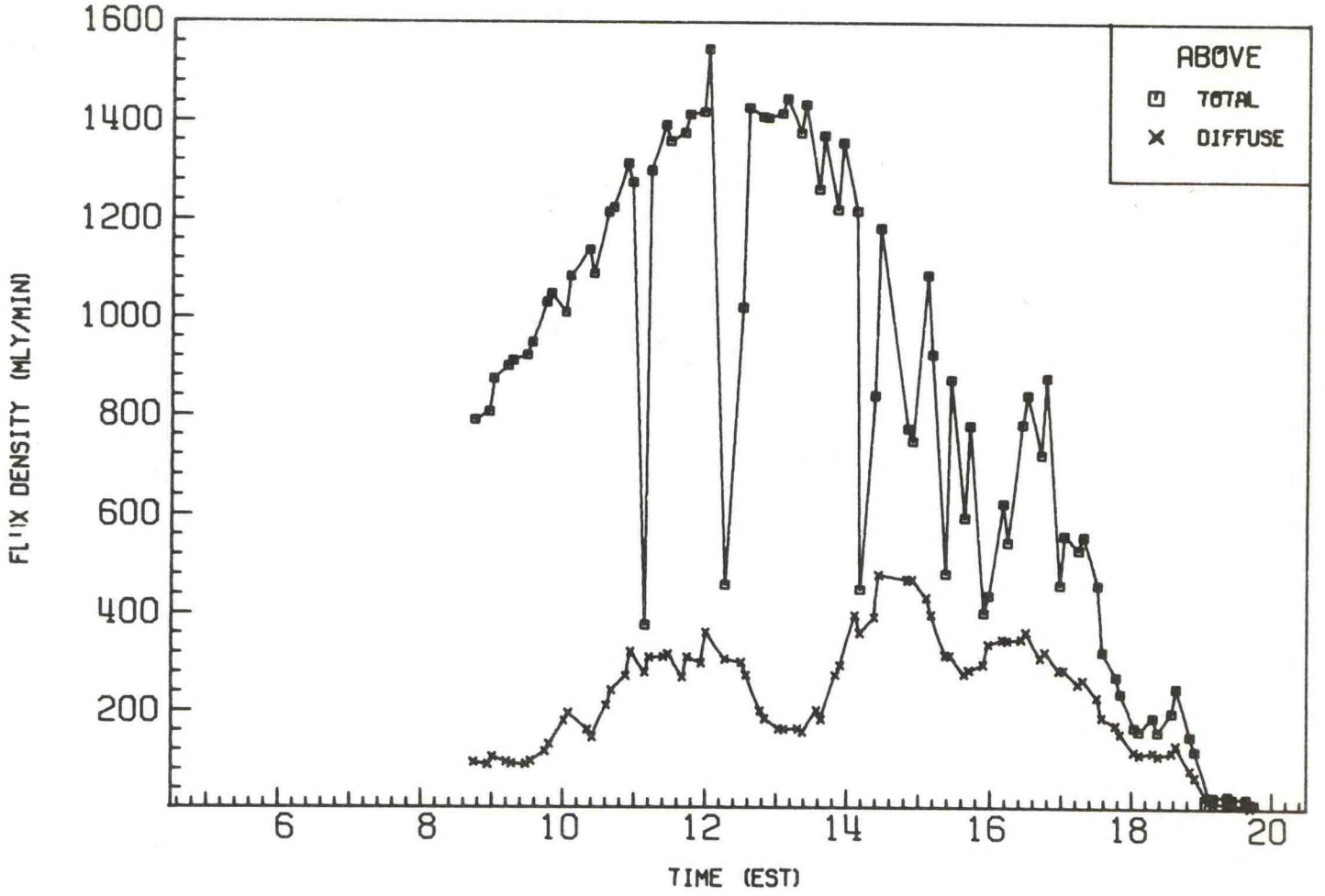


Figure 28: Partly-Cloudy Day Radiation Incident Upon Forest (June 26, 1972).

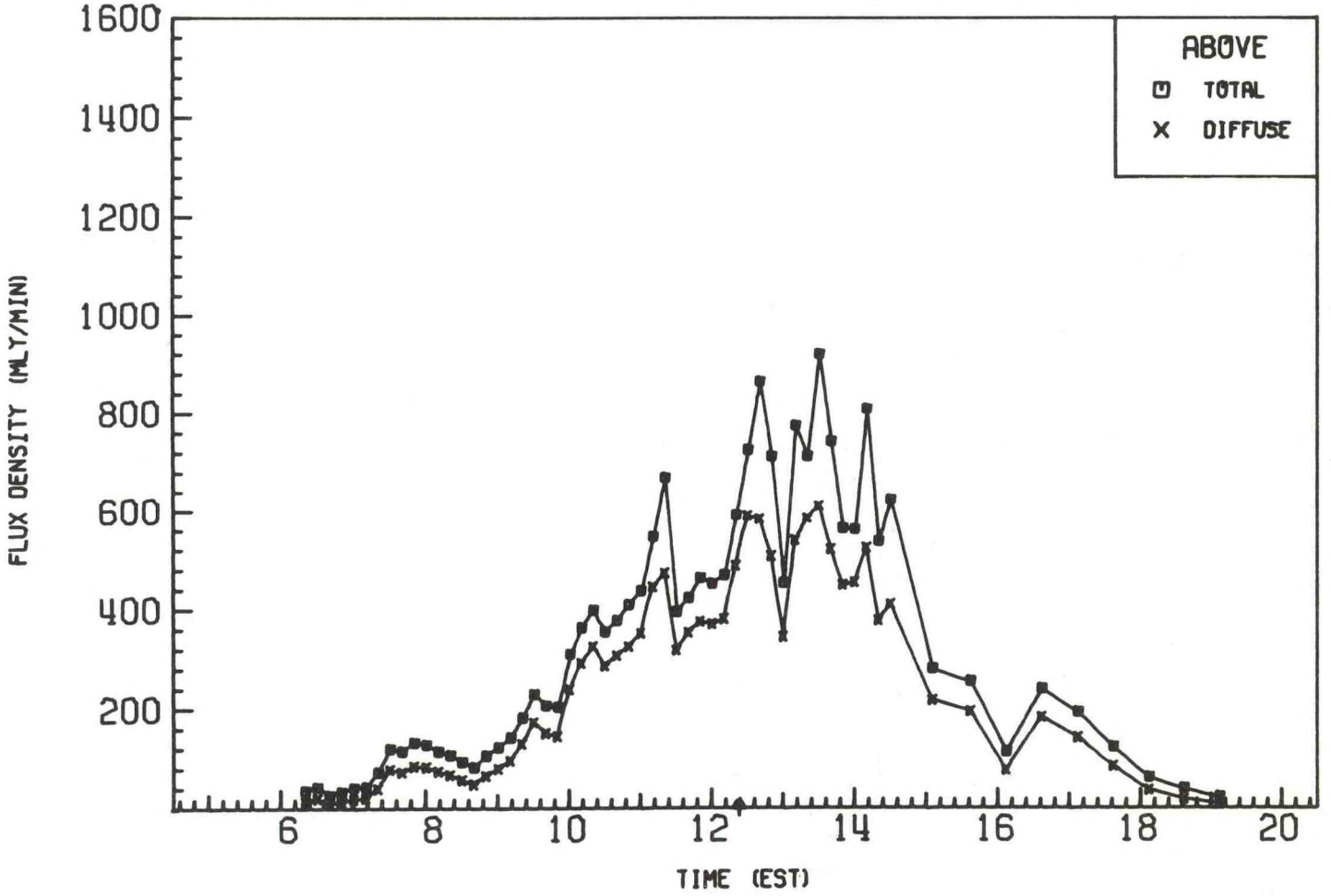


Figure 29: Overcast Day Radiation Incident Upon Forest (June 16, 1972).

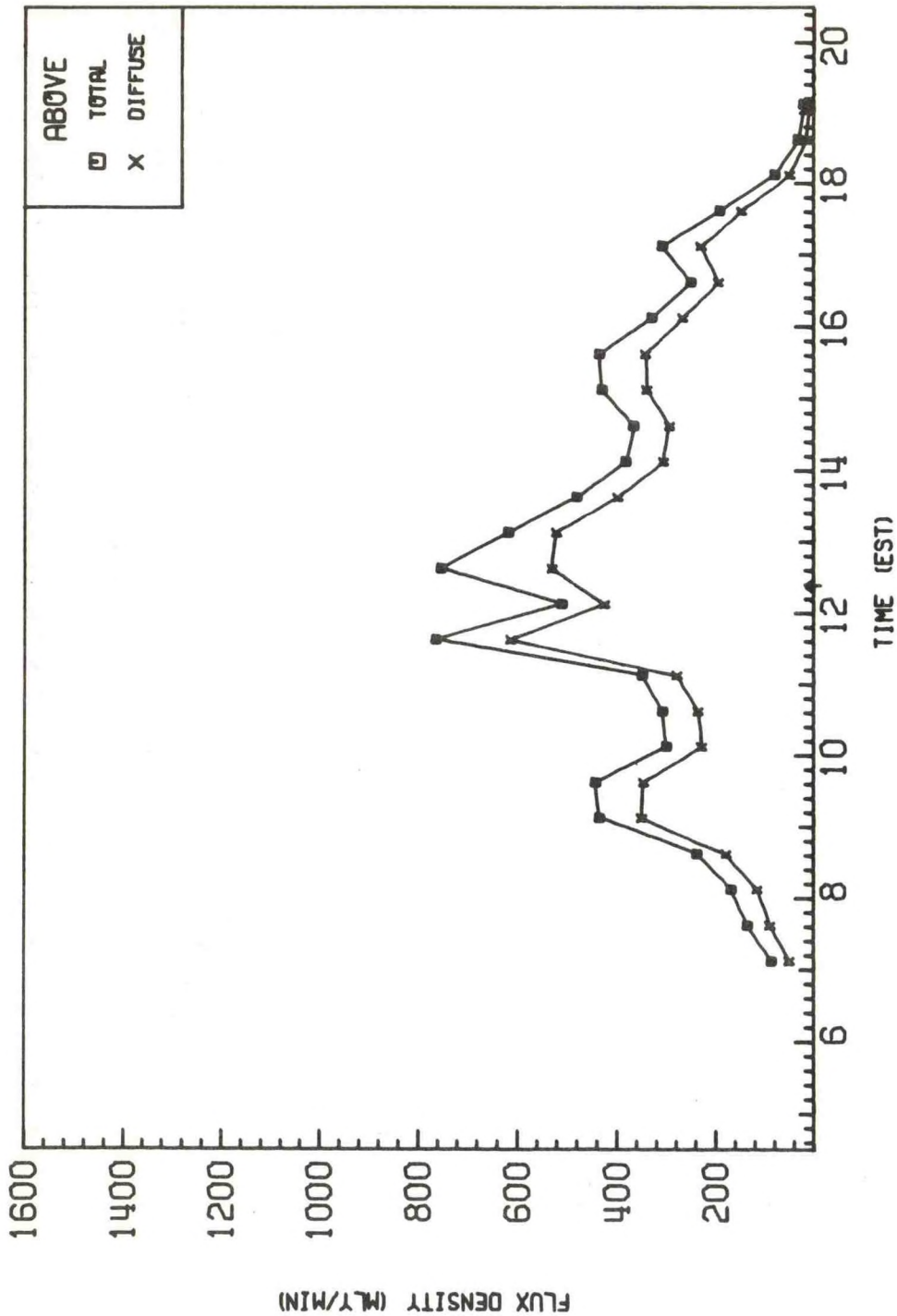


Figure 30: Overcast Day Radiation Incident Upon Forest (June 17, 1972).

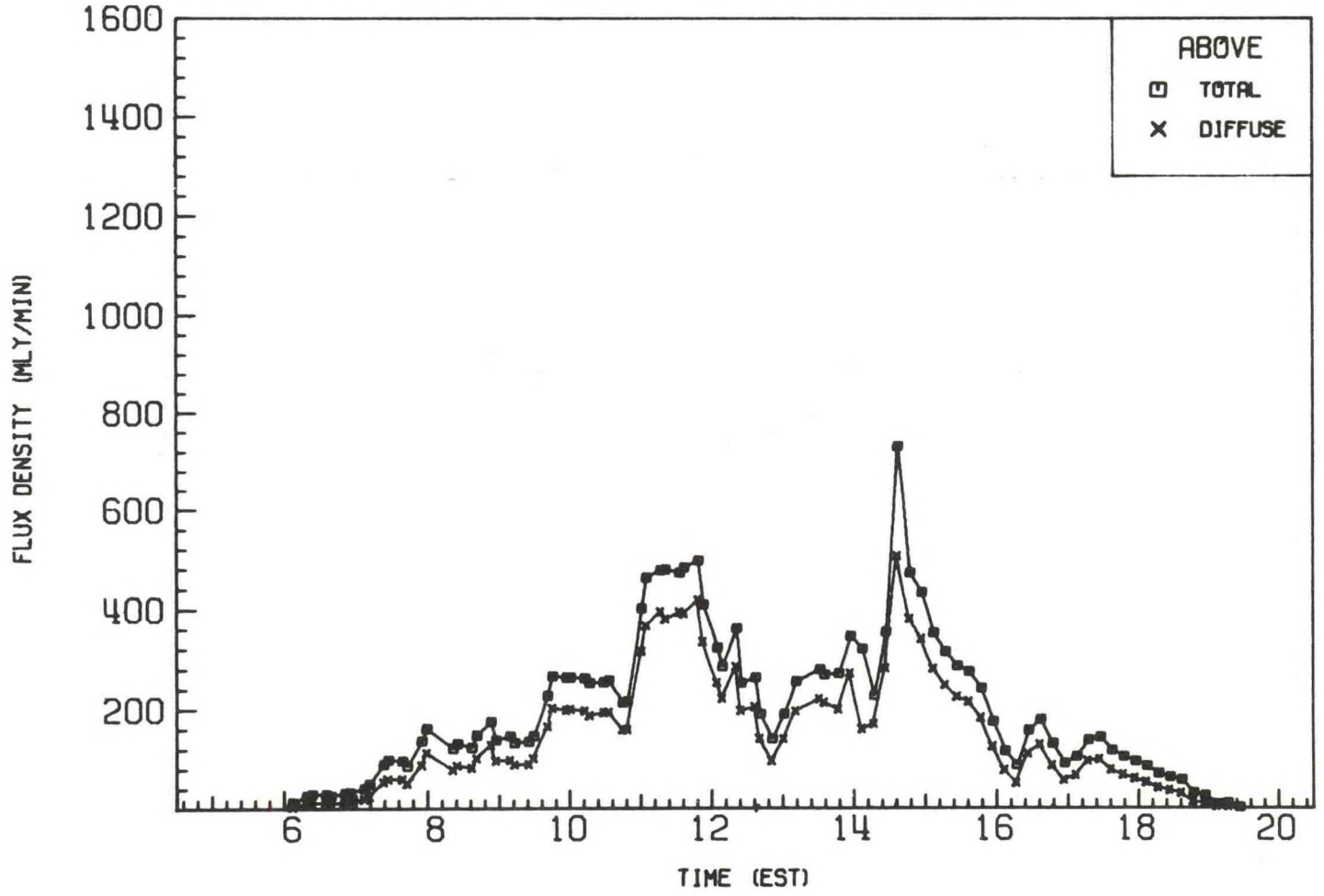


Figure 31: Overcast Day Radiation Incident Upon Forest (June 20, 1972).

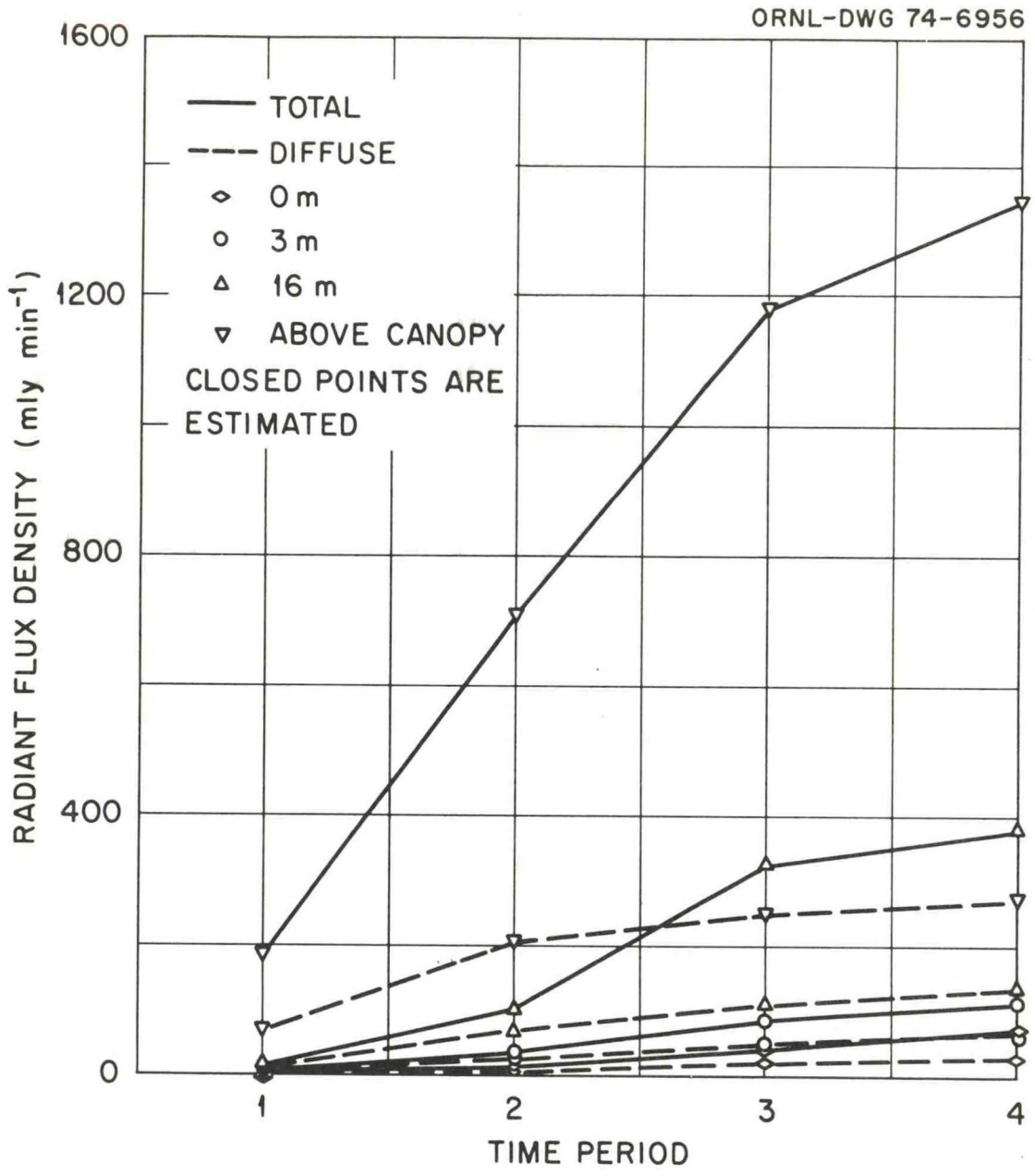


Figure 32: Clear Day Observed Data (June 8, 1972).

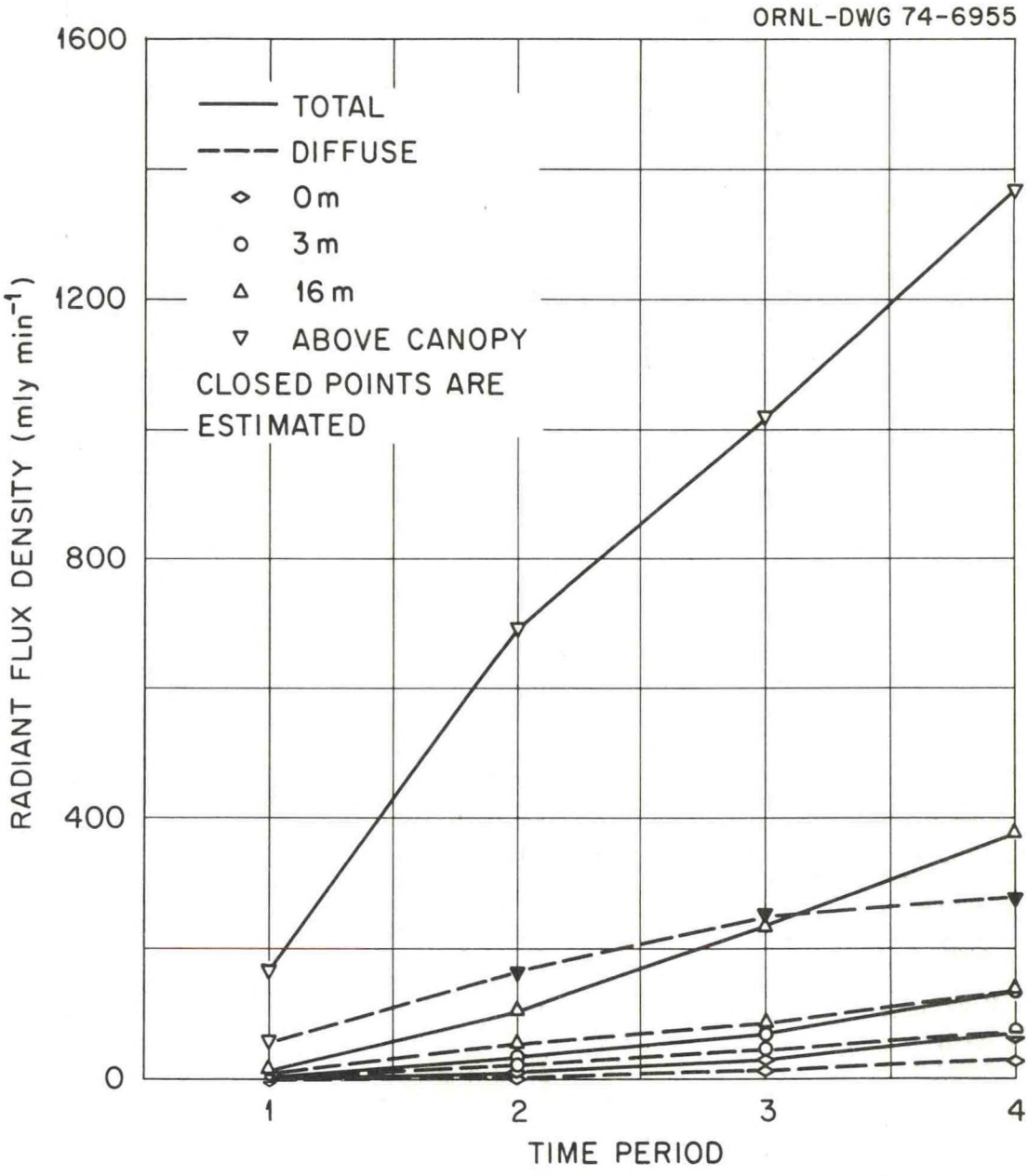


Figure 33: Clear Day Observed Data (June 14, 1972).

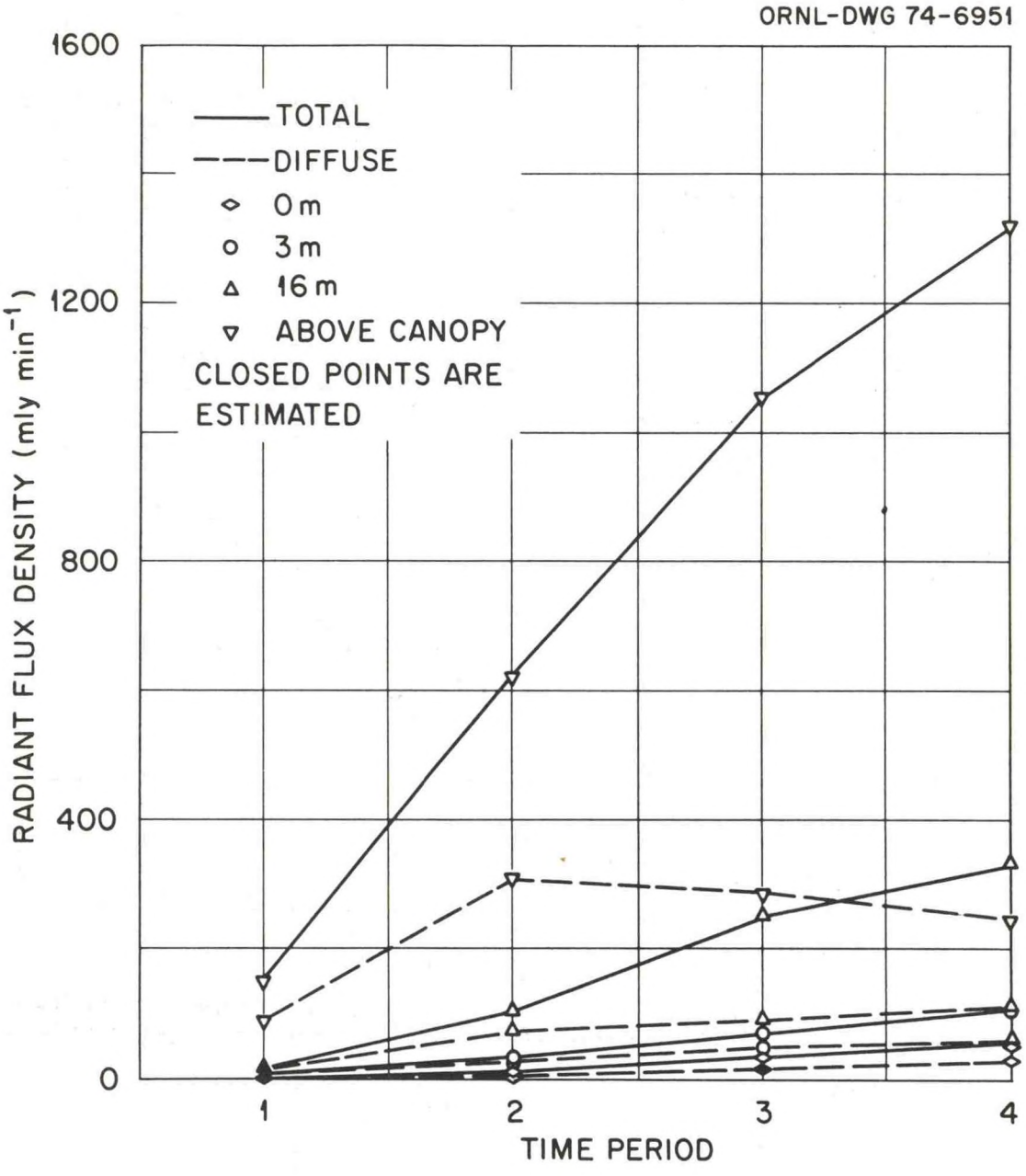


Figure 34: Partly-Cloudy Day Observed Data (June 26, 1972).

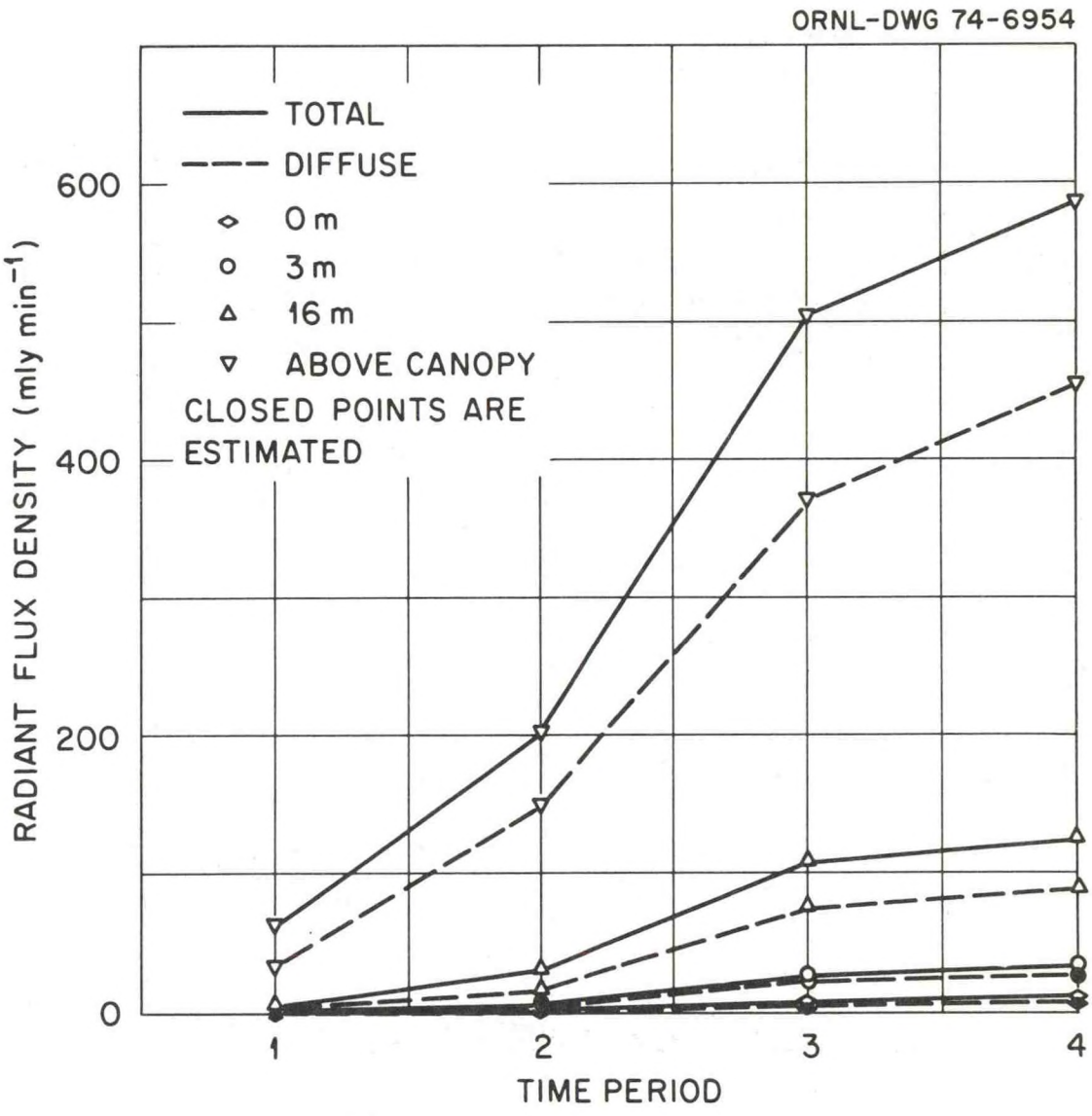


Figure 35: Overcast Day Observed Data (June 16, 1972).

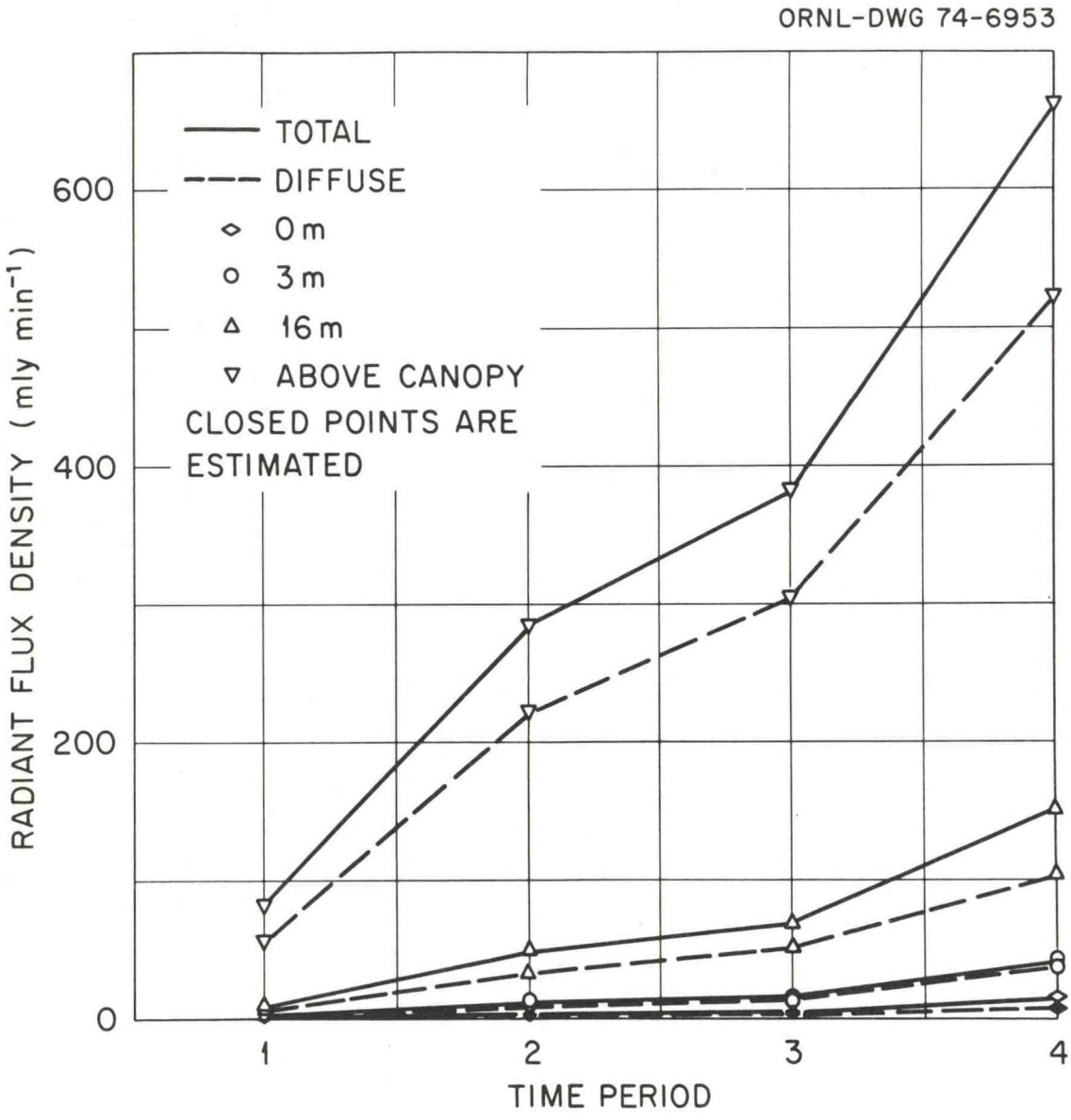


Figure 36: Overcast Day Observed Data (June 17, 1972).

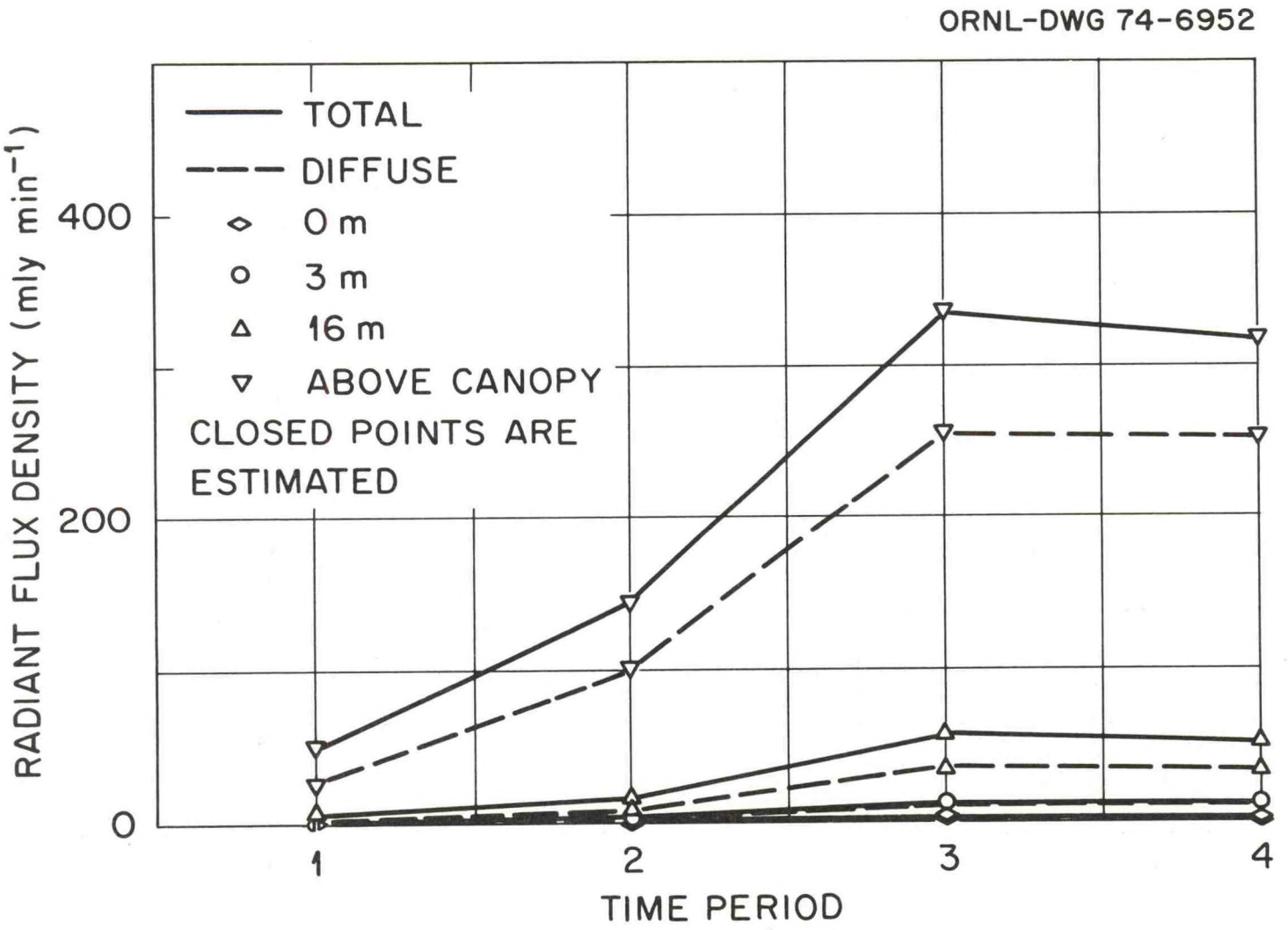


Figure 37: Overcast Day Observed Data (June 20, 1972).

Using the technique devised by Reifsnyder, Furnival, and Horowitz (1971/72), the combined down-reflected and transmitted direct beam radiation was estimated and separated from the observed diffuse radiation at each level. Thus comparisons can be made between observed and predicted diffuse radiation components as well as between observed and predicted total diffuse amounts. Figures 38 through 49 show these various comparisons for the six days. Since the transmitted and down-reflected direct beam enrichment of diffuse radiation amounts are estimated from the observed data by applying overcast day penetration rates to the incident diffuse radiation measured on clear and partly-cloudy days and subtracting this product from the diffuse radiation measured within the forest, no estimates of this enrichment can be made for the overcast days even though some direct beam radiation was present (see Figures 35, 36, and 37).

Figures 38, 39, and 40 compare observed and estimated values of $p_{z,\tau} + r_{z,\tau} + t_{z,\tau}$ for the clear and partly-cloudy days. As indicated by these figures, the photographic assessment technique used here over-estimates this sum at 0 and 3 meters through all time periods. At 16 meters, the predicted values are comparable to those observed during periods 1 and 2, but become increasingly overestimated toward solar noon. The disagreement between prediction and observation becomes more pronounced toward mid-day at all levels and generally increases with depth in the forest.

Reasons for the increasing overestimation of these diffuse radiation components toward solar noon are not clear. It may be that Pokrowski's (1929) clear sky brightness distribution does not obtain under the conditions of high humidity and haze present during the

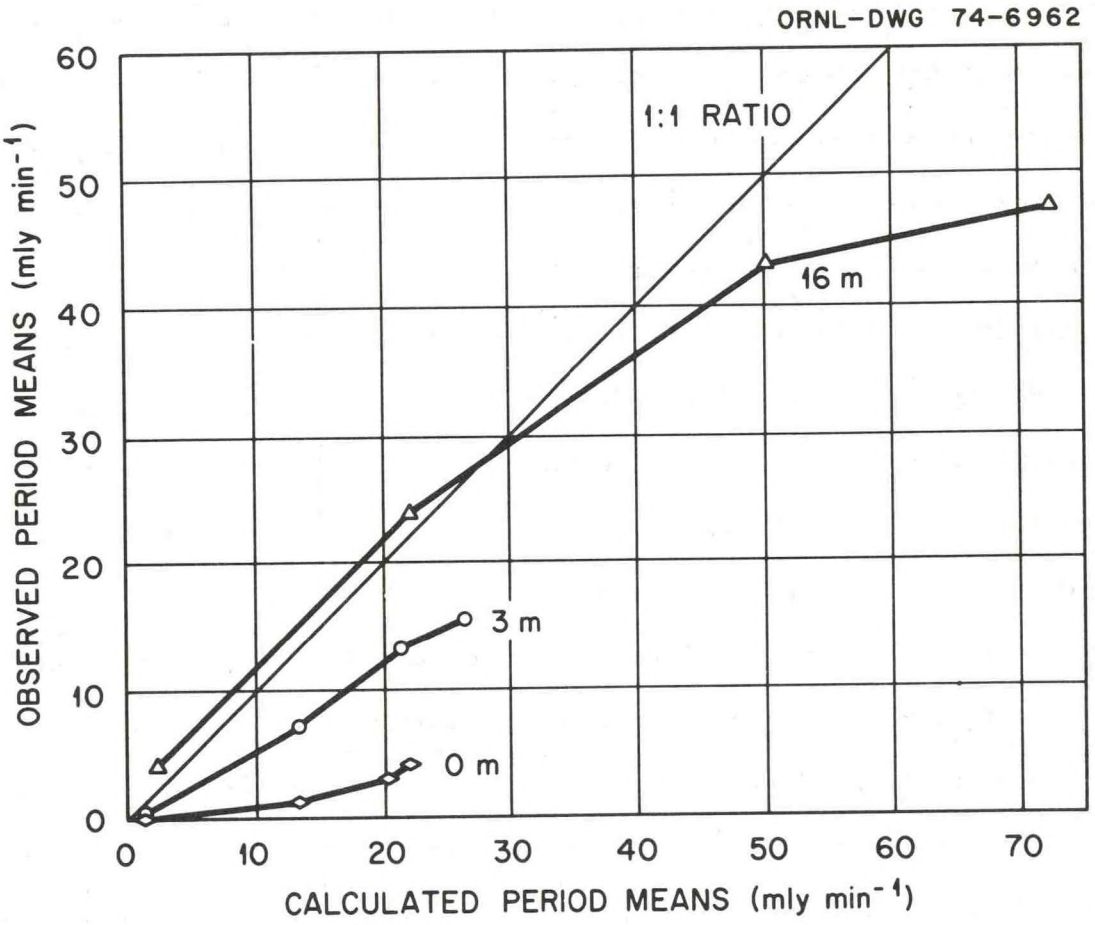


Figure 38: Observed Versus Calculated Values of $p_{z,\tau} + r_{z,\tau} + t_{z,\tau}$ in Forest on Clear Day of June 8, 1972.

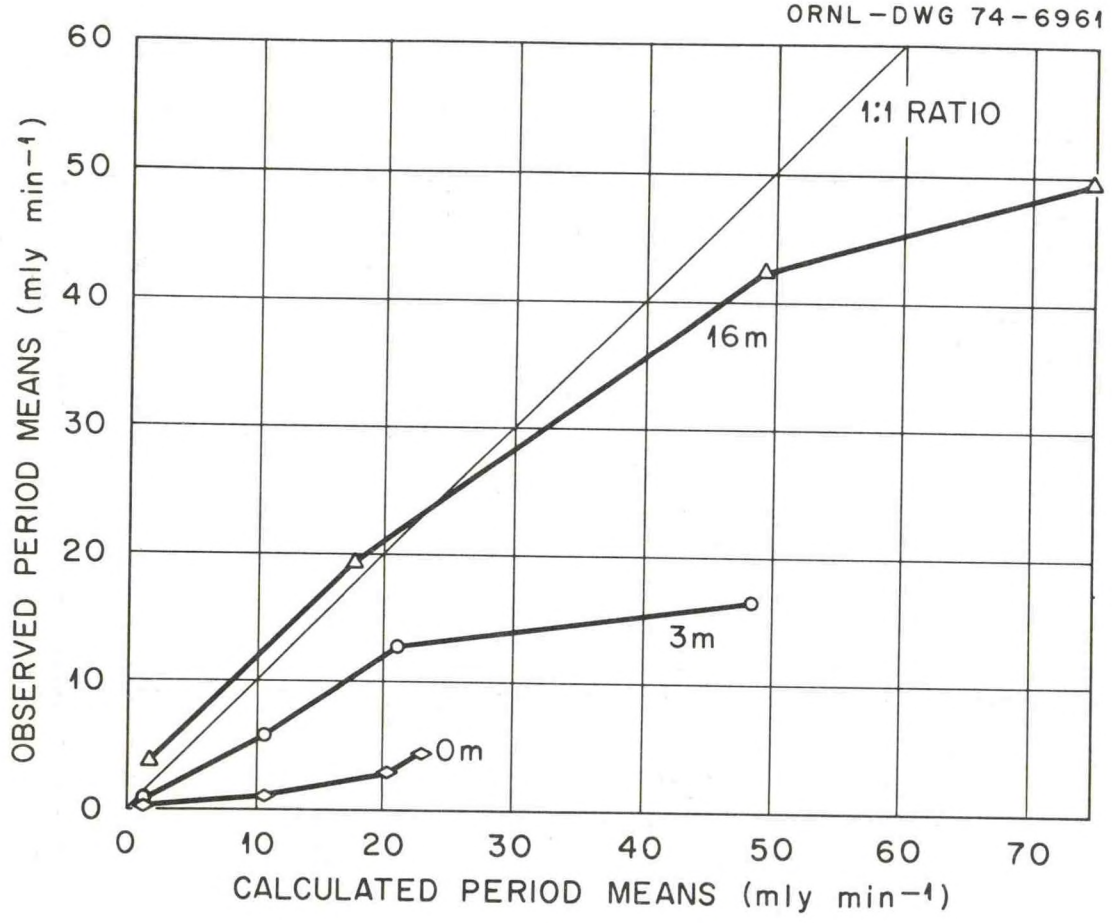


Figure 39: Observed Versus Calculated Values of $p_{z,\tau} + r_{z,\tau} + t_{z,\tau}$ in Forest on Clear Day of June 14, 1972.

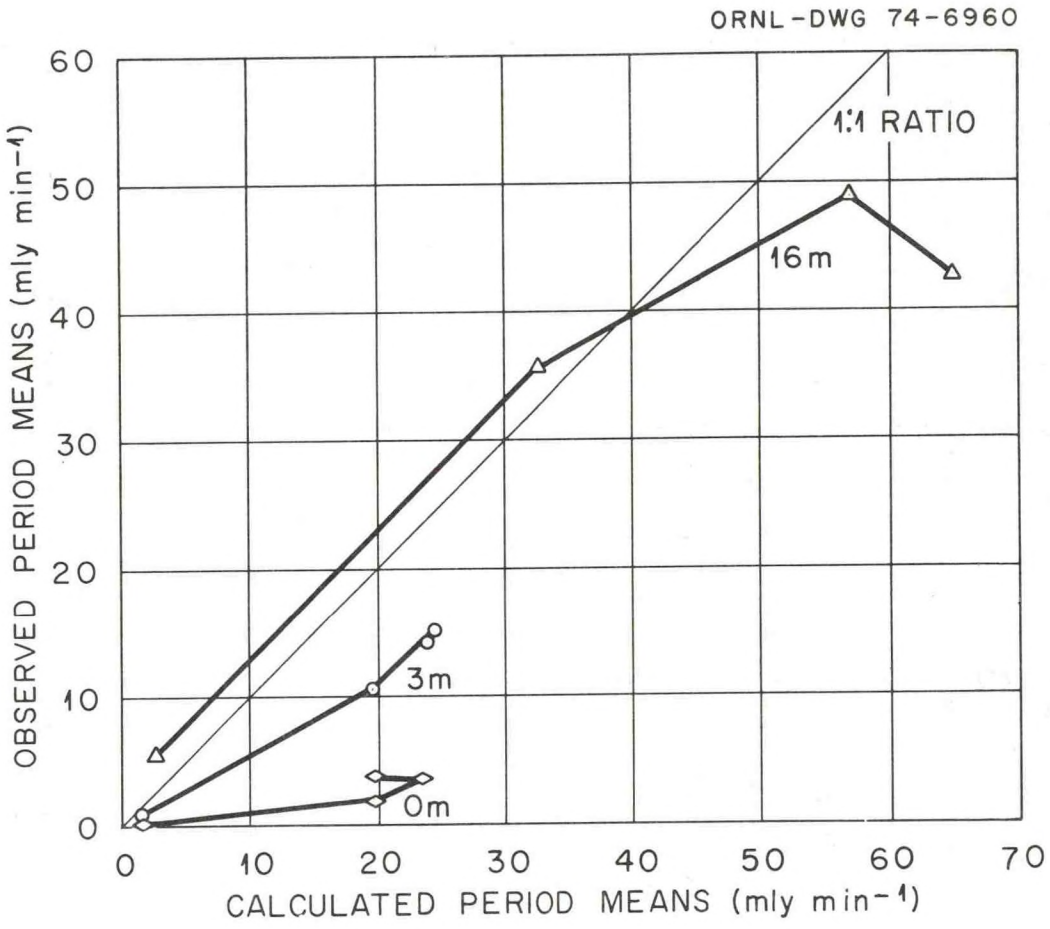


Figure 40: Observed Versus Calculated Values of $p_{z,\tau} + r_{z,\tau} + t_{z,\tau}$ in Forest on Partly-Cloudy Day of June 26, 1972.

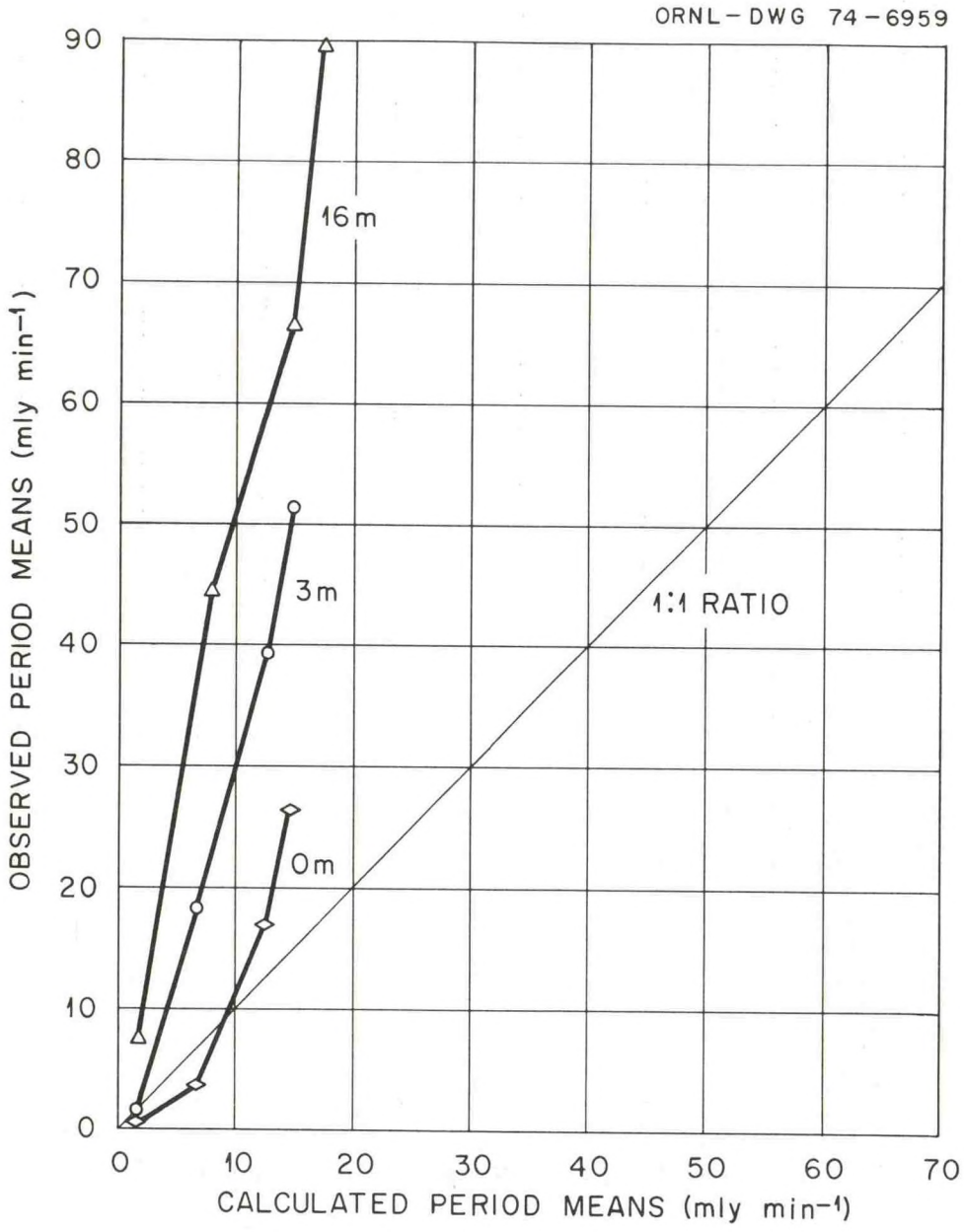


Figure 41: Observed Versus Calculated Values of $R_{z,\tau} + T_{z,\tau}$ in Forest on Clear Day of June 8, 1972

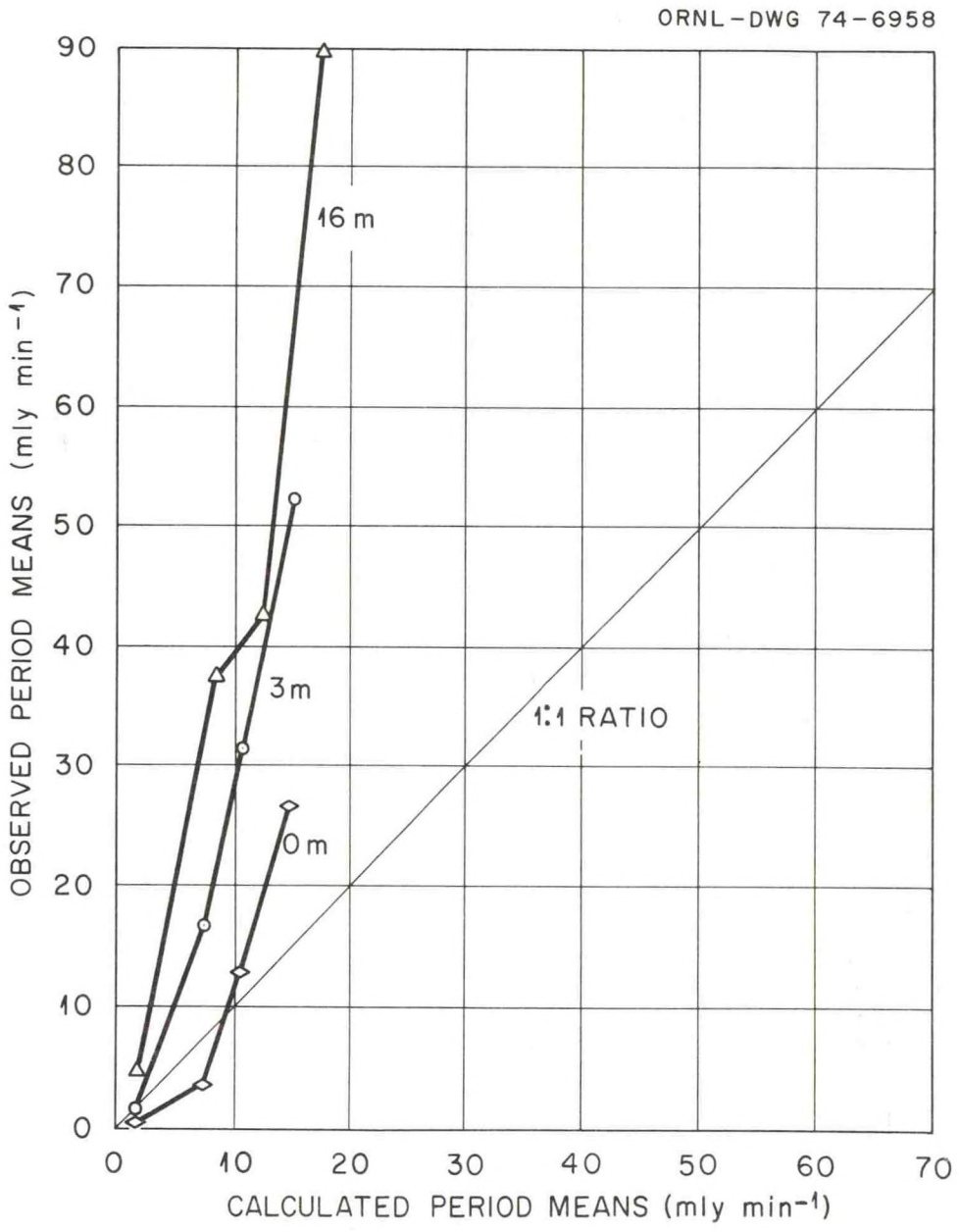


Figure 42: Observed Versus Calculated Values of $R_{z,\tau} + T_{z,\tau}$ in Forest on Clear Day of June 14, 1972.

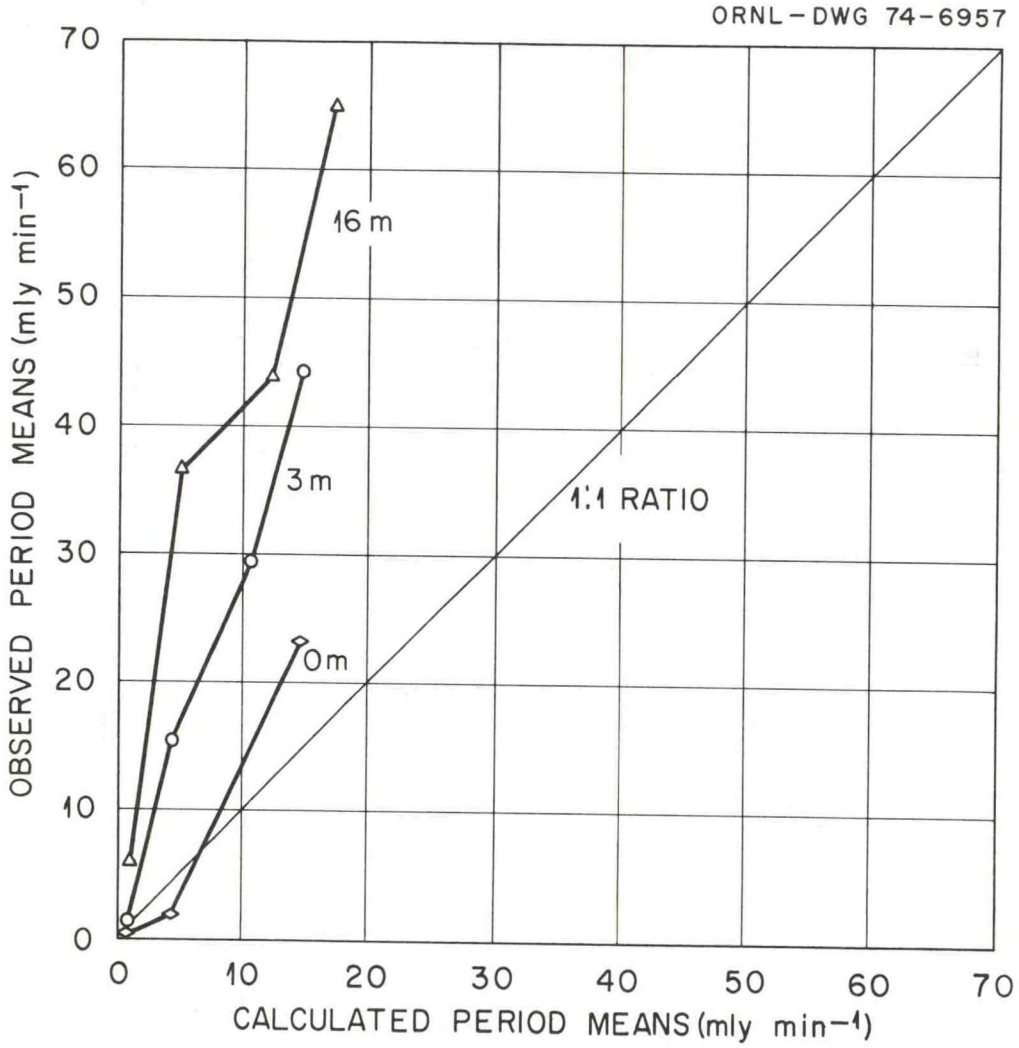


Figure 43: Observed Versus Calculated Values of $R_{z,\tau} + T_{z,\tau}$ in Forest on Partly-Cloudy Day of June 26, 1972.

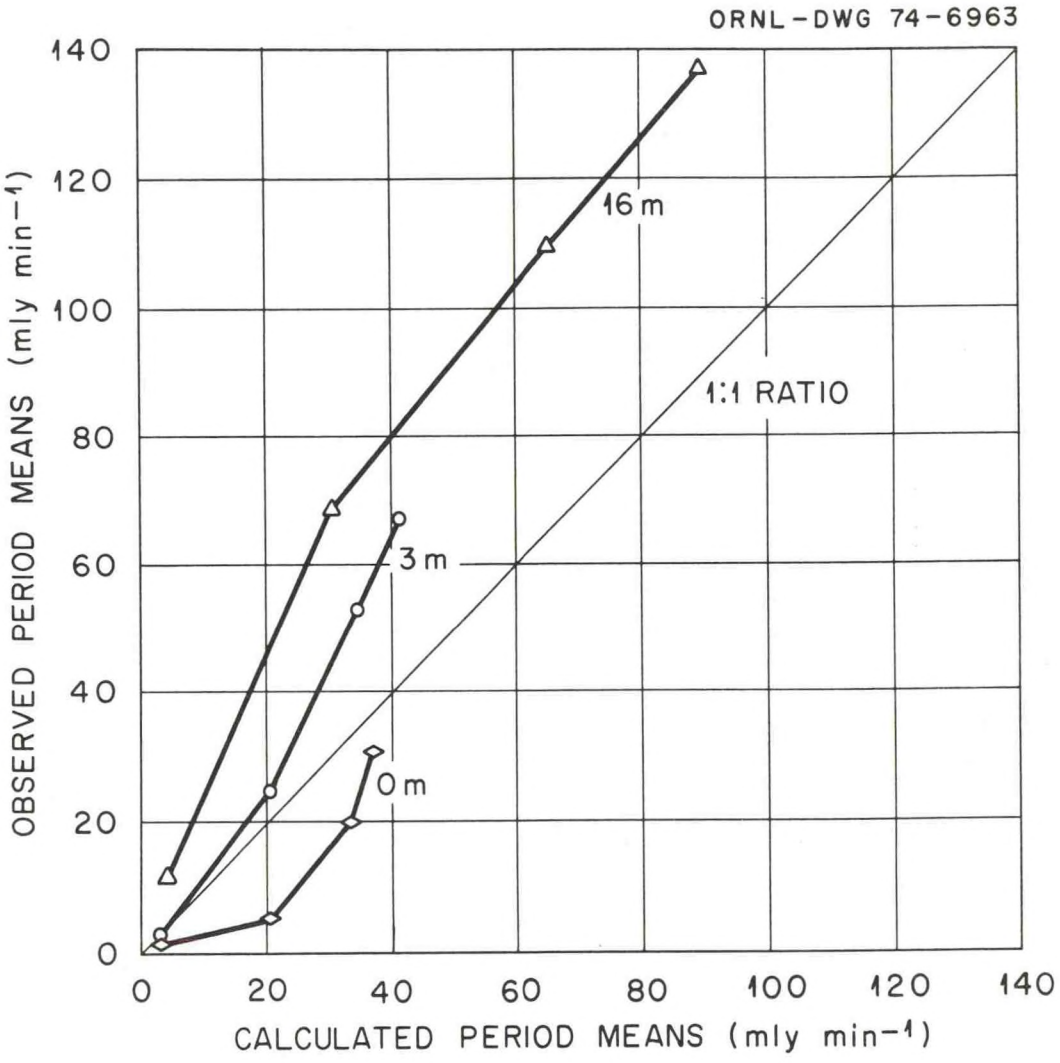


Figure 44: Observed Versus Calculated Diffuse Radiation in Forest on Clear Day of June 8, 1972.

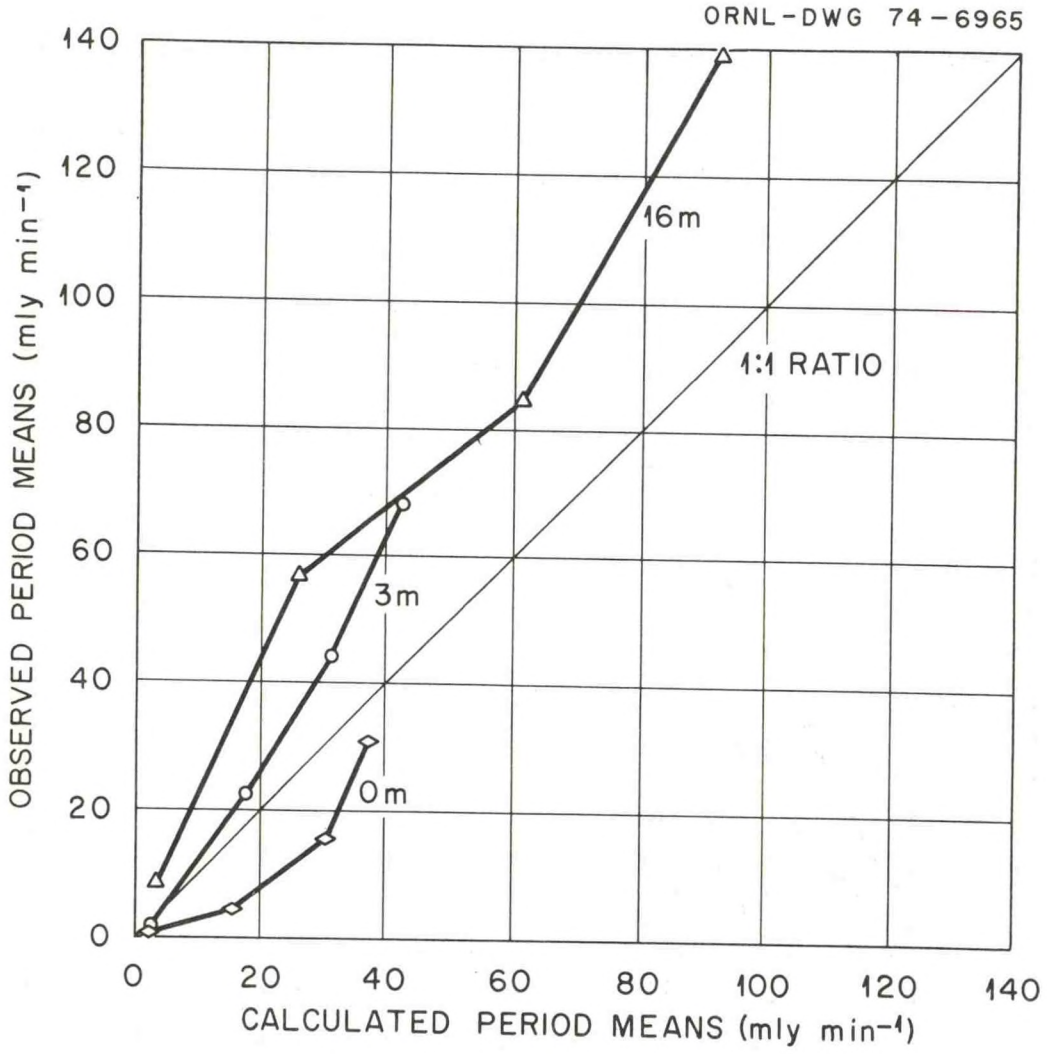


Figure 45: Observed Versus Calculated Diffuse Radiation in Forest on Clear Day of June 14, 1972.

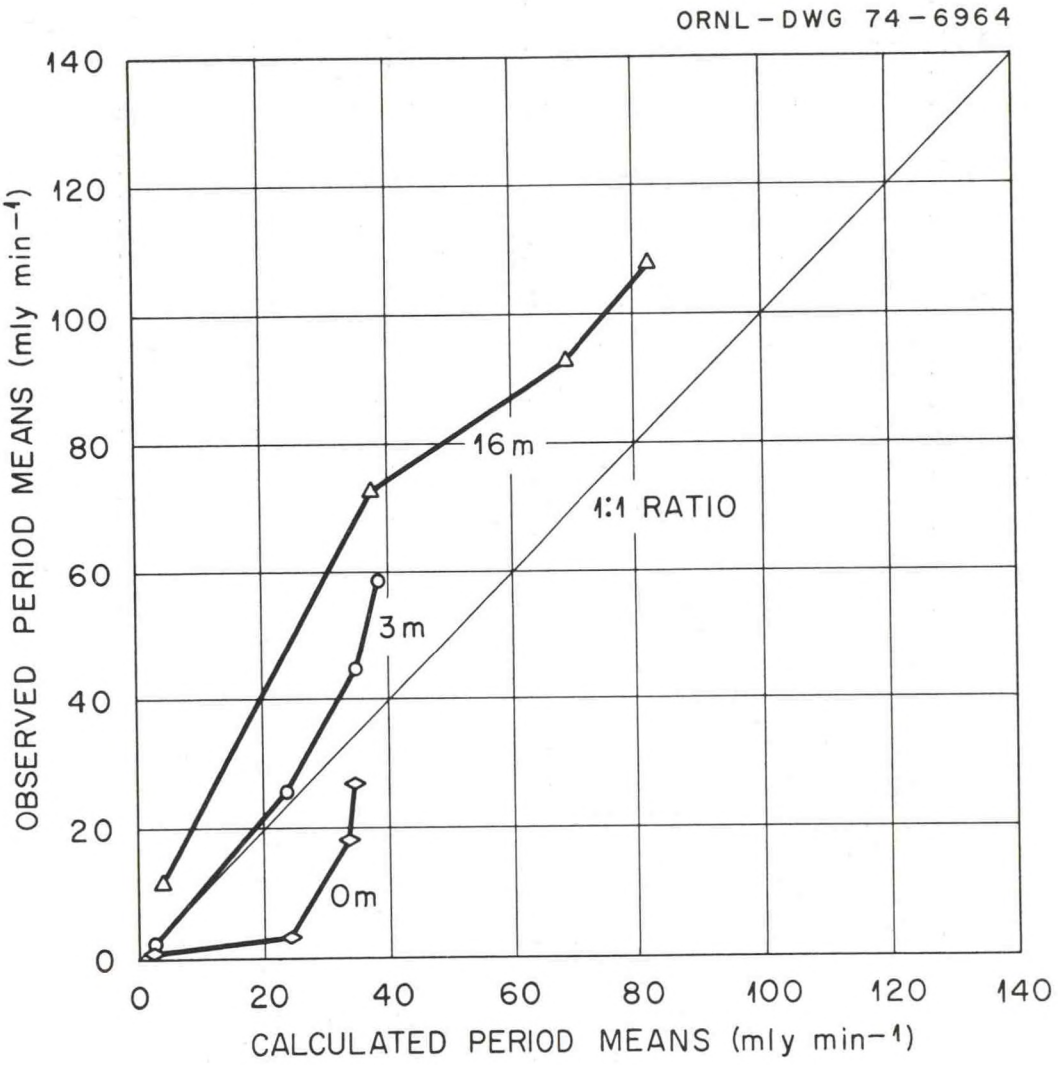


Figure 46: Observed Versus Calculated Diffuse Radiation in Forest on Partly-Cloudy Day of June 26, 1972.

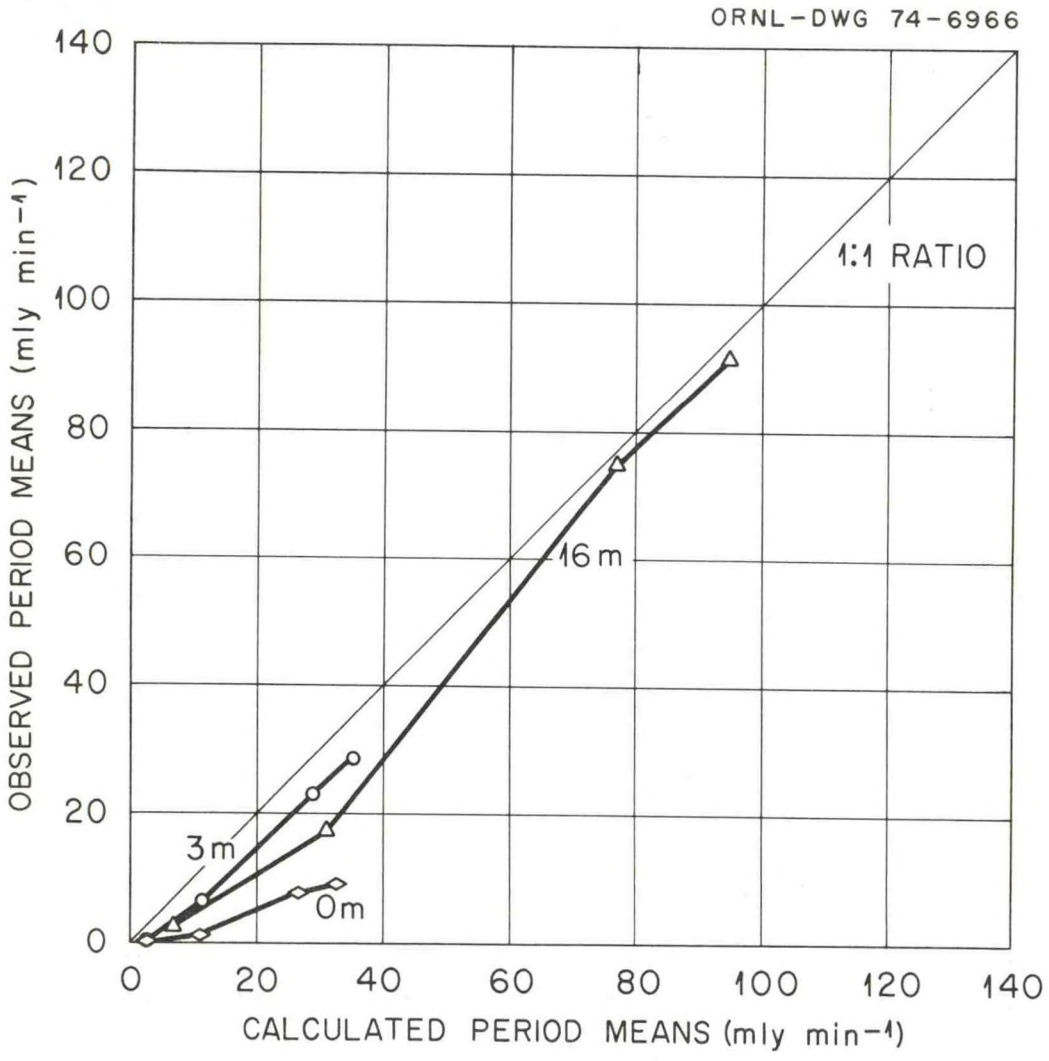


Figure 47: Observed Versus Calculated Diffuse Radiation in Forest on Overcast Day of June 16, 1972.

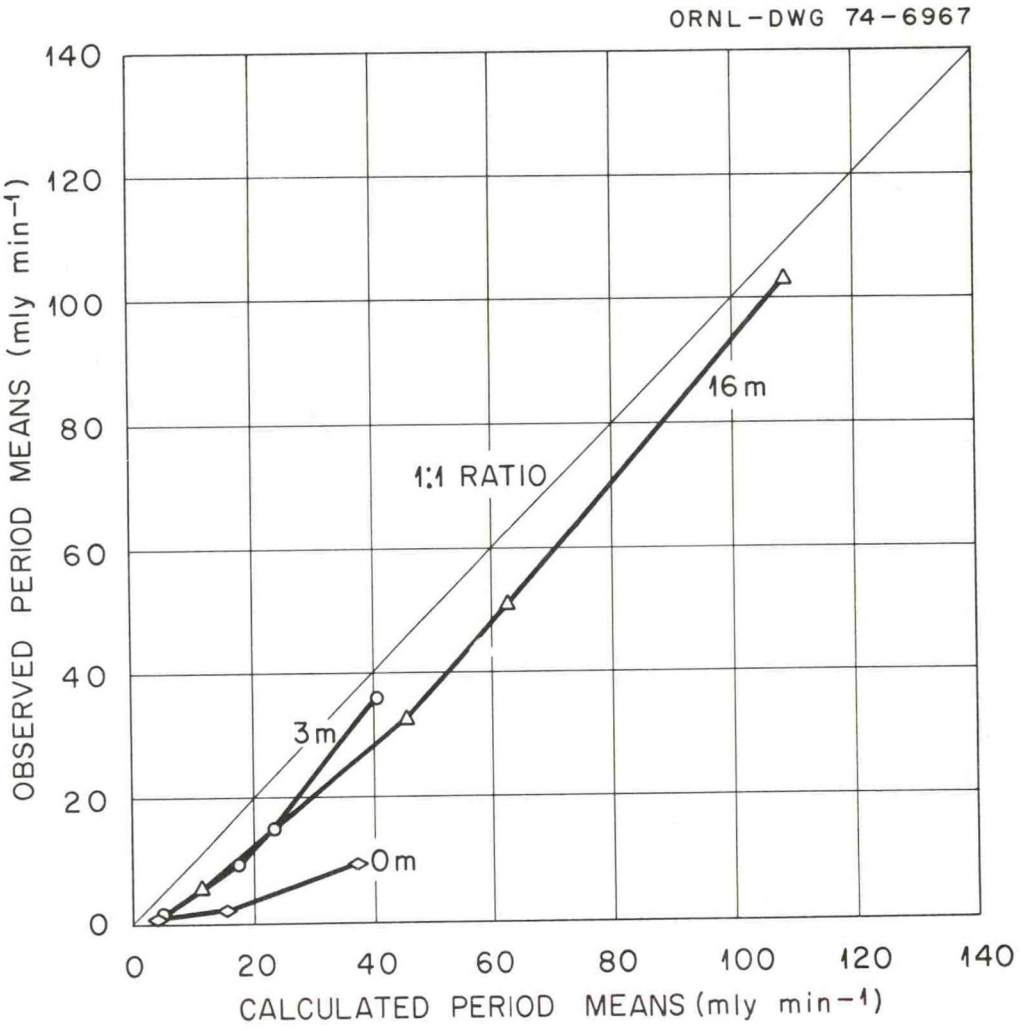


Figure 48: Observed Versus Calculated Diffuse Radiation in Forest on Overcast Day of June 17, 1972.

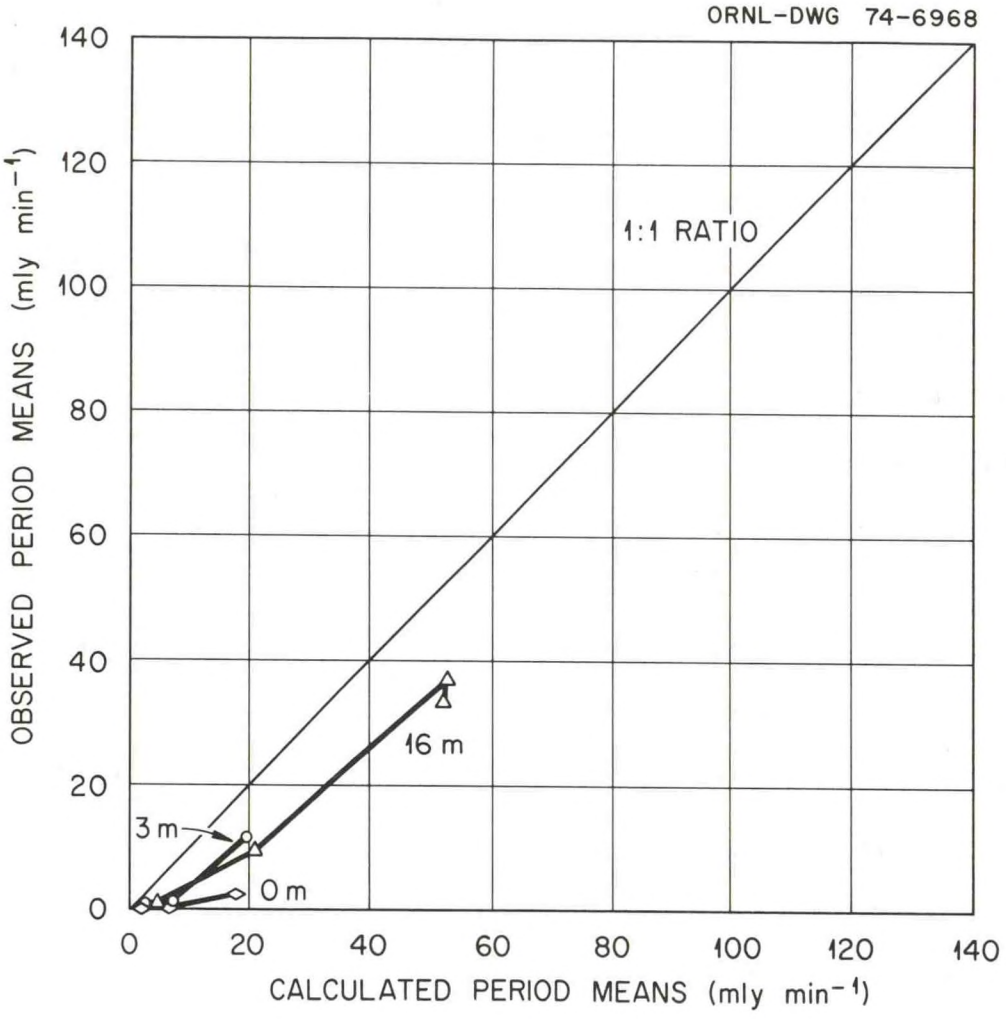


Figure 49: Observed Versus Calculated Diffuse Radiation in Forest on Overcast Day of June 20, 1972.

Appalachian summer. However, Walsh (1961) has compared sky brightness distributions measured both in Sweden and in Washington, D. C. with distributions predicted by Pokrowski's (1929) predictive equation and found good agreement between observation and prediction in both places. Thus it seems unlikely that the overestimation results from inaccuracies of this predictive equation.

More likely, this increasing overestimation results from greater halo effects at higher elevation angles in the canopy. Halos would be expected to be more pronounced around gap images backlit by brighter sky than by less bright sky. Since overcast skies tend to have brightness distributions that increase from horizon to zenith, this implies greater halo effects at higher elevation angles on these photos. Thus, the amount of canopy opening would tend to be increasingly overestimated from horizon to zenith. Now the brightest portion of a clear sky appears to move with the sun from horizon to a maximum elevation at solar noon and then back to the horizon again. Hence with the progression of time toward solar noon, canopy gaps at even higher elevation angles are responsible for the admission of greatest amounts of diffuse radiation. As the sizes of these gaps are increasingly overestimated by virtue of the halo effect, the degree of overestimation of penetrating diffuse radiation increases as well.

It is likely that differential halo effects also explain the increasing degree of overestimation with depth in the forest. As noted above, the predominant size of gap images appears to decrease with depth in the forest and because it decreases with depth, the halo effect tends to become more significant. Hence the halo effect

results in less overestimation at 16 meters than at 0 meters, i.e., the degree of overestimation increases with depth in the forest.

Figures 41, 42, and 43 present comparisons of the transmitted and down-reflected direct beam enrichment of diffuse radiation in the forest estimated from the observed data using the technique of Reifsnyder, Furnival, and Horowitz (1971/72) with those calculated from the photograph data. In this case there is a general underestimation of the calculated values except at 0 and 3 meters early and late in the day. The degree of underestimation increases toward solar noon at all levels and with height in the forest.

The overall underestimation of $T_{z,\tau} + R_{z,\tau}$ can be partially ascribed to the technique used to derive values of $n_z(\theta)$, the number of leaves through which or from which direct beam radiation is transmitted or reflected. As noted earlier, the photos were purposely underexposed to minimize halos. This resulted in a loss of canopy detail which makes the estimation of $n_z(\theta)$ even more tenuous than if good canopy detail were visible. Because of the underexposure, $n_z(\theta)$ may have been consistently overestimated. This parameter appears as an exponent in the equations used to calculate the transmitted and down-reflected radiation and hence, small errors in $n_z(\theta)$ will result in large changes in the resulting estimates of $T_{z,\tau}$ and $R_{z,\tau}$.

Furthermore, it appears that leaf inclination angles vary with height in this forest. Although our data is limited, there is an indication of increasing leaf inclination from nearly horizontal in the secondary canopy to more vertical in the upper parts of the overstory canopy. Because of this and because the elevation angle of the solar beam changes throughout the day as the sun appears to move across

the sky, the assumption that a constant proportion of the reflected direct beam radiation is reflected downward is unrealistic and may also be involved in the underestimation of $T_{z,\tau} + R_{z,\tau}$. The varying leaf inclination over height and the changing angles of incidence of the solar beam through time imply that the adjustable parameter denoted f must be assigned values which are functions of both height and time. However, I can see no method by which these values could be derived from canopy photographs. Further study of this problem is indicated.

Figures 44 through 46 show the comparisons of observed and predicted combined diffuse radiation ($p_{z,\tau} + r_{z,\tau} + t_{z,\tau} + R_{z,\tau} + T_{z,\tau}$) for clear (Figures 44 and 45) and partly-cloudy (Figure 46) days. Figures 47, 48, and 49 are comparisons of overcast day observations and predictions where $d_{z,\tau}$ is composed of $p_{z,\tau} + r_{z,\tau} + t_{z,\tau}$ only. As with the comparison of observed and predicted diffuse component, the combined diffuse radiation comparisons are similar on the clear and partly-cloudy days. Predicted values of diffuse radiation reaching the forest floor are consistently overestimated while those at higher levels are increasingly underestimated.

As with the comparison of the $p_{z,\tau} + r_{z,\tau} + t_{z,\tau}$ predictions and observations on clear and partly-cloudy days, the predicted values of this sum are overestimated on overcast days also as shown on Figures 47, 48, and 49. However, on the overcast days, the predicted values are increasingly overestimated toward solar noon only at 0 meters. At the upper two levels, the degree of overestimation remains reasonably constant over time. At all levels, however, the resultant curves are reasonably linear. This indicates that the degree of overestimation at 0 meters is reasonably constant over time and the predicted values

diverge from observation by virtue of the increasing amounts of incident diffuse radiation over time. The 3 and 16 meter level curves have slopes approximating that of the 1:1 ratio. Thus, despite the time variation in observed penetration rates, it appears that a constant diffuse site factor can predict diffuse radiation penetration from an overcast sky through time which agrees satisfactorily with observation.

The overestimation at 0 meters can be explained by the same arguments set forth in regard to diffuse radiation penetration on clear and partly-cloudy days. That is, the overestimation of canopy opening owing to halo effect causes predicted values to far exceed observed values. The reversal of the position of the 3 and 16 meter curves on overcast days in relation to their position on clear and partly-cloudy days is not explained by these arguments however. Apparently the underexposure of the 3 meter level photos yields diffuse site factors at this level which more closely approximate the actual overcast day penetration of diffuse radiation. Needless to say, comparison of clear and partly-cloudy day curves with the overcast day curves indicate that differences in the penetration processes of diffuse radiation occur that are not recognized by this model. Again, further study is indicated.

Direct Beam Component:

Figures 50 through 53 show the size distribution of canopy openings visible on the photographs in each of the annular bands corresponding to the solar elevations at each of the four mid-period times ± 20 minutes on the summer solstice. Canopy openings are relatively sparse

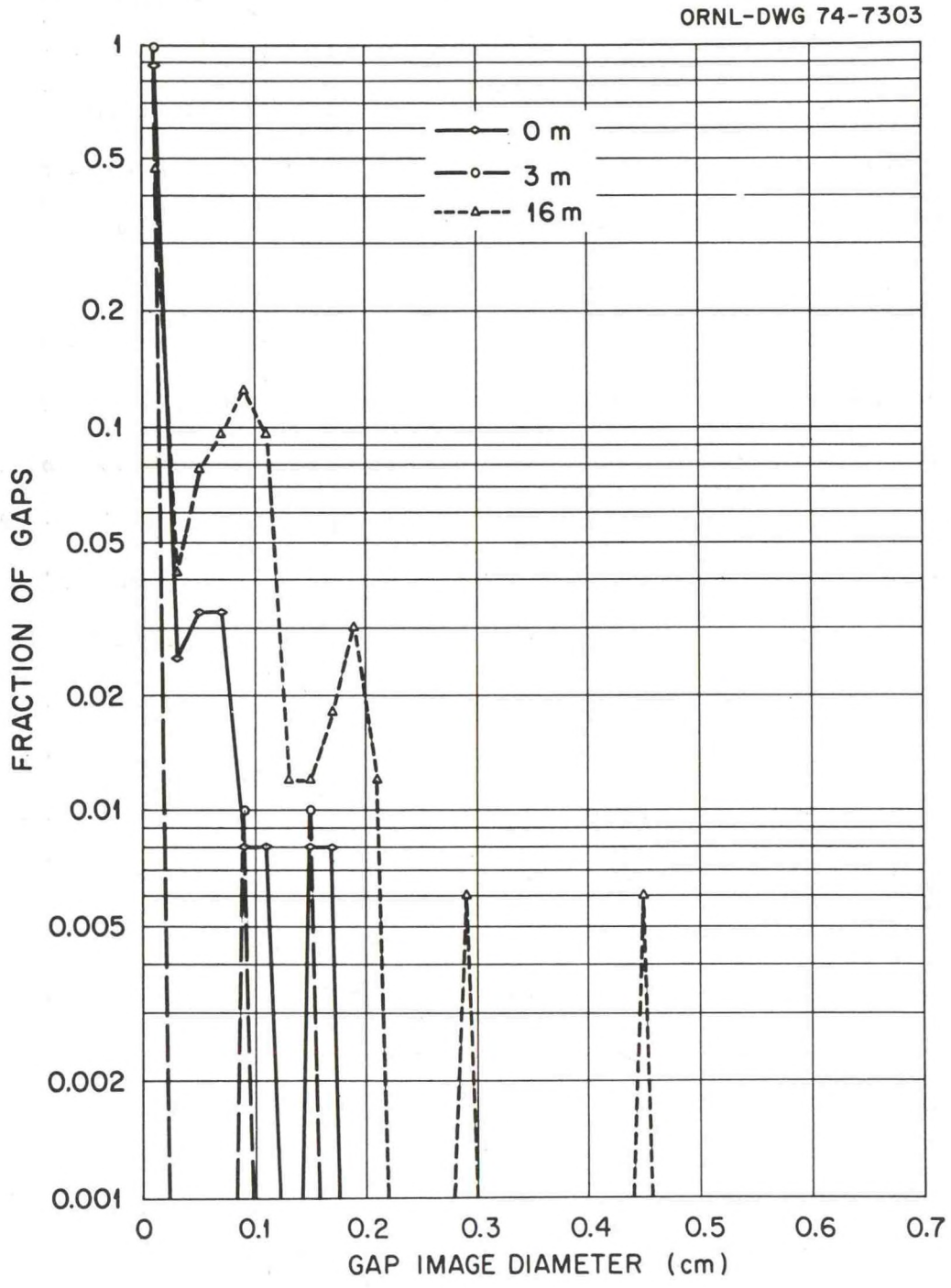


Figure 50: Gap Image Diameter Distribution - Period 1.

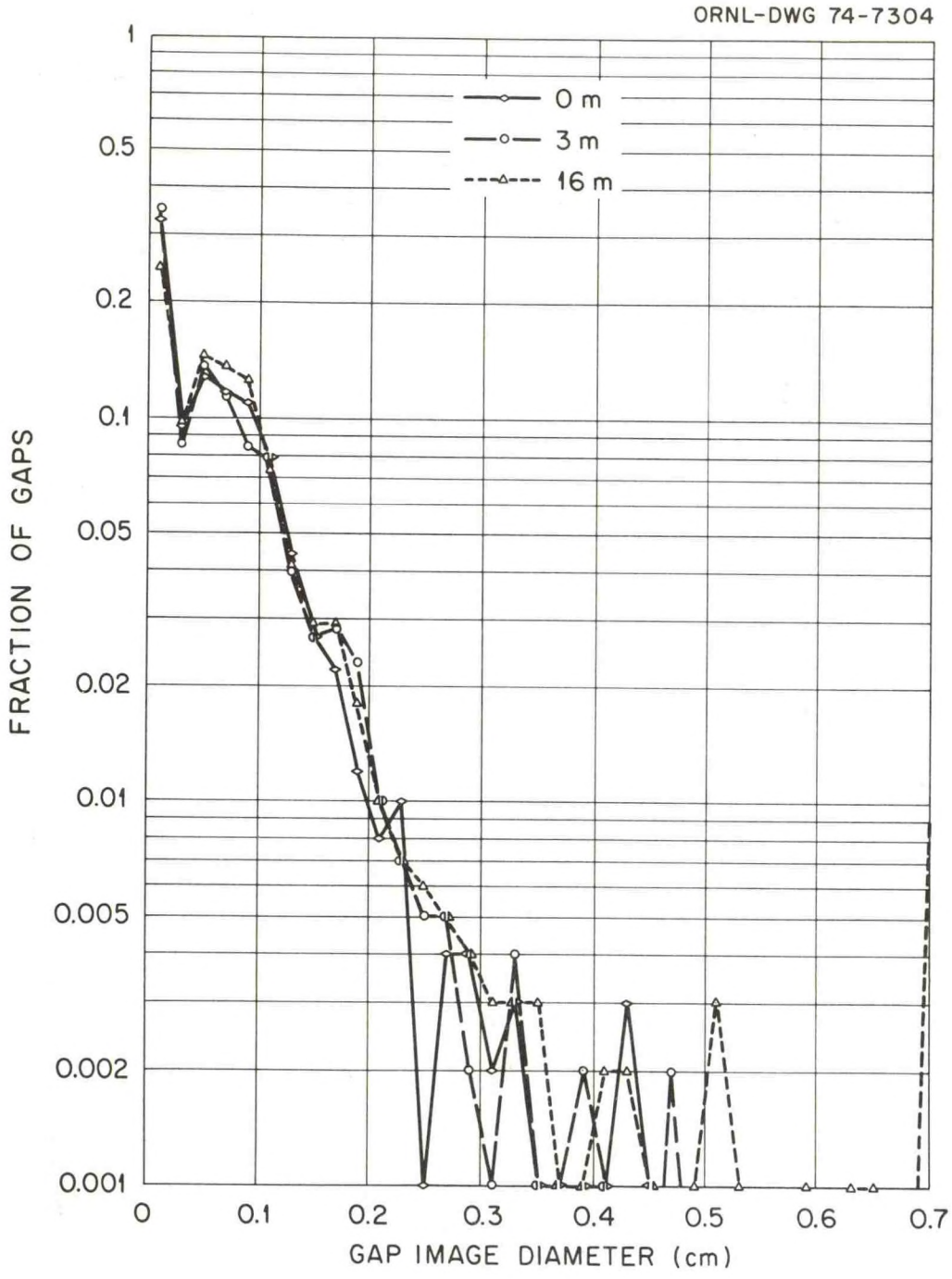


Figure 51: Gap Image Diameter Distribution - Period 2.

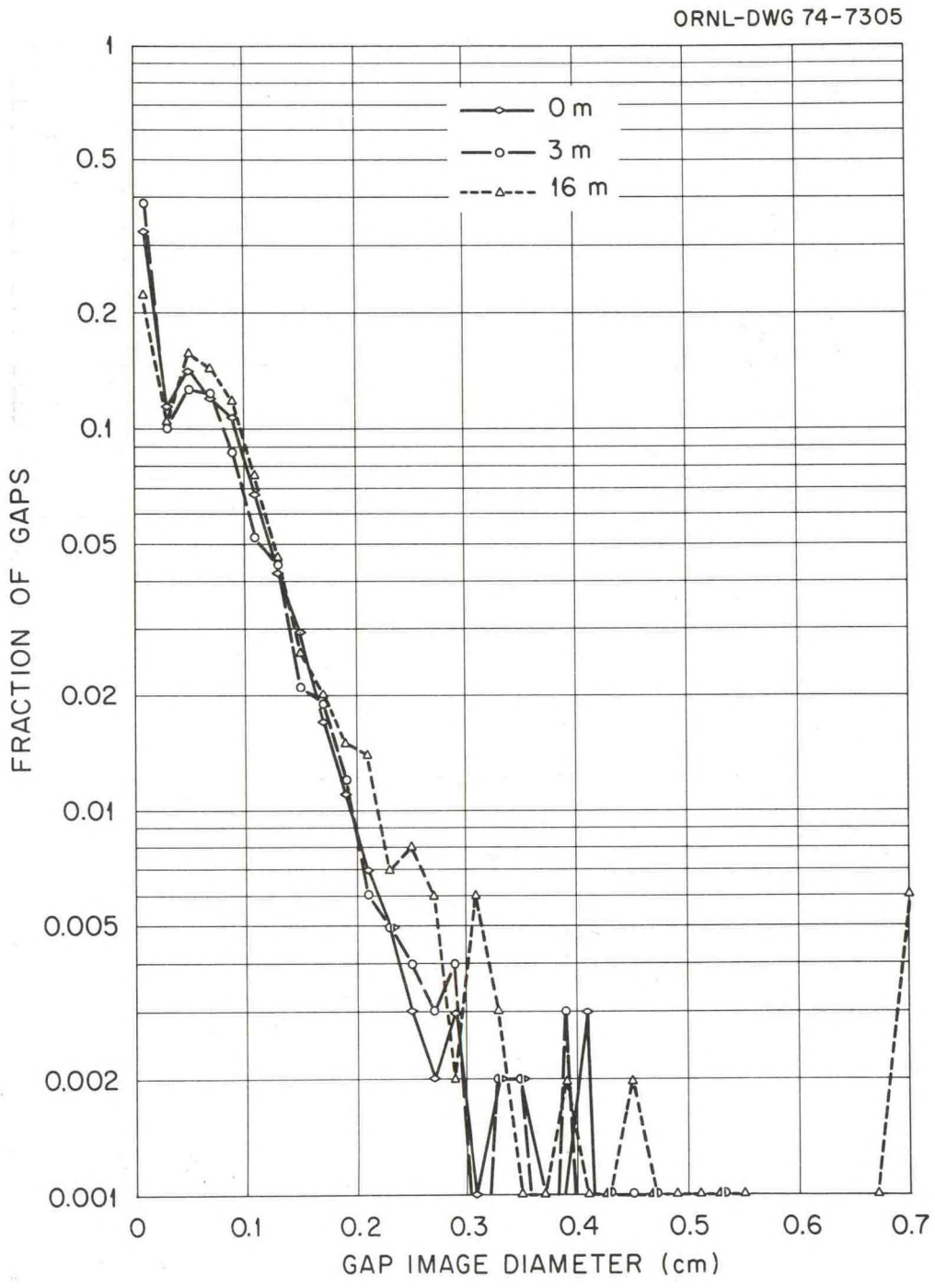


Figure 52: Gap Image Diameter Distribution - Period 3.

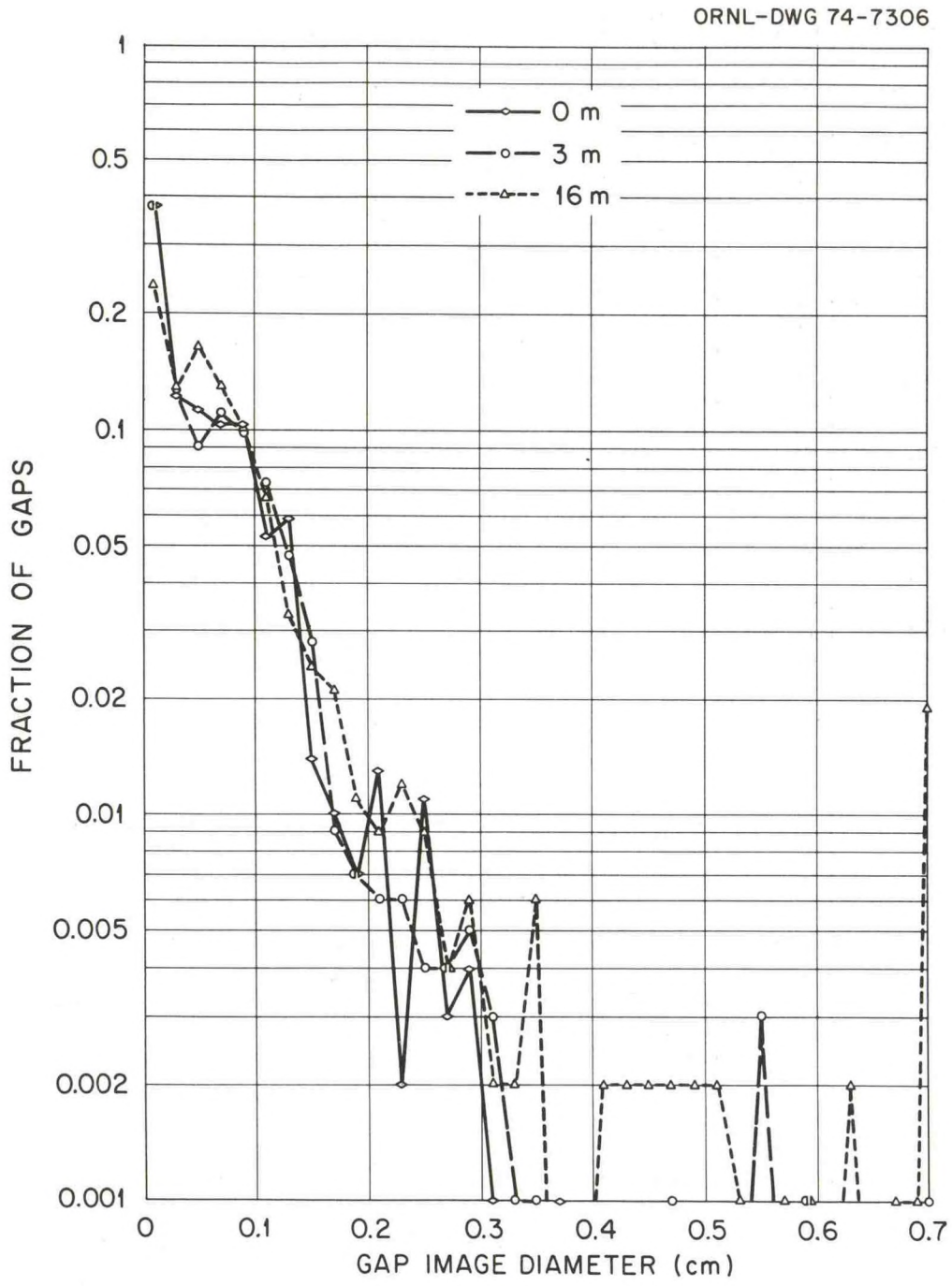


Figure 53: Gap Image Diameter Distribution - Period 4.

at the solar elevation corresponding to period 1. Hence the distribution curves are discontinuous on Figure 50. On Figures 51, 52, and 53, sufficient numbers of gaps are present that the distribution curves produced are reasonably smooth and continuous out to fairly large gap diameters. Surprisingly, little difference is found between gap diameter distributions over height or over time, except for period 1. Relatively large differences in the proportion of gaps contained in size classes occur only in the smallest gap image diameter class (0 to 0.02 cm).

Also, the proportion of openings contained in this class at 3 meters exceeds that at 0 meters which seems unlikely. This reversal in curve position is probably another result of the underexposure of the 3 meter photos which reduces the halo effect on these photos thus reducing the degree of overestimation of gap diameters. Hence more gaps visible from 3 meters fall into this diameter class than at 0 meters where the gaps generally appear somewhat larger owing to the more pronounced halos on the 0 meter photos.

On the scale of the photographs used in this study, the solar disk diameter would appear to be 0.056 cm. Hence it is obvious from these four figures that a considerable fraction of the gaps visible in the forest during all periods appear larger than the solar disk. According to the model under test, this implies that significant amounts of full incident direct beam radiation should penetrate to all levels in the forest on clear days. As will become evident below, this is not observed in the forest.

Using the procedures for deriving sunfleck areas and proportional distributions of direct beam intensities described above in the methods

section, space distributions of direct beam flux densities were predicted from the gap size distributions and plotted for each of the four periods. These predicted distributions are shown on Figures 54 through 57.

Figure 54 shows the predicted space distributions of flux densities at each of the three levels during period 1. At 0 and 3 meters, the entire area is predicted to be irradiated by direct beam flux densities between 0 and 0.1 times that incident upon the forest. Despite the presence of some gaps larger than the apparent diameter of the solar disk, so few openings are present that the degree of canopy opening during period 1 is zero, according to the technique used to estimate this. Hence, $G_{z,\tau} = 0$ in the equation

$$P_{z,\tau} = (A_{\sigma,z,\tau}/A_{g,z,\tau})\ G_{z,\tau} .$$

Therefore, $P_{z,\tau}$, the fraction of area in sunfleck, is zero and the entire area is predicted to fall in the first direct beam flux density class because this class includes the possibility of no direct beam radiation. Only at 16 meters is there any area predicted to receive direct beam radiation at higher flux densities than 0 to 0.1 times incident but, in total, this amounts to less than 2 percent of the total area. Hence the model predicts little direct beam radiation at any level in the forest during period 1.

Throughout the other three periods, by far the greatest fractional area is predicted to be irradiated by 0 to 0.1 times the incident direct beam radiation as shown on Figures 55, 56, and 57. A sharp decline in the fractional area contained is predicted in the 0.1 to 0.2 class over that contained in the 0 to 0.1 class at all levels

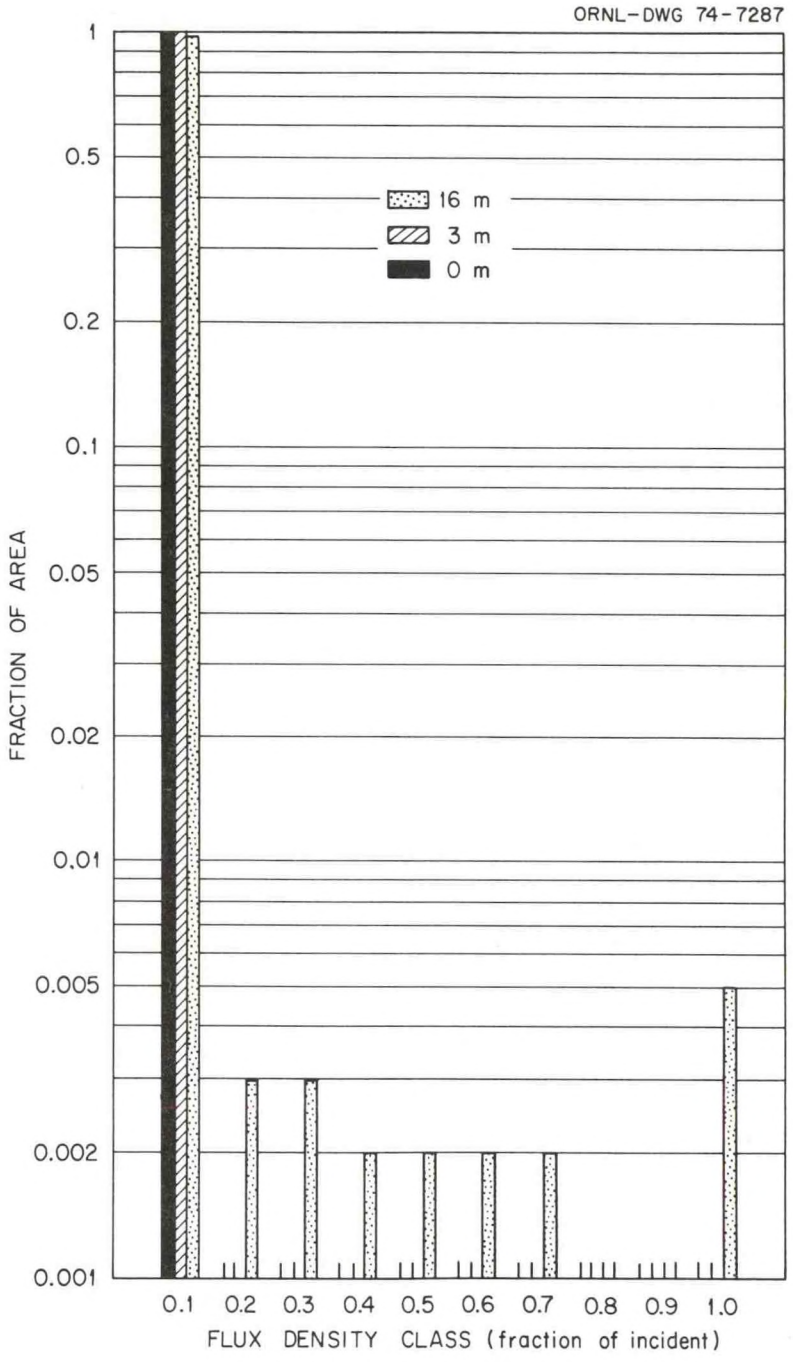


Figure 54: Predicted Space Distribution of Direct Beam Flux Densities During Period 1.

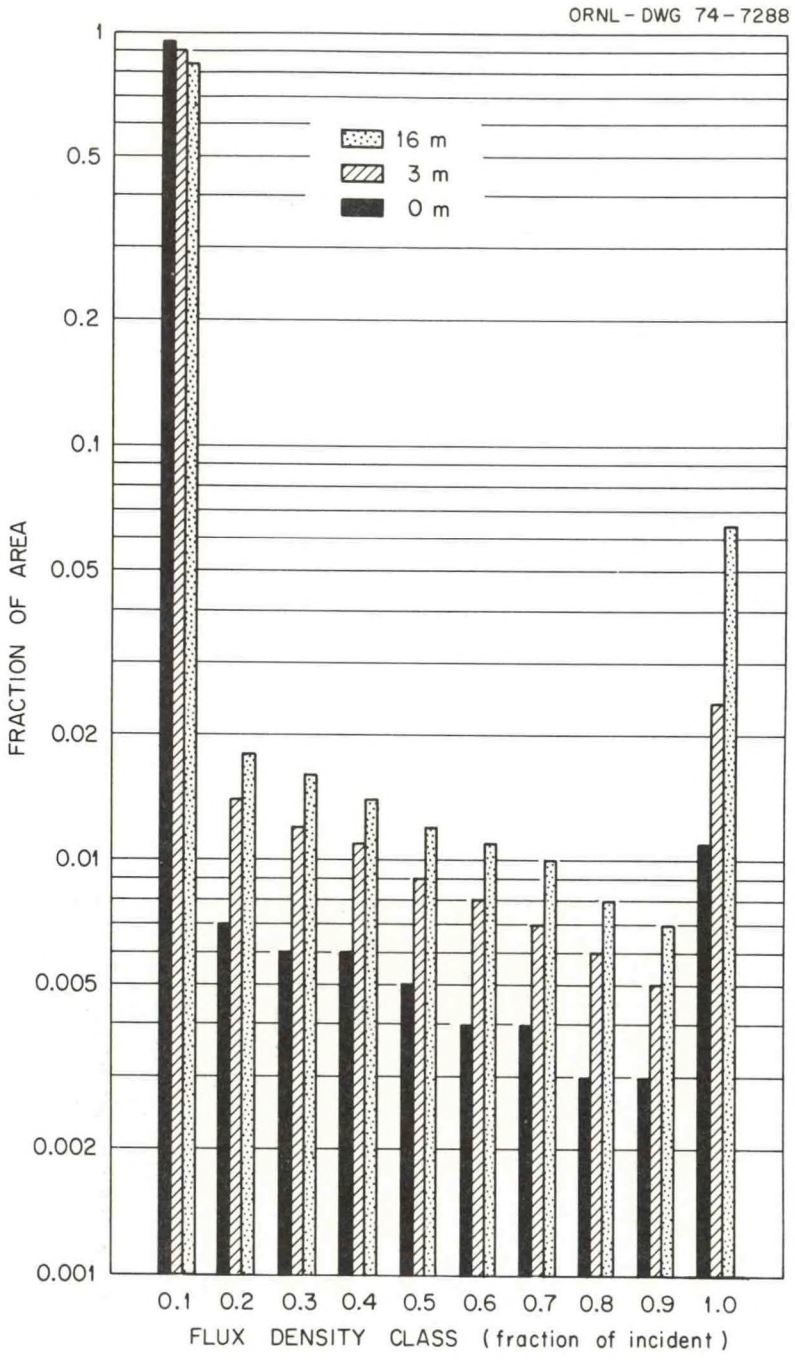


Figure 55: Predicted Space Distribution of Direct Beam Flux Densities During Period 2.

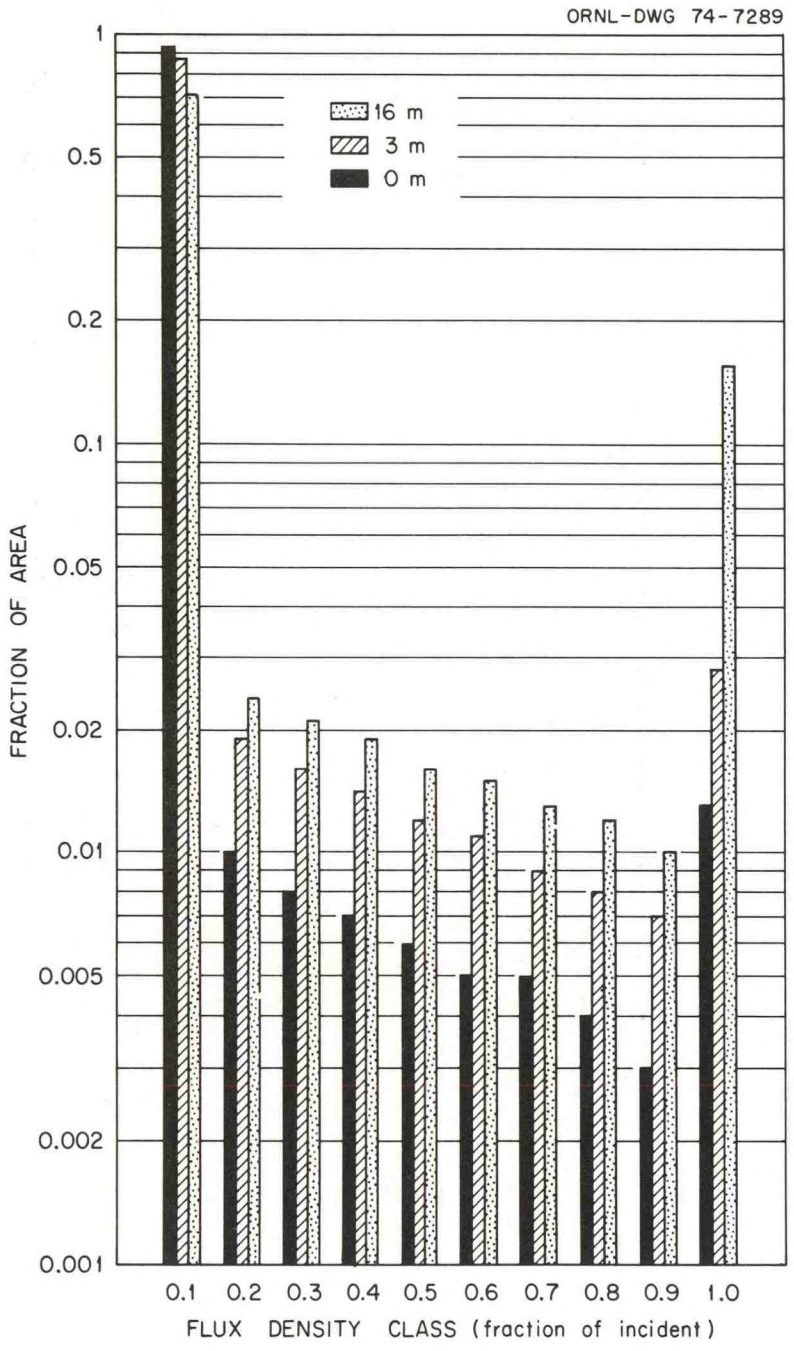


Figure 56: Predicted Space Distribution of Direct Beam Flux Densities During Period 3.

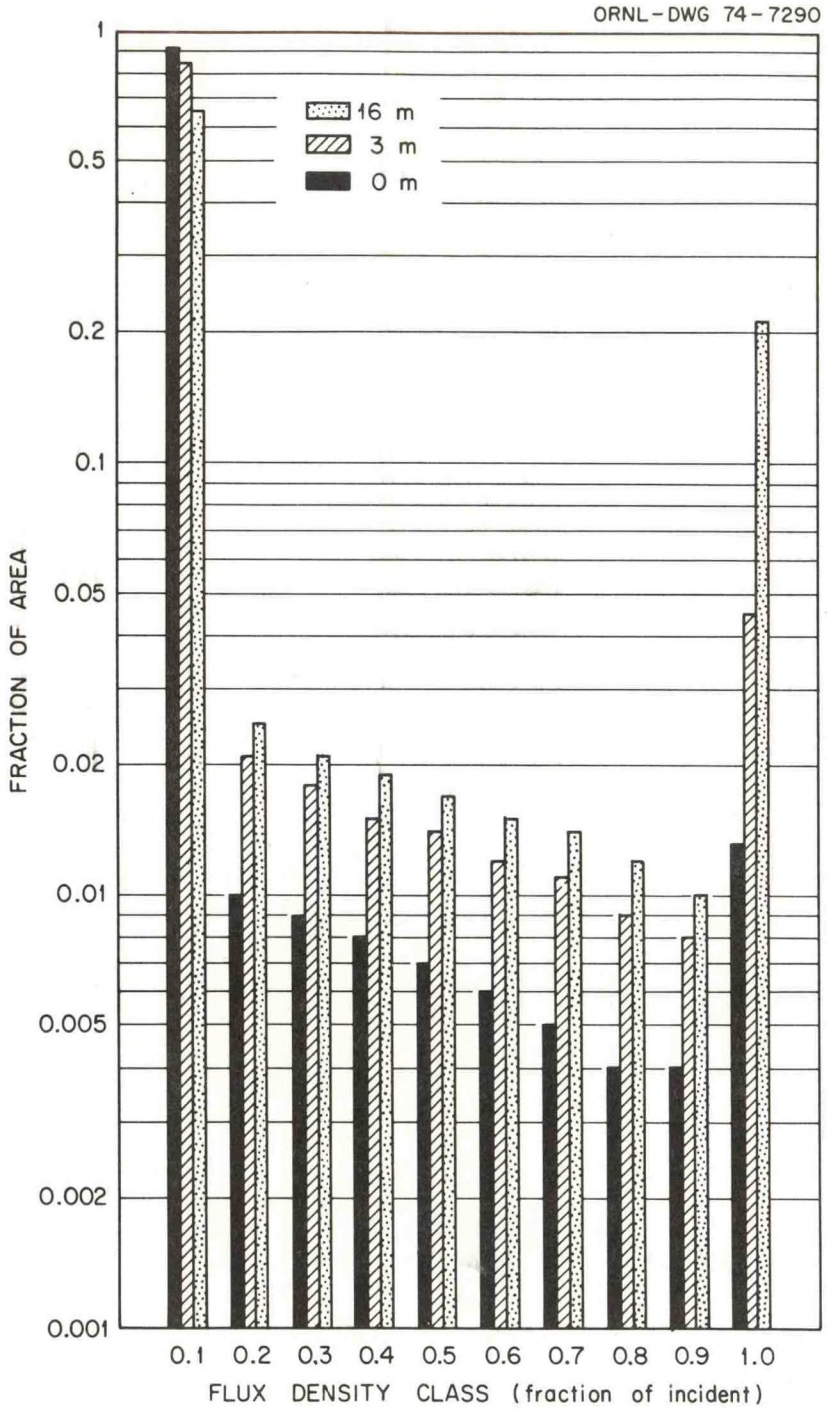


Figure 57: Predicted Space Distribution of Direct Beam Flux Densities During Period 4.

during each of these three periods. From 0.2 to 0.9 times the incident direct beam radiation, a further, gradual decline in fractional area is predicted and a secondary mode in the 0.9 to full incident direct beam radiation class is indicated at all levels in each of these three periods. This secondary mode reflects the significant fraction canopy openings having diameters which appear much larger than that of the solar disk.

Figures 58 through 69 present the observed space distributions of direct beam flux densities by periods for the two clear days of June 8 and 14, 1972, and for the partly-cloudy day of June 26, 1972. Comparison of the figures representing each of the four periods on these three days shows that no characteristic difference in the space distribution of direct beam flux densities present in each period are apparent among these three days. Thus, for purposes of discussion of direct beam penetration, these three days will be considered as being similar.

Comparison of Figure 54, the predicted period 1 space distributions of direct beam flux densities with Figures 58, 59, and 60, the observed period 1 space distributions on June 8, 14, and 26, 1972, indicates reasonable agreement between prediction and observation. Only on June 26 (Figure 60) is there any appreciable amount of direct beam irradiation in classes above the 0 to 0.1 times incident and then, only at the 16 meter level. Slightly more than 20 percent of the area is shown to have been irradiated by direct beam flux densities in excess of one-tenth of the amount incident upon the forest. Reasons for this difference are not apparent.

Figures 61, 62, and 63 present the observed space distributions

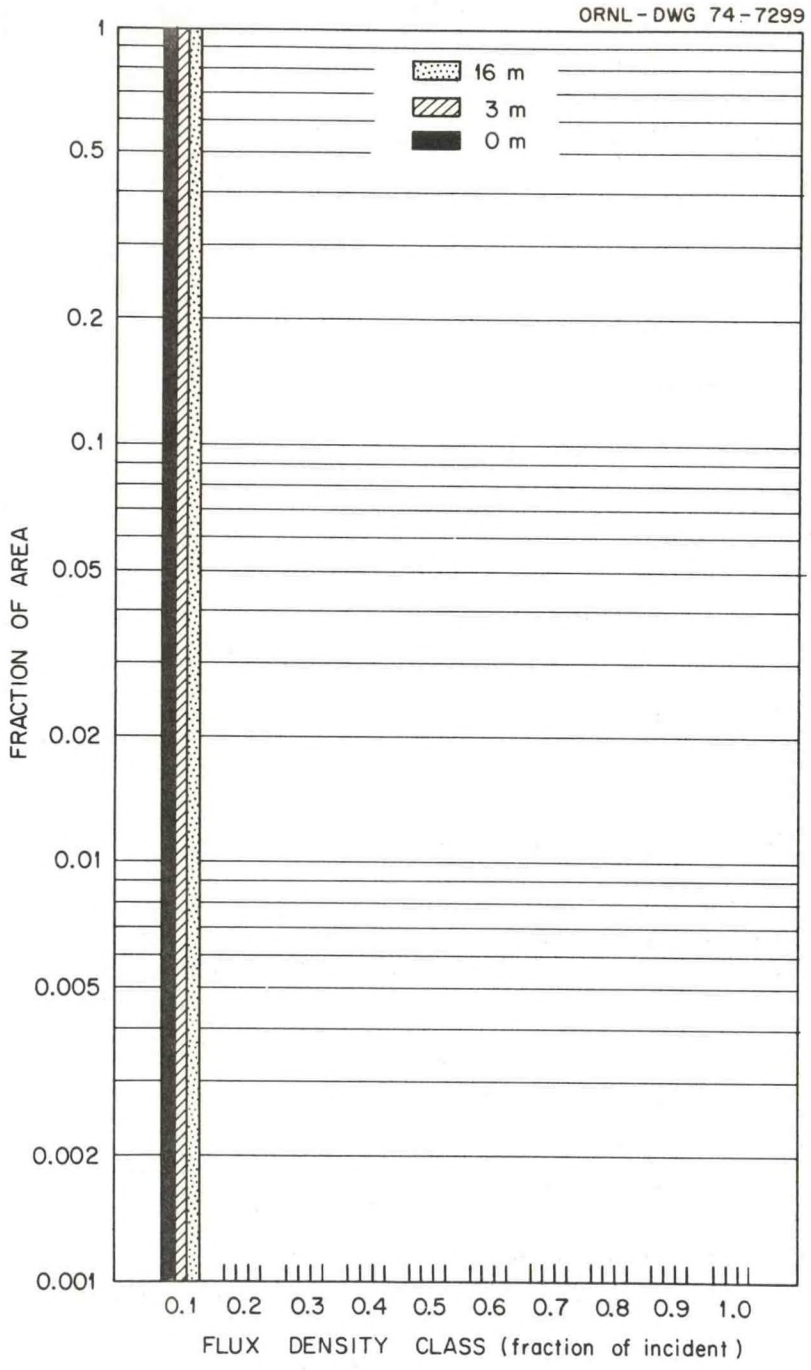


Figure 58: Observed Space Distribution of Direct Beam Flux Densities During Period 1 on June 8, 1972.

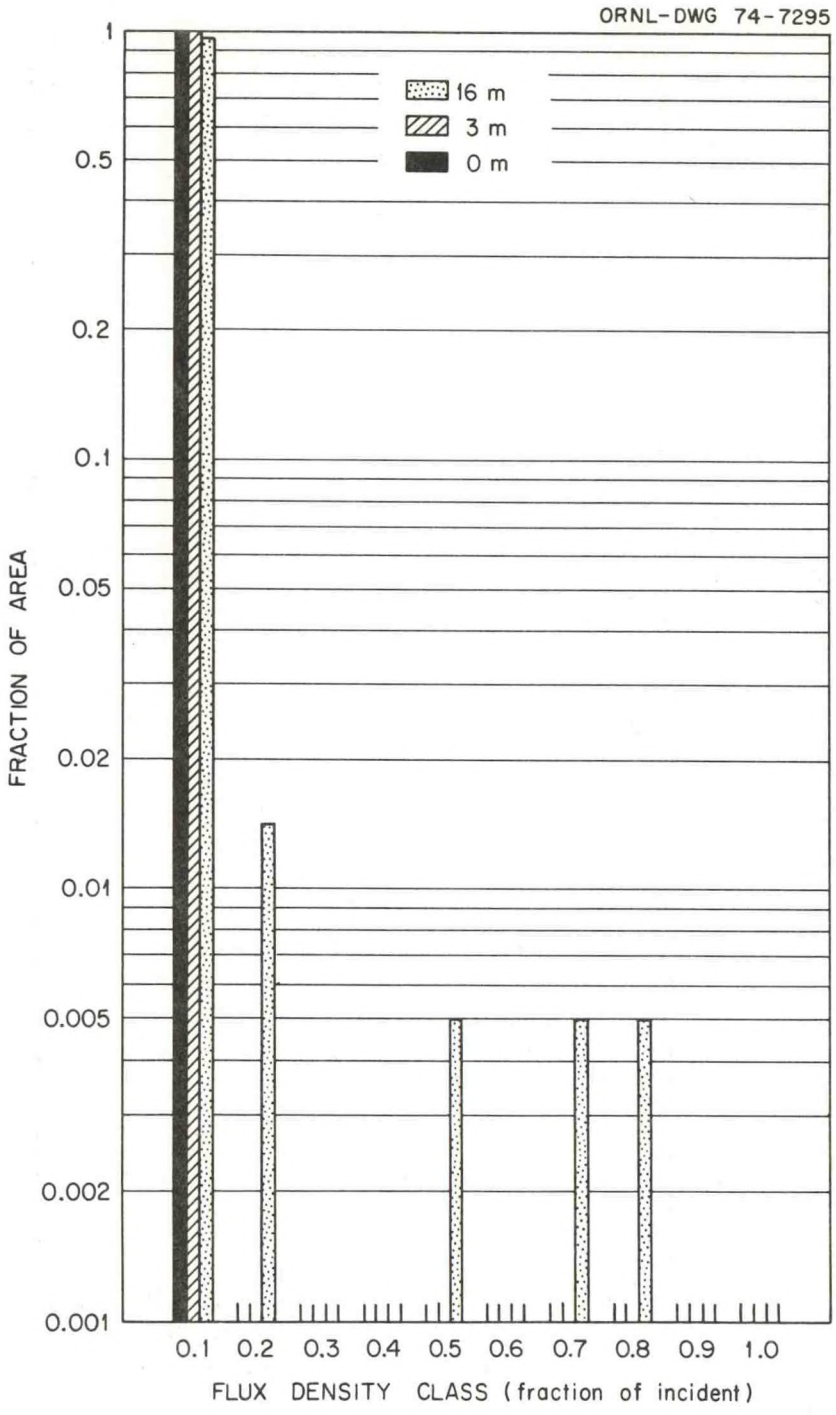


Figure 59: Observed Space Distribution of Direct Beam Flux Densities During Period 1 on June 14, 1972.

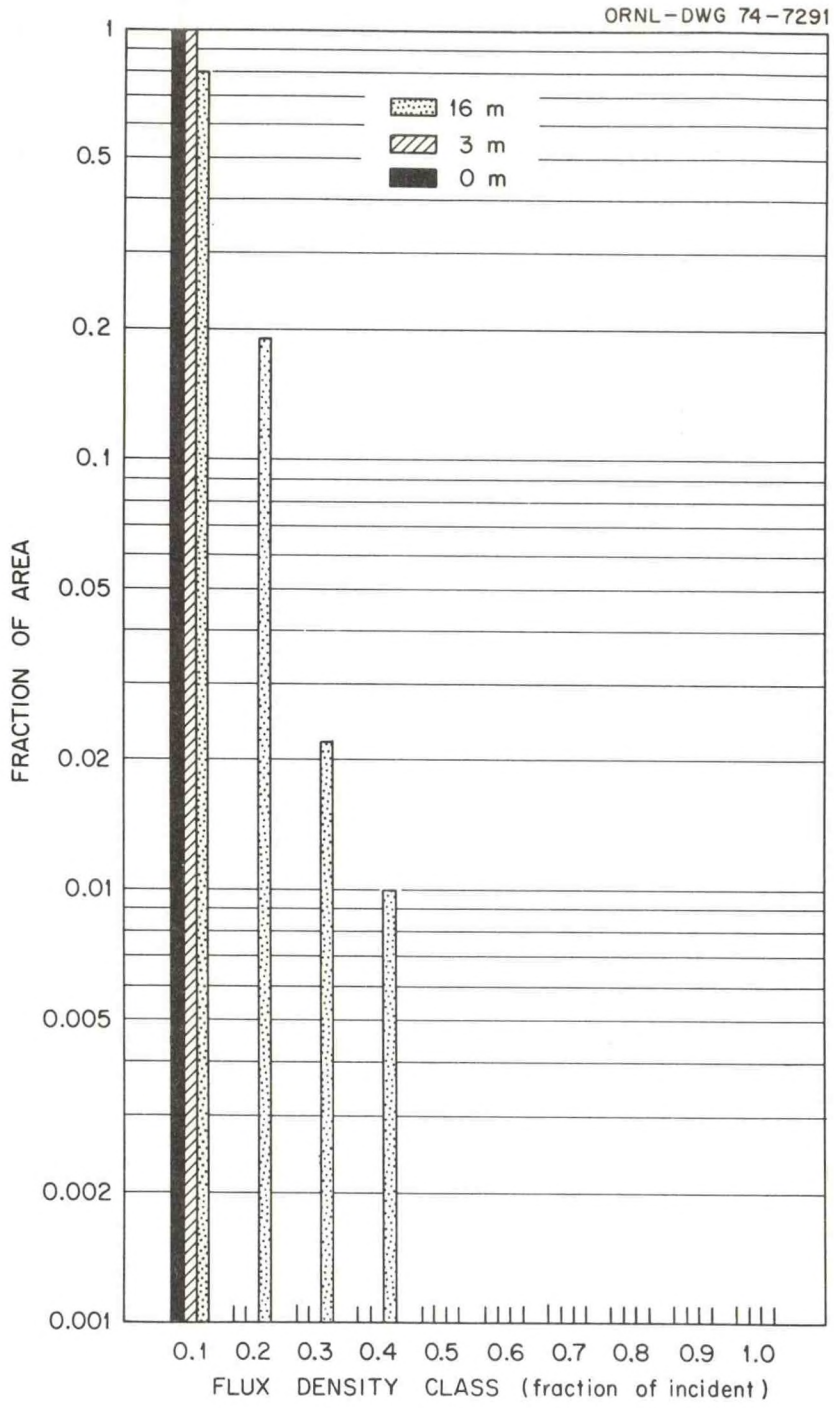


Figure 60: Observed Space Distribution of Direct Beam Flux Densities During Period 1 on June 26, 1972.

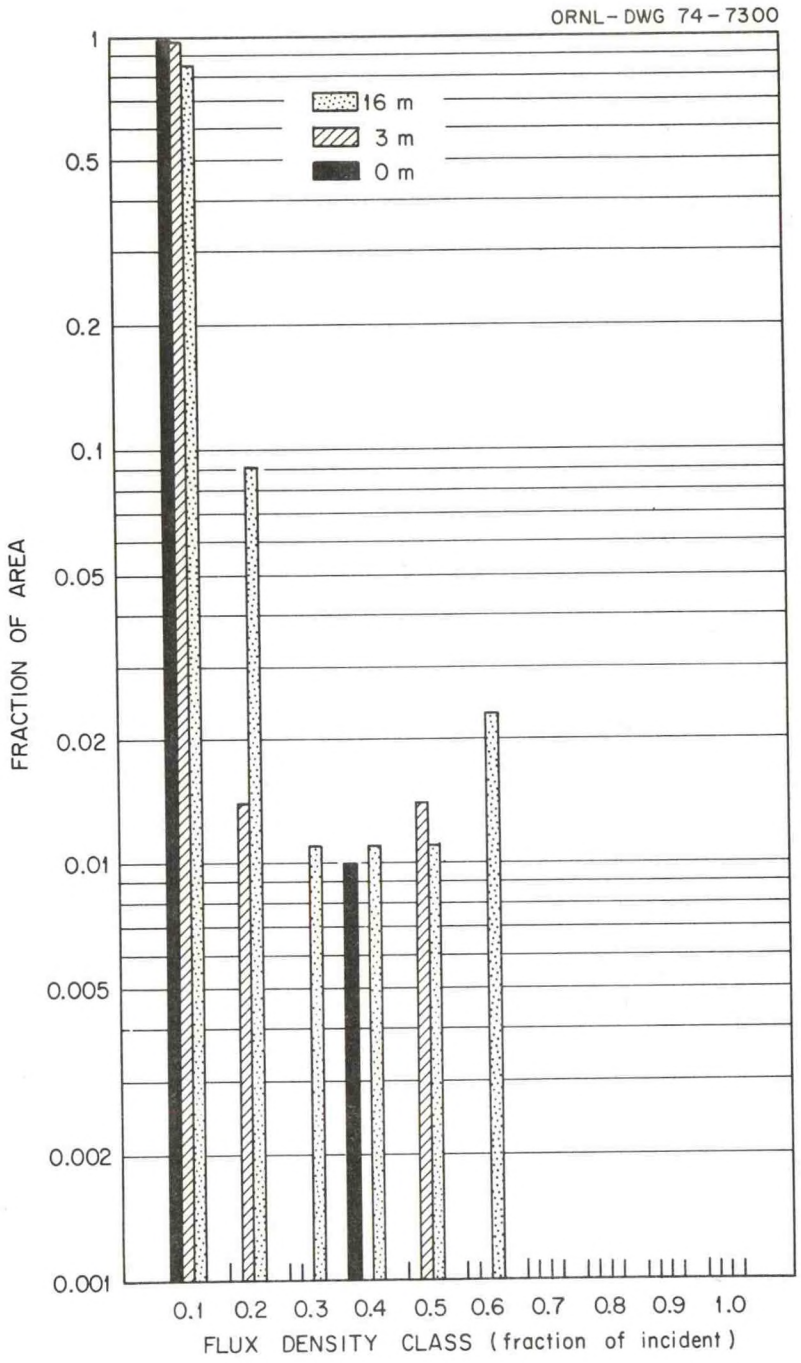


Figure 61: Observed Space Distribution of Direct Beam Flux Densities During Period 2 on June 8, 1972.

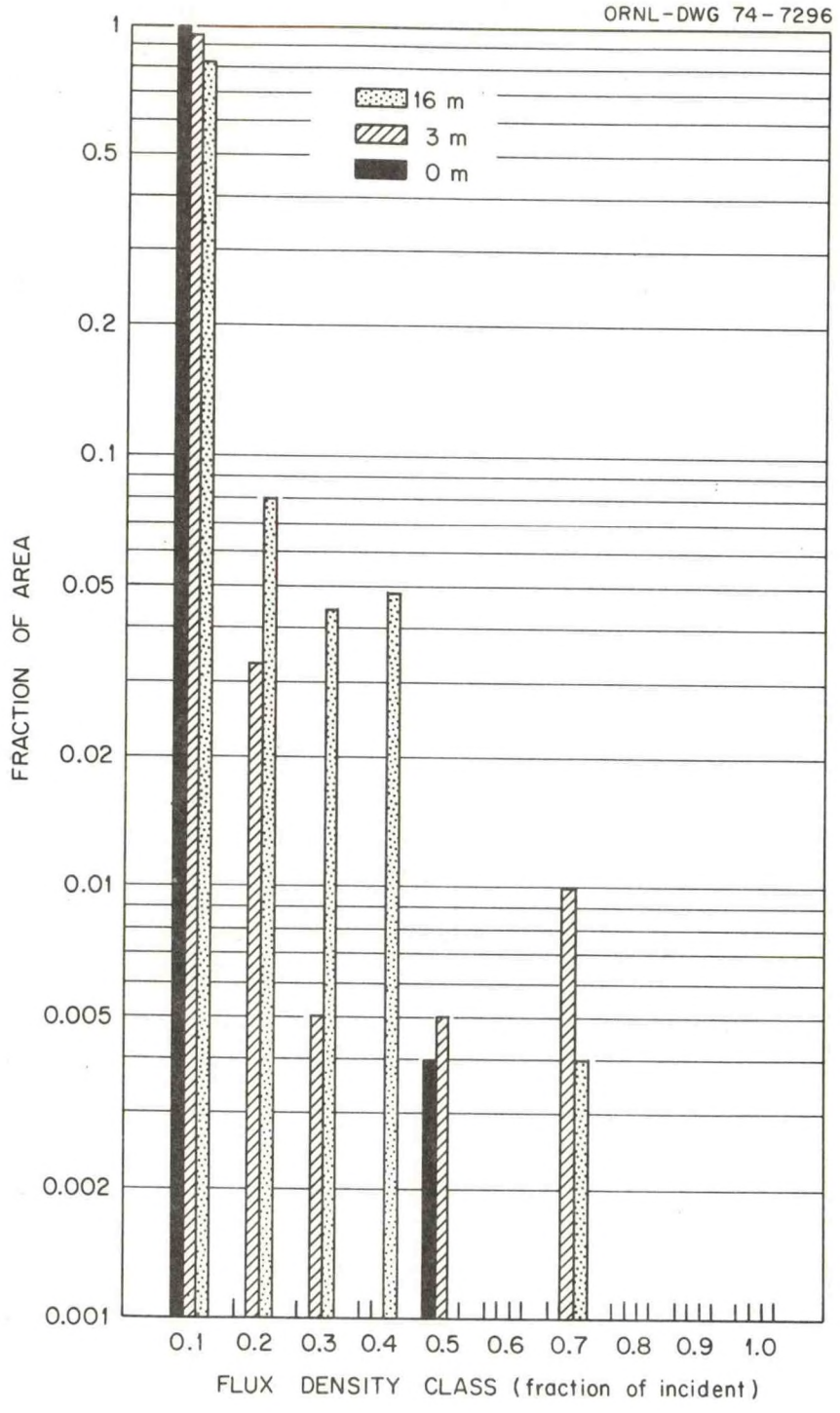


Figure 62: Observed Space Distribution of Direct Beam Flux Densities During Period 2 on June 14, 1972.

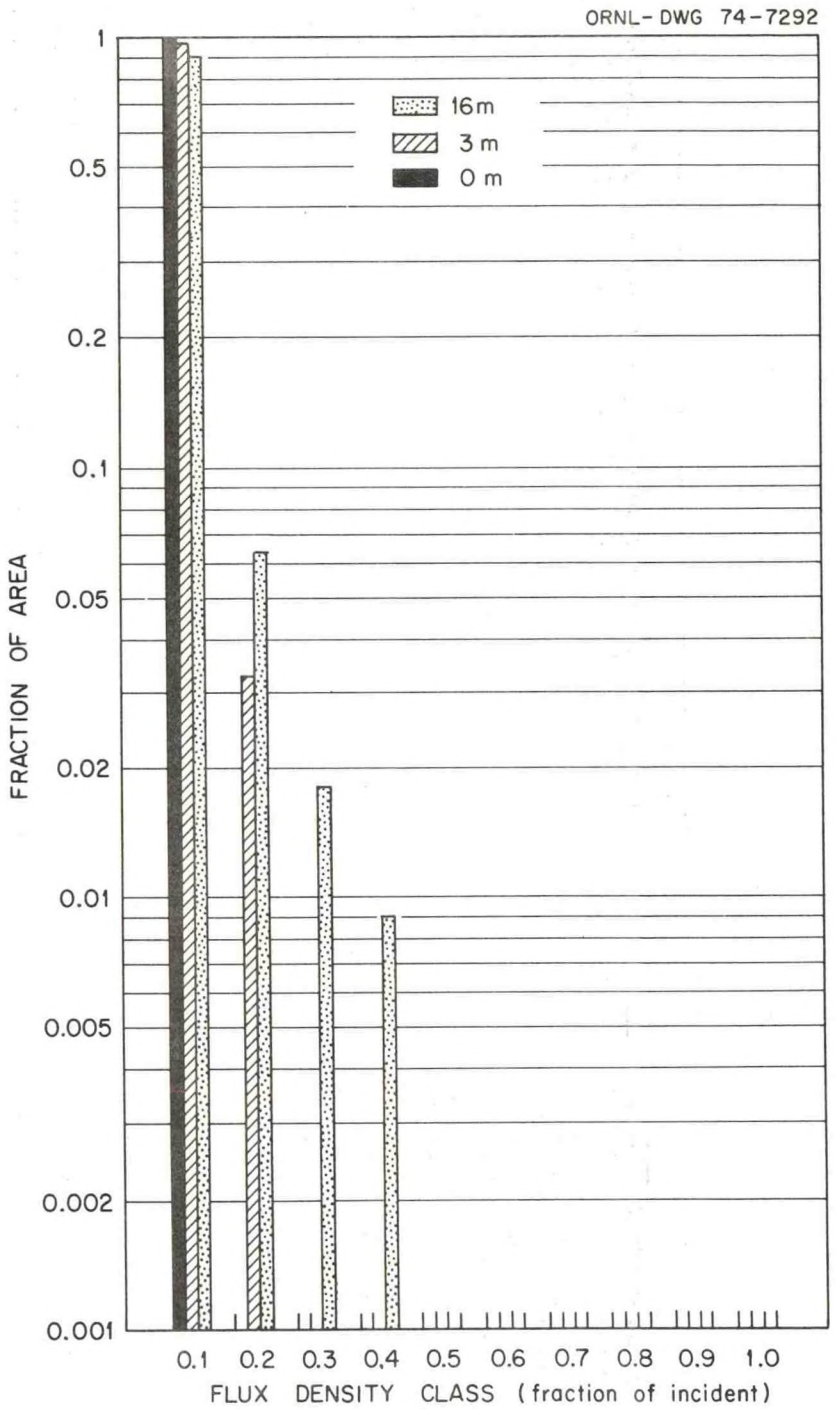


Figure 63: Observed Space Distribution of Direct Beam Flux Densities During Period 2 on June 26, 1972.

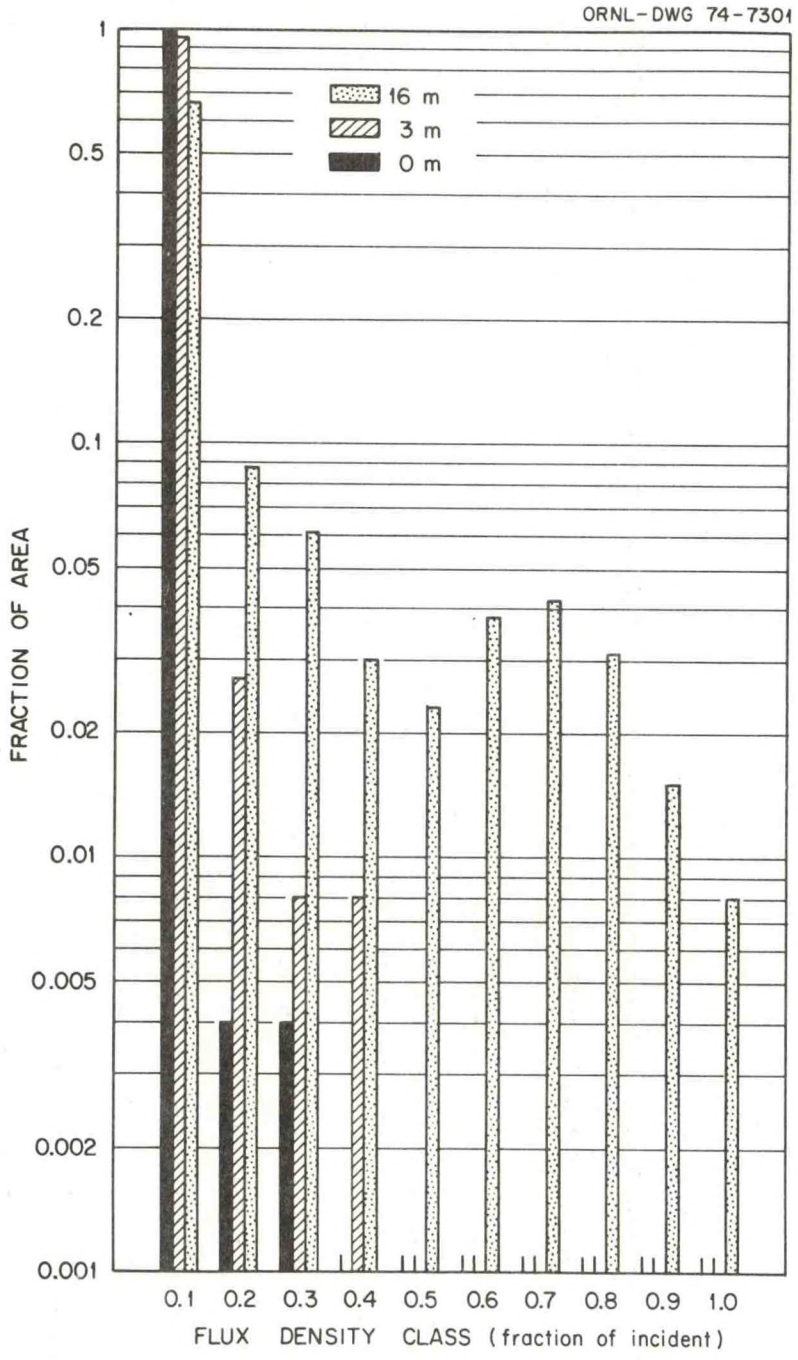


Figure 64: Observed Space Distribution of Direct Beam Flux Densities During Period 3 on June 8, 1972.

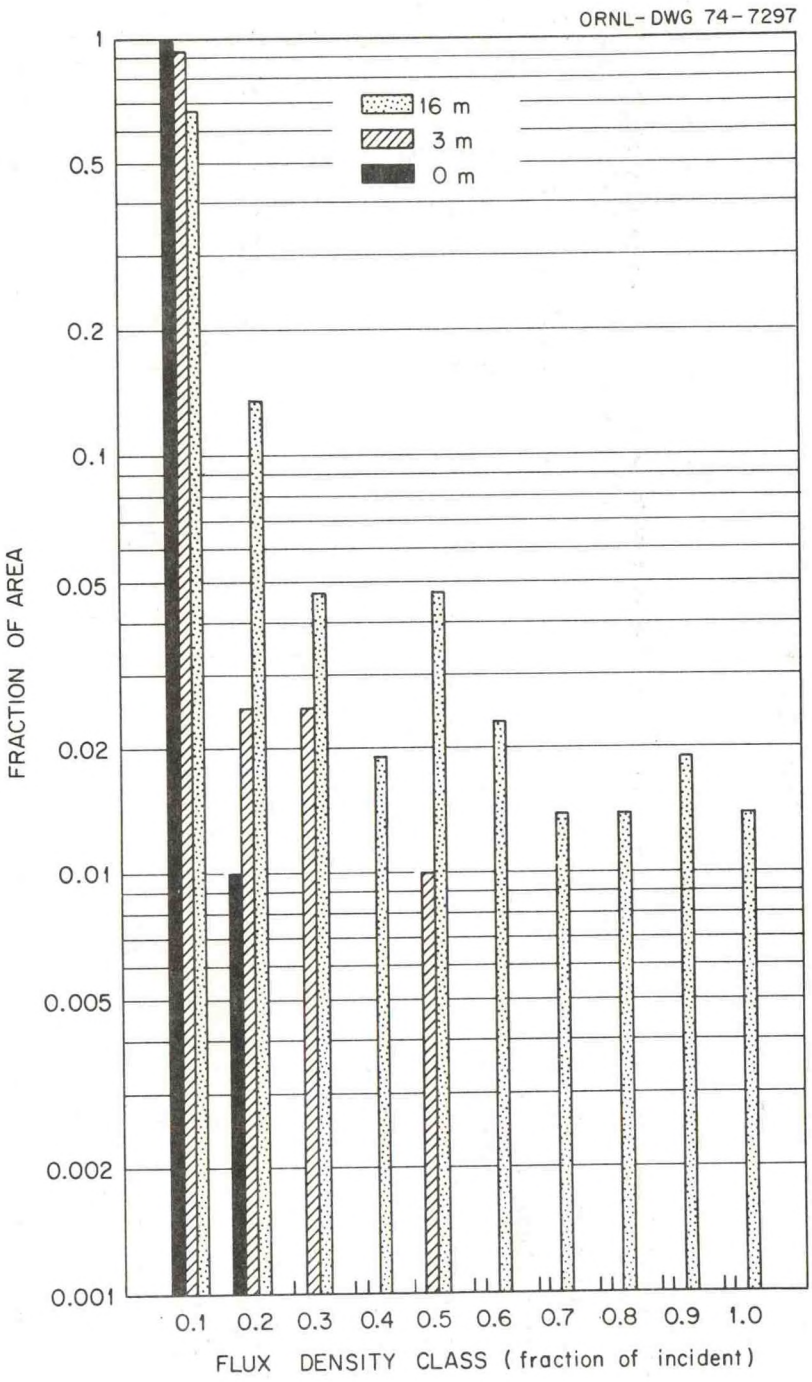


Figure 65: Observed Space Distribution of Direct Beam Flux Densities During Period 3 on June 14, 1972.

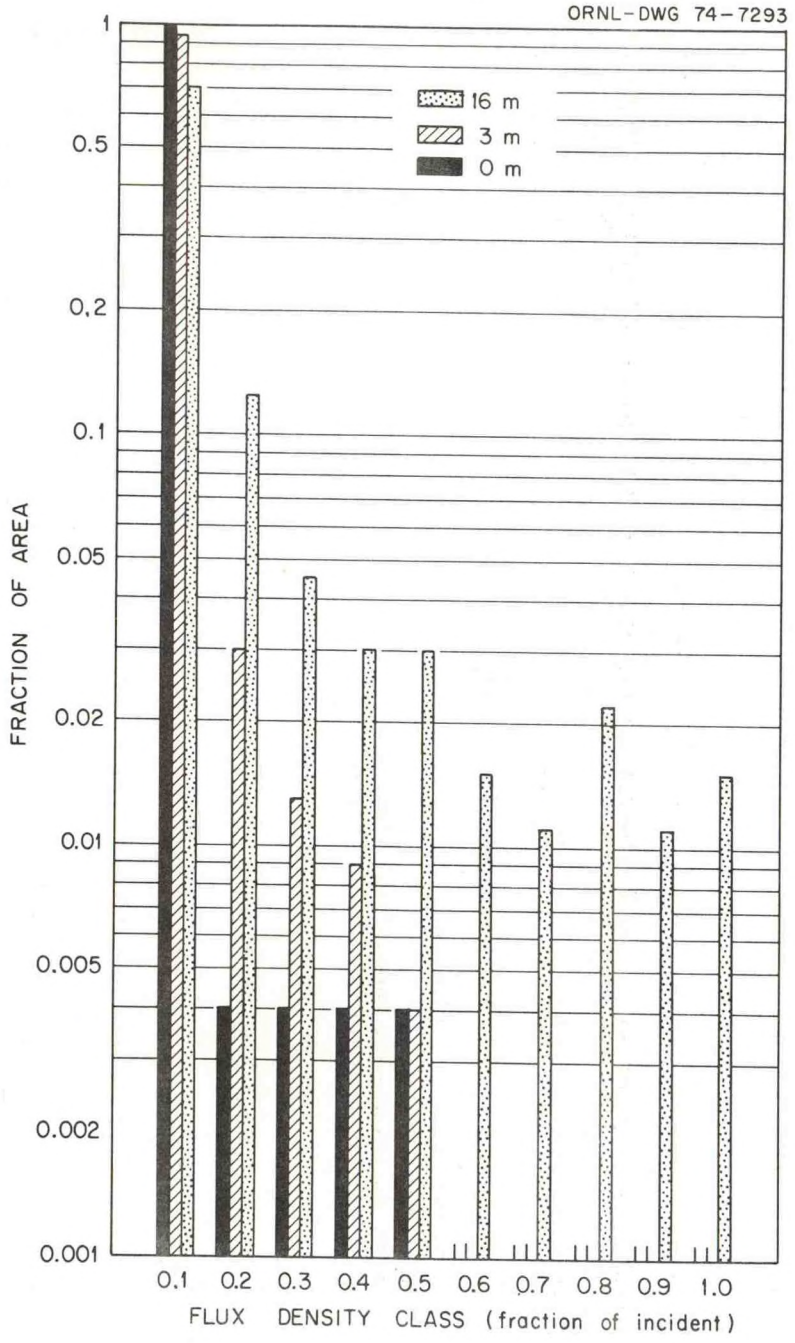


Figure 66: Observed Space Distribution of Direct Beam Flux Densities During Period 3 on June 26, 1972.

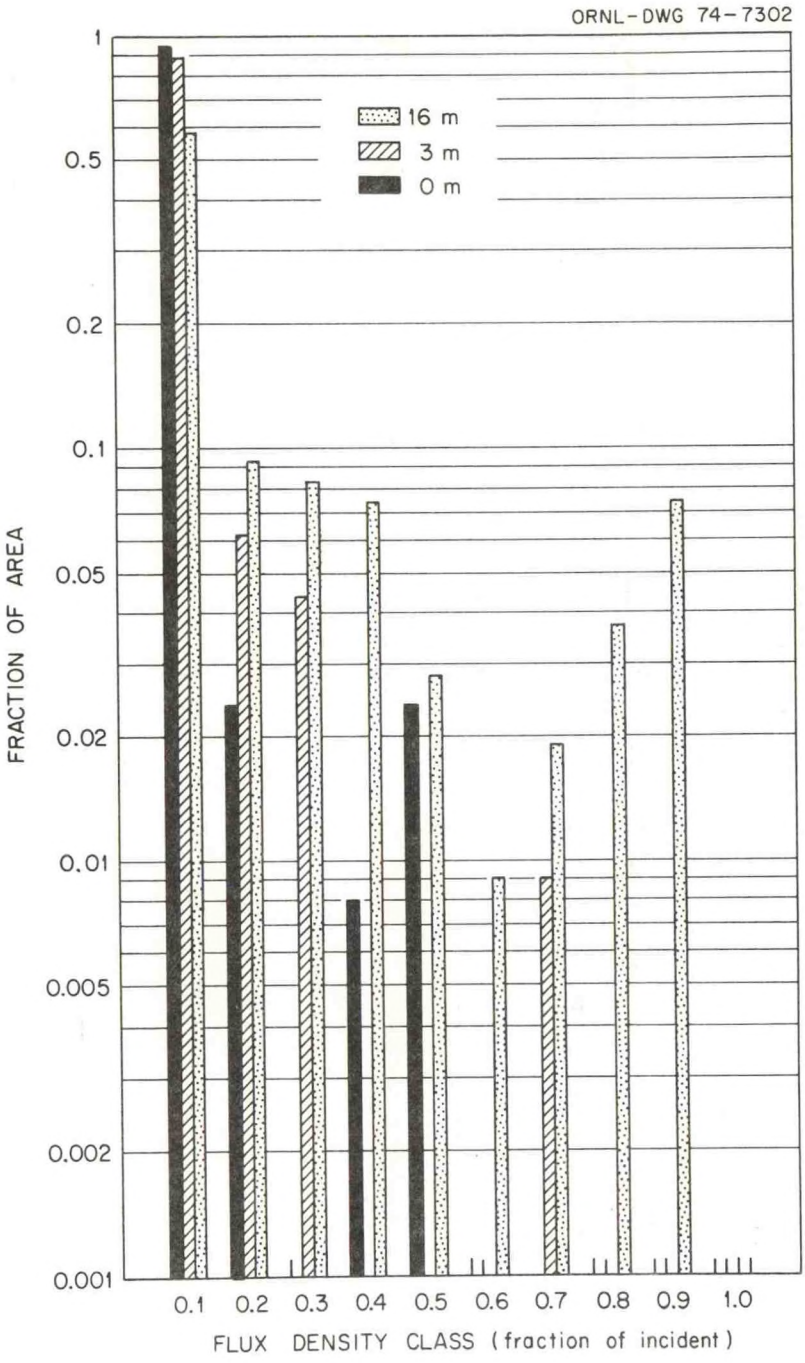


Figure 67: Observed Space Distribution of Direct Beam Flux Densities During Period 4 on June 8, 1972.

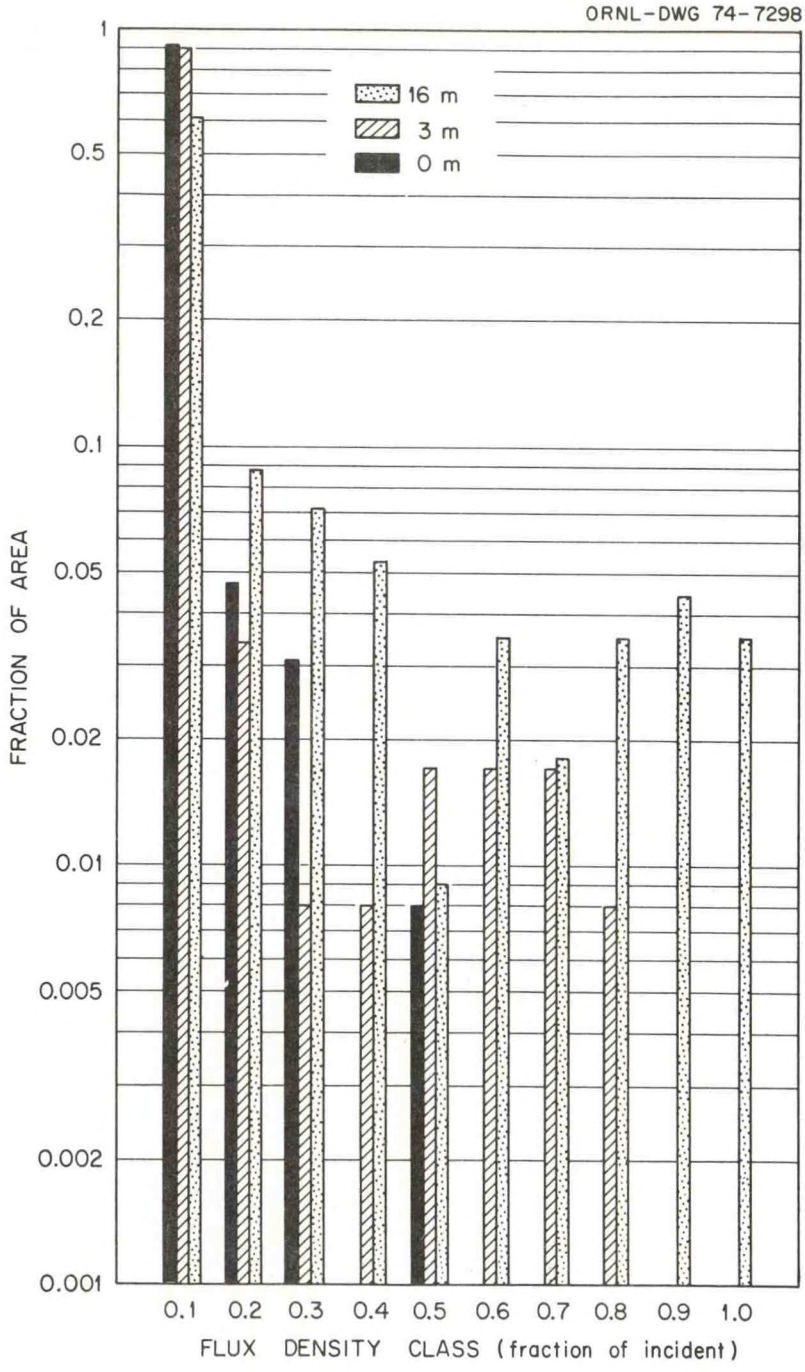


Figure 68: Observed Space Distribution of Direct Beam Flux Densities During Period 4 on June 14, 1972.

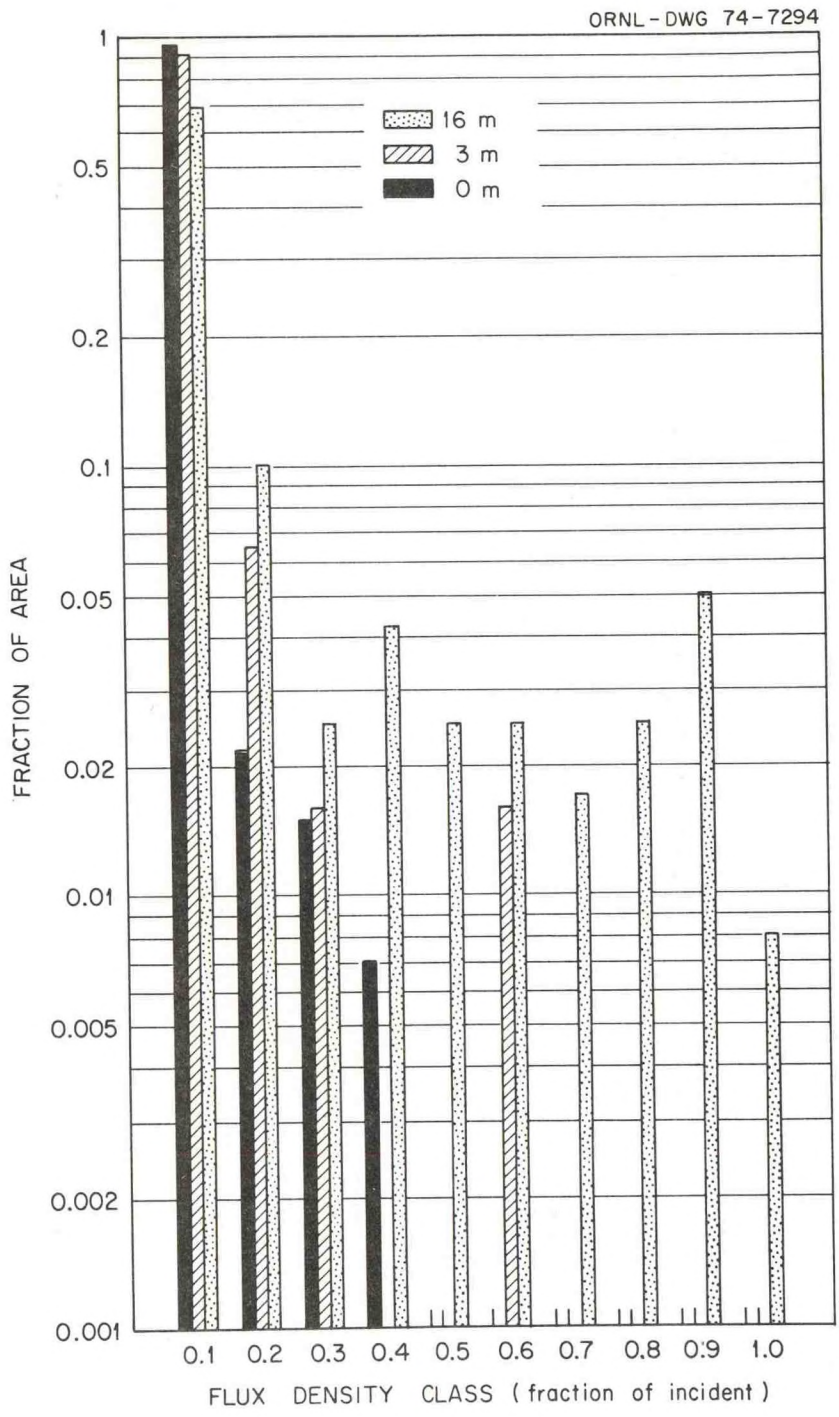


Figure 69: Observed Space Distribution of Direct Beam Flux Densities During Period 4 on June 26, 1972.

for these same days during period 2. Comparison of these figures with Figure 55, the predicted distributions during period 2, shows that the predicted bimodality of Figure 55 is not evident in the observed data as shown on these three figures. The observed distributions drop to zero at low flux densities and no secondary mode is present. Furthermore, the fractional areas observed in the first four direct beam classes is greater than is predicted, especially at 3 and 16 meters. During period 3, comparison of observation (Figures 64, 65, and 66) with prediction (Figure 56) indicates behavior similar to that of period 2.

Only during period 4 is there any evidence of bimodality in the observed data (Figures 67, 68, and 69) and then only at the 16 meter level. The predicted secondary mode always falls in the tenth and highest flux density class. On the other hand, the observed secondary mode at 16 meters on Figures 67, 68, and 69 occurs consistently in the 0.8 to 0.9 times incident flux density class.

From these comparisons it is obvious that the techniques used to calculate sunfleck dimensions yield results which overestimate the area at each level irradiated by full incident direct beam and underestimate penumbral areas. Three factors may combine to cause this behavior of the assessment technique.

First, the assumption of circular canopy openings may be involved since an irregularly shaped opening of a given area will tend to produce a sunfleck with proportionally more penumbral area and less full sun area than a circular opening of equal area. It appears that accurate characterization of sunflecks produced by irregularly shaped openings would be exceedingly difficult because the real shapes of

canopy gaps are complex and because of the distortion of image shapes produced by the Hill lens. Although the equidistant projection yields an image where a given radial increment represents an arc segment of equal length no matter where the radial increment is situated on the photo, the dimension of the image transverse to the photo radius is lengthened from the center of the photo to the edge. That is, a circle at the center of a photo obtained using a lens producing an equidistant projection would appear as a circle. This same circle at the edge of the photo would appear as an ellipse with the length of the minor axis equal to the diameter of the circular image when at the center of the photo. The major axis of this ellipse would be $\pi/2$ times the diameter of the circular image. This problem might be circumvented using a photo densitometer to obtain measurements of the shapes and sizes of canopy gaps and through development of computer programs which would correct the dimensions for radial position on the photo and calculate sunfleck dimensions produced.

The second factor that may be involved here is a further limitation of the photographic assessment approach. I have assumed that all canopy gaps are centered at one of these discrete levels in the forest and furthermore that each gap is bounded on all sides by foliage at this level. Actually the gaps are continuously distributed with height and may be bounded on different sides by foliage at different heights. I can see no possibility of accurately characterizing the vertical distribution of gap boundaries from photographs. Hence, if this source of error is significant, the use of the photographic approach for predictions of space distributions of direct beam flux densities is

probably impossible. However, further study is needed at this point to establish the significance of errors arising from this source.

Finally, the problems of nonuniform photo exposure may also be involved here. Because of the extreme contrast between foliage in the forest and that in the top of the canopy in full sun, an area of illuminated foliage may appear as a gap on a photo obtained at some level below unless the photo is severely underexposed. Hence, some apparent openings visible on the photos used may actually be foliage in the upper canopy that is receiving full illumination from the overcast sky (all photos were obtained on overcast days). Furthermore, the halo effect may also be involved here. Although the halo effect would lead to minimal errors of overestimation of gap dimensions with larger openings, another source of error may be involved. Consider a large opening that is partially obscured by illuminated foliage beyond the gap. Because of the degree of contrast and the halo effect, a larger, partially occluded gap may actually appear as a large gap with no occlusions. Again, the use of substantially underexposed photos for this portion of the analysis should minimize this source of error.

## Summary and Conclusions

To summarize, these assessment techniques predict clear to partly-cloudy day radiation regimes in the forest which do not agree well with observed regimes. Predicted sums of penetrating, transmitted, and down-reflected diffuse radiation are generally overestimated and the degree of overestimation increases with depth in the forest and with time toward solar noon. The predicted enrichment of diffuse radiation in the forest by transmitted and down-reflected radiation is, on the

other hand, generally underestimated and here the degree of underestimation decreases with depth in the forest while the relative amount of underestimation increases toward solar noon. The total amount of diffuse radiation reaching a level in the forest is represented by the sum of these two groups of components. Comparison of these sums of predicted values with those observed in the forest shows that the predicted diffuse radiation exceeds that measured at 0 meters but becomes increasingly less than that observed at higher levels.

On overcast days, the predicted values are always greater than those observed in the forest but only the 0 meter level exhibits serious disagreement. Estimated values for both the 3 and 16 meter level approximate the observed values to a fair degree.

With the space distribution of direct beam radiation, the predicted distributions extend to higher values than those observed while the mid-range flux density classes are underestimated.

Defects of the forest radiation model developed in this study along with limitations of the photographic assessment approach are thought to be involved in the overall disagreement between prediction and observation. One weakness of the model used involves the assumption of a constant proportion of down-reflected radiation. This proportion, for direct beam radiation at least, must vary with height in the forest since leaf inclination angles vary with height and with time owing to the changing angles of incidence of the solar beam.

Major limitations of the photographic assessment of canopy structure include the problem of limited contrast latitude of photographic emulsions, the inability to accurately assess canopy density, i.e., number of leaf layers in canopy which strongly control the

amount of radiation reaching a level through transmission of radiation through leaves, and the inability to derive height distributions of leaf inclination angles which affects the amount of radiation that is reflected downward into the forest.

The problems engendered by photo exposure seemingly could be avoided in the future by obtaining two sets of canopy photos for each level of interest. One set should be severely underexposed and used for the estimation of the degree of canopy opening and the determination of the size distribution of canopy gaps. The other set should be exposed to yield maximum canopy detail and used for the estimation of parameters needed for the prediction of the transmitted and down-reflected enrichment of diffuse radiation at any level.

Further field study is needed of the relative importance of transmitted and down-reflected radiation in the forest. The actual transmissivities and reflectivities of leaves of the tree species comprising the forest should be measured and used in the model presented here rather than average values for deciduous species as were used here.

With regard to the penetration of direct beam radiation, other deficiencies exist in the model as presented here. These include the assumption of circular canopy openings and the assumption that such openings are situated entirely at one of three discrete levels in the forest. The relative significance of these two sources of error cannot be assessed with the data at hand but my feeling is that the former is the more important. Again, the problems of photo exposure as described previously are involved here as well as the image distortion produced by the Hill lens.

Originally I had planned to compare the results of this assessment technique with those obtained driving the model with values derived from a densiometric analysis of the canopy photos. This would have allowed quantification of error arising from observer bias. This proved unfeasible since the only photodensitometer in the Oak Ridge area was unavailable for my use at the time I made these analyses. Hopefully this test of the model and measurement techniques will be made at some future time.

The possibility of characterizing shapes as well as sizes of canopy gaps from photodensiometric data is an important direction for future work of this nature and may allow quantification of the magnitude of error associated with the assumption of circular canopy gaps.

To conclude, this model and assessment technique attempts to predict height and time variations in the radiation regimes of a summer, deciduous forest within a single day. While the predicted regimes do not agree well with those observed in the forest, modification of the model and of the analytical techniques suggest themselves which may improve the predictive capability of this approach. The ability of the photographic approach to predict mean radiation conditions in forests for longer periods of time is well established (Anderson, 1964a; Bonhomme and Chartier, 1972; Evans and Coombe, 1959; Madgwick and Brumfield, 1969; and Tamai and Shidei, 1972). I have been unable to find any reference to past study using or testing a technique of photographic assessment of radiation regimes within single days. Hence, despite the poor agreement between prediction and observation, I believe that the results are sufficiently favorable to warrant further tests of this approach. In the meantime, those who require a

means of predicting forest radiation regimes within time periods of less than a day or of predicting space distributions of direct beam radiation within plant stands are referred to the excellent work of Norman (1971) which shows good agreement between predicted and observed radiation conditions in a sumac stand.

List of Symbols

$A$ = area

$A_p$ = sunfleck penumbral area outside geometric sunfleck

$B$ = relative sky brightness

$C$ = average reflectivity of leaves over entire solar spectrum

$C_d$ = sunfleck center major axis

$D$ = direct beam radiation

$D_r$ = direct beam flux density in penumbra at r units from sunfleck center

$D_s$ = direct beam flux density in penumbral overlap of sunfleck s

$E$ = average transmissivity of leaves over entire solar spectrum

$F$ = total leaf area index in stand above level in question

$F_{i,\beta}$ = fractional canopy opening in annuli comprising brightness class i for solar elevation $\beta$

$G$ = proportional canopy opening

$G_d$ = geometric sunfleck major axis

$I$ = average total (global) radiation

$K$ = extinction coefficient

$L$ = clear sky brightness at two points on horizon at 90 degrees from sun

$N$ = number of grid segments

$O_d$ = gap image diameter on photo

$P$ = fractional area in sunfleck

$R$ = down-reflected direct beam radiation

$S_d$ = sunfleck major axis

$T$ = transmitted direct beam radiation

$T_{pen}$ = fractional area of solar disk visible through canopy gap

$U$ = fraction of sun's angular radius visible through gap

$U_r$ = fraction of sun's angular radius visible from a point r units from sunfleck center

$X$ = fractional area

$c_d$ = sunfleck center minor axis

$d$ = diffuse radiation

$e$ = base of natural logarithms

$f$ = proportion of reflected radiation that is reflected downward into stand

$g_d$ = geometric sunfleck minor axis

$g$ = subscript denoting geometric sunfleck

$h$ = height

$i$ = relative brightness class

$j$ = fractional opening class

$k$ = annulus number

$n$ = number of leaves through which or from which radiation is transmitted or reflected

$o$ = subscript denoting level of top of forest canopy

$p$ = diffuse radiation penetrating canopy openings

$r$ = down-reflected diffuse radiation

$s_d$ = sunfleck minor axis

$s$ = subscript denoting sunfleck number

$t$ = transmitted diffuse radiation

$w_r$ = distance from inside edge of penumbra to a point r units from center of sunfleck

$w_t$ = width of penumbra

$x$ = x coordinate

$y$ = y coordinate

$z$ = level in forest

$\Delta$ = angular distance from sun

$\beta$ = solar elevation angle

$\gamma$ = subscript denoting zenith

$\delta$ = solid angle subtended by solar disk as viewed from earth

$\theta$ = elevation angle

$\nu$ = solid angle subtended by canopy gap as viewed from level in question

$\xi$ = direct beam flux density

$\rho$ = scattering coefficient

$\sigma$ = subscript denoting totality of all sunflecks s

$\tau$ = time

$\phi$ = azimuth angle

$\psi$ = canopy gap distribution function

## Literature Cited


Akulova, E. A., V. W. Khazanov, Y. L. Tsel'niker, and D. N. Shishov. 1964. Light transmission through a forest canopy depending upon the incident radiation and density of tree crowns. Soviet Plant Phys. 11: 694-698.

Alekseev, V. A. 1963. Light measurements under a forest canopy. Soviet Plant Phys. 10: 109-201.

Allen, L. H., C. S. Yocum, and E. R. Lemon. 1962. Photosynthesis under field conditions: radiant energy exchanges with a corn crop canopy and implications in water use efficiency. U. S. Agric. Res. Service, Soil and Water Conservation Division Interim Rpt. 62-4, for Met. Dept., U. S. Army Electric Proving Ground, Fort Huachuca.

Anderson, M. C. 1964a. Studies of the woodland light climate. 1. The photographic computation of light conditions. J. Ecology 52: 27-41.

Anderson, M. C. 1964b. Studies of the woodland light climate. II. Seasonal variation in light climate. J. Ecology 52: 643-663.

Anderson, M. C. 1964c. Light relations of terrestrial plant communities and their measurements. Biol. Rev. 39: 425-486.

Anderson, M. C. 1966. Stand structure and light penetration. II. A theoretical analysis. J. Appl. Ecology 3: 41-54.

Anderson, M. C. 1969a. A comparison of two theories of scattering of radiation in crops. Agr. Met. 6: 399-405.

Anderson, M. C. 1969b. Radiation climate, crop architecture, and photosynthesis. In Prediction and Measurement of Photosynthetic Productivity. Center for Agric. Pub. and Documentation, Wageningen, The Netherlands, pp. 71-78.

Anderson, M. C. 1970. Interpreting the fraction of solar radiation available in forest. Agr. Met. 7: 19-28.

Anderson, M. C. and O. T. Denmead. 1969. Short wave radiation on inclined surfaces in model plant communities. Agron. J. 61: 867-872.

Atkins, W. R. G., H. H. Poole, and F. A. Stanbury. 1937. The measurement of the intensity and colour of the light in woods by means of emission and rectifier photoelectric cells. Proc. Roy. Soc. B. 121: 427-450.

Baumgartner, A. 1955. Licht und Naturverjungung am Nordrand eines Waldbestandes. Forstwissenschaftlich Zentralblatt 74: 59-64.

Berger, P. 1953. Radiation in forest at Willamette Basin Snow Laboratory. U. S. Army Corps. of Eng. Snow Invest. Res. Note 12. 17 pp.

Bonhomme, R. and P. Chartier. 1972. The interpretation and automatic measurement of hemispherical photographs to obtain sunlit foliage area and gap frequency. Israel J. Agr. Res. 22(2): 53-61.

Brecheen, K. G. 1951. Transmission of shortwave radiation through forest canopy. Coop. Snow Invest., Corps. of Eng., U. S. Army Res. Note SPDGC 627-51. 18 pp.

Brown, G. S. 1958. Light in the forest. Empire Forestry Rev. 37: 222-232.

Brown, P. S. and J. P. Pandolfo. 1969. An equivalent-obstacle model for the computation of radiative flux in obstructed layers. Agr. Met. 6: 407-421.

Carter, G. S. 1934. Illumination in the rain forest at ground level. (Reports of the Cambridge expedition to British Guiana, 1933). Linnain Soc. of London Zoological J. 38: 579-589.

Chartier, P. 1966. Etude du microclimate lumineux dens la vegetation. Ann. Agron. 17: 571-602.

Cowan, I. R. 1968. The interception and absorption of radiation in plant stands. J. Appl. Ecology 5: 367-379.

Cowan, I. R. 1971. Light in plant stands with horizontal foliage. J. Appl. Ecology 8: 579-580.

Czarnowski, M. and J. Slomka. 1959. Some remarks on the percolation of light through the forest canopy. Ecology 40: 312-315.

Davidson, J. L. and J. R. Philip. 1956. Light and pasture growth. UNESCO Symp. Arid Zone Climatology, Canberra.

Dinger, B. E., C. J. Richardson, and R. K. McConathy. 1972. Dynamics of canopy leaf area development and chlorophyll phenology in yellow poplar. East. Deciduous Forest Biome Memo Rpt. 72-164. 15 pp.

Duncan, W. R., R. S. Loomis, W. A. Williams, and R. Hanau. 1967. A model for simulating photosynthesis in plant communities. Hilgardia 38: 181-205.

Evans, G. C. 1956. An area survey method of investigating the distribution of light intensity in woodlands, with particular reference to sunflecks. J. Ecology 44: 391-428.

Evans, G. C. 1966. Model and measurement in the study of woodland light climates. In Light as an Ecological Factor. Backwell Sci. Pub., Oxford, England. pp. 53-76.

Evans, G. C. and D. E. Coombe. 1959. Hemispherical and woodland canopy photography and the light climate. J. Ecology 47: 103-113.

Fairbairn, W. A. 1961. Light intensity measurements in Bowmont Forest. Scottish Forestry 15: 153-159.

Federer, C. A. 1971/72. Solar radiation absorption by leafless hardwood forest. Agr. Met. 9: 3-20.

Fritz, S. 1958. Transmission of solar energy through the earth's clear and cloudy atmosphere. Trans. of the Conf. on the Use of Solar Energy: The Scientific Basis ed. by E. F. Carpenter. Univ. Ariz. Press, Tucson. Vol. 1: 17-36.

Gatherum, G. E. 1961. Variation in measurements of light intensity under forest canopies. For. Sci. 7: 144-145.

Gay, L. W. and K. R. Knoerr, 1970. The radiation budget of a forest canopy. Arch. Met Geoph. Biokl. 18: 187-196.

Gay, L. W., K. R. Knoerr, and M. O. Braaten. 1971. Solar radiation variability in the floor of a pine plantation. Agr. Met. 3: 39-50.

Geiger, R. 1957. The Climate Near the Ground. Trans. from German by M. N. Stewart, et al. Harvard Univ. Press, Cambridge. 494 pp.

Geiger, R. 1965. The Climate Near the Ground, Revised Edition. Trans. from German by Scripta Technica, Inc. Harvard Univ. Press, Cambridge. 611 pp.

Hill, R. 1924. A lens for whole sky photographs. Royal Met. Soc. Quarterly J. 50: 227-235.

Horn, H. W. 1971. The Adaptive Geometry of Trees. Princeton Univ. Press, Princeton, N. J. 144 pp.

Horowitz, J. L. 1969. An easily constructed shadow-band for separating direct and diffuse radiation. Solar Energy 12: 543-545.

Hutchison, B. A. 1971. Spatial and temporal variation in the distribution and partitioning of solar energy in a deciduous forest ecosystem. East. Deciduous Forest Biome Memo Rpt. 71-82. 40 pp.

Hutchison, B. A., D. R. Matt, S. Y. Shieh, M. Breed, C. J. Payne, and R. C. Clayburn. 1972. Spatial and temporal variation in the distribution and partitioning of solar energy in a deciduous forest ecosystem. East. Deciduous Forest Biome Memo Rpt. 72-148. 14 pp.

Hutchison, B. A. and D. R. Matt. 1973. Distribution of solar radiation within a deciduous forest. East. Deciduous Forest Biome Memo Rpt. 72-170. 26 pp.

Impens, I., R. Lemeur, and R. Moermans. 1971. Spatial and temporal variation of net radiation in crop canopies. Agr. Met. 7: 335-337.

Isobe, S. 1962. Preliminary studies on physical properties of plant communities. Bull. of the Nat'l. Inst. Agr. Sci., Toyko. Series A 9: 29-66.

Jackson, L. W. R. and R. S. Harper. 1955. Relation of light intensity to basal area of shortleaf pine stands in Georgia. Ecology 36: 158-159.

Jahnke, L. S. and D. B. Lawrence. 1965. Influence of photosynthetic crown structure on potential productivity of vegetation, based primarily on mathematical models. Ecology 46: 319-326.

Kasanaga, A. and M. Monsi. 1954. On the light transmission of leaves and its meaning for the production of matter in plant communities. Jap. J. Bot. 14: 304-324.

Khazanov, V. S. and Y. L. Tsel'Niker. 1968. Measurements of the photosynthetically active radiation in forests with an intensity meter. In Actinometry and Atmospheric Optics ed. by V. K. Pyldmaa. Trans. from Russian by Israel Program for Scientific Translations TT 70-50159. pp. 373-376.

Kornher, A. and N. Rodskjer. 1967. Uber die Bestimmung der Globalstruhlung in Pflanzenbestanden. Flora (Abt. B.) 157: 149-164.

Loomis, R. S., W. A. Williams, and W. G. Duncan. 1967. Community architecture and the productivity of terrestrial plant communities. In Harvesting the Sun ed. by A. San Pietro, F. A. Green, and R. J. Army. Academic Press, New York. pp. 291-308.

Madgwick, H. A. I. and G. L. Brumfield. 1969. The use of hemispherical photographs to assess light climate in the forest. J. Ecology 57: 537-542.

Matt, D. R. and B. A. Hutchison. 1974. Response of Lintronic Dome Solarimeters to varying solar radiation flux densities. East. Deciduous Forest Biome Memo Rpt. 74-1. 13 pp.

Miller, D. H. 1955. Snow cover and climate in the Sierra Nevada, California. Univ. Calif. Publ. in Geography 11. 218 pp.

Miller, D. H. 1959. Transmission of insolation through pine forest canopy, as it affects the melting of snow. Mitt. Schweiz Zent Anst. Forstl. Versuchw. 35: 57-79.

Miller, D. H. 1965. The heat and water budget of the earth's surface. In Adv. in Geophys. 11: 175-302. Academic Press, New York.

Miller, E. E. and J. M. Norman. 1971a. A sunfleck theory for plant canopies. I. Lengths of sunlit segments along a transect. Agron. J. 63: 735-738.

Miller, E. E. and J. M. Norman. 1971b. A sunfleck theory for plant canopies. II. Penumbra effect: Intensity distributions along sunfleck segments. Agron. J. 63: 739-743.

Miller, P. C. 1969. Solar radiation profiles in openings in canopies of aspen and oak. Science 164: 308-309.

Monsi, M. and T. Saeki. 1953. Uber den Lichtfaktor in den Pflanzengesellschaften and seine Bedeutung fur die Stoffproduction. Jap. J. Bot. 14: 22-52.

Monteith, J. L. 1959. Solarimeter for field use. J. Scientific Inst. 36: 341-346.

Monteith, J. L. 1965. Light distribution and photosynthesis in field crops. Ann. Bot. (New Series) 29: 17-37.

Moon, P. and D. E. Spencer. 1942. Illumination from a non-uniform sky. Illuminating Eng. 37: 707-726.

Nageli, W. 1940. Licht Messungen in Freiland und in geschlossenen Altholzbestanden. Mitt. Schweiz Zent Anst forstl. Versuchw. 21: 250-306.

Newton, J. E. and G. E. Blackman. 1970. The penetration of solar radiation through leaf canopies of different structure. Ann. Bot. 34: 329-348.

Nilson, T. 1971. A theoretical analysis of the frequency of gaps in plant stands. Agr. Met. 8: 25-38.

Norman, J. M. 1971. Sunfleck-size and light-intensity distributions in plant canopies. Ph.D. Thesis, Univ. Wisc. Univ. Microfilms, Ann Arbor, Mich.

Norman, J. M., E. E. Miller, and C. B. Tanner. 1971. Light intensity and sunfleck-size distributions in plant canopies. Agron. J. 63: 743-748.

Ovington, J. D. and H. A. I. Madgwick. 1955. Comparison of light in different woodlands. Forestry 28: 141-146.

Pokrowski, G. I. 1929. Uber die Helligkeitsverteilung am Himmel. Phys. Zeits. 30: 697.

Ramaan, E. 1911. Lichtmessungen in Fichtenbestanden. Allg. Forst.-u Jagdztg. 87: 401-406.

Rauner, Y. L. and N. I. Rudnev. 1962. Some results of actinometric measurements in a forest. Canada, Meteorology Branch, Meterological Translations 14: 45-54. Trans. by A. Nurklik.

Reifsnyder, W. E. and H. W. Lull. 1965. Radiant Energy in Relation to Forests. USDA Forest Service Tech. Bull. 1344. 111 pp.

Reifsnyder, W. E., G. M. Furnival, and J. L. Horowitz. 1971/72. Spatial and temporal distribution of solar radiation beneath forest canopies. Agr. Met. 9: 21-37.

Ross, J. K. 1968. The present-day status of studies of the radiation regime of vegetation. In Actinometry and Atmospheric Optics ed. by V. K. Pyldmaa. Trans. from Russian by Israel for Scientific Translations. TT 70-50159. pp. 245-252.

Ross, J. K. and T. A. Nilson. 1968. A mathematical model of the radiation regime of vegetation. In Actinometry and Atmospheric Optics ed. by V. K. Pyldmaa. Trans. from Russian by Israel Program for Scientific Translations. TT 70-50159. pp. 253-270.

Ross, J. K. and H. G. Tooming. 1968. Attenuation of direct and total solar radiation in crops and the corresponding semiempirical relations. In Actinometry and Atmospheric Optics ed. by V. K. Pyldmaa. Trans. from Russian by Israel Program for Scientific Translations. TT 70-50159. pp. 272-277.

Roussel, L. 1953. Recherches theoriques at pratiques sur la prepartition en quantite et en qualite de la lumiere dens le milieu forestier influence sun la vegetation. Ann. L'Ecole Nationale Des Eaux et Forests 13: 291-400.

Sachs, J. von. 1887. Lectures on the Physiology of Plants. Trans. by H. M. Ward. Oxford Univ. Press, Oxford, England (cited by Anderson, 1964c).

Saeki, T. 1960. Interrelationships between leaf amount, light distribution and total photosynthesis in a plant community. Bot. Mag. Tokyo 73: 55-63.

Salisbury, E. J. 1916. The oak-hornbeam woods of Hertfordshire, Parts I and II. J. Ecology 4: 83-117.

Salisbury, E. 1949. Leaf form and function. Nature 163: 515-518.

Schomaker, C. E. 1968. Solar radiation measurements under a spruce and a birch canopy during May and June. For. Sci. 14: 31-38.

Shirley, H. L. 1935. Light as an ecological factor and its measurement. Bot. Rev. 1: 355-381.

Shirley, H. L. 1945. Light as an ecological factor and its measurement, II. Bot. Rev. 11: 497-532.

Shul'gin, V. M. 1961. Light and shade determination in tree stands. (Raschet sveta i teni v drevesnykh nasazh deniyzkh) Vestnik Sel'skokhozyaistrennoi Nauki 5: 111-116.

Sollins, P., N. T. Edwards, and W. F. Harris. in press. Simulating the physiology of a temperate deciduous forest. In Systems Analysis and Simulation in Ecology, Volume 3 ed. by B. C. Patten. Academic Press, New York.

Spoehr, H. A. 1926. Photosynthesis. The Chemical Catalog Co., New York. 393 pp.

Tamai, S. and T. Shidei. 1972. Light intensity in the forest. II. The hemispherical photographic computation of light intensity. Bull. Kyoto Univ. Forests no. 44: 100-110. (in Japanese).

Tranquillini, W. 1960. Das Lichtklima wichtiger Pflanzengesellschaften. In Handb. Pflanzenphysiologie ed. by W. Ruhland. Springer, Berlin. pp. 304-338.

Trapp, E. 1938. Untersuchungen uber die Verteilung der Helligkeit in einem Buchenbestand. Meterologische Zeitscrift Bioklmatische Beiblatter 5: 153-158.

Verhagen, A. M. W., J. H. Wilson, and E. J. Britten. 1963. Plant production in relation to foliage illumination. Ann. Bot. (New Series) 27: 627-640.

Verhagen, A. M. W. and J. H. Wilson. 1969. The propagation and effectiveness of light in leaf canopies with horizontal foliage. Ann. Bot. 33: 711-727.

Vezina, P. E. and G. Pech. 1964. Solar radiation beneath conifer canopies in relation to crown closure. For. Sci. 10: 443-451.

Walsh, J. W. T. 1961. The Science of Daylight. MacDonald, London. 285 pp.

Watson, D. J. and K. J. Witts. 1959. The net assimilation rates of wild and cultivated beets. Ann. Bot. 23: 431-439.

Weisner, J. 1907. Der Lichtgenuss der Pflanzen. Englemann, Leipzig, Germany. 322 pp. (cited by Anderson, 1964c).

Wellner, C. A. 1948. Light intensity related to stand density in mature stands of western white pine type. J. For. 46: 16-19.

Warren Wilson, J. 1959. Analysis of the distribution of foliage area in grassland. In The Measurement of Grassland Productivity ed. by J. D. Ivins. Butterworth, London. pp. 51-61.

Warren Wilson, J. 1960. Inclined point quadrats. New Phytologist 59: 1-8.

Wit, C. T. de. 1959. Photosynthesis of leaf canopies. Agr. Res. Rpts. no. 663. Center for Agr. Pub. and Documentation, Wageningen, The Netherlands. 57 pp.

Yocum, C. S., L. H. Allen, and E. R. Lemon. 1964. Photosynthesis under field conditions. VI. Solar radiation balance and photosynthetic efficiency. Agron. J. 56: 249-253.

# MODELING SMOG ALONG THE LOS ANGELES - PALM SPRINGS TRAJECTORY*

by

Steven R. Hanna

Air Resources

Atmospheric Turbulence and Diffusion Laboratory

National Oceanic and Atmospheric Administration

Oak Ridge, Tennessee 37830

* To be published in "Advances in Environmental Science and Technology," M. Suffet, Ed., John Wiley, New York

ATDL Contribution File No. 75/4

Abstract

Observations of smog concentrations and wind patterns during the summer of 1973 in Los Angeles, Pomona, Riverside, Banning, and Palm Springs are presented which show that high oxidant concentrations at Banning and Palm Springs are often due to advection of smog from source regions in the more densely populated western part of the Los Angeles basin. At Pomona and Riverside, advection from upwind source regions combines with the effects of local emissions to cause long durations of high oxidant concentrations with peak times in the mid afternoon. An empirical model for the diurnal oxidant variation is suggested which satisfactorily simulates observed concentrations. More complex models which include chemical kinetics systems do not perform very satisfactorily at the rural stations of Banning and Palm Springs, especially at night when observed oxidant concentrations remain high.

## I. Introduction

The problem of photochemical smog in the Los Angeles basin has been recognized for many years (U.S. D.H.E.W. Consultation Report[1]) and has been the subject of many research and observation programs. As a result of these studies, various kinds of emissions controls have been suggested and implemented, and smog concentrations in the basin have been observed to decrease significantly (Altsuller[2]). It has been recognized that, while oxidant concentrations have decreased in the central areas of the basin characterized by high emissions, oxidant concentrations are increasing in the areas of Southern California that do not have very high emissions (Gloria et al.,[3] Drivas and Shair,[4] Metronics,[5] Altshuller,[2]). In this paper, measurements along a trajectory from Los Angeles to Palm Springs are presented which show that as the smoggy air is advected towards the east, the time of peak oxidant concentration is delayed towards evening, and the duration of high oxidant concentrations increases. The roles of advection, diffusion, and chemical reactions are discussed.

Observations are reported as either ozone or oxidant. While ozone is the chief oxidant in the air, small amounts of other substances such as PAN (peroxyacetyl nitrate) are represented in the oxidant observation. The presence of ozone or oxidant in regions outside primary source areas has been observed in several regions of this country. Stasiuk and Coffee[6] reported ozone concentrations of 8 pphm (parts per hundred million) in rural New York State. The typical background concentration reported by the U. S. D.H.E.W.[7] is 3 pphm. Although at any given time,

local sources or infusions of stratospheric ozone can cause variations in the background. The National Air Quality Criterion[8] for oxidant states that an hourly average concentration of 8 pphm may be exceeded no more than once a year. Cleveland and Kleiner[9] discuss observations of ozone concentrations exceeding the Air Quality Criterion in small towns about 50 km from Philadelphia, and show that the highest concentrations occur when the wind is blowing in a direction from Philadelphia to the towns. Richter[10] and Research Triangle Institute[11] report high values of oxidant measured in mountainous regions in the eastern U. S. This may be partly due to hydrocarbon emissions from the forests. The occurrence of high ozone concentrations in Livermore Valley, east of San Francisco, is shown by Ludwig and Kealoha[12] to be caused by chemical reactions in air advected from the more populated areas of San Francisco and San Jose.

Many studies have been made of the three dimensional distribution of ozone or oxidant in Southern California (e.g. Gloria et al.,[3] Miller and Ahrens,[13] Lea,[14] Edinger,[15]). The studies all find that layers of ozone exist, and that often the highest ozone concentrations occur near the top of the mixed layer. These elevated layers of ozone can stretch with little variation across the Los Angeles basin, and impact upon the forested slopes of the mountains to the east and north of the basin. Ozone concentrations in these elevated layers do not vary much with time of day.

A tracer study by Drivas and Shair[4] shows that pollutants emitted in the more populous western part of the Los Angeles basin can be advected through the passes in the hills into the eastern part of the basin. Another tracer study by Metronics[5] found that considerable transport of material from Los Angeles to Riverside took place, but suggested that the main cause of high pollutant concentrations in Riverside is local emissions. The Los Angeles Reactive Pollutant Program, which took place in late summer, 1973, also used tracer techniques to follow air parcels across the basin (see Angeli, et al.[16]). Constant level balloons were flown, as on other occasions (e.g., Angell et al.[17]) in order to more accurately determine air trajectories. The tetroon flights verify that the sea breeze regime often dominates the air flow (DeMarrais et al,[18]), causing pollutants to drift inland during the day and out to sea at night. These patterns were also confirmed by the study by Edinger et al.[19] Mountain valley breezes dominate the flow near the large mountain ranges to the east of the basin (U.S.,[1]). It will be shown later in this paper that the sea breeze and mountain breeze interact to form a smog front which flows to the east during the afternoon and reaches Palm Springs in the early evening. Climatological summaries show that this air can have its origins either in Los Angeles or Orange Counties. For the episode analyzed here, the origin is Los Angeles.

Occasionally, the smog front is a very striking visible phenomenon. Stephens[20] provides photographs and documentation for a smog front on 16 March, 1972, as it passes Riverside. He states that such extremely

sharp demarcations between the polluted marine air and the clean desert air occur about a dozen times per year, and are most common during October.

Once the phenomenon of smog advection is documented, the next question is whether it can be modeled. Urban diffusion modeling of Los Angeles has progressed from Frenkiel's [21] simple model to the complex models of, for example, Pandolfo and Jacobs,[22] Reynolds et al,[23,24] and Roth.[25] These simple models have been validated so far only in the parts of the basin where local emissions are significant. A simple model developed by Hanna[26] was found to yield useful results where local emissions and meteorological conditions do not vary by more than an order of magnitude over time periods of several hours and distances of several kilometers. But the pollution episodes discussed here occur over regions where local emissions are insignificant and when meteorological conditions are changeable. In the model developed here, several chemical kinetic schemes are tried, in an attempt to simulate the observed smog patterns.

## 2. Observations during the Summer of 1973.

To illustrate the variations in smog concentrations across Southern California, the five stations shown in Figure 1 were used. The distances between Downtown Los Angeles, Pomona, Riverside, Banning, and Palm Springs are 46, 29, 51, and 26 km, respectively. These stations are along the trajectory of an air parcel flowing eastward from Los Angeles, through the San Gorgonio Pass (near Banning) to Palm Springs. The San Gorgonio Pass (el 500m), which is about 3 km wide, is the only low passage through the steep San Bernardino, San Jacinto, and Santa Rosa Mountains on the north and east sides of the Los Angeles basin.

Emissions characteristics of the areas around the five stations are listed in Table 1. These emissions represent an average over about 100 $km^2$

Table 1

Emissions Characteristics in Southern California

| | | Average Daily Emissions ($cm^3/m^2 sec$) | | | |
|---|---|---|---|---|---|
| Station | City Population | CO | Reactive Hydrocarbons | NO | $NO_2$ |
| Los Angeles | 2,816,000 | .11 | .021 | .004 | $3x10^{-4}$ |
| Pomona | 87,000 | .014 | $2.7x10^{-3}$ | $1.7x10^{-3}$ | $10^{-4}$ |
| Riverside | 140,000 | .014 | $2.7x10^{-3}$ | $1.7x10^{-3}$ | $10^{-4}$ |
| Banning | 12,000 | $1.4x10^{-3}$ | $2.7x10^{-4}$ | $1.7x10^{-4}$ | $10^{-5}$ |
| Palm Springs | 21,000 | $1.4x10^{-3}$ | $2.7x10^{-4}$ | $1.7x10^{-4}$ | $10^{-5}$ |

The emissions for the first three stations are estimated from the data published by Weisburd et al.[27] Emissions were estimated for Banning and Palm Springs on the basis of population, compared with Riverside, since there were no published emission data available.

Based on emissions data analyzed by Roth et al (1974), the average daily emissions reported in Table 1 must be multiplied by the following factors to obtain hourly values:

| | | | | | |
|---|---|---|---|---|---|
| hr 0-5 | .173; | hr 9 | 1.56; | hr 16-18 | 1.92; |
| hr 6 | .295; | hr 10 | 1.24; | hr 19 | 1.36; |
| hr 7 | 1.06 ; | hr 11-14 | 1.31; | hr 20-22 | .73; |
| hr 8 | 1.70 ; | hr 15 | 1.41; | hr 23-24 | .173. |

The most severe smog episode during 1973 occurred during the four day period from 23 July through 26 July. The hourly oxidant concentrations, averaged over the four days, are plotted in Figure 2. The Los Angeles, Pomona, and Riverside curves are all typical for an urban location with strong local emissions, increasing from near zero during the night to a peak near mid-day. However, the time of the peak oxidant concentration occurs later in the afternoon for the more easterly stations, due to advection of smog from Los Angeles. Furthermore, the duration of high oxidant concentrations is longer for the more easterly stations. This is also evident in the oxidant summary in Table 2.

Table 2

Time, Magnitude, and Duration of Observed Oxidant Peaks along the Los Angeles-Palm Springs Trajectory for 23-26 July 1973*

| Date | Time (hr.) and Magnitude (pphm, in parentheses) of Oxidant Peak | | | | | Duration (hr.) of Ox. Conc. > 10 pphm | | | | |
|---|---|---|---|---|---|---|---|---|---|---|
| | LA | POM | RIV | BAN | PS | LA | POM | RIV | BAN | PS |
| 23 July 73 | 12(10) | 14(23) | 13(26) | 17(30) | 18(25) | 4 | 8 | 12 | 23 | 23 |
| 24 July 73 | 12(27) | 15(31) | 14(37) | 22(25) | 24(19) | 6 | 10 | 14 | 14 | 11 |
| 25 July 73 | 11(31) | 12(26) | 16(33) | 19(37) | 21(24) | 5 | 8 | 11 | 15 | 9 |
| 26 July 73 | 13(17) | 13(16) | 12(26) | 15(21) | 19(15) | 5 | 6 | 10 | 15 | 15 |
| Average | 12(21) | 14(23) | 14(30) | 18(28) | 20(21) | 5 | 8 | 12 | 17 | 14 |

*Data supplied by the California Air Resources Board and the Riverside County Air Pollution Control District.

The observation that the oxidant concentration begins its rise later in the morning at the Los Angeles station is probably due to the persistence of low level clouds close to the coast in the early morning. At the rural stations in Banning and Palm Springs, in contrast, the oxidant concentrations remain above the National Air Quality Criterion,[8] 8 pphm, at night. There are not enough nitrogen oxides in the advected air or local emissions of nitrogen oxides to scavenge the oxidant. The oxidant concentrations in Banning and Palm Springs rise sharply at 4 pm and 8 pm, respectively, as the smog front passes through.

Meteorological conditions during the period 23-26 July 1973 were typical of those occurring in Los Angeles during the summer. The winds were generally from the west during this period at all stations except Banning and Palm Springs, where easterly winds during the afternoon were replaced by westerly winds at night. Detailed data are given in Figures 8 and 9. With the switch to westerly winds, the "smog front" arrived and oxidant concentration increased noticeably. An analysis of 24 days during June and July when the "smog front" was noticeable shows that the peak at Banning occurs an average of 3 1/4 hours later than that at Riverside, and the peak at Palm Springs occurs an average of 2 1/4 later than that at Banning. These times are nearly equal to the distance between the stations divided by the average wind speed at the two stations. Wind measurements refer to anemometer height and averages are taken over three hour periods and for the two stations at either end of the trajectory. In Figure 3, the time delay between peak oxidant at Riverside and Banning is plotted against wind speed, illustrating the good agreement.

In Table 2, it is seen that the peak oxidant concentration in the 23-26 July 1973 period does not decrease much between the urban source areas and Palm Springs. If diffusion were the dominant mechanism affecting the oxidant concentration, then it would be expected that the oxidant concentration would decrease as the smog front flowed towards Palm Springs. Perhaps the oxidant concentrations remain high because the peak occurs in the evening when atmospheric stability is higher and diffusion rates are low. Or, as suggested by the USDHEW [1] in its consultation report, the continual chemical production of oxidant proceeds at a greater rate than the diffusion.

In order to broaden the data base for these conclusions, data from each day of June and July 1973 were also analyzed. The results are summarized in Table 3.

**Table 3**

Time, Magnitude, and Duration of Observed Oxidant Peaks along the Los Angeles-Palm Springs Trajectory for June-July 1973.

| Month | Time (hr.) and Magnitude (pphm, in parentheses) of Oxidant Peak | | | Duration (hrs) of Ox. Conc. > 10 pphm | | |
|---|---|---|---|---|---|---|
| | LA | RIV | PS | LA | RIV | PS |
| June 1973 | not available | 14(21) | 17(15) | not available | 7 | . 8 |
| July 1973 | 12(12) | 14(22) | 18(18) | 2.5 | 8 | 12 |

On some days included in this analysis, the smog front never reached Palm Springs, and a local oxidant peak occurred at noon. However, the general results in Table 3 support the conclusions based on the smog episode data in Table 2. Peak oxidant concentrations occur six hours later at Palm Springs than at Los Angeles, and the duration of high oxidant concentrations is greater at Palm Springs.

Figures 4 through 9 contain hourly measurements of wind speed and direction, and concentrations of oxidants, CO, NO, and $NO_2$, for the five stations during the period from 23 July through 26 July, 1973. Hydrocarbon concentrations were also measured at the Los Angeles and Pomona stations, but are not plotted because they generally were about one half the magnitude of the CO concentrations. The main purpose of including all of these data is to provide a comprehensive set of measurements for others to use in validating models. Also, it is interesting to follow the concentration curves and compare curves for different stations.

For example, the CO and NO concentrations at Los Angeles and Pomona are nearly the same, even though the emissions at Los Angeles are reported to be almost an order of magnitude greater than those at Pomona. This inconsistency could be due to advection of CO from Los Angeles

to Pomona, errors in reported emissions rates, or unrepresentative placement of the measuring stations. The CO concentration at Palm Springs tends to increase in the evening, as does the oxidant concentration, when the smog front arrives. However, the $NO_2$ peak at Palm Springs tends to occur in early morning, suggesting that it is a local phenomenon due to local emissions. The low $NO_2$ concentration at the time of the passage of the smog front verifies the hypothesis that the smoggy air contains much oxidant but very little nitrogen oxide. Otherwise the oxidant would disappear.

There is an inconsistency in that carbon monoxide, a nearly inert gas, is not present in significant amounts in the air accompanying the smog front in Palm Springs, whereas the oxidant arrives virtually undepleted from its value in Los Angeles. We can conclude that oxidant arriving at Palm Springs is the result of chemical reactions in the presence of diffusion. Diffusion is sufficient to dilute the CO, but evidently the production of oxidant by chemical reactions balances the dilution by diffusion.

The relation between oxidant peak at Banning and Palm Springs and wind direction is strikingly illustrated by Figures 4 and 9. For example, in Banning on July 23, when the wind direction switched sharply to WNW at 3 pm, the oxidant concentration jumped to 30 pphm. The wind then shifted to SW at 5pm, and oxidant concentration fell.

From the wind speed traces in Figure 8, it is seen that relatively strong winds usually mark the passage of the smog front at Banning and Palm Springs. This is normally followed by a gradual decrease in both wind speed and oxidant concentration.

It is evident from figures 4 through 9 that the daily cycles of pollutant concentrations and meteorological variables are fairly regular. The regularity of wind patterns in the Los Angeles basin is mentioned by Anderson[28] and De Marrais et al.[18] On this basis the simplified wind speed record in Table 4 has been developed from the data in Figure 8, for use in an empirical model.

Table 4

Smoothed Component towards the East of the Wind Speed along a Trajectory Connecting the Five Stations in Figure 1, for the Period 23-26 July 1973.

| Station | | | | |
|---|---|---|---|---|
| Los Angeles | Pomona | Riverside | Banning | Palm Springs |
| 7 pm-8 am 1 m/s; | 7 pm-9 am .5 m/s; | 7 pm-9 am .5 m/s; | 2 am-7 am 2 m/s; | 8 am-7 pm -2.5 m/s; |
| 8 am-7 pm 3.5 m/s; | 9 am-7 pm 2.5 m/s; | 9 am-7 pm 4 m/s; | 7 am-2 pm -1 m/s; | 7 pm-1 am 3 m/s; |
| | | | 2 pm-2 am 2.5 m/s; | 1 am-8 am 1 m/s. |

The use of a smoothed wind record is justified by experience with the application of the ATDL simple urban dispersion model (Hanna,[29] and Gifford and Hanna[30,31]). Individual station wind records are generally not truly representative of the integrated air flow across a region. We find (Nappo,[32] Gifford[33]) that when wind speeds are averaged somewhat over time and space in order to smooth unrepresentative observations, better agreement between concentrations and those calculated by means of a simple urban pollution model is obtained.

## 3. A Simple Empirical Model for Oxidants

The oxidant patterns in Figure 2 appear so smooth and regular that it should be possible to reproduce the curves through a simple empirical formula. The empirical model should account for oxidant production due to local emissions and due to advection from upwind regions. Based on the results reported in the earlier articles by Hanna,[26,34] the local contribution to oxidant concentration, $OX_1$ (pphm), is assumed to be directly proportional to the rate constant for photochemical dissociation of $NO_2$ (denoted by $r_1$ ($sec^{-1}$) in most reports) and to the square root of emissions of reactive hydrocarbons, $Q_{RH}$ ($cm^3/m^2 sec$), but is inversely proportional to the wind speed, U (m/s).

$$OX_1(x,t) = \frac{c r_1 Q_{RH}^{1/2}(x,t)}{U(x,t)} ; \qquad (1)$$

where c is a dimensional constant, determined by comparisons with data to be equal to about $7.0 \times 10^4$ $m^2 s^{1/2}$ $cm^{-3/2}$, x is location on the trajectory, and t is time. The constant $r_1$ is assumed to be proportional to the sine of the sun's elevation angle.

The advection contribution, $OX_a$ (pphm), should account for dilution and chemical reactions. It has been shown that horizontal diffusion is not important in most urban regions (e.g., Gifford and Hanna,[30]).

Therefore only vertical dispersion need be accounted for, and it is assumed that the pollutant is well mixed up to a lid at height Z(m). Furthermore, the expression to be proposed should satisfy the conditions that during the night and at the eastern end of the trajectory, chemical reactions are insignificant. The following expression is proposed for the contribution of advection to oxidant concentrations, $OX_b$ (pphm):

$$OX_a(x,t) = \frac{OX(x_o,\ t-(x-x_o)/U)}{Z(x,t)/Z(x_o,t_o)} \left[1 - \left(1 - \frac{r_1(t)}{r_1(\text{noon})}\right) \frac{Q_{RH}-\text{lim}}{Q_{RH}}\right] \quad (2)$$

where U is wind speed, $x-x_o$ is the distance from one station (position $x_o$) to the next downwind station (position x), and lim is the reactive hydrocarbon source strength at Banning and Palm Springs. The total oxidant concentration is given by adding equations (1) and (2) to the background oxidant concentration, $OX_b$ (pphm):

$$OX(x,t) = OX_b + \frac{cr_1\ Q_{RH}^{1/2}(x,t)}{U(x,t)} + \frac{OX(x_o,t-(x-x_o)/U)}{Z(x,t)/Z(x_o,t_o)} \left[1- \left(1-\frac{r_1(t)}{r_1(\text{noon})}\right) \frac{Q_{RH}-\text{lim}}{Q_{RH}}\right] \quad (3)$$

This empirical equation was applied to the five stations in Southern California which are studied in this report, in an attempt to simulate the four day average diurnal oxidant curves drawn in Figure 2. Emissions given in Table 1, a sinusoidal variation of $r_1$ with time (with $r_1(\text{noon}) = .006\ \text{sec}^{-1}$), and wind speeds given in Table 4 were assumed. The mixing height Z was assumed to equal 200m, 300m, 450m, 900m, and 1800m

over Los Angeles, Pomona, Riverside, Banning, and Palm Springs, respectively (Holzworth,[35] and U.S.D.H.E.W.[1]). Furthermore a background oxidant concentration of 10 pphm was assumed for Banning and Palm Springs, and zero for the other stations, as suggested by the observations at these stations during smog episodes. The calculated oxidant concentration at the upwind station at time $t-(x-x_o)/U$, beginning with Los Angeles, was used as input to the advective portion of equation (3). The results of applying this model at each of the five stations are presented in Figures 10a through 10e (the dashed curves).

In Figure 10a, for Los Angeles, the calculated OX curve is a sine curve which agrees fairly well with observations at midday but exceeds the observations in the early morning and late afternoon. The error in the early morning may be due to the presence of stratus clouds which are not accounted for in the model. The error in the late afternoon is probably due to failure of the model to account satisfactorily for scavenging of oxidants by nitrogen oxides, which are emitted in large quantities in the area around this station. The agreement between observed and calculated curves in Pomona in Figure 10b is remarkable and probably somewhat fortuitous. The forms of the curves for Riverside in Figure 10c are similar, but the magnitude of the calculated concentrations is only about 50 to 60 percent of the observations. The calculated curves for Banning and Palm Springs in Figures 10d and 10e are in good agreement with the observed curves. The times of peak oxidant concentration are calculated to be within about one hour of the observed times.

We can conclude that the simple empirical model given by equation (3) is a good predictor of oxidant concentrations for these data. The model should of course be tested with other independent observations (as should those of all smog models). However, we can state with some confidence, based on the present study, that oxidant episodes in Los Angeles are due to local emissions, those at Pomona and Riverside are due partly to local emissions and partly to advection from upwind areas, and those at Banning and Palm Springs are almost entirely due to advection from upwind areas.

## 4. Numerical Models of Photochemical Smog.

Modeling of photochemical smog in Los Angeles has recently received a great deal of attention, mainly due to the encouragement of the Environmental Protection Agency. The characteristics of the models depend upon the needs for which they were developed, EPA needs are related to environmental legislation, implementation, planning, impact assessment, transportation planning, and episode controls. Photochemical diffusion models were developed independently by Sklarew et al.,[36] Roth et al.,[25] Reynolds et al.,[23,24] Weisburd etal.,[27] and Eschenroeder et al.[37] Each of thes models uses a slightly different system of approximate chemical kinetic equations. The number of chemical reactions accounted for ranges from about ten to about thirty. The diffusion methods and meteorological input to these models are relatively crude when compared to the methods used in the models for inert substances developed by, for example, Pandolfo and Jacobs[22] and the very detailed model presented by Hilst et al.[38] In the first group of models listed above, grid squares which either move with the air or are stationary are used, and atmospheric diffusion enters the problem only through a vertical diffusivity coefficient, K, and fluctuations in wind velocity. After considerable "tuning" of these models with the observations, these investigators generally can show rather good agreement between calculated and observed concentrations of CO, OX, NO, $NO_2$, and reactive hydrocarbons.

A simpler model of diffusion of photochemical smog was suggested by Hanna (1973a, 1973b). In this model, the pollutants are assumed to be well mixed throughout the volume of air passing over a grid square, and the basic simple model for inert pollutants,

$$X_i = C \frac{Q_i}{U} \qquad (4)$$

is used as a normalizing factor in the model (see Hanna,[29] and Gifford and Hanna[31]). In equation (4), $X_i$ is concentration of species i, in ppm or $cm^3/m^3$, C is a dimensionless constant found to equal about 200 on the average, and $Q_i$ is the area source emissions of species i, in $cm^3/m^2 sec$. When the equation for the time rate of change of pollutant concentrations is normalized by the factor on the right hand side of (4), several dimensionless numbers are produced which describe the relative influence of chemical reactions, advection, and emissions on the change of pollutant concentration. The chemical reactions used are those suggested by Friedlander and Seinfeld,[39] although other reactive schemes could be used. From these dimensionless numbers, which are functions of emissions rate, wind speed, mixing depth, and chemical rate constants, it is possible to estimate the deviation of the actual concentration given by the equation for the time rate of change of pollutant concentrations from the equilibrium inert concentration given by equation (4).

One valid objection to the original model by Hanna[26] for photochemical smog is that it can not be used for situations in which local emissions are not strong and advection from upwind polluted areas is important, which is exactly the type of situation described in Section 2. The original model is accordingly modified in the following manner to account for these processes. As before, it is assumed that horizontal diffusion is insignificant, due to the broad extent of the emissions region. Concentrations within boxes of length 40 km, centered nearly over each station, are assumed uniform. A schematic drawing of the location of the boxes is given in Figure 11. The continuity equation for the time rate of change of concentration of pollutant $X_i$ ($cm^3/m^3$ or ppm) in one of the boxes is

$$\bar{Z}DX \frac{\partial X_i}{\partial t} = -DX \frac{\partial}{\partial x} \bar{Z}UX_i + Q_i DX + \bar{Z}DX \sum_j R_j \qquad (5)$$

where $\bar{Z}$ is the average height of the mixing layer over the grid block, and $R_j$ is the rate of change of concentration of pollutant $X_i$ due to reaction j. Written in the finite difference form used in the numerical solution, and assuming positive U for the purpose of illustration, equation (5) becomes:

$$X_i(k,t_0+DT) = X_i(k,t_0) + DT\left[\frac{Q_{ik}}{\bar{Z}_k} + U_{k-1}\, X_i(k-1,t_0)\frac{Z_{k-1}}{DX\bar{Z}_k}\right.$$

$$\left. - U_k\, X_i(k,t_0)\frac{Z_k}{DX\bar{Z}_k} + \Sigma_j R_j,\right] \qquad (6)$$

where DT is the time step, k is the grid block number, and $t_0$ is an initial time at which all quantities are assumed to be known. As an example, to calculate the CO concentration in grid block 3, with all wind speeds U constant, the following equation would be used:

$$X_{CO}(3,t_0 + DT) = X_{CO}(3,t_0) + DT\left[\frac{Q_{CO\,3}}{\bar{Z}_3} + U\, X_{CO}(2,t_0)\frac{Z_2}{DX\bar{Z}_3}\right.$$

$$\left. - U\, X_{CO}(3,t_0)\frac{Z_3}{DX\bar{Z}_3}\right] \qquad (7)$$

Note that for steady-state conditions with no upwind sources, this equation reduces to the Gifford-Hanna simple model, $X_{CO} = CQ/U$, where C is equivalent to the ratio $DX/\bar{Z}$.

In this study, the differential equation (6) is solved for the variable pollutants CO, NO, $NO_2$, oxidant, and reactive hydrocarbons. For more detailed chemical kinetics systems, additional differential equations would be required for other chemical substances. Many important chemical substances can simply be assumed to be in steady-state equilibrium. The chemical kinetics systems used is that proposed by Friedlander and

Seinfeld [39], which is based on the work by Leighton[40]. In Friedlander and Seinfeld's seven step scheme, oxidants are assumed to be in steady-state equilibrium. In the present study this restriction is removed during the night, because it is not valid then.

The partial differential equation for oxidant concentration will, I hope, permit advection but not much chemical conversion at these stations at night. The reader should refer to Friedlander and Seinfeld's [39] paper for details of the chemical kinetics systems.

Additonal specific conditions are imposed as follows. Noon mixing heights of 200m, 400m, 800m, 1600m, and 1600m are used for the five stations; at night the mixing depth is then assumed to fluctuate as a sine curve between sunrise and sunset. A time step, DT, equal to 60 seconds, is used. To prevent computational instabilities in solving equation (6) for the concentration $X_i$ at time ($t_0$ + 60 sec), values of $X_i$ at time $t_0$ and values of all other species concentrations $X_j$ at time ($t_0$ - 60 sec) are used in $R_j$ on the right hand side of equation (6). Observed initial concentration values are those for midnight on June 22-23, 1973.

Resulting concentrations for Pomona on 23 July are shown in Figure 12a through 12d. It is seen that agreement is fair for all pollutants, considering that no adjustments have yet been made in the "tunable parameters" such as mixing depth and rate constants. Unfortunately, the calculated oxidant curve misses the observed curve significantly, both in terms of magnitude and time of peak.

For the stations at Banning and Palm Springs, the model results differ significantly from observations. With an initial oxidant concentration of 12pphm and initial NO and $NO_2$ concentrations of 1 pphm, the oxidant concentration rapidly decreases with a half life of about two hours. In contrast to observations, the calculated oxidant is almost completely eliminated by sunrise. Thus this system is not satisfactory for modeling smog at night in rural areas.

Since the Friedlander and Seinfeld seven-step kinetic mechanism has been criticized for being too short, and it does not yield very satisfactory results in this application, the Systems Applications, Inc. 15 step (Roth et al, [41]) and 19 step (Reynolds et al, [23]) kinetic mechanisms were tested. The difference between these two mechanisms is that the 15 step mechanism uses only a single hydrocarbon class, while the 19-step mechanism uses two hydrocarbon classes, based on reactivity. It is assumed here that hydrocarbon emissions are divided equally between the two classes. The result of both of these applications, using equation (6), is, perhaps, a slight improvement over the results using the Friedlander and Seinfeld scheme. But the most important observations from our point of view, namely the high background oxidant and smog front at Banning and

Palm Springs, are poorly simulated even by these more comprehensive chemical kinetics systems. In all cases the observed background oxidant concentration is whittled away at night to near zero in a few hours. Furthermore, the high oxidant concentrations associated with the smog front are not evident in the model, even though the front does arrive at the proper time, as insured by the input wind observations. Further research on chemical reactions in smoggy atmospheres during the night is necessary.

We plan to continue testing variations of this model. The next step will be to use the Lagrangian or trajectory approach suggested by Eschenroeder and Martinez[37] and applied to the San Francisco basin by Ludwig and Kealoha[12]. The more recent chemical kinetic scheme proposed by Hecht et al.[42] may be used, since this scheme divides the hydrocarbons into classes according to their chemical composition, rather than according to their reactivity. However, since the first three equations in the chemical kinetics system are nearly the same in all the models, we do not foresee much improvement over the results of the other models. It is wise not to spend too much time cross-checking each model with the same set of observations. The more this is done, the more "tuning," with the large number of adjustable parameters in these models, is involved. The end result is a model which is not independent of the data set used in its validation.

## 5. Conclusions

Observations of smog concentrations during the summer of 1973 in Los Angeles, Pomona, Riverside, Banning, and Palm Springs show that smoggy air is often advected eastward from its source region in Los Angeles and Orange counties towards the more rural areas of Banning and Palm Springs. As a result of the interaction of sea breeze and mountain breeze effects, a smog front is formed which causes abrupt increases in oxidant concentration as it passes the rural stations. On the average, the time of peak oxidant concentration occurs six hours later at Palm Springs than at Los Angles. Oxidant episodes at Palm Springs and Banning are almost entirely due to advection from the urban area, while episodes at Los Angeles are almost entirely due to strong local emissions. At Pomona and Riverside, both local emissions and advection play an important role, often resulting in days with a long duration of high oxidant concentrations, having a peak during mid-afternoon.

An empirical model of the diurnal oxidant variation is shown to agree fairly well with the observations. This model accounts both for local emissions and advection from upwind areas. In contrast, solutions to the partial differential equations for the time rate of change of pollutant concentrations due to emissions, advection, vertical mixing, and chemical reactions, could not satisfactorily simulate the observed high oxidant concentrations in Banning and Palm Springs at night.

After this work was completed, a report entitled "Comparison of Oxidant Calibration Procedures" by the Ad hoc Oxidant Measurement Committee of the California Air Resources Board (Feb. 3, 1975) was sent to me. This committee believes that the oxidant measurement reported from Riverside, Banning and Palm Springs are consistently 25 to 30% too high. These errors do not affect the basic conclusions of this paper. In future work using these data, however, the oxidant concentrations at Riverside, Banning, and Palm Springs should be reduced by 25%.

Acknowledgements: Data were provided by the California Air Resources Board and the Riverside County Air Pollution Control District. This research was performed under an agreement between the National Oceanic and Atmospheric Administration and the Energy Research and Development Administration.

References


1. U. S. Dept. of Health, Ed., and Welfare, Report for Consultation on the Metropolitan Los Angeles Air Quality Control Region. Pub. Health Serv., 79pp, Nov. 1968.

2. A. P. Altshuller, J. Air Poll. Cont. Assoc., 25, 19 (1975).

3. H. R. Gloria, J. N. Pitts, G. Bradburn, R. F. Reinisch and L. Zafonte, J. Air Poll. Cont. Assoc., 24, 645 (1974).

4. P. J. Drivas and F. H. Shair, Atmos. Environ. 8, 1155 (1974).

5. Metronics Assoc., Inc., Field Study of Air Pollution Transport in the South Coast Basin, Tech. Rept. No. 186 (May 1973).

6. W. N. Stasiuk and P. E. Coffey, J. Air Poll. Cont. Assoc., 24, 564 (1974).

7. U. S. Dept. of Health Ed., and Welfare. Air Quality Criteria for Photochemical Oxidants. NAPCA Publ. AP-G3 ($1.75), Pub. Health Serv., (March, 1970).

8. Nat. Primary and Secondary Ambient Air Quality Standard for Photochemical Oxidants. .08ppm maximum one hour concentration not to be exceeded more than once per year. Fed. Reg., 36(84), 8187 (Jan. 1973).

9. W. S. Cleveland and B. Kleiner, The Transport of Photochemical Air Pollution from the Camden-Philadelphia Urban Complex. Report from Bell Laboratories, Murray Hill, N.J. 07974, 12 pp. (1975).

10. H. G. Richter, Special Ozone and Oxidant Measurements in Vicinity of Mount Storm, West Virginia. Res. Tri. Inst., N.C. (1970).

11. Research Triangle Institute, Investigation of High Ozone Concentration in the Vicinity of Garrett County, Maryland and Preston County, West Virginia. Res. Tri. Inst. publ. NTIS-PB-218540 (1973).

12. F. L. Ludwig and J. H. Koeloha, Present and Prospective San Francisco Ray Area Air Quality, SRI project 3274 Final Report, by Stanford Research Institute, Menlo Park, Cal. 94025, for Wallace, McHarg, Roberts, and Todd and Metropolitan Transportation Commission, 110p. (1974).

13. A. Miller and C. P. Ahrens, Tellus, 22, 328 (1970).

14. D. A. Lea, J. Appl. Meteorol., 7, 252 (1968).

15. J. G. Edinger, Environ. Sci. and Tech., 7, 247 (1973).

16. J. K. Angell, C. R. Dickson, and W. H. Hoecker, Relative Dispersion within the Los Angeles Basin as Estimated from Tetroon Triads. NOAA Tech. Memo. ERL ARL-46, 34 pp. (1974).

17. J. K. Angell, D. H. Pack, L. Machta, C. R. Dickson, and W. H. Hoecker, J. Appl. Meteorol., 11, 451 (1972).

18. G. DeMarrais, G. C. Holzworth, and C. R. Hosler, Meteorological Summaries Pertinent to Atmospheric Transport and Dispersion over Southern California. Tech. Paper No. 54, Weather Bureau, U. S. Dept. of Comm. (1965),

19. J. G. Edinger, M. H. McCutchan, P. R. Miller, B. C. Ryan, M. J. Schroeder, and J. V. Behar, J. Air Poll. Cont. Assoc., 22, 882 (1972).

20. E. R. Stephens, J. Air Poll. Cont. Assoc., 24, 521 (1975).

21. F. Frenkiel, Smithsonian Inst. Report for 1956, 269 (1957).

22. J. P. Pandolfo and C. A. Jacobs, Tests of an Urban Meteorological-Pollutant Model using CO Validation Data in the Los Angeles Metropolitan Area, Vol. I, CEM Rept. 490a, Cont. No. 68-02-0223 by The Center for the Environment and Man, Inc., 275 Windsor St., Hartford, Conn. 06120, prepared for U. S. EPA, 176pp. (1973).

23. S. D. Reynolds and P. M. Roth, Atmos. Environ., 7, 1033 (1973).

24. S. D. Reynolds, M. K. Liu, T. A. Hecht, P. M. Roth, and J. H. Seinfeld, Atmos. Environ., 8, 563 (1974).

25. P. M. Roth, P. J. Roberts, M. K. Liu, S. D. Reynolds and J. H. Seinfeld, Atmos. Environ., 8, 97 (1974).

26. S. R. Hanna, Atmos. Environ., 7, 803 (1973).

27. M. I. Weisburd, L. G. Wayne, R. Danchick, and A. Kokin, Development of a Simulation Model for Estimating Ground Level Concentrations of Photochemical Pollutants, Final Report NAPCA Contract CPA 70-151. System Development Corporation, Santa Monica, Cal. (Jan. 1971).

28. G. E. Anderson, A. Mesoscale Windfield Analysis of the Los Angeles Basin, Cont. No. 68-02-0223 by the Center for The Environment and Man, Inc., 275 Windsor St., Hartford, Conn. 06120, for the U.S.E.P.A., 113 pp., (1973).

29. S. R. Hanna, J. Air Poll. Control Assoc., 21, 774 (1971).

30. F. A. Gifford and S. R. Hanna, Urban Air Pollution Modeling, 1970 Meeting of the Int. Union of Air Poll. Prev. Assoc., Washington, 11 Dec., 17 pp + 7 figs. (1970).

31. F. A. Gifford and S. R. Hanna, Atmos. Environ., 7, 131 (1973).

32. C. J. Nappo, A Method for Evaluating the Accuracy of Air Pollution Prediction Models, Proceedings of the Symposium on Atmospheric Diffusion and Air Pollution, held 9-13 Sept. 1974 in Santa Barbara, Cal., Am. Meteorol. Soc., 325 (1974).

33. F. A. Gifford, Further Comparison of Urban Air Pollution Models. Report to the 5th Meeting of NATO/CCMS Expert Panel on Air Pollution Modeling, Roskilde, Denmark, 8 pp. (1974).

34. S. R. Hanna, Application of a Simple Model of Photochemical Smog. Proceedings of 3rd Clean Air Congress, Dusseldorf, Germ., (1973)

35. G. Holzworth, Mixing Depths., Wind Speeds and Potential for Urban Air Pollution throughout the Contiguous United States. Environ. Prot. Agency Pub. No. AP-101, 118 p. (1972).

36. R. C. Sklarew, A. J. Fabrick, and J. E. Prager, J. Air Poll. Cont. Assoc., 22, 865 (1972).

37. A. Q. Eschenroeder, J. R. Martinez, and R. A. Nordsieck, Evaluation of a Diffusion Model for Photochemical Smog Simulation, Final Rept. Cont. No. 68-02-0336 by Gen. Res. Corp., P. O. Box 3587, Santa Barbara, Calif. 93105, for Environ. Prot. Ag., 212 pp. (1972).

38. G. R. Hilst, C. duP. Donaldson, M. Teske, R. Contiliano, and J. Freiberg, A Coupled 2-D Diffusion and Chemistry Model. EPA Cont. Rept. EPA-R4-73-016C (1973).

39. S. K. Friedlander and J. H. Seinfeld, Environ. Res. and Tech. 3, 1175 (1969).

40. P. A. Leighton, Photochemistry of Air Pollution, Academic Press, New York (1961).

41. P. M. Roth, S. D. Reynolds, P. J. Roberts, and J. H. Seinfeld, Development of a Simulation Model for Estimating Ground Level Concentrations of Photochemical Pollutants. Final Report, Cont. No. CPA 70-148 by Systems Appl. Inc., Beverly Hills, Cal. 90212 for the Environ. Prot. Ag., 55 pp + 6 Appen. (May 1971).

42. T. A. Hecht, J. H. Seinfeld, and M. C. Dodge, Environ. Sci. and Tech., 8, 327 (1974).

Figure 1. Map of Southern California, illustrating the cities and mountains that are important for this study.

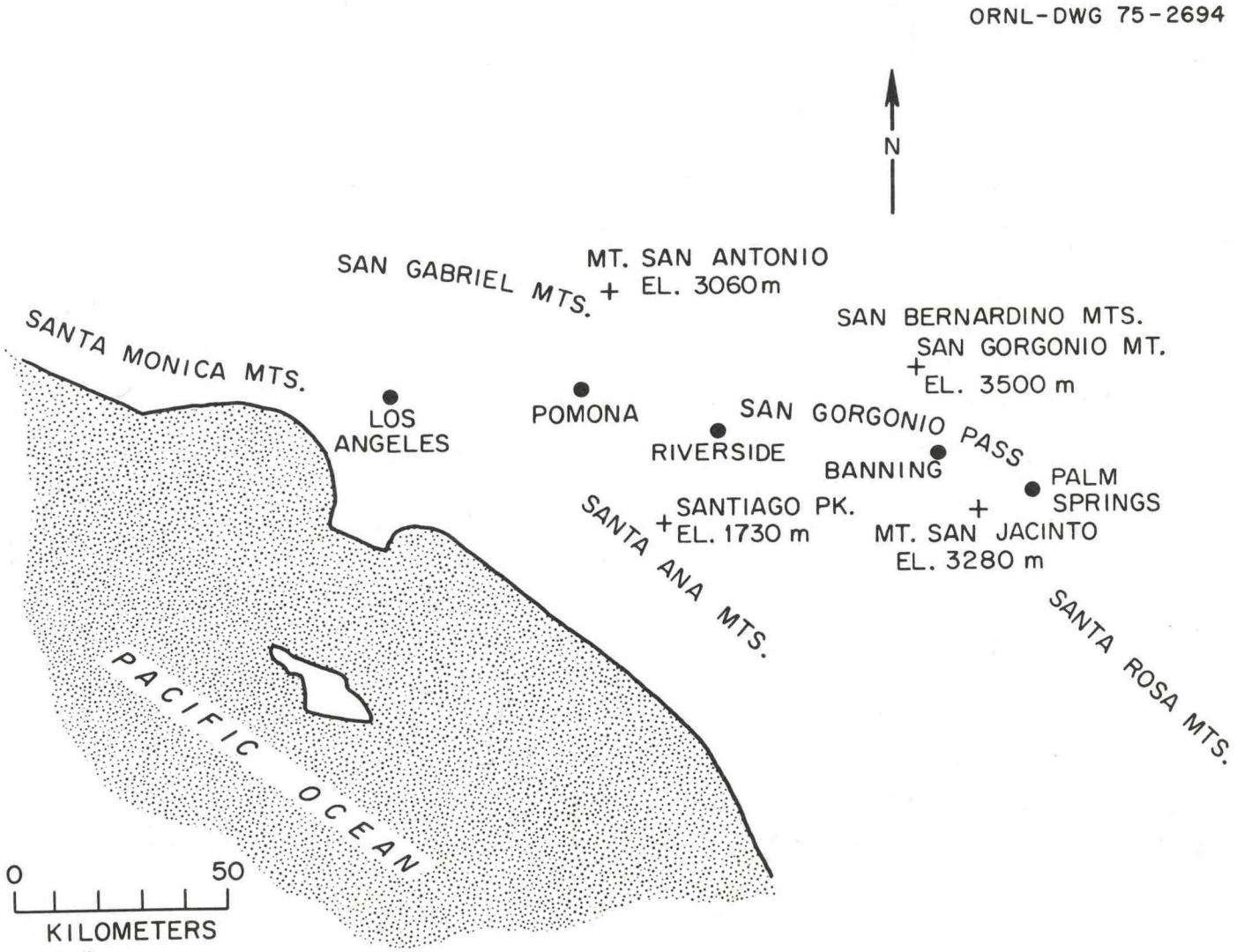

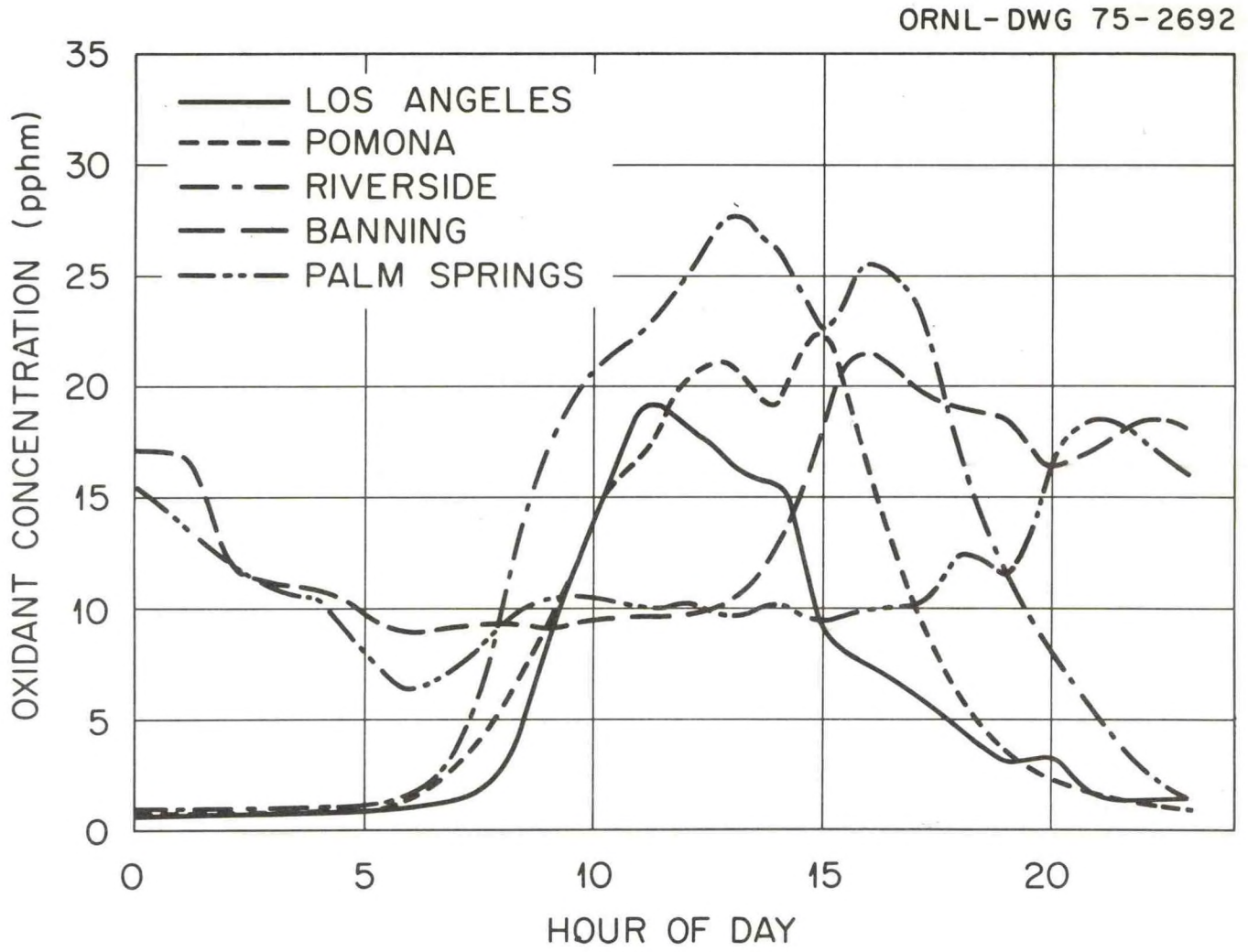


Figure 2. Average hourly oxidant concentrations for the period 23 through 26 July 1973.

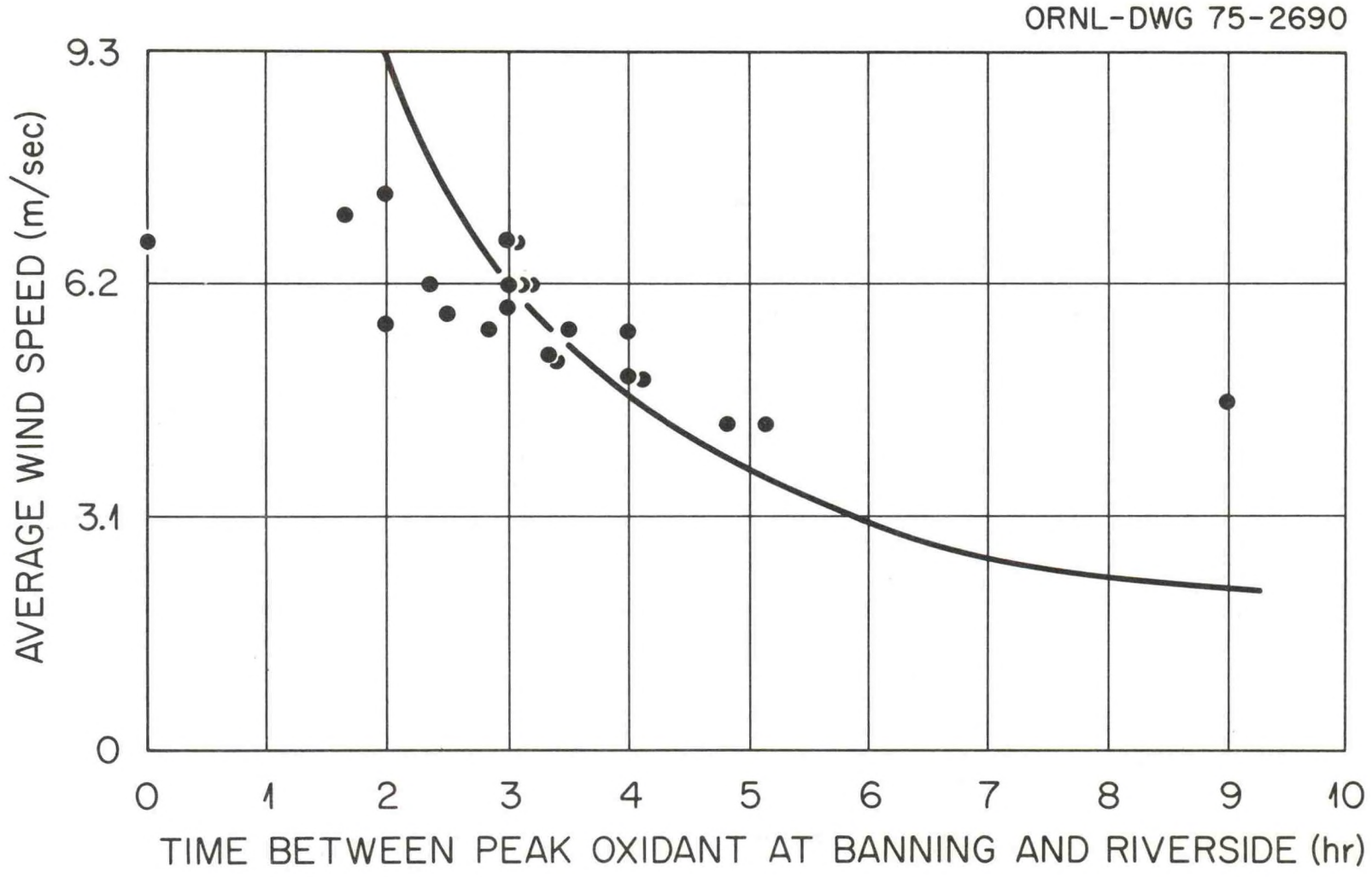


Figure 3. The time between peak oxidant concentrations at Banning and Riverside, as a function of the average wind speed at the two stations. The curve given by the time = distance/wind speed is also shown.

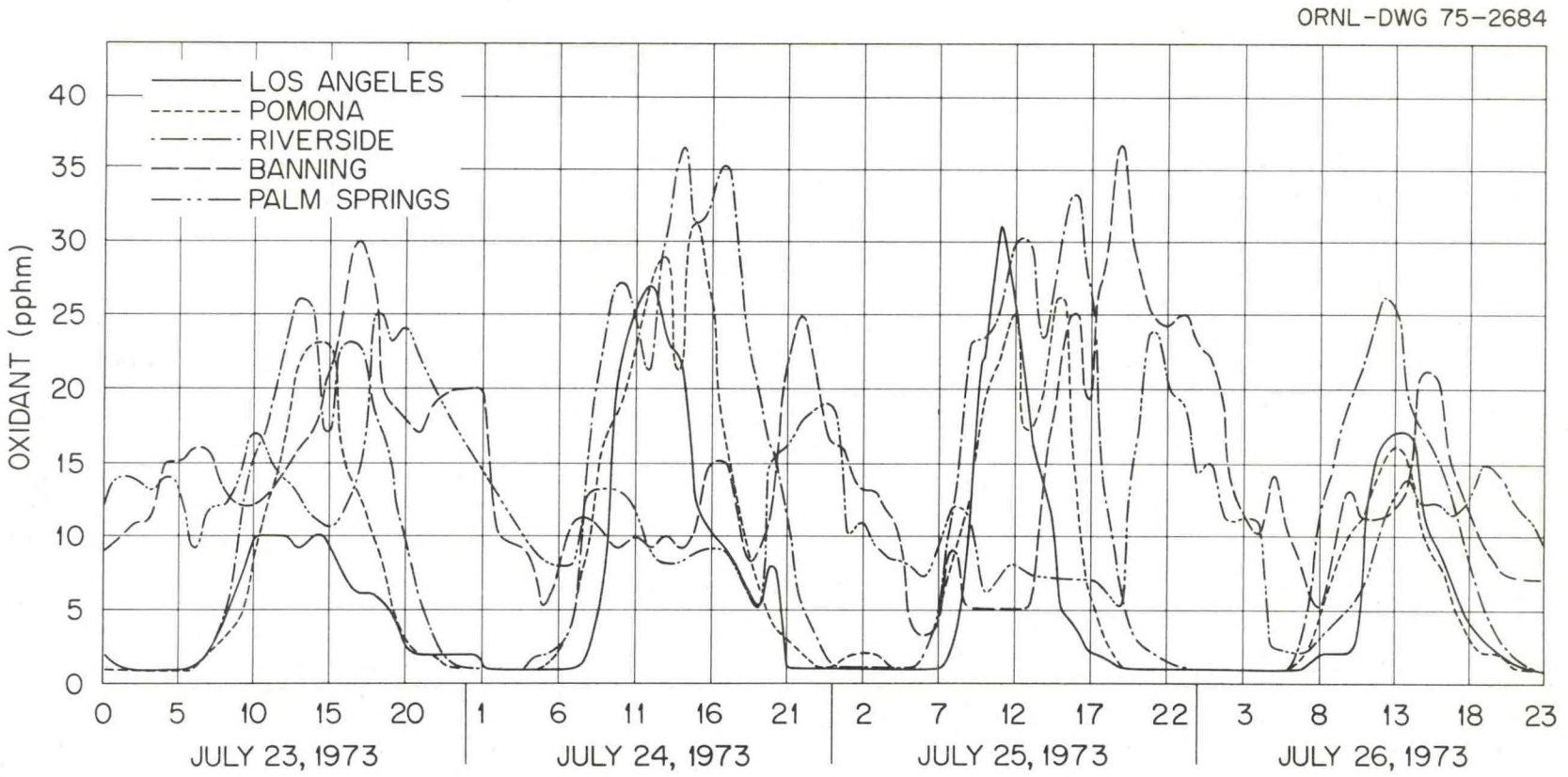


Figure 4. Hourly oxidant concentrations for the period 23 through 26 July 1973.

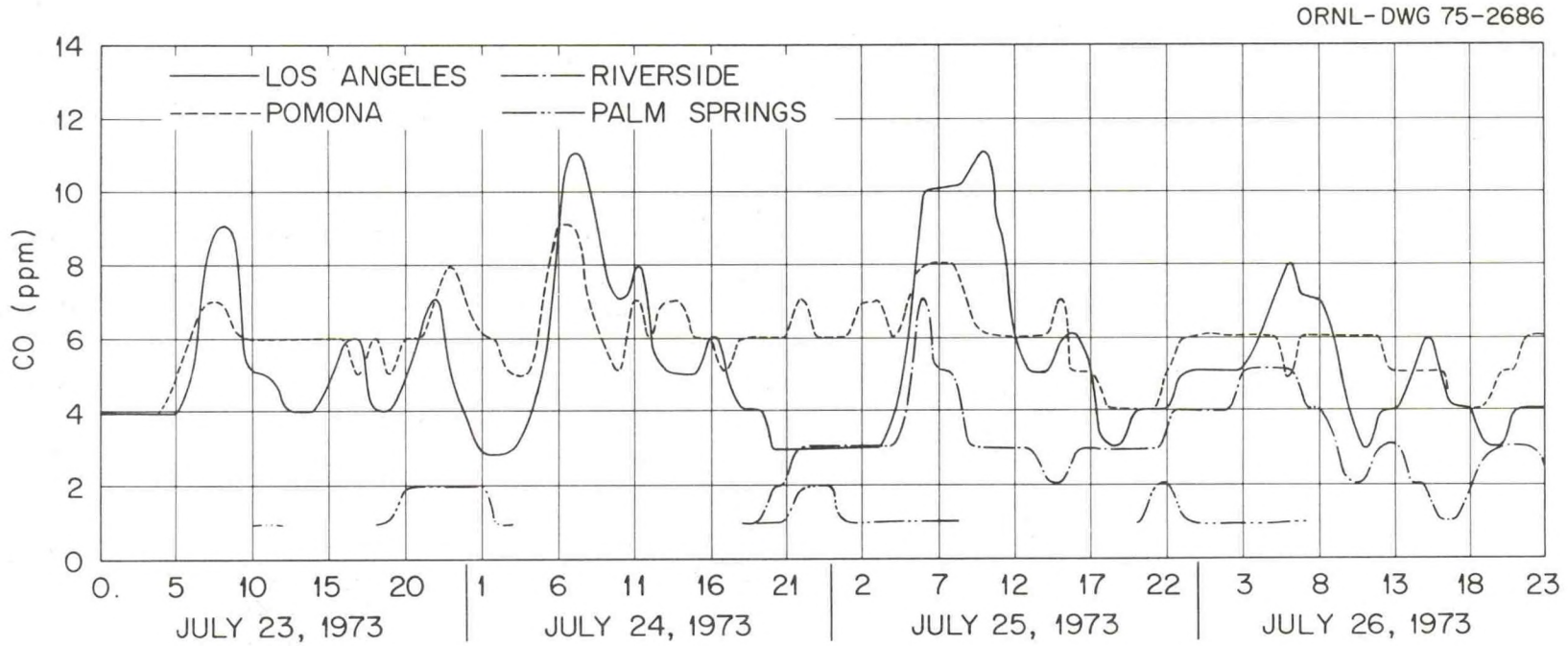


Figure 5. Hourly CO concentrations for the period 23 through 26 July 1973.

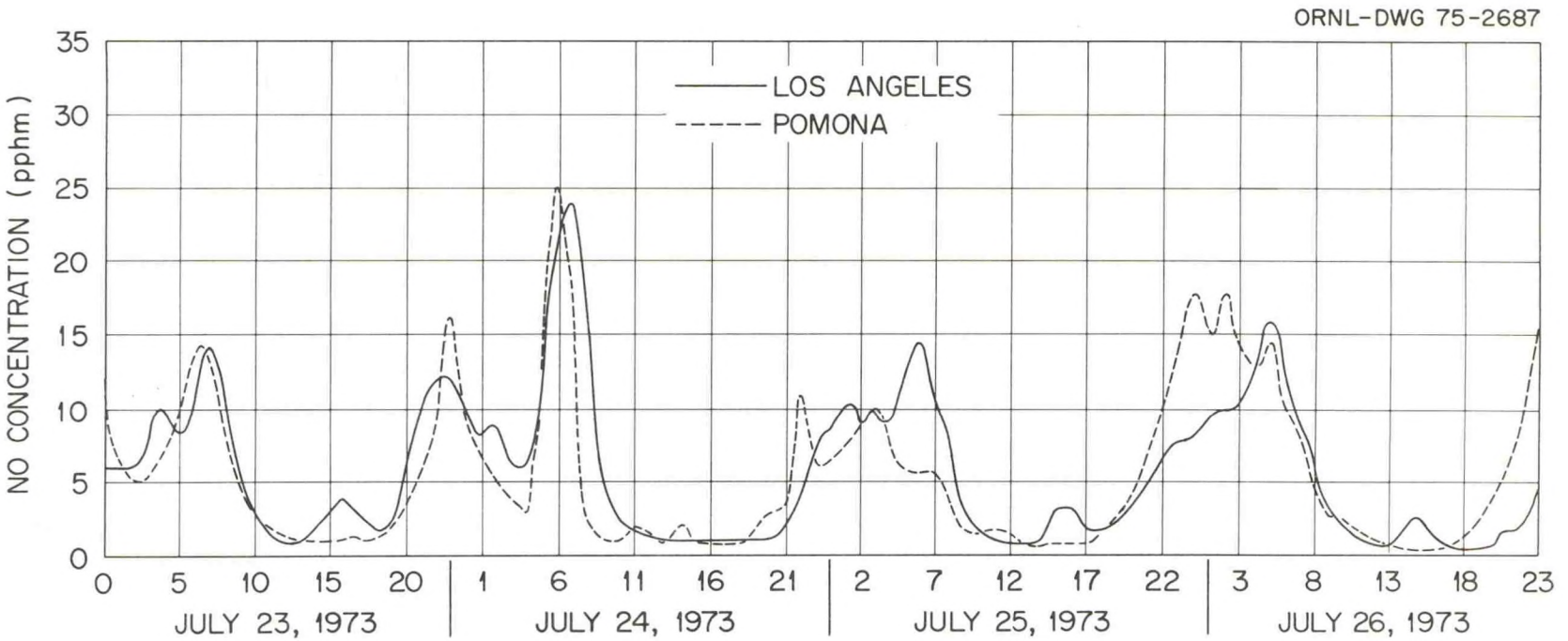


Figure 6. Hourly NO concentrations for the period 23 through 26 July 1973.

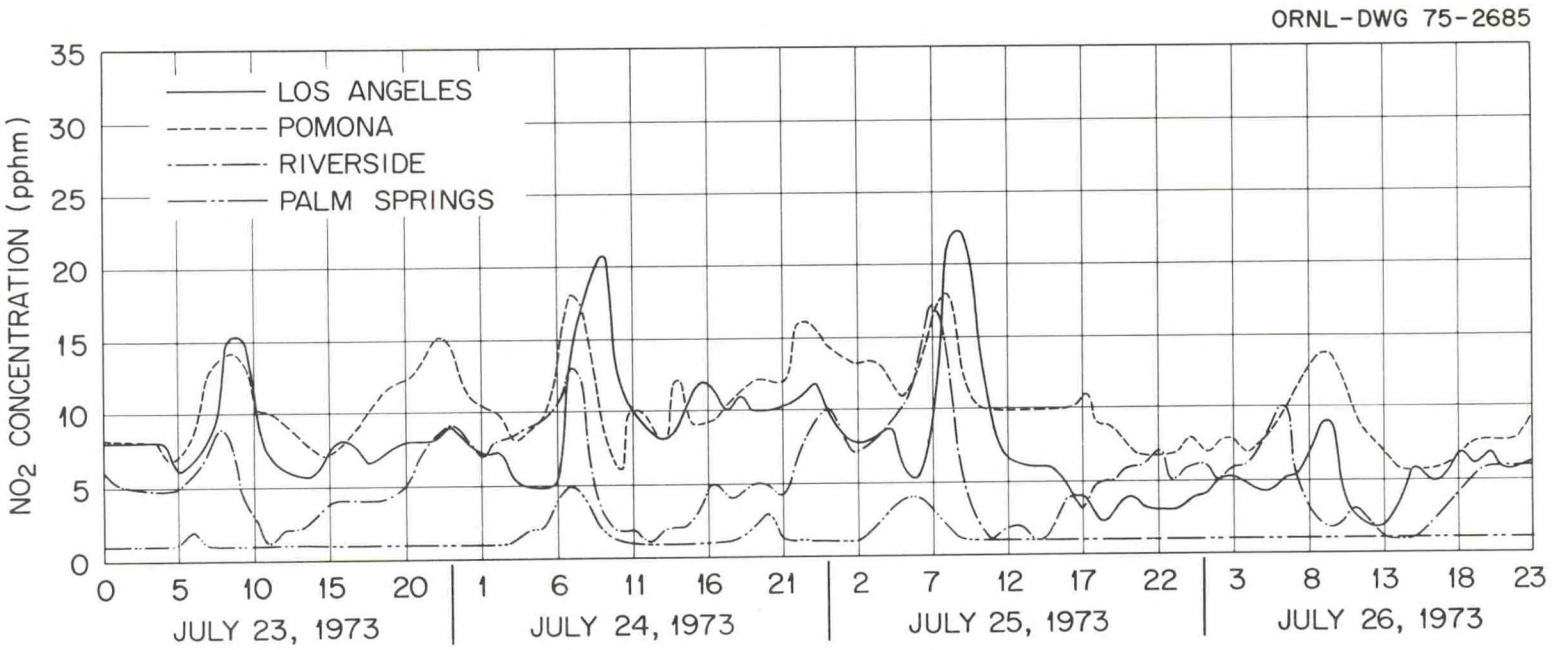


Figure 7. Hourly $NO_2$ concentrations for the period 23 through 26 July 1973.

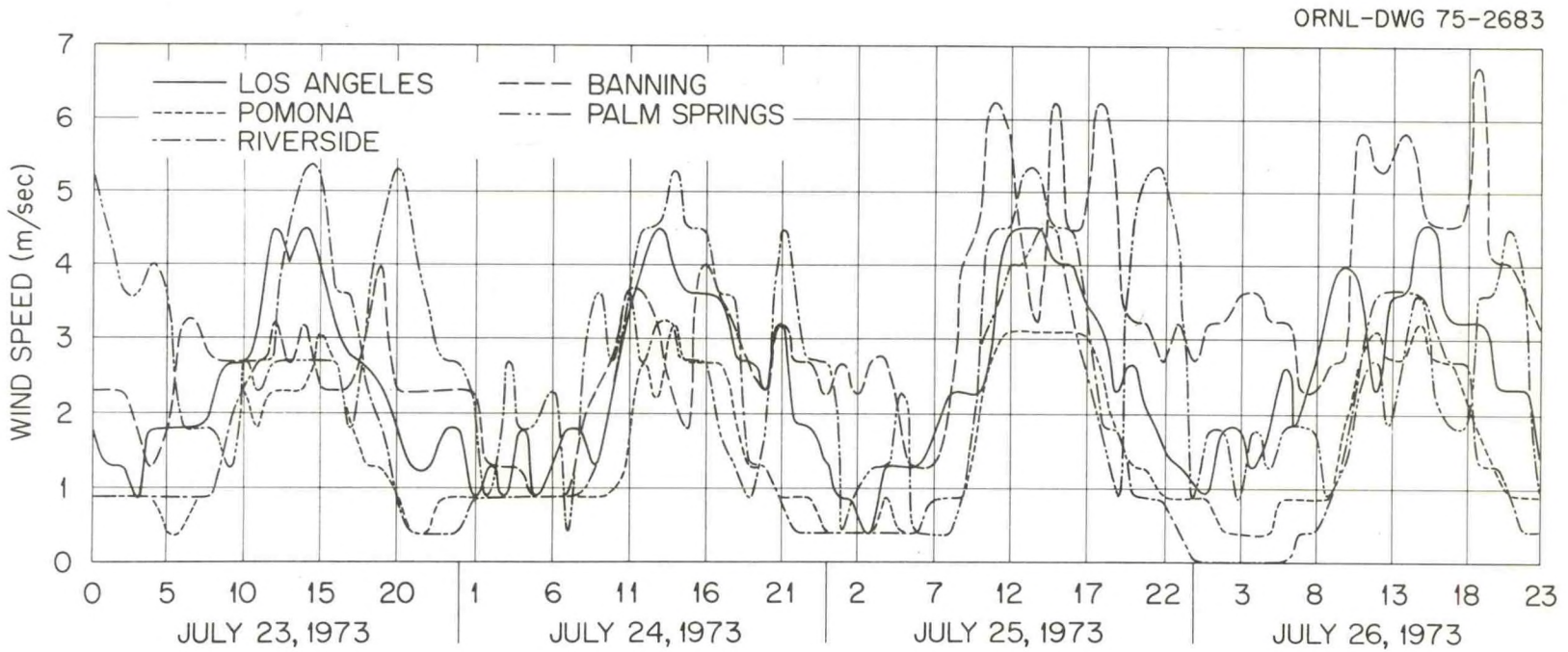


Figure 8. Hourly wind speeds for the period 23 through 26 July 1973.

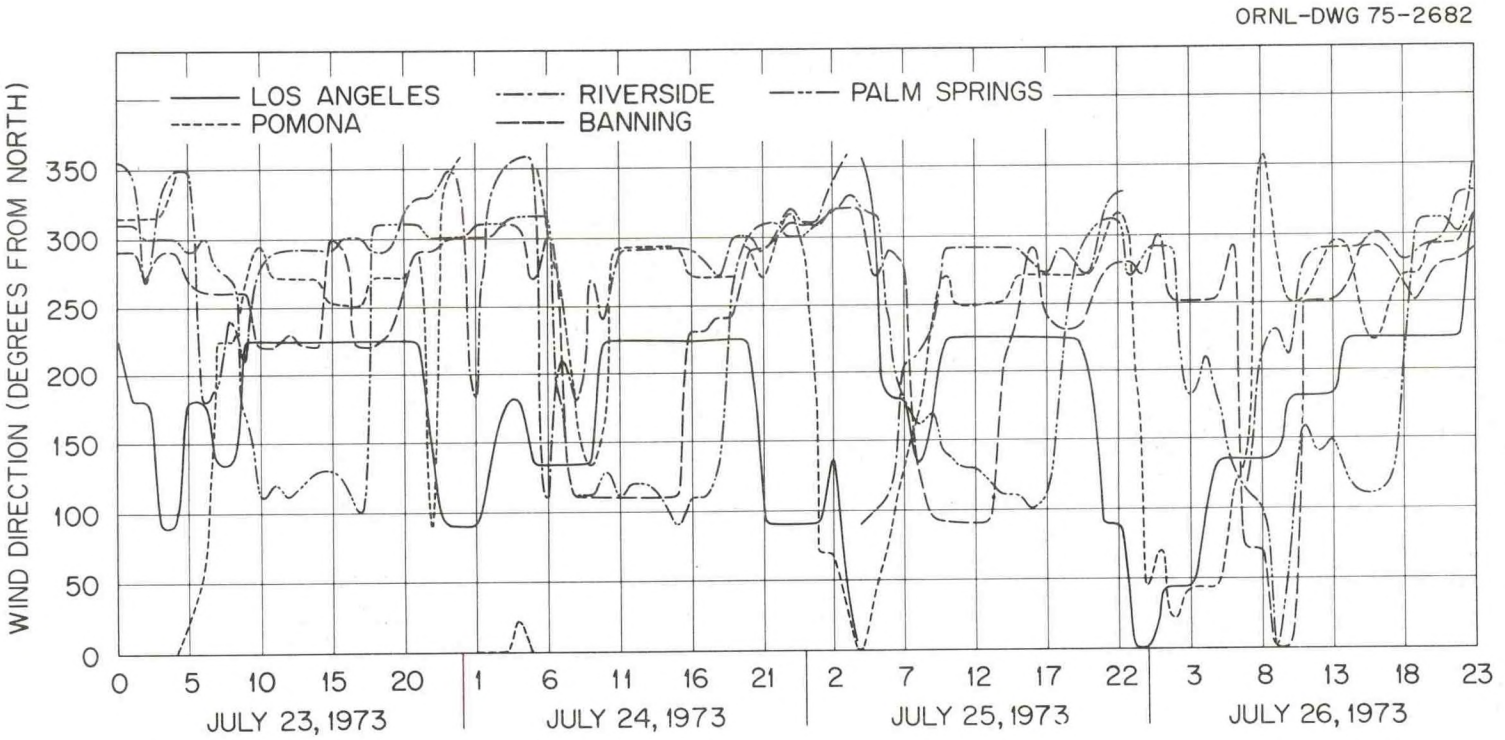


Figure 9. Hourly wind directions for the period 23 through 26 July 1973.

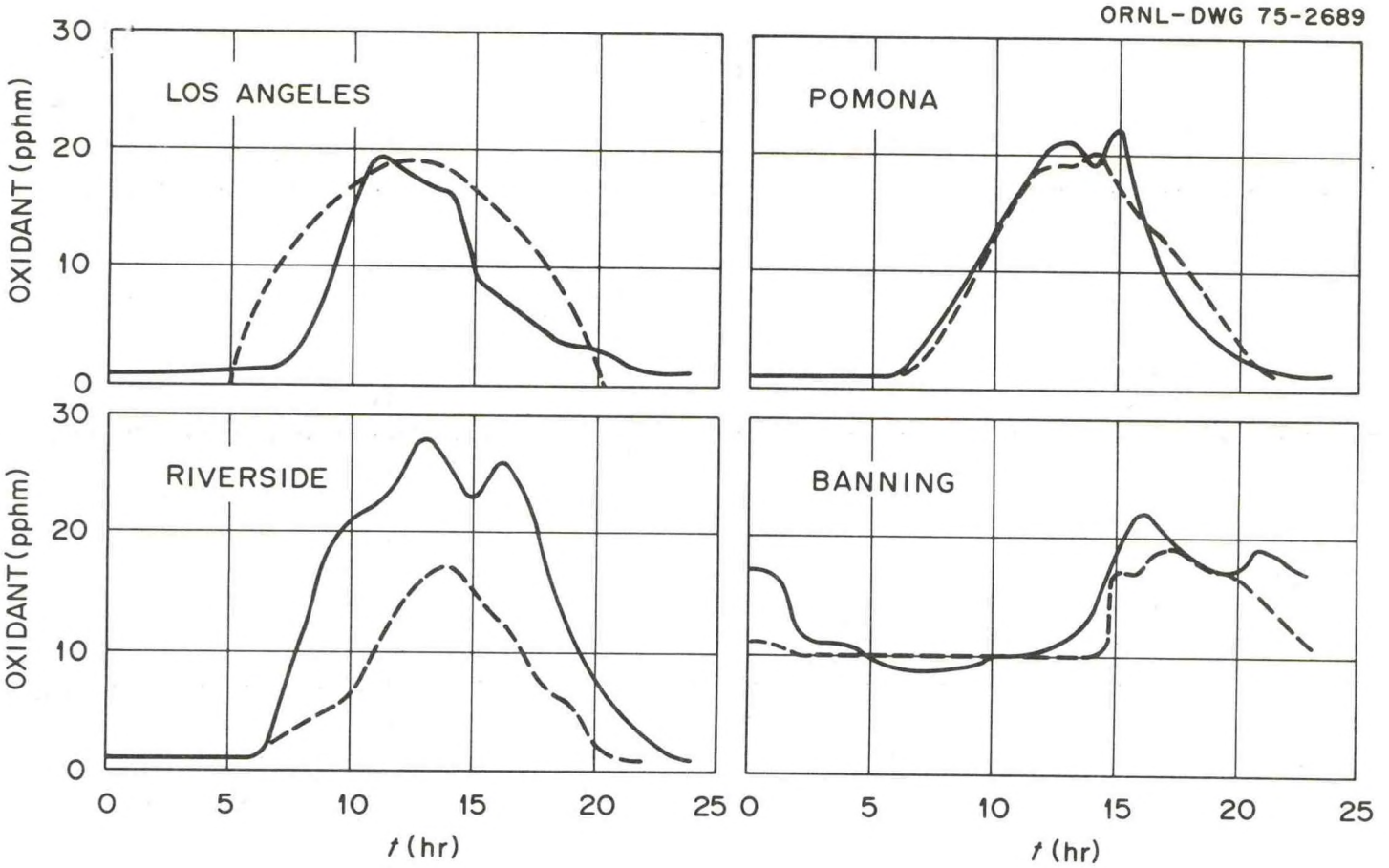


Figure 10. Observed (solid line) and calculated (dashed line, using eq. (3)) average hourly oxidant concentrations for the period 23 through 26 July 1973. The observed curves are the same as in Figure 2.

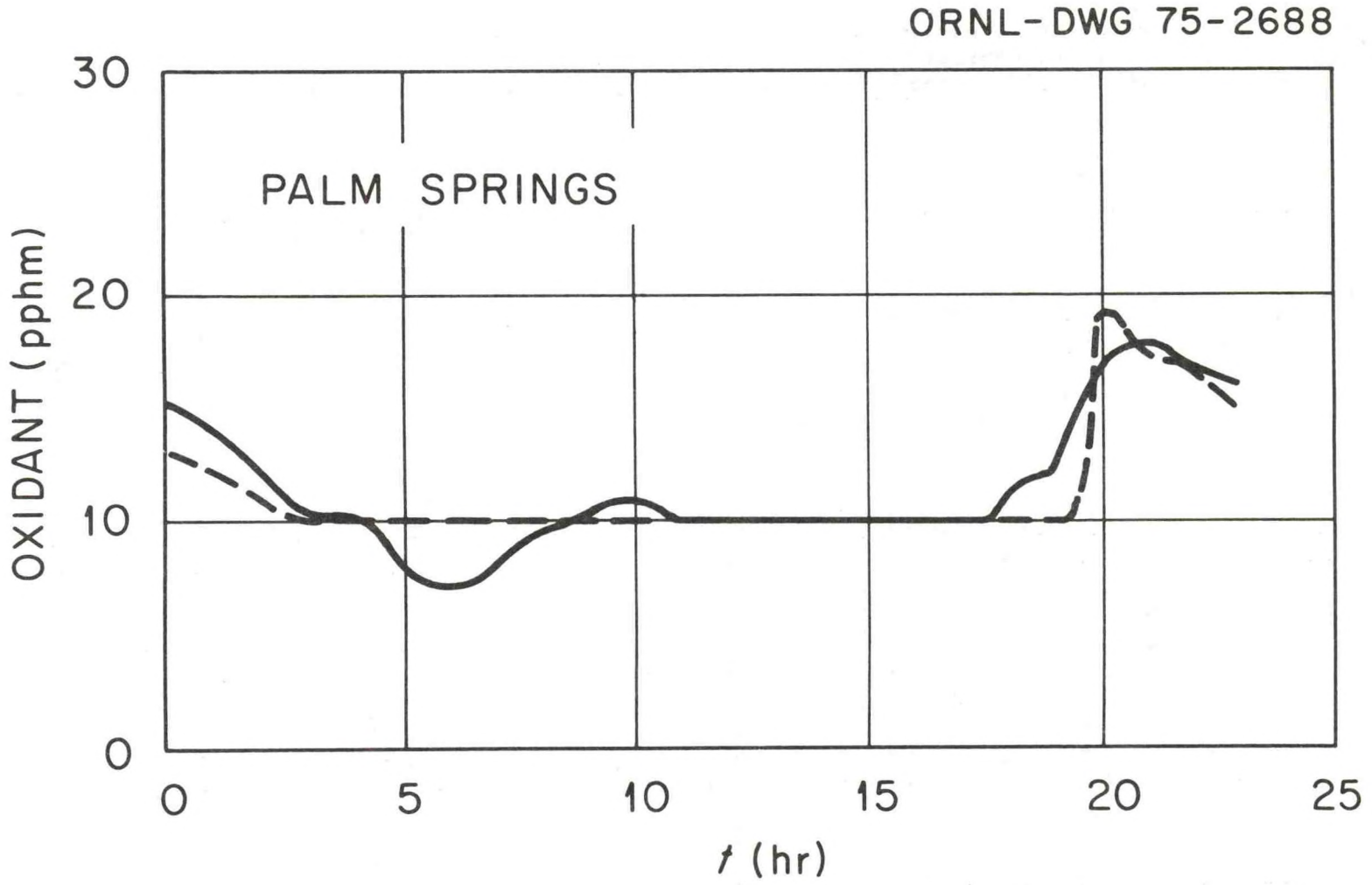
ORNL-DWG 75-2688
PALM SPRINGS
OXIDANT (pphm)
30
20
10
0
0
5
10
15
20
25
t (hr)

Figure 10e

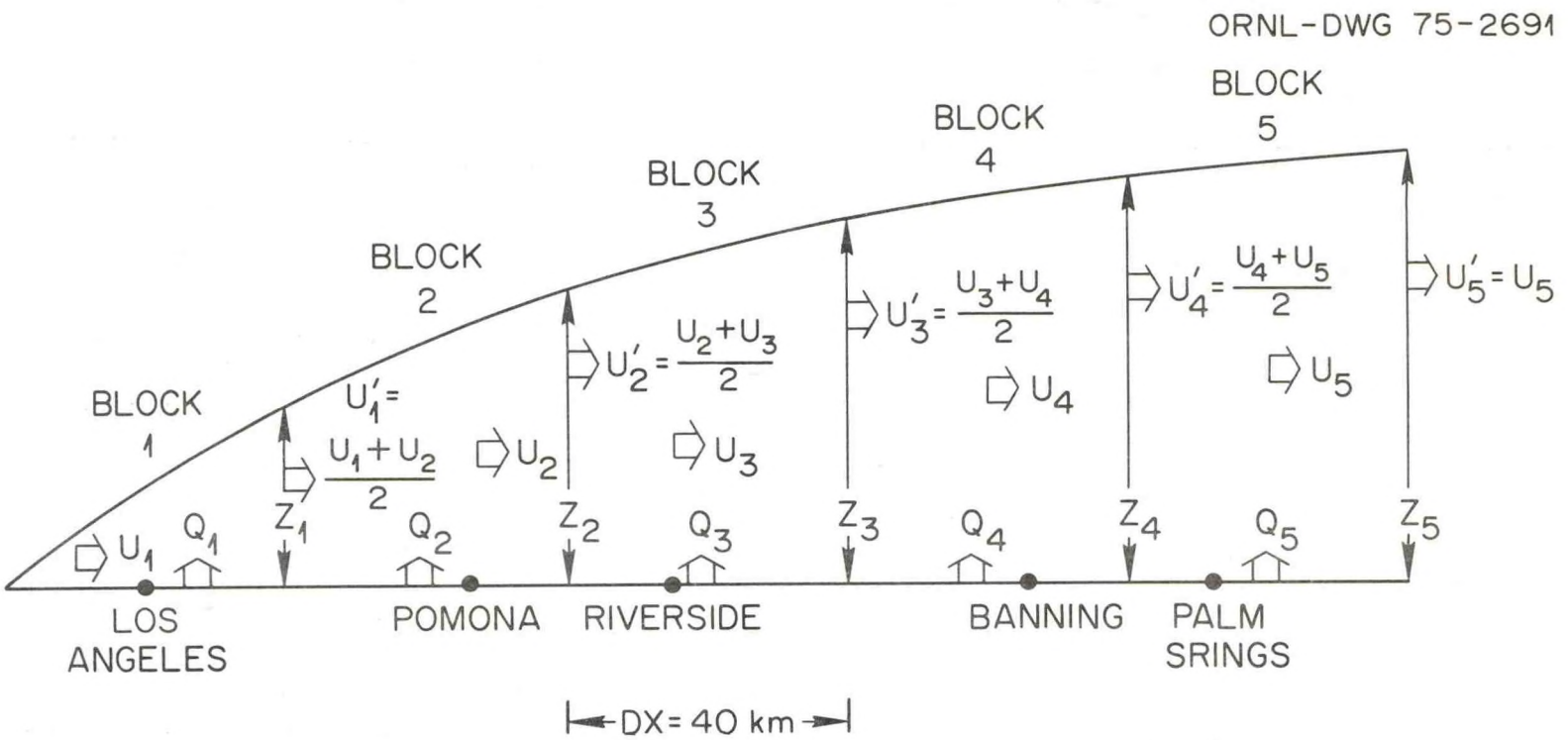


Figure 11. Schematic cross section of boxes used in numerical diffusion model.

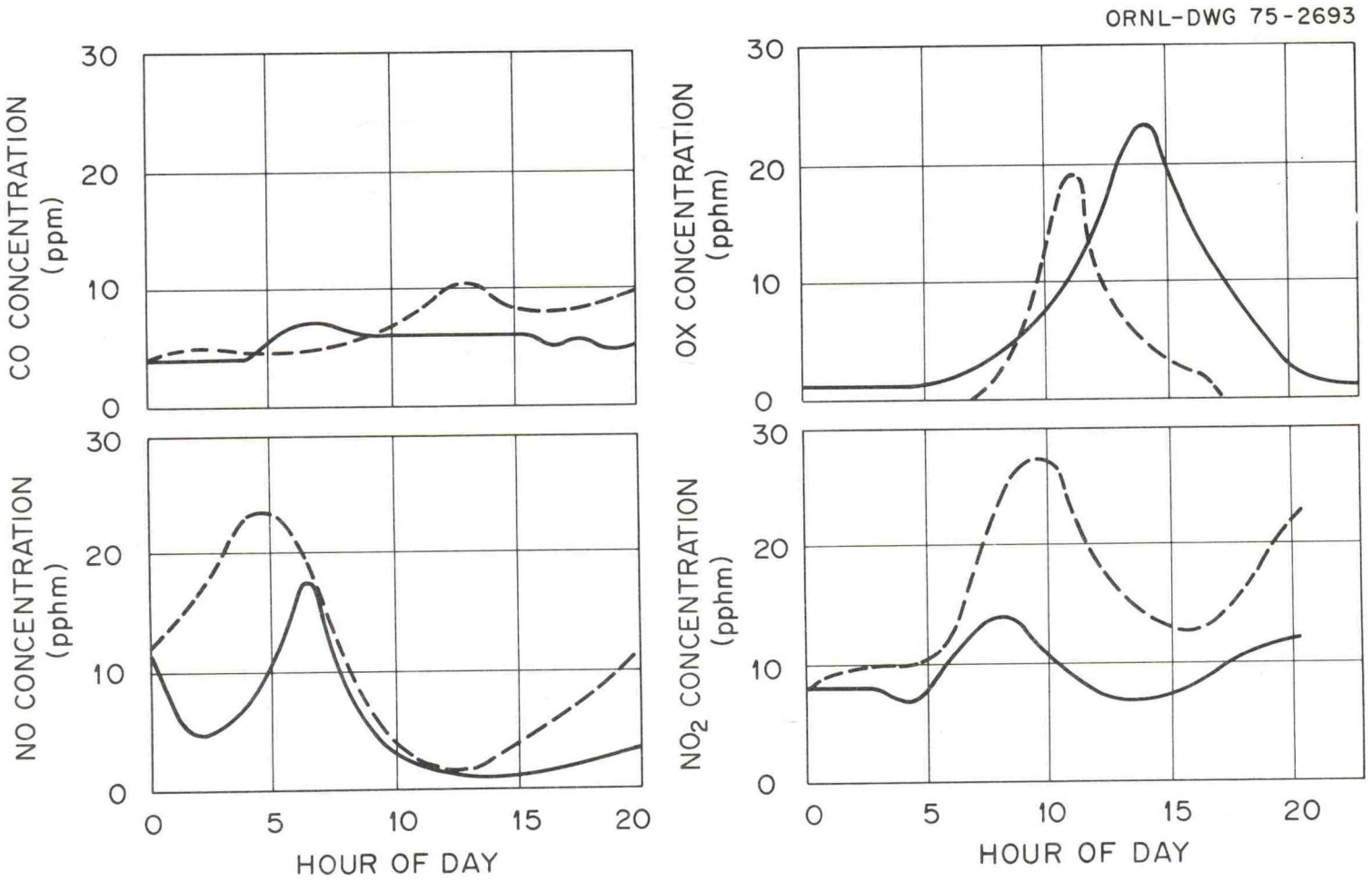


Figure 12. Observed (solid line) hourly concentrations at Pomona on 23 July 1973, compared with calculated (dashed line) concentrations, made using the numerical model with the Friedlander and Seinfeld (1969) chemical kinetics system.

# Research Required for Predicting the Behavior of Pressurized Gases Escaping into the Atmosphere

Gary A. Briggs

ATDL
February, 1975

The prediction of the behavior of pressurized gases accidentally released into the atmosphere requires many considerations, among which are thermodynamics, momentum, buoyancy (positive and negative), entrainment, and ambient wind and temperature structure. I have had relatively little time to consider these, and have not undertaken any search of the literature. This needs to be done, and will require considerable time. In what follows, I have merely outlined the areas that I think need to be considered and possible lines of research if the literature indicates the present state of knowledge is inadequate.

The problem can be divided into four parts:

1. Thermodynamics of expanding gases.
2. Diffusion of jets (momentum effects dominate).
3. Diffusion of light gases (positive buoyancy).
4. Diffusion of dense gases (negative buoyancy).

ATDL Contribution File No. 75/5

I. Thermodynamics of Expanding Gases

Gases under high pressure expand when released into the atmosphere, so there is a possibility of cooling. This can greatly affect subsequent behavior of the gas, particularly if cooling causes it to become denser than air. While classical thermodynamics should be adequate to predict the approximate results, the analysis is made complicated by the non-ideal nature of the release. The container of the gas is more often than not a good conductor of heat, not a nonconductor, and the opening through which the gas escapes seldom resembles the "porous plug" of the standard description of the throttling process. Furthermore, the process is not constant with time.

The gas which first escapes is pushed out by the gas behind it, so does little or no work itself. Except for the facts that the opening may be made of a conducting material and that the gas may escape at a high velocity, this approximates a throttling process. For an <u>ideal</u> gas, in a throttling process there is no drop of temperature, because both the internal energy (U) and pressure times volume (PV) are functions only of temperature. Because the throttled gas does no work itself, its initial and final enthalpy (U + PV) are the same, and so then must be the temperature. When the gas escapes at high velocity, it acquires kinetic energy probably at the expense of internal energy, so some initial cooling is likely.

However, as soon as the jet mixes with ambient air this energy is transformed into kinetic energy of turbulent motion, and this transforms back into heat, so there is no net effect on the gas's buoyancy. It can be shown that the temporary loss of buoyancy has negligible effect on the motion of the gas (as long as the radius of the jet is small compared to the scale height of the atmosphere!)

At the same time that something like throttling is occuring at the escape point, the gas remaining in the container is doing work to push the escaping gas out, so it does cool. For an ideal gas, the temperature of the gas remaining in the enclosure is $T = T_o(p/p_o)^{R/c_p}$, if negligible heat is transferred from the enclosure; p is the pressure in the enclosure, R is the gas constant, and $c_p$ is the specific heat at constant pressure for the gas. Subscript "o" refers to the initial conditions. The final pressure equalizes with the atmospheric value $p_a$, so if $p_o >> p_a$, the "last gas out" can be quite cool, and possibly is negatively buoyant.

Many releases occur fast enough that the gas within the container cools adiabatically while the gas escaping essentially is throttled. For an ideal gas, the temperature of the escaping gas is then effectively (after it slows down) given by

$$T = T_a \, (M/M_o)^{R/c_v}$$

where M is the mass of gas remaining in the container and $c_v$ is the specific heat at constant volume. Since $R/c_v = 0.4$ for diatomic

ideal gases, the gas coming out becomes cooler rather gradually, but can eventually be quite cold if there is little conduction of heat and $p_o/p_a$ is large. Under these conditions, the average temperature of the escaped gas approaches $(c_v/c_p)T_o$, but the "last gas out" has a temperature approaching $(p_a/p_o)^{R/c_p} T_o$.

Because there are many possible escape configurations (leaks, splits, breaks, and so on), many possible container configurations (tanks, fat pipes, skinny pipes, distant cut-off valves, etc.) and different container conductivities, one can not always approximate the process by assuming adiabatic pressure reduction within the container and throttling at the escape point. Especially in the case of marginally buoyant gases, one should ask the following questions:

1. Is the cooling of the gas at the escape point negligible?
2. Is there any significant heat transfer from the container to the gas? This applies especially to the "last gas out," which cools the most.
3. How does the temperature and rate of release of the escaping gas change with time? This is needed to define the source strength and the basic character of the source (jet, light gas, dense gas).

Usually, these questions can be answered from established thermodynamic theory, but often computer power will be required. For some configurations, a physical experiment (perhaps on a reduced scale) would be desired.

II. Diffusion of Jets

The behavior of momentum-dominated flows exiting from round openings or slots has been studied in some detail (see Pai, 1954). The final rise of such flows is not so well known, but usually buoyancy becomes an important factor before a final rise is obtained. What little is known about the rise of pure jets (no buoyancy) is summarized in Plume Rise (Briggs, 1969).

If the gas has any buoyancy, in most cases it is conserved, so the buoyant force adds (or subtracts) vertical momentum at a constant rate (Newton's second law). The buoyancy-induced momentum then exceeds the initial momentum at a time after release $T = F_m/F$, where $F_m$ is the initial flux of momentum divided by $\pi\rho_a$, where $\rho_a$ is the ambient density, and F is the flux of buoyant force divided by $\pi\rho_a$ (see Briggs, 1970). The distance at which this occurs can be estimated from the calculated jet trajectory as a function of time, neglecting buoyancy. For a jet bent over in a crosswind u, it is approximated simply by $x = ut$. Beyond this distance, the flow can no longer be considered momentum-dominated

The essential feature of a jet in the absence of crossflow is that it expands conically (dr/ds is constant, where r is the jet radius and s is the axial distance from the virtual origin). With momentum conserved, for a point source this results in a centerline velocity $\propto F_m^{1/2} r^{-1} \propto s^{-1}$ and a volume flux (dilution) $\propto F_m^{1/2} r \propto s$. For a slot jet of length L, and $s < L$, the centerline velocity $\propto (F_m/L)^{1/2} r^{-1/2} \propto s^{-1/2}$ and the volume flux $\propto (F_m Lr)^{1/2} \propto s^{1/2}$.

The jet in a crosswind is more complex (see Briggs, 1969 and 1970) but the rate of dilution is generally greater than in calm air except at large axial distances ($s > \sim 100 (w_o/u) D$, where $w_o$ is the efflux velocity and D is the source diameter).

The diffusion of a jet directed horizontally near the ground is somewhat more complex, since it may attach to the ground and become a wall jet. Positive buoyancy may cause it to lift-off at some point, and negative buoyancy will cause it to settle with less dilution than for a pure wall jet. These phenomena could be studied in a wind tunnel or water channel, but it is important to include surface layer turbulence. Engineering approximations could also be made on the basis of free jet behavior, but this involves a larger uncertainity.

As for the diffusion of a jet directed downward into the ground, this can be very difficult as the source configuration can be irregular and it involves soil mechanics as well as fluid mechanics. Lacking experience or experiment, it is probably best to assume no residual momentum and no initial mixing in estimating diffusion; i.e., assume a passive point or line source, with only buoyancy of the gas conserved.

Some particularly relevant questions are:

1. What are the possible initial source configurations?
2. At what point does the plume or cloud behave more as a light gas or a dense gas?
3. What is the dilution at the end of the momentum-dominated stage?

## III. Diffusion of Light Gases

The behavior of light (buoyant) gases is relatively well-researched (see Briggs, 1969), at least for point or small-diameter sources. No further survey of the problem will be attempted here. However, there are other aspects of buoyant gas behavior which still need study.

One is the case of buoyant gas initially attached to the ground, as may happen with horizontal ejection at the ground or in the cavity region of a building or other obstacle. As far as ground exposure is concerned, it is critical to predict whether or not the gas will lift off the ground. A systematic approach towards this prediction is suggested in a memo by Briggs (1973 ), but experiments are needed. Lift-off capability depends on the buoyancy, the wind, the plume width (but not the depth), and the friction velocity in the surface layer, $u^*$. If the plume does not lift off, it diffuses more like a passive gas (non-buoyant).

Sometimes gas under pressure ruptures a pipe along a longtidinal seam, creating a line source of buoyancy of strength F/L. The rise of buoyant gases from line sources is another area that needs more work. Briggs (1974 ) published an analysis of data from lines of discrete, continuous sources consisting of 2 to 9 power plant stacks of equal height and spacing.

This approach could be applied to a continuous line source by approximating it with N evenly spaced discrete sources of strength F/N and letting N approach infinity. However, considering the small number of discrete sources analyzed, caution is advised in extending this result to a true line source.

For cases in which the point-source plume rise $\Delta h_{pt}$ is proportional to $F^{1/3}$, the result is $\Delta h = \Delta h_{pt}/(1 + 6\ (L/\Delta h_{pt})^{3/2})^{1/3}$. If $\Delta h_{pt} \leq 3.3L$, $\Delta h \simeq 0.55\ \Delta h_{pt}^{3/2}/L^{1/2}$. This result applies to the rising stage of a buoyant plume trajectory, the "2/3 law" for a point source. For $\Delta h_{pt} < 3.3L$, the plume has a constant rate of rise with a slope proportional to $(F/L)^{1/2}\ u^{-3/2}$. A similar result also applies to the final rise in stable conditions with wind (see Briggs, 1972). With a slight modification, the approach can also be applied to final rise in stable conditions with no wind, in which case $\Delta h_{pt} \propto F^{1/4}$. Similarly results are obtained, with the line source approximation being preferred only when $\Delta h_{pt} < 3.3L$, as before. However, by the "rule of least rise," the "calm" formula is used only when u is less than $\sim 0.1(F/L)^{1/3}$, a very low wind speed for most sources.

The most relevant questions are:

1. Does the plume have enough buoyancy or vertical momentum to lift off the ground and become a "free plume"?
2. If it does, does its configuration most resemble that of a point source, for which much information exists, or that of a line source of buoyancy?

## IV. Diffusion of Dense Gases

The diffusion and spread of dense gases released near the ground is much more complicated than the behavior of free plumes because of the inhibiting effects of the ground. This means that the vertical growth of the gas is restricted, so it can not be assumed proportional to the horizontal growth, as for a free plume. Furthermore, the ground can inhibit the horizontal spread through the influence of drag. On the other hand, atmospheric effects are relatively simplified, since the gas usually sinks down into the inertial surface layer where all turbulent velocities scale to the friction velocity, $u^*$, and stratification is a minor or negligible effect. However, even in the absence of atmospheric effects, mathematic modeling of dense gas behavior over a rough surface will be more complicated than for free plume behavior.

Because of these complicating factors, complete understanding of dense gas behavior will come slowly. A few of the more simple areas have received study already. The rise and descent of a continuous dense gas plume has been investigated, including the effect of cross-wind (Hoot, Meroney and Peterka, 1973). This study includes measurements of the attenuation of concentration with distance, both for the lofted continuous plume and the ground source. For the ground source, vertical and lateral spread with distance were also measured. Several empirical studies have been made on the spread of dense gas over a

smooth surface, namely, water, but with little theoretical foundation to permit generalization of the results ( e.g. Bureau of Mines, 1972). A phenomenon similar to the spread of dense gases on a smooth surface has received considerable attention, the spread of buoyant thermals under the surface of water (Shirazi and Davis, 1974). This is almost the same problem viewed upside-down, the main difference being that the surface of the water is a free surface, whereas gas velocity must be zero next to a solid or liquid surface.

The diffusion of dense gas can be divided into up to six stages, the number depending on the strength of the source, the nature of the underlying surface, and ambient turbulence and stratification. Table I illustrates the complexity of the problem, since it constitutes a very compact summary of a host of possibilities. Only buoyancy-conserving sources are considered. There are 4 basic source types. The first two are "instantaneous" sources, identifiable by a short release time compared to the diffusion time. Type A is a compact source, more of a puff than a line, and Type B is a line source, described in terms of momentum, buoyancy, or material per unit length of the source. In general, when one considers distances out from the line source greater than the line length, the diffusion gradually becomes more and more like that of a type A source. This generalization also applies to the type D source, which diffuses more like a type C

source at great distances out. The C and D sources are designated as "continuous" sources, meaning that the release time, or characteristic decay time of source strength, is large compared to the diffusion time being considered. Of course there is a broad area between "instantaneous" and "continuous" releases; I can only suggest that if the behavior in this transition area is unknown that the pure source type prediction which gives the least amount of spreading is the most appropriate. A similar approach can be used to decide whether to treat a finite line source as a point source.

The effect of wind is not considered directly in Table 1, although it is strongly related to the friction velocity $u_*$, the effects of which are considered in stages 5 and 6. For the instantaneous sources, when the wind speed u is less than the frontal velocity $v_e$, the wind only distorts the gas, making the growth lopsided. When the component of u perpendicular to the gas boundary exceeds $v_e$, the entire cloud moves in the direction of the wind, and the diffusion is somewhat enhanced along that direction due to the presence of wind shear near the ground. A continuous point source, type C, is transformed into a type B source when the gas becomes elongated by a crosswind. The material released in a unit of time $\Delta t$ is carried along wind in a segment of plume of horizontal length $\Delta tu$, so the source strengths that were original specified per unit time are transformed to source strengths per unit length. This is done mathematically simply by dividing the source strengths (momentum, buoyancy, or material) by u. A continuous

## Table I - Stages of Dense Gas Diffusion

| | Type of source | Instantaneous point (thermal) A | Instantaneous line (line thermal) B | Continuous point (plume) C | Continuous line (slot plume) D |
|---|---|---|---|---|---|
| 1. | Buoy. $B_o = g\Delta_o V_o$, $V_o$ is a | volume | area* | volume per time | area per time |
| 2. | Dimensions of B are | $\ell^4/t^2$ | $\ell^3/t^2$ | $\ell^4/t^3$ | $\ell^3/t^3$ |
| 3. | Buoy. conserved: $B/g = \Delta V \propto$ | $\Delta r_e^2 \bar{h}$ | $\Delta r_e \bar{h}$ | $\Delta rhv$ | $\Delta hv$ |
| | Stage 1 (forced rise) | | | | |
| 4. | If upward thrust $w_o$, $\Delta h \propto$ | $B^{1/4} (w_o/g\Delta_o)^{1/2}$ | $B^{1/3} (w_o/g\Delta_o)^{2/3}$ | $B^{1/4} (w_o/g\Delta_o)^{3/4}$ | $B^{1/3} (w_o/g\Delta_o)^{1}$ |
| | Stage 2 (ground contact) | | | | |
| 5. | V at ground contact $\propto$ | $(h_s + 2\Delta h)^3$ | $(h_s + 2\Delta h)^2$ | $B^{1/3}(h_s + 2\Delta h)^{5/3}$ | $B^{1/3}(h_s + 2\Delta h)^{1}$ |
| 6. | If $h_s = 0$, $V = V_2 \propto$ | $B^{3/4} (w_o/g\Delta_o)^{3/2}$ | $B^{2/3} (w_o/g\Delta_o)^{4/3}$ | $B^{3/4} (w_o/g\Delta_o)^{5/4}$ | $B^{2/3} (w_o/g\Delta_o)^{1}$ |
| 7. | Dilution $= V_2/V_o \propto$ | $Fr_o^{3/4}$ | $Fr_o^{2/3}$ | $Fr_o^{1/2}$ | $Fr_o^{1/3}$ |
| | Stage 3 (dragless spread) | | | | |
| 8. | Frontal displacement $r_e \propto$ | $B^{1/4} t^{1/2}$ | $B^{1/3} t^{2/3}$ | $B^{1/4} t^{3/4}$ | $B^{1/3} t^{1}$ |
| 9. | Frontal velocity $v_e \propto$ | $B^{1/2} r_e^{-1}$ | $B^{1/2} r_e^{-1/2}$ | $B^{1/3} r_e^{-1/3}$ | $B^{1/3}$ |
| 10. | Dilution V $\propto$ | $r_e^{2\alpha}$ | $r_e^{\alpha}$ | $r_e^{2(\alpha-2/3)}$ | $r_e^{(\alpha-1)}$ if $\alpha > 1$ |
| 11. | Mean height $\bar{h} \propto$ | $r_e^{2(\alpha-1)}$ | $r_e^{\alpha-1}$ | $r_e^{2(\alpha-1)}$ | $r_e^{(\alpha-1)}$ if $\alpha > 1$ |
| 12. | Fr $\propto$ | $(\alpha-1/2)^{-1}$ | $(\alpha- 1/2)^{-1}$ | $(1-\alpha)/(\alpha -5/6)$ | 1/8 |
| 13. | Satisfactory values of $\alpha$: | $1/2 < \alpha < 1$ | $1/2 < \alpha < 1$ | $5/6 < \alpha < 1$ | $0 < \alpha < 1$ |

| | | A | B | C | D |
|---|---|---|---|---|---|
| | **Stage 4 (ground friction)** | | | | |
| 14. | If no mix, $(B\ V_4/C_D) \propto$ | $v_e^2\ r_e^5$ | $v_e^2\ r_e^3$ | $v_e^4\ r_e^3$ | $v_e^4\ r_e$ |
| 15. | Then $r_e \propto$ | $(B\ V_4/C_D)^{1/7} t^{2/7}$ | $(B\ V_4/C_D)^{1/5} t^{2/5}$ | $(B\ V_4/C_D)^{1/7} t^{4/7}$ | $(B\ V_4/C_D)^{1/5} t^{4/5}$ |
| 16. | And $V_e \propto$ | $(B\ V_4/C_D)^{1/2} r_e^{-5/2}$ | $(B\ V_4/C_D)^{1/2} r_e^{-3/2}$ | $(B\ V_4/C_D)^{1/4} r_e^{-3/4}$ | $(B\ V_4/C_D)^{1/4} r_e^{-1/4}$ |
| 17. | And $\bar{h} \propto$ | $V_4/r_e^2 \propto t^{-4/7}$ | $V_4/r_e \propto t^{-2/5}$ | $V_4/(r_e\ v_e) \propto t^{-1/7}$ | $V_4/v_e \propto t^{+1/5}$ |
| 18. | $Fr = v_e^2/(g\Delta_4\bar{h}) \propto$ | $(r_4/r)^3$ | $(r_4/r)^2$ | $(r_4/r)^{5/4}$ | $(r_4/r)^{3/4}$ |
| | **Stage 5 (edge diffusion)** | | | | |
| 19. | Stage 4 to stage 5 at $r_5 \propto$ | $(B\ V_4/C_D u^{*2})^{1/5}$ | $(B\ V_4/C_D u^*)^{1/3}$ | $(B\ V_4/C_D u^{*4})^{1/3}$ | $(B\ V_4/C_D u^{*4})^1$ |
| 20. | $v_e \propto u^*$, $Fr^* \propto$ | $u^{*2} r_e^2/B$ | $u^{*2} r_e/B$ | $u^{*3} r_e/B$ | $u^{*3}/B$ |
| | **Stage 6 (passive diffusion)** | | | | |
| 21. | Stage 3 or 5 to 6 at $r_6 \propto$ | $(B/u^{*2})^{1/2}$ | $B/u^{*2}$ | $B/u^{*3}$ | Depends on $B/u^{*3}$ |
| | **Stage 6a (buoyancy nulled)** | | | | |
| 22. | Buoyancy destroyed at $r_d \propto$ | $(v_e\ B/H)^{1/3}$ | $(v_e\ B/H)^{1/2}$ | $(B/H)^{1/2}$ | $(B/H)$ |

*A continuous point source stretched horizontally by wind is equivalent to a line thermal, type B.

line source is practically unaffected by a wind parallel to it until $u\Delta t$ exceeds the length of the line, L; after that, the gas moves downwind behaving similarly to gas released over a time $\Delta t = L/u$, ultimately behaving like a type B source. A wind perpendicular to the type D source has only a distorting effect if $u<v_e$. If $u>v_e$, the gas is advected as a sheet of dense gas with practially no horizontal diffusion at first, gradually it behaves like a type B source in the lateral direction, with its original source strengths multiplied by L/u.

Line 1 of Table I describes the buoyancy source term, which is the total buoyant force divided by the ambient density, $\rho_a$. It is given by $B = g\ \Delta_o\ V_o$, where g is gravitational acceleration, $\Delta_o$ is the initial relative density difference, $(\rho_o - \rho_a)/\rho_a$, and $V_o$ is the initial gas volume, generalized. For a type A source $V_o$ is a volume, but for type B it is a volume per unit length, i.e., an area. For types C and D it is given in terms of volume (or area) emitted per unit time. These various "volume" types for $V_o$ result in different dimensions of B for each source type, shown on line 2. This will result in different power law solutions for the asymptotic result of each diffusion stage, since in every case the units should balance. The basic requirement for all sources, that the total buoyancy be conserved, is expressed in line 3, where $\Delta$ is the averaged relative density difference $(\rho - \rho_a)/\rho_a$. In general, both $\Delta$ and the concentration of the gas are inversely proportional to V, i.e., $\Delta/\Delta_o = (V/V_o)^{-1}$. For the instantaneous

sources the volume after release can be described by the radius or distance of the "front" from the origin, $r_e$, and the mean height of the gas, $\bar{h}$. For the continuous source, once the front passes a radius or a point the integrated flux of buoyancy equals the source term. The flux can be stated in terms of the local height, h, the mean local outward velocity, v, and the local radius in the case of type C. Alternatively, integrating over time after the gas is "turned on," t, we have $(B/g)t \propto \Delta r_e^2 \bar{h}$ and $\Delta r_e \bar{h}$ for types C and D, just as we had for (B/g) in the case of types A and B.

The first two "stages" of diffusion apply only to dense gases given an initial upward thrust velocity $w_o$. In the first stage the gas rises due to its initial upward momentum, and in the second stage it falls back to the ground due to its negative buoyancy. Newton's second law states that the rate of change of momentum of a body equals the force acting on it. For a gas of negative buoyancy, this implies that the gas will reach its peak rise (momentum equals zero) at a time after release equal to its initial vertical momentum divided by its buoyancy: $t_m = w_o/(g\ (\rho_o - \rho_a)/\rho_o)$. Applying this time to momentum-dominated stage of rise, we can predict the rise above the source height with dimensional analysis, since $\Delta h$ is a function of M and $t_m$, where M is the initial upward momentum. Since $t_m = M/B$, $\Delta h$ can also be written as a function of B and $t_m$. Looking at the various dimensions of B shown in line 2, the power laws shown in line 4 must result. The constants of proportionality must be determined by experiment. This has been done by Hoot et al. for type B and C sources (the constants measured were 1.43 and 3.15, respectively).

The importance of the first stage is that the higher the gas is lofted, the more dilute it will be by the time it contacts the ground. Hoot et al. found that a type B source, as it approaches the ground, grows and behaves very much like a free buoyant plume viewed upside down. For instance, it grows linearly with distance of fall. An important finding is that the virtual origin, the height at which the extrapolated radius equals zero, is about 2 $\Delta h$ above the source height, $h_s$. In line 5 I have assumed that this result is true, at least approximately, for all source types, since geometrically it seems reasonable. For type B, the volume at ground contact is proportional to $(h_s + 2\Delta h)^2$, as implied by ground concentration measurements in the above experiment. For the other types, I have assumed the same volumes, or volume fluxes as found for free buoyant plumes at a height $(h_s + 2\ h)$; these relationships follow from dimensional analysis also. Line 6 gives the resultant V's for ground sources, and line 7 gives the resultant dilution of the original concentration, $V_2/V_o$. Every one of these depends on the source Froude number, the ratio of inertial forces to buoyancy forces. $Fr_o = w_o^2/(g \Delta_o r_o)$. where $r_o$ is equal to $V_o^{1/3}$ and $V_o^{1/2}$ for types A and B and is the outlet radius or half-width for types C or D.

Stage 3 assumes that the gas spreads initially with its own inertial being more important than friction or shear forces. The frontal displacements predicted in line 8 follow from dimensional

analysis, assuming that $r_e$ is a function only of B and t. Except for the proportionality constants, these are the same predictions as given for the rise of a free plume (see line 4), but here they apply to the spread of a dense gas along the ground. The same results are obtainable from an equation for the total spreading momentum, $v_e V$, where $v_e = dr_e/dt$ and it is assumed that the outward velocities behind the front all scale to the frontal velocity $v_e$. The outward force at the front is due to the hydrostatic pressure difference, which is proportional to $g\Delta\bar{h}$. It follows that, regardless of the source type,

$$d(v_e V)/dt \propto g\Delta\bar{h} \text{ (frontal area)} \propto (\bar{h}/r_e)B.$$

This is very similar to the equation for the upward momentum of a free plume, except for the term $(\bar{h}/r_e)$, which in this case acts like an effective "slope" governing horizontal acceleration due to gravity. In every case, V is proprotional to $\bar{h}$. If $\bar{h}$ is proportional to any power of t or any power of $r_e$, in effect it cancels out of the equation and asymptotically the result of line 8 is obtained. Note in line 9 that the frontal velocity decreases as the gas spreads out, except for the type D source, where it remains constant. The dilution is proportional to V, which is related to the entrainment constant $\alpha$ This is defined as the rate at which ambient gas becomes mixed into the dense gas compared with the volume being swept by the advancing

front. V cannot decrease (this would be diffusion in reverse), so in all cases $\alpha > 0$. For the continuous sources, the meaning of $\alpha < 2/3$ for type C or $\alpha < 1$ for type D is not that V decreases, for the statement of line 10 is not valid in that case. Instead, it means that the entrained volume flux becomes of diminishing importance compared to the supply volume flux, $V_2$, so $V_3 \simeq V_2$ and the mixing that occurs is insignificant. Line 11 gives the resulting behavior of the mean gas height as a function of frontal displacement. Again, the exponents of the power laws depend on $\alpha$. If the mean height $\bar{h}$ is to subside, $\alpha$ must be less than 1, except for type D. If $\alpha < 1$ for type D, $V \simeq V_2$, = constant, and since $v_e$ = constant, so is $\bar{h}$ constant.

A basic property of stage 3 is that the bulk Froude number of the flow is constant ($Fr = v_e^2/g\Delta\bar{h} = v_e^2(V/\bar{h})/B$). This follows from dimensional considerations, since $v_e^2$ and $(V/\bar{h})$ are functions of B and $r_e$; Fr, being dimensionless, then must be proportional to $B^\circ\ r_e^\circ$, a constant. Fr tends toward a constant value because of a negative feedback mechanism present. Fr can be interpreted as the ratio of shear forces, which tend to generate turbulence, to buoyant forces, which tend to hold down turbulence in this case (denser fluid on the bottom). If Fr increases over an equilibrium valve, turbulence mixing increases, which dilutes the outward momentum and slows down the speed. Since vertical mixing has no effect on the product $(\Delta\bar{h})$, the diminishing of $v_e$ decreases Fr. Conversely, if Fr decreases below its equilibrium values, turbulence decreases and the spreading rate increases, which increases Fr.

More information about Fr can be drawn by substituting the line 10 expressions into the momentum equation. Except for type D, Fr depends on $\alpha$. It is interesting to find for the instantaneous sources, types A and B. that Fr $\to \infty$ at $\alpha = 1/2$, and is real and positive only for $\alpha > 1/2$. For type C, a similar thing happens at $\alpha = 5/6$, but at $\alpha = 1$, Fr goes to zero, implying zero turbulence. For type D, I believe that $\alpha < 1$ and that turbulent mixing is of little consequence. With $v = v_e$ everywhere (except near the source), this results in $v_e = 1/2\ B^{1/3}$ and Fr = 1/8. At any rate, Fr $\propto v_e^3/B$ and is likely to be small, making it plausible that no significant turbulent mixing takes place behind the front itself.

Note that Fr is also the ratio of kinetic energy of mean motion to potential energy of the dense gas. Since this is constant in stage 3, the total energy is proportional to the potential energy which is proportional to $g\Delta\bar{h}\ V = B\bar{h}$. The total energy must decrease after release, in order to "feed" the turbulence, so in every case we must require that $\alpha < 1$. In the case of type D, there is probably a slight drop in the local value of h near the source to feed the turbulence at the edge, but thereafter h is almost constant. New potential energy is constantly pumped in from the center to feed the edge turbulence.

In line 13 we see the ranges of $\alpha$ which satisfy this model. Within these ranges, the relationships of lines 8 and 9 are unaffected by $\alpha$, except for the constants of proportionality. The only experimental information that I know of which may imply something about $\alpha$ is given by Hoot et al. (1974). They measured the ground concentration of a

continuous source in a crosswind (type B) after lofting from a model stack and ground contact occurred. They found that initially $\chi \propto x^{-0.65}$, where x is the downwind distance. Eventually the decrease of $\chi$ was much more rapid and was very similar to that of passive plumes measured in a wind tunnel. If indeed the above was a good representation of a type B source in stage 3 diffusion ($r_e$ and $\bar{h}$ were not measured), substituting $\chi \propto V^{-1}$ and $x = ut$ we conclude that $\alpha = 0.975$. This implies very slow subsidence of $\bar{h}$, and therefore relatively little dissipation of turbulent energy.

In stage 4 it is assumed that frictional forces become more important than inertial forces in limiting the spread of the gas. A conventional drag force assumption is made, namely, that the stress resisting horizontal motion is proportional to $C_D v_e^2$, where $C_D$ is a dimensionless drag coefficient, We then equate the integrated drag force with the outward acting hydrostatic pressure force:

$$g\Delta\bar{h} \text{ (frontal area)} \propto C_D v_e^2 \text{ (horizontal area)}.$$

Since (frontal area) ÷ (horizontal area) $\propto (\bar{h}/r_e)$ for all cases, it follows immediately that $Fr \propto (\bar{h}/r_e C_D)$. This implies that the onset of stage 4 occurs when $\bar{h} \propto C_D r_e$ and that Fr decreases thereafter. This means that as the gas spread slows down due to friction, it stabilizes more and more, so the turbulence gradually diminishes and further mixing becomes insignificant. For this stage, I have assumed a constant volume or volume flux $V = V_4$, a no-mix

assumption. Then $(B\ V_4/C_D) \propto v_e^{\ 2}\ r_e(V_4/\bar{h})^2$ is a constant, as specified for each source type in line 14. Since in each case this is a function of $r_e$ and $v_e = d\ r_e/dt$, it can be integrated to give $r_e$ as a function of $(B\ V_4/C_D)$ and t, as in line 15. Note that for each case the exponent of t is smaller than for stage 3, i.e., the spread is slower. In line 17 we see that definite predictions for $\bar{h}$, with the gas subsiding as it spreads (potential energy converting to frictional heat energy) in all cases except for type D. Here, $\bar{h}$ actually <u>increases</u>. At first this seem paradoxical, as the potential energy of gas then must slowly increase after it leaves the source. However, this is feasible, since the potential energy being supplied by the source must also be proportional to $\bar{h}$ and increases with $t^{1/5}$ (the source must push against more and more hydrostatic pressure as $\bar{h}$ builds up). The rate at which the friction dissipates energy is proportional to $v_e^{\ 3}\ r_e \propto t^{1/5}$ also, so an energy balance is maintained.

For a rough estimate of $C_D$, consider how the ground stress depends on wind speed in a neutral surface layer: $0.35\ u = u^* \ln(z/z_o)$, where 0.35 is the von Karman constant, z is the height, $z_o$ is the "roughness length" (about 1/10 the height of roughness elements), and $u^*$ is the "friction velocity," defined by the square root of stress divided by density. Assuming a similar stress is induced by the spread velocity v, we can say $C_D = (v^*/v)^2 \approx (0.35/\ln(\bar{h}/z_o))^2$;

very roughly, $C_D \simeq 10^{-2}$. In addition to this ground drag, it is possible that there exists a similar drag at the top of the gas due to waves on the interface. This is perhaps indicated by some experiments on underwater thermal plumes; in this situation, there is no "ground friction," yet an expression similar to the one above gave the best prediction of the spreading rate (Shiraze and Davis, 1974).

The nature of the final stages of dense gas diffusion depends on the stability of the ambient air. In most cases, because the dense gas settles into a thin layer near the ground, it can be considered to be within the inertial layer, where the ambient turbulence is mechanically induced. Here, all turbulent velocities scale to $u^*$, the friction velocity ($u^* = 0.35u/\ln(\bar{h}/z_o) \simeq 0.1u$). The transition from stage 4 to stage 5 occurs when $v_e = u^*$ (see line 19 of Table I). After this transition, ambient turbulence continues to diffuse the gase at a rate $v_e \simeq u_*$ in the horizontal, so there is no further ground friction effect except in the generation of of ambient turbulence. However, if stage 4 was of significant duration, the ambient turbulence will not be effective in the vertical direction initially in stage 5 because of the low Froude number and the vertical stability it implies. Diffusion initially occurs only horizontally, at the edges. We may replace $v_e$ with $u^*$ in the Froude number, since $u^*$ governs both the rate of horizontal spreading

and the velocity of turbulent motions attacking the gas. This Fr is shown in line 20, and is seen to grow as the gas spreads except it remains constant for type D source.

When the Fr* becomes large enough, of order unity, the ambient turbulence can work into the dense gas from above. As the turbulence comtinues to spread the gas horizontally, the influence of buoyancy weakens and the gas gradually becomes "passive," diffusing like a non-buoyant gas. The radius at which this occurs is given in line 21. Note that this is the same radius (except for proportionality constant) for which $v_e \simeq u^*$ in stage 3. If this occurs before the onset of stage 4, then $Fr^* \simeq 1$ and the diffusion shifts from stage 3 to stage 6 directly, bypassing stages 4 and 5. The type D source is a special case, because if $B/u^{*3}$ exceeds a certain critical value it never attains stage 6 diffusion. However, if $B/u^{*3}$ is small, $v_e < u^*$ from the very outset of stage 3 and stage 6 diffusion developes immediately.

What if there is convective turbulence present, as there nearly always is in the daytime? It will have a greater effect than the mechanical turbulence if the convective velocities are larger than u* at height $\bar{h}$. In free turbulence, the convective velocity scale near the ground is proportional to $(Hz)^{1/3}$, where $H = gH_o/(c_p \rho_a T_a)$. $H_o$ is the upward sensible heat flux, and $T_a$

is the absolute ambient temperature. The convective turbulence is then more important than the mechanical if $(H\bar{h})^{1/3} > \simeq u^*$, or if $(\bar{h}/L)^{1/3} > \simeq 1$, where $L \propto u^{*3}/H$ is the Monin-Obukov length. Another possibility is for the gas density difference to become smaller than the natural density differences due to convection This turns out to occur at about the same time. In either case, if $(\bar{h}/L)^{1/3} > \simeq 1$, a stage analogous to stage 6 occurs when $Fr_c = (H\bar{h})^{2/3}/(g\Delta\bar{h})$ becomes of order unity.

Another distinct possibility when H is positive is that the dense gas absorbs enough heat flux from the ground to warm up and lose its density difference entirely. Since there is a hydrostatically stable interface at the top of the gas, it is likely to absorb nearly 100% of the heat flux. Complete buoyancy destruction occurs when $\int H$ (horizontal area) dt = B for the instantaneous sources, or at the radius for which H(horizontal area) = B for the continuous sources. Which happens first, buoyancy destruction by H or erosion by convective turbulence? At the time of buoyancy destruction, we can show that $Fr_c \propto (\bar{h}/r_e)^{2/3}$ if it occurs during stage 3. Since $\bar{h}/r_e$ is quite small, we anticipate that $Fr_c$ is too small for convective turbulence to be effective. This is even more true if buoyancy destruction occurs in stages 4 or 5, where $Fr_c \propto (\bar{h}/r_e)^{2/3}$ times $(\bar{h}/C_D r_e)^{1/3}$ or times $Fr^{*1/3}$. Both these parameters are less than of order unity in their respective stages. Thus, buoyancy destruction occurs first in convective conditions. The radius at which it occurs is shown in line 22 of Table 1 (for instantaneous sources, $\int$ (horizontal area) dt $\propto$ horizontal area $(r_e/v_e)$ in each stage).

If the ambient turbulence level is low, the air is stably stratified, and the spreading dense gas is mixing with the air, it carries the mixed air to levels of lower potential density as it subsides. This produces a counter-buoyancy which may eventually cancel out the initial negative buoyancy of the gas. In stage 3 the rate of buoyancy change $dB/dt$ is $-sV\, d\bar{h}/dt$, where $s = (g/\theta)\partial\theta/\partial z$ and $\theta$ is the ambient potential temperature. This is analogous to $dB/dt = -sVd\bar{z}/dt$ for a free plume (Briggs, 1969). In conjunction with the momentum equation for state 3, the above equation predicts equilibrium with ambient density after a time proportional to $(r_e/\bar{h})(m\ s)^{-1/2}$, where $\bar{h} \propto r_e^{-m}$. This compares to an equilibrium time equal to $\pi\ s^{-1/2}$ for a free plume, which itself is usually of the order of several minutes. Since $(r_e/\bar{h})$ is large by this time and m may be small, the equilibrium time is probably very large indeed for a spreading dense gas. It is very likely that the diffusion would be well out of stage 3 this time, either into stage 4, where there is little mixing and the change in buoyancy is negligible, or into stages 5 and 6, where ambient turbulence already has a dominant effect. It would appear that ambient stable stratification rarely, if ever, affects the diffusion of a dense gas, except inasmuch as it affects ordinary passive diffusion .

It is obvious that the behavior of dense gas releases includes many areas that have not yet been researched. The unexplored areas are numerous. However, for a specific release, the following questions are good ones to ask:

1. Which source type does this release most closely approximate? (Keep in mind that finite line sources approximate line source behavior when $r_e < L$ and point source behavior when $r_e > L$, where L is the line length. Also, finite time releases approximate continuous source behavior when $t < \Delta t$ and instantaneous source behavior when $t > \Delta t$, where $\Delta t$ is the duration of release).
2. How much initial dilution of the gas is likely?
3. In a zero wind, zero u*, zero H condition (the worst situation), how does $\chi$ attenuate with increasing $r_e$? (This depends on stage 3 behavior which needs to be researched, and on how quickly stage 4 occurs. Paradoxically, the rougher the surface, the less the ultimate dilution.)
4. When u* and H are not both zero, at what point does the dense gas become "passive," diffusing like a non-buoyant gas?

References

Briggs, G. A. (1960), Plume Rise, TID-25075.

Briggs, G. A. (1970), Some recent analyses of plume rise observations, 2nd International Air Pollution Conference, Washington, D. C.

Briggs, G. A. (1973), Lift-off of buoyant gas initially on the ground (draft).

Briggs, G. A. (1974), Plume rise from multiple source, proceedings "Cooling Tower Environment - 1974" Symposium, TID -

Bureau of Mines (1972), Hazards of spillage of LNG into water. Final report supporting investigation MIPR No. 2-70099-9-12395 prepared for U.S. Coast Guard, Hazardous Materials Division.

Hoot, T. G., Meroney, R. N. and Peterka, J. A. (1973), Wind tunnel tests of negatively buoyant plumes. Fluid Dynamics & Diffusion Laboratory, Colorado State University CER73-74TGH-RNM-JAP-13.

Pai, S. I. (1954), Fluid Dynamics of Jets, D. Van Nostrand Company, Inc., New York.

Shirazi, M. A. and Davis, L. R. (1974), Workbook of Thermal Plume Prediction Vol. 2 - Surface Discharge, EPA-R2-72-0056.

# Time Dependent Mesoscale Wind Fields Over Complex Terrain*

Carmen J. Nappo, Jr.

Air Resources
Atmospheric Turbulence and Diffusion Laboratory
National Oceanic and Atmospheric Administration
Oak Ridge, Tennessee

## Abstract

Wind soundings simultaneously made at five stations over a mesoscale region of complex terrain during the Eastern Tennessee Trajectory Experiment (ETTEX) are objectively analyzed, vertically averaged and interpolated over a uniform grid. The temporal and spatial variability of the resulting mesoscale wind field are examined for several observation periods, each lasting about six hours. Finally, the observed trajectories of tetroons are compared with trajectories computed using wind fields measured during the tetroon flights.

A result of the analysis is that during stable night time conditions, the wind field has marked horizontal variability which diminishes with the development of convective boundary layer. Hence terrain effects may be more significant in their effect on the mesoscale flow at night than during the day.

*Presented at the First Conference on Regional and Mesoscale Modeling, Analysis, and Prediction of the American Meteorological Society, Las Vegas, Nevada, May 6-9, 1975.

ATDL Contribution File No. 75/6

# Time Dependent Mesoscale Wind Fields Over Complex Terrain

Carmen J. Nappo, Jr.

Air Resources
Atmospheric Turbulence and Diffusion Laboratory
National Oceanic and Atmospheric Administration
Oak Ridge, Tennessee

## INTRODUCTION

The present stage of the ETTEX data analysis allows some qualitative judgements concerning large-scale topographic effects on stable and unstable mesoscale flows and the ability to predict observed trajectories of tetroons during these conditions. Large-scale topographic features are those features with horizontal dimensions comparable with the mesoscale and vertical dimensions comparable with the mixing depth. In the eastern Tennessee region, the large-scale topographic features are the Great Smoky Mountains, the Cumberland Plateau and the Tennessee Valley.

Our initial assumptions concerning mesoscale dynamics over complex terrain are:

(1) A strongly convective boundary layer with light winds will tend to obscure any large-scale topographic effects.

(2) Convective activity in the unstable boundary layer is more or less homogeneously distributed throughout the mesoscale area, and wind profiles taken at different locations will be similar and show little vertical shear.

(3) During stable conditions, large-scale topographic features should have a strong influence on the mesoscale flow through a depth of not more than about 1000 m.

(4) During stable conditions, wind profiles taken at different locations should be highly dependent on local topography; however, winds are expected to be uniform in the free atmosphere about 1000 m.

(5) Homogeniety of the convective boundary layer and similarity of the wind profiles throughout the mesoscale area suggest that trajectory calculations using interpolated winds from widely spaced stations should compare well with observed trajectories.

(6) Under stable conditions with highly localized winds, interpolated winds are not expected to agree well with the actual winds and hence trajectory calculations will agree poorly with observed results.

## THE ETTEX REGION

The ETTEX area is shown in figure (1) where the observation stations are indicated. Single theodolite pibal observations were made at each station every hour or half hour during a trajectory experiment. Tetroons were released at or near the "0800" site. The contour lines represent surface elevations in meters above sea level (ASL). The Great Smoky Mts. are off to the south-east and the Cumberland Plateau is off to the north-west. The Tennessee Valley lies along the line joining New Tazewell, "0800," and Athens. For a more detailed description of the ETTEX region and experiment, see Hanna et al. (1974).

## OBJECTIVE ANALYSIS PROGRAM

To objectively analyze the wind field, wind soundings are vertically smoothed, using a three point smoothing, and interpolated to 100 meter levels above sea level. Horizontal winds are then interpolated and extrapolated at each level to a 20 x 20 grid with a uniform grid spacing of 10 km. The weighting function used in the interpolation scheme is $a^2/(a^2 + r^2)$, where 'a' is a constant and r is the distance from an observation station to a grid point. The interpolation scheme is able to work around vertical boundaries by setting the velocity component normal to the boundaries equal to zero.

## MESOSCALE WIND FIELDS DURING UNSTABLE CONDITIONS

The wind field at various elevations for a typical unstable period is shown in figure (2). This case is for July 16 at 1400 EDT. The arrows indicate the direction of the wind while the length of each arrow is proportional to the wind speed. The observation stations are also indicated and the observed wind for each station is given. Little change in wind direction is noted as we move downward through the mixing layer. At 1200 m (ASL) and again at 500 m (near the ground surface) we see what appears to be channeling of the wind by the valley. These channeling effects are not large and appear to be confined to low elevations; we can conclude then, that when the flow is along the valley topographic effects are slight. These observations would appear to justify assumption (1).

Another unstable case is shown in figure (3). This case is for July 18 at 1800 EDT. At 2000 m the flow is from the west, off the Cumberland Plateau. At this level, noticeable turning down the valley is seen over Athens. At 1200 m, this down-valley component has disappeared but an up-valley turning is seen over the north-eastern end of the valley. At 1000 m, a noticeable steering of the wind up the valley is seen, but east of the valley the original easterly flow is recovered. Continuing downward, we see ever increasing channeling of the wind along the valley. In view of these observations, assumption (1) is apparently not justified, and we must conclude that large-scale topographic effect are important during unstable conditions.

MESOSCALE WIND FIELDS DURING STABLE CONDITIONS

An example of a stable period is shown in figure (4). This case is for August 8 at 0500 EDT. At 2000 m, we have a uniform southerly flow east of the Smoky Mts. Just over and downwind of the Smokies, the winds are near calm; further north there appears to be valley channeling over New Tazewell. At 1500 m this channeling has increased, and the "wind shadow" over Sevierville is still present. Between 1200 and 900 m, a sharp change in wind direction and speed takes place. This change actually occurred between 1000 and 900 m suggesting a strong layering between a free atmosphere, with relatively slight terrain effects, and a surface layer, with strong terrain effects. Note that over New Tazewell a 90° change

in wind direction takes place. At 700 m, a cross-valley flow exists and this persists almost to the ground. This flow may be due to a large-scale drainage wind from the Smoky Mts. Over New Taxewell at 500 m (almost at the ground), the wind direction is down the valley. This is apparently a valley drainage wind. Analysis of surface winds verifies the existence of this drainage wind. Hence we conclude that assumption (3) is justified, and that topographic features may even dominate mesoscale flow during stable conditions.

## WIND PROFILES DURING UNSTABLE CONDITIONS

Vertical wind profiles for each station are shown in figure (5), for the same time period as figure (2). The profiles are more or less similar. They show little shear and contain much vertical structure (kinks) which may reflect the turbulent structure of the mixing layer. From this and other observations, it is concluded that assumption (2) is valid.

## WIND PROFILES DURING STABLE CONDITIONS

Figure (6) displays the wind profiles for the same time period as figure (4). The profiles show a linear shear layer the ground and smooth profiles above. The profiles are distinct from station to station, reflecting a highly local character. Wind speeds tend to be equal in the free atmosphere except for the stations down wind from the Smoky Mts., i.e. Sevierville and New Tazewell, Hence we conclude that assumption (4) is valid with topographic effects extending to elevations higher than expected.

## TRAJECTORY CALCULATIONS DURING UNSTABLE CONDITIONS

A trajectory calculation was made for the July 18 period from 1400 to about 1700 EDT. The observed vertical positions of the tetroon were used to determine the averaging thickness of the winds for the calculations. The average elevation was 950 m (ASL) with a standard deviation of 250 m. Hence the averaging layer extends from 700 to 1200 m. The calculated and observed trajectories are shown in figure (7a). In an effort to improve the calculations, a frequency distribution of the vertical position of the tetroon was plotted. This revealed that the variance is not normally distributed about the mean, but is skewed, such that most of the time the tetroon is below the mean elevation. This is due to thermal updrafts intermittently carrying the tetroon to high elevations. As an extreme alternative, the averaging layer was decreased to 100 m between 900 and 1000 m (ASL). The resulting calculation is shown in figure (7b). While the result is much improved, the sudden departure of the calculated and observed trajectories at 120 minutes still persists. It is believed that the kink in the observed path is due to a large eddy which quickly blew the tetroon northward. From then on, the tetroon path is smooth and parallels the calculated trajectory. It appears that assumption (5) is valid, but more cases must be studied before a definite conclusion can be stated.

## TRAJECTORY CALCULATIONS DURING NEAR STABLE CONDITIONS

Unfortunately, at this time a trajectory calculation has not been made for stable conditions; however, a calculation has been made for what is believed to be near-stable conditions. This was for July 19 from 1600 to 2100 EDT. Winds were averaged from 700 to 1000 m (ASL). The results are shown in figure (8). It is seen that the path of the tetroon is well simulated, but the speed of the tetroon is underpredicted. The tetroon was launched from the "0800" site. As it moved away from this site, it entered regions of different wind speeds but equal wind directions, so that the local "0800" winds no longer applied. Hence we conclude that assumption (6) may be valid, although more testing must be done.

## CONCLUSION

From the above observations we may conclude the following: Large-scale topographic features always affect the mesoscale flow. The effect is very strong during stable conditions and extends to elevations and distances larger than originally anticipated, i.e. greater than 2000 m above the ground and further than 50 km. Convective turbulence is uniformly distributed throughout the region during unstable conditions, and trajectory calculations agree with observations for these cases. During stable conditions, wind profiles are local, and trajectory calculations are questionable. These conclusions are based on limited analyses of the data, and are, of course, subject to possible revision as additional cases are examined.

REFERENCE

Hanna, S. R., C. J. Nappo, R. P. Hosker, and G. A. Briggs, 1974, Description of the eastern Tennessee trajectory experiment (ETTEX). Air Resources, Atmospheric Turbulence and Diffusion Laboratory, ATDL Contribution No. 103.

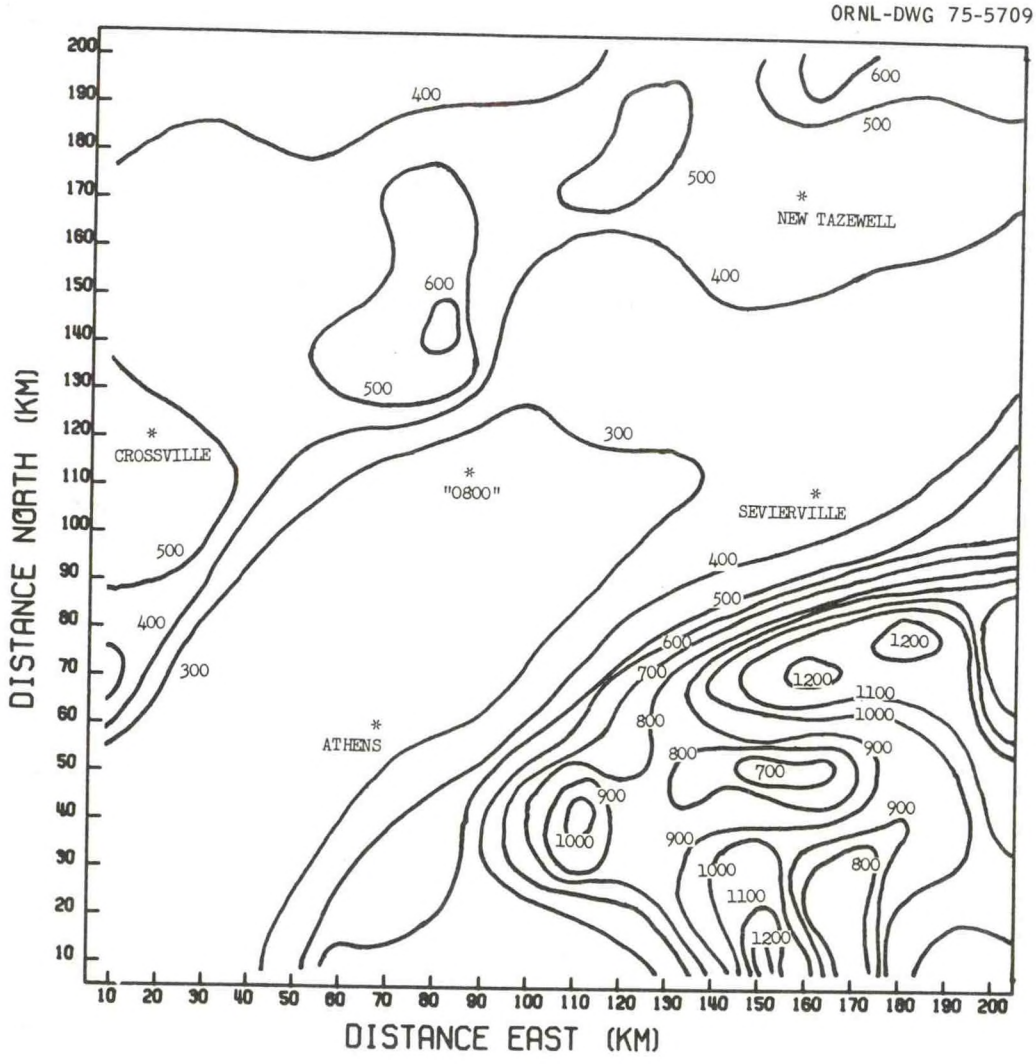


Fig. 1. The ETTEX region. Height contours are shown as solid lines, with the elevations shown in meters above sea level. Pilot balloon stations are indicated by asterisks.

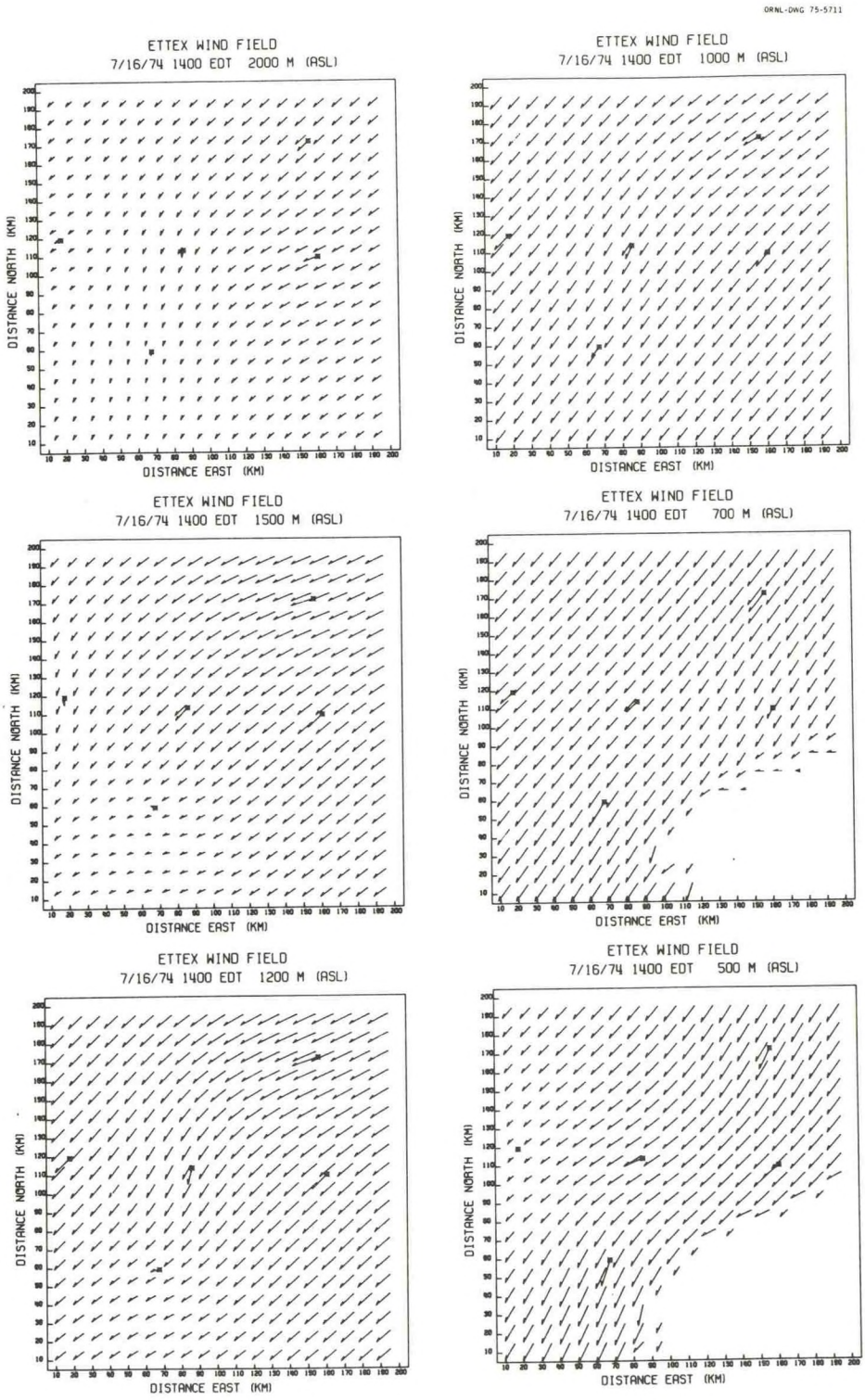


Fig. 2. Mesoscale wind fields for various altitudes, in unstable conditions (July 16, 1974; 1400 EDT).

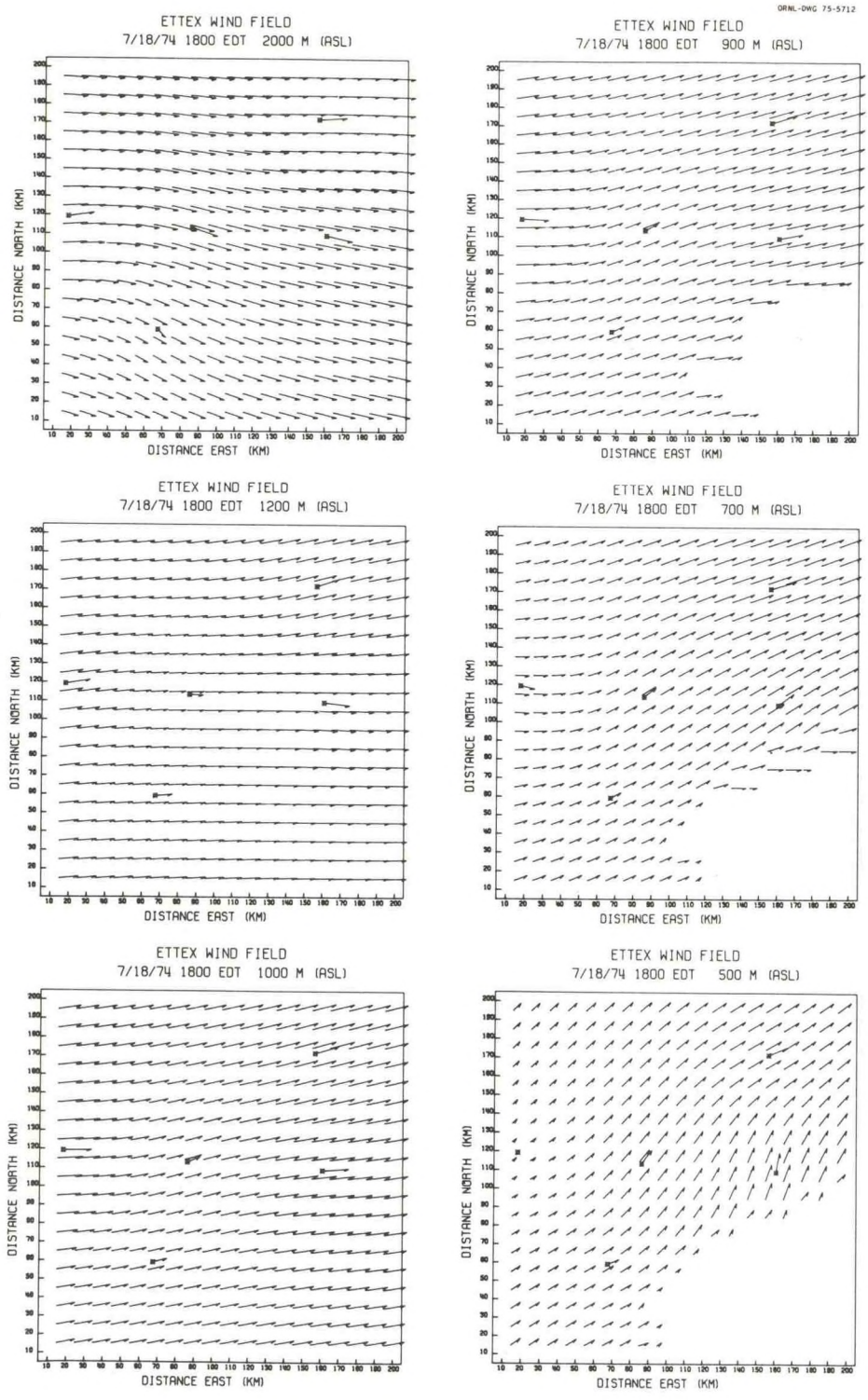


Fig. 3. Mesoscale wind fields for various altitudes, in unstable conditions (July 18, 1974, 1800 EDT).

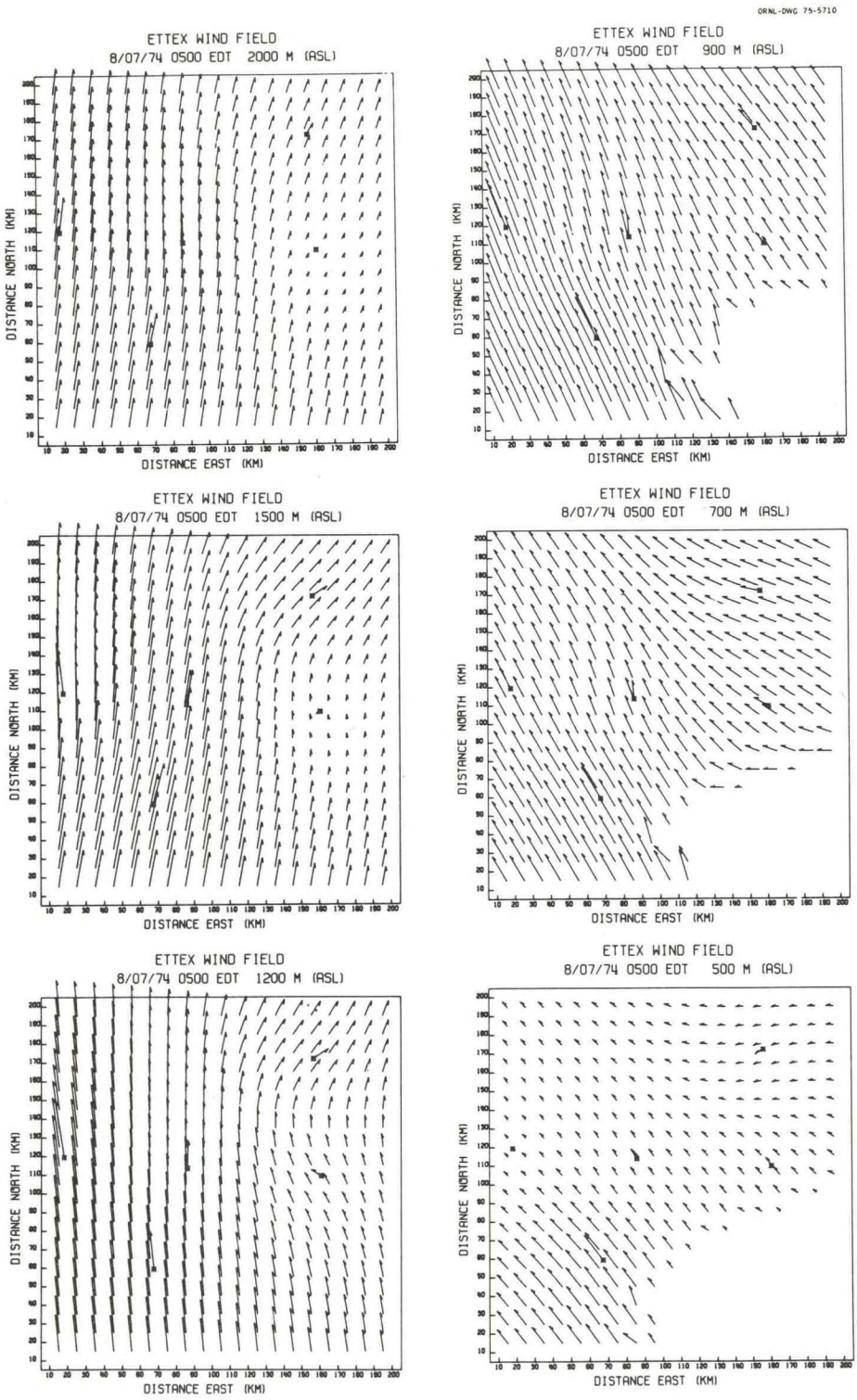


Fig. 4. Mesoscale wind fields for various altitudes, in stable conditions (August 7, 1974; 0500 EDT).

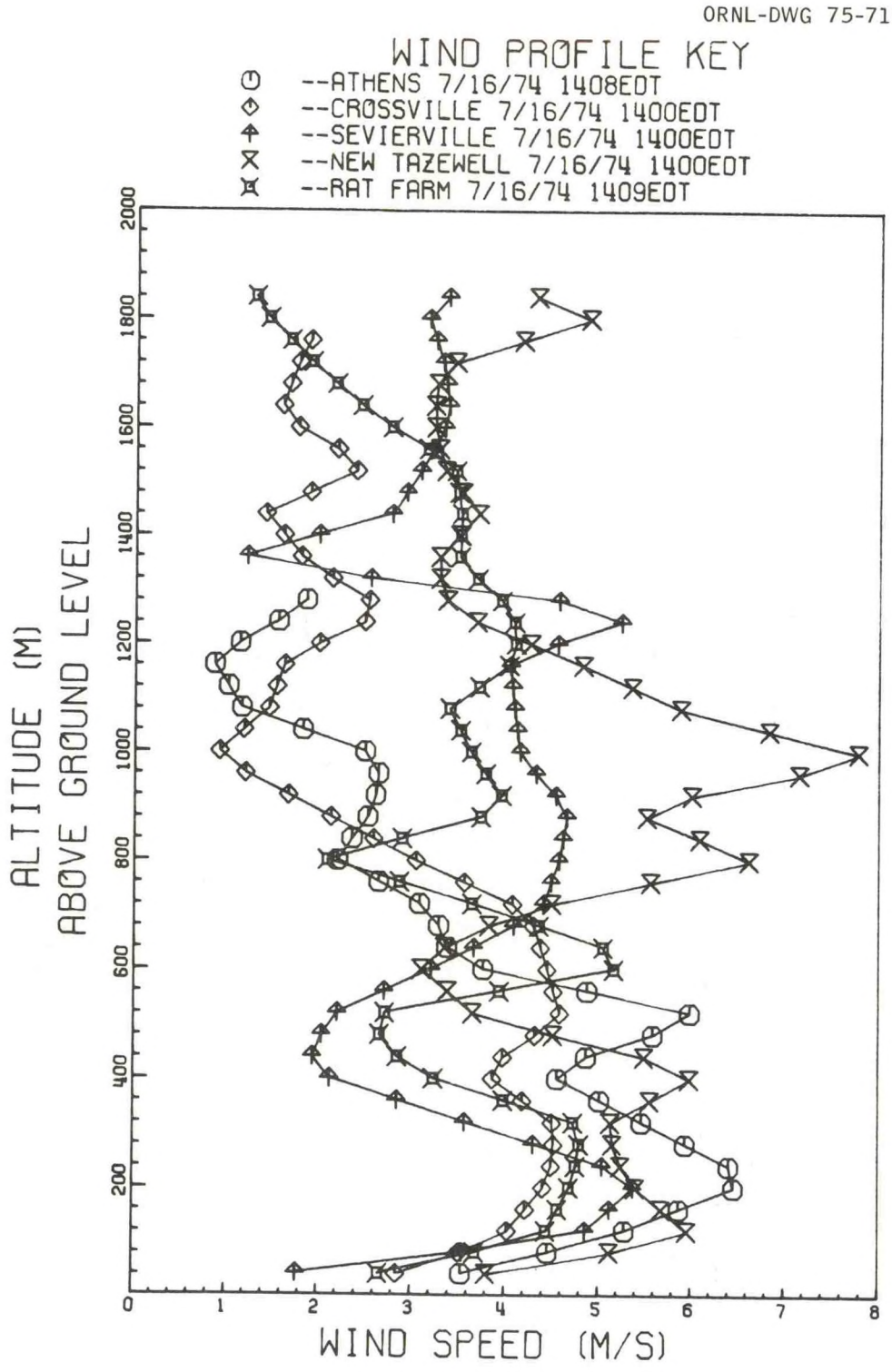


Fig. 5. Wind profiled in unstable conditions.

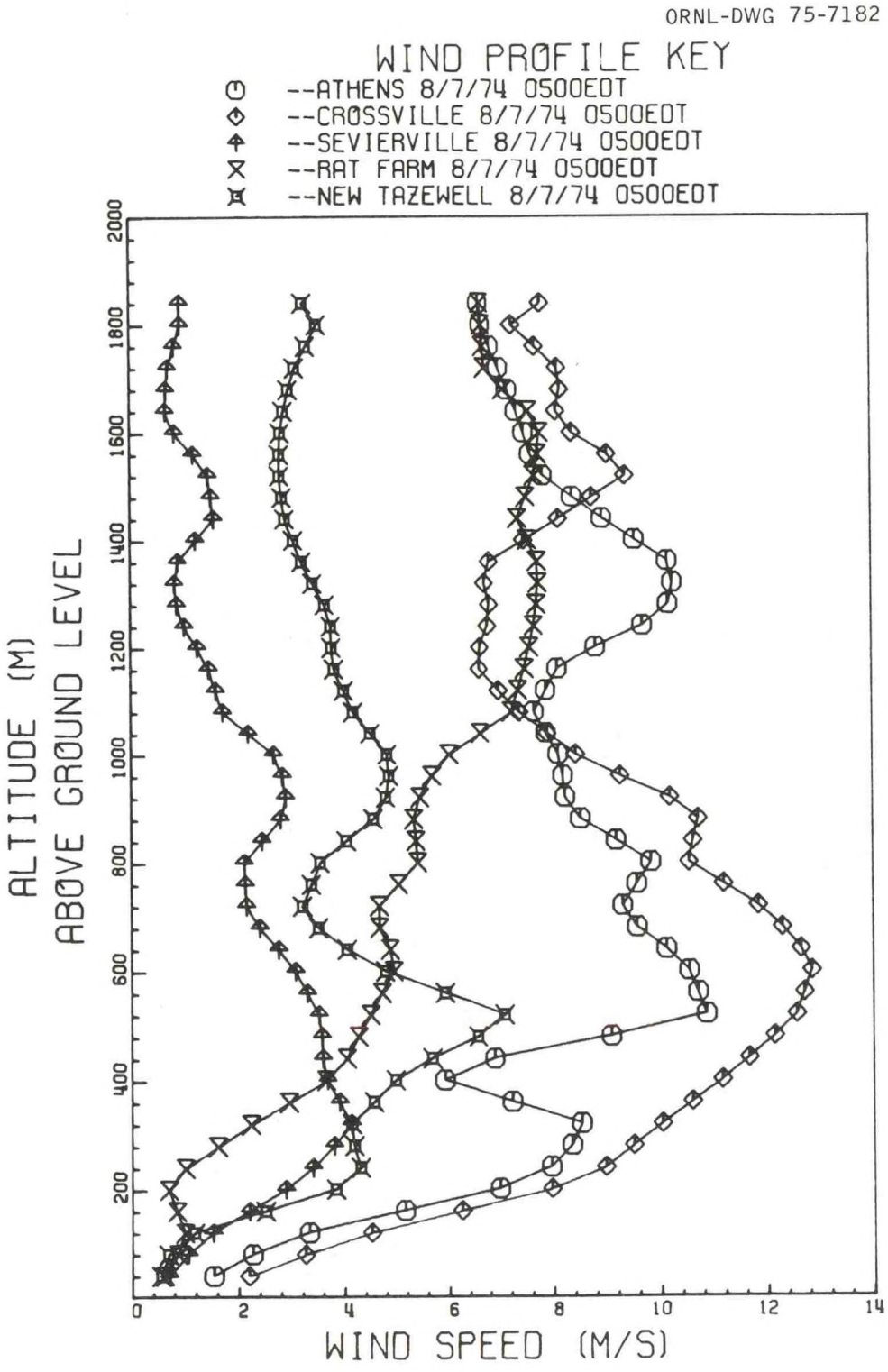


Fig. 6. Wind profiles in stable conditions.

ORNL-DWG 75-7179

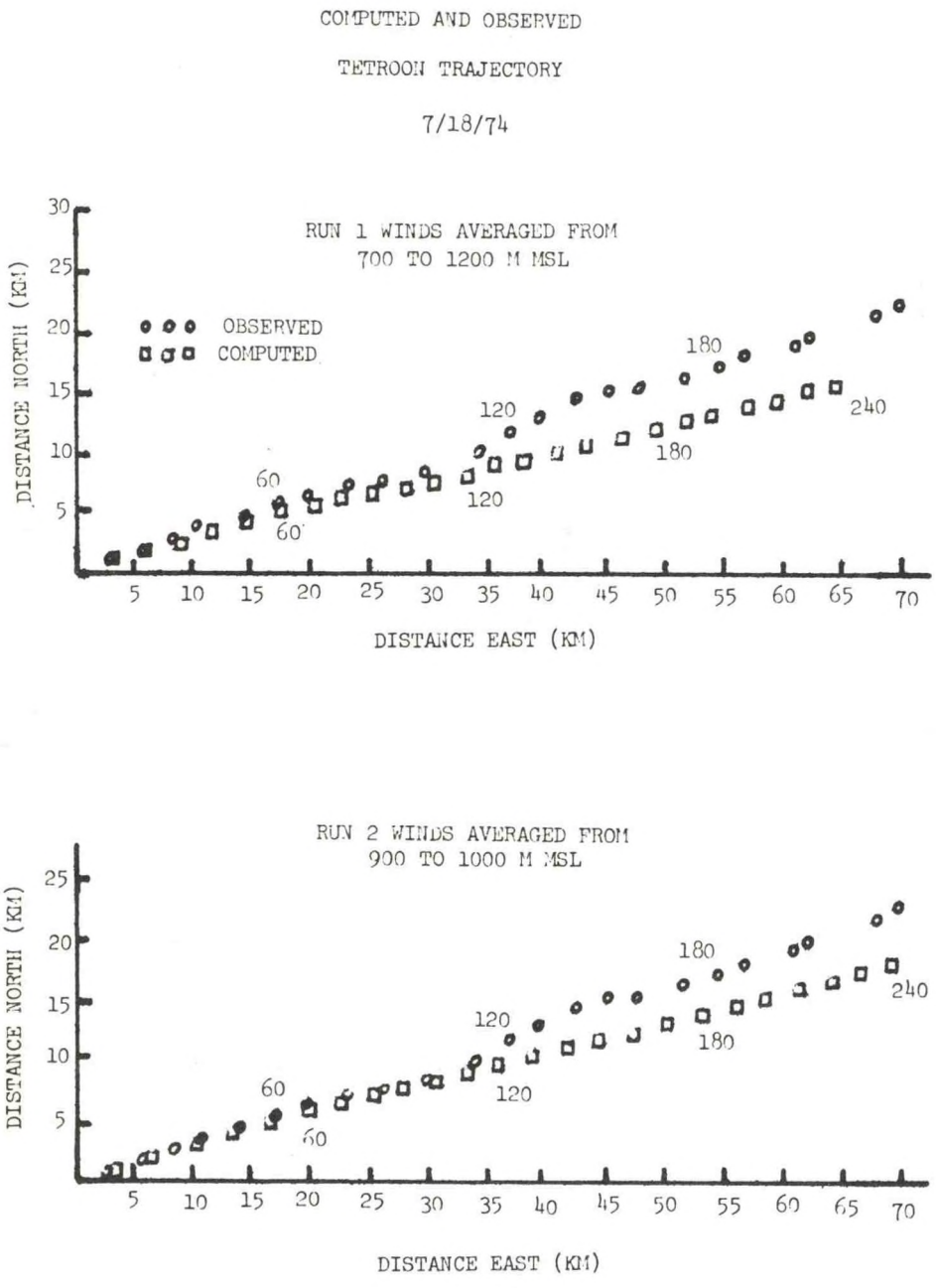


Fig. 7. Comparison of observed and predicted tetroon trajectories in unstable conditions (July 18, 1974; 1400 - 2100 EDT).

ORNL-DWG 75-7180

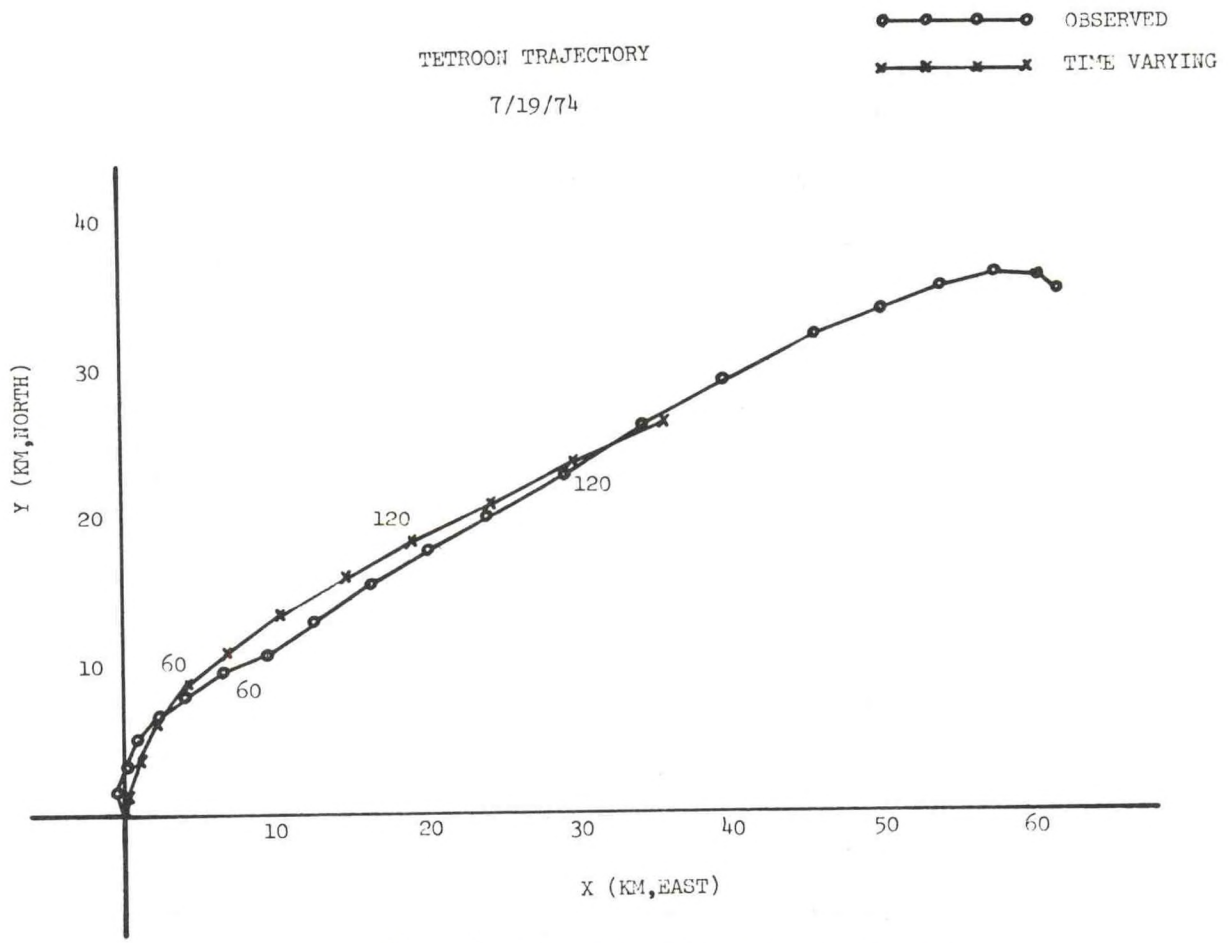


Fig. 8. Comparison of observed and predicted tetroon trajectories in stable conditions (July 19, 1974; 1600 - 2100 EDT).

# LECTURES ON AIR POLLUTION AND ENVIRONMENTAL IMPACT ANALYSES

Sponsored by the

AMERICAN METEOROLOGICAL SOCIETY

29 September - 3 October 1975
Boston, Massachusetts

Duane A. Haugen
Workshop Coordinator

The tutorial lectures reproduced in this collection are unedited manuscripts of the material presented at the AMS Workshop on Meteorology and Environmental Assessment; their appearance here does not constitute formal pbulication.

ATDL Contribution File No. 75/7

AMERICAN METEOROLOGICAL SOCIETY
45 Beacon Street, Boston, Massachusetts, 02108 U.S.A.

# CHAPTER 2

## ATMOSPHERIC DISPERSION MODELS FOR ENVIRONMENTAL POLLUTION APPLICATIONS

F. A. Gifford

Air Resources
Atmospheric Turbulence and Diffusion Laboratory
National Oceanic and Atmospheric Administration
Oak Ridge, Tennessee

### 1. INTRODUCTION

Pollutants are introduced into the air by many of man's activities. The potentially harmful effects these can cause are, broadly speaking, of two kinds: long-term, possibly large-scale and wide-spread chronic effects, including long-term effects on the earth's climate; and acute, short-term effects such as those associated with urban air pollution. This section is concerned with mathematical cloud or plume models describing the role of the atmosphere, primarily in relation to the second of these, the acute effects of air pollution, i.e. those arising from comparatively high concentration levels. The need for such air pollution modeling studies has increased spectacularly as a result of the National Environmental Policy Act of 1968 and, especially, two key court decisions; the Calvert Cliffs decision, and the Sierra Club ruling on environmental non-degradation. This increase is being met in several ways. Many more individuals and companies, a large number, have entered the environmental consulting field.* Similarly many more universities now offer special training in atmospheric diffusion. This workshop itself is a response to the greatly increased demand that exists for information on applications of diffusion modeling to a wide variety of urgent, practical, air-pollution problems.

#### 1.1 Modeling Requirements of Environmental Pollution Problems

Transport and dilution of pollutants by air motions goes on constantly; and all of humanity, particularly that large and increasing segment inhabiting cities and industrial areas, depends strongly on this capability of the air to carry away and dilute the pollutants it receives. What we call "air pollution" occurs when too much waste material is emitted into an air volume for the air's capacity to carry it away and dilute it. Thus we must be able to control the amounts of pollutants emitted into the atmosphere to levels which will not harm people, plants, or animals or cause damage to property. This requires that we understand the atmospheric mechanisms that result in transport and dilution, as well as the roles played by various kinds of sources and by processes that remove pollutants from the atmosphere.

The atmosphere is a carrier as well as a modifier of pollutants. In this respect its role is rather different from the other great carriers or sinks of pollutants, namely the water and the land, in one significant respect. Once introduced into the atmosphere, a pollutant spreads rapidly and cannot very well be removed except by naturally occurring processes, such as deposition on natural or manmade surfaces, washout by precipitation, or radioactive decay or chemical reaction. These removal processes themselves may have undesirable effects, for instance the creation of new pollutants through chemical reaction (i.e. photochemical oxidants), or undesirable surface effects such as "acid rain."

#### 1.2 Sources of Pollution

Pollution is emitted into the atmosphere from a large number of different kinds of sources, which can conveniently be classified into 4 groups: 1) isolated, tall-stack sources such as the stacks of large electricity generating stations; 2) lower single- or multiple-stack sources from isolated industrial process emissions of all kinds; 3) area sources, representing the conglomerate, net effect of the multitudes of small single sources, mainly from domestic heating, that occur at or near the ground surface; and 4) the non-stationary sources such as automobiles, trucks, and airplanes. Atmospheric dilution in the first hundred meters or so of air above the ground can vary over fairly wide limits, because the vertical temperature gradient, which governs the rate of diffusion, is strongly controlled by the daily march of solar radiation at these elevations. Higher up changes are not normally so marked, and it is for this reason that a distinction is made between tall-stack sources and process emission sources in the above source listing.

Large electric power plants are very localized sources of air pollution, approximating

*This trend can readily be documented from the directory section of the Bulletin of the American Meteorological Society. For many years the number of advertisers of air pollution or environmental services in the Bulletin was about 10% of the total number; 2 out of 20 in January, 1961; and 4 out of 46 in January of 1968. By April, 1975, not only had the number of advertisers offering this service increased to the remarkable total of 27, but this represented over 40% of all BAMS advertisers.

continuous point sources. Conventional (i.e. fossil-fueled) plants release waste gases and particles from tall stacks. The trend to large, conventional units, producing power in the 1000 MW range, has been accompanied by an increase in stack heights to around 300 meters. This is because the amount of waste emitted from the stacks of these plants is very large, and the elevated release is required to keep the maximum ground level concentration below permissible control limits. The waste emitted from a nuclear power plant to the atmosphere is on the other hand much smaller in volume. Where stacks are used they are not usually very tall, and roof-level vents have been found adequate at some nuclear plants.

Releases from conventional power plant stacks are at a comparatively high temperature, because a large fraction of the combustion heat is emitted directly to the air. In standard, U.S. (i.e. water-cooled) nuclear plants, on the other hand, all the heat generated within the reactor core is exchanged with water or steam and does not have any direct contact with the atmosphere. Consequently airborne wastes from nuclear plants are usually considered to be emitted at ambient temperature. For this reason the behavior of stack plumes in the two cases is quite different. Hot buoyant plumes from conventional power plants rise appreciably in the atmosphere, to heights approximating twice the original stack height or more. Conventional plants take advantage of this added rise in order to control the maximum ground-level concentrations experienced in their vicinity. The small, low-volume effluent plume from a nuclear plant is on the other hand assumed to be non-buoyant, and any possible plume rise is usually ignored.

Process emission sources, such as short stacks or chimneys on buildings, roof vents, and the like, are much more numerous than isolated tall stacks. The gross tonnage of air pollution from such sources is also very high; it probably exceeds that from tall stacks. Plumes emanating from such low-level sources are nearly always more-or-less deformed and sometimes radically altered by aerodynamic wake effects near adjacent buildings. This greatly complicates the problem of determining pollution patterns.

Area sources, the multitude of very small, low-level pollution sources, including residential and industrial space-heating chimneys and other such sources, are most conveniently dealt with as total emissions per unit area. A significant part of the problem is to establish the area source strength, and systematic procedures for doing this have formulated.

## 1.3 The Nature of Atmospheric Dispersion of Pollutants; Some Generalities

Given sources of all the above kinds, emitting pollutants into the lower levels of the atmosphere, we can conceive the meteorological effect as follows. Wind blowing over the surface of the earth sets up a turbulent, well-mixed layer, similar in many ways to the boundary layer in a wind tunnel or over an airplane wing. This layer is the meteorologists' "planetary boundary layer." Air pollution investigators frequently refer to it as the "mixing layer" and to its top as the "mixing height." Detailed tabulations of mixing height as a function of time of day and season for the U.S., have been made by Holzworth (1972). The boundary, or mixed layer is usually of the order of a kilometer or so in depth. Though it can extend to several kilometers in the presence of active thermal convection, it can be restricted to only a few hundred meters in the presence of an active subsidence inversion. Practically all air pollution is emitted into this boundary layer, and its properties govern how serious air pollution problems are in a given locality.

If the mixing layer is about a kilometer deep, and if pollution from any plume emitted into it near the ground is spreading upward at the rate of, say, about 1/4 meter per second, then it will reach the top of this layer in about an hour. During this time the polluted air will have travelled about 10 or 15 km downwind. Thus it can be seen that the mixing-height, that is the depth of the planetary boundary layer, exerts a degree of control over air pollution over a fairly broad area, such as a municipality, city, or air quality region.

This simple, order-of-magnitude line of reasoning can also be used to determine another important atmospheric aspect of pollution. Consider emissions from a source 100 meters high, a more-less typical tall stack. Vertical plume dispersion at the above rate will cause the lower edge of this plume to reach the ground after about 400 seconds, i.e. 2 kilometers, of downwind travel, in the absence of any especially intense vertical mixing. The maximum ground-level concentration point will be found near that distance, which is thus very significant in determining the contribution of this source to the ambient air quality. From this and the preceding example it is clear that mixing depth is important in limiting the overall burden of air pollution in a region. However the effect of mixing depth on the contribution of any particular source to ambient air quality is as a rule small and indirect. Exceptions to this statement, which are rare, occur only when the (effective) source height is very great or the mixing depth is quite low. Normally, for tall-stack sources the pollutant appears at the ground only after considerable downwind plume travel and dilution. For low-level sources vertical mixing also produces considerable dilution before the plume reaches the mixing height.

For each of the source-types enumerated above, methods for the calculation of air concentration levels are available. Useful guidance, including many nomograms, can be found in the reviews by Slade (1968), Smith (1968), and Turner (1969). In general these methods all depend on knowledge of the vertical and lateral atmospheric diffusion coefficients. The theoretical basis of our knowledge of these has been reviewed by Pasquill in the preceding lecture. Our practical knowledge of these transfer coefficients, which is based on experimental diffusion trials, is far from complete, particularly for large distances

from sources. Also the diffusion experiments have for the most part been performed under somewhat idealized conditions as compared with those governing real pollution sources. Notwithstanding these uncertainties, we possess a considerable capability to calculate air concentration (ambient air quality), with precision at least compatible with our present imperfect knowledge about pollutant source strengths.

This scheme of analyzing the meteorology of air pollution can be used in many ways to help restore and conserve the environment. It can be used on a short-term "real-time" basis to forecast air concentration levels for pollution alerts and emergencies. Restrictions to industrial, domestic, and vehicle emissions can be planned on this basis. The contribution of any source or group of sources to the general background of air pollution can be determined. This can facilitate siting of industries, urban planning and zoning, and the design of air pollution monitoring networks. The methodology can also assist designers to determine permissible levels of industrial process emissions and requirements for air cleaning equipment. Finally the calculations, which can be extended to seasonal and annual periods, can assist in studying long-term air pollution trends, knowledge of which is urgently needed in air resources management.

## 2. DIFFUSION MODELS APPLICABLE TO ENVIRONMENTAL PROBLEMS

For all the applications mentioned above we need first to determine the mean field of concentration, $\bar{C}$, which in general is a function of position and time, $\bar{C}(x,y,z,T)$. Moreover, as Monin and Yaglom (1971) remarked, "The determination of this function is the most important . . . problem of the theory of turbulent diffusion." Thus both for practical and theoretical reasons it seems that the determination of this quantity is quite urgent. Since this is a problem involving the phenomenon fluid turbulence, any solution at present necessarily contains hypothetical or empirical elements, because the fluid turbulence problem has up to the present resisted all attempts at a general solution. Choice among the various approximate possibilities normally reflects the empirical or theoretical bias of the investigator, which in turn is to a great extent determined by whether the particular application is to an applied or a theoretical diffusion problem. But because of the need of all current theories to rely on empiricism or hypotheses, or both, the quality of results can in the final analysis only be judged by comparison with data. Models having a high empirical content will be stressed in the following, as seems appropriate to the applied nature of air pollution problems. As pointed out by Pasquill in the previous presentation, there are three main bases for determining pollutant spreading in the atmosphere; statistical theory, gradient - transport theory, and similarity theory.

### 2.1 Models Based on the Statistical Theory of Turbulence

For the special case of a homogeneous turbulent flow, G. I. Taylor (1921) proved the well-known result that

$$\overline{y^2}(T) = 2\overline{v^2} \int_0^T \int_0^\tau R(\xi)\, d\xi\, d\tau \qquad (1)$$

where $\overline{y^2}$ is the mean square particle displacement relative to a fixed axis, T(sec) is the time of travel of diffusing material from a source, $\overline{v^2}$ is the mean square value of the y-directed wind speed fluctuations that diffuse the particles, and $R(\xi)$ is the single-point Lagrangian autocorrelation coefficient; that is, $R(\xi)$ is the correlation coefficient formed from successive values of the velocity of a single diffusing particle, separated in time by the value $\xi = T_2 - T_1$. Similar expressions can be derived for $\overline{x^2}$ and $\overline{z^2}$. Since $R(0) \equiv 1$ it follows that, for small values of T, $\overline{y^2} \propto T^2$. At the other extreme, that is for large values of diffusion time, $\overline{y^2} \propto T$ since the inner integral in (1) is necessarily bounded.

These particle variances are related to the particle distribution function, as Frenkiel (1953) pointed out, by expressions such as

$$\overline{y^2}(T) = \int_{-\infty}^{\infty}\int\int y^2 P_i(x,y,z,T)\,dx\,dy\,dz \Big/ \int_{-\infty}^{\infty}\int\int P_i(x,y,z,T)\,dx\,dy\,dz \qquad (2)$$

where the particle probability density function, $P_i$, is given by $P_i \equiv \bar{C}_i/Q_i$; $Q_i$ is the strength of an instantaneously created point source of particles, and the diffusing particles have been assumed to behave just like ideal fluid points, i.e. like very small, marked volumes of fluid.

The next step is to assume that the form of the distribution of diffusing particles, is normal, or Gaussian. In the case of homogeneous turbulence, strong theoretical and experimental evidence for this can be cited. A time scale characteristic of the diffusion process, the Lagrangian integral time scale, $t_L$, can be defined by

$$t_L = \int_0^\infty R(\xi)\, d\xi \quad . \qquad (3)$$

For small values of the diffusion time, $T \ll t_L$, the trajectories of diffusing particles are straight lines through the point of origin. In this case the particle distribution coincides with the local, i.e. Eulerian, velocity distribution, which is observed to be Gaussian in a homogeneous turbulent flow. For large T, i.e. $T \gg t_L$, the particle distribution is normal by an application of the central limit theorem. There is experimental evidence that at intermediate times the particles distribution is also nearly Gaussian. The arguments have been

summarized by Monin and Yaglom (1971). Similar results can be adduced for $\overline{x^2}$ and $\overline{z^2}$.

For the case of an isotropic homogeneous flow, i.e. one for which $\overline{y^2} \equiv \overline{z^2} \equiv \overline{x^2}$, $(m^2)$, the mean concentration field, $\bar{C}_i$ (mass units $cm^{-3}$), relative to a fixed axis, due to an instantaneous point emission of strength $Q_i$ (mass units), is consequently given by the normal, or Gaussian equation,

$$\bar{C}_i(x,y,z,t)/Q_i = \tag{4}$$
$$(2\pi\overline{y^2})^{-3/2}\exp(-(x^2+y^2+z^2)/2\overline{y^2}].$$

Equation (4) can be integrated over all time to get the equation for the mean concentration distribution due to a steady, continuous point source, $\bar{C}$, of strength Q; x in (4) is first replaced by $x - \bar{u}T$ so that the coordinate origin can be located at the source. Both these results can be extended to the case of anisotropic turbulence, for which $\overline{y^2} \neq \overline{z^2} \neq \overline{x^2}$. The resulting equation for a steady, continuous point source is

$$\bar{C}(x,y,z)/Q = \tag{5}$$
$$[2\ (\overline{y^2}\overline{z^2})^{1/2}\bar{u}]^{-1}\exp\ [-(y^2/2\overline{y^2}+z^2/2\overline{z^2})\ ],$$

where $\bar{C}$ (mass units $cm^{-3}$) is the mean concentration distribution and Q(mass units $sec^{-1}$) is the continuous source strength. The term containing $\overline{x^2}$ has been ignored compared with transport in the x-direction by the mean wind in the derivation of (5). Consequently the dispersing cloud elements have the form of contiguous disks of width $dx = \bar{u}\,dt$, spreading in the y- and z-directions. A discussion can be found in Frenkiel's (1952) (1953) papers and a detailed summary of the literature appears in Hinze's (1959) book.

As Pasquill has previously pointed out, the turbulence structure of the atmospheric boundary layer is strongly inhomogeneous in the vertical direction. The assumption of turbulence homogeneity can be useful, if at all, only in the horizontal. Boundary layer turbulence inhomogeneity in the vertical was in fact the main subject of the previous workshop in this series, Haugen (1973). Sutton (1932, 1953) attempted to adapt the statistical theory of diffusion to the case of a stratified boundary layer with vertical wind shear. He assumed the mean concentration distribution to be Gaussian but derived expressions for the particle variances whose parameters depended on a vertical thermal stratification parameter, n, which was derived from the wind profile. These results were of great interest and considerable practical utility; but Barad and Haugen (1959) showed that they did not in general fit the results of careful field diffusion trials beyond a few hundred meters downwind distance, without empirical adjustment of parameters.

On the other hand in flows which approximate homogeneous turbulence, for instance in properly adjusted wind tunnel flows, and in the atmosphere for limited downwind distances, plumes from pollutant sources often exhibit the initially linear, later parabolic average outline predicted by equation (1); and the mean concentration distribution is close to the Gaussian. For inhomogeneous flows such as the planetary boundary layer the point made by Obrien (1964) is worth repeating. Namely, equation (1) becomes

$$\overline{y^2} = \int_0^T\int_0^T \overline{v(T_1)v(T_2)}\ d\,T_1\ d\,T_2\ . \tag{6}$$

Although this can not be simplified as in the case of (1) because of lack of turbulence homogeneity, nevertheless something like the asymptotic results Taylor derived for the homogeneous case may still apply. That is, the correlation $\overline{v(T_1)\ v(T_2)}$ should tend to be constant for small values of time and to approach zero for large ones.

## 2.2 Models Based on Gradient Transport Theory

Atmospheric diffusion is frequently described by means of the following equation,

$$\partial\bar{C}/\partial t + \bar{u}\partial\bar{C}/\partial x = \tag{7}$$
$$K_{yy}\partial^2\bar{C}/\partial y^2 + \partial/\partial z(K_{zz}\ \bar{C}/\partial z);$$

the quantities $K_{yy}$ $(cm^2sec^{-1})$ and $K_{zz}$ $(cm^2sec^{-1})$ are eddy-diffusivity coefficients applying to their respective directions. This equation is derived from consideration of mass continuity, on the assumption that the flux, $F_i$ (mass units $cm^{-2}sec^{-1}$), of the pollutant is proportional to the mean concentration gradient, i.e.

$$F_i = -\ K\ \partial\bar{C}/\partial x_i \tag{8}$$

where the subscript i refers to one of the directions y or z. Diffusion in the x-direction is negligible compared to transport in that direction, i.e. $\bar{u}\ \partial\bar{C}/\partial x >> \partial/\partial x(K_{xx}\ \bar{C}/\partial x)$, and this term is accordingly omitted.

Equation (7) with various initial boundary conditions has been solved for a wide range of atmospheric diffusion problems. The simplest possible case of (7), that is the constant -K, or Fickian case, $K_{yy} = K_{zz} = K$ = constant, has the following solution for instantaneous point source boundary conditions:

$$\bar{C}(r,t)/Q_i = (4\pi KT)^{-3/2}\ \ \exp(-r^2/4KT), \tag{9}$$

where $r^2 = x^2+y^2+z^2$. Note that equation (9) is Gaussian in form. The closely related problem with constant but not necessarily equal K-values was solved for horizontal mean flow on a spherical earth, Machta (1958). This proved to be a useful model of global-scale diffusion, one which also is, essentially, characterized by Gaussian symmetry. It is worthwile considering the reason for this success. At the scale of global diffusion the asymptotic limit $T >> t_L$ certainly applies. Consequently the assumption of constant values of horizontal and vertical diffusivities should be a good one and in fact proves to be so

in practice. The same solution could have been reached by means of equations (1) through (4) by applying the large-time limit.

At a much smaller atmospheric scale, the gradient transport equation has been extensively studied for the problem of diffusion in the atmosphere's surface layer. Solutions for the half-space $z > 0$ have been sought for various reasonable assumptions about the vertical variation of $\bar{u}$ and $K_{zz}$ involving the state of thermal stratification of the surface layer. Results for point, line, and area sources have been summarized by Csanady (1973) and Pasquill (1974). There have been extensions of this work to the entire boundary layer, usually by using a two-layer model, see Monin and Yaglom (1971) and Berlyand (1972a, b) for summaries. Monin and Yaglom show that in general solutions to equation (7) are asymptotically correct for the case $T >> t_L$. Although $t_L$ can be considered to be of the order of a few seconds in the atmospheric surface layer, its value reaches tens of minutes on occasion, considering the boundary layer as a whole. At this scale in, for instance, conditions of active large-scale buoyant convection in the boundary layer, $T \simeq t_L$; and so the general applicability of the gradient transport equation in the boundary layer is open to some question on fairly fundamental grounds.

At scales intermediate between the two extremes, of "close-in" boundary-layer diffusion and, say, regional to global-scale diffusion, it thus becomes necessary to consider further generalization of the gradient-transport equation to describe diffusion. Because of the strong influence, at these intermediate scales, of mean wind shear effects, equation (8) must be replaced by the more general expression

$$F_i = - K_{ij} \, \partial \bar{C} / \partial x_j \, . \qquad (10)$$

The terms $K_{ij}$ are the 9 components of the eddy-diffusivity tensor of which only 2 appear in equation (7). The resulting diffusion equation contains in addition terms including $K_{xz}$ and $K_{zx}$. The importance of such terms in shear-flow diffusion was first pointed out by Lettau (1952) and the subject has recently been reviewed by Yaglom (1972). Few solutions have been obtained to the diffusion equation for this case. But the conclusion as pointed out by Pasquill (1974) is that the pattern of atmospheric diffusion at distances greater than a few kilometers is strongly influenced by wind shear, and pollutant clouds tend to become elongated in the direction of the shear.

### 2.3 Models Based on Similarity Theory

Because of the inherently limited applicability of the assumption of turbulence homogeneity to atmospheric diffusion problems, and the mathematical complexity of concentration equations derived by K-theory except in very simple special cases, as well as concerns for the general validity of the gradient transfer hypothesis, alternative approaches are of great interest. An important one is provided by the hypothesis of Lagrangian similarity, according to which the Lagrangian (particle-attached) characteristics of the flow depend only on basic flow parameters such as are known to characterize Eulerian properties like the boundary-layer mean wind and temperature distributions. Various applications of this theory to the determination of vertical spreading rates in the boundary layer were reviewed by Pasquill in the previous lecture, and summaries of available theoretical results can be found in Pasquill (1974) and Monin and Yaglom (1971).

As applied for instance in the surface layer, the basic assumption of similarity theory is that the mean concentration distribution for an instantaneous point source has the following form:

$$\bar{C}_i(x,y,z,T) = (Q_i/\bar{z}^3) f([x-\bar{x}]/\bar{z}, y/\bar{z}, [z-\bar{z}]/\bar{z}, \bar{z}/L) \, . \qquad (11)$$

The quantities $\bar{x}$ and $\bar{z}$ are the coordinates of the mean position, or centroid, of the diffusing cloud; and these depend only on the basic flow parameters of the surface layer, e.g. on $u_*$, $z_o$, and the Monin-Obukhov stability length L, as previously defined by Pasquill. Expressions for $\bar{x}$ and $\bar{z}$ are derived by dimensional analysis ($\bar{y} = 0$ of course); and it is then possible to derive specific results for some properities of mean concentration distributions from equation (11), integrating it to obtain other source configurations in the usual way.

When these results are extended above the surface layer, additional flow parameters, the geostrophic wind and Coriolis parameter, become involved which of course greatly add to the complexity of the dimensional analysis and reduce the definiteness of the results obtained. From the standpoint of determining the mean concentration distribution, it is important to notice that nothing in the theory specifies the form of the unknown, universal function f. Consequently only the downwind or central concentration distribtuion, but not the form of the crosswind cloud (or puff) distribution, is determined. Nevertheless several useful applications to diffusion problems have been made using this approach, including the interesting study of urban pollution by Friedlander and Seinfeld (1969).

## 3. PLUME MODELING APPLICATIONS TO VARIOUS SPACE AND TIME SCALES

### 3.1 Applicability of a Simple, Empirical Diffusion Model

From the brief sketch of theoretical results contained in the preceding section it can be appreciated that "solutions" to the problem of modeling atmospheric turbulent diffusion are characterized by various limitations, restrictions, and degrees of empiricism; indeed they are quite analagous in this respect to solutions to many, probably most other turbulent flow problems. On the other hand the introductory section stressed the great need for diffusion models, in applications to a large and growing number of air pollution problems. In this situation it has seemed best to develop diffusion models that are

consistent with whichever theoretical expectations are believed to apply to a given problem but that are also strongly rooted in empirical diffusion data, particularly certain key sets of diffusion trials, which have been summarized in detail by Islitzer and Slade (1968) and Pasquill (1974). These diffusion data include measurements of clouds from surface level and elevated point sources, mainly of the continuous type although some instantaneous-source data exist, and extend to downwind distances of the order of a few kilometers from the source.

The diffusion data have been organized into a form suitable for application to a wide variety of air pollution modeling problems by assuming that the distribution of pollutant clouds is Gaussian. This assumption has been seen to be in accord with various theoretical results, for instance for diffusion in homogeneous turbulent flows and for the case, $T >> t_L$, of very large downwind distances and travel times. In the planetary boundary layer, in which the wind is strongly sheared and skewed, the Gaussian assumption is in principle faulty from the theoretical point of view; but even here it is a good approximation in certain conditions, i.e. for small values of travel time T. Strictly speaking the Gaussian equation, as a solution to the parabolic equation of diffusion, implies an infinite speed of propagation of pollutants, which is physically unrealistic. Accordingly several writers, e.g. Monin (1955), have derived a diffusion equation of hyperbolic type, the telegrapher's equation, to remove this difficulty. But Monin and Yaglom (1971) have demonstrated that infinite speed of propagation is in general a secondary problem to shear effects on diffusion. Pasquill (1974) stressed that the exact form of the tails of the cross-wind distribution formula is not very important as a practical matter.

The important point is that the Gaussian formula, properly used, is peerless as a practical diffusion modeling tool. It is mathematically simple and flexible, it is in accord with much though not all of working diffusion theory, and it provides a reliable framework for the correlation of field diffusion trials as well as the results of both mathematical and physical diffusion modeling studies. An interesting example of the latter is the recent study by Deardorff and Willis (1975) which uses a Gaussian plume formulation to correlate laboratory modeling and theoretical results on diffusion in the daytime mixing layer.

### 3.2 The Gaussian Plume Model

Gaussian diffusion formulas appear in the early work by Roberts (1923), in which they are derived from K-thory, and in the papers by Sutton (1932) and Frenkiel (1953), based on statistical theory. However they were first used by Cramer (1957) and Hay and Pasquill (1957), as mathematical diffusion models to correlate empirical data. The most usual form is the so-called Gaussian plume model, Gifford (1960), which applies to the ground level concentration due to a source at the (effective) height z = h;

$$\bar{C}/Q = (\pi\sigma_y\sigma_z\,\bar{u})^{-1} \cdot \exp\,[-(y^2/2\sigma_y{}^2 + h^2/2\sigma_z{}^2)]. \qquad (12)$$

In this formula $\bar{u}$ is the mean wind speed at plume height; $\sigma_y$ and $\sigma_z$, having units of length, are the standard deviations of the cloud distribution in the y- and z-directions; and h is the elevation of the source above the ground surface, which is assumed to coincide with the x - y plane. Equation (12) can be obtained for instance from equation (5), with $\sigma_y{}^2 \equiv \overline{y^2}$ and $\sigma_z{}^2 \equiv \overline{z^2}$, simply by multiplying by 2 to account for the presence of the ground surface; that is, the ground is assumed (for the moment) to be a perfect "reflector" of pollutant species. Different symbols for the variances are introduced partly to emphasize that these are to be determined in a different way, namely by data correlation.

Several systems have been used to incorporate empirical diffusion and meteorological data directly into equation (12). The most widely used scheme is the one proposed by Pasquill (1961). Alternatives have been proposed by Cramer (1957), Singer and Smith (1953), and Carpenter, et al. (1971), among others. An extended review of these turbulence typing schemes has been given by Gifford (1975). Their great merit is that they incorporate to the maximum extent our direct, observational knowledge of atmospheric diffusion, in a manner consistent with our understanding of stratified boundary layer shear flow, into an equation for the mean concentration distribution that, while not theoretically exact, is both reasonable and consistent with much of the existing body of theory of turbulent diffusion.

Curves of $\sigma_y$ and $\sigma_z$ based on Pasquill's original scheme are included as Figure 1. The dashed portions of these curves indicate the tentative nature of the extrapolation beyond about 1 km, owing to limited data. These curves apply to diffusion from a source near the surface; A through F are atmospheric stability categories, from unstable to very stable. For details see Pasquill (1974) or the summary review by Gifford (1975).

### 3.3 Diffusion Modeling at Distances Beyond a Few Kilometers

Beyond a few, at most 10, kilometers from the source, use of empirically-based diffusion categories based on local meteorological data with a Gaussian plume equation becomes seriously inadequate for several reasons. First, there are very few reliable diffusion data for distances greater than about 10 km. Second, the effect of wind shear on horizontal diffusion, through terms omitted in the usual theoretical treatments, becomes large; and they do not directly provide a viable alternative. Finally, large scale air motions affect the trajectories of diffusing plumes and puffs, and the assumption of constant $\bar{u}$ is rarely adequate.

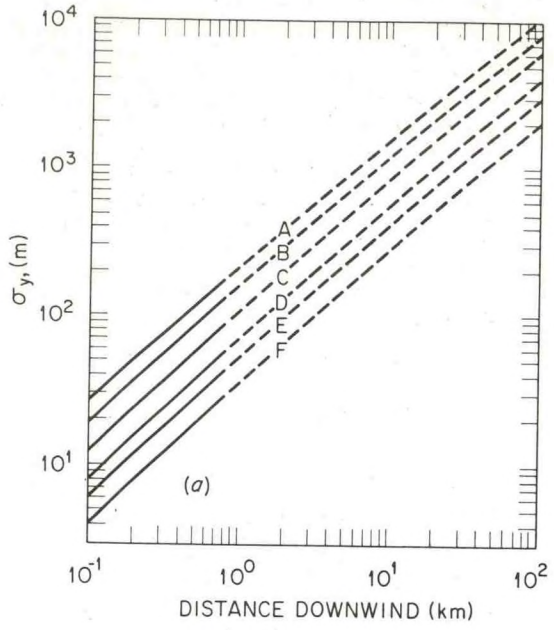


(a)

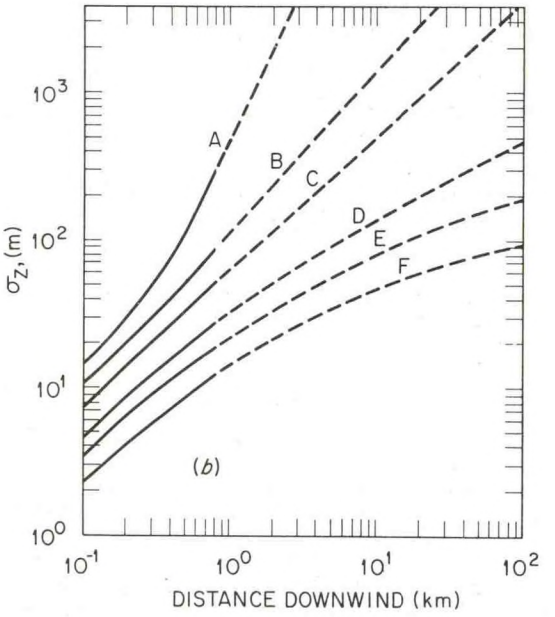


(b)

Figure 1. Curves (a) of $\sigma_y$ and (b) of $\sigma_z$ for Pasquill's turbulence types, based on Pasquill (1961) [see also Gifford (1960), Slade (1968), and Turner (1969)].

Various authors, including Frenkiel (1957) Start and Wendell (1974), Roberts (1970), and others have used Gaussian "puff" models, that is models of the form of equation (4), combined with air trajectory estimates, to estimate longer-range diffusion. In such studies, the horizontal air trajectory is calculated, or estimated, from a suitably weighted average of the observed horizontal wind field at elevations of interest. The diffusing cloud, which is assumed to have Gaussian symmetry, is then advected along this trajectory; and the instantaneous concentration field, $C_i$, is calculated from an equation of the form

$$C_i / Q_i = (2\pi)^{-3/2}(\sigma_y \sigma_z \sigma_x)^{-1} \cdot \exp\left[-(x^2/2\sigma_x^2 + y^2/2\sigma_y^2 + z^2/2\sigma_z^2)\right] \quad (13)$$

the coordinates being located at the centroid, along the trajectory. Distance along the trajectory is calculated by $x = \bar{u}T$, and the contributions of puffs passing any point are integrated to find the average plume concentration distribution.* As discussed in many references, for instance Gifford (1968), the form of the instantaneous cloud spreading relative to its centroid, i.e. relative diffusion, differs from average diffusion relative to a fixed coordinate axis. The reason is that only eddies whose size is of the order of the cloud size contribute to relative diffusion, whereas eddies of all sizes contribute to the average diffusion. The $\sigma$-values of equation (13) have usually been adjusted in practice so as to reflect the best available empirical diffusion information.

Start and Wendell (1974) compared the mean concentration field, calculated from a Gaussian puff equation like (13), using a year's trajectories from a detailed wind observation network, to that based on equation (12) using "straight-line" winds. They found significant differences beyond distances of several kilometers from the source, especially in areas where the mesoscale wind field was strongly influenced by topographic flows.

At distance beyond a few hundred km, that is for $T >> t_L$, a Gaussian model can once again be used with little or no theoretical apology, if only because there is no obviously superior alternative. At the global limit, as has been mentioned, constant-K solutions work quite well, see Machta (1973).

*As a practical matter there is no particular need to introduce a "puff" model for the purpose of calculating long-distance, trajectory-driven plumes. A version of Frenkiel's spreading-disk model, i.e. of equations (5) or (12), with the disk-centroid positioned by the trajectory wind, gives identical results, without the need to specify $\sigma_x$, about which it should be emphasized virtually nothing is known. The Argument that a 3-dimensional Gaussian puff model is needed, different, or somehow "better" is mistaken. Appreciable savings of computer time could probably be realized by using a spreading-disk trajectory model.

### 3.4 Time Averages of Diffusion

Point source diffusion models, such as eqs. (4), (9), (11), and (12) attempt to define the mean concentration field, relative to a spatially fixed point or axis, over some more-or-less extended period of time. The averaging time of Gaussian models, in particular, is that of the diffusion data upon which they are based; and this is usually a period of the order of 20 or 30 minutes, i.e. generally longer than $t_L$. The steady state contemplated in these equations is in effect assumed to obtain over periods of this length of time, that is, about an hour. But the meteorological processes driving boundary layer diffusion vary in time both diurnally and with changes in the large-scale meteorological field. For averaging times shorter than an hour concentration fluctuations also occur owing to the inherently irregular nature of turbulence, even in the presence of a (temporarily) steady state of the mean flow.

Various theoretical difficulties associated with this problem, that is with the specification of the frequency distribution of pollutant concentrations in addition to the mean, are described by Csanady (1973), who discusses several possible lines of approach. Gifford (1959) employed a version of the Gaussian plume, equation (12), which takes into account short-period meandering of the mean plume axis to derive the concentration distribution. In this model the coordinates y and z of equation (5) are replaced by $(y - D_y)$ and $(z - D_z)$, where $D_y$ and $D_z$, the displacements of the fluctuating plume axis, are assumed to be normally distributed. Even in this special case (constant mean wind directed toward the sampling station) the mathematical expression for the concentration distribution is quite complex.

Barry (1971) (1975), based on a long series of short period observations of ground-level concentration values from continuous, isolated, elevated source, concluded that the form of the concentration frequency distribution is exponential, a property earlier noticed by Gartrell (1966). Barry's equation for the concentration frequency distribution from such a source, F, can be written (in the present notation)

$$F(C/Q) = F(0) \exp\left[-F(0)(C/Q)/(\overline{C/Q})\right]. \qquad (14)$$

In this equation $(\overline{C/Q})$ is the long-period mean value of the short period concentration from an isolated elevated plume, normalized by source strength (both can vary). F(0) is the frequency with which C/Q exceeds the zero value at a given surface level sampling point.

Equation (14) corresponds to the ordinary, single, point-source situation in which there is a fixed receptor. For this reason it is of potentially great use in correlating pollution data from sources of this kind. Barry (1975) finds that F(0) increases very nearly as the cube root of averaging time, that is, of the interval over which the concentration data are gathered. F(0) reaches its theoretical limit of unity for an averaging time of about four days, which means that within this period, the average time of passage of low and high pressure regions over a point in mid latitudes, the wind will blow from source to sampler some fraction of the time with a high probability.

Various authors have attempted to account for the effect of time averaging on the concentration distribution by a modification of the plume formula. This has been done in two ways, either by operating directly on the concentration, C, or else indirectly, by modifying $\sigma_y$ and $\sigma_z$. In the first method the assumption is that

$$C_A/C_B = (t_B/t_A)^p \quad . \qquad (15)$$

Here $C_A$ is the concentration value averaged over some time period of interest, $t_A$; and $C_B$ is that for some basic averaging time period, $t_B$, often an hour; i.e. $C_B$ is usually taken to be identical with $\bar{C}$ of equation (12). The averaging effect has also been introduced by a similar modification of $\sigma_y$ in equation (12). The idea is that the controlling influence is that of horizontal wind fluctuations. Since $\sigma_y/x \simeq \sigma_\theta$ where $\sigma_\theta$ is the horizontal wind direction standard deviation, the averaging effect on $\sigma_y$ has been studied by means of the relation

$$\sigma_{yA}/\sigma_{yB} = \sigma_{\theta A}/\sigma_{\theta B} = (t_A/t_B)^q \quad . \qquad (16)$$

Based on experimental studies it can be concluded [Csanady (1973)] that the range q = 0.25 to 0.3 is a reasonable approximation for 1 hr < $t_A$ < 100 hrs. Similar considerations should apply to $\sigma_z$, except the effect of variations of $\sigma_z$ should not extend to downwind distances beyond a few kilometers. Thus the value p = 1/2, found by Hino (1968) for the maximum concentration variation, which reflects dependence of the concentration on $(\sigma_y\sigma_z)^{-1}$, would not be expected to extend to much greater downwind distances. For $t_A$ ranging downward from an hour to a few minutes, most authors agree on a q-value of 0.2, as originally suggested by Stewart, et al. (1953).

Average concentrations over very long periods of time, like a season or a year, have been calculated by simply weighting the concentration $\bar{C}$ at a point by the frequency, f, with which the wind blows toward that point, according to climatological records (the wind rose). Thus the annual or long term average concentration, $\bar{C}_{avg.}$, is taken to be

$$\bar{C}_{avg.}/Q = (2/\pi)^{1/2} f[\sigma_z \bar{u}(2\pi x/n)]^{-1} \cdot \exp(-h^2/2\sigma_z^2)] \qquad (17)$$

where $2\pi$ x/n is the width of a standard angular (wind-rose) sector, usually 22.5°; i.e. n usually equals 16. Formulas of this type employing Sutton's diffusion model were first introduced by Holland (1953) and Meade and Pasquill (1958).

As Barry (1975) points out, these long period averages must necessarily be approached asymptotically by the shorter period values given above. At the values of q that have been quoted this point should be reached in no more than several hundred hours.

## 4. BUOYANCY EFFECTS

### 4.1 Buoyant Plume Models

Many, if not most pollutant sources are positively buoyant. (Some are negatively buoyant and probably very few are exactly neutrally buoyant). The source of this buoyancy is the waste heat accompanying energy generation, some industrial process, or space heating. As many authors have pointed out (cf for instance Briggs (1969)) buoyancy has a profound effect on plumes. At first, near the source of a buoyant plume, the plume rises above the source level, at a rate and to a height controlled at first by the buoyancy excess and later by atmospheric stability. This stage of plume rise and spread is controlled by the rate of entrainment into the plume of ambient air, a phenomenon that takes place as a result of fine-scale turbulence generated by the wind shear at the rising plume's edge. This phenomenon, which is quite different in structure and in its plume-spreading properties from the general, random turbulent diffusion of the boundary layer, persists for considerable distances downwind, of the order of 10 times the stack height in the case of tall, electric power-plant stacks. Passive diffusion, the ordinary atmospheric diffusion considered in all the previous sections, becomes the dominant factor in the spreading of such plumes only at greater downwind distances.

Further properties of buoyant plumes will be discussed in detail by Briggs; I only wish to point out here that the current, standard method of accounting for this in calculating the buoyant-plume concentration distribution is to adjust the source height, h, in the plume formula, equation (12), as follows:

$$h = h_s + \Delta h. \qquad (18)$$

The Gaussian form is retained; $h_s$ is the physical source elevation, the stack height; $\Delta h$ is the buoyant rise. Plume formulas of this type, i.e. equation (12) combined with equation (18), have provided quite acceptable estimates of for instance the maximum ground-level concentration, $\bar{C}_{max}$, where

$$\bar{C}_{max}/Q = 2\sigma_z/\pi h^2 e\bar{u}\ \sigma_y \qquad (19)$$

obtained from (12) by setting $y = 0$ and $h^2 = 2\sigma_z^2$. However the location of this concentration maximum, which can also be derived from (12), is in practice much less successfully predicted. The probable reason is that at the distance of ground-level concentration maxima, a few source-heights downwind, the plume's behavior is still dominated by buoyant rise, and not by the diffusion process assumed in (12). The concentration is well-predicted because the values of $\sigma_y$ and $\sigma_z$ are in part adjusted to assure this; that is, the $\sigma_y$ and $\sigma_z$ values at these distances reflect actual observed plume maximum concentrations from elevated sources.

Pasquill (1974) and in the previous section has emphasized that diffusion, particularly the vertical component, is quite different for sources located near the surface as compared with elevated sources like tall stacks because of boundary-layer turbulence inhomogeneity. Furthermore the buoyancy of most tall-stack plumes itself controls their spreading rate, as Briggs will point out. To make reliable estimates of concentration patterns using the Gaussian plume model requires adjustment of the $\sigma$-curves of Figure 1 to compensate for these effects. Briggs (1973) considered all available diffusion data, including surface-level sources, elevated sources, and strongly buoyant sources, and proposed the formulas for $\sigma_y$ and $\sigma_z$ that are summarized in Table 1.

Table 1

Formulas recommended by Briggs (1973) for $\sigma_y(x)$, m, and $\sigma_z(x)$, m; $10^2 < x < 10^4$ m, open country conditions.

| Pasquill Type | $\sigma_y$(m) = | $\sigma_z$(m) = |
|---|---|---|
| A | $.22x(1+.0001x)^{-1/2}$ | $.20x$ |
| B | $.16x(1+.0001x)^{-1/2}$ | $.12x$ |
| C | $.11x(1+.0001x)^{-1/2}$ | $.08x(1+.0002x)^{-1/2}$ |
| D | $.08x(1+.0001x)^{-1/2}$ | $.06x(1+.0015x)^{-1/2}$ |
| E | $.06x(1+.0001x)^{-1/2}$ | $.03x(1+.0003x)^{-1}$ |
| F | $.04x(1+.0001x)^{-1/2}$ | $.016x(1+.0003x)^{-1}$ |

Graphs of these formulas are reproduced as Figure 2.

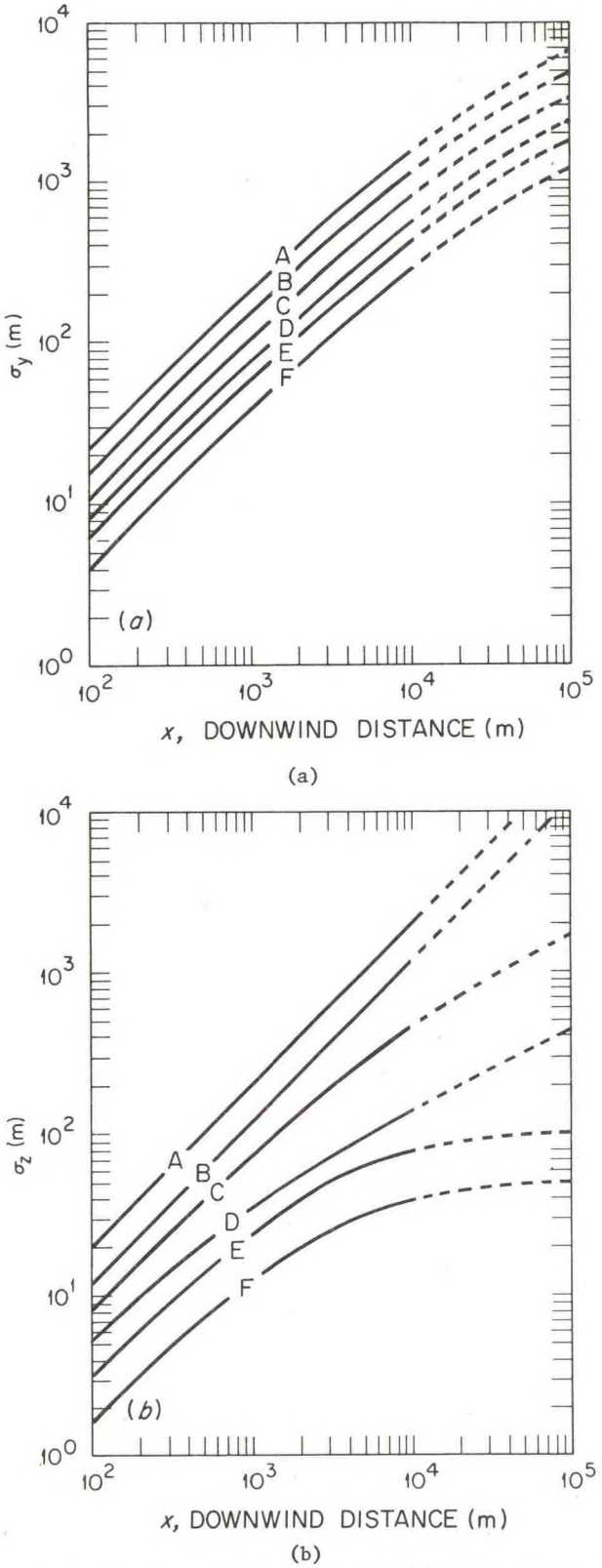


Figure 2. Curves (a) of $\sigma_y$ and (b) of $\sigma_z$ based on Briggs (1973) interpolation formulas for flow over open country, see Table 1; from Hosker (1974).

The intent of these formulas must be stressed. Briggs' $\sigma$-curves are meant to be used in connection with formulas such as equation (19), or those of the following section, to estimate the maximum ground level concentration. Since this will be located farther downwind the greater the source height is, the curves reflect diffusion data for higher sources at greater x-values [cf Gifford (1975)]. If for some reason it is required to model the axial, or plume-level concentration, for a tall-stack source, plume spreading values given by buoyant plume rise formulas must be used.

### 4.2 Processes Carrying Buoyant Plumes to the Ground; "Fumigations"

The appearance of plumes from tall stacks has often been classified in terms of their physical form during various typical turbulence conditions of the planetary boundary layer. Plumes are said to be "fanning," "coning," or "looping." In the fanning condition, which would correspond to diffusion category E or F, vertical diffusion is sharply suppressed by a certain amount of stabilization but there is still some horizontal plume spreading. Looping, on the other hand, is associated with category A or B, that is, with unstable lapse rates. Coning occurs during category C or D conditions.

Plumes can be brought to the surface by several of these processes. Such occurrences are collectively called "fumigations." This term was coined by Hewson and Gill (1944) in the Trail Smelter report. The original idea was that material from an elevated, possibly buoyant source is carried down to the ground when the nocturnal surface inversion is dissipated by daytime heating up to the level of the plume. When this happens, the shallow, ribbon-like "fanning" plume, which is characteristic of nocturnal, stable conditions, changes over to a "looping" type as a result of the destruction of the nocturnal surface inversion by daytime heating. Figure 3 illustrates these various plume types schematically.

The fumigation concept has been extended to cover several distinct types of events. In the case of a buoyant plume there is competition between the tendency of the plume to rise because of its buoyancy and any tendency for it to be carried to the ground by a fumigation process. The various possibilities have tentatively been classified as follows, cf Briggs (1969), Pooler (1965). If a buoyant plume fails to penetrate an elevated inversion and is trapped aloft, an inversion breakup fumigation (IBF) occurs when the lapse-rate below the inversion becomes neutral or unstable. This is the classical case, for which Holland (1953) reasoned that the effluent must be rapidly mixed in the vertical. The concentration equation is obtained by integrating the Gaussian plume equation with respect to z, and dividing by the effective stack height (plume height) h:

$$\bar{C}_{IBF} = Q/[(2\pi)^{1/2}\ \bar{u}\ h\ \sigma_y] \qquad (20)$$

This condition is, as Briggs (1969) pointed out, particularly serious when it takes place in a deep valley. This was the case at Trail, B.C. If the plume does not rise out of the valley an appropriate concentration equation is obviously

$$\bar{C}_{IBF} = Q/(\bar{u}\ h\ W) \qquad (21)$$

where W is the width of the valley up to height h. Smith (1968) points out that the inversion break-up type of fumigation should not, in the case of a buoyant, tall-stack plume, be expected to occur at a distance downwind much less than $x = 20\ h_s$, because of the dominance of plume behavior by buoyant rise at smaller distances.

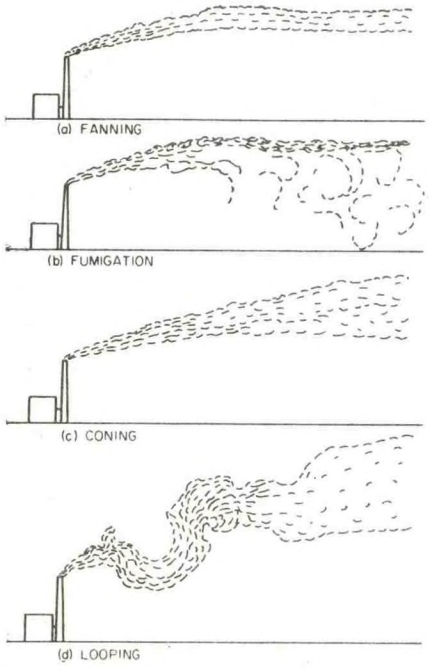


Figure 3. Schematic illustrations of various characteristic plume types; from Briggs (1969).

For strongly buoyant plumes from tall power plant stacks, the maximum concentration value may occur at distances up to 20 miles down wind according to Carpenter, et al. The duration of the maximum condition is inherently short, from a few minutes in the case of smaller, less buoyant plumes, to 30 to 45 minutes for the tall-stack TVA plumes. The absolute frequency, without respect to particular location, of this kind of fumigation is probably fairly high. However, the frequency at any particular downwind location is likely to be low, because the type occurs over a large range of downwind distances.

A second fumigation type, the high wind fumigation, occurs as a result of the relatively straightforward plume behavior known as "coning," This happens when the atmosphere is well mixed by turbulence at all heights encountered by the plume. Equation (12) applies; $\sigma_y$ and $\sigma_z$ are Pasquill types C or D, and the relevant equations for $\Delta h$ must be included. When the coning plume has grown to the point where it reaches the ground, the maximum ground level concentration occurs. In terms of equation (12) this happens when $h = 2^{1/2}\sigma_z$. Since for a coning plume $\sigma_z \simeq \sigma_y$, the equation for the maximum concentration, from (12) is seen to be

$$\bar{C}_{max} = 2Q/(\pi h^2 \bar{u}\ e) \qquad (22)$$

Air pollution regulations are usually written in terms of controlling the maximum ground concentration level, and so this is an important formula. If $\sigma_y$ differs from $\sigma_z$, the formula

$$\bar{C}_{max} = (2Q/(\pi h^2 \bar{u}\ e))(\sigma_z/\sigma_y) \qquad (23)$$

applies.

Calculations and observations of buoyant plumes show that as a rule the coning value at which $\sigma_z$ equals the effective stack height, h, occurs at considerable downwind distances, of the order of 10 times the stack height, $h_s$.

The so-called high-wind fumigation (HWF) occurs because of the competition between the maximum concentration defined by equation (23), which is lowest for high winds, and the value of $\Delta h$ in the buoyant plume rise formula,

$$\Delta h = c_1/\bar{u}\ , \qquad (24)$$

where $c_1$ is obtained from whichever plume rise equation applies (cf. Briggs (1969) and his later presentation here). This leads to a high value of $\bar{C}_{max}$ when h, and consequently $\Delta h$, are small. If we eliminate $\bar{u}$ between equations (24) and (23) and maximize the resulting expression it turns out that the maximum condition is $\Delta h = h_s$, and it follows that

$$\bar{C}_{HWF}/Q = (\sigma_z/\sigma_y)(2\pi e h_s c_1)^{-1} = (\sigma_z/\sigma_y)(\pi e h c_1)^{-1} \qquad (25)$$

for the maximum concentration under this fumigation condition. Because it occurs with high winds, this condition can persist for several hours at a time. The required wind speed value is

$$\bar{u}_{HWF} = c_1/h_s \qquad (26)$$

and the downwind distance at which it occurs is obtained from the condition that $h = \Delta h + h_s = 2h_s = 2^{1/2}\sigma_z$. Because the high-wind fumigation results from coning, which is caused by a comparatively steady turbulence process, it can be quite persistent, for instance under cloudy, windy conditions. Also it is for the same reason much more likely to occur at a given location than the inversion breakup type of fumigation.

A third type of fumigation is called the limited mixing (LMF) or trapping type. This type occurs when upward diffusion or penetration of the plume is restricted by an inversion, below which strong mixing is occurring. The most important case is that of a subsidence inversion. Because such inversions (stable layers) are associated with anticyclones, their lifetime is measured in days. Consequently this kind of fumigation can be quite persistent, lasting for several hours through the mid-day, well-mixed stage of development of the boundary layer.

Because of the mode of development of this condition, mixing below an inversion, it should be described by a formula similar to equation (20), namely

$$\bar{C}_{LMF} = Q/[(2\pi)^{1/2}\bar{u}\, H\, \sigma_y]. \qquad (27)$$

The difference is that H now refers to the limited inversion height. It appears that Holland (1953) was the first person to propose this kind of a formula. More complicated formulas for "trapping," involving infinite series of plume "reflections" have been derived but their superiority to Eq. (27) has never been established.

For tall-stack, strongly buoyant plumes, high-wind and limited mixing types are most important, the inversion breakup tending to be in any particular spot a rare and transient condition. TVA experience is that the LMF results in maximum concentrations up to three times that of the HWF at their plants. The reason for this is easy to see, because since $h = 2^{1/2}\sigma_z$, from equations (25) and (27),

$$\bar{C}_{LMF}/\bar{C}_{HWF} = (\pi^{1/2}e/2)(h/H) \simeq 2.4h/H. \qquad (28)$$

Of course, the depth H of a persistent subsidence inversion that is low enough to restrict the rise of a buoyant plume must necessarily be somewhat less than h, the effective stack height of the plume, and so $\bar{C}_{LMF}/\bar{C}_{HWF}$ must be greater than about 2.4.

Naturally if either the LMF or the IBF occurs with essentially calm conditions, the resulting concentrations will be especially high. Briggs (1969) says that a fumigation occurring under calm conditions in the presence of a subsidence inversion has led to the highest ground-level concentrations experienced around a TVA plant, and is moreover quite persistent. Fortunately the frequency of the required meteorological conditions, which incidentally are those that accompanied major air pollution disasters such as the Donora and the Meuse Valley incidents, is low. Briggs proposes formulas for this calm subsidence fumigation type which he will discuss.

## 5. MODIFICATION OF PLUME MODELS TO ADAPT THEM TO VARIOUS ENVIRONMENTAL PROBLEMS AND EXCEPTIONAL ATMOSPHERIC FLOWS

Boundary layer turbulence is governed by the mechanical and thermal properties of the underlying surface. The relationship between mean values and vertical gradients of such properties as wind, temperature, and humidity, and surface mechanical and thermal properties was the principal subject of the preceding Workshop in this series [Haugen (1973)]. These same properties are assumed, in the diffusion models described above, to affect the mean concentration distribution through their control of atmospheric diffusion. In the case of Gaussian diffusion models this influence occurs on the diffusion lengths, chiefly $\sigma_z$, and hence on the Pasquill diffusion categories.

The Monin-Obukhov stability-length L,

$$L \equiv -(u_*^3 c_p \rho \bar{T})/kgF_H, \qquad (29)$$

where $\bar{T}$ is average surface layer temperature, $c_p$ is specific heat at constant pressure $\rho$ is air density, k is von Karman's constant, $F_H$ is the vertical heat flux, and $u_*$ is the friction velocity as determined from the surface shear stress, $u_* = (\tau/\rho)^{1/2}$, is a fundamental index of the state of the boundary-layer turbulence. All of these parameters can usually be assumed to be constants or to vary only slowly in a steady-state boundary layer, over time periods of the order of a typical averaging time for diffusion formulas like equation (12), i.e. 30 minutes to an hour.

The connection between the stability parameter, L, surface roughness, $z_o$, and empirical stability categories has been studied by Golder (1972), who obtained the relationship displayed in Figure 4. Golder also provided nomograms relating Richardson number, Ri, and the more easily measured bulk Richardson number, B, (Lettau and Davidson (1957), where

$$B \equiv (g/\bar{\theta})(\partial\theta/\partial z)(z/\bar{u})^2, \qquad (30)$$

$\theta$ being potential temperature, to the quantity $z/z_o$, where $z_o$ is the roughness length. Relationships between Ri and L are discussed in detail in several papers from the previous Workshop. Thus the applicable diffusion category can be determined, with the help of these equations and nomograms,

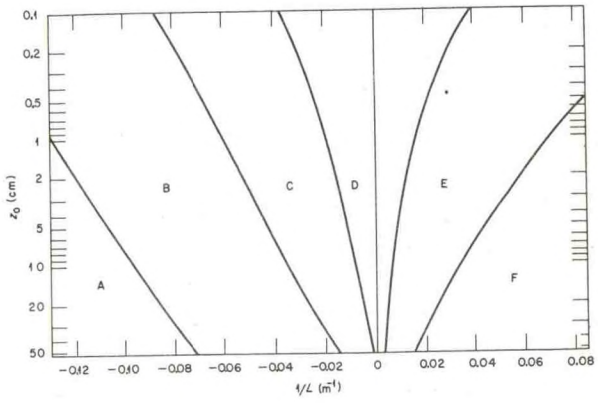


Figure 4. Golder's (1972) curves showing Pasquill's turbulence types as a function of the Monin-Obukhov statility length L, m, and the aerodynamic roughness length $z_o$, cm.

from thermal and mechanical properties of the surface layer. In particular equation (30) requires only measurements of mean wind, $\bar{u}$, and the vertical temperature gradient.

For diffusion over distances greater than a few kilometers, and even in some situations at smaller distances, changes in roughness and thermal properties of the underlying surface occur and these must necessarily modify diffusion models. In addition, flows exist for which diffusion is not controlled solely by direct thermal and mechanical turbulence generation as conceived in diffusion typing schemes. Examples are: flows over cities, flows over large bodies of water, wake flows, and very light wind, stable flows such as occur on calm, clear nights. In all such cases modifications of the basic plume model must be considered.

## 5.1 Diffusion Categories at Distances Beyond a Few Kilometers

Diffusion beyond a few kilometers from a source, even in the relatively straightforward case of "open country" that is assumed in typing schemes, is complicated by a number of effects that are not particularly important at short distances. The underlying surface type changes, introducing changes in roughness and thermal conditions. Vertical diffusion ultimately extends through the entire boundary layer, which is usually surmounted by a stable layer. This limits $\sigma_z$ to the values of the mixing depth, [Holzworth (1972)]. As travel time (downwind distance) increases, diurnal changes in governing parameters such as stability also become important.

In order to account for these problems F. B. Smith (1972), see also Pasquill (1974), and Pasquill and Smith (1974) has enlarged upon Pasquill's original turbulence typing scheme as follows. He obtained numerical solutions to the diffusion equation for downwind distances up to 100 km, using wind speed and diffusivity values based on actual experience over a range of stability conditions. He then used these results to define $\sigma_z$-values based on: i) the stability of the lower layers, as ordinarily determined in Pasquill's method; and ii) the overall stability of the planetary boundary layer. Provision is also made to introduce the "typical" roughness length over the plume path, the incoming solar radiation, the upward heat flux, the mixing depth, and variation of stability along the path. The method is not yet complete (curves for $\sigma_y$ have not yet been published), but will ultimately provide a way to extend the basic typing scheme to distances up to 100 km. Curves of $\sigma_z$ computed by Hosker (1974) according to Smith's procedure for $z_o$ = 10 cm and $z_o$ = 100 cm are shown in Figure 5.

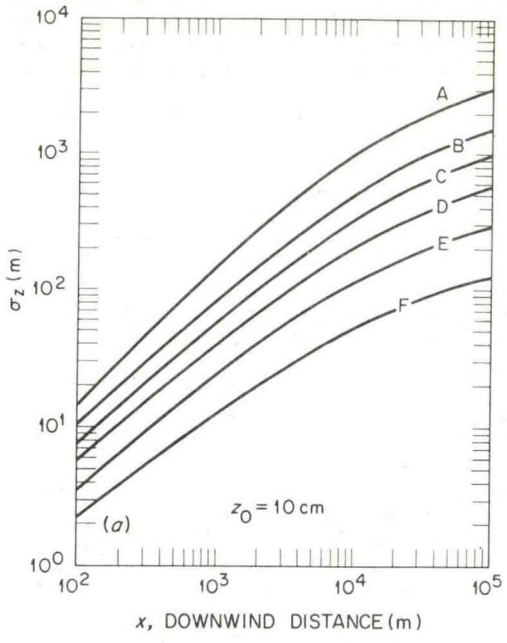


(a)

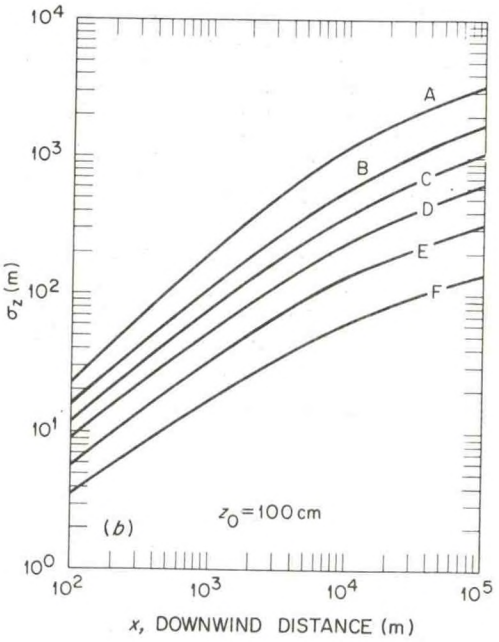


(b)

Figure 5. Curves (a) of $\sigma_z$, $z_o$ = 10 cm, and (b) of $\sigma_z$, $z_o$ = 100 cm based on F. B. Smith's (1972) method, after Hosker (1974).

## 5.2 Diffusion in Near-Calm, Very-Stable Conditions

Beattie (1963) determined the frequency of occurrence of Pasquill's stability categories at eight British meteorological stations, and results for others were reported by Bryant (1964). Others have since repeated this determination at various locations. The results are as a rule similar, although there is some variation with locality. Categories A and B provide together around 10%, C and D around 60%, E about 10%, and the remaining 20% of the time category F applied, at least at the British stations.

However, included in the latter 20% are a number of near-calm situations typically ocurring on clear nights with frost or heavy dew. Such conditions were specifically excluded by Pasquill from the original categories because the diffusing plume could be expected to be very variable, with "little definable travel." As these conditions occurred some 5 to 8% of the time in Beattie's study, they have considerable practical importance. Beattie assigned to them the designation G, without proposing any σ-curves

On the not unreasonable assumption that actual diffusion under category G conditions would be less than under F conditions, users have arbitrarily assigned diffusion values; see for instance U.S. NRC Regulatory Guide 1.21, which indicates that category G diffusion has been assumed to be appreciably slower than category F. Atmospheric diffusion experiments, reported by Sagendorf (1974), suggest however than under category G conditions the plume is subject to a good deal of irregular horizontal "meander," or swinging. When averaged over an hour, the concentration values at a point are much lower than was at first assumed under these conditions. Nickola, et al. (1974), based on the results of two low-wind ($\bar{u}$ = 1.5 m sec$^{-1}$) diffusion experiments in which the tracer was released for 30 minutes from a point quite near the ground, come to similar conclusions. In the test run under stable conditions, varying between types E and G, the averaged concentration values corresponded approximately to category C. In the test run under unstable conditions, varying between types A and D, the average concentration values were found to be a factor of two below category A values.

A review of several sets of diffusion data for such light wind, stable condtions by Van der Hoven (1975) indicates that the effective σ-values can correspond to anything between categories A and F. This supports Pasquill's original assertion, that diffusion under these conditions will be very irregular and indefinite. In dealing with these conditions at any site, it will clearly be necessary as a minimum to have measurements or estimates of horizontal plume meander, as well as the usual quantities required to define the turbulence type.

## 5.3 Diffusion Over Water

Flow over bodies of water has long been known to be characterized by greatly reduced turbulence intensity [Slade (1962], and a correspondingly decreased diffusion rate [Van der Hoven (1967)]. According to Kitaigorodskii (1970), in order to describe the neutral boundary-layer wind profile over a water surface, account has to be taken of the fact that the waves are in motion relative to the air. Consequently they do not act as ordinary, land-surface, fixed roughness elements except in the initial states of wave development.

In engineering terms, the roughness length $z_o$, which serves to characterize the wind profile and turbulence, depends on an "equivalent sand roughness" of the sea surface, $h_r$, which is in turn a function of the stage of wave development. The exact form of this dependence is determined by the Reynolds number at the surface [Kitaigorodskii (1970)]:

$$z_o/h_r = f(u_* h_r/\nu) \tag{31}$$

where $\nu$ is the kinematic viscosity. If the surface is aerodynamically "smooth," such that $u_* h_r/\nu < 5$ or so, then $z_o \simeq 0.12\nu/u_*$. If the surface is "fully rough," with $u_* h_r/\nu > 50$ to 100, say, then $z_o \simeq h_r/30$, just as in flows over fixed roughness elements [Schlichting (1962)]. Within the transition range $5 < u_* h_r/\nu < 50$ to 100, a simple expression for $f(u_* h_r/\nu)$ is not available.

In order to evaluate this surface Reynolds number and to compute $z_o$, it is necessary to determine $h_r$. Kitaigorodskii (1970) considers the flow over individual waves of phase velocity c, taking into account all possible values of c. He finds that

$$h_r \simeq \left[ 2 \int_0^\infty S(\omega) \exp\left( -\frac{2kg}{\omega u_*} \right) d\omega \right]^{1/2} . \tag{32}$$

S (ω) is the frequency spectrum of the waves, such that the rms wave height is given by

$$\sigma = \left[ 2 \int_0^\infty S(\omega) \, d\omega \right]^{1/2} . \tag{33}$$

The wave frequency ω and the phase velocity are related, for deep water gravity waves, by $c = g/\omega$ [Stoker (1957)]. The frequency spectrum will typically have a peak at some frequency $\omega_o$ (phase speed $c_o$). Using the experimentally and theoretically supported assumption that only "steep" waves (i.e., those with $\omega > \omega_o$) can contribute to the drag, Kitaigorodskii (1970) finds:

$$h_r \simeq \begin{cases} \sigma, \text{ if } \omega_o u_*/g \gg 1 \\ \sigma \, e^{-kg/\omega_o u_*}, \text{ if } \omega_o u_*/g \sim O(1) \\ 0.38 \, u_*^2/g, \text{ if } \omega_o u_*/g \ll 1, \end{cases} \tag{34}$$

We can interpret these equations as follows. When $\omega_o \bar{u}/g \equiv u_*/c_o \gg 1$, so that $u_*$ is much greater than the phase speeds of all the waves which contribute to the drag, the waves all behave as immobile roughness elements, and so the equivalent sand roughness of the sea surface is approximately equal to the rms value of the wave heights. This corresponds to the very early stages of wave development. At the other extreme, where $\omega_o u_*/g \equiv u_*/c_o \ll 1$, $h_r$ is independent of the state of wave development and, in fact, is determined only by the aerodynamic quantity $u_*$. Note that for these fully-developed waves, $h_r$ is quite small; if $u_*$ = 50 cm/sec, a fairly large but realistic value, $h_r$ is less than one centimeter. For the intermediate stages of wave development, corresponding to usually observed

situations, $\omega_o u*/g \equiv u*/c_o \simeq 0.01$ to 1.0, and $h_r$ depends on the wave spectrum parameters $\sigma$ and $\omega_o$, as well as on $u*$. Hence $h_r$ can be expected to vary with factors such as fetch and duration of the wind. In these cases of intermediate wave development, $h_r$ can be much smaller than the rms wave height. It seems quite possible, therefore, that even for large waves on a rough sea, the surface may not be fully rough, in the usual aerodynamic sense. This may be the reason why diffusion observations over the sea such as those reported recently by Raynor, et al. (1974) show little spreading and marked departure from the standard, over-land diffusion curves.

The effect of mechanical roughness can be introduced into the marine boundary layer as outlined above, although the details are somewhat complex as compared with the situation over land. Another major difference arises from the intense evaporation of water that takes place from the sea surface most of the time. Density stratification over water is controlled not only by the heat flux, as over land, but also depends on the water-vapor flux. By considering fluctuations of virtual temperature, rather than those of temperature as ordinarily defined (Lumley and Panofsky, 1964, p. 95) the vapor flux can be taken into account. This leads (see for instance Monin (1970)) to a redefinition of the stability parameter L for over-water flows, as follows:

$$Ri_w = Rf\ (1 + m/B_o) \qquad (35)$$

where $m = 0.61\ c_p \theta/\bar{\ell}$, $\bar{\ell}$ being the latent heat of vaporization (for $\theta \sim 300°K$, $m \simeq 0.075$) and

$$L_w = L\ (1 + m/B_o)^{-1} \qquad (36)$$

where $L_w$ is the Monin-Obukhov length over water. Rf is the usual flux form of Richardson number, and $B_o$ is the Bowen ratio;

$$B_o = (c_p/\bar{\ell})(\theta_a - \theta_w)/(e_a - e_w) \qquad (37)$$

where e stands for specific humidity. Over the ocean, $|B_o|$ usually ranges between 1/4 and 1/20 [Thompson (1972), Warner (1973)] so that the term $m/B_o$ is quite significant.*

The above presents at least a general framework for including the complexities present in flows over water into the determination of the characteristics of turbulent diffusion. Pasquill's turbulence types could, in principle at least, be determined over over-water flows by calculating the appropriate roughness, $h_r$, and stability-length, $L_w$, and then referring to Golder's (1972), or F. B. Smith's (1972) nomograms.

### 5.4 Diffusion in the Lee of Flow Obstacles (Wake Diffusion)

By far, most sources of airborne contaminants are located on or near buildings or other structures, such as cooling towers. Isolated tall stacks which, when properly designed, do as a practical matter approximate the point source assumed in diffusion theory are the exception, rather than the rule, among pollutant sources. This being so, it is a matter of concern that so little is known about the properties of diffusion in the wakes which exist in the atmosphere downwind of such structures.

A wake is a region of low-speed flow that extends downwind from a flow obstacle. Within the wake the flow is turbulent, having properties at first strongly conditioned by the size and shape of the obstacle. The lowered wind speed in the wake creates shear at its boundary; and the resulting fine-scale turbulence entrains air from the ambient atmospheric flow into the wake, gradually expanding it, reducing the velocity deficit, and ultimately dissipating the wake. Thus dilution downwind of a source like a roof vent or a building leak is, nearby, strongly influenced by the building and then farther downwind comes to be dominated by atmospheric diffusion in the ordinary sense.

For this reason, an early proposal was to combine the building and atmospheric effects into the following expression for the downwind concentration, $\bar{C}$;

$$\bar{C}/Q = [\ (\pi\ \sigma_y\ \sigma_z + c\ A)\ \bar{u}\ ]^{-1}, \qquad (38)$$

where Q is the source strength, A is the area of the building cross-section normal to the flow, and c represents the fraction of A over which the plume is dispersed by the wake. Gifford (1960) suggested that $1/2 < c < 2$. These limits were proposed on purely intuitive grounds but have been widely quoted. Halitsky's (1968) detailed wind-tunnel studies of the near-wake region, as well as Barry's (1964) summary of both atmospheric and wind-tunnel tests, in general give support for c-values near 1/2, and this values has moreover been assigned on grounds of conservatism. This simple scheme permits wake effects to be combined with turbulence types in a logical way, but in practice has two defects.

*The water vapor flux may well, at times, exert a noticeable influence on diffusion over heavily vegetated land also. Lowry (1972), quoting Knoerr, gives values of the Bowen ratio over a spruce forest that vary from 0.80 to 0.15 with time of day, and from 0.35 to 2.50 with season over a deciduous forest. A calculation with equation (36) shows that $L_w$ can be as much as 30% less than the corresponding L-value for $B_o$ equal to 0.15. In fact a certain amount of this effect has necessarily been incorporated directly into empirical diffusion categories. Rough calculations based on Bowen ratios presented with the Prairie Grass data, see Lettau and Davidson (1957), indicate that this may correspond to a reduction in L of around 5%.

The first problem relates to wake diffusion under low wind speed, stable ambient turbulence conditions, mainly type G but also types E and F to some extent. Under these conditions the plume from a release in a building wake, although it may spread slowly by diffusion, undergoes erratic larger-scale horizontal "meanders" due to flow fluctuations not accounted for in the usual typing schemes. The result is that hourly-averaged concentration values much lower then eq. (11) would indicate are experienced. Halitsky and Woodard (1974) give an example of wake concentration measurements at one site, in an effort to resolve this question. These observations show that under stable, light-wind conditions, wake plumes do meander horizontally. A firm, general plume model for these conditions that correctly combines the wake effect, the ambient turbulence type, and the ensuing plume meander, has yet to be formulated and tested, but the common assumption of very slow dispersion in category G conditions together with the building effect of equation (38), is certainly quite conservative.

The second problem occurs in higher wind-speed, less stable conditions, i.e. types B through D, when wakes are steadier. Wind-tunnel studies by Meroney and Symes (1971), and Meroney and Yang (1971) indicate that building wakes persist far downstream in neutral and stable conditions, much farther than equation (38) would indicate. The wake persists as an entity, and grows slowly by the entrainment process, to downwind distances greater than 30 times the building height, in their tests. Analogous atmospheric experiments, reported by Dickson, et al. (1967), confirm this result, at least out to 23 times the characteristic building dimension.

The decrease in axial, ground-level concentration in wake plumes is therefore small, varying as distance raised to the power -0.6 to -0.7, according to Meroney and Yang, and the effect on this of ambient stability variation is slight. This contrasts with the usual, open-country diffusion categories which imply concentration variation with distance to the power -1.5 or thereabout, with a strong stability dependence. However, before we can make a suitable interpolation formula between these two cases, more research on wake behavior needs to be done. Meroney's wind-tunnel work needs to be extended to various building shapes and arrays and to downwind distances adequate to define the end of the far-wake region, where ambient diffusion begins to dominate the flow. Likewise, parallel atmospheric experiments, greatly extending those begun by Dickson, et al., should be carried out. Until then it should be realized that formulas like eq. (38) or the equivalent curves recently presented by Bowne (1974) may somewhat under-predict concentration values at large downwind distances in well-developed wake plumes. On the other hand at small distances under stable conditions, when the wake is poorly developed, the meandering effect results in lower concentration values than eq. (38) would indicate.

## 5.5 Line Source Models - The Highway Problem

An environmental problem that is receiving an increasing amount of attention is that of pollution near highways. A straight, level highway can be approximated as a continuous infinite line-source whose source strength is derived from the traffic density. By integrating equation (12) with respect to the direction of the highway's orientation, Calder (1973) derived the approximate line-source formula

$$\bar{C}_L(\alpha, X_o)/Q_L = (2/\pi)^{1/2}[(\bar{u}/\cos\alpha)\sigma_z(\xi)]^{-1} \cdot \exp[-h^2/2\sigma_z^2(\xi)] \qquad (39)$$

where $\xi \equiv X_o/\cos\alpha$, subscript L refers to a line source, $X_o$ is the perpendicular distance of a receptor from the highway, and $\alpha$ is the angle made by the wind direction with this perpendicular.

Several recent studies, e.g. Johnson (1974) and Clarke and Zeller (1974) have reported patterns of concentrations within a few hundred meters of highways. Concentrations measured near highways do not conform to values that would be expected from application of a line source formula such as eq. (39). Johnson's comparison of curves of $\sigma_z$ vs. downwind distance (from a highway), inferred from concentration data, showed that: a) there is little if any organization of the data by stability classes; and b) the vertical diffusion is considerably enhanced over the usual point-source values. This should certainly be interpreted as a wake effect, although of a more complicated kind, involving penetration and interaction of successive vehicle wakes. Moving vehicles generate wakes, about which even less is known than the wakes behind buildings. Dabbert et al., (1974) conducted a literature survey and concluded that there is very little definite information on vehicle-wake properties.

The strength, and the distance from the highway to which this complex effect dominates diffusion, and beyond which presumably the line-source Gaussian formula, suitably adjusted for initial wake diffusion, will then apply will be determined by extension of the above and related studies, such as those summarized by Ludwig, et al. (1975).

## 5.6 Area Sources Models

The contribution to environmental pollution resulting from the many, small sources typical of a city comprises the area source. The strength and distribution of urban area sources are established indirectly, from indices such as area fuel consumption and traffic counts. Systematic procedures for making the necessary estimates have been formulated. Based on these the pollutant emissions per unit area, by species, have been established for every city large enough to have significant air pollution. The source strengths are available on a checker-board grid whose squares are as a rule 5 km on a side.

A detailed description of various urban pollution models will be given later by Hanna. It is noted here only that a quite successful area source model follows by integration over the area source of a point-source plume formula, or a line source formula. For instance integration of equation (12) with respect to y gives the line source formula

$$\bar{C}_{Line}/Q = (2/\pi)^{1/2}(\sigma_z \bar{u})^{-1} \exp(-h^2/2\sigma_z^2) \qquad (40)$$

On integrating this equation with respect to distance, x, from the upwind edge of a city to some urban receptor point, for a checkerboard source of grid spacing $\Delta x$, and assuming the grid orthogonal to the wind direction, with h = 0, the simple urban area source formula proposed by Gifford and Hanna (1970) is obtained:

$$\bar{C}_{AO} = (2/\pi)^{1/2}(\Delta x/2)^{1-b}[a(1-b)\bar{u}]^{-1}\{Q_o + \sum_{i=1}^{n} Q_i[(2i+1)^{1-b} - (2i-1)^{1-b}]\} \qquad (41)$$

where $\bar{C}_{AO}$ is the surface-level concentration. In this equation the diffusion length $\sigma_z$ has been assumed to follow a power law, i.e. $\sigma_z = ax^b$; x equals $(n\Delta x + \Delta x/2)$ where n is the number of upwind source squares of strength $Q_i$, and the receptor is at the center of the square having strength $Q_o$. Such a simple assumption works well for urban diffusion because the surface-level concentration at an urban receptor point is primarily determined by the nearby upwind sources. The numerical coefficients in the sum term of (41) drop off very quickly with distance. Also, the form of this equation is considerably simplified as a result of assuming that the source distribution varies only with x. This is not a particularly restrictive assumption because the concentration in real point-source plumes is observed to decrease very rapidly with distance from the plume centerline. Those source points that influence $\bar{C}_{AO}$ appreciably will consequently lie in a fairly narrow, plume-shaped upwind sector whose width is much less than $\Delta x$. The angular width of this sector will depend on atmospheric stability, but that it is always small as a practical matter is shown by the ordinary, elongated appearance of plumes.

Diffusion over cities is enhanced, compared with that over open country, not only because the surface roughness is greatly increased but also because of cities' great heat capacity. Thus both mechanical and thermal turbulence are increased. The net increase in turbulence intensity is evidently about 40%, as compared with open country, according to Bowne, et al. (1968). This study and other material on atmospheric transport and dispersion over cities were summarized by Gifford (1972).

Estimates of turbulence types for urban diffusion have been based on the series of observations, reported by McElroy and Pooler (1968), of diffusion over St. Louis. Based on these data, Pasquill (1970) compared diffusion types in open country and over a city, as in Table 2. Johnson, et al. (1971) analyzed additional urban tracer experiments and presented revised estimates of $\sigma_z$. Considering these data and analyses, Briggs (1973) proposed the urban $\sigma_y$- and $\sigma_z$-curves that are shown in Table 2 and in Figure 6. These are based on Figures 9 and 10 of the paper by McElroy and Pooler; the $\sigma_z$-curves are in essential agreement with those of Johnson, et al. For a

Table 2

Formulas recommended by Briggs (1973) for $\sigma_y(x)$, m and $\sigma_z(x)$, m; $10^2 \leq x \leq 10^4$ m, urban conditions.

| Pasquill Type | $\sigma_y$(m) = | $\sigma_z$(m) = |
|---|---|---|
| A-B | $.32x(1+.0004x)^{-1/2}$ | $.24x(1+.001x)^{1/2}$ |
| C | $.22x(1+.0004x)^{-1/2}$ | $.20x$ |
| D | $.16x(1+.0004x)^{-1/2}$ | $.14x(1+.0003x)^{-1/2}$ |
| E-F | $.11x(1+.0004x)^{-1/2}$ | $.08x(1+.0015x)^{-1/2}$ |

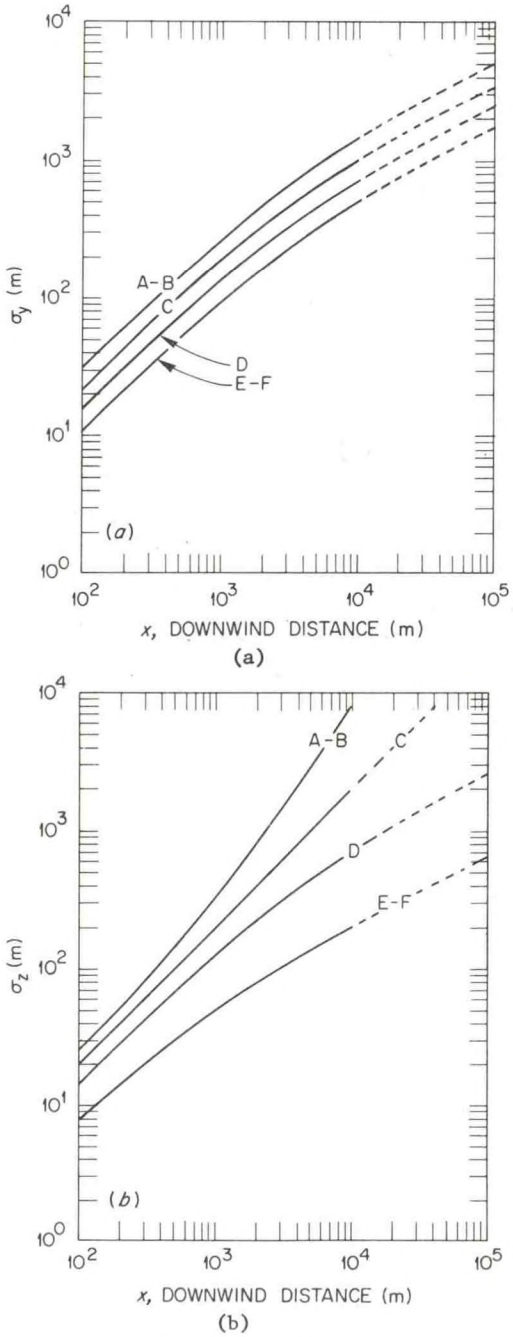


Figure 6. Curves (a) of $\sigma_y$ and (b) of $\sigma_z$ based on Briggs' (1973) interpolation formulas for flow over urban areas, see Table 2; from Hosker (1974).

treatment of the complicated problem of calculating air concentrations within city street canyons, see Johnson, et al. (1971).

### 5.7 Diffusion Over Irregular and Rugged Terrain

Flows in rugged terrain have irregular, often turbulent features that originate otherwise than with boundary-layer turbulence and heat transfer. Among the possibilities that can be mentioned are drainage (katabatic) winds, vortices shed from terrain obstacles, channeling effects, and flow separations of various kinds. None of these was contemplated in the original typing systems, and so departures under such conditions can and do occur.

Methods of calculating diffusion over hills and terrain obstacles, based on the assumption of the mean motion, have been discussed by Stumke (1964) (1966) (1973 a,b), and Berlyand (1972 a,b). As to diffusion categories under such flow conditions, several papers at the recent AMS Symposium on Atmopsheric Diffusion and Air Pollution, Santa Barbara, September 9-13, 1974, touched on this topic. Start, et al. (1974) reported results of a series of diffusion measurements conducted in a deep, steep-walled canyon system in southern Utah. They found that diffusion rates are systematically greater within these deep canyons, implying departures from the usual Pasquill categories. These departures resulted in low concentrations, compared with those calculated from the standard values. The differences ranged from a factor of 1.4 in category B conditions, through 4 in weak lapse to near-neutral conditions, to 15 in category F conditions. The authors state that most of the phenomena mentioned earlier, i.e. greatly enhanced roughness, density flows, wake flows, and channeling effects, were probably operating. Similar results were reported by Hovind, et al. (1974). Start, et al. believe that their canyon results represent a fairly extreme example of the terrain effect on diffusion categories, and speculate that less rugged terrain should lead to departures intermediate between these results and the open-country values. More experimental work clearly is needed.

## 6. MODELING REMOVAL, TRANSFORMATION AND RESUSPENSION

Various complicated process act to transform atmospheric pollutants, remove them from the diffusing cloud, deposit them on the earth's surface, and also to pick them up again once deposited, i.e. to resuspend them. Hales will discuss these processes in some detail and here I only wish to indicate briefly how they can be accounted for in plume models. Further information can be found in the reviews by Van der Hoven (1968), Healy (1968), and Engelmann (1968), and in the proceedings of two recent symposia, U.S.AEC's Precipitation Scavenging (1970), and U.S. ERDA's Atmosphere-Surface Exchange of Particulate and Gaseous Pollutants - 1974 Symposium.

### 6.1 Radioactive Decay

This phenomenon proceeds according to the familiar exponential decay scheme

$$\bar{C}_R = \bar{C} \exp(-\lambda_R t) \qquad (42)$$

where $\bar{C}$ is the quantity of a radioactive species that would have been present in the absence of decay, calculated for instance according to equation (12). The constant $\lambda_R$ is the fraction of the species that decays per unit time. One half of the nuclei of the species will decay in a time $T_R = 0.693/\lambda_R$; $T_R$ is called the half-life. Radioactive species have widely varying half-lives and, moreover, decay to other species that may also be radioactive. The resulting decay "chains," as well as the variety of species originally present, makes for a complex situation the details of which are set out in Healy's review. As a practical matter equation (42) may also be of use in approximating some simple non-radioactive chemical transformations.

### 6.2 Dry Deposition

Air pollution involves particles of a large range of sizes and shapes, from aerosols in the micron range to large particles several hundred micrometers across. Particles or droplets at the larger end of this range fall fairly quickly from a plume and contaminate the ground near the source. Aerosols may be retained in the atmosphere for long periods of time.

Particles or droplets larger than about 100 μm in diameter settle according to Stokes' law at a velocity $v_g$, the gravitational settling speed. A simple modification of the plume formula, the so-called "tilted-plume model," consists in replacing h in equation (12) by the quantity $(h - xv_g/\bar{u})$. The resulting formula should describe the behavior of large particles from a stack plume reasonably well, and has also been of use in studies of the behavior of "drift" droplets, the large droplets that are formed in cooling towers and carried out in their plumes, see Pena and Hosler (1974) for instance. Note that the deposition of particles having a settling velocity $v_g$ occurs at a distance $x = \bar{u}h/v_g$, usually within a few stack heights.

A more general treatment of deposition is afforded by means of a modification to the plume equation, [cf. Van der Hoven (1968)] which assumes that the rate at which material is deposited on the surface, $\omega$(g sec$^{-1}$ m$^{-2}$), is just proportional to the airborne concentration close to the ground, i.e. that

$$\omega = v_d \bar{C}(x, y, 0) \quad . \qquad (43)$$

The proportionality parameter, $v_d$, has the dimensions of velocity, m sec$^{-1}$, and is called the deposition velocity. It is in general not identical to $v_g$, the particle's gravitational settling speed. Detailed information on values of $v_d$, can be found in a recent survey paper by Sehmel (1974).

The chief problem in applying the above concept lies in accounting for the effect of the deposited materials on $\bar{C}(x,y,z)$. Two procedures have been used, termed source-depletion, and

surface-depletion. The first and more traditional of these, originally suggested by Chamberlain (1953) and described by Van der Hoven (1968), consists in calculating the total deposition at each downwind distance, x, and then subtracting this from the source. The second, recently proposed by Horst (1974), represents the surface deposition flux as a material sink, i.e. a negative source for diffusion downwind of the point of deposition. This is the more realistic procedure, in that it permits the form of the cloud concentration function $\bar{C}$ to be modified by deposition. It seems from Horst's calculation that, whereas the source depletion model is quite adequate for a range of small values of $v_d$, corresponding to small particles, the surface depletion model must be invoked for larger $v_d$ values.

If the source is depleted by deposition, $Q = Q(x)$, and [Van der Hoven (1968)]

$$dQ(x)/dx = -(2/\pi)^{1/2} v_d Q(x) (u\sigma_z)^{-1} \cdot \exp(-h^2/2\sigma_z^2) \quad . \tag{44}$$

This equation follows, by definition, from integrating equation (12) with respect to y (i.e. crosswind) after substituting from equation (43), to determine the total deposition at each distance x. Thus

$$Q(x)/Q(0) = \left[ \exp \left( \int_0^x \sigma_z^{-1} \cdot \exp(-h^2/2\sigma_z^2)\, dx \right) \right]^{-(2/\pi)^{1/2} v_d/u} . \tag{45}$$

From this it follows that the flux to the surface can be determined by integration, given a suitable expression for $\sigma_z$.

The corresponding result for the surface-depletion model is

$$\omega(x,y,z_d) = v_d \bar{C}(x,y,z_d) = \tag{46}$$

$$= v_d \left[ Q(0)\, D(x,y,z_d) - \int_{-\infty}^{\infty} \int_0^x v_d \bar{C}(\xi,\eta,g_d) D(x-\zeta, y-\eta, z_d)\, d\xi\, d\eta \right] ;$$

here $D(x,y,z) \equiv \bar{C}(x,y,z)/Q(x)$, and $z_d$ is a reference height near the ground. This differs from the source depletion result not only in the presence of the integral term, but also in that the form of the concentration distribution, $\bar{C}$, in equation 46 is itself modified by surface deposition and hence is not known a priori. Horst has presented the results of a series of calculations which show that the two models do not differ significantly if $v_d/\bar{u} < 10^3$. For somewhat larger values of this ratio, $10^{-3} < v_d/\bar{u} < 10^{-2}$, the difference is tolerable except under rather stable vertical atmospheric temperature stratification. For $v_d/\bar{u}$ greater than $10^{-2}$ it is advisable to use the surface depletion model in all conditions.

### 6.3 Resuspension

Horst (1975) has extended his surface-depletion model to account for resuspension of deposited surface materials, as follows. If $\bar{C}_c$ is the crosswind-integrated air concentration, obtained by integrating eq. (12) with respect to y, and if $\psi \equiv \bar{u}\,\bar{C}/Q$, then

$$\psi(x,z) = \psi_c(x,z,h) + \int_0^x S(\zeta)\, {}_o(x-\zeta,z,h=0)\, d\zeta \tag{47}$$

where $S(\zeta)$ is the net flux of material upwards from the surface, per unit source strength Q. The air concentration due to resuspended material, given by $\psi_r$, is

$$\psi_r = \psi_T - \psi_d \tag{48}$$

where $\psi_T$ is the total air concentration and $\psi_d$ is the air concentration considering only deposition. The flux $S_T$ corresponding to $\psi_T$ is given by

$$S_T(x) = \Lambda G/Q - v_d\, \psi_T\, (x,\, z_d) \tag{49}$$

where $\Lambda$ is the resuspension rate and G is the ground concentration of material; G/Q is calculated from

$$\partial/\partial t\ (G/Q) = v_d \psi_T(z_d)/u - (\Lambda+\alpha) G/Q \tag{50}$$

where $\alpha$ is an empirical weathering factor, representing the rate at which material becomes permanently fixed in the soil. Further details can be found in Horst, et al. (1973), and in the Proceedings of the Atmospheric-Surface Exchange Symposium.

### 6.4 Washout

A falling droplet sweeps out an air volume. Paths of some pollutant particles in this volume will cross the air streamlines and intersect the droplet. The fraction of the particles in the droplet's path that will do this is called the target efficiency, E. The fraction of these contacting particles that actually "stick" is called the retention efficiency, R. The collection efficiency, C, equals ER. E can be calculated but not much is known about R. It is often assumed that R = 1, i.e. that E = C. The washout coefficient, $\Lambda_w$, is given by

$$\Lambda_w = \int F\, E\, A\, d(D) \tag{51}$$

where D refers to the diameter of the scavenging droplets; A is the cross-sectional area of drops of diameter D, and F is the flux density of drops, i.e. drops per unit area, time, and interval of

diameter, d(D). Then it is assumed that

$$\bar{C}_w = \bar{C} \exp(-\Lambda_w t) \qquad (52)$$

similar to the case of radioactive decay. The meaning of this assumption is that the washout process occurs uniformly over the plume volume, and so the shape of the plume is not changed. Washout is however not irreversible. Gases washed out of a tall-stack plume can be desorbed into the air below the plume, see Slinn (1974). This and many other aspects of these complicated processes will be discussed by Hales.

## 7. SOME COMMENTS ON THE POSSIBILITIES OF FUTURE RESEARCH

These are exciting times for theoreticians of turbulent diffusion. Based on 3-dimensional numerical models of turbulent boundary-layer flows, such as Deardorff's, or higher order closure models of turbulence such as Donaldson's, both of which were discussed at the previous Workshop, it seems we are on the threshold of basic new insights into the turbulence problem. The situation with respect to applications of diffusion modeling, on the other hand, could most charitably be described as frustrating. Practical diffusion problems have proliferated far faster than our ability to model them. We don't even know, just to take an example, how long a turbulent wake is; and so our models of a whole class of important applied diffusion problems are necessarily uncertain. Similar difficulties exist for models of diffusion over water, irregular or rugged terrain, in very stable conditions, and in various other situations of great practical importance, some of which have been described above.

In spite of recent advances, little immediate reflief from turbulence theory should be expected. The problem is that practical diffusion modeling involves an assortment of exceptional flows and conditions that are not yet fully accessible to theoretical treatment. Rather it seems that some mix of physical (i.e. wind tunnel and water tank) and mathematical modeling studies of the many special, exceptional cases, backed up by adequate experimental diffusion trials in the real atmosphere, are going to be necessary before many outstanding modeling problems can be fully resolved. Sponsors of research in this area should plan on support of such projects. Particularly, regulatory agencies must realize that our environmental modeling needs exceed our capability in many of these special problem areas. These must be resolved by adequate research programs before reliable modeling estimates can be given.

Acknowledgement

This research was performed under an agreement between the National Oceanic and Atmospheric Administration and the U. S. Energy Research and Development Administration.

## REFERENCES

Barad, M. L., and D. A. Haugen, 1959: A preliminary evaluation of Sutton's hypothesis for diffusion from a continuous point source. J. Meteor., 16, 12-20.

Barry, P. J., 1964: Estimation of downwind concentration of airborne effluents discharged in the neighborhood of buildings. Canada, Rep. No. AECL-2043.

Barry, P. J., 1971: Use of Argon-41 to study the dispersion of effluent from stacks. Nuclear Techniques in Environmental Pollution, Int. Atomic Energy Agency, Vienna, pp 241-245.

Barry, P. J., 1975: Stochastic properties of atmospheric diffusivity. Rep. AECL-5012, Chalk River Nuclear Labs., Ontario.

Beattie, J. R., 1963: An assessment of environmental hazard from fission product releases. UK Atomic Energy Authority, Rep. No. AHSB(S) R64.

Berlyand, M. E., 1972a: Atmospheric diffusion investigation in the USSR. In World Meteor. Organiz. Tech. Note. No. 121, Dispersion and forecasting of air pollution.

Berlyand, M. E., 1972b: Investigations of atmospheric diffusion providing a meteorological basis for air pollution control. Atmospheric Environment, 6, 379-388.

Bowne, N. E., 1974: Diffusion rates. J. of the Air Poll. Control Assoc., 24, 832-835.

Briggs, G. A., 1969: Plume Rise, USAEC, Div. of Tech. Info., TID-25075, vi and 81 pp.

Briggs, G. A., 1973: Diffusion estimation for small emissions, in Environmental Res. Lab., Air Resources Atmos. Turb. & Diffusion Lab., 1973 Annual Rep., ATDL-106, USDOC-NOAA.

Bryant, P. M., 1964: Methods of estimation of the dispersion of windborne material and data to assist in their application. U.K. Atomic Energy Authority Report No. HSSB(RP) R42.

Calder, K. L., 1973: On estimating air pollution concentrations from a highway in an oblique wind. Atmos. Environ., 7, 863-868.

Carpenter, S. B., T. L. Montgomery, J. M. Leavitt, W. C. Colbaugh, and F. W. Thomas, 1971: Principal plume dispersion models: TVA power plants, J. Air Poll. Control Assoc., 21, 491-495. (See also, TVA and PHS, Full-scale Study of Dispersion of Stack Gases (5 vols.), Chattanooga, TN, 1964).

Clarke, J. F., and K. F. Zeller, 1974: Tracer study of dispersion from a highway. Symp. on Atmos. Diff. and Air Poll., American Meteor. Soc., Sept. 9-13, 1974, Santa Barbara, Cal.

Csanady, G. T., 1973: Turbulent diffusion in the environment, x and 248 pp, D. Reidel Pub. Co., Dordrecht, Holland.

Chamberlain, A. C., 1960: Aspects of the deposition of radioactive and other gases and particles. Int. J. Air Poll., 3, 63-88.

Cramer, H. E., 1957: A practical method for estimating the dispersal of atmospheric contaminants. Proc. First National Conf. on Applied Meteor., pp C-33 to C-55, Am. Meteor. Soc., Hartford, Conn., Oct. 1957.

Dabberdt, W.F., D. C. Cagliostro, and W. S. Meisel, 1974: Analyses, experimental studies, and evaluations of control measures for air flows and air quality on and near highways. Quart. Prog. Rep. 2, Stanford Res. Inst., Menlo Park, Cal., 25 Jan. 1974.

Deardorff, J. W., and G. E. Willis, 1975: A parameterization of diffusion into the mixed layer. To be published in J. of Appl. Meteor.

Dickson, C. R., G. E. Start, and E. H. Markee, 1967: Aerodynamics effects of the EBR-II containment vessel complex on effluent concentration. Proc. USAEC Meteorological Information Meeting (C. A. Mawson, ed.), Chalk River, Canada, Sept. 11-14, 1967, pp 87-101.

Engelmann, R. J., 1968: Precipitation scavenging. Meteorology and Atomic Energy 1968, D. Slade, ed., 208-221, USAEC, TID-24190.

Friedlander, S. K., and J. H. Seinfeld, 1969: A dynamic model of photochemical smog. Environmental Res. and Tech., 3, 1175-1180.

Frenkiel, F. N., 1952: On the statistical theory of turbulent diffusion, Int. symp. on atmospheric turbulence in the boundary layer, Geophys. Res. Paper No. 19, USAF, Geoph. Res. Directorate, Cambridge, Mass.

Frenkiel, F. N., 1953: Turbulent diffusion, in Adv. in Appl. Mech., 3, Academic Press, N.Y.

Frenkiel, F. N., 1956: Atmospheric pollution in growing communities. Annual Report of the Smithsonian Inst. for 1956, Washington, 1957.

Gartrell, F. E., 1966: Control of air pollution from large thermal power stations. Rev. Mensuelle 1966 de la Soc. Belge des Ingénieurs et des Industriels de Bruxelles, pp 1-12.

Gifford, F. A., 1959: Statistical properties of a fluctuating plume model. Adv. in Geophysics, 6, 117-137, Academic Press, N.Y.

Gifford, F. A., 1960: Atmospheric dispersion calculations using the generalized Gaussian plume model. Nuclear Safety, 2, 56-59.

Gifford, F. A., 1968: An outline of theories of diffusion in the lower layers of the atmosphere. In Meteorology and Atomic Energy 1968, D. Slade, ed., USAEC, TID-24190, 65-116.

Gifford, F. A., and S. R. Hanna, 1970: Urban air pollution modeling. Proc. Second Int. Clean Air Congress, Washington, Dec. 6-11, 1970. H. M. Englund and W. T. Beery, eds., 1146-1151, Academic Press, N.Y. (1971).

Gifford, F. A., 1972: Atmospheric transport and dispersion over cities. Nuclear Safety, 13, 391-402. (See also World Meteor. Organization Tech. Note, No. 121, Chapter 4.)

Gifford, F. A., 1975: Turbulent diffusion typing schemes: a review. To be published in Nuclear Safety.

Golder, D., 1972: Relations among stability parameters in the surface layer. Boundary Layer Meteor., 3, 47-58.

Halitsky, J., 1968: Gas diffusion near buildings. In Meteor. and Atomic Energy 1968 (D. Slade, ed.), pp 221-225.

Halitsky, J., and K. Woodard, 1974: Atmospheric diffusion experiments at a nuclear plant site under light wind inversion conditions. Symp. on atmos. diff. and air poll., pp 172-179, American Meteor. Soc., Sept. 9-13, 1974, Santa Barbara, Cal.

Haugen, D. A., 1973: Workshop on micrometeorology, American Meteorol. Soc., xi and 392 pp.

Hay, J. S., and F. Pasquill, 1957: Diffusion from a fixed source at a height of a few hundred feet in the atmosphere. J. Fluid Mech., 2, 299.

Healy, J. W., 1968: Radioactive cloud-dose calculations. Meteorology and Atomic Energy 1968, D. Slade, ed., 301-377, USAEC, TID-24190.

Hewson, E. W., and G. C. Gill, 1944: Meteorological investigations in Columbia River Valley near Trail, B.C., U.S. Bur. of Mines Bull. 453, Washington.

Hino, M., 1968: Maximum ground-level concentration and sampling time. Atmos. Env., 2, 149-166.

Hinze, J. O., 1959: Turbulence, ix and 586 pp, McGraw-Hill, N. Y.

Holland, J. Z., 1953: A meteorological survey of the Oak Ridge area. USAEC report ORO-99.

Holzworth, G. C., 1972: Mixing heights, wind speeds, and potential for urban air pollution throughout the contiguous United States. Envir. Protection Agency, Office of Air Programs, Pub. No. AP 101, xi and 118 pp.

Horst, T. W., 1974: A surface depletion model for deposition from a Gaussian plume. In Proc. of Atmosphere-Surface exchange of particulates and gaseous pollutants - 1974 Symposium, U.S. ERDA Symposium Series (in press).

Horst, T. W., J. G. Droppo, and C. E. Elderkin, 1973: An assessment of the long-term exposure due to resuspension. Battelle Northwest Laboratories BNWL-1850 Pt. 3, 1974.

Horst, T. W., 1975: The resuspension rate for a Gaussian plume. Battelle Northwest Laboratories BNWL-1950 Pt. 3, 204-242.

Hosker, R. P., 1974: Estimates of dry deposition and plume depletion over forests and grassland. Proc. Symp. on Physical Behavior of Radioactive Contaminants in the Atmosphere. (Paper No. IAEA-SM-181/19), 291-308, IAEA, Vienna.

Hovind, E., T. C. Spangler, and A. J. Anderson, 1974: The influence of rough mountainous terrain upon plume dispersion from an elevated source. Symp. on Atmos. Diff. and Air Poll., pp. 214-217. American Meteor. Soc., Sept. 9-13, Santa Barbara, Cal.

Islitzer, N., and D. Slade, 1968: Diffusion and transport experiments. In Meteorology and Atomic Energy 1968, D. Slade, ed., pp 117-188, USAEC TID-24190.

Johnson, W. B., W. F. Dabberdt, F. L. Ludwig, and R. J. Allen, 1971: Field study for initial evaluation of an urban diffusion model for carbon monoxide. Stanford Res. Inst. Report, SRI Project 8563, June 1971.

Johnson, W. B., 1974: Field study of near-roadway diffusion using a fluorescent dye tracer. Symp. on Atmos. Diff. and Air Poll.,pp 261-266. American Meteor. Soc., Sept. 9-13, 1974, Santa Barbara, Cal.

Kitaigorodskii, S. A., 1970: The physics of air-sea interaction. Trans. from Russian and publ. by Israel Program for Scientific Translations, TT72-50062, Jerusalem, v and 237 pp, (1973).

Lettau, H., 1952: On eddy diffusion in shear zones. Geoph. Res. Papers No. 1, Report NP-1761, Air Force Cambridge Res. Labs.

Lettau, H., and B. Davidson (eds.), 1957: Exploring the atmosphere's first mile. Pergamon Press, N.Y.

Lumley, J. L., and H. A. Panofsky, 1964: The structure of atmospheric turbulence. xi and 239 pp, Interscience Pub., N.Y.

Lowry, W. P., 1972: Weather and life, xii and 305 pp, Academic Press, N.Y.

Ludwig, F. L., J. H. Smith, W. B. Johnson, and R. E. Inman, 1975: Air quality impact study for proposed highway widening near Ojai. Stanford Research Inst. report, SRI Project 2852, 11 pp.

Machta, L., 1958: Global scale dispersion by the atmosphere. Proc. Second U.N. International Conf. on the Peaceful Uses of Atomic Energy, 1958, 18, 519-523, U.N., N.Y.

Machta, L., 1973: Global scale atmospheric mixing, in Turbulent diffusion and environmental pollution, Adv. in Geoph., Vol. 18B, F. N. Frenkiel and R. E. Munn, eds., Academic Press, N.Y.

McElroy, J. L., and F. Pooler, 1968: St. Louis dispersion study, vol. II, analysis. USDHEW, Report AP-53.

Meade, P. J., and F. Pasquill, 1958: A study of the average distribution of pollution around Staythorpe. Int. J. of Air Poll., 1, 60.

Meroney, R. N., and C. R. Symes, 1971: Entrainment of stack gases by buildings of rounded geometry. Conference on Air Poll. Meteorology, pp 132-135, American Meteor. Soc., April 5-9, 1971, Raleigh, N.C.

Meroney, R. N., and B. T. Yang, 1971: Gaseous plume diffusion about isolated structures of simple geometry. Proc. 2nd Int. Clean Air Congress (H. M. Englund and W. T. Beery, eds.) pp. 1022-1029, Academic Press, N.Y.

Monin, A. S., 1955: Diffusion with finite velocity, Izvestiya AN SSSR, Ser. geofiz., No. 3, 234-248.

Monin, A. S., and A. M. Yaglom, 1971: Statistical fluid mechanics, xii and 769 pp, MIT Press, Cambridge, Mass.

Monin, A. S., 1970: The atmospheric boundary layer. Annual Review of Fluid Mechanics, 2, 225-250.

Nickola, P. W., G. H. Clark, and J. D. Ludwick, 1974: Frequency distribution of atmospheric tracer concentration during periods of low winds. Pacific Northwest Laboratory Annual Report for 1974 to the USAEC Div. of Biomedical and Environmental Research, Part 3, Atmos. Sciences, BNWL-1950, Pt. 3, (pp 51-55).

Obrien, E. E., 1964: Discussion presented at Conf. on AEC Meteorological Activities, May 19-22, 1964. I. A. Singer, M. E. Smith, and E. W. Bierly, eds. (see pp 104-106), Brookhaven Nat. Lab., Pub. BNL 914 (C-42).

Pasquill, F., 1961: The estimation of windborne material. Meteorological Magazine, 90, 33-49.

Pasquill, F., 1970: Prediction of diffusion over an urban area-current practice and future prospects; in Proc. of Symposium on Multiple-source Urban Diffusion Models. USEPA, Research Triangle Park, N.C.

Pasquill, F., 1974: Atmospheric diffusion (2nd Ed.), xi and 429 pp, John Wiley and Sons.

Pasquill, F., and F. B. Smith, 1974: Eddy coefficients for vertical diffusion in the neutral surface layer. Boundary Layer Meteor., 7, 227-288.

Pena, J. A., and C. L. Hosler, 1974: Influence of the choice of the plume diffusion formula on the salt-deposition-rate calculation. Cooling Tower Environment-1974, U.S. ERDA Conf. Proceedings, CONF-740302, Tech. Info. Center, 1975.

Pooler, F., 1965: Potential dispersion of plumes from large power plants. U.S. PHS Pub. No. 999-AP-16.

Raynor, G. S., P. Michael, R. M. Brown, and S. SethuRaman, 1974: A research program on atmospheric diffusion from an oceanic site. American Meteor. Soc. Symposium on Atmospheric Diffusion and Air Pollution, Santa Barbara, Cal., Sept, 9-13, 1974, pp 289-295.

Roberts, J. J., E. J. Croke, and A. S. Kennedy, 1970: An urban atmospheric dispersion model. In Proc. Symp. on Multiple-source urban diffusion models. U.S. EPA, Res. Triangle Park, N.C.

Roberts, O. F. T., 1923: The theoretical scattering of smoke in a turbulent atmosphere. Proc. Roy. Soc., London, A., 104, 640-654.

Sagendorf, J., 1974: Diffusion under low wind speed and inversion conditions, USDOC-NOAA, Environmental Res. Labs Report ERL-ARL Tech. Memo.

Schlichting, H., 1962: Boundary layer theory (4th ed.), McGraw-Hill, N.Y., xx and 647 pp.

Sehmel, G. A., 1974: Particle dry deposition velocities. In Proc. of Atmosphere-surface exchange of particulates and gaseous pollutants - 1974 Symposium, ERDA Symposium Series (in press).

Singer, I. A., and M. E. Smith, 1953: Relation of gustiness to other meteorological parameters. J. of Meteor., 10, 121-126.

Slade, D. H., 1962: Atmospheric diffusion over Chesapeake Bay. Monthly Weather Rev., 90, 217-224.

Slade, D. H. (ed.), 1968: Meteorology and Atomic Energy 1968, x and 445 pp., USAEC TID-24190.

Slinn, W. G. L., 1974: The redistribution of a gas plume caused by reversible washout. Atmos. Env., 8, 233-240.

Smith, F. B., 1972: A scheme for estimating the vertical dispersion of a plume from a source near ground level. Proc. of the Third Meeting of the Expert Panel on Air Pollution Modeling, NATO-CCHS Report No. 14, Brussels.

Smith, M. E. (ed.), 1968: Recommended Guide for the prediction of the dispersion of airborne effluents. Am. Soc. of Mech. Engineers, ix and 85 pp.

Start, G. E., C. R. Dickson, and N. R. Hicks, 1974: Effluent dilutions over mountainous terrain and within mountain canyons. Symp. on Atmos. Diff. and Air Poll., pp 226-232, American Meteor. Soc., Sept. 9-13, 1974, Santa Barbara, Cal.

Start, G. E., and L. L. Wendell, 1974: Regional effluent calculations considering spatial and temporal meteorological variations. Symp. on Atmos. Diff., and Air Poll., Am. Meteor. Soc., Boston, 202-208.

Stewart, N. G., H. G. Gale, and R. N. Crooks, 1954: The atmospheric diffusion of gases discharged from the chimney of the Harwell pile (BEPO). Int. J. of Air Poll., 1, 87-102.

Stoker, J. J., 1957: Water waves, Interscience Pub., N.Y., xxiv and 567 pp.

Stumke, H., 1964: Correction of the chimney height due to an influence of terrain. Staub, 24, 525-528.

Stumke, H., 1966: Investigations on the turbulent dispersion of stack gases over uneven terrain. Staub, 26, 97-104.

Stumke, H., 1973a,b: Dispersion of stack gases over a plain with a long valley of basin-shaped valley perpendicular to the wind field - Parts I and II. Staub, 33, 312-316 and 336-340 (Translated edition).

Sutton, O. G., 1932: A theory of eddy diffusion in the atmosphere. Proc. Roy. Soc. London, A., 135, 143.

Taylor, G. I., 1921: Diffusion by continuous movements. Proc. London Math. Soc., 20, 196-212.

Thompson, N., 1972: Turbulence measurements over the sea by a tethered-balloon technique. Quarterly J. of the Roy. Meteor. Soc., 98, 745-762.

Turner, D.B., 1969: Workbook of Atmospheric Dispersion Estimates. vii and 84 pp, USDHEW, PHS Pub. No. 995-AP-26.

U. S. Atomic Energy Comm., 1970: Precipitation Scavenging (1970), Proc. of a symp. at Richland, Wash., June 2-4, 1970, xii and 499 pp, USAEC, CONF-700601

U. S. ERDA, 1970: Proc. of Atmosphere-Surface Exchange of particulate and gaseous pollutants - 1974 Symposium, ERDA Symposium Series (in press).

U. S. Nuclear Regulatory Commission, 1974: Regulatory Guide 1.21, Measuring, evaluating, and reporting radioactivity in solid wastes and releases of radioactive materials in liquid and gaseous effluents from light-water-cooled nuclear power plants, 21 pp.

Van der Hoven, I, 1968: Deposition of particles and gases. Meteorology and Atomic Energy 1968, D. Slade, ed., 202-208, USAEC, TID-24190.

Van der Hoven, I., 1967: Atmospheric transport and diffusion at coastal sites. Nuclear Safety, 8, 490-499.

Van der Hoven, I., 1975: "A Survey of Field Measurements of Atmospheric Diffusion Under Low Wind Speed, Inversions Conditions." To be published.

Warner, J., 1973: Spectra of the temperature and humidity fluctuations in the marine boundary layer. Quarterly J. of the Roy. Meteor. Soc., 99, 82-88.

Yaglom, A. M., 1972: Turbulent diffusion in the surface layer of the atmosphere. Izvestiya, Atmos. and Oceanic Physics, 8, 579-593.

# LECTURES ON AIR POLLUTION AND ENVIRONMENTAL IMPACT ANALYSES

Sponsored by the

AMERICAN METEOROLOGICAL SOCIETY

29 September - 3 October 1975
Boston, Massachusetts

Duane A. Haugen
Workshop Coordinator

The tutorial lectures reproduced in this collection are unedited manuscripts of the material presented at the AMS Workshop on Meteorology and Environmental Assessment; their appearance here does not constitute formal pbulication.

ATDL Contribution File No. 75/8

AMERICAN METEOROLOGICAL SOCIETY
45 Beacon Street, Boston, Massachusetts, 02108 U.S.A.

# CHAPTER 6

## URBAN DIFFUSION PROBLEMS

Steven R. Hanna

Air Resources
Atmospheric Turbulence & Diffusion Laboratory, NOAA
Oak Ridge, Tennessee

### 1. INTRODUCTION

Most of the basic concepts that are needed to make calculations of urban diffusion are summarized in other papers at this workshop. Therefore this paper is not planned to be a long review of basic techniques. Instead, emphasis will be on the factors that cause diffusion in urban areas to present special problems or to differ from diffusion in other environments.

Because of the obvious problems of urban air pollution and the stringent regulations laid down by governments, there has been a great increase in the number of observation programs and theoretical and applied studies of urban diffusion. But since most of this work has been directed towards solving local problems, there have been relatively few advances in the science of estimating urban air pollution. Studies tend to concentrate on monitoring programs or on straightforward application of existing techniques. Many of these studies are quite complex, due to the large number of computer calculations which must be made in the process of insuring numerical stability or accounting for the multiple sources and receptors.

It is hoped that urban diffusion models can eventually confidently be used to make major decisions, such as in planning the layout of a new industrial park, determining the effects of a new highway on air quality, or estimating the results of a new automobile emissions exhaust system. The first major input to the urban diffusion model is emissions. Because of the nearly linear dependence of pollutant concentrations on emissions strength, it is important to know precisely the time and space variations of emissions. Likewise, mixing depth, atmospheric stability, and wind speed and direction also have a strong influence on concentrations and should be carefully measured. Since diffusion is due to atmospheric turbulence, measures of this quantity are desirable throughout the region. Observations of pollutant concentrations throughout space at initial time and on the boundaries of the region at all times should be made.

The urban diffusion model itself should be able to account for point, line, and area sources, and the local aerodynamic effects of street canyons and building wakes. Removal or transformations due to dry or wet deposition and chemical reactions are often important. It would be best if the model included meteorological parameters such as wind speed and temperature as dependent variables, since these parameters vary significantly when air passes from rural surfaces over urban surfaces. Because of the extra computing time necessary to predict these parameters, they are usually assumed to be already known, based on a few sets of observations in urban areas. Furthermore, in any model it is necessary to know the dispersion parameters beforehand, whether they are the $\sigma$'s of the Gaussian plume equation or the K's of the so-called diffusion equation. These too must be based on previous observation programs.

The final set of problems involves the form of the output of the urban diffusion models and the statistical analysis of the results. The methods of comparisons of estimated with observed concentrations depend to some extent on our confidence in the observations. In this sense the placement of the monitoring stations, their accuracy, and their averaging times are important. Ultimately models should be able to guide in decisions regarding the placement of the monitoring stations. It is hoped that the detailed monitoring systems of the Regional Air Pollution Study (RAPS) in St. Louis will help answer some of these questions.

### 2. INPUT PROBLEMS

The quality of the output of an urban diffusion model can be no better than the input. By definition, "input" is all the information that must be provided to a model before it can operate. It includes parameters such as emissions, chemical rate constants and eddy diffusivities, initial and boundary values of pollutant concentrations, and space and time variations of meteorological variables. Uncertainties in any of these parameters can cause unacceptable errors in estimates of pollutant concentrations.

#### 2.1 Emissions

The process of estimating emissions is straightforward but very tedious, because of the large number of pollution sources in an urban area. Detailed descriptions of emissions in Los Angeles (Roth et al., 1974), Reading (Marsh and Foster, 1969), and Chicago (Roberts et al., 1970) are available for those who wish examples of the results of emissions surveys. By law, emissions surveys were made in each air pollution

"airshed" in the United States (U.S.D.H.E.W. Consultation Reports, 1968). In these reports, emissions are divided among point sources (units of mass per unit time) and area sources (units of mass per unit time per unit area). Generally a limit is set, such as .1 ton/day, so that there are, at most, a few dozen point sources with emissions above this limit. All other point sources, including small industries, schools, commercial establishments, and homes, are lumped together as area sources. It is then assumed that area source emissions are constant over square or rectangular blocks of area from 1 $km^2$ to 500 $km^2$. In a study in Reading, England, Marsh and Withers (1969) find that the best size for an area source grid square is about 10 $km^2$. This figure is obtained by correlating observed concentrations at a monitoring station with area source emissions averaged over various sizes of grid blocks around that station.

In the original 1968 round of consultation reports there was very little information on the time variability of emissions. Since the air over a city can be exchanged or "flushed" every few hours, it is important to know the hour by hour variation of emissions. The most detailed studies in this respect have been in Los Angeles (Roth et al., 1974), where, for example, the hour by hour emissions due to motor vehicles are given. These estimates result from long, painstaking observations of traffic patterns throughout the city and of exhaust characteristics of a wide variety of engines. Even so, these researchers state that more detailed data are needed. The diurnal emissions cycle in Table 1, based on the work of Roth et al. (1974) is clearly not applicable to every street on every day.

A new round of Consultation Reports is now coming out in which local pollution control officials and industries are updating the emissions data in the 1968 reports. The original data were often based on very crude or non-existent emissions data. In any sensitivity study that one would care to apply, it is clear that pollutant concentrations are nearly always more strongly correlated with emissions than with any other variable. It is not consistent to use detailed meteorological data or boundary conditions if emissions are not well known. In comparing the results of the models of Roth et al. (1971) and Reynolds et al. (1974), as applied to Los Angeles, one finds that the 1974 model is more satisfactory, even though it is somewhat simpler (e.g., fewer vertical levels). However, the emissions data used in the 1974 model are much better than those used in the earlier model.

## 2.2 Boundary and Initial Pollutant Concentrations

In any diffusion model based on time and space derivatives of pollutant concentration, it is necessary to prescribe the boundary conditions. In all models, either a background or initial concentration must be taken into account. Ideally, these values should be known at the grid points used in the model and at the monitoring stations being studied. This ideal situation has never been realized, however, and modelers always have to interpolate or arbitrarily prescribe the boundary values.

Table 1

The Diurnal Distribution of Traffic in Los Angeles (Roth et al., 1974)

| Hourly Period (local time) | Fraction of Daily Traffic per one hour period | |
|---|---|---|
| | Freeways | Surface Streets |
| 0-5 | .0077 | .0068 |
| 5-6 | .0178 | .0068 |
| 6-7 | .0591 | .0293 |
| 7-8 | .0768 | .0651 |
| 8-9 | .0648 | .0651 |
| 9-10 | .0536 | .0502 |
| 10-11 | .0494 | .0502 |
| 11-14 | .0494 | .0608 |
| 14-15 | .0569 | .0608 |
| 15-16 | .0779 | .0608 |
| 16-18 | .0779 | .0820 |
| 18-19 | .0598 | .0540 |
| 19-20 | .0302 | .0540 |
| 20-24 | .0302 | .0308 |

The upper boundary conditions are most difficult to measure because of their relative inaccessibility. Remote sensing techniques, such as the lidar (Johnson et al., 1973) may provide good upper boundary measurements once the remote sensing instruments can be satisfactorily calibrated. In cases where there is a significant amount of pollutant advected into the upper regions of the urban mixing layer, such as reported by Stasiuk and Coffee (1975) or Edinger (1973), it is possible that the concentration at the ground is strongly dependent on material mixed to the ground from aloft.

## 2.3 Meteorological Conditions

In order to operate, any urban diffusion model requires knowledge of at least one meteorological variable. The most important of these is wind speed, due to its obvious diluting effect. It is possible to add the equations of motion, mass continuity, and the first law of thermodynamics to the system of diffusion equations and "predict" meteorological conditions along with pollutant concentrations, given suitable boundary conditions. The only time that this was done in an application specifically to urban diffusion was in the model of diffusion in Los Angeles by Pandolfo and Jacobs (1973). Unfortunately, some of their meteorological predictions were not very realistic and pollutant predictions were not improved over other models. A possible reason for this lack of improvement is the inability of the model to account satisfactorily for the rugged topography at the edges of the Los Angeles basin.

The equation of mass continuity is used in the diffusion models developed at Lawrence Livermore Laboratory (Knox, 1974, and Dickerson, 1973). Measured wind fields are "adjusted" in the model so that the requirement of mass continuity is satisfied. This adjustment eliminates the chances for unrealistic local accumulations of pollutants which invariably occur in models using a network of wind observations.

The required input for most models is observations of wind speed at all grid points at hourly intervals, at least. But since these observations must be representative of the grid square in which they are located, it is important that monitoring sites be chosen which are free of local flow obstructions. Gifford (1974) has used observations from Los Angeles to show that predictions of pollutant concentrations are more accurate when space averaged wind speeds are used than when single station winds are used. Presumably there are errors in single station measurements which are cancelled when the measurements from several nearby stations are averaged.

In several urban diffusion models (e.g., Eschenroeder, 1972) it is necessary to know the trajectory of air parcels. Often serious air pollution episodes in rural areas are caused by the transport of polluted air originating in upwind urban areas (Hanna, 1975). In order to estimate the trajectory, wind velocities can be interpolated from a network of stationary monitoring sites. More accurately, a climatology of trajectories can be built up by observing the paths of constant density balloons. For example, Angell et al. (1972, 1974) describe the use of this technique to estimate typical trajectories in the Los Angeles basin. They were able to trace the motion of air through mountain passes using their radar transponder system.

It is known that urban areas alter the air flowing over them (Peterson, 1969). Surface temperature, stability, and mixing heights are the variables which experience the greatest change. Of these, stability and mixing height have a strong influence on pollutant concentration. Clarke (1969) and McElroy (1971) report measurements of temperatures at night over urban areas showing that stable air from rural areas is modified as it flows over an urban area. An adiabatic or mixed layer forms near the surface, and the height of the mixed layer increases with downwind distance. The rate at which the mixing height, Z, increases with distance, x, from the city edge depends on the wind speed, U, the stability of the rural air and the rate of heat input, H, from the surface of the city. From thermodynamic considerations, Summers (1965) derived an equation illustrating this dependence:

$$Z = (2Hx/c_p \rho\, U(\partial\theta/\partial z))^{1/2} \qquad (1)$$

where $\partial\theta/\partial z$ is the vertical gradient of potential temperature, $\rho$ is air density, and $c_p$ is the specific heat of air at constant pressure. This equation has been applied with success by Leahey and Friend (1971) to New York City and by Leahey (1975) to Edmonton. It is observed by McElroy (1971) that the stability near the city surface is nearly neutral or adiabatic, no matter how stable the rural air is.

During the daytime the sun warms the urban surface and the mixing height rises to an equilibrium value. This equilibrium mixing height is nearly the same in the urban area and the rural area, and can be estimated from charts published by Holzworth (1972). For regions where afternoon mixing heights vary markedly across the region, such as the Los Angeles basin, reports are sometimes available (e.g., Edinger, 1958) in which measurements of this variation are given. Or, more accurately, the afternoon mixing height can be predicted if the morning temperature profile and predicted afternoon surface temperatures are known, and it is assumed that the mixed layer is adiabatic (Holzworth, 1972). Currently there are also several theoretical methods under development (e.g., Carson, 1973) for estimating the rise of the morning mixing layer, but these methods generally require more information than is usually available.

Urban areas also alter the turbulence characteristics of the air, because of their increased roughness and their effects on stability. The intensity of turbulence is measured in Ft. Wayne to be about 40% greater in the urban area than in the surrounding rural areas (Graham, 1968). The rate of diffusion, which is dependent on the turbulent intensity, is measured by McElroy, (1969) in St. Louis to be about twice that expected from the standard "Pasquill-Gifford curves" at short distances ($x < 200$m) from the source, and then asymptotically approach the standard curves at greater distances. McElroy (1969) suggests that the initial difference is mostly due to the effects of turbulence in building wakes and in street canyons. Gifford (1972) suggests that the increased turbulence in an urban area be approximated by first estimating the standard Pasquill (1962) letter stability class by the usual techniques, then shifting the class to the next higher letter. The Pasquill letter stability classes are being modified by Smith (1973) to include effects of variations in surface roughness. He uses K theory to estimate diffusion in the planetary boundary layer under a variety of conditions, and then derives the distribution functions $\sigma_y$ and $\sigma_z$ from the results. The eddy diffusivity is estimated from the relation

$$K = .1\, \sigma_w\, \lambda_m \qquad . \qquad (2)$$

Where $\sigma_w$ is the is the standard deviation of vertical speed fluctuations, and $\lambda_m$ is the wavelength at which maximum energy occurs in the vertical velocity spectrum. These similarity laws for the eddy diffusivity were derived independently by Pasquill (1968) and Hanna (1969). As yet, no observation program has taken place over urban areas which verifies the validity of this or any other form for K. In such a program, observations should be made of the turbulent fluctuations of the wind velocity and the turbulent flux of a pollutant.

## 2.4 Removal Mechanisms

An urban diffusion model also requires as input some estimation of removal by dry or wet deposition, and transformation by chemical reactions. Some of these topics will be covered by other papers presented at this workshop. Generally dry deposition of a pollutant is described by a deposition speed, $V_d$, which has been roughly determined by previous experiments. Likewise, wet deposition or rainout is described by the frequency, $\Lambda(\text{sec}^{-1})$, which is approximately the inverse of the half life of the pollutant in the presence of a given rain intensity. Neither of these parameters is very

well known in ideal conditions, such as in the case of a uniform pollution cloud over a flat, grassy, surface. (Van der Hoven, 1968; Precipitation Scavenging-1970 Symposium). Even less is known about these parameters in the complicated conditions over an urban surface. However, during special conditions a large fraction of the pollutant cloud can be removed by these processes.

Chemical transformations in an urban atmosphere are very complex, and advances have been made only by determining simplified chemical kinetic mechanisms and their appropriate rate constants. This is true both for photochemical smog and $SO_2$-sulfate atmospheres. For example, to model photochemical smog in Los Angeles it is necessary to account for from seven (Friedlander and Seinfeld, 1969) to 19 (Hecht et al., 1974) or more chemical equations. The rate constants for each of these reactions must be input to the urban diffusion model. Some of these rate constants are not very accurate, since they were determined from smog chamber experiments with simplified mixtures. A major unsolved problem of urban diffusion is the accurate specification of chemical reactions.

It is clear from the above listing of input data and their problems that in each case meteorologists and engineers have a fair idea of what is happening in idealized or simplified cases. But much more observation and analysis must be done before we can confidently prescribe all the input parameters to an urban diffusion model. Until that time, we must at times use the time-worn expression "garbage in--garbage out."

## 3. MODELING

There are many types of urban diffusion models, each with its own special problems. First are the rollback models, which assume a straightforward relationship between emissions and pollutant concentrations (e.g. Barth, 1973). Next are statistical models, which provide statistical relationships between pollutant concentrations and variables such as temperature, emissions, wind direction, etc. (e.g. Peterson, 1972). Next are analytical models, which are of necessity simple (e.g. Lettau, 1970; Gifford and Hanna, 1970). And finally are models solved by finite differencing techniques on computers (e.g., Reynolds et al., 1973). This final class of models can be further subdivided into those which use K theory and those which assume Gaussian plumes, and those which treat changes in pollutant concentrations at a fixed point or along a parcel trajectory. The special problems of each of these models will be treated in the following sections.

### 3.1 Rollback Models

The rollback philosophy assumes that pollution concentration is proportional to emissions. Consequently, if a 50% reduction in concentration is desired then emissions should be reduced by 50%. There is assumed to be no variability in the net effect of diffusion. Barth (1973) used the rollback model to examine federal motor vehicle emission goals for primary pollutants. For secondary pollutants he developed a "modified rollback" technique. With these modifications the model could better be classed as a statistical model.

A valid criticism of the rollback model is that it does not give proper credit to tall stacks, which may account for most of the total emissions of, say, $SO_2$, but are designed so that ground level $SO_2$ concentrations are within acceptable limits. Under regulations using the rollback method, a source releasing $SO_2$ at ground level and a tall stack must reduce their emissions by the same amount.

On the other hand, the rollback method gets to the root of our air pollution problem, namely emissions. This world has seen many stagnating highs, inversion layers, and G stability classes. But these do not by themselves cause air pollution episodes. The necessary ingredient is emissions. Furthermore, in terms of synoptic or global scale air pollution, the initial height of the source makes no difference. Global air pollution problems can be solved only by the rollback method.

### 3.2 Statistical Models

Given a set of observations from air monitoring stations and meteorological stations in urban areas, it is possible to calculate some statistical relationships among the variables. This procedure requires little physical insight and is limited to the region in which the observations were taken, but has the advantage of revealing the true relationships among variables at a specific location.

Statistical models of this type include those by Bezuglaya (1971), Peterson (1972), Bruntz et al. (1974) and McCollister et al. (1975). Peterson (1972) analyzes daily average $SO_2$ concentrations from St. Louis and Bruntz et al. (1974) use ozone concentrations from New York City. In the analysis by Bruntz et al. (1974) it is found that ozone concentrations $O_3$ (parts per billion average from 1 pm to 3 pm each day) on Welfare Island are best estimated by the following equation:

$$\log_{10}(O_3 + 5) = -3.29 + .21 \log_{10} S - .61 \log_{10} U + 2.65 \log_{10} T \qquad (3)$$

where S (langleys, averaged from 8 am to noon) is solar radiation, U (mph, averaged from 7 am to 10 am) is wind speed, and T (°F, maximum daily) is temperature. There is no significant relationship between ozone concentration and mixing depth evident in these observations. The relationships with solar radiation and wind speed in equation (3) are roughly what one would expect intuitively. But the dependence of ozone concentration on temperature is stronger than expected. The next step in this analysis would be to apply equation (3) to a new, independent set of observations at this site.

Another purely statistical scheme was developed by Smith and Jeffrey (1973) for cities in England. Their formula for estimated 24 hour average $SO_2$ concentration, $C_{est}$, is:

$$C_{est} = 0.085 \quad (1 + (\delta_m/6))(1 - (T - t)/28) \cdot (5\overline{C} + 4C_p) + 0.15\ \overline{C} \qquad (4)$$

where $\delta_m$ = 1 if the mixing depth is low for London only, and is 0 otherwise.

$T(°C)$ = minimum temperature from 9 am to 9 am.

$t$ = hours when mean wind falls below 5 kts.

$\overline{C}$ = mean concentration.

$C_p$ = yesterday's concentration.

The major factors entering equation (4) are mixing depth, wind speed, persistence, and minimum temperature (presumably related to emissions). In a comparison of the model predictions with observations, it is found that the mean concentration (about 200 gm/m$^3$) is predicted within 30% and that the correlation between observations and predictions is about .7.

Statistical analysis of observations should be a required step in the development and analysis of any urban diffusion model. Knowing the relationships among observed variables, it may be possible to use this information to strengthen or possibly eliminate certain features of the model.

### 3.3 Analytical Models

If one accounts for all of the possible physical and chemical effects and requires information at many grid points in an urban area, a computer model is necessary. But if one can be satisfied with treating urban diffusion as an integral problem, not requiring detailed spatial pollutant information, then analytical solutions are possible. The most elegant of these is the solution for concentrations due to area sources proposed by Lettau (1970), which is analogous to solutions based on conservation of momentum or heat. The relative influences of city size, wind speed, and source strength can be readily determined using this approach.

The geometry of this box model is illustrated in Figure 1, where $\Delta X$ is urban diameter, $Z$ is urban mixing depth, $U$ and $V$ are components of the horizontal wind speed, $w$ is vertical wind speed, $S$(gm/sec) is internal source or sink, and $c$ (gm/m$^3$) is local pollutant concentration. The simplified version of the primitive equation is:

$$\partial\overline{c}/\partial t + \partial(\overline{Uc})/\partial x + \partial(\overline{Vc})/\partial y = \overline{S} - \partial(w'c')/\partial z \qquad (5)$$

where the bars indicate a time average and the primes indicate turbulent fluctuations from the time average. In words, equation (5) states that the local change of concentration plus horizontal advection balances the change due to sources or sinks minus the local change due to convergence of the vertical turbulent flux. Let the average of any function g be denoted by the symbol

$$[\,g\,] = (1/Z\Delta X)\int_Z \int_{\Delta X} g\ dx\ dz \quad . \qquad (6)$$

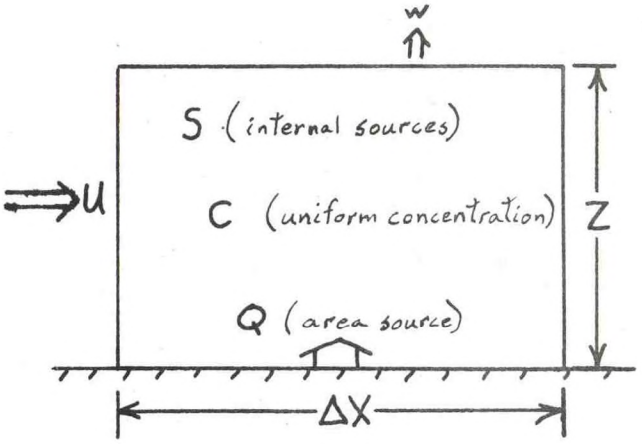


Figure 1. Geometry of Urban Box Model

Dependence on crosswind distance, y, could be included but is suppressed in order to simplify the discussion. The area source strength itself is the lowest boundary value of $\overline{w'c'}$; i.e. the vertical turbulent flux of pollutant at height z equal to zero. The source function is therefore defined as

$$Q(t) = [(\overline{w'c'})_o] + [Z\overline{S}] \quad . \qquad (7)$$

The dependent variable of interest is the area average concentration, C,

$$C(t) = [\,\overline{c}\,] \quad . \qquad (8)$$

Horizontal advection is expressed by a bulk wind speed, U*, defined by

$$U^*(t) = (\Delta X/C)\,[\partial(\overline{Uc})/\partial x + \partial(\overline{Vc})/\partial y] \quad . \qquad (9)$$

The flushing frequency, $f^*(\text{sec}^{-1})$, which is the most often quoted parameter from Lettau's paper, is defined with the aid of the bulk wind speed, U*, and vertical eddy flux $\overline{w'c'}$ at the top of the box.

$$f^* = U^*/\Delta X + (1/ZC)[(\overline{w'c'})_Z] \quad . \qquad (10)$$

From these definitions, the box model of urban

diffusion results:

$$\partial C/\partial t = Q/Z - Cf^* \quad . \qquad (11)$$

To further transform this equation, Lettau defines the quasi-equilibrium value of pollutant concentration, C*:

$$C^* = Q/Zf^* \quad , \qquad (12)$$

and the dimensionless time, t'

$$dt' = f^* dt \quad . \qquad (13)$$

The governing equation can be written as

$$\partial C/\partial t' = C^* - C \qquad (14)$$

which has the solution

$$C = e^{-t'}\left(C_o + \int_o^{t'} e^{t'} C^* \, dt'\right) \qquad (15)$$

where $C_o$ is the initial value of concentration.

In the simplest application of this model, it can be assumed that there are no internal sources or sinks (S=0), the vertical eddy flux at the top of the box vanishes ($[\overline{(w'c')}_Z = 0$), that $\bar{U}$ is constant, and that the background concentration is zero. Therefore the functions in equations (7) through (15) become:

$$Q(t) = [\overline{(w'c')}_o] \qquad (7a)$$

$$C(t) = [\bar{c}] \qquad (8a)$$

$$U^*(t) = \bar{U} \qquad (9a)$$

$$f^* = \bar{U}/\Delta X \qquad (10a)$$

$$\partial C/\partial t = Q/Z - C\bar{U}/\Delta X \qquad (11a)$$

$$C^* = Q\Delta X/\bar{U}Z \qquad (12a)$$

$$dt' = \bar{U}\, dt/\Delta X \qquad (13a)$$

$$\partial C/\partial t' = Q\Delta X/\bar{U}Z - C \qquad (14a)$$

$$C = e^{-t'}\left(C_o + Q\Delta X(e^{t'}-1)/\bar{U}\, Z\right) \quad . \qquad (15a)$$

In this simplified case, the flushing frequency f* is the inverse of the time necessary for the air to pass over the urban area and the equilibrium concentration C* is the steady-state concentration obtained by mixing the material through a box of depth Z, and length ΔX, with wind speed $\bar{U}$. From equation (15a) it is seen that the actual concentration approaches this equilibrium concentration as time increases, no matter what the initial concentration is.

While Lettau's (1970) model reduces to the well known box model in its simplest application, it is also capable of handling internal sources and sinks, fluxes of pollutant from the top of the box, and variable advection patterns. Lettau plotted the solution to equation (15) for several typical forcing functions, Q. An example of a solution is plotted in Figure 2. It is assumed that the forcing function or rate of pollutant release has a diurnal variation over a factor of twenty. The resulting pollutant concentrations over the six day period vary by a factor of twenty also. Lettau finds that a larger city is slower to respond to changes in rate of pollutant release or forcing function, and smooths out the changes that do occur, as we would expect intuitively.

Lettau (1970) goes on to show how his model can be applied to thermal pollution and momentum drain over urban areas. Knowledge of the momentum drain or surface roughness allows the wind speed to be determined, for use in determining the flushing frequency. It is clear that the major advantage of this model is that it permits a relatively quick analysis of urban diffusion problems, while still accounting for the major physical factors.

Adapted from Lettau's Figure 2.7 :

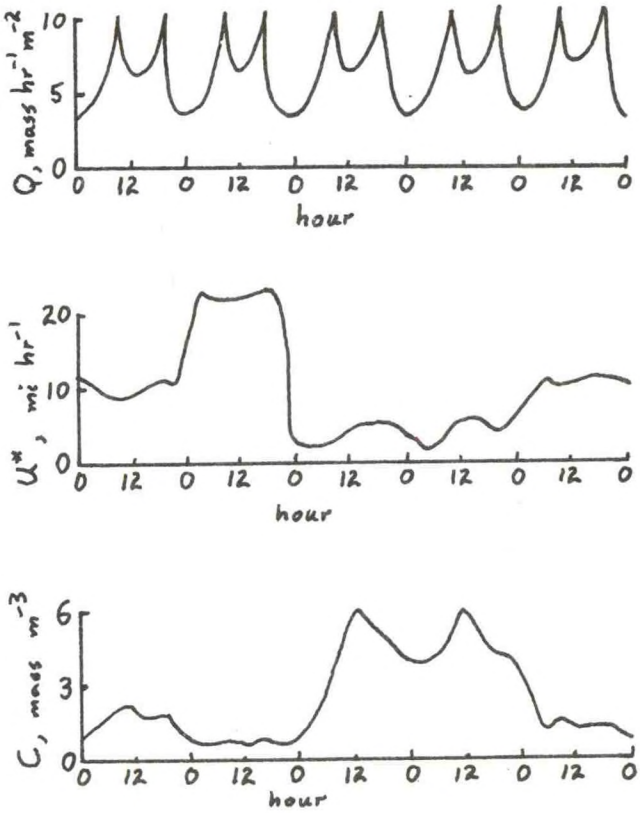


Figure 2. Trends of pollutant concentration in response to indicated forcing function for typical variation of atmospheric flushing parameters. City size ΔX is 20 miles.

Another study which discusses the physical basis for the box model is summarized by Hanna (1971) and Gifford and Hanna (1973). Their model is intended to be applied to urban area sources, where emissions are given as uniform over grid squares. As stated in section 2, the typical size of a grid square is one to ten kilometers. But instead of assuming that the pollutant cloud at all locations extends to the mixing height, it is assumed that the pollutant is well mixed to a height Z(x), given by

$$Z(x) = ax^b \qquad (16)$$

where a and b are parameters dependent on stability. It is most convenient to assume that the vertical distribution of pollutants is Gaussian, and that the parameters a and b are as suggested by Smith (1968):

Table 2

| Meteorological conditions | a | b |
|---|---|---|
| Very Unstable | 0.40 | 0.91 |
| Unstable | 0.33 | 0.86 |
| Neutral | 0.22 | 0.80 |
| Estimated Pasquill "D" | 0.15 | 0.75 |
| Stable | 0.06 | 0.71 |

Gifford's "reciprocal plume" hypothesis (1959) permits the solution for the case of steady state conditions, no internal sources and sinks, no vertical turbulent advection, and constant wind speed $\bar{U}$, to be written in the form

$$C = \int_0^\infty \int_{-\infty}^{\infty} (Q/\pi U \sigma_z \sigma_y) e^{y^2/2\sigma_y^2} dy\, dx \qquad (17)$$

where $\sigma_y$ and $\sigma_z$ are the standard deviations of the horizontal and vertical crosswind distributions of pollutant in a plume at distance x from a point source. Integration is over the upwind half plane.

Next the "narrow plume" hypothesis permits the dependency of Q on y to be removed. Since most plumes include an angle of approximately 20°, then sources outside of a 20° sector in the upwind direction from the receptor have little influence on the concentration at the receptor. In this case equation (17) becomes:

$$C = \int_0^\infty (Q\sqrt{2/\pi} / U \sigma_z)\, dx \quad . \qquad (18)$$

Note that equation (18) can be written in the form

$$C = \sqrt{2/\pi}\ (\Delta X/U)\ (\overline{Q/\sigma_z}) \qquad (19)$$

which is equivalent to Lettau's equilibrium concentration (12a).

If the source strength, Q, varies according to the typical grid pattern illustrated in Figure 3, the parameter $\sigma_z$ varies as in equation (16) and Table 2, and the grid size is $\Delta X$ then the solution is obtained by piecewise integration:

$$C = \left( \sqrt{2/\pi}\ (\Delta X/2)^{1-b}/Ua(1-b) \right) \cdot \left( Q_o + \sum_{i=1}^{N} Q_i \left( (2i+1)^{1-b} - (2i-1)^{1-b} \right) \right). \qquad (20)$$

In equation (19), N is the number of upstream gridblocks, generally extending to the city's edge.

A constant wind direction is required for application of equation (20). Extension to monthly or annual average conditions is made by solving equation (20) for a variety of wind directions, then weighting each result by the frequency with which the wind blows in that direction. Solutions obtained in this manner for several urban areas have been reported by Gifford and Hanna (1970) and Hanna (1972). After comparison with observations it was soon discovered that variations in the source terms $Q_i$ outside of the receptor grid square do not have a great influence on the concentration in the receptor square. This is because area source distributions are generally fairly smooth and the coefficients of the $Q_i$ terms in equation (20) are significantly less than the coefficient of the $Q_o$ term. Therefore for most applications it is sufficient to assume that all source terms equal the receptor source term, and equation (20) becomes:

$$C = \left( \sqrt{2/\pi}(\Delta X(2N+1)/2)^{1-b}/a(1-b) \right) Q_o/U = A\, Q_o/U \qquad (21)$$

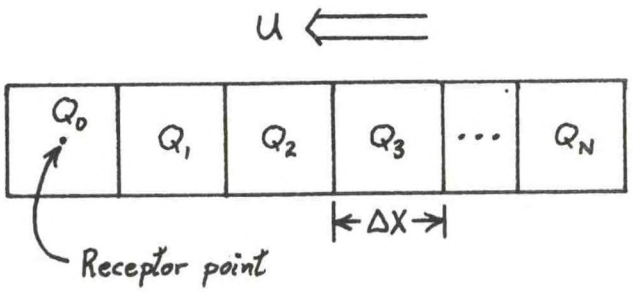


Figure 3. Area source grid pattern used in Eq. (20).

where $\Delta X(2N+1)/2$ is the distance to the upwind edge of the urban area. For class "D" conditions and typical urban sizes, the dimensionless constant "A" in brackets is calculated to equal about 200, in agreement with observations from many urban areas (Gifford and Hanna, 1973). For stable conditions it is about 60. Note that this constant is defined by the integral

$$A = \sqrt{2/\pi} \int_{0}^{\text{edge}} dx/\sigma_z \quad , \qquad (22)$$

Thus this method reduces to the familiar box model. In an analysis by Gifford (1970), it was shown that the form of the vertical distribution of pollutant does not significantly influence the ground level pollutant concentration. It is the integral of the distribution curve rather than the shape of the curve which is important. Consequently it does not matter whether the distribution is assumed to be Gaussian, linear, or top hat, as long as the integral height scale of the distribution is consistent. Furthermore, for most low and mid latitude cities it is found that the daytime mixing height or inversion height is generally much greater than the height of the pollutant cloud, Z, as calculated above, and is not well correlated with pollutant concentrations.

Similar analytical calculations, differing slightly from each other, but all yielding what would be called a box model, are reported by Calder (1970), and Lebedeff and Hameed (1975). A basic result of these models is that urban pollutant concentrations depend most strongly on source emissions and on wind speed. Generally, correlations between predicted and observed concentrations are about .5 to .9 in applications of these models. There are no definite time or space limitations to the box model. Any time or space scale can be used, as long as the period or region does not experience abrupt changes in meteorological conditions or emissions which would make the steady state assumption invalid.

It is also possible to obtain a simple analytical solution for the more general case, which includes the effects of dry deposition, washout, and chemical reactions. The flux of pollutant to the ground due to dry deposition is given by $CV_d$, where $V_d$ is the dry deposition speed (Van der Hoven, 1968). Removal by washout equals $\Lambda_w ZC$, where $\Lambda_w$ is the washout coefficient, defined in the relation:

$$\partial C/\partial t(\text{washout}) = - \Lambda_w C \quad . \qquad (23)$$

Similarly, removal by chemical reactions can be approximated by $\Lambda_c ZC$. The fraction $1/\Lambda_c$ is proportional to the chemical half life of the pollutant. None of the parameters $V_d$, $\Lambda_w$, and $\Lambda_c$ is well known, particularly over urban areas. Average values for $V_d$ and $\Lambda_w$ are 1 cm/sec and $10^{-4}$ $sec^{-1}$, respectively. The conservation equation for material uniformly distributed in an urban box of height Z and length $\Delta X$ is:

$$Z\,\Delta X\,\partial C/\partial t = Q\,\Delta X - U\,CZ - V_d\,\Delta X - \Lambda_w\,CZ\,\Delta X - \Lambda_c\,CZ\,\Delta X \quad . \qquad (24)$$

In steady state conditions this equation becomes

$$C = (Q\,\Delta X/UZ)/(1 + (\Delta X/U)/(Z/V_d) + (\Delta X/U)/(1/\Lambda_w) + (\Delta X/U)/(1/\Lambda_c)) \quad . \qquad (25)$$

The quantity in the numerator is Lettau's equilibrium concentration (equation 12a). In the denominator the terms are the ratios of the characteristic times:

- $\Delta X/U$ : (flushing frequency)$^{-1}$. The timefor the air to pass over the urban area.
- $Z/V_d$ : The time for the pollutant to settle a distance equal to the depth of the pollutant cloud.
- $1/\Lambda_w$ : The characteristic time for washout.
- $1/\Lambda_c$ : The characteristic time for chemical reactions.

Because it is assumed that the pollutant is well mixed throughout the volume, the approximations in equation (25) are most valid if the terms in the denominator are not much greater than unity. The gross effects of deposition, washout, and chemical reactions can be easily estimated from equation (25). Numerical methods for obtaining more detailed results are discussed in the next section.

## 4. NUMERICAL URBAN DIFFUSION MODELS

Numerical urban diffusion models begin with a set of governing equations and suitable input parameters, and then estimate pollutant concentrations by means of many calculations on a computer. The complexity is generally due to the large number of receptor grid points and point and area source emissions. While there are several different types of numerical models available, the choice of "best" model must wait until a good set of observations in an urban area is available. Some models are based on K theory and others on the Gaussian plume concept. Some are based on a fixed grid system and others on a parcel of air which travels with the wind. Rather than give a point by point review of these numerical models, since this has been done by Eschenroeder (1975), this paper will stress the problems of the models.

### 4.1 Gaussian Models

The first urban diffusion model was the one prepared by Frenkiel (1956) for Los Angeles, using the Gaussian kernel. Subsequently a series of simple Gaussian type models were developed by researchers at the National Center for Air Pollution Control (Pooler, 1961; Turner, 1964; Clarke, 1964; Miller and Holzworth, 1967). These numerical models were quite simple in their approach, but

produced fair correlations between predictions and observations. At that time, emissions and pollutant concentrations were not well known.

Similarly, Davidson (1967) and Bowne (1969) applied the Gaussian formula to dispersion over New York City and the state of Connecticut respectively. In Bowne's model the state of Connecticut was broken up into one mile grid squares and predictions of $SO_2$ and CO made at hourly intervals. The superposition of Gaussian plumes from the many point sources was assumed. To save computer time, backward trajectories were calculated from each receptor point. These calculations could be done by hand, but would take forever.

The model by Martin and Tikvart (1968) is the forerunner of the Air Quality Display Model (AQDM, TRW, 1969) currently in use by the EPA. It is nearly the equivalent of the model by Hanna (1971), in which large point sources are handled by the Gaussian plume formula:

$$C = (Q_p/2\pi\, U\, \sigma_y\, \sigma_z)\, \exp(-y^2/2\sigma_y^2)$$
$$\exp(-(z-h)^2/2\sigma_z^2 - (z+h)^2/2\sigma_z^2) \qquad (26)$$

where $Q_p$(g/sec) is the point source strength, y(m) is horizontal crosswind distance from the plume axis, z(m) is height above ground and h(m) is effective plume height, which is the sum of stack height $h_s$(m) and plume rise $\Delta h$(m). Equation (26) is thoroughly discussed by Gifford and Pasquill in other papers presented at this workshop. Formulas for calculating plume rise $\Delta h$ are given by Briggs (1969). Area sources are handled in this model by the technique summarized by equation (20) of the last section. As input to the model, joint frequency distributions of wind direction, wind speed, stability, and emissions strength are desirable. Also, as mentioned in section 2, it is desirable to use values of the dispersion parameters $\sigma_y(x)$ and $\sigma_z(x)$ which are suitable for urban areas (see Gifford's (1975) review of turbulence typing schemes.) The specification of $\sigma$ is clearly an important unsolved problem in urban diffusion modeling. More experiments such as the ones in St. Louis reported by McElroy (1969) should be performed.

Dabberdt et al. (1973) applied Clarke's (1969) simple Gaussian model, with modifications for street canyon effects, to the problem of estimating CO concentrations. Buildings and streets do modify the air flow in urban areas and at times cause significant deviations from the predictions of pollutant concentrations by means of simple models. To be strictly correct, the influences of a specific city surface can be determined through wind tunnel tests (e.g. Chaudry et al., 1971). Dabberdt et al. observed air circulations and CO concentrations in street canyons in San Jose and St. Louis, and suggest that the amount of CO that should be added ($\Delta C$) to the roof top concentration for the side of the street in which the buildings face the wind is:

$$\Delta C = (\, A\, Q_L/W(U + 0.5)\,)\,(\,(H - z)/H\,) \qquad (27)$$

where the constant, A, is determined to be 7, $Q_L$($gm^{-1}s^{-1}$) is line source strength, U($ms^{-1}$) is roof top wind speed, H(m) is street canyon depth, and W(m) is the street width. On the upwind side of the street, $\Delta C$ is given by

$$\Delta C = A\, Q_L/r(U + 0.5) \qquad (28)$$

where r is the slant distance from the receptor to the nearest traffic lane. When the wind is parallel to the street, $\Delta C$ is described by the average of equations (27) and (28). This model was applied to an independent set of data from St. Louis, and the root mean square difference between predicted and observed CO concentrations was 3ppm (parts per million). These empirical formulas must be further refined using observations in other street canyons.

There are at least two Gaussian models available (Roberts et al., 1970; Start et al., 1974) which employ puffs, rather than plumes. They argue correctly that a plume model cannot handle wind direction changes on time scales less than a few hours. Serially released puffs, on the other hand, can be made to follow the wind trajectory. In some calculations the expanding puff blows right back over the source point. The difficulty with puffs is that very little is known about their dispersion characteristics. A graph summarizing the few observation programs is given by Islitzer and Slade (1968). But the dispersion functions $\sigma_y(t)$ and $\sigma_z(t)$ for puffs and plumes are different. Thus the applications by Roberts et al. (1970) and Start et al, 1974) using plume $\sigma$'s are not strictly correct. The method developed by Roberts et al. and applied to $SO_2$ in Chicago contains many parameterizations and assumptions besides the questionable puff assumption. For example, area sources are approximated by virtual point sources. Virtual sources are not necessary if the basic integral equation (17) for area sources is used. A danger with large computer urban diffusion models is that there are so many steps and calculations that many "tunable" or empirical parameters enter the system. If one works with the same urban observations for long enough, the model no longer is independent of the observations used to test it.

Rather than using a puff model, it is more valid to use a spreading disc model. The discs, or wafers, diffuse in the crosswind directions. The axis connecting the discs can bend or meander due to changes in wind direction.

As the Gaussian model is applied to a wide range of new problems, it is sometimes criticized because it does not produce concentration estimates which agree well with observations. In most cases, this is not the fault of the model but of the person making the application. In the standard references which explain the Gaussian model (Pasquill, 1962; Gifford, 1968) it is made clear that the suggested dispersion parameters are derived from experiments over flat terrain over short to moderate distances (no greater than a few hundred meters). Emissions were from point sources near the ground. It is not expected that these dispersion parameters would strictly apply

to different source conditions, long distances, or over a very rough surface. For these conditions, new sets of σ graphs should be constructed from detailed observations of that particular case. The Gaussian model has proven to be a powerful tool when applied to point sources over smooth terrain. It can also be very powerful for special case of diffusion over urban surfaces, once the required empirical parameters are determined.

4.2 K Models

Through analogy with the molecular diffusivity, it can be assumed that the vertical turbulent or eddy flux of material, $F_z$ ($gm^{-2}s^{-1}$), is proportional to the gradient of material:

$$F_z = - K_z \, \partial C/\partial z \qquad (29)$$

where $K_z$ ($m^2 s^{-1}$) is defined as the vertical eddy diffusivity coefficient. Similar definitions apply for the diffusivities, $K_x$ and $K_y$, in the horizontal directions. The so-called diffusion equation can be written:

$$\partial C/\partial t + \partial(uC)/\partial x + \partial(vC)/\partial y + \partial(wC)/\partial z$$

$$= \partial(K_x \, \partial C/\partial x)/\partial x + \partial(K_y \, \partial C/\partial y)/\partial y +$$

$$\partial(K_z \, \partial C/\partial z)/\partial z + S \quad . \qquad (30)$$

The last term, S, represents all sources and sinks. In most problems, the first term on the right hand side of equation (30), involving the along wind diffusion, is neglected, on the grounds that it is much less than along wind advection.

If there are no sources or sinks, the wind blows constantly from one direction, steady state conditions are achieved, and K's are constant, then equation (30) becomes the Fickian diffusion equation. The solution is Gaussian with standard deviations $\sigma_y$ and $\sigma_z$ equal to $(2 K_y x/U)^{1/2}$ and $2 (K_z x/U)^{1/2}$ respectively. Unfortunately the diffusivity K is rarely constant. The magnitude and functional form for $K_z$ can be estimated by assuming that it is equal to the diffusivity for water vapor or heat, which have been shown to equal the diffusivity for momentum $K_m$ divided by the dimensionless wind shear, $\phi$ (Pasquill, 1974), where $\phi$ is defined by:

$$\phi = (1 - 16 \, z/L)^{-1/4} \quad \text{unstable} \qquad (31)$$

$$\phi = (1 + 4.5 \, z/L) \quad \text{stable}$$

The Monin Obukhov length L is defined by

$$L = - \rho \, c_p \, T \, u_*^3 / .4 g \, H \qquad (32)$$

where $u_*$ is friction velocity, g is the acceleration of gravity and H is the upward heat flux. A general form for the diffusivity for momentum, $K_m$, in the air layer within 100 m of the ground, is given by the relation

$$K_m = .4 \, u_* \, z/\phi \quad . \qquad (33)$$

At heights above about 100 m the diffusivity for momentum ceases its linear variation with height and approaches a constant which equals about $.005 \, u_*^2/f$ for Clarke's (1970) near-neutral data. The parameter f is the Coriolis parameter. In general, this value of $K_m$ depends on the friction velocity or free stream wind speed and the stability. There are presently very few data available which permit calculation of $K_m$ at heights between 100 m and 1000 m. Above about 1000 m, $K_m$ generally decreases again.

If measurements of the vertical velocity spectrum are available, then the techniques suggested by Hanna (1969) or Pasquill (1967) (see equation (2) ) can be used to estimate $K_m$. It is clear, however, that the vertical eddy diffusivity coefficient $K_z$ is a highly empirical parameter which is difficult to specify, especially at heights above about 100 m. No matter how elegant the mathematical solution to equation (30), the final result always depends on the highly elusive eddy diffusivity coefficient.

The crosswind horizontal diffusivity, $K_y$, is even more difficult to estimate because of possible influence of mesoscale meanders in wind velocity. In most studies, $K_y$ is simply assigned a constant value, such that the estimated concentration distribution will agree as well as possible with the observed distribution.

For K theory to be strictly valid it is necessary that the length scale of the diffusing cloud of pollutants be greater than the length scale of the turbulence. Otherwise the full spectrum of turbulence does not take part in the diffusion. Modifications to K can be made to account for this, but this generally adds an unacceptable amount of complication to the model. As Pasquill (1974) shows, K theory is most applicable to ground level sources, where the criterion regarding length scales of the cloud and the turbulence is satisfied.

Analytical solutions to several greatly simplified forms of equation (30) are summarized by Pasquill (1974). It has already been mentioned that the solution to the Fickian simplification of equation (30) can be shown to be equivalent to the Gaussian plume formula. The simplest steady state solution for diffusion from a very broad ground level area source is obtained from

$$\partial(K_z \, \partial C/\partial z)/\partial z = 0 \qquad (34)$$

where $- K_z \, \partial C/\partial z = Q$

and $C(z = 0) = C_o$

If it is assumed that $K_z = .4 \, u_* \, z$, then the solution to equation (34) is

$$C = C_o - (Q \ln z/z_o)/.4\, u_* \qquad (35)$$

where $z_o$ is the roughness length. Because $K_z$ is assumed to be proportional to z, then this solution is valid only in the surface layer; i.e., at heights less than about 100 m. Not many of the recent group of K models for urban diffusion employ an analytical solution. Instead, a computer is used to solve the general form of equation (30).

There are well-known numerical instabilities associated with the solution of the finite difference approximation to equation (30). In particular, errors in approximating the advective terms on the left hand side of the equation lead to a pseudo-diffusion which is at times greater than the real diffusion. Methods of eliminating these problems include using as small time and space increments as possible and using a finite difference approximation based on higher order terms in the Taylor series expansion of C. However these techniques may cause computer costs to rise to an unacceptable level. Two alternative ways for correcting for pseudo-diffusion are the moment method of Egan and Mahoney (1971) and the particle-in-cell (PICK) method of Sklarew et al. (1972). In the moment method, the moments of the concentration distribution are used in the governing equations, and the distribution is recovered using the first and second moments. In the particle-in-cell method, single particles at the centers of grid squares are advected by a velocity which is the sum of the true velocity and a diffusive velocity (i.e., $-(K/C)\ \partial C/\partial y$ ). The advection of many such particles is calculated and the concentration estimate is based on the resulting distribution of these particles. The ADPICK code used by Ludwig and Keoloha (1974) to estimate smog concentrations in the San Francisco area is also based on this concept.

An attempt should be made to insure that the wind field that is being used in the model conserves mass. Otherwise, unrealistic accumulations and deficits of pollutants are apt to occur. Knox (1974) and Dickerson (1973) describe their technique for calculating a mass-consistent wind field from the observed wind field. Basically the model adjusts the observed winds in order to make sure that the continuity equation is nearly satisfied at each grid point. Ideally, a model should predict the wind field as well as the pollutant concentration distribution. Pandolfo and Jacob's (1973) model for CO in the Los Angeles basin included predictions of winds, temperatures, and CO concentrations. The effects of topography were also included. Because of the large number of variables in the model, the grid spacing (8 miles) had to be larger than that of other models of the region (e.g., Roth et al. (1971) use a 2 mile grid spacing). The predictions of CO, however, were no better than those of other models which did not predict winds. This may be due to the fact that the other models used observed winds, which as any weather forecaster knows can differ significantly from predictions.

Shir and Shieh (1974) hope to minimize the numerical error in their study of $SO_2$ dispersion in St. Louis by using a fine grid (16,800 points) system and by using the Crank-Nicolson technique for approximating vertical dispersion. The vertical diffusivity, $K_z$, is linear with height near the surface, but approaches a constant as height increases. The horizontal diffusivity, $K_y$, is set equal to 200 $m^2$/sec, but it is found that $K_y$ has little influence on the results. The lack of importance of horizontal diffusion processes in most urban areas was first suggested by Gifford and Hanna (1970). The final test of the Shir-Shieh model must await the results of the large Regional Air Pollution Study, RAPS, (Pooler, 1974) presently underway in St. Louis.

The final set of models which will be discussed has been designed specifically to study the Los Angeles smog problem. These models are generally intended to satisfy a need of the Environmental Protection Agency. The general philosophy of these models is discussed by Reynolds et al. (1973) and Eschenroeder (1975). The first group of EPA contractor reports appeared in 1971. Wayne et al. (1971) used a box which moved with the wind. Pollutants entered the box at the bottom and concentration distributions were uniform within the box. Eschenroeder et al. (1971) also used a moving box, but accounted for vertical gradients by means of a simplified K formulation. Roth et al. (1971) employed stationary boxes, of width 2 miles, and also used a simplified $K_z$. Thus the diffusion techniques and kinematics of these models are quite simple. The complexity enters due to the emissions, the chemistry, and the large number of calculations which must be made.

Detailed emissions specifications are discussed by Roth et al. (1974), who account for such seemingly minor points as the differences between cold-start and hot-start auto emissions. Furthermore, since most of the ozone and $NO_2$ in Los Angeles air are formed through chemical reactions originating with NO and reactive hydrocarbons at the mouth of exhaust pipes, these models contain detailed chemical kinetics mechanisms. The large number of possible reactions in a smoggy atmosphere are boiled down to about 15 or 20 reactions. Thus the reaction rate given for a chemical equation in the model represents the average reaction rate for a system of fundamental equations. The choice of reactions and their rates is based on smog chamber experiments (e.g., Altshuller and Bufalini, 1974). As these experiments are refined and as research continues, the chemical kinetics schemes are being updated (see Reynolds et al., 1973; Hecht, 1973; and Hecht and Seinfeld, 1974). As new problems arise, such as the advection of ozone to rural areas at night, it is found that chemical kinetics systems formulated for daytime conditions over the source region do not apply well to the new problem (Hanna, 1975).

In the current versions of the Los Angeles smog models, much more attention is paid to chemical reactions than to meteorological factors such as diffusion and advection.

Hanna (1973) describes a box model which can be used to determine the relative importance of source terms, advection, and chemical reaction terms in the equation for pollutant conservation in a well-mixed box with no upwind sources:

$$Z\,\Delta X\,\partial C_i/\partial t = Q\,\Delta X - UZC_i + R_i \qquad (36)$$

where $R_i$ represents the rate of change of pollutant concentration $C_i$ due to chemical reactions. If a dimensionless time $t^*$ is defined as the time t times the flushing frequency $U/\Delta x$ (equation 10a), a dimensionless concentration $C_i^*$ is defined as the concentration $C_i$ divided by the equilibrium concentration $Q\Delta x/UZ$ (equation 12a), and the 7 step chemical kinetics system proposed by Friedlander and Sienfeld (1969) is used, then equation (36), as applied to, e.g., NO, becomes:

$$\partial\, \ell n\, C^*_{NO}/\partial t^* = 1/C^*_{NO} - 1 - C^*_{NO_2} C^*_{RH}{}^{\alpha}$$

$$Q_{NO_2}\, Q_{RH}\, \Delta X^3/U^3\, Z^2 \quad . \qquad (37)$$

The rate constant $\alpha$ has the value 1/600 $ppm^{-2}s^{-1}$. All of the terms but the last in equation (37) have a coefficient of unity. Therefore if the dimensionless number

$$Cl = \alpha\, Q_{NO_2}\, Q_{RH} \Delta X^3/U^3\, Z^3 \qquad (38)$$

is much less than unity, then chemical reactions are unimportant. If Cl is much greater than unity, then chemical reactions are more important than advection. Clearly the flushing frequency $U/\Delta X$ has a great influence on whether chemical reactions are important. In the wind tunnel simulation of photochemical smog proposed by Hoffert et al. (1975), dimensionless formulations such as equation (37) can assist in the comparison of model results with full scale atmospheric results.

There is a new technique called second order closure (see Donaldson, 1973 and Hilst et al., 1973) which is being applied to atmospheric turbulence and diffusion problems and may prove to be more useful than the Gaussian plume model or K theory. Whereas K theory provides empirical approximations to second order terms in the governing equations, second order closure provides empirical approximations to the third order terms. Thus more details of the flow can be modeled, such as turbulent folding of parcels of air containing different amounts of pollutants (O'Brien, 1971). However, at the present time, this technique is still in the development stage. A major problem is the specification of the empirical length required for closure.

The material covered in this section indicates that there are currently many different types of models, with many different purposes and assumptions. In the next section the output of some of these models will be discussed and compared with observation.

## 5. OUTPUT AND OBSERVATIONS

Some urban diffusion models are used as research tools in order to understand the physical and chemical processes that are going on. But most models have the ultimate purpose of predicting pollutant concentrations, whether for episode control, industrial planning, or many other important applications. Looking at the comparisons of model output with observations that have been reported so far, it seems that we deserve only a "fair" rating. With good input, the correlations between the estimates of our models and independent observations averages about .6, implying that we can explain 36% of the variance of the observed concentrations. In some cases, the correlation is .8 or higher. Correlations of.9 or higher are probably fortuitous and should be carefully examined. Of course, the correlation coefficient itself is not a sufficient measure of model "goodness" and is often misleading. For example, a good correlation is possible between two data sets whose average values differ widely. Or, a single outlier point in a set of otherwise uniform data may almost completely determine the value of the correlation all by itself. As an example of problems that are encountered, a model might be used to estimate concentrations in an urban area at five stations where mean concentrations are very close. Here the model might predict the mean concentrations and their diurnal variability quite well, but the spatial correlation is bad. For these reasons, and because they do not trust the current observations, Reynolds et al. (1974)do not calculate any estimate of the statistical relationship between predictions and observations. They do plot predictions and observations together on the same graph, however.

For the purposes of testing urban diffusion models, monitoring stations should be placed in and around an urban area so that the measurements of each station are representative of the average ground level pollutant concentration in the rest of that grid square. Most monitoring stations are in reality placed according to criteria such as accessibility or nearness to a significant source which is under surveillance. For example, CO monitors tend to be located near busy streets. As a result, the observed CO concentrations in most cities are about twice the magnitude of the regional value (Dabberdt et al., 1973). One justification for modeling is that the model can be used to determine the best location for monitoring stations. In St. Louis, where the Reginal Air Pollution Study (Pooler, 1974) has been underway for over a year, the monitoring sites have been chosen with the purpose of using the observations to test urban diffusion models. But in most of the urban areas to be discussed next, monitoring stations were poorly located for testing diffusion models.

A detailed review of the performance of prediction techniques is contained in the review by Eschenroeder (1975) of models for predicting air quality. His review, in turn, summarizes other model comparisons by Gifford (1973), Koch and Thayer (1971), Sklarew (1975), Lamb et al. (1973), Turner et al.(1972), and Nappo (1974). It must be mentioned that at no time has an urban diffusion model "olympics" been held,wherein each model is

Table 3. COMPARISON OF SIMPLE URBAN POLLUTION MODEL WITH VARIOUS OTHER MODELS (GIFFORD, 1973)

| City | Concentration value modelled | Period | Pollutant | Correlation Coefficient | | Model |
|---|---|---|---|---|---|---|
| | | | | ATDL (Hanna, 1971; Gifford & Hanna, 1970, 1973) | Other | |
| Chicago | Point | 24 hr (for 18 days) | $SO_2$ | .67 | .69 | Roberts, et al., 1970 |
| Chicago | Point | 6 hr (for 4 days) | $SO_2$ | .66 | .80 | " |
| Memphis | Area Pattern | Annual | Particle | .68 | .73 | AQDM TRW, 1969 |
| Nashville | " | " | " | .91 | .80 | " |
| Ankara | " | Seasonal | " | .63 | .59 | Climatological dispersion model Calder, 1971 |
| Bremen | " | " | $SO_2$ | .65 | .05 | Fortak, 1970 |
| "Test City" | " | Annual | Particle | .98 | .96 | AQDM |
| L.A. | Point | 1 hr (for 17 hrs) | CO | .89 | .48 | PICK Sklarew et al., 1972 |
| San Francisco | " | 1 hr | CO | .74 | .66 | McCracken et al., 1971 |
| L.A. | Area Average | 1 hr (for 7 hrs) | NO | .97 | .91 | PICK Sklarew et al., 1972 |
| " | " | " | $NO_2$ | .05 | -.42 | " |
| " | " | " | Reactive Hydrocarbons | .61 | .55 | " |
| London | " | 24 hr avg | $SO_2$ | .76 | .87 | Smith and Jeffrey, 1973 |

required to make the same calculations based on an independent set of input parameters. Usually in model comparisons we are comparing the results of a fresh or independent model with the results of a model which has been specially turned to the input data of that particular urban area. Again, the RAPS program in St. Louis will be very valuable in this regard, for it will provide a new set of independent data for model comparison.

In Gifford's (1973) review the correlation coefficients between predicted and observed concentrations for the Hanna (1971) model and other models, are compared at nine cities as summarized in Table 3. It is seen that the correlation coefficients for the simple model and the other models are similar at any city. Very high correlations such as .98 at the AQDM "test city" are due to a choice of sampling stations such that the observed concentrations at all but one of them are moderate and nearly equal. At one station the concentration is quite high. Consequently if the model predicts that the concentration at the one station is high whereas the concentrations at the other stations are low and equal, a high correlation results. This illustrates how the use of correlation coefficients can be deceiving.

The comparison by Gifford (1973) in Table 3 includes correlations of diurnal variations of hourly average concentrations at a single site or over an area, and of spatial variations of hourly average concentrations at multiple sources in an urban region. Also, time series of daily averages at a single site and spatial variations of seasonal averages at multiple sites were anlyzed.

Turner et al. (1972), however, looked at the spatial variations of annual average $SO_2$ measurements at 75 locations and suspended particulate matter at 113 locations in New York City. So-called climatological models, such as the EPA Air Quality Display Model (AQDM, TRW, 1969) and the simple Hanna (1971) model were used to estimate average annual concentrations at each site. The AQDM, in contrast to the Hanna model, uses joint frequency distributions of wind direction, wind speed and stability. Correlations between observations and predictions ranged between .57 and .89 for all the models and all the data. There was not a significant difference in the correlations produced by the simple models and the models requiring joint frequency distributions. The simple models had the largest mean absolute error, however. Turner et al. conclude that:

> "It seems reasonable when attempting to validate a dispersion model to compare results with the results obtained with simple models applied to the same data. If the performance of the model considered does not exceed that of the simple model(s), it probably should be discarded."

Of course, Turner et al. (1972) are thinking only of the practical applications of models. A model may have valid uses for research purposes even if it is not the best model for prediction purposes.

In addition, Turner et al. (1972) calculated linear correlation coefficients of measured air quality data with predictions of the model using emission rates averaged over circles of radius 3, 5, 10, 20, 30, and 40 km about each receptor. In rough agreement with Marsh and Withers' (1969) and Marsh and Fosters' (1969) findings in Reading, the optimum radius for the emissions estimate is about five to 20 km.

The survey by Sklarew (1975) evaluates three photochemical models which have been developed for the Los Angeles basin. The models by Reynolds et al. (1973), Wayne et al. (1973), and Eschenroeder et al. (1972) were evaluated. For CO, each model yields a correlation coefficient of about .8 between prediction and observations. For ozone, correlation coefficients of .92, .69, and .49 are obtained for the models by Eschenroeder et al. (1972), Reynolds et al. (1973) and Wayne et al. (1973), respectively. The difference among the ozone predictions can be attributed to differences in the chemical kinetics systems.

Table 4

**MODEL EVALUATION BASED ON TEMPORAL CHARACTERISTICS**

| Model | Average Temporal Correlation Coefficient | Computer Time for 24 Hour Prediction (min) | Computer Cost for 24 Hour Prediction (dollars) |
|---|---|---|---|
| MacCracken *et al* (1971) multi-box | 0.37 | 106 | 350 |
| 24 Hour Persistence | 0.47 | None | None |
| Roth *et al* (1971) primitive equation | 0.52 | 60 | 200 |
| Hanna (1973) ATDL simple model | 0.60 | None | None |
| Sklarew *et al* (1972) particle-in-cell | 0.65 | 49 | 160 |
| Pandolfo and Jacobs (1973) primitive equation | 0.66 | 20 | 70 |
| Reynolds *et al* (1973) primitive equation | 0.73 | 30 | 100 |
| Lamb and Neiburger (1971) trajectory | 0.90 | 35 | 115 |
| Eschenroeder *et al* (1972) trajectory | 0.73 | 15 | 50 |

(Nappo, 1974)

In Nappo's (1974) comparison of eight models and persistence, computer time and the ratio of predicted to observe CO concentrations were estimated, along with the usual space and time correlation coefficients. Some results of Nappo's evaluations are listed in Table 4. In addition, it is found that temporal correlation coefficients are better than spatial correlation coefficients in all but one model (McCracken et al., 1971). The most interesting and unique aspect of Nappo's paper is his calculation of the mean and standard deviations of the ratios of predicted to observed concentrations. These ratios and their standard deviations for spatial and temporal averages are shown in Figure 4. On this figure it is seen that the simpler the model, the greater the expected error in mean magnitude. But Gifford (1974) showed that Hanna's (1973) simple model for CO in Los Angeles could be considerably improved in this respect if regional average wind speeds were used for each receptor, instead of local wind speeds. He argues that the local wind speed is often unrepresentative because of poor instrument location.

The Regional Air Pollution Study (RAPS, Pooler, 1974) will provide high quality air pollution concentration data for further testing and development of urban diffusion models. The St. Louis urban area was chosen as the site for this study. It is planned that the various aspects of the study will be performed in the best way possible, resulting in a significant increase in our knowledge of urban diffusion. For example, very detailed and comprehensive emissions data and models are being compiled. The atmospheric transformation of oxides of sulfur and the dynamics of aerosol formation are being studied. The effects of the urban surface on the overlying air structure will be elucidated. The greatest effort, however, has gone into the design and construction of the Regional Air Monitoring Station (RAMS) network, which consists of 25 fixed stations under the control of a central computer. At every station, CO, NO, $NO_2$, $O_3$, total hydrocarbon, total sulfur and dew point are being measured. In addition, $SO_2$ and total gaseous sulfur are being measured at 13 of the stations. Turbulence, vertical temperature gradient, solar radiation, and suspended particle data are obtained at a few of the stations. The basic sampling interval is one minute. During special purpose expeditionary studies, mobile measurements will also be made.

Using this unified approach and with the cooperation of all persons and measuring instruments, it is planned that by June, 1977, the primary models will be developed and validated. Everyone hopes that the experiment will be a success, since never before has such a comprehensive study of urban diffusion been carried out. At least, when the RAPS project is completed, we should have a better idea of the quantitive aspects of urban diffusion problems,even if we do not have foolproof models.

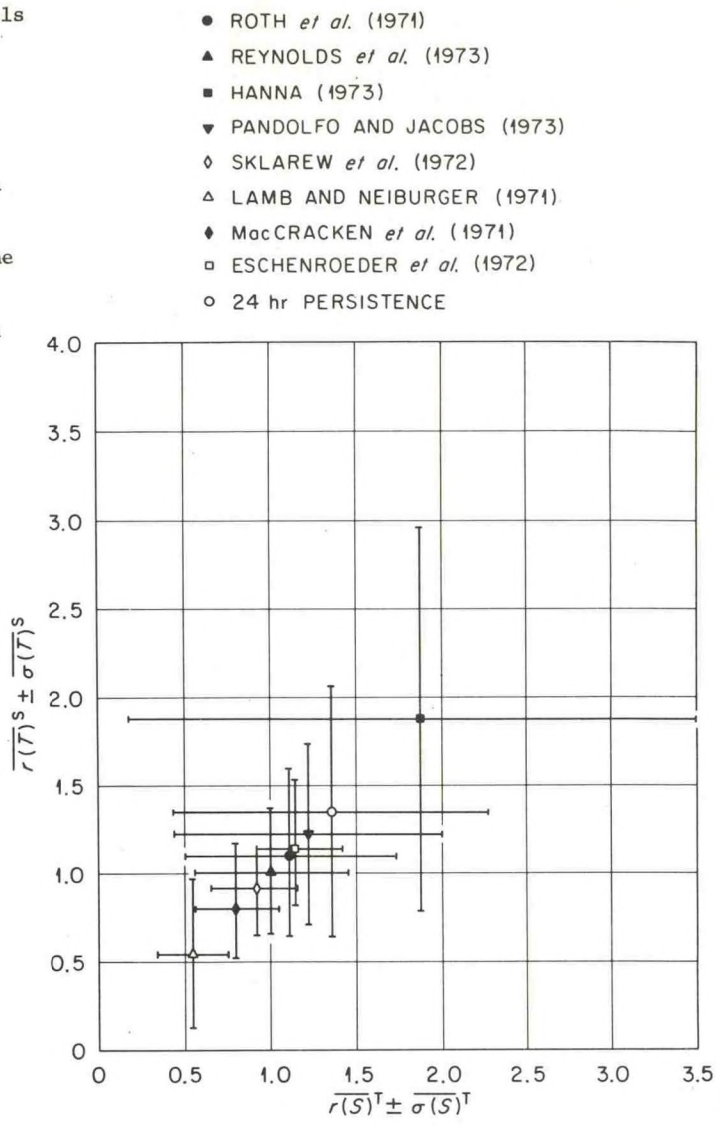


Figure 4. Average result for each model tested. r is the ratio of predicted to observed concentrations. σ is the standard deviation of r. S is space and T is time. (Nappo, 1974).

Acknowledgements: The review of models for predicting air quality by Dr. Alan Eschenroeder (1975) has been of great help in compiling these notes. This research was performed under an agreement between the National Oceanic and Atmospheric Administration and the Environmental Research and Development Administration.

REFERENCES


Altshuller, A. P., and P. Bufalini, 1971: Photochemical aspects of air pollution: A review. Env. Sci. and Tech., 5, 39-63.

Angell, J. K., C. R. Dickson, and W. H. Hoecker, 1974: Relative Dispersion within the Los Angeles Basin as Estimated from Tetroon Triads. NOAA Tech. Memo. ERL ARL-46, 34 pp.

Angell, J. K., D. H. Pack, L. Machta, C. R. Dickson, and W. H. Hoecker, 1972: Three dimensional air trajectories determined from tetroon flights in the planetary boundary layer of the Los Angeles basin. J. Appl. Meteor., 11, 451-471.

Barth, D. S., 1971: Federal motor vehicle emission goals for CO, HC, and $NO_x$ based on desired air quality levels. J. Air Poll. Cont. Assoc., 20, 519-523.

Bezuglaya, E. Y., 1971: Statistical Determination of Mean and Maximum Values of Pollution Concentration. Leningrad. Glavnaya Geofizicheskaya, Observatoriya, Trudy, No. 254, p. 138-139.

Bowne, N. E., 1969: A simulation model for air pollution over Connecticut. J. Air Poll. Cont. Assoc., 19(8), 570-574.

Briggs, G. A., 1969: Plume Rise, AEC Critical Review Series, TID-25075, 81 pp.

Bruntz, S. M., W. S. Cleveland, B. Kleiner, and J. L. Warner, 1974: The Dependence of Ambient Ozone on Solar Radiation, Wind, Temperature, and Mixing Height. Proc. Symp. on Atmos. Turb. and Diffusion, AMS, Santa Barbara, Cal., Sept. 9-13, pp 125-128.

Calder, K. L., 1971: A Climatological Model for Multiple Source Urban Air Pollution. Proceed. of the Sec. Meeting of the Expert Panel on Air Poll. Modeling, NATO Committee on the Challenges of Modern Society, Paris, pp I-1 to I-33.

Carson, D. J., 1973: Development of a dry inversion-capped convectively unstable boundary layer. Q.J. Roy. Meteorol. Soc., 99, 450-467.

Chaudry, F. H., and J. E. Cermak, 1971: Wind Tunnel Modeling of Flow and Diffusion over an Urban Complex. USAECOM, R and D Tech. Rep. ECOM-C-0423-7.

Clarke, J.F., 1964: A simple diffusion model for calculating point concentrations from multiple sources. J. Air Poll. Control Assoc., 14, 347.

Clarke, J. F., 1969: Nocturnal urban boundary layer over Cincinnati, Ohio. Mon. Wea.Rev. 97, 582-589.

Clarke, R. H., 1970: Observational studies in the atmospheric boundary layer. Quart. J. R. Met. Soc., 96,91-114.

Dabberdt, W. F., F. L. Ludwig, and W. B. Johnson, 1973: Validation and applications of an urban diffusion model for vehicular pollutants. Atmos. Environ., 7, 603-618.

Davidson, B., 1967: A summary of the New York urban air pollution dynamics research program. J. Air Poll. Cont. Assoc., 17, 154-158.

Dickerson, M. H., 1973: A mass-consistent wind field model for the San Francisco bay area. Lawrence Livermore Lab., Univ. of Cal., Livermore, Cal. Presented at the WMO/IAMAP Symposium, Reading, Eng., 14-18 May, 30 pp.

Donaldson, C. du P., and G. R. Hilst, 1972: Effect of inhomogeneous mixing on atmospheric photochemical reactions. Envir. Sci. and Tech., 6, 812-816.

Edinger, J., 1958: The Meteorology of Los Angeles' Polluted Layer. Prepared by Univ. of Cal. Dept. of Meteorol. for Los Angeles Co. Air Poll. Cont. Dist., 22 pp + 119 figs.

Edinger, J. G., 1973: Vertical Distribution of Photochemical Smog in the Los Angeles Basin. Environ. Sci. and Tech., 7 (3), 247-252.

Egan, B. A., and J. R. Mahoney, 1972: Numerical modeling of advection and diffusion of urban area source pollutants. J. Appl. Meteorol., 11 (3), 312-322.

Eschenroeder, A. Q., J. R. Martinez, and R. A. Nordsieck, 1972: Evaluation of a Diffusion Model for Photochemical Smog Simulation, Final Rept. Cont. No. 68-02-0336 by Gen. Res. Corp., P. O. Box 3587, Santa Barbara, Cal. 93105, for Env. Prot. Agency, 212 pp.

Eschenroeder, A., 1975: Models for Predicting Air Quality. 121 pp. To be published by EPA.

Fortak, H., 1970: Numerical simulation of the temporal and spatial distribution of urban air pollution concentration. Proceedings of Symp. on Multiple-Source Urban Diffusion Models, A. Stern, ed. U.S. EPA Publ. No. AP-86, Ch. 9.

Frenkiel, F. N., 1957: Atmospheric pollution in growing communities. Smithsonian Institute Report for 1956, 269-299.

Friedlander, S. K., and J. H. Seinfeld, 1969: A dynamic model of photochemical smog. Environ. Res. and Tech., 3, 1175-1180.

Gifford, F. A., 1959: Computation of pollution from several sources. Int. J. Air Pollut., 2, 109-110.

Gifford, F. A., 1968: An outline of theories of diffusion in the lower layers of the atmosphere. Ch. 3 in Meteorology and Atomic Energy - 1968. TID-24190, USAEC Tech. Inf. Center, Oak Ridge, TN, pp 66-116.

Gifford, F. A., 1970: Atmospheric Diffusion in an Urban Area. Presented at 2nd IRPA Conf. in Brighton, England, 5 pp.

Gifford, F. A., 1973: The simple ATDL urban diffusion model. Proceedings of the Fourth Meeting of the NATO/CCMS Expert Panel on Air Pollution Modeling, Paris, France, Oct. 2-3, 1972. Ch. XVI.

Gifford, F. A., 1974: Further Comparison of Urban Air Pollution Models. Proceedings of the Fifth Meeting of NATO/CCMS Expert Panel on Air Pollution Modeling, Roskilde, Denmark, 8 pp. June 4-6.

Gifford, F. A., 1975: Turbulent diffusion typing schemes: A review. To be published in Nuclear Safety.

Gifford, F. A., and S. R. Hanna, 1970: Urban Air Pollution Modeling, presented at 1970 Meeting of the Int. Union of Air Poll. Prev. Assoc., Washington, 17 pp, Dec. 11. Proceedings published by Nat. Air Poll. Cont. Assoc.

Gifford, F. A., and S. R. Hanna, 1973: Modeling urban air pollution. Atmos. Environ., 7, 131-136.

Graham, I. R., 1968: Analysis of turbulence statistics at Ft. Wayne, Indiana. J. Appl. Meteorol., 7, 90-93.

Hanna, S. R., 1969: Urban micrometeorology. Trans. Am. Nucl. Soc., 12, 815.

Hanna, S. R., 1971: A simple method of calculating dispersion from urban area sources. J. Air Poll. Control Assoc., 21, 774-777.

Hanna, S. R., 1973: Simple dispersion model for the analysis of chemically reactive pollutants. Atmos. Environ., 7, 803-817.

Hanna, S. R., 1973: Description of ATDL Computer Model for Dispersion from Multiple Sources. Industrial Air Pollution Control, Ann Arbor Science, Ann Arbor, Mich., 23-32.

Hanna, S. R., 1975: Modeling smog along the Los Angeles - Palm Springs trajectory. Presented at Am. Chem. Soc. Meeting, Philadelphia, April 7, to be published in Advances in Environ. Sci. and Tech., I. Suffett, Ed., John Wiley & Sons, New York.

Hecht, T. A., 1973: Generalized Mechanism for Describing Atmospheric Photochemical Reactions, App. B of Urban Air Shed Photochemical Simulation Model Study, Cont. No. 68-02-0339, by Systems Appl., Inc., Beverly Hills, Cal. 90212, for Environ. Prot. Agency, 79 pp, July 1973.

Hecht, T. A., J. H. Seinfeld, M. C. Dodge, 1974: Further Development of Generalized Kinetic Mechanism for Photochemical Smog. Environ. Sci. and Tech., 8 (4), 327-339, April 1974.

Hilst, G. R., C. du P. Donaldson, M. Teske, R. Contiliano, and J. Freiberg, 1973: A Coupled 2-D Diffusion and Chemistry Model. EPA Cont. Report EPA-R4-B-73-016c.

Holzworth, G., 1972: Mixing depths, wind speed, and potential for urban air pollution throughout the contiguous United States. Environ. Prot. Agency Pub. No. AP-101, 118 pp.

Hoffert, M. I., W. G. Hoydysh, S. Hameed, and S. A. Lebedeff, 1975: Laboratory simulation of photochemically reacting atmospheric boundary layers: A feasibility study. Atmos. Environ., 9 (1), 33-48.

Islitzer, N., and D. Slade, 1968: Diffusion and Transport Experiments, in Meteorology and Atomic Energy 1968, D. Slade, Ed., USAEC Rep. No. TID-24190, 117-188.

Johnson, W. B., R. J. Allen, and W. E. Evans, 1973: Lidar Studies of Stack Plumes in Rural and Urban Environments, PB 227-347, by Stanford Res. Inst., Menlo Park, Cal., for Environ. Prot. Agency, 65 pp. + append.

Johnson, W. B., F. L. Ludwig, A. E. Moon, 1970: Development of a Practical, Multipurpose Urban Diffusion Model for Carbon Monoxide, in Proc. Symp. on Multi-Source Urban Diffusion Models, USEPA Publ. No. AP-86.

Knox, J. B., 1974: Numerical modelling of the transport, diffusion, and deposition of pollutants for regions and extended scales. J. Air Poll. Control Assoc., 24 (7), 660-664.

Koch, R. L., and S. D. Thayer, 1971: Validation and Sensitivity Analysis of the Gaussian Plume Multiple-Source Urban Diffusion Model. Geomet Report No. EF-60.

Lamb, D. V., F. I. Badgley, and A. T. Rossano, Jr., 1973: A Critical Review of Mathematical Diffusion Modeling Techniques for Air Quality with Relation to Motor Vehicle Transportation. Washington State Highway Dept. Research Report 12.1, Research Proj. Y-1540, Univ. of Wash., Seattle.

Lamb, R. G., and M. Neiberger, 1969: An interim version of a generalized urban air pollution model. Atmos. Environ., 5, 239-264.

Leahey, D. M., 1975: An application of a simple advective pollution model to the city of Edmonton. Atmos. Environ., 9,

Leahey, D. M., and J. P. Friend, 1971: A model for predicting the depth of the mixing layer over an urban heat island with application to New York City. J. Appl. Meteorol., 10, 1162-1173.

Lebedeff and Hameed, 1975: Steady-state solution of the semi-empirical equation for area sources. J. Appl. Meteorol, 14, 546-549.

Lettau, H., 1970: Physical and Meteorological Basis for Mathematical Models of Urban Diffusion. Proc. of Symp. on Multiple-Source Urban Diffusion Models, U.S. EPA, APCO Publ. No. AP 86.

Ludwig, F. L., and J. H. Keoloha, 1974: Present and Prospective San Francisco Bay Area Air Quality, SRI project 3274 Final Report, by Stanford Research Inst., Menlo Park, Cal. 94025, for Wallace, McHarg, Roberts, and Todd and Metropolitan Transportation Comm., 110 p.

McCollister, G. M., and K. R. Wilson, 1975: Linear stochastic models for forecasting daily maxima and hourly concentrations of air pollutants, to be published in Atmos. Environ.

MacCracken, M. C., T. V. Crawford, K. R. Peterson, and J. B. Knox, 1971: Development of a Multi-Box Air Pollution Model and Initial Verification for the San Francisco Bay Area. Lawrence Rad. Lab. No. UCRL-73348, Livermore, Cal.

McElroy, J. L., 1969: A comparative study of urban and rural dispersion, J. Appl. Meteorol., 8 (1), 19-31.

McElroy, J. L., 1971: An experimental and numerical investigation of the nocturnal heat island over Columbus, Ohio. Ph.D. Thesis, Dept. of Meteorol., Penn. State Univ.

Marsh, K. J., and M. D. Foster, 1967: An experimental study of the dispersion of the emissions from chimneys in Reading - I. Atmos. Environ., 1, 527-550.

Marsh, K. J., and V. R. Withers, 1969: An experimental study of the dispersion of the emissions from chimneys in Reading - III: The investigation of dispersion calculations. Atmos. Environ., 3, 281.

Martin, D. O., and J. A. Tikvart, 1968: A general atmospheric diffusion model for estimating the effects on air quality of one or more sources. Air Poll. Control Assoc. Paper 68-148.

Miller, M. and G. Holzworth, 1967: An atmospheric diffusion model for metropolitan areas. J. Air Poll. Control Assoc., 17, 46.

Nappo, C. J., 1974: A method for evaluating the accuracy of air pollution prediction models. Proceedings of the Symposium on Atmospheric Diffusion and Air Pollution, held Sept. 9-13, 1974 in Santa Barbara, Cal. Am. Meteorol. Soc., 325-329.

O'Brien, E. C., 1971: Turbulent mixing of two rapidly reacting chemical species. Phys. Fluids, 14, 1326-1331.

Pandolfo, J. P. and C. A. Jacobs, 1973: Tests of an Urban Meteorological Pollutant Model using CO Validation Data in the Los Angeles Metropolitan Area, Vol. I, CEM Report 490a, Cont. No. 68-02-0223 by The Center for the Environment and Man, Inc., 275 Windsor St., Hartford, Conn. 06120, prepared for U.S. EPA, 176 pp.

Pasquill, F., 1962: Atmospheric Diffusion, D. van Nostrand Co. Ltd., London. 297 pp.

Pasquill, F., 1968: Some outstanding issues in the theory and practice of estimating diffusion from sources, Sandia Laboratories, Symposium on the Theory and Measurement of Atmospheric Turbulence and Diffusion in the Planetary Boundary Layer, pp. 17-30.

Pasquill, F., 1974: Atmospheric Diffusion, 2nd ed., John Wiley & Sons, New York, 429 pp.

Peterson, J., 1969: The Climate of Cities: A Survey of Recent Literature, U.S. Dept. of Health, Educ., and Welfare, Pub. Health Ser., Pub. No. AP-59, Raleigh, N.C., 48 pp.

Peterson, J. T., 1970: Distribution of sulfur dioxide over metropolitan St. Louis, as described by empirical eigenvectors and its relation to meteorological parameters. Atmos. Environ., 4, 501.

Pooler, F., 1961: A prediction model of mean urban pollution for use with standard wind roses. Int. J. of Air and Water Poll., 4, 199-211.

Pooler, F., 1974: The St. Louis regional air pollution study: A coherent effort toward improved air quality simulation models. Presented at Summer Computer Simulation Conf., Houston, July 9, Available from EPA, Research Triangle Park, N.C., 27711, 20 pp.

Precipitation Scavenging, 1970: R. J. Engelmann and W. G. N. Slinn (coordinators), Richland, Wash., June 2, AEC Symposium Series, No. 22 (CONF-700601).

Reynolds, S. D., and P. M. Roth, 1973: Mathematical modelling of photochemical air pollution, Pt. 1 Formulation of the model. Atmos. Environ., 7, 1033-1061.

Reynolds, S. D., M. K. Lin, T. A. Hecht, P. M. Roth, and J. H. Seinfeld, 1974: Mathematical modelling of photochemical air pollution, Part 3, Evaluation of the model. Atmos. Environ., 8, 563-596.

Roberts, J. J., E. J. Croke, A. S. Kennedy, J. E. Norco, and L. A. Conley, 1970: A Multiple Source Urban Atmospheric Dispersion Model, Report ANL/ES-CC-007, Argonne Nat. Lab., 9700 S. Cass Ave., Argonne, Ill. 148 pp.

Roth, P. M., S. D. Reynolds, P. J. Roberts, and J. H. Seinfeld, 1971: Development of a Simulation Model for Estimating Ground Level Concentrations of Photochemical Pollutants. Final Report, Cont. No. CPA 70-148 by Systems Appl. Inc., Beverly Hills, Cal. 90212 for eht Environ. Prot. Agency, 55 pp + 6 Appen.

Roth, P. M. P. J. Roberts, M. K. Liu, S. D. Reynolds, and J. H. Seinfeld, 1974: Mathematical modelling of photochemical air pollution, Pt. 2, A model and inventory of pollutant emissions. Atmos. Environ., 8, 97-130.

Sklarew, R. C., A. J. Fabrick, and J. E. Proger, 1972: Mathematical modeling of photochemical smog using the PICK method. J. Air Poll. Control Assoc., 22 (11), 865-869

Sklarew, R. C., 1975: Air Quality Simulation Models for Photochemical Pollutants. Air Pollution, A. C. Stern, Ed., John Wiley and Sons, New York, Ch. VI, (to be published).

Smith, F. B. and G. H. Jeffrey, 1973: The prediction of high concentrations of sulfur dioxide in London and Manchester air. Air Pollution: Proceedings of the Third Meeting of the Expert Panel on Air Pollution Modelling, NATO/CCMS N. 14, pp. XVIII - 1 to 6.

Smith, F. B., 1973: A scheme for estimating the vertical dispersion of a plume from a source near ground level. Air Pollution: Proceedings of the Third Meeting of the Expert Panel on Air Pollution Modelling, NATO/CCMS N. 14, pp XVII - 1 to 14.

Smith, M. E. (ed.) 1968: Recommended Guide for the Prediction of the Dispersion of Airborne Effluents, ASME, 85 pp.

Start, G. E., and L. L. Wendell, 1974: Regional effluent dispersion calculations considering spatial and temporal meteorological variation. NOAA Tech. Memo ERL ARL-44, Air Resources Lab., Idaho Falls, Idaho, 63 pp.

Stasiuk, W. N. and P. E. Coffey, 1974: Rural and urban ozone relationships in New York State. J. Air Poll. Control Assoc., 24, 564-568.

Summers, P., 1965: An urban heat island model. Its role in air pollution problems with application to Montreal. Presented at First Canadian Conf. on Micrometeorology, Toronto, April 12-14.

Turner, D. B., 1964: A diffusion model for an urban area. J. Appl. Meteorol., 3, 83-91.

Turner, D. B., J. R. Zimmerman, A. D. Busse, 1972: An Evaluation of Some Climatological Dispersion Models, Proceed. of the Third Meeting of the Expert Panel on Air Poll. Modeling, NATO Committee on the Challenges of Modern Society, Paris, pp. VIII-1 to V111-25.

U.S. DHEW, 1968-1969: Reports for Consultation (separate reports were published covering each of the major cities in the U.S.) U.S. DHEW, PHS, Nat. Air Poll. Cont. Admin.

Van der Hoven, I., 1968: Deposition of particles and gases. In Meteorology and Atomic Energy 1968, D. Slade, Ed., USAEC Rep. No. TID-24190, 202-208.

Wayne, L., R. Danchick, M. Weisburd, A. Kokin, and A. Stein, 1971: Modeling photochemical smog on a computer for decision making. J. Air Poll. Control Assoc., 21(6), 334-339.

Wayne, L. G., A. Kokin, M. I. Weisburd, 1973: Controlled Evaluation of the Reactive Environmental Simulation Model (REM), Pac. Envir. Services, Inc. (EPA R4-73-013a).

Reprinted from JOURNAL OF APPLIED METEOROLOGY, Vol. 15, No. 6, June 1976
American Meteorological Society
Printed in U. S. A.

# Relative Diffusion of Tetroon Pairs During Convective Conditions

STEVEN R. HANNA

ATDL Contribution File No. 75/9

# Relative Diffusion of Tetroon Pairs During Convective Conditions[1]

STEVEN R. HANNA

*Atmospheric Turbulence & Diffusion Laboratory, NOAA, Oak Ridge, Tenn. 37830*

(Manuscript received 25 August 1975, in revised form 15 April 1976)

ABSTRACT

Observations of the relative diffusion of 13 sets of tetroon pairs in the mixed layer during convective conditions in eastern Tennessee are reported. The root-mean-square separation $S$ is proportional to time $t$ raised to a power of 1 for times from 2 to 30 min and a power of 0.75 for times from 30 to 100 min. On the average, the observations are satisfied by the approximation $dS/dt \approx \sigma_v$, where $\sigma_v$ is the standard deviation of the lateral wind speed fluctuations, as sensed by the tetroon.

## 1. Introduction

Observations of mesoscale or regional diffusion are currently important because of our need to make estimates of the environmental impact of various effluents at these scales. The data studied here cover distances from 100 m to 50 km and times from 2 min to 2 h. The observational technique has been developed and applied several times in the past (e.g., Angell *et al.*, 1971, 1974). Two tetroons are released simultaneously and their transponders are tracked by an M-33 radar system. The relative speeds and separations of the balloons are then analyzed, and the results compared with the results of similar experiments in other locations, and with the predictions of theories developed to explain relative diffusion.

## 2. Experimental technique

The relative diffusion experiment is a small part of a comprehensive transport and diffusion experiment called the Eastern Tennessee Trajectory Experiment (ETTEX), conducted during July and August of 1974. The comprehensive experiment, described by Hanna *et al.* (1974), had as its major goal the evaluation of transport models applied to hilly eastern Tennessee terrain. Nappo (1975) discusses preliminary results in which an observed tetroon trajectory compares favorably with a trajectory calculated using an interpolated wind field from a pibal grid. As another part of ETTEX the fluctuations of pollutant concentration and turbulence in the $SO_2$ plume from TVA's Bull Run steam plant were measured. The plume experiment was prompted by a theory developed by Briggs (1975) for estimating ground level pollutant concentration during fumigation conditions on convective afternoons, when subsiding air motions between thermals bring the plume to the ground. Most of the $SO_2$ plume experiments coincided with the relative diffusion experiments described here.

The M-33 radar used for tracking the tetroons was set up at the top of Buffalo Mountain (1030 m MSL), the second highest peak in the Cumberland Mountains. The location of the radar is shown in Fig. 1. In the relative diffusion experiments, instantaneous readings of tetroon range, elevation angle and azimuth angle were taken at the radar console every 2 min for each tetroon.

Tetroons were released from either the ATDL building or the Bull Run steam plant, depending on whether an $SO_2$ plume experiment was also taking place. These locations are marked on the map in Fig. 1. The two tetroons were inflated so they would fly at the same predetermined level, based on radiosonde observations of the vertical temperature profile. The techniques recommended by Hoecker (1975) were used to determine the necessary amount of inflation. It was planned that the tetroons would fly within the afternoon mixing layer, at heights between about 500 and 1500 m above the ground. Lower flights were not practical because of the presence of 200 m high linear ridges in the Tennessee valley which would interfere with the transponder signal.

The transponders were tuned to slightly different frequencies so that the radar could tell the difference between the two tetroons. Errors in recorded tetroon position are due mainly to the inherent inaccuracy of the radar and to observer errors (Van der Hoven, 1968). We estimate that the expected error in the indicated tetroon position is about 20 m.

Radiosonde observations of vertical profiles of wet and dry bulb temperature were taken during most of

[1] Presented at the First AMS Conference on Regional and Mesoscale Modeling, Analysis and Prediction, Las Vegas, Nev., 6–9 May 1975.

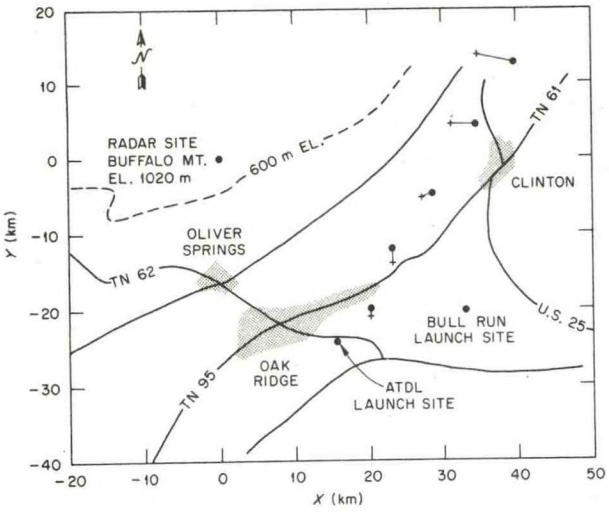


FIG. 1. Map of experiment area, showing radar and launch sites. The separations of tetroons 7293 and 7294 are shown, where the time interval between plotted separations is 15 min. Launch was from the ATDL site.

the experiments. Vertical wind profiles were obtained from either single or double theodolite pibal runs. When an $SO_2$ plume experiment was also taking place, vertical profiles of temperature, eddy dissipation rate, and $SO_2$ concentration were obtained from aircraft flights. All of the experiments took place during midday.

## 3. Observations

Some general characteristics of the data are summarized in Table 1. The month and day are given in the first three digits of the tetroon number. Potential temperature gradient $\partial\theta/\partial z$ is determined by analyzing the radiosonde and aircraft flights. Vertical shear of wind speed, $\partial V/\partial z$, and direction, $\partial\alpha/\partial z$, are obtained from pilot balloon observations, averaged over the layer in which the tetroon flew. Eddy dissipation rate $\epsilon$ is measured by an MRI universal turbulence indicator on the aircraft.

Mixing height $h$ is estimated as the average height at which discontinuities in temperature lapse rate, eddy dissipation, $SO_2$ and haze occur. The average tetroon height and mixing height refer to height above ground level at the launch sites (250 m MSL).

After about 10 min, the tetroons generally reached their equilibrium height, which ranged from 320 to 1220 m above ground for the 26 tetroons. The standard deviation of the vertical tetroon position about the average height ranged from 60 to 430 m. Some tetroons bobbed up and down in convective eddies from nearly ground level to heights of 2000 m during their flight. Due to the buoyant restoring force on the tetroon during such wide excursions, it is not possible for the tetroon to follow the vertical air motions faithfully (Hanna and Hoecker, 1971). For this reason the statistical analysis of vertical motions is not carried very far. The

TABLE 1. General characteristics of tetroon flights.

| Tetroon no. | Starting time (EDT) | Duration (min) | Average height $\bar{Z}$ (m) | $\sigma_z$ (m) | Average speed $\bar{V}$ (m s$^{-1}$) | Average direction | $\sigma_w$ (m s$^{-1}$) | $\partial\theta/\partial z$ (°C m$^{-1}$) | $\epsilon$ (cm$^2$ s$^{-3}$) | $\partial V/\partial z$ (s$^{-1}$) | $\partial\alpha/\partial z$ (deg m$^{-1}$) | Mixing height (m) |
|---|---|---|---|---|---|---|---|---|---|---|---|---|
| 7221 | 1015 | 117 | 320 | 70 | 2.1 | SW | 0.24 | — | — | — | — | — |
| 7222 | 1015 | 117 | 370 | 120 | 1.9 | SW | 0.31 | — | — | — | — | — |
| 7223 | 1303 | 120 | 340 | 120 | 3.3 | WSW | 0.59 | — | — | — | — | — |
| 7224 | 1305 | 120 | 530 | 210 | 3.6 | WSW | 0.56 | — | — | — | — | — |
| 7253 | 1620 | 56 | 660 | 180 | 2.9 | SSW | 0.59 | $4\times10^{-4}$ | 15 | 0 | 0 | 1200 |
| 7254 | 1620 | 56 | 720 | 130 | 2.5 | SSW | 0.48 | $4\times10^{-4}$ | 15 | 0 | 0 | 1200 |
| 7271 | 1208 | 126 | 890 | 250 | 1.8 | NE | 0.45 | $2\times10^{-4}$ | 20 | 0 | 0 | 3000 |
| 7272 | 1208 | 126 | 740 | 150 | 1.4 | ENE | 0.45 | $2\times10^{-4}$ | 20 | 0 | 0 | 3000 |
| 7273 | 1428 | 94 | 730 | 420 | 2.3 | NE | 0.54 | $2\times10^{-4}$ | 20 | 0 | −0.1 | 3000 |
| 7274 | 1428 | 94 | 510 | 250 | 1.4 | NE | 0.39 | $2\times10^{-4}$ | 20 | 0 | −0.1 | 3000 |
| 7291 | 1201 | 102 | 380 | 80 | 3.3 | SSW | 0.24 | — | — | 0.007 | 0.1 | 3000 |
| 7292 | 1201 | 102 | 400 | 80 | 3.2 | SSW | 0.31 | — | — | 0.007 | 0.1 | — |
| 7293 | 1401 | 82 | 420 | 160 | 4.9 | SSW | 0.42 | — | — | 0.006 | 0 | — |
| 7294 | 1401 | 82 | 410 | 110 | 4.7 | SSW | 0.32 | — | — | 0.006 | 0 | — |
| 7301 | 1109 | 100 | 770 | 370 | 2.5 | NNW | 0.26 | 0 | — | 0.005 | 0 | 1600 |
| 7302 | 1109 | 100 | 710 | 240 | 2.2 | NNW | 0.35 | 0 | — | 0.005 | 0 | 1600 |
| 7303 | 1320 | 70 | 820 | 430 | 1.1 | NE | 1.0 | 0 | — | 0 | 0 | 1600 |
| 7304 | 1320 | 70 | 480 | 60 | 0.88 | NNE | 0.41 | 0 | — | 0 | 0 | 1600 |
| 7311 | 1307 | 92 | 650 | 380 | 2.2 | NE | 1.2 | 0 | 60 | 0 | 0.06 | 2200 |
| 7312 | 1307 | 92 | 660 | 270 | 2.0 | NE | 0.82 | 0 | 60 | 0 | 0.06 | 2200 |
| 7313 | 1511 | 108 | 950 | 350 | 1.0 | E | 0.75 | 0 | 40 | 0 | 0 | 2200 |
| 7314 | 1511 | 108 | 720 | 290 | 1.2 | ENE | 0.73 | 0 | 40 | 0 | 0 | 2200 |
| 8011 | 1258 | 100 | 1220 | 320 | 0.77 | E | 0.63 | $10^{-4}$ | 25 | 0 | 0 | 2200 |
| 8012 | 1258 | 100 | 520 | 100 | 0.60 | ESE | 0.63 | $10^{-4}$ | 25 | 0 | 0 | 2200 |
| 8021 | 1311 | 100 | 670 | 86 | 3.8 | SW | 0.35 | $10^{-4}$ | 40 | 0 | 0 | 1000 |
| 8023 | 1311 | 100 | 480 | 152 | 3.4 | SW | 0.31 | $10^{-4}$ | 40 | 0 | 0 | 1000 |

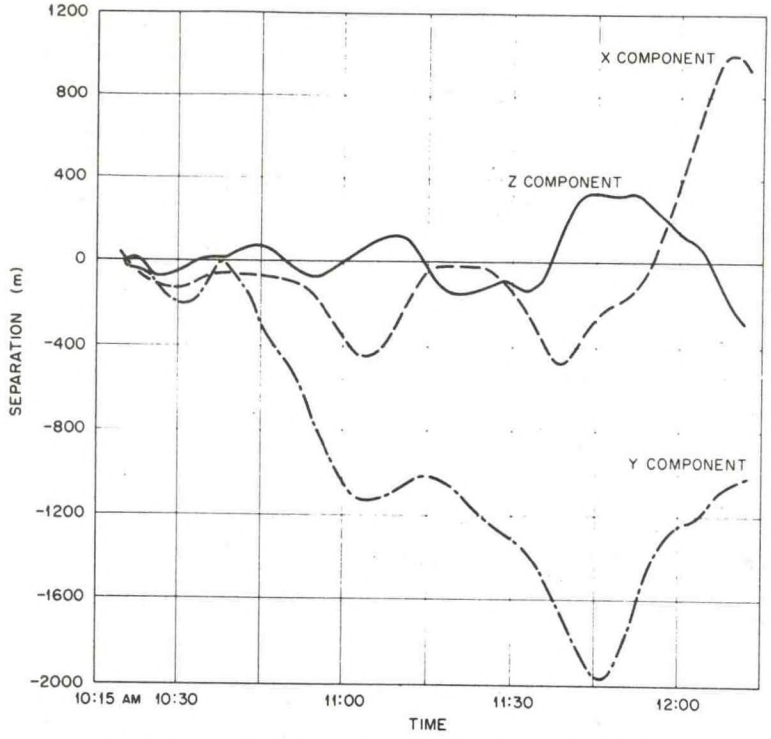


FIG. 2. Components of separation for tetroons 7221 and 7222.

average turbulence intensity $\bar{\sigma}_w/\bar{V}$ of 0.23 indicates a great deal of turbulent convection. The turbulent speed $\sigma_w$ is not significantly correlated with wind speed, a condition known to be typical of sunny days, when turbulence production is due more to convection than to wind shear. The standard deviations of the turbulent fluctuations of longitudinal or alongwind speed, $\sigma_u$, and latitudinal or crosswind speed, $\sigma_v$, are also calculated. The average values of the ratios $\sigma_v/\sigma_w$ and $\sigma_u/\sigma_w$ are 1.3 and 1.9, in rough agreement with values of these ratios reported by Lumley and Panofsky (1964), based on many other independent sets of data.

Wind velocities in Table 1 generally have a SW or NE component, corresponding to the alignment of the ridges and valleys in eastern Tennessee. Average speed of the tetroons is 2.3 m $s^{-1}$, typical of light-wind summertime conditions in this area. Since all of the runs in Table 1 occur during similar climatic regimes, averages of parameters over all the runs can be confidently made.

## 4. Relative separation of tetroons

As an example of the results, the three components (latitudinal or cross-wind, longitudinal or along-wind, vertical) of tetroon separation for tetroons 7221 and 7222 are plotted as a function of time in Fig. 2. The along-wind direction is defined by the line connecting the tetroon launch position with the averaged position of the tetroons at the time the experiment is concluded. Oscillations with periods of 10–40 min are evident, in agreement with typical periods of convective elements. Clearly there is too much variability in this individual run to permit general conclusions regarding dispersion.

When the 13 runs are averaged together, this variability nearly disappears. For example, the rms total separation is plotted in Fig. 3. At times from 2 min through about 30 min the separation is proportional to time. At times from 30 min to 90 min, the separation $S$ is proportional to time raised to a power somewhat less

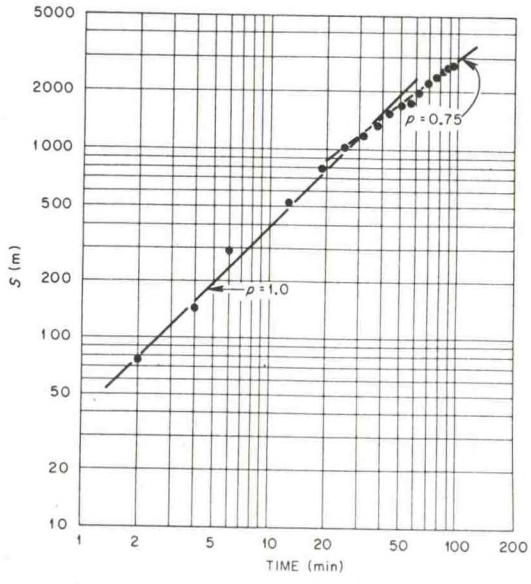


FIG. 3. Root-mean-square total separation $S$ as a function of time.

than 1. From Fig. 3 it is seen that the average rate of separation $dS/dt$ is roughly 0.5–0.7 m s$^{-1}$. Since the average value of $\sigma_v$ for the 13 runs is 0.6 m s$^{-1}$, these observations are roughly satisfied by the relation $dS/dt \approx \sigma_v$.

The rate of change of total separation $S$ with time for these data and for observations from others of the relative dispersion of tetroon pairs are plotted on Fig. 4. The power $p$ for each set of observations is close to unity ($p=1\pm0.3$). It is seen that the magnitude of the separation $S$ during ETTEX is slightly greater than the average magnitude of the separations during several experiments summarized by Islitzer and Slade (1968). This is expected, though, because our experiments were all conducted during highly dispersive summer days. However the dispersion of the tetroons released from Las Vegas (Angell *et al.*, 1971) is greater than the dispersion during ETTEX, presumably due to the greater dispersive power of the atmosphere over rugged desert terrain.

When observations of the relative dispersion of smoke puffs (e.g., Bauer, 1974) are studied, it is found that their cross-wind spread at small times is often proportional to time raised to the 1.5 power (Gifford, 1957). This power is predicted by Batchelor and Townsend's (1956) similarity theory for relative diffusion at length scales within the inertial subrange of atmospheric turbulence. But as Brier (1950) suggests, observed tetroon separations may not agree with the theoretical dependence of separation on time raised to the 1.5 power, because of the inability of the tetroons to respond to small-scale fluctuations in air motion. The small particles used in the smoke puff experiments respond well to all of the fluctuations in air motion that they encounter.

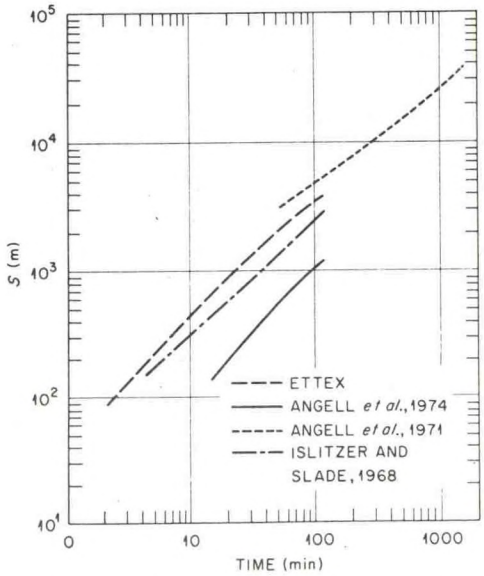


FIG. 4. Comparison of ETTEX root-mean-square total separations $S$ with the results of other experiments.

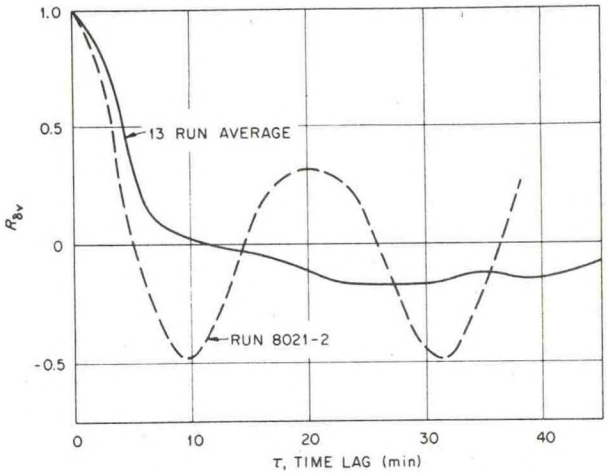


FIG. 5. Correlation coefficient $R_{\delta v}$ for the cross-wind component of the relative wind speeds.

At large times, when large scales of turbulence can take part in dispersion, the separation can be estimated from the relation

$$S=2(Kt)^{\frac{1}{2}}, \tag{1}$$

where $K$ is the eddy diffusivity coefficient (Pasquill, 1974). This formula, however, is valid only at times much greater than the period at which peak energy occurs in the cross-wind turbulent velocity spectrum. It is seen in Fig. 2 that, during the highly convective conditions of ETTEX, significant turbulent fluctuations occur even at periods of 40 min. Consequently it is doubtful that the time regime during which Eq. (1) is valid is included in our observations.

## 5. Test of the statistical theory of diffusion

According to the statistical theory of relative diffusion, as reviewed by Pasquill (1974), the cross-wind separation $Y$ of two diffusing tetroons is given by

$$\overline{Y^2}=\overline{Y_0^2}+2\sigma_{\delta v}^2\int_0^T\int_0^{t'}R_{\delta v}(\tau)d\tau dt', \tag{2}$$

where $\delta v(t)$ is the relative velocity of the balloons at time $t$ after release, $\sigma_{\delta v}^2$ is the variance of the relative velocity fluctuations, and $R_{\delta v}(t)$ is the correlation coefficient of the relative velocities at time lag $\tau$, i.e.,

$$R_v(\tau)=\overline{\delta v(t)\delta v(t+\tau)}/\sigma_{\delta v}^2. \tag{3}$$

Eq. (2) predicts that the rms separation $(\overline{Y^2})^{\frac{1}{2}}$ is proportional to time, as observed in our experiments, only when the correlation coefficient $R$ is a constant. This can be seen by integrating (2) for $R$ equal to a constant $C$:

$$\overline{Y^2}=\overline{Y_0^2}+\sigma_{\delta v}^2CT^2. \tag{4}$$

In order to determine if $R$ is indeed a constant for the ETTEX data, values of $R$ were calculated for all of the data. Fig. 5 presents the average correlation

coefficient $R(t)$ for the cross-wind component $\delta v$ of the relative velocities. The average correlation drops to zero after about 10 min and then remains slightly less than zero. The time scale at which $R=1/e$ is about 5 min. This is slightly less than the time scale of 8 min for the tetroon relative diffusion data taken in Idaho by Kao and Wendell (1968). The 13 individual correlation curves used in obtaining the average curve in Fig. 5 have many oscillations. For example, the curve for the combined tetroon run 8021-2 (randomly chosen for illustrative purposes) is shown in Fig. 5. The shapes of the individual curves are similar to this example for all of the observations, exhibiting parabolic form at small times and then sinusoidal form at large times. At any rate, none of the data suggest that $R$ is positive and nearly constant over a large range of time lag $\tau$, as is required by the statistical theory [Eq. (2)] to produce a linear dependence of the rms separation on time.

A requirement of the statistical theory is that both tetroons should remain within the same atmospheric layer. Pasquill (private communication) suggests that the ETTEX observations may not satisfy this requirement, since the tetroons are subject to such great vertical displacements. At times, one tetroon is near the ground and the other near the top of the planetary boundary layer. Twenty minutes later their positions could be reversed.

## 6. Shear diffusion

Whenever observations of relative diffusion do not agree well with the predictions of similarity or statistical theory, the differences can be blamed on shear diffusion. The tetroons can be separated due to the simple fact that they are flying at different heights and that the wind velocity is different at these heights. Angell *et al.* (1974) explain that much of the erratic behavior of their tetroons in the Los Angeles basin is due to wind shears associated with the sea breeze front. According to Smith's (1965) theory of shear diffusion, the variance of longitudinal separation ($\overline{X^2}$) due to a wind speed shear $\partial V/\partial z$ in unbounded flow is given by

$$\overline{X^2}=0.17(\partial V/\partial z)^2K_z t^3, \tag{5}$$

where $K_z$ is the vertical eddy diffusivity coefficient. Smith (1965) suggests that the eddy diffusivity $K_z$ is equal to $\sigma_w^2 t_{wL}$, where $t_{wL}$ is the Lagrangian integral time scale for the vertical motions. Thus Eq. (5) can be written

$$\overline{X^2}=0.17(\partial V/\partial z)^2\sigma_w^2 t_{wL} t^3. \tag{6}$$

Table 1 contains the observed wind speeds and direction shears, from pibal data, for the vertical layer $\bar{z}\pm\sigma_z$. During over half of the runs, no shear at all was observed in the layer in which the tetroons flew. At heights between 200 and 1200 m, the average wind speed shear for the 13 runs is about 0.005 $s^{-1}$. As an example of the application of the technique, the combined run 7301–2 is considered where the shear $\partial V/\partial z = 0.005\ s^{-1}$. The observed variance $\sigma_w^2$ is 0.1 $m^2\ s^{-2}$ and the Lagrangian integral time scale $t_{wL}$ can be estimated to equal about $10^2$ s. For these values, the variance $\overline{X^2}$ at time $t=30$ min has a value from (6) of about $3\times10^6$ $m^2$, which is close to the observed separation. Thus it is possible for shear diffusion to account for the observed tetroon separations during some of these experiments. However, there is no significant difference between the observed separations of tetroons on days when there is no wind shear and days when there is wind shear. It can be concluded that wind shear probably plays a role in separating the tetroons, but that the extent of this role is uncertain.

*Acknowledgments.* This experiment would have been impossible without the help of C. R. Dickson of the ARL Field Office in Idaho Falls, who provided the M-33 radar unit, a mobile radiosonde unit, and an enormous collection of routine but essential equipment. E. White and D. Forsythe of Idaho Falls were in charge of the radar's operation. W. Hoecker of the ARL office in Silver Spring, Md., offered invaluable aid in launching the tetroons. The Coal Creek Mining and Manufacturing Corporation and the Oliver Springs Mining Company (specifically, C. H. Smith and C. Owens) were very cooperative in helping us select and travel to and from the radar site. T. L. Montgomery and J. H. Coleman of the TVA Air Quality Branch loaned us several crucial pieces of equipment for the aircraft. Much of the data analysis was done by S. Perry, J. Pollock and S. Yeh of this office.

## REFERENCES

Angell, J. K., P. W. Allen and E. A. Jessup, 1971: Mesoscale relative diffusion estimates from tetroon flights. *J. Appl. Meteor.*, **19**, 43–46.

——, C. R. Dickson and W. H. Hoecker, Jr., 1974: Relative dispersion within the Los Angeles basin as estimated from tetroon triads. NOAA Tech. Memo. ERL ARL 46, 34 pp.

Batchelor, G. K., and A. A. Townsend, 1956: *Turbulent Diffusion. Surveys in Mechanics*, G. K. Batchelor and R. M. Davies, Eds., Cambridge University Press, 352–399.

Bauer, E., 1974: Dispersion of tracers in the atmosphere and ocean: Survey and comparison of experimental data. *J. Geophys. Res.*, **79**, 789–795.

Brier, G. W., 1950: The statistical theory of turbulence and the problem of diffusion in the atmosphere. *J. Meteor.*, **7**, 283.

Briggs, G. A., 1975: Plume rise predictions. *Lectures on Air Pollution and Environmental Impact Analyses*, D. Haugen, coordinator, Amer. Meteor. Soc., 59–111.

Gifford, F. A., 1957: Relative atmospheric diffusion of smoke puffs. *J. Meteor.*, **14**, 410–444.

Hanna, S. R., and W. H. Hoecker, Jr., 1971: The response of constant density balloons to sinusoidal variations of vertical wind speeds. *J. Appl. Meteor.*, **10**, 601–604.

——, C. J. Nappo, R. P. Hosker and G. A. Briggs, 1974: Description of the Eastern Tennessee Trajectory Experiment (ETTEX). ATDL Contrib. File. No. 103, 26 pp., [Available from ATDL, P. O. Box E, Oak Ridge, Tenn., 37830].

Hoecker, W. H., Jr., 1975: A universal procedure for deploying constant-volume balloons and for deriving vertical air speeds from them. *J. Appl. Meteor.*, **14**, 1118–1124.

Islitzer, N., and D. Slade, 1968: Diffusion and transport experiments. *Meteorology and Atomic Energy—1968*, D. Slade, Ed., USAEC Rep. No. TID-24190, 117–188.

Kao, S. K., and L. L. Wendell, 1968: Some characteristics of relative particle dispersion in the atmospheric boundary layer. *Atmos. Environ.*, **2**, 397–407.

Lumley, J. L., and H. A. Panofsky, 1964: *The Structure of Atmospheric Turbulence*. Interscience, 239 pp.

Nappo, C. J., 1975: Time-dependent mesoscale wind flows over complex terrain. Presented at the First AMS Conference on Regional and Mesoscale Modeling, Analysis and Prediction, Las Vegas, 6–9 May.

Pasquill, F., 1974: *Atmospheric Diffusion*, 2nd. ed. Wiley, 429 pp.

Smith, F., 1965: The role of wind shear in horizontal diffusion of ambient particles. *Quart. J. Roy. Meteor. Soc.*, **91**, 318–329.

Van der Hoven, 1968: Atmospheric transport and diffusion in the planetary boundary layer. Tech. Memo. ERL TM-ARL 5, 5–14.

# DISPERSION OF SULFUR DIOXIDE EMISSIONS FROM AREA SOURCES

F. A. Gifford

and

S. R. Hanna

Air Resources
Atmospheric Turbulence and Diffusion Laboratory
National Oceanic and Atmospheric Administration
Oak Ridge, Tennessee

Published as Chapter 7 of Section II in Power Generation: Air Pollution Monitoring and Control, Ann Arbor Science Publishers Inc, P. O. Box 1425, Ann Arbor, Mich. 48106, pp. 71-81.

ATDL Contribution File No. 75/10

# POWER GENERATION:

## Air Pollution Monitoring and Control

edited by

Kenneth E. Noll
Professor, Environmental Engineering
Illinois Institute of Technology, Chicago

Wayne T. Davis
Assistant Professor, Environmental Engineering
University of Tennessee, Knoxville

7

# Dispersion of Sulfur Dioxide Emissions from Area Sources

**F. A. Gifford and S. R. Hanna**
Atmospheric Turbulence and Diffusion Laboratory,
National Oceanic and Atmospheric Administration,
Oak Ridge, Tennessee

## INTRODUCTION

This chapter can be used in evaluating surface concentrations of sulfur dioxide emitted generally over an area. The most common example of an area source is provided by urban domestic and industrial heating, for which it is necessary to consider the sum of a large number of individual sources over an area of some convenient size. Given an area-source inventory, this chapter provides a simple, systematic procedure for calculating the surface concentration at any point, averaged over an hour, a day, or a year. The basic physical model of atmospheric diffusion employed is the same as for Chapter 5 on tall-stack emissions.

Area-source concentration calculations are a recent development compared with calculations of concentrations from isolated sources. There are discussions of some of the methods now available, but these all require the use of a high-speed electronic computer.[1] The method to be described, although very simple, has been shown[2] to provide results of a precision comparable with that of the more elaborate computer calculations and can be used with confidence for area-source calculations in urban air pollution and regional air quality studies. An even simpler area-source calculation[3] suitable for many air pollution control purposes is also described. The model is described here in such a way that all the calculations can be done by hand. For the purpose of making many applications of the model, it has also been programmed in Fortran.[4]

## THE AREA-SOURCE GRID

The area source strength data are assumed to be given in the form of a regular "checkerboard" grid pattern. This area-source grid pattern is the usual one in which source information is provided. If the available source strength data are given in some other pattern, for instance by counties or districts, they should be modified to approximate a regular checkerboard pattern by choosing the largest grid-square size that will give an adequate representation of the given data. Squares of 5 x 5 km are fairly standard.

## CALCULATION OF AREA-SOURCE SURFACE CONCENTRATION: ONE-HOUR PERIOD

It is assumed that the concentration is required at the center of a grid square, which is designated square "O." The procedure when the receptor is not centered on a grid square is covered under Correction Factors, below. The calculation requires evaluation of the following simple formula for the area-source concentration, $\chi_A$:

$$u\chi_A = c_oQ_o + c_1Q_1 + c_2Q_2 + c_3Q_3 + c_4Q_4 + c_5Q_5 \qquad (1)$$

The Q's are the given area source strength emissions per unit area per second in a line of source-grid squares centered on the square containing the receptor, *i.e.*, square "O" whose strength equals $Q_o$, and extending *upwind*. The c's are multipliers that depend on the meteorological conditions and the grid size. For a 5 x 5 km grid the multipliers are given in Table 7.1.

**Table 7.1.** Grid Multipliers for Meteorological Dispersion Conditions

| | *Neutral* | *Stable* | *Unstable* |
|---|---|---|---|
| $c_o$: | 153 | 331 | 137 |
| $c_1$: | 48 | 124 | 23 |
| $c_2$: | 28 | 73 | 12 |
| $c_3$: | 20 | 54 | 8.3 |
| $c_4$: | 16 | 44 | 6.7 |
| $c_5$: | 14 | 38 | 5.3 |

The area-source calculation, Equation (1), requires combination of these multipliers with upwind source strengths. Since this may have to be done for a number of receptor points and wind directions, it is convenient to introduce the multipliers by means of a multiplier grid, Figures 7.1–7.3, prepared from Table 7.1.

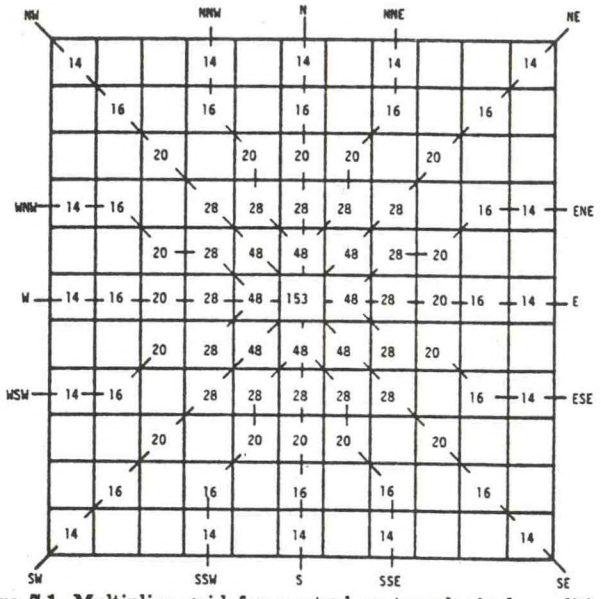


**Figure 7.1.** Multiplier grid for neutral meteorological conditions.

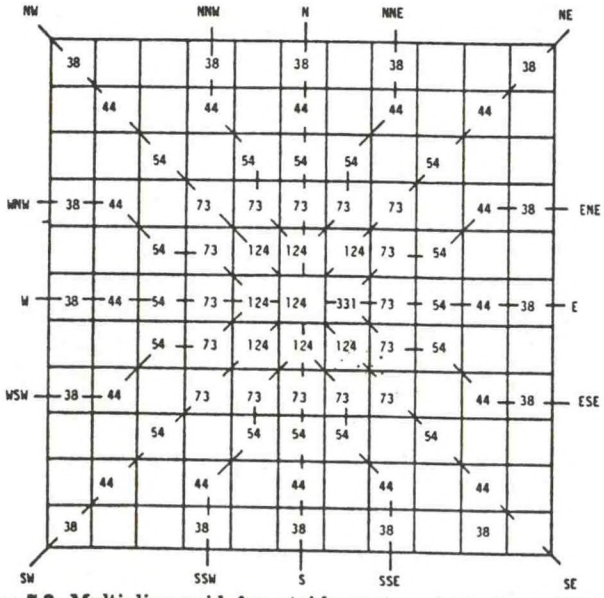


**Figure 7.2.** Multiplier grid for stable meteorological conditions.

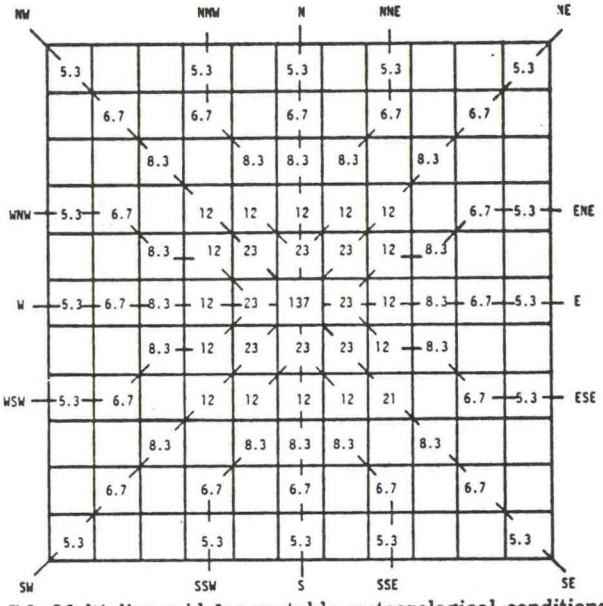


**Figure 7.3.** Multiplier grid for unstable meteorological conditions.

**Step 1** — Plot the area-source strength data at the centers of 1/2-inch squares. This is the "source grid." It is convenient for the following steps to do this on tracing paper or, better, to make a transparency.

**Step 2** — Select the multiplier grid, Figures 7.1, 7.2, or 7.3, appropriate to the given meteorological conditions. Center the source grid over the multiplier grid so that square "O" corresponds to the source grid square that contains the receptor point.

**Step 3** — Six numbers on the multiplier grid, including the central number at square "O," correspond to each wind direction. Multiply these by the six numbers in the corresponding source-grid squares and sum these products.

**Step 4** — Divide the result of Step 3 by the given mean wind speed, u. The result is the required hourly average area-source concentration value.

**Step 5** — Relocate the multiplier grid to a new receptor square and repeat Steps 1 through 5.

## EQUATIONS FOR AREA SOURCE

The equation for surface concentrations from an area source:

$$\chi_A = \left(\frac{2}{\pi}\right)^{1/2} \frac{(\Delta x/2)^{1-q}}{b(1-q)} \left[ Q_o + \sum_{i=1}^{5} Q_i \left[(2i+1)^{1-q} - (2i-1)^{1-q}\right] \right] \quad (2)$$

is based directly, on Equation (2) of Chapter 5; $\Delta x$ is the size of the source-strength grid, and the rest of the terms are defined in the nomenclature. Equation (2) must be multiplied by the frequency $f_d$ of wind from the d direction, to obtain the annual average.

Comparing Equations (1) and (2), it can be seen that the dimensionless multipliers $c_i$, i= 0, 1, . . . are given by:

$$c_o = \left(\frac{2}{\pi}\right)^{1/2} \frac{(\Delta x/2)^{1-q}}{b(1-q)} \quad (3)$$

$$c_1 = \left(\frac{2}{\pi}\right)^{1/2} \frac{(\Delta x/2)^{1-q}\ (3^{1-q}-1)}{b(1-q)} \quad (4)$$

$$c_2 = \left(\frac{2}{\pi}\right)^{1/2} \frac{(\Delta x/2)^{1-q}\ (5^{1-q}-3^{1-q})}{b(1-q)} \quad (5)$$

and so on. The values appearing in Table 7.1 were calculated from these equations.

## CALCULATION OF ANNUAL AVERAGE AREA-SOURCE CONCENTRATION

The procedure is the same as the previous one. The exception is that the annual average wind direction frequency must be included. It is assumed that a standard, 16-point wind direction frequency distribution (wind rose) is available, giving the fraction, $f_d$, of the time the wind blows *from* each direction, d. The average annual wind speed is used and neutral meteorological conditions are assumed to apply. Because the wind rose varies from place to place, it is necessary to calculate a new multiplier grid for each application (each city). The complete procedure is as follows.

**Step 1** — Form an annual average multiplier grid by multiplying each of the values in the hourly average multiplier grid for *neutral meteorological conditions,* Figure 7.1, by the corresponding numbers in the wind direction frequency grid, Figure 7.4, after first summing the $f_d$'s as indicated

in Figure 7.4; $f_1$ is the relative frequency (fraction) of winds from the NNE, $f_2$ that from NE, . . ., $f_{16}$ that from N.

| | | | | | | | | | | |
|---|---|---|---|---|---|---|---|---|---|---|
| $f_{14}$ | | | $f_{15}$ | | $f_{16}$ | | $f_1$ | | | $f_2$ |
| | $f_{14}$ | | $f_{15}$ | | $f_{16}$ | | $f_1$ | | $f_2$ | |
| | | $f_{14}$ | | $f_{15}$ | $f_{16}$ | $f_1$ | | $f_2$ | | |
| $f_{13}$ | $f_{13}$ | | $f_{14}$ | $f_{15}$ | $f_{16}$ | $f_1$ | $f_2$ | | $f_3$ | $f_3$ |
| | | $f_{13}$ | $f_{13}$ | $f_{14}$ | $f_{15}+f_{16}+f_1$ | $f_2$ | $f_3$ | $f_3$ | | |
| $f_{12}$ | $f_{12}$ | $f_{12}$ | $f_{12}$ | $f_{11}+f_{12}+f_{13}$ | 1 | $f_3+f_4+f_5$ | $f_4$ | $f_4$ | $f_4$ | $f_4$ |
| | | $f_{11}$ | $f_{11}$ | $f_{10}$ | $f_7+f_8+f_9$ | $f_6$ | $f_5$ | $f_5$ | | |
| $f_{11}$ | $f_{11}$ | | $f_{10}$ | $f_9$ | $f_8$ | $f_7$ | $f_6$ | | $f_5$ | $f_5$ |
| | | $f_{10}$ | | $f_9$ | $f_8$ | $f_7$ | | $f_6$ | | |
| | $f_{10}$ | | $f_9$ | | $f_9$ | | $f_7$ | | $f_6$ | |
| $f_{10}$ | | | $f_9$ | | $f_8$ | | $f_7$ | | | $f_6$ |

**Figure 7.4.** Wind direction frequency grid.

**Step 2** — Center the source-grid square containing the receptor point over the multiplier grid. It is convenient for this purpose to use a transparent source grid. (If the annual average source strength differs from the short period average value, then of course the annual source strengths must be used.)

**Step 3** — Multiply *all* the number pairs of these two grids, and sum. (Where a square of the multiplier overlay falls outside the source grid area, the product is zero.)

**Step 4** — Divide the result of Step 3 by the annual average wind speed to get $\chi_o$.

**Step 5** — Relocate the multiplier grid to a new receptor square and repeat Steps 1 through 5.

### Correction Factors

The following procedures should be applied, if required, to the values determined by the foregoing procedure.

*One-Hour to 24-Hour or Other Averaging Time*

To calculate average area-source concentrations for 24-hour or other (*e.g.*, monthly) periods, follow the same procedures as for the annual average except that wind direction frequencies appropriate to the period in question must be used.

*Grid Size Other Than 5 x 5 km*

Multiply the value obtained at Step 4 by the appropriate correction factor shown in Table 7.2.

**Table 7.2.** Grid Size Correction Factors–Meteorological Conditions.

| *Grid Size (km)* | *Neutral* | *Stable* | *Unstable* |
|---|---|---|---|
| 1 | .94 | .97 | .93 |
| 2 | .97 | .98 | .96 |
| 3 | .98 | .99 | .98 |
| 4 | .99 | 1.00 | .99 |
| 5 | 1.00 | 1.00 | 1.00 |
| 10 | 1.03 | 1.01 | 1.03 |
| 15 | 1.04 | 1.02 | 1.05 |
| 20 | 1.05 | 1.02 | 1.07 |
| 25 | 1.06 | 1.03 | 1.08 |

*Receptor Point Not at Center of a Source-Grid Square*

Calculate $\chi_o$ for the center of the source-grid square containing the receptor point, and for the next nearest square beyond the receptor point. Interpolate linearly between these values.

### Worked Example

*Problem*

The source inventory for sulfur dioxide assuming no decay for a (real) city is given in Figure 7.5. The grid spacing is 5 km. (1) Calculate the sulfur dioxide concentration for a receptor located at the

center of source square with the heavy outline, for the case of a WNW wind at 10 mph (3.4 m/sec) under neutral meteorological conditions. (2) Given the following annual wind frequency distribution, calculate the annual average concentration for a receptor located at the center of the same source square.

| | | | | | |
|---|---|---|---|---|---|
| .15 | .16 | .27 | .18 | .14 | .07 |
| .39 | .45 | .58 | .27 | .20 | .07 |
| .22 | .64 | 1.42 | .36 | .24 | .14 |
| .10 | .34 | .50 | .14 | .05 | .05 |
| .08 | .31 | .13 | .05 | .05 | .05 |
| .05 | .12 | .26 | .08 | .10 | .11 |

**Figure 7.5.** Source inventory grid, annual average particulate emissions ($\mu g/m^3$ sec).

| *Direction* | $f_d$ | *Direction* | $f_d$ |
|---|---|---|---|
| NNE | .02 | SSW | .05 |
| NE | .04 | SW | .05 |
| ENE | .08 | WSW | .05 |
| E | .08 | W | .05 |
| ESE | .08 | WNW | .12 |
| SE | .05 | NW | .14 |
| SSE | .04 | NNW | .07 |
| S | .04 | N | .02 |

*Solution*

*Procedure for Hourly Average Concentration.* Select the multiplier grid for neutral conditions, Figure 7.1. Center over this the square of the source inventory overlay (Figure 7.5) containing the receptor point. Corresponding to WNW wind, it is seen that Equation (1) gives:

$$\chi_o = \frac{1}{u}(153 \times .05 + 48 \times .05 + 28 \times .50 + 20 \times .34 + 16 \times .22 + 14 \times 0) = 34.4/3.4 = 10. \mu g/m^3$$

*Procedure for Annual Average Concentration.* Form an annual average multiplier grid by multiplying the corresponding numbers in Figure 7.6 and Figure 7.1. The result is Figure 7.7. Figure 7.6 was obtained by substituting the actual wind direction frequencies in the above table into the annual wind frequency grid, Figure 7.4. The receptor point of Figure 7.5 is now centered over the multiplier grid, Figure 7.7, and all corresponding numbers are multiplied and added; the result equals 24.03. The annual average concentration is:

$$24.03/3.4 = 7.1\ \mu g/m^3$$

| | | | | | | | | | | |
|---|---|---|---|---|---|---|---|---|---|---|
| .14 | | | .07 | | .02 | | .02 | | | .04 |
| | .14 | | .07 | | .02 | | .02 | | .04 | |
| | | .14 | | .07 | .02 | .02 | | .04 | | |
| .12 | .12 | | .14 | .07 | .02 | .02 | .04 | | .08 | .08 |
| | | .12 | .12 | .14 | .11 | .04 | .08 | .08 | | |
| .05 | .05 | .05 | .05 | .22 | 1.0 | .24 | .08 | .08 | .08 | .08 |
| | | .05 | .05 | .05 | .13 | .05 | .08 | .08 | | |
| .05 | .05 | | .05 | .05 | .04 | .04 | .05 | | .08 | .08 |
| | | .05 | | .05 | .04 | .04 | | .05 | | |
| | .05 | | .05 | | .04 | | .04 | | .05 | |
| .05 | | | .05 | | .04 | | .04 | | | .05 |

**Figure 7.6.** Wind direction frequency grid for example.

*A Simple Approximation to the Area-Source Calculation.* Area-source strength values do not in practice vary much from one grid square to another. Furthermore, the grid multipliers of Table 7.1 show that the contribution to $\chi_a$ from the zeroth square (strength =

$Q_o$) is weighted most heavily. This suggests the following simple approximation to Equation (1):

$$u\chi_a = CQ_o \tag{6}$$

where the coefficient C is obtained by summing the values given in Table 7.1, *i.e.*,

$$C = c_o + c_1 + c_2 + c_3 + c_4 + c_5 \tag{7}$$

thus C equals 279 for neutral conditions, 664 for stable conditions, and 192 for unstable conditions.

Corresponding to the conditions of the worked example, Equation (6) provides the result, $\chi_a = 4.1\ \mu g/m^3$. This is in reasonably good agreement with the results using Equation (1), especially the annual average value. Hanna[3] has made a number of comparisons and finds Equation (6) to be a valid, useful area-source formula.

| | | | | | | | | | | |
|---|---|---|---|---|---|---|---|---|---|---|
| 2.52 | | | .98 | | .28 | | .28 | | | .56 |
| | 2.24 | | 1.12 | | .32 | | .32 | | .64 | |
| | | 2.80 | | 1.40 | .40 | .40 | | .80 | | |
| 1.68 | 1.92 | | 3.92 | 1.96 | .56 | .56 | 1.12 | | 1.28 | 1.12 |
| | | 2.40 | 3.36 | 6.72 | 5.28 | 1.92 | 2.24 | 1.66 | | |
| .70 | .80 | 1.00 | 1.40 | 10.56 | 153 | 11.52 | 2.24 | 1.60 | 1.28 | 1.12 |
| | | 1.00 | 1.40 | 2.40 | 6.24 | 2.40 | 2.24 | 1.60 | | |
| .70 | .80 | | 1.40 | 1.40 | 1.12 | 1.12 | 1.40 | | 1.28 | 1.12 |
| | | 1.00 | | 1.00 | .80 | .80 | | 1.00 | | |
| | .80 | | .80 | | .64 | | .64 | | .80 | |
| .70 | | | .70 | | .56 | | .56 | | | .70 |

**Figure 7.7.** Annual average multiplier grid for example.

## NOMENCLATURE

$b$ = vertical dispersion coefficient corresponding to given atmospheric stability ($m^{1-q}$)
$c$ = multiplier that depends on the meteorological conditions and the grid size
$\Delta x$ = size of the source-strength grid (m)
$f_d$ = fraction of the time the wind blows from each direction (dimensionless)
$p$ = crosswind dispersion exponent corresponding to a given atmospheric stability (dimensionless)
$q$ = vertical dispersion exponent corresponding to a given atmospheric stability (dimensionless)
$Q_N$ = area source strengths of grid square N ($\mu g/m^2$ sec)
$u$ = mean wind speed in plume region (m/sec)
$\chi_A$ = area source 1-hour average surface sulfur dioxide concentrations for the center of the source-grid square A ($\mu g/m^3$)

## REFERENCES

1. Stern, A. C., (ed.) "Proceedings of Symposium on Multiple-Source Urban Diffusion Models," USEPA (1970).
2. Gifford, F. A. and S. R. Hanna. "Urban Air Pollution Modeling," *Proceedings of The Second Clean Air Conference*, H. M. England and W. T. Beery, eds. (New York: Academic Press, 1971), pp. 1146-1151.
3. Hanna, S. R. "A Simple Method of Calculating Dispersion from Urban Area Sources," *J. Air Poll. Control Assoc.*, **21**, 774-777 (1971).
4. Hanna, S. R. "Description of ATDL Computer Model for Dispersion from Multiple Sources," *Industrial Air Pollution Control* (Ann Arbor: Ann Arbor Science, 1973), pp. 23-32.

# Standard Deviation of Wind Direction as a Function of Time; Three Hours to Five Hundred Seventy-Six Hours

by

Walter M. Culkowski
Air Resources
Atmospheric Turbulence and Diffusion Laboratory
National Oceanic and Atmospheric Administration
Oak Ridge, Tennessee

## Abstract

The standard deviation of horizontal wind direction $\sigma_\theta$ increases with time of averaging up to a maximum value of 104°. The average standard deviation of horizontal wind directions averaged over periods of 3, 5, 10, 16, 24, 36, 48, 72, 144, 288, and 576 hours were calculated from wind data obtained from a 100 meter tower in the Oak Ridge area. For periods up to 100 hours, $\sigma_\theta \propto t^{.28}$; after 100 hours $\sigma_\theta \propto 6.5 \ln t$.

ATDL Contribution File No. 75/11

## Introduction

In computer modeling of continuous point source emissions, the emphasis is generally on very short (i.e. one hour) or very long (monthly or seasonal) descriptions of plume behavior. The literature on horizontal dispersion averaged over periods of 24 hours or more is sparse; comprehensive averages from appropriate observational data are few. As the averaging time increases beyond one-month, however, the problem reduces to climatological and recurrence interval estimates, rather than the continued increase of horizontal dispersion as in the daily to weekly time regime. For the shortest practical time intervals (10 seconds to 10 minutes) good evidence exists (1), (2), (3) for the relation

$$\sigma_{\theta_1}/\sigma_{\theta_2} = (t_1/t_2)^{.2} \quad ,$$

where $\sigma_{\theta_1}$ and $\sigma_{\theta_2}$ are standard deviation of horizontal wind direction which has been averaged over times 1 and 2, respectively.

For periods beyond one hour, $\sigma_\theta$ has been found in various studies to vary as $t^{.25}$ to $t^{.50}$. Slade (4) found from measurements of the range of wind direction at a height of 100 meters, that, up to eight hours, $\sigma_\theta$ varied as $t^{.25}$ during the day and $t^{.50}$ at night. Slade concluded that on this time scale, $\sigma_\theta$ varied as a function of height and surface roughness. Hino (2) concluded, from sulfur dioxide measurements, that $\sigma_\theta \propto t^{.5}$ for up to 5 hours regardless of stability; but the

applicable time scale of the power law did vary with stability. Barry (5) at Chalk River found an excellent fit to a $t^{.33}$ power law for periods up to several hundred hours.

In the Air Transport Model (8), used in Oak Ridge, we addressed ourselves to the increase of the horizontal dispersion parameter with time up to 576 hours. The study is principally aimed at determining the behavior of average concentration with time out to fifty kilometers or so. The $\sigma_\theta$'s are calculated to be applicable to the Gaussian plume formulation (3), but as a centerline (maximum) concentration only. As the time scale increases beyond one hundred hours, the constraints forced by climatological limits become increasingly obvious. The maximum possible $\sigma_\theta$ is 104°, which is the standard deviation of a wind direction that varies randomly through 360°. In Oak Ridge, the effect of the terrain appears to be to limit $\sigma_\theta$ to about 50° after 1000 hours or so.

Location and Data

The data used in this study were extracted from hourly wind records in Oak Ridge, Tennessee area. The wind data were obtained from an anemometer located at the top of a hundred meter tower, situated at one of the highest points in the area. The instruments were well above surrounding trees and other terrain features. The data thus represent, to a reasonable degree, the flow of "free" air over the area. As a result of the regional topography, a distinct northeast-southwest bias occurs in the wind frequency tables, corresponding to the orientation of the Appalachian and Cumberland Mountains.

The data are for the period 1961 thru 1962. No special significance is attached to these particular years, other than that the equipment was operating continuously and the data were accordingly easy to extract. Ideally, one might consider including the entire fifteen year history of the station, but computer time limits the practical period to two years.

The Calculations

A vector array of wind component data would have been prohibitive in terms of computer time and storage for a large body of wind data, necessitating a much simpler approach. For each 3, 5, 10, 16, 24, 36, 48, 60, 72, 144, 288, and 576 hour period (P) all 16 wind directions were examined and the highest frequency f(P) noted, a "calm" was assigned the previous hour's direction. Noting that the standard deviation of a uniform distribution 22.5° wide is 6.6°; the standard deviation for the period (P) was then computed to be

$$\sigma_\theta(P) = f(P) \cdot 6.6°/P \quad . \qquad (1)$$

The time increment between each set of observations, regardless of length of period, was one hour. Eighteen thousand eight hundred hours were examined for each interval; thus there are 18800-3 = 18797 computations of $\sigma_\theta(3)$ and 18800-576 = 18224 computations of $\sigma_\theta(576)$. The average for each $\sigma_\theta(P)$ was then computed by means of the formula

$$\bar{\sigma}_\theta(P) = \left( \sum_{1}^{n(P)} \sigma_\theta(P) \right) / n(P)$$

where n(P) is the number of computations for each period.

## Results

Table I and Figures I and II show the results of the calculations. For the first 100 hours, $\bar{\sigma}_\theta$ follows a $t^{.28}$ power law, and $\sigma_\theta \propto \ln t$ applies beyond 100 hours. Overall, from 10 to approximately 1000 hours, the equation $\sigma_\theta = 6.5 \ln t$ leads to slightly over-estimating at t - 30 hours and under estimates at t = 500 hours.

## Results from Other Stations

Two other stations in the Oak Ridge area were examined in a similar manner to that described above. Both were located well below the ridge tops and surrounding building. One station (040) has shown an extreme valley wind bias in climatological wind roses, yet it shows only a slight (about 10%) reduction of $\bar{\sigma}_\theta$ at 576 hours. By contrast, station 20 which is located only a few feet above a moderate size building shows less climatological directional bias, but a 33% reduction of $\bar{\sigma}_\theta$ at 576 hours. Apparently no a priori conclusions about $\bar{\sigma}_\theta$ can be reached by examining a wind rose.

## Conclusions

In calculating concentrations of effluent from continuous point sources, the average maximum concentration may be considered proportional to $t^{-.28}$ for averaging times from 3 up to 100 hours, and to $(\ln t)^{-1}$ for averaging times to 1000 hours. This is in excellent agreement with the results by Barry (5), who studied a fixed source point-fixed receptor geometry. For this study the receptor point was assumed to be the plume's centerline.

## Acknowledgement

This research was performed under an agreement between the U.S. Energy Research and Development Administration and the National Oceanic and Atmospheric Administration.

References


1. Stewart, N. G., H. J. Gale, and R. N. Crooks, 1958, The atmospheric diffusion of gases discharged from the chimney of the Harwell reactor BEPO, Int. J. Air Pollut. 1, 87-102.

2. Hino, Mikio, 1967, Maximum Ground-Level Concentration and Sampling Time, Atmospheric Environment, Vol 2, 1968, pp. 149-165.

3. Slade, David (Editor), 1968, Meteorology and Atomic Energy 1968, USAEC, Rep. No. TID 24190, x and 445 pp.

4. Slade, David H., 1965, Dispersion Estimates from Pollutant Releases of a Few Second to 8 Hours in Duration, Weather Bureau Washington, D. C. PB 168 335.

5. Barry, P. J., 1975, Stochastic Properties of Atmospheric Diffusivity, Atomic Energy of Canada Limited, AECL 5012.

6. McGuire, T., and K. E. Noll, 1970, Relationship Between Concentrations of Atmospheric Pollutants and Averaging Time, Atmospheric Environment, 1971, Vol. 5, pp. 291-298.

7. Larsen, R. I., 1970, Relating Air Pollutant Effects to Concentration and Control, Journal of the Air Pollution Control, Volume 20, Number 4, pp 214-225.

Table I

Average Horizontal Angular Dispersion Factor over Oak Ridge, Tennessee

| Time (Hours) | 3 | 5 | 10 | 16 | 24 | 36 | 48 | 60 | 72 | 144 | 288 | 576 |
|---|---|---|---|---|---|---|---|---|---|---|---|---|
| (degrees) | | | | | | | | | | | | |
| $\sigma_\theta$ | 11.0 | 12.3 | 15.0 | 17.2 | 19.5 | 22.2 | 24.4 | 26.3 | 28.0 | 34.1 | 39.5 | 42.9 |

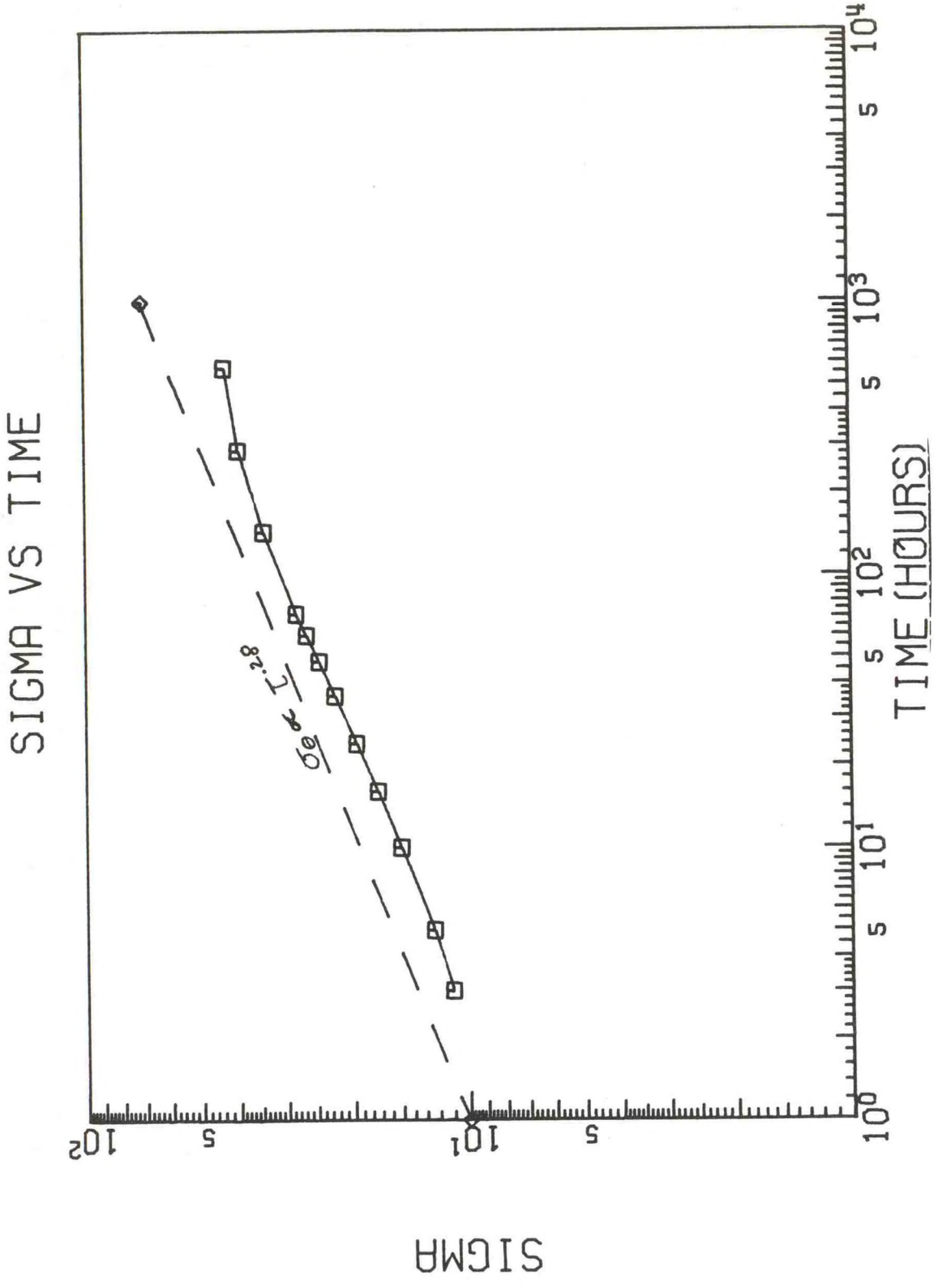


Figure 1. Log horizontal dispersion (Sigma) vs. log time in hours.

Figure 2. Horizontal dispersion (Sigma) vs. log time in hours.

# COMPARISON OF TWO PLUME DEPLETION ESTIMATION TECHNIQUES: THE ADPIC METHOD vs. THE GAUSSIAN MODEL

by

R. P. Hosker, Jr.

Air Resources
Atmospheric Turbulence and Diffusion Laboratory
National Oceanic and Atmospheric Administration
Oak Ridge, Tennessee 37830

August 29, 1975
ATDL Contribution Number 75/12

WITHDRAWN

# Validation of a Multisource Dispersion Model for Atmospheric Sulfur Concentrations

Walter M. Culkowski
Air Resources
Atmospheric Turbulence and Diffusion Laboratory, NOAA
Oak Ridge, Tennessee

Two tenths of one percent of the annual world output of $SO_2$ is generated within twenty five kilometers of the Walker Branch watershed. The prevailing wind pattern dictates that a substantial fraction of this effluent is transported to the vicinity of the Walker Branch area. As noted previously, the Air Transport Model (ATM ) is the mechanism employed to estimate the concentration and/or deposition of an effluent at any given point. A test of the validity of the ATM was undertaken, therefore, using data from $SO_2$ monitoring stations established by the Tennessee Valley Authority (TVA).

The location, and type of monitoring stations employed were far from ideal. In addition, the tabulating requirements of TVA are often an order of magnitude more gross than the model predicts. Nevertheless, comparison of the model with TVA data shows excellent agreement.

TVA supplied data for three parameters; $SO_2$ , suspended particulate and settled particulate matter. Preliminary analysis indicated that only the $SO_2$ concentrations tended to correlate with the output of the Bull Run steam plant. Accordingly the ability of the ATM to correlate with TVA $SO_2$ data was considered to be a valid test of the model.

ATDL Contribution File No. 75/13

Presented at 1974 Fall Meeting of the American Geophysical Union, San Francisco, December 12-17, 1974.

Only four monitoring stations had records long enough (8 months or longer) to be considered adequate. Two of these stations (# 13 and # 6) were located too near to automotive traffic for meaningful data to be extracted, although more will be said of these two stations below. The two "best" stations were TVA's Bull Run # 1, located approximately two and one fourth miles northeast of the plant, and Kingston # 2, located about six and one half miles north-northwest of the Kingston plant.

Table I lists the observed and predicted concentrations of $SO_2$m along with the resulting correlations. It must be noted that TVA considers any hourly reading of $SO_2$ below .01 parts per million (PPM) to be zero. The observed values in table one, therefore, may easily be a factor of two (or more) low since the cut off point is generally well above the ensuing average monthly reading.

Table I

Observed vs. Predicted Average Monthly $SO_2$ Concentrations for the Period July 1972 to August 1973. Concentration in Parts for Million

| Month | Bull Run # 1 | | Kingston # 2 | |
|---|---|---|---|---|
| | Observed* | Predicted | Observed* | Predicted |
| July 72 | .0041 | .0079 | | |
| Aug. | .0019 | .0045 | | |
| Sept. | .0033 | .0056 | | |
| Oct. | .0018 | .0042 | | |
| Nov. | .0016 | .0035 | | |
| Dec. 72 | .0033 | .0049 | | |
| Jan. 73 | .0013 | .0035 | .0054 | .0011 |
| Feb. | .0021 | .0046 | .0093 | .0023 |
| Mar. | .0006 | .0032 | .0131 | .0042 |
| Apr. | .0015 | .0044 | .0123 | .0028 |
| May | .0014 | .0032 | .0050 | .0021 |
| June | .0005 | .0028 | .0104 | .0037 |
| July | .0007 | .0044 | .0063 | .0010 |
| Aug. 73 | .0006 | .0015 | .0080 | .0018 |
| Mean | .0018 | .0042 | .0087 | .0024 |
| $\sigma$ | .0011 | .0014 | .0030 | .0010 |
| Correlation | r = 0.86 | | r = 0.85 | |

*See Text

Both correlations are excellent, particularly in view of the number of variables involved, the difficulties previously mentioned, and the problem of maintaining and calibrating a sampling network. The difference between observed and predicted values for the Bull Run # 1 gauge is largely as anticipated; the observed values lower by about a factor of two due to the rejection of observed values below .01 PPM. The similarity in standard deviations ($\sigma$) suggest that simply adding a constant (.0024) should bring "observed" vs. predicted concentrations into very good agreement. Conversely, the model underpredicts the Kingston gauge # 2 by approximately a factor of three of the many possible reasons for this anomaly, the most probable is the effect of the nearby terrain. Between the Kingston plant and gauge #2, and almost normal to the direction of travel is Walden Ridge, rising some 350 meters from the valley floor. Beyond Walden Ridge are a series of valleys, one of which leads to gauge # 2. The effect of this valley may be to lessen the assumed randomness of flow in this direction by channeling the effluent towards the gauge.

The basic ATM does not include terrain effects other than the nature of the surface (forest or grass covered) although there would be no major obstacle to employing them for specific gauges and specific sources. For complex surface features, such as the the Walden Ridge area, terrain factors are often desirable, although by no means are they always necessary. Time and distance scales may obviate the need for detailed surface features.

Before leaving the subject of correlations it is interesting to note that Bull Run Gauge # 13 and Kingston Gauge # 6 correlated not all with the ATM, but did correlate with only the amount of effluent from the Bull Run stack. Gauge # 13 located four miles east of Bull Run correlated weakly with the $SO_2$ output ($r = +0.49$), while a strong but apparently anomolous correlation was obtained with Kingston # 6 ($r = +0.70$). The concentration at Kingston #6, some 30 kilometers from Bull Run often exceeded, on a monthly basis, the yearly applicable $SO_2$ standard of 0.03 PPM. Whether this anomaly will persist in the future is being investigated, but the complexity of sulpher reactions along with our incomplete knowledge of wind levels above a few hundred meters suggest that such a strong correlation should not be summarily dismissed.

Table II, below provides the average monthly estimates of sulphur deposition using measured stability wind data, and emission strengths supplied by TVA and ORNL sources combined with deposition velocity of .10 meters per second (assumed appropriate for a forest covered terrain). Table II illustrates the dominance of the Kingston effluent over the Walker Branch Watershed. Also, the significance of the Y-12 effluent during the winter season becomes evident.

Table II

Estimates of Sulphur Deposition from Various Sources in the Walker Branch Watershed July 1972 - Aug. 1973. Values are grams/meter$^2$ x sec) x $10^{-9}$.

| | Bull Run | Kingston | Y-12 | Alcoa | Area Sources | Total |
|---|---|---|---|---|---|---|
| July 72 | 123 | 1110 | 0 | 1 | 0 | 1230 |
| Aug. | 60 | 684 | 4 | 1 | 0 | 748 |
| Sept. | 67 | 799 | 2 | 1 | 0 | 870 |
| Oct. | 122 | 405 | 52 | 3 | 13 | 594 |
| Nov. | 53 | 327 | 167 | 1 | 30 | 579 |
| Dec. 72 | 48 | 592 | 43 | 1 | 45 | 728 |
| Jan.73 | 109 | 448 | 223 | 2 | 75 | 857 |
| Feb. | 80 | 679 | 435 | 3 | 49 | 1250 |
| Mar. | 108 | 443 | 205 | 6 | 40 | 802 |
| Apr. | 60 | 595 | 76 | 2 | 9 | 743 |
| May | 40 | 751 | 5 | 1 | 4 | 801 |
| June | 0 | 886 | 6 | 2 | 0 | 895 |
| July | 1 | 1390 | 14 | 2 | 0 | 1410 |
| Aug. 73 | 0 | 471 | 3 | 3 | 0 | 478 |
| Mean | 62.2 | 684.2 | 88.2 | 2.1 | 18.9 | 856.1 |
| $\sigma$ | 43.1 | 293.4 | 127.6 | 1.4 | 24.5 | 268.7 |

The change in relative contributions from each source is readily apparent in Table II. Note that the standard deviation to the mean ratio for Kingston is some 43% in the table. This ratio is only 8% when applied to the source strength along.

It is clear from Table II that many sources must be considered when estimating the deposition over an area such as Walker Branch. Y-12, whose peak emission is never greater than fove percent of Kingston's contributes, due to its proximity, over half as the amount of the larger plant.

The ATM is being modified as outlined under II A, above. Continued input from TVA and ORNL sources will help in continuing the validation of the model and, of course, its refinement. Better wind estimates, weighting the parameters to reflect the atmospheric chemistry of sulphur, and applying, where necessary, such regional requirements as terrain will add to the model's versatility. Although sulphur has been emphasized here, the model is equally applicable to other gaseous or particulate matter.

# BEAM ENRICHMENT OF DIFFUSE RADIATION IN A DECIDUOUS FOREST[1,2]

by

BOYD A. HUTCHISON

AND

DETLEF R. MATT

Atmospheric Turbulence and Diffusion Laboratory
National Oceanic and Atmospheric Administration
Post Office Box E
Oak Ridge, Tennessee 37830

[1]This research supported in part by the Eastern Deciduous Forest Biome, US-IBP, funded by the National Science Foundation under Interagency Agreement AG-199, BMS69-01147 A09 with the U. S. Energy Research and Development Agency, Oak Ridge National Laboratory, and in part by the Division of Biomedical and Environmental Research, ERDA.

[2]Contribution No. _____, Eastern Deciduous Forest Biome, US-IBP ATDL Contribution No. 75/14.

Accepted for publication in Agricultural Meteorology, March 30, 1976.

ABSTRACT

By applying a model developed by Reifsnyder et al. (1971/72) to solar radiation data collected in and above an East Tennessee deciduous forest, solar radiation budgets are approximated for three forest levels within the winter leafless, spring leafless, summer fully leafed and autumnal fully leafed forest phenoseasons. Beam radiation dominates these budgets throughout the year and varies directly with solar elevations. Although beam radiation penetration is severely reduced in the fully leafed forest, this component still accounts for over one-half the total radiation received within the forest in early autumn, the phenoseason of minimal beam penetration. Beam enrichment of diffuse radiation within the forest is also highly dependent upon solar elevation and canopy biomass density. Maximum beam enrichment occurs in summer with the high solar elevation of that season and a fully leafed canopy. Minimum enrichment occurs in the leafless winter forest when solar elevations are lowest and canopy biomass density is minimal. The penetration of diffuse sky radiation is maximal in the leafless forest and minimal in the fully leafed forest but, because of limitations of the model used in this approximation, this quantity appears insensitive to changes in solar elevations. This limitation is a defect of the model but it should not substantially alter the indicated results.

INTRODUCTION

The solar radiation budget of a vegetative stand may be written as:

$$I_z = d_z + D_z,$$

where $I_z \equiv$ the total radiation passing downward through level z in the stand, $d \equiv$ the diffuse radiation component, and $D \equiv$ the component that penetrates to a level as a collimated beam via canopy openings. Reifsnyder et al. (1971/72) hypothesize that the diffuse radiation component is actually made up of diffused radiation from a number of sources. Using our own notation, this may be expressed as:

$$d_z = p_z + r_z + t_z + R_z + T_z,$$

where $p_z \equiv$ the sky radiation penetrating to a level z in the stand via canopy openings, $r \equiv$ the down-reflected sky radiation, $t \equiv$ the sky radiation transmitted through plant parts, $R \equiv$ the down-reflected beam radiation, and $T \equiv$ the transmitted beam radiation.

Obviously, this model assumes that beam radiation is perfectly diffused by reflection from and by transmission through plant parts. Anderson (1969) has concluded that reflected beam radiation is not directionally isotropic. However, there is no preferred orientation of plant parts in our forest; thus the reflected beam radiation should be directionally random and as such, may be considered a diffuse radiation source. Upward fluxes of radiation are ignored in this paper because, as Gay and Knoerr (1970) have reported, the

upward fluxes are necessarily small by virtue of the exponential decrease in radiant flux densities resulting from multiple reflections or transmissions.

Following the techniques of Reifsnyder et al. (1971/72), with completely overcast skies no beam radiation reaches the stand canopy and;

$$(I_z)\text{overcast} = (d_z)\text{overcast} = (p_z + r_z + t_z)\text{overcast}.$$

Defining the fractional penetration of diffuse radiation as

$$F_z = (d_z/d_o)\text{overcast}$$

where $d_o \equiv$ the diffuse radiant flux density incident on the stand, then

$$F_z \cdot (d_o)\text{clear} \equiv (\overline{p_z + \hat{r}_z + t_z})\text{clear}.$$

That is, the fractional penetration of diffuse radiation with overcast skies multiplied by the diffuse radiation incident on the stand under clear skies estimates (-^-) the amount of diffuse radiation penetrating the stand via canopy openings, down-reflection and transmission. Then by simple subtraction:

$$(d_z)\text{clear} - (\overline{p_z + \hat{r}_z + t_z})\text{clear} = (\overline{R_z} \hat{+} \overline{T_z})\text{clear},$$

where $(\overline{R_z} \hat{+} \overline{T_z})_{clear} \equiv$ the estimated enrichment of diffuse radiation at level z by down-reflected and transmitted beam radiation.

This approach can only be considered a first approximation because sky brightness distributions are greatly dissimilar on clear and overcast days. Hence, the fractional penetration of diffuse radiation under overcast skies may be a poor approximation of the penetration of such radiation under clear skies. Despite this defect, the trends and relative magnitudes of the quantities estimated in this way should approximate reality.

In this paper, the model is applied to solar radiation data collected above and within an East Tennessee deciduous forest. From the observed and derived radiative components, approximations of the incoming solar radiation budgets above and within the forest are generated for idealized clear days in the winter and spring leafless forest and in the summer and autumn fully leafed forests. Diurnal, seasonal, and vertical variation in these budgets are illustrated by comparison. Results are presented only in graphic form; however, the data used are tabulated in the appendix for those interested.

These comparisons are of interest for several reasons. The role of forest biomass distribution and geometry in the partitioning of radiation fluxes is little understood and, although this paper does not address the mechanics of such

partitioning, knowledge of the spatial and temporal variation in the relative magnitudes of solar radiation budget components will improve our understanding of forest energy relationships. Furthermore, the spectral quality of radiation is grossly altered by reflection from or transmission through tree leaves. Knowledge of the relative magnitudes of penetrating beam radiation and beam enrichment of diffuse radiation will therefore indicate changes in the spectral quality of solar radiation in the forest in the absence of actual spectral measurement.

## METHODS

Replicated measurements of total and diffuse radiation within solar wavelengths (0.3 to 3μ) were made above and within a seral, deciduous forest composed predominantly of tulip poplar. The forest is located in a moist sink on the Energy Research and Development Agency reservation near Oak Ridge, Tennessee. Radiation measurements were made using Lintronic Dome Solarimeters, a commercial modification of Monteith's (1959) field solarimeter. Sensors were randomly sited in horizontal space at the forest floor, below a shrub and sapling stratum, at the base of the secondary canopy formed by redbud and dogwood (about 3 m height) and at the base of the overstory canopy (about 16 m height). The diffuse

radiation component was measured by sensors equipped with shadow bands as designed by Horowitz (1969). A single open and shaded sensor mounted above the canopy provided records of total and diffuse radiation incident upon the forest. Output signals from all sensors were fed into a digital data acquisition system, scanned periodically through time, and recorded on punch paper tape. Data were collected sporadically over several years, such that data are now available on solar radiation in this forest under a variety of sky conditions in all seasons of the year and in all phenological phases of the forest. A more complete description of the measurement techniques and of the study site is found in Hutchison (1975) and in Hutchison and Matt (in preparation).

Temporal variation in forest radiation regimes arises from daily and annual changes in solar beam geometry as well as from phenological changes in forest structure. Time variation through single days is illustrated by time plots of composite day data. Since mornings and afternoons are equivalent with respect to solar position, each day is folded upon solar noon (SN) and average radiation values are computed for one-hour increments of time away from solar noon. That is, the value plotted at solar noon is the average for the hour centered on solar noon. The value plotted for solar noon $\pm 1$ hr is the average of 2 hr of record, 1 hr centered on time 1 hr before noon and the other centered on time 1 hr after noon.

To illustrate the effects of seasonal changes in solar geometry and of phenological changes in forest structure, seven phenoseasons have been defined as shown in Fig. 1. The derivation of these phenoseasons is described in detail elsewhere (Hutchison and Matt, in preparation). During the leafing and leaf-fall phenoseasons, forest radiation conditions change rapidly because of the rapidly changing structure of the forest and therefore, the radiation regimes are highly variable. During the winter and spring leafless forest phenoseasons however, forest structure is essentially static and solar geometry changes slowly. Then, the forest radiation regimes are relatively stable in time and seasonal comparisons can be made.

Comparison of winter and spring data shows the effect of changing solar elevation upon leafless forest radiation budgets. From summer to autumn, solar paths move southward, solar elevations decrease from maximum at the summer solstice, and comparison of summer and autumn data shows effects of changing solar elevation upon fully leafed forest radiation budgets. Since solar paths are identical on the vernal and autumnal equinoxes, comparison of spring and autumn forest radiation budgets shows the effects of the presence of tree leaves upon the partitioning and conversion of solar radiation.

A major problem became apparent when an attempt was made to calculate overcast day diffuse fractional penetration. A surprising variety of values were found for different overcast days within a phenoseason. Sky brightness distributions apparently vary significantly even with heavily overcast skies. To eliminate this source of variability, instantaneous fractional diffuse penetration values were plotted over instantaneous above-canopy diffuse-to-total radiation ratios. Since these plots appeared remarkably linear (for example, see Fig. 2, the scatter diagram of diffuse penetration values at three levels in the forest as functions of above canopy diffuse to total ratios for a summer day), overcast days' data were combined from winter and from summer; the best-fit lines were computed, using simple linear regressions and extrapolated to above canopy diffuse to total ratios of 1.0; and corresponding fractional penetration values were used from winter for winter and spring calculations. The fractional penetration values for diffuse-to-total ratios of 1.0 in summer were used for the summer and autumn calculations.

Since the sensor shaded by the shadow band "sees" less of the sky than the open sensor, empirical diffuse-to-total ratios of 1.0 would never be observed. Thus, this normalization procedure is conservative with respect to direct beam enrichment of diffuse radiation (i.e. all best fit lines had positive slopes, $F_z$ is high, and in turn $\overline{(p + \hat{r} + t)}$ is high); consequently, $\overline{(R + \hat{T})}$ is low.

Incident radiation totals and ratios of diffuse to total radiation are also variable on clear days because of differing atmospheric turbidity. An attempt was made to minimize the effects of this source of variation by combining data from several clear days or clear segments of days in each phenoseason, averaging as described above, and plotting these averages over time as in Figs. 3, 4, 5, and 6. Hand-fitted smooth curves were drawn through the data points. Examination of the plots shows that few hourly average values fall far from the smoothed curves. In general, deviations are less than 5%.

## RESULTS AND DISCUSSION

The bulk of diffuse radiation within the winter forest originates from diffuse sky radiation incident upon the leafless canopy as is evident in Fig. 3. The direct beam enrichment of diffuse is negligible at all levels within the forest and decreases with depth to essentially no enrichment at the forest floor. The small amounts of beam radiation converted to diffuse radiation increase with rising solar elevations to midday maxima. Diffuse radiation in the forest is reduced strongly from that incident upon the forest, but the attenuation of direct beam radiation by the leafless forest is much more striking. Because of the low solar elevations, optical path lengths through the forest canopy are long and, consequently, the attenuation of beam radiation by the woody forest biomass is great.

Solar elevations in early to mid-March are much higher than in the winter and, as a result, the penetration of beam radiation into the forest is greatly increased over winter amounts as shown in Fig. 4. Despite this increased penetration, conversion of beam radiation to diffuse radiation in the overstory canopy changes negligibly from winter values. At lower levels, the beam enrichment of diffuse radiation is strongly increased from the winter season and is estimated to account for over 25% of the diffuse radiation received at these levels at midday. As before, the amounts of direct beam enrichment increase with increasing solar elevation through time to midday maxima at all levels.

The amount of beam radiation converted to diffuse radiation is nearly equal at all three forest levels because of the greatly increased penetration of beam radiation in the spring leafless forest. Although estimated amounts of direct beam enrichment are significant fractions of the diffuse radiation received within the forest in this season, the amounts of beam radiation converted to diffuse radiation are negligible fractions of the total radiation received at any level by virtue of the high amounts of beam radiation penetrating the forest without conversion.

In early April, leaf expansion begins in this forest and continues until late May. With this addition of biomass to the canopy, radiation conditions within the forest change drastically. Despite maximum potential insulation around the summer solstice, the penetration of beam radiation is severely reduced from that in the spring leafless forest. As shown in Fig. 5, amounts of diffuse radiation received within the forest are increased over those in the early spring forest. Some of this increase is due to increased amounts of diffuse radiation incident upon the forest, but, according to this model, most of it is the result of greater beam enrichment in the fully leafed forest. As in the winter forest, greatest beam enrichment occurs in the overstory canopy and least in the shrub layer just above the forest floor. Nevertheless, most of the diffuse radiation reaching the forest floor is composed of down-reflected and transmitted beam radiation. Estimated midday fractions of diffuse radiation stemming from beam radiation approach 85% at the forest floor, 75% in the secondary canopy and 50% in the overstory canopy. Green and near infrared wavelengths are reflected and transmitted preferentially by leaves, and this, coupled with reduced beam penetration, implies quite different radiation spectral quality within the fully leafed forest than in the leafless forest of spring. Expressing the estimated beam enrichment of diffuse as a percent of total midday radiation amounts within the forest, we find about 40%, 40%, and 15% in the shrub layer, secondary canopy and overstory canopy, respectively.

After the summer solstice, solar paths move southward in the sky and, consequently, midday solar elevations decrease. Between the solstice and the autumnal equinox, forest structure remains relatively static as evidenced by the stabilization of leaf area indexes at 6.0 $m^2 m^{-2}$ throughout this period reported by Dinger et. al. (1972). Hence, in early September, the fully leafed forest is irradiated by an autumn sun. The radiation budgets for this period are shown in Fig. 6. Total insolation has decreased slightly while diffuse radiation amounts incident upon the forest are essentially unchanged from those of summer.

Within the autumn fully leafed forest, total radiation amounts are further reduced from those received within the summer forest by virtue of the lower solar elevations and the attendent increases in optical path lengths for beam radiation. Beam enrichment of diffuse is much reduced as well and, as a result, overall amounts of diffuse radiation received are also much reduced. While the amounts of diffuse radiation originating from down-reflected or transmitted beam radiation are small and decrease with depth in the forest, they remain significant fractions of diffuse radiation received at the lower forest levels. Over one-half of the diffuse radiation received at the forest floor is estimated to stem from such beam enrichment in the autumn fully leafed forest.

Surprisingly, comparison of the spring leafless forest data of Fig. 4 with the autumn fully leafed forest data of Fig. 6 shows comparable beam enrichment of diffuse at the upper two levels in the forest. Only at the forest floor are estimated beam enrichment amounts significantly reduced by the presence of leaves in the canopy. Beam radiation is severely reduced at all levels in the autumn forest from that in the spring as would be expected. Relative amounts of diffuse radiation received are also reduced when the much greater amounts of incident diffuse radiation in the autumn are taken into account. We conclude that the similarity in beam enrichment amounts between spring and autumn is fortuitous. Despite the limited surface areas available for reflection in the spring leafless forest, so much beam radiation is present that limited fractional conversion of beam to diffuse radiation produces small but measurable increases of diffuse radiation. In the autumn, much greater leaf surface area is available allowing higher fractional conversion of beam to diffuse radiation. However, the presence of these leaves also severely reduces the amount of beam radiation penetrating the forest and hence, the beam enrichment of diffuse radiation remains small. By chance, the magnitudes of direct beam enrichment amounts are comparable in the upper forest strata in spring and autumn.

SUMMARY AND CONCLUSIONS

With static forest structure, amounts of conversion of beam to diffuse radiation vary directly with variation in solar elevations. In the leafless forest, there is essentially no conversion of beam to diffuse radiation by transmission through biomass. Hence, the beam enrichment that does occur must arise through reflection phenomena. Because there is little reason to expect that the reflectivity of woody biomass is strongly dependent upon the angle of incidence of solar rays, we conclude that the increase in beam enrichment of diffuse radiation indicated by this model occurs because of the interaction of two factors. First, with increasing solar elevations, optical path lengths through the forest decrease and greater penetration of beam radiation results. Second, with increasing solar elevations, more reflected beam radiation is directed downward. The greater amounts of beam radiation received within the forest in spring are considered to indicate greater amounts of reflected (and therefore diffused) beam radiation. At the same time, more of the reflected radiation is directed downward, with the net result that beam enrichment of diffuse radiation increases from winter to spring.

In the summer to autumn transition, the same argument obtains. However, in this case the forest is fully leafed and both reflection and transmission phenomena are involved. Nevertheless, higher solar elevations imply shorter optical paths through the

forest which, in turn, imply reduced probabilities of interception by leaves or other biomass and greater probabilities for reflection in a downward direction. Therefore, in the summer fully leafed forest, the fractional conversion of beam radiation to diffuse radiation reaches its annual maximum. In the autumn fully leafed forest, beam penetration is minimal by virtue of the presence of leaves and the lower solar elevations. These factors, coupled with the greater possibility that reflected radiation will be directed upward out of the forest, explain the decreasing amounts of beam enrichment from summer to autumn.

The amounts of sky radiation penetrating the forest $(\overline{p + \hat{r} + t})$ estimated by this technique are comparable in winter and spring and in summer and autumn. As would be expected, the amounts are much lower relative to those incident upon the forest when the forest is fully-leafed. As estimated here, this quantity is quite insensitive to changes in solar elevation but this is an artifact of the model. An overcast sky tends to have an azimuthally isotropic brightness distribution that increases from minimum at the horizon to maximum at the zenith (Moon and Spencer 1942). Hence, solar position has no effect and since the fractional penetration of diffuse is approximated using overcast day data, the derived values show no dependence upon solar elevation. In reality, clear skies are brightest around the sun (e.g. Kimball and Hand 1921) and the sky brightness distribution changes constantly as the sun appears to move across the sky,

We would therefore expect that the quantity (p + r + t) would show diurnal and seasonal variation in response to changing solar position. Because of the limitation of the model used here, such variation is masked and this represents a major defect of this technique.

ACKNOWLEDGMENTS

We gratefully acknowlege the assistance of Barbara Rooney and John Pollock, ATDL, in this research effort.

LITERATURE CITED

Anderson, M. C., 1969. A comparison of two theories of scattering of radiation in crops. Agr. Met., 6: 399-405.

Dinger, B. E., Richardson, C. J. and McConathy, R.K. 1972. Dynamics of canopy leaf area development and chlorophyll phenology in yellow poplar. East. Deciduous Forest Biome Memo Rpt. 72-164. 15 p.

Gay, L. W.,and Knoerr, K. R. 1970. The radiation budget of a forest canopy. Arch. Met. Geoph. Biokl., 1B: 187-196.

Horowitz, J. L., 1969. An easily constructed shadow-band for separating direct and diffuse radiation. Solar Energy, 12: 543-545.

Hutchison, B. A., 1975. Photographic Assessment of Deciduous Forest Radiation Regimes. Atmos. Turb. and Diffusion Lab., NOAA. ATDL Contribution No. 75/3. 164p.

Hutchison, B. A., and Matt, D. R. to be published. The distribution of solar radiation within a deciduous forest. (submitted to Ecol. Monographs).

Kimball, H. H., and Hand, I. F. 1921. Sky brightness and daylight illumination measurements. Amer. Illumination Eng. Soc. Trans., 16: 235-275.

Monteith, J. L., 1959. Solarimeter for Field Use. J. Scientific Inst., 36: 341-346.

Moon, P., and Spencer, D. E. 1942. Illumination from a non-uniform sky. Illuminating Eng., 37: 707-726.

Reifsnyder, W. E., Furnival, G. E.and Horowitz, J.L. 1971/72. Spatial and temporal distribution of solar radiation beneath forest canopies. Agr. Met., 9: 21-37.

APPENDIX

Table 1: Tabulated values of winter leafless forest solar radiation budgets.

Table 2: Tabulated values of spring leafless forest solar radiation budgets.

Table 3: Tabulated values of summer fully leafed forest radiation budgets.

Table 4: Tabulated values of autumnal fully leafed forest radiation budgets.

Table 1: Winter leafless forest solar radiation budgets

| Level (m) | Hour centered on | Hourly average flux density (mly $min^{-1}$) Total | Diffuse | $\overline{(p + \hat{r} + t)}$ | $\overline{(R + T)}$ | Direct beam |
|---|---|---|---|---|---|---|
| 30 (Above canopy) | SN ±4 | 135 | 22 | -- | -- | 113 |
| | SN ±3 | 433 | 41 | -- | -- | 392 |
| | SN ±2 | 646 | 55 | -- | -- | 591 |
| | SN ±1 | 839 | 64 | -- | -- | 775 |
| | SN | 913 | 71 | -- | -- | 842 |
| 16 (Below overstory canopy) | SN ±4 | 12 | 8 | >8 | 0 | 4 |
| | SN ±3 | 118 | 28 | >28 | 0 | 90 |
| | SN ±2 | 328 | 44 | 41 | 3 | 284 |
| | SN ±1 | 437 | 57 | 48 | 9 | 380 |
| | SN | 467 | 66 | 53 | 13 | 401 |
| 3 (Below secondary canopy) | SN ±4 | 5 | 4 | >4 | 0 | 1 |
| | SN ±3 | 37 | 17 | >17 | 0 | 20 |
| | SN ±2 | 103 | 27 | >27 | 0 | 76 |
| | SN ±1 | 198 | 35 | 32 | 3 | 163 |
| | SN | 266 | 41 | 36 | 5 | 225 |
| 0 (Below shrub stratum) | SN ±4 | 3 | 2 | >2 | 0 | 1 |
| | SN ±3 | 20 | 11 | >11 | 0 | 9 |
| | SN ±2 | 70 | 19 | >19 | 0 | 51 |
| | SN ±1 | 140 | 24 | >24 | 0 | 116 |
| | SN | 214 | 28 | 27 | 1 | 186 |

Table 2: Spring leafless forest solar radiation budgets

| Level (m) | Hour centered on | Hourly average flux density (mly $min^{-1}$) Total | Diffuse | $\widehat{(p + r + t)}$ | $\widehat{(R + T)}$ | Direct beam |
|---|---|---|---|---|---|---|
| 30 (Above canopy) | SN ±5 | 243 | 28 | -- | -- | 215 |
| | SN ±4 | 612 | 48 | -- | -- | 564 |
| | SN ±3 | 938 | 62 | -- | -- | 876 |
| | SN ±2 | 1185 | 71 | -- | -- | 1114 |
| | SN ±1 | 1334 | 77 | -- | -- | 1257 |
| | SN | 1385 | 81 | -- | -- | 1304 |
| 16 (Below overstory canopy) | SN ±5 | 51 | 16 | >16 | 0 | 35 |
| | SN ±4 | 271 | 35 | >35 | 0 | 236 |
| | SN ±3 | 555 | 49 | 46 | 3 | 506 |
| | SN ±2 | 747 | 60 | 53 | 7 | 687 |
| | SN ±1 | 880 | 68 | 57 | 11 | 812 |
| | SN | 930 | 72 | 60 | 12 | 858 |
| 3 (Below secondary canopy) | SN ±5 | 22 | 8 | >8 | 0 | 14 |
| | SN ±4 | 177 | 25 | 24 | 1 | 152 |
| | SN ±3 | 362 | 37 | 31 | 6 | 325 |
| | SN ±2 | 586 | 45 | 36 | 9 | 541 |
| | SN ±1 | 714 | 50 | 38 | 12 | 664 |
| | SN | 770 | 52 | 40 | 12 | 718 |
| 0 (Below shrub stratum) | SN ±5 | 8 | 2 | >2 | 0 | 6 |
| | SN ±4 | 71 | 20 | 18 | 2 | 51 |
| | SN ±3 | 257 | 31 | 24 | 7 | 226 |
| | SN ±2 | 440 | 39 | 27 | 12 | 401 |
| | SN ±1 | 531 | 43 | 30 | 13 | 488 |
| | SN | 581 | 45 | 31 | 14 | 536 |

Table 3: Summer fully leafed forest solar radiation budgets

| Level (m) | Hour centered on | Hourly average flux density (mly $min^{-1}$) Total | Diffuse | $\overline{\overline{(p + \hat{r} + t)}}$ | $\overline{\overline{(R + \hat{T})}}$ | Direct beam |
|---|---|---|---|---|---|---|
| 30 (Above canopy) | SN ±7 | 15 | 7 | -- | -- | 8 |
| | SN ±6 | 135 | 56 | -- | -- | 79 |
| | SN ±5 | 368 | 133 | -- | -- | 235 |
| | SN ±4 | 680 | 188 | -- | -- | 492 |
| | SN ±3 | 978 | 221 | -- | -- | 757 |
| | SN ±2 | 1210 | 241 | -- | -- | 969 |
| | SN ±1 | 1363 | 251 | -- | -- | 1112 |
| | SN | 1412 | 253 | -- | -- | 1159 |
| 16 (Below overstory canopy) | SN ±7 | 0 | 0 | >0 | 0 | 0 |
| | SN ±6 | 7 | 5 | >5 | 0 | 2 |
| | SN ±5 | 35 | 30 | >30 | 0 | 5 |
| | SN ±4 | 97 | 61 | 51 | 10 | 36 |
| | SN ±3 | 188 | 102 | 60 | 42 | 86 |
| | SN ±2 | 322 | 122 | 66 | 56 | 200 |
| | SN ±1 | 448 | 137 | 68 | 69 | 311 |
| | SN | 510 | 143 | 69 | 74 | 367 |
| 3 (Below secondary canopy) | SN ±7 | 0 | 0 | >0 | 0 | 0 |
| | SN ±6 | 1 | 0 | >0 | 0 | 1 |
| | SN ±5 | 11 | 7 | >7 | 0 | 4 |
| | SN ±4 | 33 | 23 | 12 | 11 | 10 |
| | SN ±3 | 63 | 40 | 14 | 26 | 23 |
| | SN ±2 | 93 | 55 | 16 | 39 | 38 |
| | SN ±1 | 124 | 65 | 16 | 49 | 59 |
| | SN | 153 | 72 | 16 | 56 | 81 |
| 0 (Below shrub stratum) | SN ±7 | 0 | 0 | >0 | 0 | 0 |
| | SN ±6 | 0 | 0 | >0 | 0 | 0 |
| | SN ±5 | 3 | 0 | >0 | 0 | 3 |
| | SN ±4 | 10 | 4 | 3 | 1 | 6 |
| | SN ±3 | 24 | 12 | 4 | 8 | 12 |
| | SN ±2 | 39 | 20 | 4 | 16 | 19 |
| | SN ±1 | 58 | 27 | 4 | 23 | 31 |
| | SN | 74 | 34 | 4 | 30 | 40 |

Table 4: Autumnal fully leafed forest solar radiation budgets

| Level (m) | Hour centered on | Hourly average flux density (mly $min^{-1}$) Total | Diffuse | $\widehat{(p + r + t)}$ | $\widehat{(R + T)}$ | Direct beam |
|---|---|---|---|---|---|---|
| 30 (Above canopy) | SN ±6 | 48 | 22 | -- | -- | 26 |
| | SN ±5 | 295 | 99 | -- | -- | 196 |
| | SN ±4 | 583 | 146 | -- | -- | 437 |
| | SN ±3 | 854 | 181 | -- | -- | 673 |
| | SN ±2 | 1060 | 204 | -- | -- | 856 |
| | SN ±1 | 1168 | 218 | -- | -- | 950 |
| | SN | 1204 | 225 | -- | -- | 979 |
| 16 (Below overstory canopy) | SN ±6 | 0 | 0 | >0 | 0 | 0 |
| | SN ±5 | 12 | 10 | >10 | 0 | 2 |
| | SN ±4 | 38 | 25 | >25 | 0 | 13 |
| | SN ±3 | 80 | 42 | >42 | 0 | 38 |
| | SN ±2 | 136 | 60 | 55 | 5 | 76 |
| | SN ±1 | 194 | 73 | 59 | 14 | 121 |
| | SN | 209 | 76 | 61 | 15 | 133 |
| 3 (Below secondary canopy) | SN ±6 | 0 | 0 | >0 | 0 | 0 |
| | SN ±5 | 1 | 0 | >0 | 0 | 1 |
| | SN ±4 | 10 | 5 | >5 | 0 | 5 |
| | SN ±3 | 29 | 12 | 12 | 0 | 17 |
| | SN ±2 | 50 | 17 | 13 | 4 | 33 |
| | SN ±1 | 73 | 23 | 14 | 9 | 50 |
| | SN | 91 | 26 | 15 | 11 | 65 |
| 0 (Below shrub stratum) | SN ±6 | 0 | 0 | >0 | 0 | 0 |
| | SN ±5 | 0 | 0 | >0 | 0 | 0 |
| | SN ±4 | 2 | 0 | >0 | 0 | 2 |
| | SN ±3 | 9 | 2 | >2 | 0 | 7 |
| | SN ±2 | 20 | 6 | 3 | 3 | 14 |
| | SN ±1 | 32 | 9 | 3 | 6 | 23 |
| | SN | 41 | 11 | 4 | 7 | 30 |

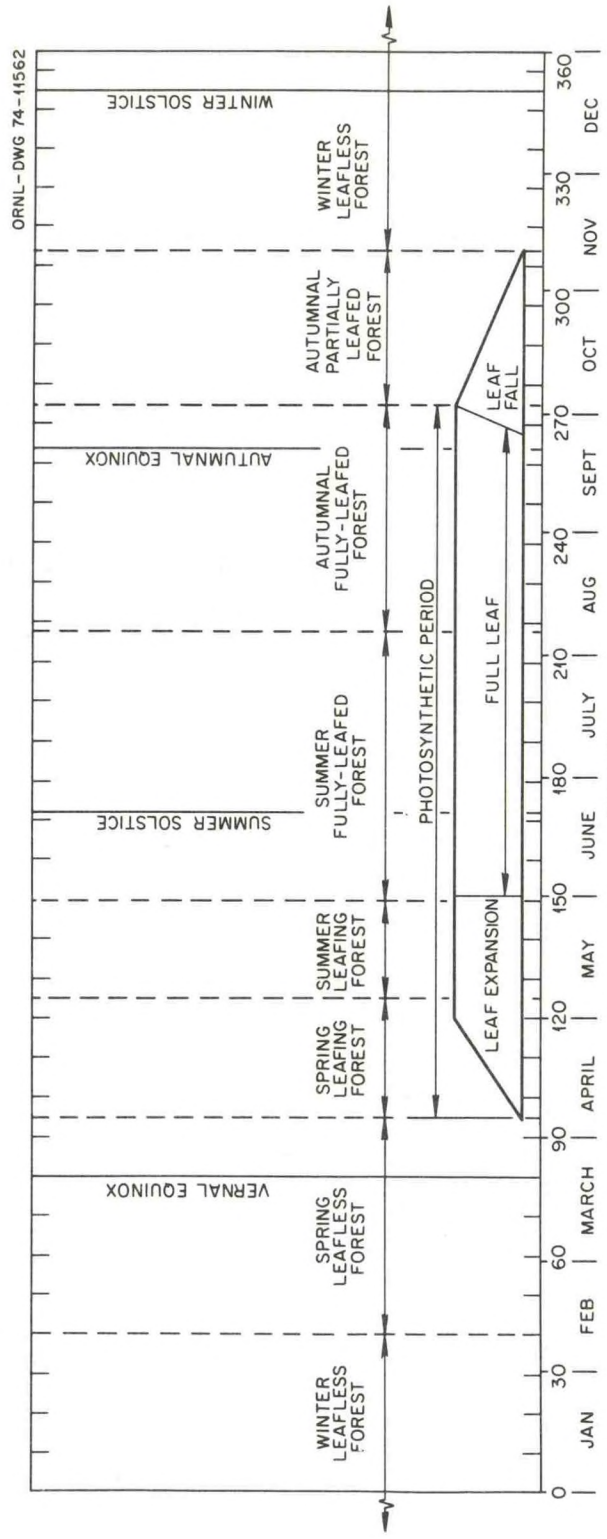


Phenoseasons in *Liriodendron* Forest.

Figure 1: Phenoseasons in the tulip poplar forest.

ORNL DWG 75-14761

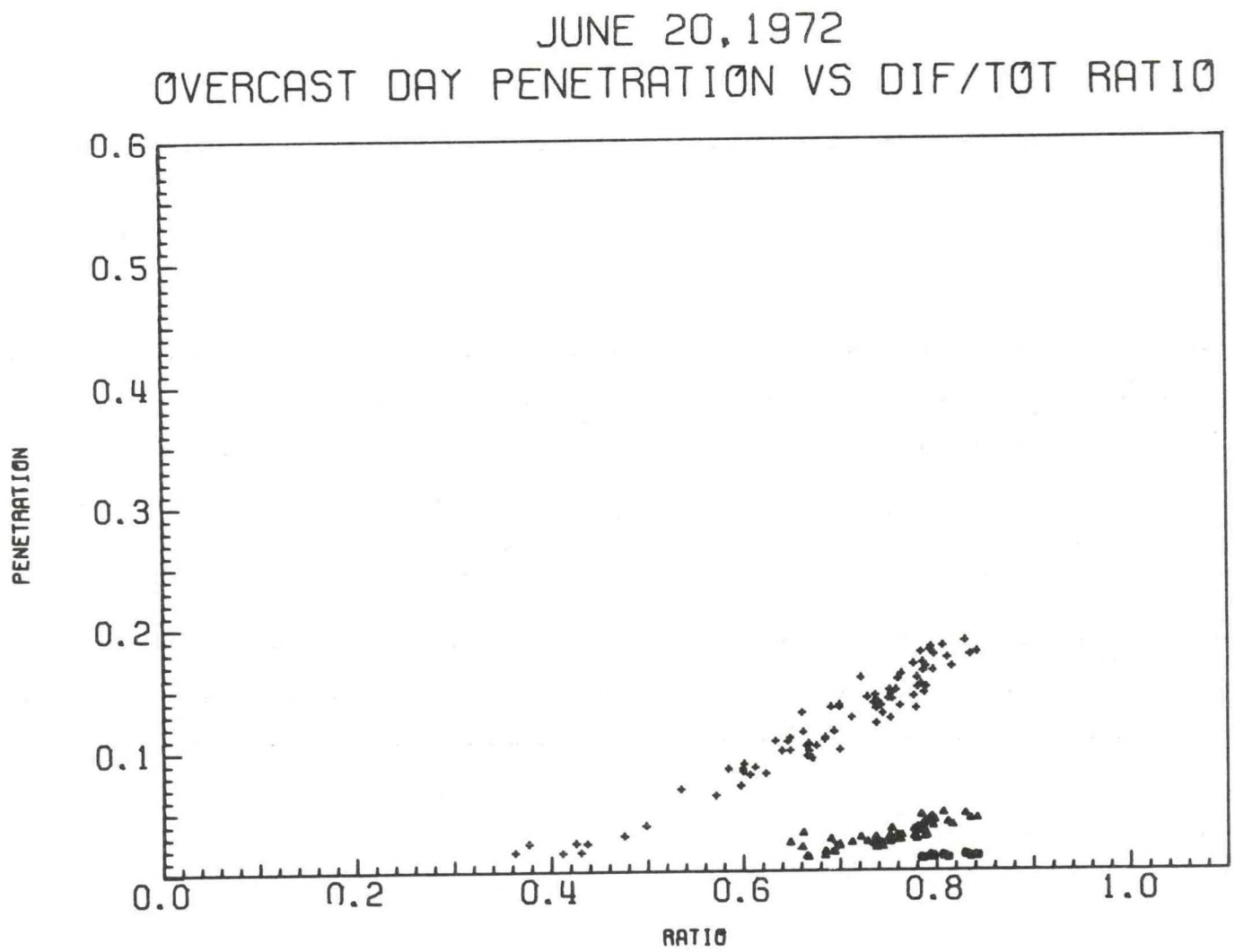


Figure 2: Overcast day fractional penetration vs. above canopy diffuse to total radiation ratio for June 20, 1972. (+ indicates overstory canopy, Δ - secondary canopy, o - forest floor)

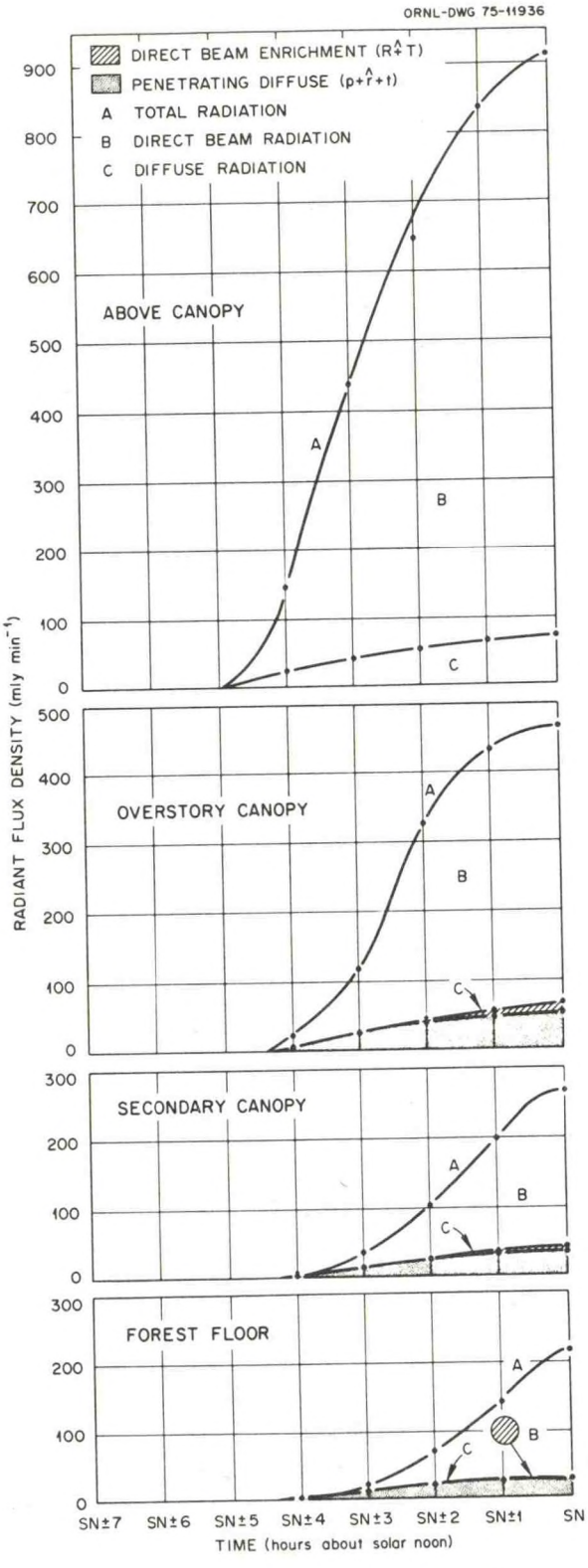


Winter Leafless Forest Solar Radiation Budget.

Figure 3: Solar radiation budgets in and above the winter leafless forest.

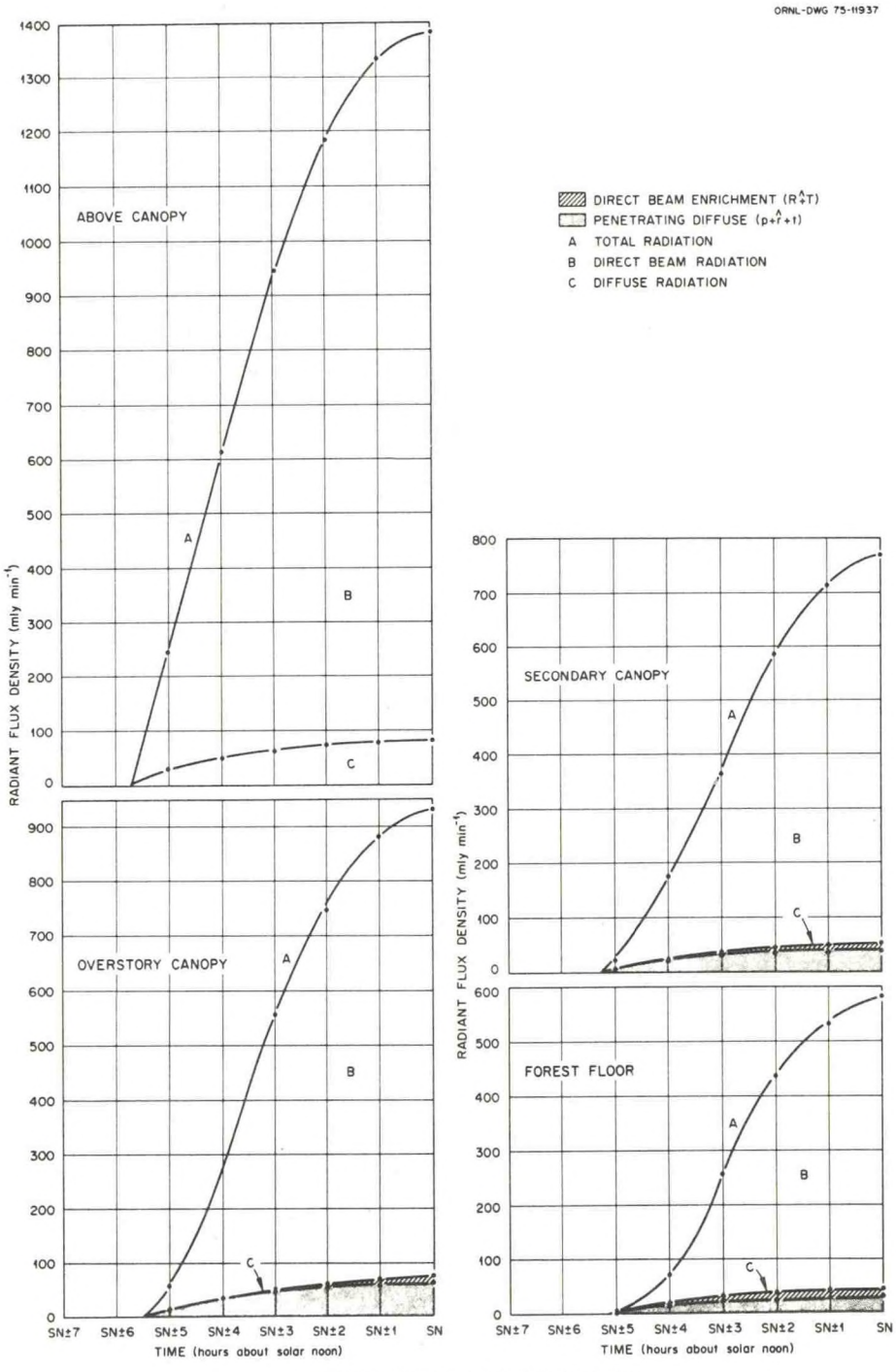


Spring Leafless Forest Solar Radiation Budget.

Figure 4: Solar radiation budgets in and above the spring leafless forest.

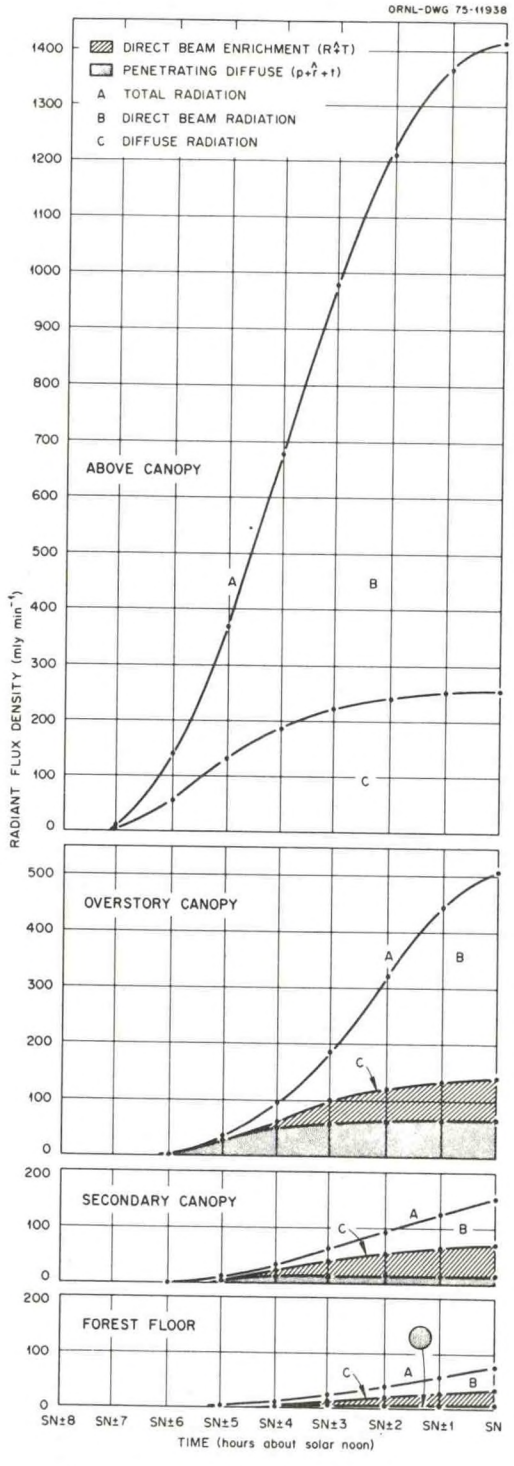


Summer Fully-Leafed Forest Solar Radiation Budget.

Figure 5: Solar radiation budgets in and above the summer fully-leafed forest.

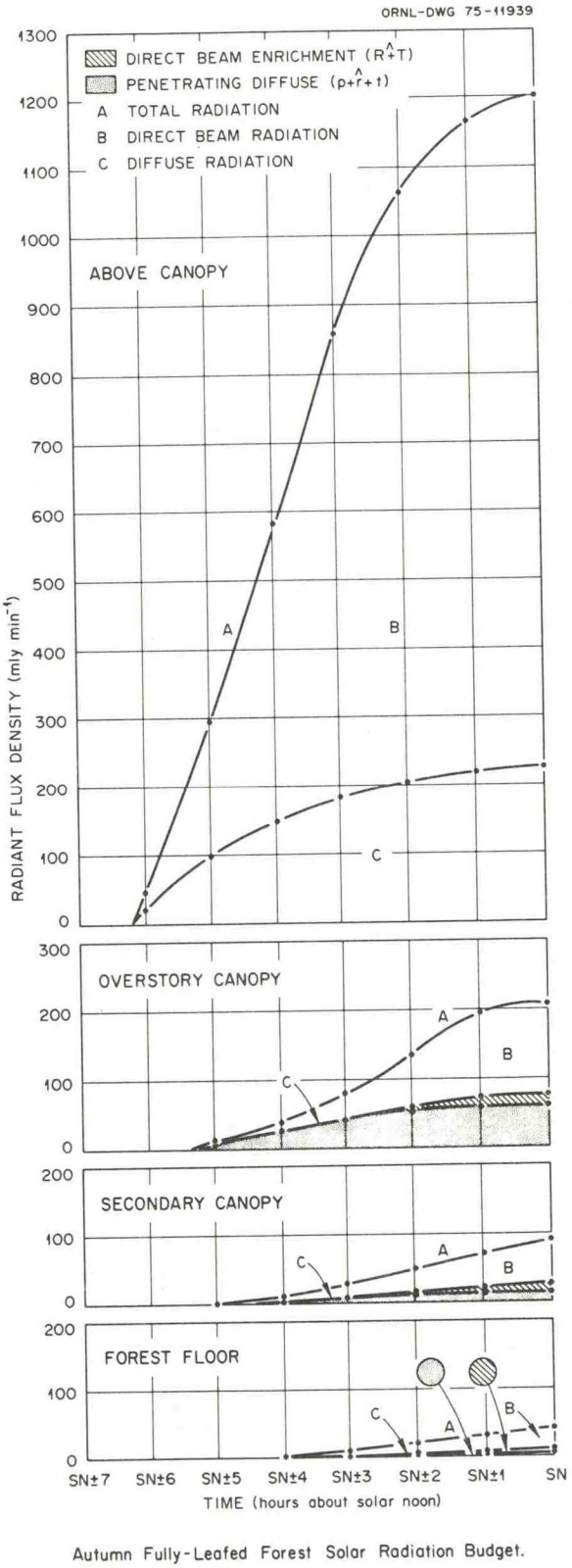


Autumn Fully-Leafed Forest Solar Radiation Budget.

Figure 6: Solar radiation budgets in and above the autumnal fully-leafed forest.

# LECTURES ON AIR POLLUTION AND ENVIRONMENTAL IMPACT ANALYSES

Sponsored by the

AMERICAN METEOROLOGICAL SOCIETY

29 September - 3 October 1975
Boston, Massachusetts

Duane A. Haugen
Workshop Coordinator

The tutorial lectures reproduced in this collection are unedited manuscripts of the material presented at the AMS Workshop on Meteorology and Environmental Assessment; their appearance here does not constitute formal pbulication.

ATDL Contribution File No. 75/15

AMERICAN METEOROLOGICAL SOCIETY
45 Beacon Street, Boston, Massachusetts, 02108 U.S.A.

# CHAPTER 3

## PLUME RISE PREDICTIONS

Gary A. Briggs

Air Resources
Atmospheric Turbulence & Diffusion Laboratory, NOAA
Oak Ridge, Tennessee

### 1. INTRODUCTION

Anyone involved with diffusion calculations becomes well aware of the strong dependence of maximum ground concentrations on the "effective stack height," $h_e$. For most conditions $\chi_{max}$ is approximately proportional to $h_e^{-2}$, as has been recognized at least since 1936 (Bosanquet and Pearson). Making allowance for the gradual decrease in the ratio of vertical to lateral diffusion at increasing heights, the exponent is slightly larger, say $\chi_{max} \sim h_e^{-2.3}$. In inversion breakup fumigation, the exponent is somewhat smaller; very crudely, $\chi_{max} \sim h_e^{-1.5}$. In any case, for an elevated emission the dependence of $\chi_{max}$ on $h_e$ is substantial.

Fortunately for people at the ground, or fortunately for people who pollute air, as the case may be, for most sources the effective stack height is considerably larger than the actual source height, $h_s$. For instance, for power plants with no downwash problems, $h_e$ is more than twice $h_s$ whenever the wind is less than 10 m/sec, which is most of the time. This is unfortunate for anyone who has to predict ground concentrations, for he is likely to have to calculate the "plume rise," $\Delta h$. Especially when using $h_e = h_s + \Delta h$ instead of $h_s$ may reduce $\chi_{max}$ by a factor of anywhere from 4 to infinity.

Presumedly, $\Delta h$ can be calculated as a function of source parameters, such as buoyancy, and meteorological conditions. Techniques for doing this have been developed by at least 50 different people and organizations, probably more than 100 (I gave up counting them six years ago). The problem is, they don't all agree. Hardly any of them agree, either with each other or with new observations if they go outside the range of variables of the observations the techniques were originally made to fit. A few of these approaches are in reasonable agreement with each other and with new sets of observations, and I will utilize them whenever they are applicable. To report on <u>all</u> the techniques for predicting $\Delta h$ would be exhausting, and totally confusing for most people including myself! I will just list all those I have come across in the extended bibliography to this paper.

Much of the confusion is due to effectively different definitions of plume rise. One common definition is that $\Delta h + h_s$ = the height of the plume at the greatest distance where it is still dectectable (by lidar, by $SO_2$ analyzer, by photography, by eye, etc.). Naturally, this would lead to different reports of the observed $\Delta h$ even for the same plume, since in more than 90% of the observations the plume has not yet leveled when it is lost sight of. This $\Delta h$ is then strongly a function of measuring technique, unless it is recognized that $\Delta h$ is a function of the downwind distance, x. This has not been the case with empirical attempts to fit plume rise observations. Without exception, they ignor x as a variable.

I prefer to define $\Delta h$ as the difference between $h_s$ and the value of $h_e$ one would need in the diffusion equation to correctly calculate $\chi_{max}$. Of course, this is only practical if we have good measurements of $\chi_{max}$ and we have adopted a specific set of diffusion coefficients to use in future calculations. One is usually most concerned with predicting $\chi_{max}$. At distances much closer in, where the plume is still rising, the ground concentration is practically zero. Sometimes we do want to know $\Delta h$ as a function of x to see whether the plume will clear close-in obstacles. At distances beyond that at which $\chi_{max}$ occurs, additional plume rise might make $\chi$ fall off a little more rapidly with x, but not much. For the plume to reach the ground in the first place, the effective diffusing velocity must considerably exceed the plume rise velocity, which diminishes with distance (for an exception, see Section 3.3).

In lieu of large sampling networks and attendent meteorological measurements to correlate $\Delta h$ with $\chi_{max}$, one is forced to detect the plume height directly and to assume that this <u>is</u> the effective stack height, or at least this approaches it. This is quite satisfactory for stable atmospheric conditions. During these, plumes are observed to rise and level off, becoming stratified and maintaining a nearly constant elevation for many kilometers downwind. However, in neutral conditions plumes never have been observed to just "level off," and very, very few observations even approach the distance at which one might expect $\chi_{max}$ to occur. In unstable conditions, the plume is even more elusive, diluting rapidly and swinging up and down enough to throw a maddening degree of scatter in the comparison with any model, no matter how elaborate. (In general, the scatter of plume rise observations compared with plume rise models is indifferent as to the complexity of the models). Occasionally, one finds in the literature an attempt to explain loops in one hour average plume trajectories in terms of plume rise theory, but my own suspicion is that these are caused by persistent areas of subsidence

or of thermal lifting or of lake/sea/river*breeze circulations - factors which are not accounted for in plume rise models at present. Not only are there many observational difficulties, but there are so many variables that $\Delta h$ could be related to - source diameter, efflux velocity, temperature elevation, stack height, wind speed, temperature profile, turbulence intensity, and so on. It is no wonder that so many plume rise formulas have been developed. What is particularly distressing is the degree to which they diverge on predicting $\Delta h$ for a given source and given conditions. See for instance Figure 1, which compares formulas of the type $\Delta h \propto U^{-1}$ times a function of the heat emission, $Q_H$.

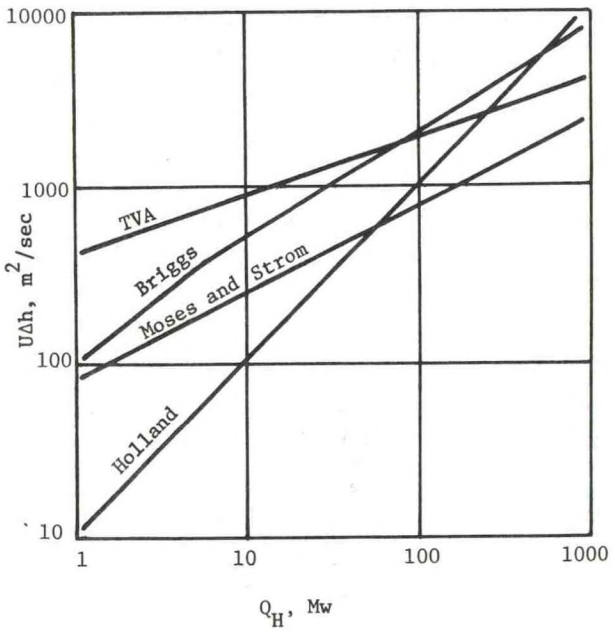


Figure 1. Plume rise times wind speed as a function of $Q_H$ according to some well-known formulas, neutral conditions.

Undoubtedly, many an engineer has felt extremely frustrated after discovering that different formulas give $\Delta h$ ranging over a factor of 10 or more! To add to his difficulties, there are other formulas which give $\Delta h$ as different powers of the wind speed, U, which give $\Delta h$ in terms of different source parameters, or which require more complex meteorological information. Then he is told that no one formula can be expected to apply in all situations. This is a sad situation indeed.

Given the apparent complexity of the problem, the only way to proceed as I see it is to build as much physical insight into one's equations as possible and to test the predictions step-by-step. This way, one may be able to dispense with many extraneous variables, ones that do not materially affect ground concentrations. Furthermore, many of the significant variables may be grouped into single variables. With these simplifications, comparisons with observations become easier, and one is more certain that the model optimumization is not being unduly influenced by a neglected or unmeasured variable.

One should be wary of allowing new dimensional constants to slip into a model, unless they are simply groups of old dimensional constants that are relevant to the problem of plume rise (e.g. gravity or specific heat capacity). If they are not, they are indicative of things going on that are not fully understood, so the assumed relationship might not be true at another time and another place. The exception to this is the discovery of new physical laws which do appear to be valid for any time and any place; an example of an old one is: gravitational force = dimensional constant x $mass_1$ x $mass_2 \div distance^2$. However, plume rise is just an application of a poorly understood branch of "old physics," namely, turbulent fluid mechanics, so I am always suspicious of new dimensional constants introduced into the problem. Unfortunately, I have resorted to such crude displays of ignorance myself in the past, when confronted with the need to specify the level of atmospheric turbulence at the plume elevation. I did not really know what was going on up there, and probably no else did either. This situation has at least improved, as you will see later.

Of course, a really clever ignorant theoretician can disguise his ignorance with <u>dimensionless</u> constants. For instance, he could say that plume rise is a function of the buoyancy parameter, F(dimensions $length^4 \div time^3$) and the eddy viscosity of the ambient turbulence, K(dimensions $length^2 \div time$). Therefore, he could say, $\Delta h$ equals a dimensionless constant times $(K^3/F)^{1/2}$. This is the only combination that works dimensionally, but who believes that plume rise is increased by more turbulence and by less buoyancy?*

---

* I have witnessed (from a small plane) a plume from a 900 MW power generating unit subside continuously for more than an hour over a river a mere 1/2 km wide - and it had to shift 1 km to the left of its original trajectory in order to come down over the river. This occurred at about 5 km downwind of the source on a sunny summer afternoon.

* The correct physical interpretation of $(K^3/F)^{1/2}$ is this. If a buoyancy-dominated plume is rising from a point source in an ambient fluid with no mean motion but possessing turbulence on scales small compared to the plume radius, the <u>internal</u> eddy viscosity of the plume dominates over K above a height proportional to $(K^3/F)^{1/2}$. In an analogous situation, it is found experimentally that an initially laminar, buoyant plume, such as a cigarette plume, breaks up into turbulence at a height $\simeq 50{,}000$ $(K^3/F)^{1/2}$, where K is the <u>molecular</u> kinematic viscosity (Yih, 1952). But this is not the plume rise height!

Someone does, or did, because this is actually the asymptotic prediction of a plume rise theory published several decades ago in a journal of high repute. Obviously, the author's physical intuition failed at some point, and the reviewer missed it. This still happens, by the way, which I guess is why our journals publish so many papers today - if you publish enough of them, a few of them are bound to contain some useful and sound information.

In what follows I try to avoid ad hoc assumptions involving previously undiscovered dimensional constants and to make qualitatively reasonable assumptions where they are required to extend previously established models. The complexities that cannot be evaded will be dealt with in as simple a manner as I believe possible, and the resulting predictions will be simplified further whenever possible. In the end we will see that the "how to" of calculating plume rise can be fairly straightforward, but getting there requires a lot of careful consideration of the problem.

## 2. THE PHYSICS OF PLUME RISE

As suggested by the introduction, the phenomenon of plume rise can be quite complex unless some simplifications can be made by careful scrutiny of the physics of the problem. Then we can judge what parameters are important, and what are not. It is also prudent to make full use of established physical laws, particularly those of fluid mechanics. We will start here with some conservation relationships. I will not develope the equations in full detail, but will describe the assumptions and theorems used to achieve the working set of equations for predicting plume rise. I hope to detail these derivations in an appendix to the planned revision of Plume Rise (Briggs, 1969).

For a qualitative description of the dynamics of plume rise, see Chapter 2 of the above reference. The treatment here will go somewhat beyond my earlier efforts in that the effect of vertical meander on determining the distance of $\chi_{max}$ will be considered (in Sections 5 and 6). This will be especially important in convective conditions.

Some will be inclined to pass over the equations in this section, but I hope that the descriptive parts of it will be given attention.

### 2.1 Conservation of Mass

As an adjunct to the other conservation equations, plume rise models make use of the continuity equation. This assumes that the rate at which the fluid mass within any element of space changes is equal to the net flow of mass across the boundaries of the element:

$$\partial\rho/\partial t = - \nabla \cdot (\rho \vec{v}) \quad , \qquad (1)$$

where $\rho$ is the local fluid density and $\vec{v}$ is the local velocity. This simply means that mass is not created or lost within the element. In some papers in the literature, however, the equation described as "conservation of mass" is really an entrainment assumption, and does not describe the conservation of anything.

We may use the continuity equation in the above form, but usually it is assumed that density variations are negligible in the inertial terms of the equations (but not in the buoyancy term). This is the Boussinesq approximation. With $\rho \simeq$ constant, the above becomes

$$\nabla \cdot \vec{v} \simeq 0 \qquad (2)$$

This greatly simplifies the development of the buoyancy, momentum and energy equations, but the use of the Boussinesq approximation is occasionally questioned (see, for instance, Ooms, 1972). From Eq. (1) we see that actually $\nabla \cdot \vec{v} = - d \ln \rho/dt$, where d/dt is the Lagrangian time derivative (it follows the fluid element). At low Mach numbers, the only occasion for significant divergence is the rise of a plume to very great altitudes, where the plume gases expand due to lower ambient pressure. In our own atmosphere, for adiabatic rise there is about a 50% drop in density for about every 7 km of additional rise. This is certainly of no concern for ordinary man-made plumes. My own feeling is that even when the rise goes to 7 km and beyond, the effect of divergence is to widen the flow at the top of the plume somewhat, thus distorting the geometry of the plume, but that the dynamics of the rise are only slightly changed by this distortion. Indeed, an ordinary plume rise equation gave quite a reasonable estimate of the rise height of the Surtsey volcano plume (Briggs, 1969).

For a vertical, axisymmetric, plume Eq. (2) can be integrated over a horizontal plane intersecting the plume to give

$$dV/dz = 2 \pi r v_e \quad . \qquad (3)$$

where r is the radius of the plume, $v_e$ is the radial inflow into the plume and $V = \rho \iint w \, d S$, where w is the vertical component of $\vec{v}$. This equation just says that the increase of the plume volume flux with height equals the total inflow at the periphery. We call $v_e$ the "entrainment velocity." It is not specified by the conservation of mass equation, but is very important because it determines the growth of the plume, which in turn determines the dilution of the buoyancy, momentum, energy, and concentration.

### 2.2 Conservation of Buoyancy

For most types of plumes, one can assume that buoyancy is conserved in the sense that the potential temperature of the each element of gas is constant. That is, the motion is assumed to be adiabatic, with the gas cooling only due to expansion as it rises to heights of lower ambient pressure. This assumes that the plume does not radiate significant heat, or absorb much solar radiation. It is possible for these factors to become significant at great distances for very opaque plumes, but such plumes are a rarity these days. Plumes have been observed to stratify in

stable air and maintain a constant level ($\pm$ 1%) for up to 15 km downwind (Gartrell, Thomas, and Carpenter, 1961).

Two kinds of plumes which do not conserve potential temperature are very radioactive plumes, which generate their own heat continuously, and plumes in which condensation or evaporation are taking place. For the ordinary stack plume,

$$d\theta/dt = \partial\theta/\partial t + ( (\vec{U} + \vec{v}) \cdot \nabla )\theta = 0 , \qquad (4)$$

where $\theta$ is the potential temperature of the gas and the velocity has been divided into two components: an ambient crosswind velocity, $\vec{U}$, and a velocity caused by the presence of the plume, $\vec{v}$. We will assume $\vec{U}$ to be constant in time and in space and horizontal. It will define the x-direction (also we will use $\vec{U} = U\vec{i}$ where $\vec{i}$ is a unit vector).

It is customary to assume the plume motion stationary, so that the average values do not change in time, and then to take a time average of the equations (this operation is assumed in the rest of this section). After this operation on Eq. (4), $\partial\theta/\partial t = 0$. We define $\theta = \theta_a + \theta'$, where $\theta_a$ is the ambient potential temperature and varies significantly only in the vertical (z) direction. This gives

$$U \frac{\partial}{\partial x} \theta' + (\vec{v} \cdot \nabla)\theta' = - w \frac{\partial}{\partial z} \theta_a , \qquad (5)$$

where w is the vertical component of the plume-induced motion. This says that the potential temperature of a gas relative to the ambient value changes only at minus the rate the ambient value is changing; its absolute value does not change, which is just exactly the adiabatic assumption.

Equation (5) can be best applied to a whole plume by intersecting the plume with a flat plane (a mathematical one, of course) and then integrating over it. For a vertical or a quasi-vertical plume, it is most convenient to use a horizontal plane. By definition, $\theta' = 0$ outside the plume. Also, if $\nabla \cdot \vec{v} \simeq 0$ we may write $( \vec{v} \cdot \nabla)\theta' = \nabla \cdot (\vec{v}\,\theta')$. This gives

$$d/dz \iint_P w\,\theta'\,dS = - \partial\theta_a / \partial z \iint_P w\,dS, , \qquad (6)$$

where $\iint_P$ signifies an integral over the plume cross-section. For convenience later on, we multiply both sides by $g/\theta_a$, which is approximated as a constant in a fashion similar to the Boussinesq approximation ($g/\theta_a$ decreases only to 15% less than the surface value at a height of ~ 10 km, near the top of the troposphere). The result is written

$$dF_z/dz = - s V, \qquad \text{where} \qquad (7)$$

$$\pi F_z = \iint_P w\, g(\theta'/\theta_a)\,dS$$

$$s = (g/\theta_a)\, \partial\theta_a/\partial z$$

$$\pi V = \iint_P w\,dS$$

$F_z$ is called the "buoyancy flux," or the buoyancy parameter, and s is the stability parameter. For a neutral atmosphere (s = 0), Eq. (7) says that the buoyancy flux of the plume does not change with height. It is then equal to the value at the source.

Equation (7) could also be applied to a bent-over plume, as long as it can be completely intersected with a horizontal plane. However, it is customary to intersect bent-over plumes with vertical planes so the normal to the plane is oriented in the downwind direction, $\vec{i}$. This makes the plume cross-section more nearly circular. We also will assume that $\partial\theta_a/\partial z$ is approximately constant through the layer occupied by the plume, and will evaluate it at the plume centerline height, $z_c$. Eq. (5) upon integration becomes

$$d/dx \iint_P (U + u)\,\theta'\,dS = - \iint_P w(\partial\theta_a/\partial z)\,dS \simeq$$

$$- \partial\theta_a/\partial z \iint_P w\,dS \quad . \qquad (8)$$

Again, we multiply both sides by $(g/\theta_a)$, which is assumed constant, so the integral on the left becomes the buoyancy flux through the plane. Also, we define $t = x/U$ so that $dx = U\,dt$ and

$$dF_z/dt = - s M, \qquad \text{where} \qquad (9)$$

$$\pi F_z = \iint_P (U + u)\, g(\theta'/\theta_a)\,dS$$

$$\pi M = U \iint_P w\,dS \quad .$$

For the bent-over plume we will see that $u \ll U$, so that M is approximately the flux of vertical momentum within the plume. This term will appear in the vertical momentum equation for a bent-over plume, but there will also be a term for the momentum of the effective mass outside the plume.

Exactly similar equations can be written for the conservation of mean molecular weight, m, and $m'/m$ can be added to $\theta'/\theta_a$ to produce a more complete definition of $F_z$. The main difference is that $\partial m_a/\partial z = 0$ in our atmosphere up to a height of

about 90 km, so the stability parameter is unaffected. We have Eqs. (7) and (9) for the variation of $F_z$, so all we need now is an initial value, F. For this calculation I like to assume that the efflux volume is mixed with a large volume of ambient air, because this is what quickly happens within the plume. When this is done for an ideal gas, we find that initially

$$F_z = F = g(1 - m_o/28.9)(T_a/T_o)V_o + g\, Q_H/(\pi\, c_p\, \rho_a\, T_a) \quad , \qquad (10)$$

where $m_o$ is the mean molecular weight of the efflux gas and 28.9 is that of air, $T_o$ is the absolute temperature of the efflux and $T_a$ is that of the ambient air, $V_o$ is the initial volume flux divided by $\pi$, g is gravity, $Q_H$ is the sensible heat emission of the stack gases, and $c_p$ is the specific heat capacity of air. If $|m_a - m_o|/m_a$ is less than 10% of $|T_o - T_a|/T$, we can neglect the molecular weight term. This is true of the emissions from most combustion processes, unless they have been cooled considerably. The second term, the buoyancy due to heat emission, can be handily approximated by

$$g\, Q_H/(\pi\, c_p\, \rho\, T) \simeq 3.7 \cdot 10^{-5} (m^4/sec^3)(p_s/p_a)\, Q_H/(cal/sec) \simeq 8.9\ (m^4/sec^3)(p_s/p_a)\, Q_H/MW \quad , \qquad (11)$$

where $p_s$ is the standard sea level pressure. For emissions with heat capacity and mean molecular weight close to those of air, this reduces to

$$F = g\,(T_o - T_a)\, V_o/T_o \quad . \qquad (12)$$

In other theoretical papers and comparisons with observations one sometimes finds F defined with $T_a$ instead of $T_o$ in the denominator. This, of course, affects the comparison of observations with models using F, so due allowance should be made for the difference. A physical interpretation of the difference between the two definitions is discussed in a footnote to Briggs (1972). I will denote this alternative definition of the buoyancy parameter by F*, after Csanady (1973, appendix).

## 2.3 Conservation of Momentum

Some form of the momentum conservation equation is required in any plume trajectory model in order to describe how the rise velocity is affected by mixing with the ambient fluid and by buoyancy force, if present. Sometimes this equation seems to just appear out of nowhere, with ad hoc terms thrown in by the modeler to satisfy his own intuition. An example is the "drag force" term, which characteristically assumes a force (per unit area of plume surface) proportional to the square of the plume's relative velocity. However, the momentum conservation equation can be derived as a special form of Newton's second law. When one does this assuming that each element of fluid experiences only pressure and buoyancy forces, one finds that terms resembling "drag force" can be eliminated.

Viscous forces are generally neglected because they act effectively on only the very smallest scales of motion, primarily on the turbulent microstructure. These forces are important as initiators of turbulent motion and as dissipators of turbulent energy. However, it appears that in order to predict the effect of viscosity directly we must predict the whole turbulent flow, a task that is beyond the capacity of computers for some time to come.* In order to make expedient predictions of the gross features of plume motion, plume rise theories have always neglected the viscous force term. As a result, they always have one more unknown than they have conservation equations, and the system of equations is not closed. This happens because the effect of turbulent mixing has not been accounted for, since the computation of turbulent motion has been bypassed. In order to close the equations, some assumption about the bulk effect of turbulent mixing must be made. This is the "closure problem" to be discussed in Section 2.5.

We assume that the only significant forces acting on any small element of fluid are pressure and gravity. The pressure force consists of two parts, one part due to hydrostatic force. The hydrostatic pressure is assumed to be the same inside the plume as it is outside the plume at the same height; $\partial p_a/\partial z = -\rho_a g$, where $p_a$ and $\rho_a$ are the ambient values of pressure and density. This is an expression of Archimedes' Principle, and will be combined below with gravitational force ($\rho$ g) to form a buoyancy term. The second pressure force is the perturbation due to the plume-induced motion, designated here as p. For convenience, let us again write the total velocity as a sum of

*"Second-order closure" methods, used on large computers, currently are capable of predicting large scale turbulent structure. However, the effect of sub-grid scale turbulence is parameterized with closure assumptions and no attempt is made to compute turbulent microstructure. Present computers are simply orders of magnitude too small to do this.

a uniform, horizontal crosswind $\vec{U}$ and a plume perturbation velocity $\vec{v}$. We can set $\vec{U} = 0$ later for the case of no crosswind. Our starting equation is then

$$d(\vec{U} + \vec{v})/dt + \rho^{-1} \nabla p = g(\rho'/\rho)\vec{k} \quad , \qquad (13)$$

where $\rho' = \rho_a - \rho$ and $\vec{k}$ is a unit vector pointed upward.

When the plume gas is mostly entrained air, $\rho'/\rho \simeq \theta'/\theta_a + m'/m_a$, which appears in the full definition of the buoyancy flux $F_z$ discussed at the end of Section 2.2. The definitions given in Eqs. (7) and (9) included only the potential temperature term, $\theta'/\theta_a$.

The Lagrangian time derivative can be expressed as the sum of the partial derivative with respect to time at a fixed point and advection terms. Utilizing some vector relationships, we may write

$$d(\vec{U} + \vec{v})/dt = \partial(\vec{U} + \vec{v})/dt + ((\vec{U} + \vec{v}) \cdot \nabla)\vec{v}$$

$$((\vec{U} + \vec{v}) \cdot \nabla)\vec{v} = U \partial\vec{v}/\partial x$$

$$+ \nabla(1/2\ \vec{v}^2) - \vec{v} \times (\nabla \times \vec{v}) \quad , \qquad (14)$$

where x is the space coordinate in the $\vec{U}$ direction and X is the vector cross product. We will assume a stationary process and take a time average, so the partial time derivative term will be zero. We could do Reynolds' averaging at this point by dividing $\vec{v}$ into a mean value and a fluctuation from the mean. This won't be necessary here as the Reynolds stresses affect only the internal distribution of momentum in the plume, and we aim only to describe the mean plume momentum.

We will make use of a theorem that states that any inviscid fluid that is initially in potential flow, that is, with $\nabla \times \vec{v} = 0$, remains so until acted upon by a non-potential force (Lamb, 1932, p 18). Since pressure force is given by a potential, i.e., $\nabla p$, the only non-potential force in Eq. (13) is buoyancy. Since, by definition, $\rho' = 0$ outside the plume, the above theorem implies that $\nabla \times \vec{v} = 0$ outside the plume. Only inside the plume is the motion rotational ($\nabla \times \vec{v} \neq 0$)*. Then outside the plume we can say that

$$\vec{v} = -\nabla\phi \qquad (15)$$

$$p = \text{constant} + \partial\phi/\partial t - (1/2)\ \rho\ \vec{v}^2 \quad ,$$

where $\phi$ is a potential function. Since we assume stationarity, $\partial\phi/\partial t = 0$.

To make Eq. (13) into a plume equation, we simply intersect the plume with a flat plane and integrate over its surface, S. Let $\int\int_p$ indicate integration over the plume cross section only, $\int\int_A$ indicate integration over any area which includes the plume, and $\int\int_\infty$ indicate integration over an infinite plane. We make use of Green's theorem to evaluate the pressure force acting in the S-plane: $p \int\int_S \nabla_S\ p\ dS = p \oint p\ d\vec{s}$, where $d\vec{s}$ is an element of the plume periphery and is directed inward. This integral is just the resultant external pressure force pushing against the plume.

There is one more step that can be taken to simplify the momentum equation for a plume, and that is to assume that $\int\int_A \vec{v}^2\ dS$ is bounded as $A \to \infty$. That is, the kinetic energy of the plume-induced motion cannot be infinite on any plane intersecting the plume. This is common sense, and also could be proven mathematically by using the simple-source theorem (see p 58 of Lamb, 1932). By making this step, we can transform the rotational motion term into an axial derivative:

$$\int\int_p \vec{v} \times (\nabla \times \vec{v})\ dS$$

$$= (\partial/\partial n) \int\int_\infty (1/2\ \vec{v}^2\ d\vec{S} - v_n \vec{v}\ dS) \quad , \qquad (16)$$

where n is the space coordinate normal to S and $\vec{S}$ is also aligned in this direction.

When we do this, terms resembling "drag force" drop out. This happens because potential flow is frictionless. High Reynolds number drag is due to the advection of momentum by a turbulent wake, but we have assumed irrotational motion outside the plume; this cannot be turbulent. In order for this assumption to be valid, either the plume has no turbulent wake, or it has a finite wake which is included as part of the plume in the integral equations. Let us consider the mechanism of wake development.

The velocity next to the surface of a solid object is zero, so rotational motion must develope due to velocity shear. This vorticity diffuses outward by molecular diffusion. At high Reynolds number, this boundary layer flow, which is viscous and rotational, is completely arrested at some point along the backside of the object by the adverse pressure gradient, and a counterflow developes to the lee of this point. This forces the boundary layer to separate from the object and to enter the free flow, carrying its accumulated vorticity with it and creating a wake region.

---

* Outside fluid that is "entrained" by the plume does not immediately acquire rotationality. It must first be so stretched and twisted by the chaotic, turbulent motion of the surrounding plume that it becomes thin enough for density differences and vorticity to diffuse into it by molecular diffusion.

A plume is quite different, since it is fluid and its surface is a free surface, so the "no slip" condition present at a solid boundary does not apply. More important, if a viscous, rotational boundary layer did develop along the "skin" of the plume, at high Reynolds number this layer thickens at a rate much slower than the rate at which the plume expands due to turbulent entrainment.* It seems likely then that the plume would envelope shear layer vorticity just as fast as it is created, so there would be none available for the formation of a wake.

There is ample evidence that bent-over plumes have no wake under them. Tsang (1971) found concentrated vorticity only towards the rear half of a laboratory thermal, with practically none outside it and surprisingly little vorticity in the leading half of the thermal. Briggs (1970) noted that the average shape of Fan's channel plumes, defined by above ambient salt concentrations (Fan, 1967), was identical to the average shape of the turbulent region of Richards' laboratory thermals (Richards, 1963). Both were kidney shaped. In the case of a non-buoyant jet, the introduction of a drag force term proportional to $C_D$ into the momentum equation results in an altered trajectory equation; rise would be proportional to downwind distance raised to the power $+(1/3 + \text{constant} \cdot C_D)$, instead of $+ 1/3$. However, the data shown in Section 3.2 lend good support to the "1/3 law" of rise, implying that $C_D \simeq 0$.

The case of a quasi-vertical plume in a crossflow may be complicated by the presence of a stack wake. At low ratios of efflux velocity, $w_o$, to U, the stack wake quickly overtakes the plume and downwash may occur due to the low pressure in the lee of the stack and to descending ambient streamlines. At high values of $w_o/U$, it is possible that a stack wake will be drawn upwards by the plume, since rising, bent-over plumes induce substantial vertical motion underneath themselves. This would not be a plume wake, but it is unclear to me what effect it would have on the plume trajectory. This type of wake interaction is not accounted for in present plume rise theories, but there is no evidence that it is of any practical consequence.

*Roughly speaking, the thickening rate is $\sim(\nu u/b)^{1/2}$, where $\nu$ is the kinematic viscosity, u is the velocity shear, and b is the plume radius, whereas the plume growth rate is $\sim u$. The ratio of these is $\sim Re^{-1/2}$, where Re is the Reynolds number. Re is of the order of $10^5$ to $10^7$ for full-sized plumes.

Accepting the above assumptions, the resulting momentum equation is

$$U\Big[\underset{A}{\iint}\frac{\partial}{\partial x}\vec{v}\,dS - \underset{A-P}{\iint}\frac{\partial}{\partial n}u\,d\vec{S} - \underset{A}{\oint}u\,d\vec{s}\Big] \qquad \text{(a) (b) (c)}$$

$$+\rho^{-1}\underset{P}{\iint}\frac{\partial}{\partial n}p\,d\vec{S} - \underset{\infty-P}{\iint}\frac{\partial}{\partial n}(1/2\,\vec{v}^2)d\vec{S} \qquad \text{(d) (e)}$$

$$+\underset{\infty}{\iint}\frac{\partial}{\partial n}(v_n\vec{v})dS = \vec{k}\underset{P}{\iint}g(\rho'/\rho)dS \quad . \qquad \text{(f)} \qquad (17)$$

This does not appear simple at first, but it is in a completely generalized form. Certain terms will drop out as we orientate $\vec{S}$ either vertically ($\vec{S} = S\vec{k}$) or parallel to $\vec{U}$ ($\vec{S} = S\vec{i}$). The lateral component of this equation is identically zero if the plume is symmetric about the x - z plane, which is true if the initial boundary condition is symmetric on the x - z plane. If there is no crossflow, U = 0 and the first three terms are dropped. Note that Eq. (17) applied to an arbitrary choice of A, as long as A includes P. Some of the terms already cancelled outside the plume, so only $\iint_P$ is left.

For a vertical plume in no wind, the first three terms of Eq. (9) are zero, and the non-vertical components cancel due to symmetry. We chose to intersect the plume with horizontal planes, so $\vec{S} = S\vec{k}$, $\partial n = \partial z$, and $v_n = w$. It is possible to show that terms (d) and (e) are both of the order $\alpha^2$ times term (f), where we define the entrainment coefficient $\alpha = v_e/\bar{w}$ and $\bar{w}$ is defined below. Experimentally, $\alpha \simeq 0.1$, so terms (d) and (e) are negligible. If $\alpha$ is assumed constant, which will be the closure assumption chosen in Section 2.5, these terms could easily be combined with term (f) under conditions of similarity, but no significant change in the plume rise prediction would result. Term (f) just represents the total flux of vertical momentum. Since $w^2$ is much larger inside a vertical plume than outside of it, most of this flux occurs within the plume (a crude calculation shows that just outside the plume boundary, $w \simeq 2\alpha^2\bar{w} \simeq 0.02\,\bar{w}$).

In order to put the momentum equation for a vertical plume into the familiar form appearing in classical "top hat" plume models (Morton, Taylor and Turner, 1956), it will be convenient to define

$$\pi\bar{w}V = S_1\underset{\infty}{\iint}w^2\,dS \qquad (18)$$

$$S_1 = \left[\frac{\iint_P wg\,(\rho'/\rho)\,dS}{\iint_P g\,(\rho'/\rho)\,dS}\;\frac{\iint_P w\,dS}{\iint_\infty w^2\,dS}\right]^{1/2}$$

$S_1 = 1$ if $\rho' = 0$ (no buoyancy)

where V is defined in Eq. (7) and $S_1$ is just a shape factor. These are just definitions, but now I would like to assume that the variation of $\ell n S_1$ with height is very small compared to the variation of $\ell n(\int\int w^2 \, d\, S)$. This permits us to reduce Eq. (17) to

$$d(\bar{w}\, V) \,/\, \partial z = F_z \,/\, \bar{w} \qquad (19)$$

$$\pi F_z = {}_P\int\int w\, g\, (\rho'/\rho)\, d\, S \; .$$

The variation of $F_z$ with height was given by Eq. (7), and the initial value was given by Eqs. (10) - (12). Note that the validity of Eq. (19) does not require constant profile shapes (similarity), as long as they change sufficiently slowly with height.

Suppose now that we have a quasi-vertical plume in a crosswind, that is, a plume that is just starting to bend over. For this case we can still use a horizontal plane of integration, but we must include terms (a) and (b) of Eq. (17). The vertical component of term (c) is zero. The sum of terms (a) and (b) is the same regardless of the choice of A. We can remove one of these terms by letting A = P (this eliminates term (b)) or by letting A = $\infty$ (this eliminates term (a) as a result of the boundedness of $\int\int w^2 \, d\, S$). In the latter case, before taking d/dz the ratio of term (f) to term (b) is $\int\int w w \, d\, S \div {}_{\infty}{}_P\int\int u\, U \, d\, S$. Since the perturbation velocity u outside the plume should be less than the mean value inside the plume, $\bar{u}$, the above ratio should be larger than $\bar{w}^2/(\bar{u}\, U)$. The slope of the plume centerline is $\bar{w}\,/(U + \bar{u})$, so we can show that $\bar{w}^2/(\bar{u}U) \approx R^2/(1 + R/\text{Slope})$ for a non-buoyant plume (with $\bar{w}\, V \approx w_o\, V_o$, $u\, V \approx - U\, V_o$, and R is defined $= w_o/U$). It should be larger for a buoyant plume. Then as long as R is fairly large, say >2, and the plume is not bent-over, say that the slope >1, term (b) has only a small effect and Eq. (19) is approximately valid for the quasi-vertical plume.

For the $\vec{i}$ component of Eq. (17), with $\vec{S} = S\,\vec{k}$ we find that all the terms except for term (f) are zero or cancel out, so

$$d/dz \int\int_{\infty} u\, w \, d\, S = 0 \; . \qquad (20)$$

This just states that the flux of horizontal momentum is constant, and is analogous to Eq. (19) in the absence of buoyancy. For a vertically oriented emission of volume flux $\pi\, V_o$, the initial value of the above integral is $- U\, V_o$ and

$$\bar{u}\, V = - U\, V_o \qquad (21)$$

$$\bar{u} = \int\int_{\infty} u\, w \, d\, S \,/\, {}_P\int\int w \, d\, S$$

Finally, for a bent-over plume let us use a plane of integration oriented parallel to the crossflow ($\vec{S} = S\vec{i}$). For the vertical component we have from Eq. (17)

$$U\,[d/dx\; {}_A\int\int w \, d\, S - {}_A\oint u \, d\, y] + d/dx \int\int_{\infty} u\, w \, d\, S =$$
$$\text{(a)} \qquad\qquad \text{(b)} \qquad\qquad \text{(c)}$$

$${}_P\int\int g\, (\rho'/\rho)\, d\, S, \qquad (22)$$

where y is the lateral space coordinate. Outside the plume terms (a) and (b) cancel, for we can write $\vec{v} = - \nabla\, \phi$ and $\oint u \, d\, y = - d/dx \oint \phi \, d\, y = d/dx \int\int w \, d\, S$ (in this case $d\, S = d\, y\, d\, z$). Term (c) is of the order $\bar{u}/U$ times term (a), and can generally be neglected for bent-over plumes because $|\bar{u}/U| = V_o/V$ and $V/V_o$ is large (see Eq. (27)).

For the bent-over case, let us define a time $t = x/U$, so that $U\, d/dx = d/dt$, and use the relation $u = - \partial\phi/\partial x$ around the periphery of the plume. Dropping term (c) of Eq. (22), we have

$$d/dt \; ({}_P\int\int w \, d\, S - {}_P\oint \phi \, d\, y) = {}_P\int\int g(\rho'/\rho)\, d S. \qquad (23)$$

A very similar equation can be developed for the purely two-dimensional case, such as for a line thermal in a fluid at rest. The main difference is that such a flow is not stationary, so $\partial/\partial t$ terms must be retained. The resulting equation is identical to Eq. (23) with d/dt replaced by $\partial/\partial t$. However, the above definition of t means that d/dt in this context is Lagrangian only in the sense that the observer moves downwind at the free stream velocity, U. This forms the mathematical basis for the notion that a bent-over, continuous plume is practically equivalent to a horizontal instantaneous line thermal. Hence the relevance of line thermal laboratory models such as those of Richards (1963) and of Tsang (1971).

For the purely two-dimensional case, we can express the mean velocities as derivatives of a stream function, $\psi$. Then $w = \partial\psi/\partial y$, and the first integral of Eq. (23) becomes $p\oint \psi \, d\, z$. This has a form similar to the second term. If the velocity profiles maintain similarity, these two terms will maintain a constant ratio. The first term has been related to the flux of vertical momentum within the plume in Eq. (9). In the context of two-dimensional motion we see that the second term is $- {}_P\oint(\partial\phi/\partial t) d\, y$. This is just the pressure force on the plume due to accelerative motion outside the plume, which is due to the effective mass of fluid outside the plume which must get out of the way. Then it seems appropriate to define an effective vertical momentum flux by

$$\pi\, M_{eff} = U\, ({}_P\int\int w \, d\, S - {}_P\oint \phi \, d\, y) \; . \qquad (24)$$

For the streamlines of buoyant thermals measured by Richards (1963), the ratio $M_{eff}/M \approx 2.3$. This ratio explains most of the discrepancy between the visible plume radius and the effective plume radius that determines rise (see Briggs, 1972).

Multiplying Eq. (23) by U, and assuming that $u << U$ so that $_p\iint U\, g(\rho'/\rho)\, d\, S \simeq F_z$, we have finally

$$d\, M_{eff} / d\, t = F_z \quad . \qquad (25)$$

The variation of $F_z$ with height was given by Eq. (9) and the initial value was given by Eqs. (10) - (12). Note that if the variation of $\ell n\, (M_{eff}/M)$ is much less than the variation of $\ell n\, (M_{eff})$, $d\, M_{eff}/d\, t = (M_{eff}/M)\, d\, M/d\, t$, forming an equation pair with Eqs. (25) and (9) similar to Eqs. (19) and (7) for vertical plumes. Since we would like to use Eq. (25) for predicting the centerline rise of a bent-over plume, let z designate this rise. Define $\bar{w} = dz/dt = U\, dz/dx$ for a bent-over plume. Finally, define an effective volume flux V and effective plume radius r by

$$M_{eff} = \bar{w}\, V = \bar{w}\, (U\, r^2) \qquad (26)$$

Lets take a quick look at the $\vec{i}$ component of momentum for a bent-over plume. The terms (a) and (b) of Eq. (17) combine, term (c) drops out, and terms (d), (e) and (f) are all of the order $\bar{u}/U$ times the first terms, so we will neglect them. All this is left is

$$d/dx\ _p\iint u\, U\, d\, S = 0 \qquad (27)$$

which says that the horizontal momentum deficit is conserved and is analogous to Eq. (20). For a vertically oriented emission we have $p\iint u\, U\, d\, S = - U\, V_o$. Since $_p\iint U\, d\, S \simeq V$, and since $V >> V_o$ in the bent-over stage of rise (except for very close in when $w_o < U$), the assumption that $|u| << U$ appears to be justified.

Finally, from Eq. (18) we find the initial values of $(\bar{w}\, V)$ or of $M_{eff}$, designated by $F_m$:

$$F_m = (\rho_o/\rho_a)\, w_o\, V_o \qquad (28)$$

$F_m$ is the initial vertical momentum flux. To allow for the possibility that initially $\rho$ may not be approximated by $\rho_a$, as assumed with the Boussinesq approximation, the ratio of the initial density, $\rho_o$, to $\rho_a$ is included in the above definition. It is applicable non-vertically oriented emissions also, as long as $w_o$ is the vertical component of efflux velocity. In this case, an initial horizontal momentum flux for use in Eqs. (20) and (26) can be defined just as in Eq. (28), using $(u_o - U)$ instead of $w_o$.

This section has been lengthy, but the momentum equation is central to plume rise models and we would like to put it on firm ground. The resultant equations, (19) and (20) for a vertical or quasi-vertical plume and Eqs. (25) and (26) for a bent-over plume, are quite simple, yet are rigorous statements with the limitations described.

## 2.4 Conservation of Energy

The mass, buoyancy, and momentum equations constitute a complete set of conservation equations, but sometimes a fourth one is obtained for kinetic energy. (Note that in some papers, what is labeled the "energy conservation" equation corresponds to the "buoyancy conservation" equation here. It basically refers to heat energy, where in this section we are going to refer to kinetic energy. Of course, the kinetic energy of turbulent motion in a plume is eventually dissipated into heat energy by viscosity effects, but this can double the original plume buoyancy only when the rise exceeds $(T_a\, c_p/g)$, about 30 km in our atmosphere). Basically, the energy equation is obtained by multiplying the momentum equation by $\vec{v}$ and simplifying the result by using the continuity equation (Eq. (1) or (2)). Since it is derived from other conservation relations, the energy conservation equation can not give any new information. However, it does offer alternative possibilities for closure of the set of equations. These are to be discussed in the next section.

There are two forms of the energy conservation equation, one for the total kinetic energy and one for the kinetic energy of the mean motion only. The first is obtained by multiplying Eq. (13) by $\vec{v}$ and then taking an average. For a vertical plume, the result is often approximated by

$$d/dz\ _p\iint (1/2\ \vec{v}^2)\, w\, d\, S = F_z \qquad (29)$$

where $1/2\ \vec{v}^2$ is the total kinetic energy, consisting of the sum of the turbulent kinetic energy, $1/2\ q^2$, and the kinetic energy of the mean motion. Since the latter is primarily vertical, it can be approximated by $1/2\ \bar{w}^2$ times a profile shape factor. This is the equation used by Telford (1966) to determine the turbulent energy, which he uses in his closure assumption. It appears in the form which he gives only after substituting $F_z$ from the momentum equation (Telford, 1968). Wang (1973) also uses this equation to determine $q^2$, but the model is already closed without it.

However, Eq. (29) is a questionable approximation because it neglects a term that is of the same order as the $(q^2\, w)$ part of the equation. This term is minus the vertical component of the Reynolds stress tensor times the mean velocity. Assuming the vertical mean velocity to be dominant, this term is properly accounted for by replacing $1/2\ q^2$ with $(1/2\ q^2 + \overline{w'^2})$, where $\overline{w'^2}$ is the variance of the vertical component of turbulent velocity. Other terms have also been neglected, namely those involving the axial gradient of pressure, but this may be justified.

For a bent-over plume, an equation identical to Eq. (29) with w replaced by U can be derived. In this case, however, dz must be defined as $(\bar{w}_b/U)\, dx$ with $\bar{w}_b$ defined by $p\iint g(\rho'/\rho)\, wdA \div F_z/U)$. In other words, $\bar{w}_b$ is the mean vertical velocity within the plume weighted by the local buoyancy. The objections raised in the above paragraph do not apply to the bent-over plume, because $U >> |\vec{v}|$, so the other terms are negligible.

Shwartz and Tulin (1971) use a form of this equation for a bent-over plume with similarity of velocity and temperature profiles assumed. It is also assumed that $q \propto \bar{w}$. Their Eq. (3) appears to me to require the approximation $\Delta\theta/\theta << \rho'_o/\rho_a$ in order to be correct, where $\Delta\theta$ is the change in ambient potential temperature through the whole layer of rise and $\rho'_o$ is the initial density difference of the effluent. The above approximation is valid for a plume, but it was not stated by the authors.

The alternative form of the energy equation is obtained by multiplying Eq. (13) by the mean plume-induced velocity $\vec{\bar{v}}$, then taking an average. The result for a vertical plume is approximated by

$$d/dz \int\int_P (1/2\, \vec{\bar{v}}^2)\, w\, d\, S = \int\int_P (\nabla \cdot \vec{\tau}_z)\, w\, d\, S, \qquad (30)$$

where $\vec{\tau}_z$ is the vertical part of the Reynolds stress tensor; the other parts are neglected, since $\bar{w}$ is much larger than the other components of mean plume motion. The above equation is used in the models of Priestley and Ball (1955) and of Fox (1970).

Note that either form of the energy conservation equation, Eq. (29) or Eq. (30), introduces a new unknown into the problem that does not appear in the other conservation equations, i.e. either $q^2$ or $\tau$, Thus adding this conservation equation to the others does not close the equations, It does permit closure by means of assumptions about $q^2$ or $\tau$, as opposed to, say, assumptions that the entrainment velocity, $v_e$. This was done in the above-mentioned theories, except that Telford used all four conservation equations and assumed something about both $v_e$ and q, namely, $v_e \propto q$. The choice of closure assumption is arbitrary, but the resulting predictions are different, as we will see in the next section.

Several models include an additional term in the energy equation for dissipation of turbulent energy (Shwartz and Tulin, 1971; Tulin and Shwartz, 1970, Wang , 1973). This is a valid consideration, but this term is not derivable because it arises from the viscous dissipation of small-scale turbulence. However, experience with turbulent flows has shown that the dissipation rate tends to be proportional to the rate of production of turbulent energy. For a vertical plume, this is given approximately by subtracting Eq. (30) from Eq. (29). Thus the turbulent dissipation is of the same form as the last term of Eq. (30), which involves $\vec{\tau}$; when dissipation is included, it just increases the size of this term, but does not change the character of the solution. In the above models, equations similar to Eq. (29) are used with a dissipation term added. Implicity, $\tau \propto \bar{w}^2$ is assumed in these theories, as the dissipation is assumed to be $C_d|\bar{w}|^3 r$, where $C_d$ is a dimensionless dissipation constant and r is a characteristic plume radius. (Wang includes also a "form drag" term, which is probably unnecessary, but at any rate is identical in form to the dissipation term).

When Eq. (29) is used without a dissipation term, as in Telford's model, reasonable asymptotic results are obtained for buoyant plumes, probably because asymptotically $|\bar{w}|^3 r \propto F_z$ and so the character of the solution is unchanged by neglecting this term. However, in the absence of buoyancy, the asympototic prediction of Telford's model is $b \propto z^2$, in great contrast to the observation that $b \sim z$. This happens because the scale of energy-containing turbulent eddies is implicitly assumed to be $\propto b$, which grows; if no turbulent energy dissipation is assumed, then one, in effect, assumes a "reverse cascade" of turbulent energy, progressing from small eddies to large eddies. This is the reverse of what actually happens in turbulent flows (see, for instance, Tennekes and Lumley, 1972). In fairness, it must be said that Telford intended his model for convective plumes only, not for jets.

## 2.5 Closure Methods

As discussed in Section 2.3, regardless of the choice of conservation equations, they do not provide a complete plume rise model because there is always at least one more unknown than there are conservation relationships. This results from our failure so far to calculate the entire turbulent motion, including turbulent eddies down to the scale where molecular diffusion occurs. No present plume rise theory, indeed, no turbulence theory, has gotten around this stumbling block. In order to make a model predict the gross dynamics of the plume, one is forced to make up some relationship among the unknowns already present in the conservation equations. Once such a "closure assumption" is made, the set of equations is mathematically closed; given initial conditions and the ambient parameters, the equations can be solved for real cases.

In addition, there is the problem of ambient turbulence, which is not even properly dealt with in the conservation equations. Most theories assume, with good observational support, that the plume's own turbulence far overrides the effects of ambient turbulence in the early, more vigorous stage of rise. What happens when the internal turbulence loses dominance over the ambient turbulence seems to be anybody's guess. At least, many people, including myself, have speculated about this stage of rise. The lack of any complete set of measurements of plume rise and ambient turbulence parameters at this stage of rise has been discouraging, but is no deterrent to plume rise modelers. After all, in the absence of stable stratification one simply does not get any final rise unless one makes a fairly strong assumption about the effect of ambient turbulence.

The problem with the need for closure is that there are so many ways to do it, as Table I will show. Most distressing, different closure schemes give different answers. Sometimes the available data make the choice clear, but often the choice is left ambiguous. Sometimes one must choose on the basis of convenience; many of the models are not readily applicable to real cases.

Table I summarizes most of the basic rise plume rise models (not the variations on them) in the literature. I have probably overlooked a few, and wish to apologize if any

Table I - Summary of Basic Plume Rise Models

| Models for U = 0 | Ambient Conditions $\partial\theta_a/\partial z$ | Ambient Conditions Turbulence | Conservation Equations | Method of Closure |
|---|---|---|---|---|
| Morton, Taylor, Turner 1956 | Yes | --- | CBM | $v_e = \alpha \bar{w}$ |
| Abraham 1963 | Yes | --- | CBM | $r \propto s$ |
| Priestley and Ball 1955 | Yes | --- | (C)BM$\bar{K}$ | $\tau \propto \bar{w}^2$ |
| Telford 1966 | Yes | Yes | CBMK | $v_e \propto q$, extrainment $v_{ex} \propto u'$ |
| **Models for U ≥ 0** | | | | |
| Bryant 1949 | --- | --- | CBM* | dr/ds = function $(R, r/r_o, \theta_{e\ell})$ For U = 0, $r \propto z$. For U > 0, $r \propto x^{1/3}$ |
| Sutton 1950 | --- | Yes | None | $\bar{w} \propto (F/s)^{1/3}$, terminate at $\bar{w} \propto U$ |
| Bosanquet 1957 | Yes | Yes | CBM | $v_e = \alpha\|v_r\|$, $v_e \propto u' \propto U$ |
| Scorer 1959 | --- | Yes | CBM | $r \propto z$, terminate at $\bar{w} \propto u' \propto U$ |
| Briggs 1964 | Yes | Yes | CBM | $v_e = (\alpha \sin\theta_{e\ell} + \beta \cos\theta_{e\ell})\bar{w}$, $v_e = \gamma(\varepsilon r)^{1/3}$ |
| Fan 1967 | Yes | --- | CBM* | $v_e = \alpha\|v_r\|$ |
| Hoult, Fay, Forney 1969 | Yes | --- | CBM | $v_e = \alpha\|v_p\| + \beta\|v_t\|$ |
| Abraham 1971 | --- | --- | CBM* | $v_e = \alpha v_p + \beta v_t \cos\theta_{e\ell}$ |
| Hirst 1971 | Yes | --- | CBM($\bar{K}$) | $v_e = \alpha\|v_p\| + \beta\|v_t\|$, α and β both functions of Fr |
| Ooms 1972 | Yes | Yes | CBM* | $v_e = \alpha\|v_p\| + \beta\|v_t\| \cos\theta_{e\ell} + \gamma u'$ |
| Campbell and Schetz 1973 | --- | --- | CBM* | $v_e = \alpha(v_s - U)$ |
| **Models for U > 0** | | | | |
| Priestley 1956 | Yes | Yes | CBM | $r = \alpha z$, $\alpha \propto u^{1/2}$, decay time $\propto (\alpha\Delta h)^2/K_d$ |
| Schmidt 1965 | --- | Yes | CB | $r^2 \propto x^{2-m}$, m as for passive plumes |
| Moore 1968 | --- | Yes | CBM | $r = \beta z$, $\beta \propto (U^2 w_o r_o/F)^{1/6}$ puff buoy. $\approx (F/U)(6r_o + x/4)$. terminate at $x \propto h_s^{4/9}$ |
| Slawson and Csanady 1967 | --- | Yes | CBM | $v_e = \beta\bar{w}$, $dr^2/dt \propto \varepsilon^{1/3} r^{4/3}$, $dr^2/dt = K_d$ |
| Slawson and Csanady 1971 | Yes | Yes | CBM | Same, except $v_e = \beta\|\bar{w}\|$ |
| Tulin and Shwartz 1970 | --- | --- | CMK'$V_{or}$ | Similarity of internal velocities; similarity of external velocities. |
| | Yes | --- | CBK' | $r = \beta z$ |
| Shwartz and Tulin 1971 | Yes | --- | CBK' | $v_e = \beta\|\bar{w}\|$ |

Conservation equations: C = continuity, B = buoyancy, M = momentum, K = total kinetic energy (K' includes dissipation), $\bar{K}$ = kinetic energy of mean motion, $V_{or}$ = vorticity.

Closure notation: $v_e$ = entrainment velocity, defined by $dV/ds = 2r\, v_e$, V = effective volume flux of plume ÷ π, s = distance along plume axis, r = effective plume radius, defined by $V = v_s r^2$, $\theta_{e\ell}$ = slope of plume axis above horizontal. Mean velocities of the plume are as follows: $v_s$ = total = $(\bar{w}^2 + (U + \bar{u})^2)^{1/2}$, $\bar{w}$ = vertical, $\bar{u}$ = relative horizontal, $v_r$ = relative total = $(\bar{w}^2 + \bar{u}^2)^{1/2}$, $v_p$ = shear parallel to plume axis = $v_s - U\cos\theta_{e\ell}$, $v_t$ = transverse shear = $U \sin\theta_{e\ell}$.

Other parameters: α, β and γ = dimensionless constants, τ = Reynolds stress in plume, q = variance of plume turbulent velocity, u' = variance of ambient turbulent velocity, $v_{ex}$ = "extrainment" velocity, $R = w_o/U$, ε = ambient turbulent energy dissipation rate, Fr = local Froude number of plume = $v_r^2 v_s\, r/F_z$, $K_d$ = ambient eddy diffusivity.

* Includes a drag force term. The following values of the coefficient of drag $C_D$ were suggested: Bryant, $C_D = 1$. Fan, $C_D = 0.1$ to 1.7. Abraham (1971), $C_D = 0.3$. Ooms, $C_D = 0.3$. Campbell and Schetz, $C_D = 1.6$.

misrepresentations have been made (the present author admits that he has not studied all of these references in detail, and wonders whether anyone else has either!) The table lists the conservation equations used in each model in an abbreviated form. A parentheses indicates an equation used to solve for a specific variable, but not used to obtain closure. In the final column, the essential closure assumptions of each model are given in a very abbreviated form.

This table is by no means exhaustive, but certainly is exhausting enough. It is no wonder that there are such a variety of theoretical predictions for plume rise. There are even more empirical schemes, which make little attempt to account for the physics of the problem. Obviously, a full discussion of each model and its relative merits could occupy a book. I will attempt a brief discussion of the main ideas.

Note that most of the models use only the continuity equation, buoyancy conservation and some form of momentum conservation equation. Every one of these obtains closure with an assumption about the entrainment velocity or about the growth of the plume radius, r. The rate of growth of r is related to the entrainment velocity by

$$dr/dt = v_e - (r/2)\, d\, v_s/ds, \qquad (31)$$

where dt has been consistently defined by $dt = ds/v_s$. The second term on the right is the change of the plume radius due to change of velocity along the axis, and causes no change in the flux of plume volume. For a bent-over plume, $v_s \approx U$ and $dr/dt \approx v_e$.

Of the models for the calm case, the model of Morton, Taylor and Turner (1956) is now a classic, being the take-off point for many subsequent plume rise models. Actually it originated with G. I. Taylor (1945) and was re-invented by Morton and Turner, so it goes back at least 30 years. This will be referred to as the MTT model. The closure assumption is that the entrainment velocity, which arises quite naturally from the continuity equation, scales to the mean vertical velocity at any height. For a jet, a plume of zero buoyancy, this combines with the momentum equation to give $dr/dz = 2\alpha$, while for a purely buoyant plume $dr/dz = (6/5)\alpha$ in neutral surroundings. In stable surroundings, $dr/dz \to \infty$ at the height where $\bar{w} \to 0$.

Abraham (1963) believed that experimental evidence indicated much less difference between dr/dz for jets and for buoyant plumes than predicted by the MTT model, and opted for simply $r \propto z$. To apply the model to non-vertically oriented plumes, he generalized this approach with $r \propto s$.

Instead of assuming something about the rate of plume growth, Priestley and Ball (1955) used the conservation equation for kinetic energy of the mean motion and closed it by assuming $\tau \propto \bar{w}^2$. This will be referred to as the PB model. The result is a straight-sided plume with $r \propto z$ even if $\bar{w} \to 0$, which it does if $\partial\theta_a/\partial z > 0$. The unrealistic result that the plume volume flux goes to zero at this point can not be interpreted as being due to material leaving the plume to spread horizontally, although this does happen. The fact is that the PB model and all other present models do not attempt to describe the flow pattern near the top of the rise, where the flow that had been predominantly vertical must become predominantly horizontal. At this point, pressure distribution would become very important and any closure assumption would have to be strongly modified to allow for the inhibiting effect of stable stratification on the plume turbulence. Much of this has been pointed out by Morton (1971) in a discussion of a paper by Fox (1970). The PB and MTT models do give quite good predictions of the maximum rise in stable ambients, however, in spite of these limitations (see Section 4.1).

Telford (1966) suggested a rather unique model in that it uses four conservation equations, and ties the unknown entrainment velocity from the continuity equation to the unknown plume turbulent velocity from the total kinetic energy equation with $v_e \propto q$. Since no turbulent energy dissipation is included, it cannot realistically be applied to jets, as was already pointed out. Another feature of this model that is unique, which is not to say realistic, is that it is assumed that ambient turbulence will cause negative entrainment, i.e. fluid leaving the plume ("extrainment" is my word for it, not Telford's). But can buoyant fluid cross the plume boundary? Most modelers assume that the buoyant fluid <u>is</u> the plume, by definition.

With the exception of the two earliest models, most of the models for plumes bending over in a crosswind ($U > 0$) are variations on the MTT model. Some have added assumptions to account for the effect of ambient turbulence on the rise. Bryant (1949) used the same conservation equations, but suggested a rather complicated function for dr/ds in order to best fit the observed bending over stage of heated jets. Again, $r \propto z$ for the vertical case, but $r \propto x^{1/3}$ for large values of x when $U > 0$. This would result in a proper prediction for jet trajectories ($\Delta h \propto x^{1/3}$), but would give $\Delta h \propto x^{4/3}$ instead of $x^{2/3}$ for buoyant plume trajectories. The Sutton (1950) model really uses no conservation equations, but borrows a result for vertical buoyant plumes from the early model of W. Schmidt (1941), a mixing-length theory. This model predicted that $\bar{w} \propto (F/z)^{1/3}$, as is also given by the MTT and PB models. Sutton applied this to a bent-over plume by replacing z with s, the distance along the plume axis. This fortuituously predicts the now well-established "2/3 law" for large values of x/L, where $L = F/U^3$ (both $\Delta h$ and x scale to L at the point that a buoyant plume becomes just bent-over, say at $\theta_{e\ell} = 45°$). Sutton suggested that the rise be terminated when some small values of the plume inclination $\theta_{e\ell}$ is obtained. This gives $\Delta h \propto L = F/U^3$, another formula which has appeared again and again in many subsequent models. This goes to show, I suppose, that a plume rise model does not have to be complicated if it is adequately inspired.

The Bosanquet (1957) model is the most complete of the early models and has received wide use. It resembles the MTT model for the vertical case. It uses the same entrainment assumption for the bent-over stage of rise, and differs from

later models in that it assumes the same entrainment constant, $\alpha$, for both vertical and bent-over stages of rise. Later investigators, notably Briggs (1969) and Hoult and Weil (1972), showed that the entrainment coefficient for the bent-over stage, $\beta$, is at least 5 times $\alpha$. This happens because the plume is able to entrain ambient fluid much more efficiently when its' relative velocity is directed perpendicular to its axis instead of parallel to it. For this reason, most of the later models assume different entrainment constants for the vertical and bent-over stages (Briggs, 1964, Hoult, Fay and Forney, 1969, Abraham, 1971, Hirst, 1971, Ooms, 1972).

Hirst (1971) assumed that the entrainment coefficients $\alpha$ and $\beta$ are not constants, but are functions of the local Froude number of the plume ($Fr = \infty$ if $F_z = 0$, and tends towards a constant value ~ 1 if $F_z$ is constant). This is implied for $\alpha$ by the PB model, as was shown by Fox (1970), because PB predicts the same value of dr/dz for both jets and buoyant plumes. However, the PB approach has no more validity a priori than the MTT model; if one applies MTT to the energy equation just as Fox applied PB to the continuity equation, one finds that $\tau/\bar{w}^2$ is not a constant, but a function of Fr! There is obviously a law of reciprocity operating here. What this suggests to me is that both $\alpha = v_e/\bar{w}$ and $\tau/\bar{w}^2$ may be functions of Fr. Only a very well designed experiment could resolve this question. This area of incompatibility between the MTT and PB models, which is discussed further by Morton (1971), shows that it does matter somewhat what one choses for a closure assumption. Fortunately, the resultant plume rise predictions of these two models do not differ very much.

For a bent-over plume, the Taylor assumption that $v_e = \beta\bar{w}$ gives immediately $dr = \beta\, dz$. Two investigators (Briggs (1969), Bringfelt (1969)) have confirmed a linear relationship between photographically measured plume radii and height above the stack, z. Both note that the best fit line passes close to r = 0, z = 0, so for a bent-over plume in its early stage of rise $r \approx \beta z$. This assumption was first utilized by Scorer (1959) for bent-over plumes. Many of the more recent models use $v_e = \beta|\bar{w}|$, to account for the continued growth of the plume in its oscillatory stage after maximum rise is obtained in stable conditions.

One point remains to be discussed, and that is the various attempts to account for the effect of ambient turbulence on rise. The earliest goes back to Bosanquet, Carey and Halton (1950). In this model there was assumed a component of the entrainment velocity proportional to the variance of ambient turbulent velocity, which was assumed proportional to the windspeed. This results in a final rise for a jet proportional to $(u/u')^{1/2}\, R\, r_o$, but for a buoyant plume the rise is asymptotically $\propto L\, \ell n\, (x/L)$. The Ooms (1972) model is very similar, with refinements in the earlier stages of rise. Scorer (1959) also uses u' as a turbulence parameter, but simply terminates the plume rise when $\bar{w} \approx u' \propto U$. This results in the same prediction for final jet rise, but for a buoyant plume $\Delta h \propto L = F/U^3$.

Bosanquet (1957) recognized that the most effective scale of eddy rise which dilutes plume buoyancy and momentum is of the order of the plume radius. Smaller eddies only "fuzz" the plume boundary, and very large eddies move the whole plume; they cause meander, but do not dilute the plume. Briggs (1964) implemented this idea by assuming these effective eddies to be in the inertial subrange of the turbulence spectrum, where their energy is a function only of their size and of the turbulent energy dissipation rate, $\varepsilon$. Since the inertial subrange effectively extends to eddy wavelengths considerably larger than the height above the ground (see Lumley and Panofsky (1964), Fig. 5.2), plume radii are normally well within this range. Dimensional analysis then suggests that $v_e \propto (\varepsilon r)^{1/3}$ for atmospheric turbulence-induced entrainment. Slawson and Csanady (1967) proposed an equivalent relation for the second stage of their bent-over plume model.

In addition, Slawson and Csanady proposed a third stage of rise in which the plume would have to be larger than the eddies containing the greater part of the ambient turbulent energy. In this stage, the effect of ambient turbulence on entrainment is parameterized with a constant eddy diffusivity, $K_d$. At large distance, this results in $r \propto (K_d\, t)^{1/2}$, which results in continued rise for a buoyant plume with a constant vertical velocity $\propto F/(U\, K_d)$. One difficulty with this proposal is that the internal eddy diffusivity of a buoyant plume would grow with $t^{1/2}$, so it would eventually dominate over the ambient value $K_d$; this would put the plume back into the first stage of rise, where internal turbulence overrides the ambient turbulence. Another difficult is that in the atmosphere the maximum turbulent energy is contained in wavelengths equal to about 2 to 5 times the height above the ground, at least up to a height of 500 m (see Lumley and Panofsky (1964), Fig. 5.4). It seems unlikely that the plume size could exceed this wavelength.

Table 2 - Comparison of Assumptions about Entrainment Velocity due to Ambient Turbulence

| | $v_e \propto (\varepsilon r)^{1/3}$ | $v_e \propto u'$ | $v_e \propto K_d/r$ |
|---|---|---|---|
| Scaling implied | $r \ll \ell$ | $r \simeq \ell$ | $r \gg \ell$ |
| Asymptotic behavior: | | | |
| Growth | $r \propto \varepsilon^{1/2} t^{3/2}$ | $r \propto u't$ | $r \propto (K_d t)^{1/2}$ |
| Jet rise | $\Delta h \propto \left(\frac{F_m}{U}\right)^{3/7} \varepsilon^{-1/7}$ | $\Delta h \propto \left(\frac{F_m}{Uu'}\right)^{1/2}$ | $\Delta h \propto \frac{F_m}{UK_d}\, \ell nx$ |
| Buoyant rise | $\Delta h \propto \left(\frac{F}{U}\right)^{3/5} \varepsilon^{-2/5}$ | $\Delta h \propto \frac{F}{Uu'^2}\, \ell nx$ | $\Delta h \propto \frac{F}{U^2 K_d}\, x$ |

$\ell$ = dominant scale of ambient turbulence.

The three assumptions about how plume entrainment velocity relates to ambient turbulence are compared in Table 2. If $\varepsilon$ is chosen as the ambient turbulence parameter, the entrainment velocity

increases with plume size, while it is constant if u' is chosen and it decreases if $K_d$ is chosen. The choice of $\varepsilon$, u', or K is strictly valid only if the plume radius is respectively much smaller than, of the same order as, or much larger than the dominant scale of ambient turbulence, $\ell$. The plume growth is respectively proportional to $t^{3/2}$, $t^{2/2}$, or $t^{1/2}$, so the effect on the plume trajectory is progressively weaker. I prefer to use only the $\varepsilon$ assumption for the ambient turbulence effect, because in any situation in which ambient turbulence is important it seems likely that $r << \ell$, or at least r is less than $\ell$. In fact, in neutral and in convective conditions it seems clear that r can not exceed $\ell$ until distances much greater than the distance of maximum ground concentration.

## 2.6 Values of Entrainment Constants

The majority of plume rise models to date use the continuity, buoyancy and momentum conservation equations, as can be seen in Table I. This is a versatile set of equations, easy to extend to three dimensions and to a variety of boundary conditions, such as emission at arbitrary angles. For closure, these equations require only some assumption about the entrainment velocity or the growth of the plume radius, which are related to each other as shown by Eq. (31). Entrainment is relatively easy to visualize mentally, so many possible closure assumptions suggest themselves. The predicted plume growth can be easily checked against the growth of the visible boundaries of a real plume, but since the effective radius may be different from what we see, the best test of a model is the accuracy of the predicted centerline trajectory, velocity, or the rate of dilution.

In the last decade there has been general agreement among plume rise modelers that in the early stage of rise plumes grow due to self-induced turbulence, not ambient turbulence. Furthermore it is agreed that for vertically-emitted plumes in this stage: (1) $v_e \propto \bar{w}$, or, equivalently, $r \propto z$; (2) the entrainment or proportionality constant is much larger for a bent-over plume than for a vertical plume. Diverse assumptions have been made about how to apply these results to the bending-over stage of rise or to the trajectories of non-vertically oriented emissions (see, for instance, Abraham (1963), Fan (1967), Anwar (1969), Hirst (1971), and Campbell and Schetz, 1973). We will consider only the "pure cases" of vertical or bent-over stages of rise. It is quite possible to approximate the plume trajectory in the intermediate bending-over stage ($\theta_{el} \simeq 45°$) by matching the vertical and bent-over plume solutions, as was done by Scorer (1959). In addition to estimating the entrainment rate for vertical plumes and for the early stage of bent-over plume rise, we want some estimate of the entrainment rate in the ambient turbulence-dominated stage of rise.

Estimates for the entrainment coefficient $\alpha$ for the vertical plume as appears in the Taylor entrainment assumption, i.e., $v_e = \alpha \bar{w}$, have been made by Morton, Taylor and Turner (1956), Morton (1959), Fan (1967), Briggs (1969), and Hoult and Weil (1972). The latter concluded that $\alpha = 0.11 \pm 20\%$, on the basis of a survey of past estimates.

All the estimates for $\alpha$ for non-buoyant jets are based on the work of Ricou and Spalding (1961), since they measured entrainment directly by determining the inflow into a jet in a specially constructed chamber. They found a constant rate of inflow per unit length of jet, as predicted by the MTT and other theories ($dV/dz = 2\alpha \bar{w} r$, and for a jet $\bar{w} r = w_o r_o$, from the vertical momentum conservation equation). This gives the value $\alpha = 0.080$ for a jet. This rate of jet growth has been confirmed by Hill (1972) in a similar experiment, in which it was found that it takes 10 diameters of rise for the entrainment coefficient to reach this constant value; it is smaller than this very close to the source, in the zone of flow establishment.

Many of the estimates of $\alpha$ for buoyant plumes are based on profiles of temperature and velocity measured in a vertical, buoyant laboratory plume by Rouse, Yih, and Humphreys (1952). They found that

$$w = 4.7\ (\pi F)^{1/3} z^{-1/3}\ \exp\ (-96\ y^2/z^2) \qquad (32)$$

$$g(\rho'/\rho) = 11.0\ (\pi F)^{2/3} z^{-5/3}\ \exp\ (-71\ y^2/z^2),$$

where y is the radial distance off-axis. Integrating $g(\rho'/\rho)w$ over an infinite plane, we find that 97% of the initial buoyancy flux is accounted for, so these look like reasonably careful measurements. Even more gratifying, checking our approximation for vertical momentum flux conservation, Eq. (19), we find $d/dz \iint_\infty w^2\ d\ S \div \iint_\infty g(\rho'/\rho)\ dS = 0.99$. The measured change in vertical momentum flux is 99% of what we predict. Using the above profiles, we find that the shape factor defined by Eq. (18) is $S_1 = 0.92$ (this factor is directly related to the factor $\lambda$ defined by MTT; here we have chosen to incorporate the shape factor into the definition of the mean vertical velocity, $\bar{w}$, so the equations can take the same form as those for the simple "top-hat" profile assumption). Using the definitions given by Eqs. (3) and (18), $\alpha = v_e/\bar{w}$, and $r = (V/\bar{w})^{1/2}$, we find for the Rouse et al. profiles $\alpha = 0.125$. Incidently, I would like to point out that the predicted rise is very insensitive to profile shapes. $S_1$ depended only on the square-root of the dimensionless integrated flux ratios, $\alpha$ is proportional to $S_1^{-1/2}$, and the final rise in stable conditions depends on $\alpha^{-1/2}$.

There are some alternative ways to optimize $\alpha$ for a buoyant plume. For the same observations used above, we find that the integrated volume flux divided by $\pi$ is

$$V = \iint_\infty w\ d\ S \div \pi = 0.0717\ F^{1/3} z^{5/3}. \qquad (33)$$

Using the MTT model to predict this, we find that we require $\alpha = 0.124$, which is almost identical to the value given by the strict definition of $\alpha$. Another way to optimize $\alpha$ is to make theoretical predictions fit observed find rises. For rise through a constant density gradient with no crossflow, a number of different experiments indicate that $\Delta h \simeq 5\ F^{1/4} s^{-3/8}$ for the top of the

plume (see Section 4.1). To fit MTT model to this, using the height where $\bar{w} \to 0$, requires $\alpha = 0.132$. Alternatively, I will suggest an "unaltered volume flux" model in which an equation like Eq. (33) is assumed to hold even in stable surroundings. This is much easier to apply, and gives the correct prediction for $\bar{w} \to 0$ with $\alpha = 0.124$, the same value required to give Eq. (33) exactly.

In summary, I would like to recommend $\alpha = 0.080$ for a jet and $\alpha = 0.125$ for a buoyant plume. For plumes going through a transition in which both the buoyancy and the initial momentum flux may be constant, $\alpha = 0.1$ is the logical compromise, being the geometric mean.

Alternatively, we note that in the MTT formulation $dr/dz = 2\alpha = 0.16$ for a jet rising in neutral surroundings, while for a buoyant plume $dr/dz = (6/5)\ \alpha = 0.15$ with our present estimates of $\alpha$. This is consistent with Scorer's report (1959) that buoyant plumes appear to be only slightly more slender than jets (half-cone angles of 11° and 12°, respectively). Then a more accurate compromise for vertical plumes in neutral conditions is $dr/dz = 0.155$, which follows the logic used by Abraham (1963). One difficulty with this is that $dr/dz$ cannot remain constant as $\bar{w} \to 0$, as near the final rise in stable conditions. Indeed, conservation of plume mass requires $dr/dz \to \infty$, as in the MTT model.

Another alternative is to assume that $\alpha$ is a function of the local Froude number of the plume, $Fr = \bar{w}^3\, r/F_z$, as was suggested by Fox (1971). For a buoyant plume in neutral surroundings Fr approaches a constant value, and for a jet $Fr = \infty$. Fox assumed $\tau \propto \bar{w}^2$, which results in $dr/dz =$ constant and implies that $\alpha =$ constant + constant/Fr. The trouble is that this implies negative entrainment near the top of the rise, since $F_z < 0$ due to "overshoot" and $\bar{w} \to 0$. Also, there is no a priori reason for expecting that $\tau$ is not a function of Fr, especially near the top of the rise when entrained stable fluid must have some effect on the plume turbulence. As suggested earlier, both $\alpha$ and $\tau$ might be functions of Fr. Unfortunately, we have determined reliable values of $\alpha$ for only 2 values of Fr, which is certainly not enough points to define a complete function.

For the bent-over plume, it is commonly assumed that in the early rising stage $dr/dz = \beta$, or equivalently, $v_e = \beta\bar{w}$. For photographically determined radii, defined by 1/2 the visible plume depth, it has been found that plots of r vs z are linear and pass near the origin, so we can say simply $r = \beta z$ (Briggs (1969), Bringfelt (1969)). For the visible radius, Briggs found $\beta \simeq 0.5$ for TVA power plant plumes while bringfelt found average values of $\beta$ to be 0.52 and 0.45 for neutral and stable conditions, respectively. The Bringfelt observations were mostly on plumes from small industrial sources. Tsang (1971) also found that $\beta \simeq 0.5$, for the radius of an "equivalent circle" approximating the outline of his 2-dimensional laboratory thermals. However, we expect that the effective plume radius is larger than the visible radius , since it must include the effective mass of fluid pushed aside to make way for the plume

Indeed, Hoult and Weil (1972) report that $\beta = 0.6$ gives the best prediction of the rising trajectories of buoyant, laboratory plumes. This is the same value recommended by Briggs (1972) on the basis of best fits to the "2/3 law" of buoyant rise. This study surveyed the results of 10 different sets of published observations, 9 of which were on full-scale plumes. The best fits for individual studies ranged from 0.3 to 0.9. For the laboratory plumes there was about ±25% scatter about the rise predicted with $\beta = 0.6$. Briggs (1969) reported about the same scatter for full-scale plumes when comparing the average rise at one plant with that at other plants; the scatter for individual runs would have been much larger. In a detailed study of TVA and Bringfelt (1968) field data, Fay, Escudier and Hoult (1969) found lower rise when $R = w_o/U < 1.2$, indicating a stack downwash effect, but found no correlation of the best-fit value of $\beta$ with stack Froude number, stack height, heat emission rate, or stratification parameter $U^4 s^{-1/2}/F$ (this is proportional to the ratio of the leveling-off distance to the bending-over distance of a buoyant plume). Disregarding runs in which $R < 1.2$, they found a best fit to the "2/3 law" with $\beta = 0.81$, using $F^*$ instead of F for the buoyancy parameter (see the end of Section 2.2). Had F been used, the best fit $\beta$ would be about 0.65. The geometric standard deviation of best fit values of $\beta$ was almost a factor of 2. The best fit to the predicted rise in the leveled-off region of rise in stable stratification was $\beta = 0.55$. This discrepancy can be accounted for in the context of the present theory by allowing for the difference between the "effective," or inertial mass of the plume, which determines the "2/3 law" rise, and the actual rise within the plume itself, which determines the rate of buoyancy decay and the height of leveling-off. The above results imply that $M_{eff}/M = (0.81/0.55)^2 \simeq 2.2$. Using the streamlines around two-dimensional line thermals measured by Richards (1963) to directly determine this ratio from the definitions given in Eqs. (9) and (24), we find that $M_{eff}/M \simeq 2.3$, an encouraging correlation.

In other respects, the correlation of the line thermal data of Richards with data from bent-over plumes is not so good. For the visible radius, as defined above, $\beta \simeq 0.6$, instead of 0.5. For the best fit to the "2/3 law" based on the centerline rise rate, we find $\beta \simeq 1.0$. Determining $\beta$ directly from the streamlines and the definition of $M_{eff}$, we find $\beta \simeq 0.7$, but only 60% of the predicted rate of change of momentum flux is accounted for. There is a better correlation with the line thermal laboratory data of Tsang (1971), with the best fit to the "2/3 law" with $\beta = 0.66$.

For the observed rise trajectories of bent-over jets, Hoult and Weil (1972) show that the "1/3 law" is fit reasonably well with $\beta = 0.6$ again. The velocity ratio R ranged from 3 to 27, and the average scatter was roughly 20%. The laboratory data of Vadot (1965), Fan (1967), and Barilla (1968) were used. However, Briggs (1970) noted a correlation of $\beta$ with R in comparing the results of six different laboratory experiments with the "1/3 law" (see Section 3.2). For values of R ranging from 2 to 40, he suggested $\beta = 1/3 + R^{-1}$ (when R is less than 2, jets strongly interact with the stack wake). This value is based on jet trajectories determined by maximum concentration, velocity, heat or temperature. The centerline of the visible jet is about

10 to 20% lower (see Figure 3), so for consistency I would suggest $\beta = 0.4 + 1.2\ R^{-1}$. If we accept this value, $\beta = 0.6$ should give the rise to an adequate approximation (±25%) in the range R = 3 to 40.

In summary, it appears that for bent-over plumes $r = \beta z$ in the early part of the rise, with $\beta \simeq 0.5$ for the visible plume half-depth and $\beta \simeq .0.6$ for the radius of the effective mass of the plume. For non-buoyant jets, slightly better correlation is obtained with observed trajectories with $\beta = 0.4 + 1.2\ R^{-1}$. The radius of the effective plume mass within the plume boundary is only $(M/M_{eff})^{1/2}$ times the effective radius; for buoyant plumes, this appears to be $r \simeq (2.25)^{-1/2}\ 0.6z = 0.4z$.

For ambient turbulence-dominated entrainment for bent-over plumes, Briggs (1964, 1969, 1970) and Slawson and Csanady (1967) assumed that $v_e = dr/dt = \gamma(\varepsilon r)^{1/3}$, where $\varepsilon$ is the turbulent energy dissipation rate in the ambient and $\gamma$ is a dimensionless constant. (It is doubtful that ambient turbulence is of any significance to plume rise for vertical plumes, since their own velocities greatly exceed at least the horizontal ambient velocities.) The only past estimate of $\gamma$ was made on the basis of observed short range expansion of puffs of smoke (Frenkiel and Katz, 1956) and Lycopodium spores (Smith and Hay, 1961) by Briggs (1969). Since $\varepsilon$ was not determined in these experiments, it was estimated by means of an empirical function using only height and windspeed. In spite of this crude expediency, the analysis indicated that $\gamma \simeq 0.7$ within ±15%.

Hanna, Hutchison and Gifford (1969) photographed short, continuous plumes released from the 16 m level of a 61 m meteorological tower and made simultaneous estimates of $\varepsilon$ from the wind and temperature profiles. The diffusion rate was analysed from the photographs assuming a Gaussian density distribution with the plume standard deviation given by $d\sigma/dt = \gamma'(\varepsilon\sigma)^{1/3}$ and a visible plume boundary at some theshold density per unit area in the line of sight. The results indicated that $\gamma' = 1.8 \pm 10\%$.

Interpreting such observations made on passive puffs and plumes in terms of entrainment into a rising plume is full of uncertainities. Csanady (1965) derived streamlines of mean flows induced by a Gaussian distribution of plume buoyancy, finding a mean centerline velocity as given by the vertical momentum equation, Eq. (25), with $r = (2)^{1/2}\sigma$. This assumes that plume-induced velocities are much smaller than the rate of plume spreading due to ambient turbulence, however. In the case we are interested in, plume velocities are at least of the same order as entrainment velocities. It seems likely too, that the double vortex rotation within the plume resists erosion by outside turbulence; since organized rotations in fluids tend to dampen turbulence; examples are vortex rings and tornadoes. This stability arises when the relative circulation increases with distance from a point; in such a flow, an angular momentum-conserving element of fluid that is displaced outwards tends to be pushed back by the pressure gradient that balances the mean centriptal acceleration. This restoring force acts much in the same way that hydrostatic stability acts, except that it tends to suppress radial motions rather than vertical motions.


Figure 2. Structure of a line thermal. Solid lines show thermal shape at two successive times. Dashed line shows advance of thermal boundary due to mean motion. Remainder of advance assumed due to turbulent entrainment, shown by curls. Arrows show streamlines of mean motion relative to center of widest part of the thermal. Horizontal hatching indicates high vorticity regions. Cross hatching indicates concentration maximums.

It might be helpful at this point to look at the internal sturcture of a rising plume. Some of the details of structure within a rising plume are indicated by laboratory measurements on horizontal thermals, which closely resemble bent-over plumes in cross-section. Figure 2 shows the dominant features; it is a composite of the streamline measurements of Richards (1963), the vorticity measurements of Tsang (1971), and the concentration measurements in a bent-over laboratory plume of Fan (1967). We see that almost all of the entrainment occurs across the top part of the plume. Part of the rise is due to mean vertical motion, but 75% of it is due to turbulent entrainment. There is a secondary zone of entrainment under the middle of the plume, where induced velocities are very much higher than anywhere else around the boundary. This may be due to the low hydrostatic pressure underneath the buoyant fluid, and might not be so pronounced in a bent-over jet. Turbulence is generated here due to a strong shear of the vertical motion, evidenced by closeness of the streamlines near the center and by the flanking areas of high vorticity. This turbulence is advected upward through the middle of the plume, where is bisects the concentration maximum. The intensity it developes as it spreads across the top of the plume is partly due to horizontal divergence, which stretches vortex filaments in a direction almost tangent to the upper surface, thereby intensifing turbulent velocities perpendicular to the surface by the "skater effect." In a buoyant plume, turbulence is also generated due to unstable internal density stratification above the concentration maxima, which are density minima. The marked decrease in turbulent entrainment around the lower flanks of the plume is probably due to the small amount of shear with the ambient at these points (it appears that the plume almost

"rolls" up an imaginary inclined plane tangent to these points), and also is due to the proximity of the larger regions of high mean vorticity. In this region the plume should possess rotational stability similar to that in vortex rings.

When a plume or a thermal as described above enters into a fluid having ambient turbulence, it seems likely to me that the ambient turbulence must first mix its way into the plume by means of a "frontside attack," since the lower flanks and underside possess more inherent stability. Also, there is a strong convergence of ambient streamlines under the plume, which tends to relax turbulence velocities that are perpendicular to the surface.

If this analysis is true, and ambient turbulence must first break into the plume in the frontal region , then its effectiveness will be delayed due to the relatively high plume turbulence in this same region. In effect, the plume will at first advance into the ambient faster than the ambient can advance into the plume. Once the balance is reversed, as the plume motions weaken, it is quite easy to conceive that the ambient turbulence may move downward and destroy the stable double vortex structure from within, making the plume vulnerable from all sides. In other words, plume "breakup" may occur relatively quickly, as has been suggested by Csanady (1973) and others. If so, then entrainment assumptions of the form $v_e$ = maximum ($\beta\bar{w}$, $\gamma\ \varepsilon r^{1/3}$) may give too gradual a transition from the self-structured plume to the passively diffusing plume. Indeed, the transition derived by Briggs (1969, 1970b) on the basis of the above assumption is so gradual for a buoyant plume that at 3 times the transition distance the plume rise departs only 8% from the "2/3 law" governing the first stage of rise, and at 10 times the transition distance only 81% of the asymptotic rise has been reached.

This seems too gradual to me now. It seems more likely that the self-structured rising plume resists transition to the passive growth regime, then succombs rather rapidly to erosion by ambient turbulence and experiences a breakdown of it structure. Then asymptotic rise may be approached more quickly than in my earlier model and the rise trajectory might be more closely approximated by abrupt termination of the first stage rise at an appropriate point.

One way to estimate this breakdown point is to compare the plume's inertial subrange turbulence with that of the ambient. This is done by comparing turbulent energy dissipation rates. In the self-structured stage of rise we can assume for the effective dissipation rate of the plume

$$\bar{\varepsilon} = \eta\ \frac{\bar{w}^3}{z} \qquad (34)$$

since turbulence velocities have been assumed to scale to the centerline rise velocity, $\bar{w}$, and the plume geometry scales to the centerline rise, z. We then terminate the first (self-structured) stage of rise when $\bar{\varepsilon} = \varepsilon$, the ambient value. This assumption will give the same asymtotic rise formulas, excepting for proportionality consists, as my earlier model. It has three desirable characteristics over the earlier model, though. The first is simplicity. The second is the rapid decay of $\bar{\varepsilon}$ with rise, which makes the transition from $\bar{\varepsilon} > \varepsilon$ to $\bar{\varepsilon} < \varepsilon$ relatively sharp. For a buoyant plume, $\bar{\varepsilon} \propto z^{-5/2}$, and for a jet $\bar{\varepsilon} \propto z^{-7}$. In contrast, with $\bar{w} \propto (\varepsilon r)^{1/3}$ for a transition criterion, we have $\bar{w}/r^{1/3} \propto z^{-5/6}$ and $\propto z^{-7/3}$, respectively. Finally, while only crude estimates can be made of either $\gamma$ or $\eta$ at present, the predicted plume rise is much less sensitive to $\eta$.

Let us make some estimates of $\eta$. For a buoyant plume, potential energy is released as the plume rises. It is transformed into kinetic energy of mean motion, which in turn is transferred into kinetic energy of turbulent motion, which is finally dissipated. The total rate of potential energy release is approximately F $\bar{w}$, if we consider the buoyant force to be effectively centered at the centerline height. Richards (1963) measured the total kinetic energy of mean motion, and found it to increase at a rate $\simeq$ 0.3 F $\bar{w}$. This means that about 0.7 F $\bar{w}$ must go into turbulent kinetic energy and dissipation. We do not know how this breaks down, but often in nature we find an equipartition of energy, so this seems to be a reasonable first guess. We then assume an integrated dissipation rate $\simeq$ (1/3) F $\bar{w}$. This is not spread evenly through the plume, but is probably concentrated near the upper surface, where the most vigorous turbulent entrainment is. This is the region where plume turbulence is most in competition with ambient turbulence. I will assume that the plume turbulence effectively occupies only the upper one-half of the plume, and that the plume's total cross-sectional area is $\simeq \pi(0.5z)^2$. These assumptions result in $\bar{\varepsilon} \simeq$ (8/3) F $\bar{w}$/(U $z^2$). Substituting the "2/3 law" of rise, this transforms into Eq. (34) with $\eta = 4\beta^2 = 1.44$. This is probably accurate within a factor of 2. For perspective, note that buoyant plume rise $\sim\eta^{2/5}$, maximum ground concentration in neutral conditions $\sim\eta^{-2/9}$, and as a result the required stack height $\sim\eta^{-2/15}$.

A second estimate of $\eta$ can be made for bent-over jets. In this case there is no new supply of energy, but the total kinetic energy of the jet diminishes as it rises, feeding into turbulent dissipation. Very roughly, the total kinetic energy is $\sim$ 1/2 $\bar{w}^2$ ($\pi r^2$), where r is the effective plume radius (part of the kinetic energy is outside the jet, in the ambient fluid being moved by the jet). If dissipated over the area ($\pi r^2$), we find in the "1/3 law" regime of jet rise that $\bar{\varepsilon} \sim$ (d/dt (1/2 $\bar{w}^2$ $\pi r^2$)) $\div$ $\pi r^2 = \bar{w}^3/z$. Very likely it is larger than this because all the turbulent dissipation must take place inside the jet, so the actual cross-sectional area should be used rather than the effective area. The jet turbulence may be concentrated in the frontal regional also, but probably not so much as in a buoyant plume. For consistency, let us assume for now that $\eta \simeq 1.5$ for both buoyant plumes and jets. For a jet, the final rise $\sim\eta^{1/7}$, so this estimate is not very critical.

## 2.7 Summary of Equations

Here is a recapitulation of the equations that will be used for predicting plume rise. First, let us review some of the definitions used.

For a vertical plume, we define

$$V = {}_{P}\iint w \, d S \div \pi$$

$$\bar{w} = S_1 \iint_{\infty} w^2 \, d S \div {}_{P}\iint w \, d S$$

$$S_1 = {}_{P}\iint g(\rho'/\rho) w \, d S \div (\bar{w} \, {}_{P}\iint g(\rho'/\rho) d S)$$

$$= 1 \text{ if } \rho' = 0$$

$$r = (V/\bar{w})^{1/2}$$

$$dt = dz/\bar{w} \qquad (35)$$

where V is the vertical volume flux, $\bar{w}$ is a mean vertical velocity, $S_1$ is a dimensionless shape factor, and r is an effective radius. These quantities are based on integrals taken over horizontal planes intersecting the plume. All of them can vary with the height above the source, z, but we will assume that the variation in $S_1$ is insignificant compared to the variation in $\bar{w}V$.

For a bent-over plume, we define z to be the height of the centerline of the plume. We also define t = x/U and

$$\bar{w} = dz/dt = U \, dz/dx$$

$$M = U \, {}_{P}\iint w \, d S \div \pi$$

$$M_{eff} = U({}_{P}\iint w \, d S - {}_{P}\oint \phi \, dy) \div \pi$$

$$V = M_{eff}/\bar{w}$$

$$r = (V/U)^{1/2}$$

$$dt = dx/U \qquad (36)$$

In both cases, we define an ambient stability parameter by

$$s = \frac{g}{\theta_a} \frac{\partial \theta_a}{\partial z} = \omega^2 \qquad (37)$$

which is recognized as the square of the Brunt-Väissälä frequency, ω. Physically, s is the restoring acceleration per unit vertical displacement of a potential density-conserving element in a stable fluid (for an incompressible fluid, such as in a modeling tank, we replace $\theta_a$ with $-\rho_a$ in this definition). This restoring force is analogous to that acting on a weight hung on a spring, and ω is just the natural angular frequency of vertical motions in a stable fluid, such as the motion of air moving through a gravity wave in the lee of an obstacle.

Finally, we can restate our working equations. In terms of space derivatives, we have

| Vertical Plumes | Bent-over Plumes |
|---|---|
| $d F_z/dz = -s V$ | $d F_z/dz = -s (M/M_{eff})V$ |
| $d(\bar{w} V)/dz = F_z/\bar{w}$ | $d(\bar{w} V)/dz = F_z/\bar{w}$ |
| $d V/dz = 2\alpha \bar{w} r$ | $d V/d\lvert z\rvert = 2\beta U r$ |
| $= 2\alpha (\bar{w} V)^{1/2}$ | $= 2\beta (U V)^{1/2}$ |
| (38) | or $V = Ur^2$ with $\lvert dr/dz\rvert = \beta$ (39) |

The equations for vertical and bent-over plumes are shown side-by-side in order to demonstrate their similarity. The only major difference between them is in the volume flux equations, which are the closure assumptions. The only other difference is that s is multiplied by $(M/M_{eff})$ in the buoyancy flux equation for bent-over plumes. This will have the effect of expanding the time scale of stability effects by a factor $(M_{eff}/M)^{1/2}$.

An alternative form of these equations that will be especially convenient when considering rise in stratified surroundings is given in terms of time derivatives:

| Vertical Plumes | Bent-over Plumes |
|---|---|
| $d F_z/dt = -s(\bar{w} V)$ | $d F_z/dt = -s(M/M_{eff})(\bar{w} V)$ |
| $d(\bar{w} V)/dt = F_z$ | $d(\bar{w} V)/dt = F_z$ |
| $d V/dt = 2\alpha (\bar{w} V)^{3/2}/V$ | $d V/dt = 2 (\bar{w} V)(U/V)^{1/2}$ |
| (40) | or $V = Ur^2$ with $dr/dt = \beta\lvert w\rvert$ (41) |

When s is a constant, or if s can be expressed as a function of time, in this formulation the buoyancy and vertical momentum equations can be solved independently of the plume growth assumption.

For bent-over plumes rising through a turbulent ambient with a turbulent dissipation rate ε, we will simply terminate the rise when

$$\varepsilon = \eta \, \bar{w}^{\,3}/z \qquad (42)$$

The recommended constants for vertical plumes are α = 0.08 for a jet, α = 0.125 for a buoyant plume and α = 0.1 for a mixed case. Alternatively, we may use r = α'z with α' = 0.16 for a jet, α' = 0.15 for a buoyant plume, and α' = 0.155 for a mixed case.

The recommended constants for bent-over plumes are $\beta = 0.6$ and $\eta = 1.5$. For bent-over jets, a somewhat better fit to the "1/3 law" is obtained with $\beta = 0.4 + 1.2/R$, as will be seen in the next section.

For plumes in the bending-over stage inbetween vertical and bent-over, we can add a horizontal momentum conservation equation, such as Eq. (20), but will also require a modified entrainment assumption to account for the additional mixing induced by the crossflow. For this stage I recommend the model developed by Hoult, Fay and Forney (1969).

## 3. RISE NEAR THE SOURCE

It will be shown in Section 4 that ambient stratification has little effect on plume trajectories when t is less than $|\omega|^{-1}$, which ranges from about 20 seconds in strong stratification to 100 seconds in weak stratification. Furthermore, in Section 5 it will be seen that strongly buoyant plumes rise for a considerable distance before ambient turbulence diminishes the rise. For conventional power plants, this distance is of the order of 10 stack heights. Sometimes it is desirable to compute the rise at a closer point, for instance, to see if the plume will clear an obstacle. Occasionally, one is concerned with the possible effect of vertical velocities induced by a plume on aircraft.

### 3.1 Rise in a Calm

When $U = 0$, or at least $U \ll \bar{w}$, we can use the equations for vertical plumes to compute how vertical velocities and the plume volume flux changes with height. Past work on plumes in calm surroundings has been reviewed by Turner (1969).

An extended survey on the dynamics of jets was given by Pai (1954). For the incompressible axi-symmetric jet in a calm fluid he notes that it takes about 10 diameters of travel for similarity of the flow profiles to get established, and then the jet expands conically from an apex near the center of the source. We then find $r = 0.16z$, in terms of the effective radius. The mean velocity at the centerline is $13.0\, w_o\, r_o/z$, according to Pai. With the present model, with $F_z = 0$ momentum conservation requires that $(\bar{w}\, V)^{1/2} = \bar{w}\, r = \text{constant} = w_o r_o$ for a round source with $\rho_o = \rho_a$. Then $\bar{w} = w_o r_o / r = 6.25\, w_o r_o / r$, about 1/2 the centerline velocity. The total upward volume flux is just $\pi\, \bar{w}\, r^2 = \pi\, V_o (r/r_o) = 0.5\, w_o r_o z$.

For a buoyant plume with $F_z = F = \text{constant}$, the momentum equation of Eqs. (40) integrates immediately to

$$\bar{w}\, V = F_m + F\, t \quad . \tag{43}$$

Transition to a "buoyancy-dominated" plume occurs at $t = F_m/F$. To interpret this in terms of height, the best approximation for V in this transition zone is $V = \bar{w}\, (0.155z)^2$, provided that this is not in the zone of flow establishment. Substituting this into Eq. (43), taking the square root, and integrating, we find that transition to buoyancy domination takes place at

$$z \simeq 2\, D\, (Fr_o)^{1/2} \tag{44}$$

where D is the source diameter and $Fr_o$ is the source Froude number: $Fr_o = w_o^2/(r_o\, g\, \rho'_o/\rho_a)$.

Above this height, we can increasingly neglect the source momentum flux. For a "purely buoyant" plume, $\bar{w}\, V = F\, t$. We can easily solve this equation using the entrainment assumption, but since the entrainment constant was chosen to be consistent with the measurements of Rouse, Yih and Humphreys (1952), we might as well use these measurements directly. The centerline velocity and density (or temperature) can be calculated from Eq. (32). We found an effective radius $r = 0.15\, z$ and a shape factor $S_1 = 0.92$, which makes $\bar{w}$ equal to 0.46 times the centerline velocity. An important quantity for estimating the ability of large sources to entrain ambient air and to carry it upwards, possibly even through elevated inversions, is the total volume flux. This is obtained by multiplying Eq. (33) by $\pi$. To get the rate of ambient inflow at each level, simply differentiate this. We find that the total inflow increases with height, being proportional to $z^{2/3}$; this is in contrast to the jet, which induces a constant total inflow $d\, V/dz$.

### 3.2 Momentum Conservation and the "1/3 Law"

Next, consider the rise of a bent-over jet. By definition, $F_z = 0$, so momentum conservation requires that $\bar{w}\, V$ remains constant (see Eq. (39)). $V = U\, r^2$, and in the first stage of rise $r = \beta\, z$, so we have simply $\bar{w}\, V = \beta^2\, U\, z^2\, dz/dt = F_m$, the source value of the vertical momentum flux. This integrates quite readily to predict

$$z = \left( \frac{3}{\beta^2}\, \frac{F_m}{U}\, t \right)^{1/3} = \left( \frac{3}{4\beta^2} \right)^{1/3} (R\, D)^{2/3} x^{1/3} \tag{45}$$

where in the last expression we use $t = x/U$, $R = w_o/U$, and assume $\rho_o = \rho_a$. This is the "1/3 law" for bent-over jets.

Patrick (1967) carried out extensive measurements on jets in a crossflow but only to about 25 diameters downstream. In this region he found best fits to $z \propto x^n$ with $n = 0.34$ for the centerline based on maximum concentration, $n = 0.38$ based on maximum jet velocity, and $n = 0.45$ based on Schlieren photographs. Thus, the experimental trajectory depends a lot on what is being measured in this region. Other researchers cited by Patrick found n ranging from 0.32 to 0.36.

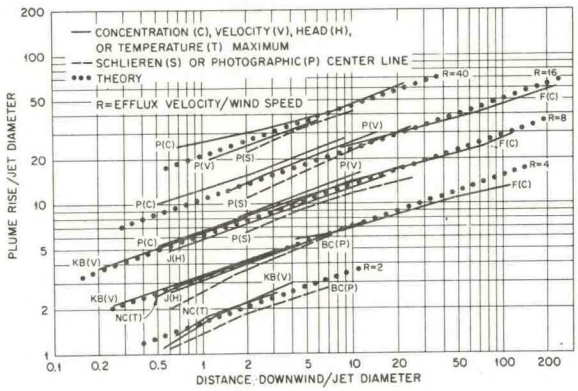


Figure 3. Rise vs. distance downwind for jets in a crossflow. $R = w_o/U$. Observations shown are by: P - Patrick (1967), KB - Keffer and (1963), J - Jordinson (Patrick, 1967), NC - Norster and Chapman (Patrick, 1967), BC - Bryant and Cowdry (1955), F - Fan (1967).

Figure 3 shows plots of z/D vs x/D for representative values of R on log-log coordinates. Six different experiments are represented. Overall, there is a good fit to $z \propto x^{1/3}$, as predicted. There is even a reasonably good fit in the part of the figure where z > 10 x, which must be purely fortuituous since the model used to derive the "1/3 law" is based on the "bent-over" plume concept. However, there is more of a dependence on the velocity ratio R than is predicted by Eq. (45) if $\beta$ is assumed constant. Eq. (45) can be made to give a good fit by setting $\beta = 1/3(1 + 3/R)$, which is the formulation represented by the dotted lines. The visible centerlines (dashed lines) are somewhat lower, and could better be represented by $\beta = 0.4(1 + 3/R)$, as suggested earlier.

This apparent dependence of $\beta$ on R might be due to interaction with the stack wake, which would tend to pull the plume downwards when R is small. At large values of R, the plume should rise well above the region affected by the stack wake. Alternatively, it is conceivable that a jet has some "memory" of its bending over stage, in which it acquires some mean vorticity due to the stronger mixing of the outside edges with the crossflow. Kamotani and Greber (1972) found a strong, self-preserving double vortex at axial distances of 15 to 70 diameters downstream in a jet when R = 7.7, but found only a very poorly organized double vortex when R = 3.9. In addition, they found a region of reduced velocity, presumedly a wake, underneath the plume at x = 7 D for R = 3.9. There was no trace of this for R = 7.7. It seems, then, that their measurements could support either hypothesis above about the decreased rise at low values of R. At R = 2, Keffer and Baines' plume photographs show a very ragged appearing plume bottom, which dips somewhat below the stack top level, so there is definitely interaction with the stack wake at this value of R. In contrast, at R = 8 both the top and the bottom of the plume take on an irregular, but relatively sharp, appearance.

Before leaving the subject of bent-over jets, it should be mentioned that the Hoult, Fay, and Forney (1969) model predicts a "1/2 law" for the rise very close in, when the jet is quasi-vertical. Both the axial and the transverse shear may be important, as the effective entrainment coefficient is $(\alpha + \beta/R)$. Specifically, their prediction is

$$z = \left( \frac{R\, r_o\, x}{\alpha + \beta/R} \right)^{1/2} . \qquad (46)$$

Hoult and Weil (1972) demonstrated a good correspondence between this equation and the observations of Keffer and Baines (1963), Bryant and Cowdry (1955), Jordinson (1956) and Gordier (1959) when z > x and R > 6. Actually, the agreement was fairly good for R = 2 and 4 except extremely close in (z < D). The fit would be improved if $\beta = 0.4\ (1 + 3/R)$ were used in place of the fixed value ($\beta = 0.6$) used by Hoult and Weil, but the latter assumption is quite adequate.

### 3.3 Buoyancy Conservation and the "2/3 Law"

When the stability is neutral (s = 0) or $t < |\omega|$, the buoyancy conservation equation implies that $F_z \simeq$ constant = F. Then for a bent-over plume the momentum equation of Eqs. (41) integrates immediately to $\bar{w}\, V = F_m + Ft$. For the first stage of rise we substitute $r = \beta z$, so $\bar{w}\, V = U(\beta z)^2 dz/dt$. Then we are able to integrate again to derive the centerline trajectory:

$$z = \left( \frac{3}{\beta^2} \frac{F_m}{U} t + \frac{3}{2\beta^2} \frac{F}{U} t^2 \right)^{1/3} . \qquad (47)$$

This equation includes both the effect of source vertical momentum and of buoyancy. At small values of t, momentum dominates and we have the "1/3 law" again, but buoyancy dominates when t exceeds $2F_m/F = 2w_o/(g\rho'_o/\rho_o)$. For many sources, this is about 10 seconds, so buoyancy becomes dominant rather close in to the source. Briggs (1970) tested the laboratory data of Fan (1967) against Eq. (47), using $\beta = 1/3 + R^{-1}$ for the momentum term and $\beta = 0.5$ for the buoyancy term. The comparison is shown in Figure 4

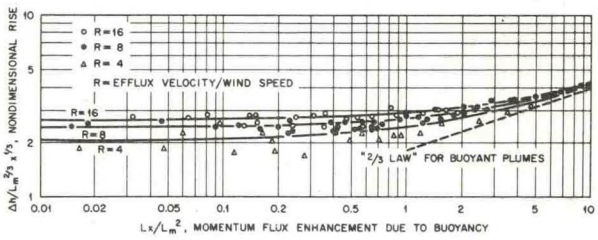


Figure 4. Transition from the "1/3 law" for jets to the "2/3 law" for buoyant plumes vs. theory (Eq. 47). $L = F/U^3$, $L_m = F_m^{1/2}/U$, $Lx/L_m^2 = Ft/F_m$.

When $Ft/F_m$ is large, Eq. (47) reduces to the well known "2/3 law" for the rise of buoyant plumes:

$$z = \left(\frac{3}{2\beta^2}\ \frac{F}{U}\right)^{1/3} t^{2/3}$$

$$= 1.6\ F^{1/3}\ U^{-1}\ x^{2/3} \qquad (48)$$

The coefficient 1.6 corresponds to the recommended value of $\beta$, 0.6. This equation is the asymptote of Sutton's (1950) formulation, and was first predicted explicitly by Scorer (1958, 1959). It has been confirmed by many experients since then, both in the field and in the laboratory. Briggs (1972) summarized many of the best fit values of the constant $C_1 = z \div (F/U)^{1/3}\ x^{2/3}$ This summary is extended in Table 3

Table 3 - Experimental Values of $C_1 = z \div (F/U)^{1/3}\ t^{2/3}$

| Investigator | Data Source | $C_1$ |
|---|---|---|
| Slawson and Csanady (1967) | Lakeview P.P. | 2.6* |
| Csanady (1961) | Tallawarra P.P. | 2.5* |
| Briggs (1965) | Tallawarra, Stewart et al. (1958) | |
| | Bosanquet et al. (1950), Ball (1950) - smudge | |
| | pots, Von Vleck and Boone (1964) - rocket motors | 2.0 |
| Bacci et al. (1974) | Ostiglia P.S. - neutral | 1.7 |
| Bringfelt ($1969_a$) | 17 chimneys - slightly stable | 1.8 |
| | - very stable | 1.7 |
| Briggs (1969) | Lakeview, Tallawarra, Stewart et al., | |
| | Bosanquet et al., Rauch (1964), | |
| | 3 CEGB plants - Lucas et al. (1963), Hamilton (1967), | |
| | 6 TVA plants - Carpenter et al. (1967) | 1.6 |
| Briggs (1970a and b) | All of the above plus Bringfelt (1968) | 1.6 |
| Hoult and Weil (1972) | Laboratory studies of Vadot (1965), Fan (1967), | |
| | Barilla (1968) and Weil (1968) | 1.6 |
| Humphries | Komati and Hendria P.P., x = 1500 m | 1.6[a] |
| Hewett et al. (1971) | Wind tunnel plumes | 1.6*[b] |
| Carpenter et al. (1971) | 6 TVA plants, x = 1200 m - neutral | 1.6 |
| | slightly stable | 1.5 |
| Tsang (1971) | Laboratory, 2-D thermal | 1.5 |
| Richards (1963) | Laboratory, 2-D thermal | 1.2 |
| Thomas et al. (1970) | 6 TVA plants, x = 1200 m | 1.2* |

* - Indicates that $F^*$ was used in original analysis (see end of Section 2.2 and Briggs (1972)) - an adjustment for the average $F/F^*$ has been made here.

[a] - The author gave his data in terms of the Lucas, Moore and Spurr (1963) formula, so I assumed $Q_H$ = 85 MW and x = 1500 m for this comparison.

[b] - With an assumed $\rho'_o/\rho_a = 0.3$

We see in Table 3 that experimental values of $C_1$ range from 1.2 to 2.6. However, the great majority of values cluster in the range 1.5 to 1.8, and the suggested value $C_1 = 1.6$ appears to be very satisfactory on the whole.

One factor that the model presented here does not take into account is the effect of wind shear on plume trajectories, since the crossflow velocity U has been assumed constant. In reality, U usually increases with height in the atmosphere, in which case the best fit exponent to $z \propto x^n$ would be somewhat less than 2/3 for a buoyant plume. This should be especially so when z is large compared to $h_s$ and in stable conditions, since more shear is possible when ambient stratification suppresses turbulent mixing. Indeed, the optimized value of n shows considerable variation for buoyant plume trajectories in the real atmosphere, ranging generally between 1/2 and 3/4. For instance, Bringfelt (1969a) found that n = 0.73 gave the best fit to trajectories in neutral conditions, while n = 0.62 fit better in stable conditions. In a later analysis (Bringfelt, 1969b), n = 0.66 fit in the range x = 250 to 500 m, while n = 0.50 fit best in the range 500 to 1000 m (this possibly could reflect some tendency toward leveling).

Murthy (1970) developed a form of the bent-over plume model that allows U to vary with height, but still assumed that dr/dz is constant. For $U \propto z^p$, the model predicts for a buoyant plume in neutral conditions $z \propto x^{(2/3)/(1+p)}$. Murthy tested this model by releasing buoyant plumes from a model stack in a wind tunnel, where it was possible to adjust the wind profile so that $p \simeq 1/3$. For this profile, the model predicts $n = (2/3)/(1+p) = 0.5$. Regression analysis of seven experimental trajectories gave values of n ranging from 0.35 to 0.52; the median value was 0.45.

Moore (1974a) argued that wind shear also induces increased entrainment due to axial shear as the bent-over plume rises into a faster airstream. In a discussion of this point, Briggs (1975) showed that the ratio of axial to transverse shears in a bent-over plume following the "2/3 law" is approximately

$$\bar{u}/\bar{w} \simeq \frac{1}{2} \frac{x}{U} \frac{\overline{\partial U}}{\partial z} \quad . \tag{49}$$

For the neutral surface layer, the result is that $\bar{u} < \bar{w}$ as long as x is less than the distance to the maximum ground concentration. In this case, the axial shear is unimportant, since the ratio of entrainment velocities is $\alpha\, \bar{u}/(\beta\, \bar{w}) \simeq 0.2\, \bar{u}/\bar{w}$. In a convective mixing layer, there is even less wind shear. However, $\partial U/\partial z$ can be much larger in stable air. As a crude approximation $U \propto (h_s + z)^{0.5}$ (ASME, 1973). This gives $\bar{u}/\bar{w} \simeq 0.5\, (x/h_s)\, (h_s/h)^{1.5}$. In this case, the shear-induced entrainment should remain unimportant unless $us^{-1/2} > 10\, h_s$ or so (it will be shown in Section 4.1 that the plume levels at $x \simeq 4\, us^{-1/2}$).

### 3.4 Buoyancy Generation and the "3/3 Law"

Although conservation of buoyancy has been assumed here, it is conceivable to have a buoyancy-generating effluent, such as in the case of strongly radioactive plumes. Such plumes were considered by Gifford (1967), who assumed that the plume generated new buoyancy at a constant rate ($\partial F/\partial t$). For this case, disregarding the factor $M/M_{eff}$, the buoyancy equation becomes

$$d F_z/dt = - s\, (\bar{w}\, V) + \partial F/\partial t \quad . \tag{50}$$

The result in neutral conditions, after the buoyancy flux has increased many times over its initial value, is

$$z = \left( \frac{\partial F/\partial t}{2\beta^2\, U} \right)^{1/3} t \quad , \tag{51}$$

rise with a constant upward slope. This plume also has the interesting property that it does not level off in stable conditions. Instead, at large values of $ts^{1/2}$, the two terms on the right side of Eq. (50) balance, so

$$z = \left( \frac{3(\partial F/\partial t)\, t}{\beta^2\, U\, s} \right)^{1/3} \quad . \tag{52}$$

## 4. RISE LIMITED BY STABLE STRATIFICATION

When the air is stable ($\partial \theta_a/\partial z > 0$), as it is at night and also is above the mixing layer during the day, ambient turbulence is greatly diminished or even absent. However, plume rise is limited for buoyancy-conserving plumes because of the loss of relative buoyancy as the plume rises into regions of lower potential density. The time scale of the rise is independent of the plume growth rate, and is found by differentiating the momentum equations and substituting the buoyancy equation of Eqs. (40) and (41):

$$d^2(\bar{w}V)/dt^2 = - s'(\bar{w}V) \quad , \tag{53}$$

where s' = s for a vertical plume and $s' = s\, M/M_{eff}$ for a bent-over plume.

Thus, the time scale of momentum flux change is $s^{-1/2}$, and plumes level off in stable air after a rise time proportional to an average value of $s^{-1/2}$. This was first recognized by Bosanquet (1957). As has been already mentioned, $s^{1/2} = \omega$ is the natural frequency of vertical oscillations in a stable fluid. Since the volume flux V is monotonically increasing, for constant s Eq. (53) implies that a plume is a damped harmonic oscillator. Indeed, on some occasions we can see plumes that overshoot their equilibrium height and display a quickly-damped oscillation before becoming completely level (watch for this especially just around sunrise on calm, clear mornings).

One also may observe that such plumes, while appearing turbulent and sharply defined in the rising stage, become smooth and fuzzy appearing a little after leveling occurs. This indicates very effective suppression of the internal turbulence due to mixing with stable air, which

resists all vertical motions. Usually, such plumes are seen to drift downwind with no further increase in thickness. This indicates complete absence of ambient turbulence (the plume may diffuse laterally due to inertial, 2-dimensional, horizontal eddies, but these are not regarded as "turbulence" in the strict sense of the word).

### 4.1 Rise Through a Constant Density Gradient

When s is approximately constant, as it often is in elevated layers and in the lowest 100 m or so at night, Eq. (53) is the equation of a harmonic oscillator. Recognizing that at t = 0 we have $\bar{w}V = F_m$ and $d(\bar{w}V)/dt = F$, we can write the solution as

$$\bar{w}V = F_m \cos(\omega' t) + (F/\omega') \sin \omega' t \quad , \qquad (54)$$

where $\omega' = s'^{1/2}$. This implies that the maximum rise, where $\bar{w}V$ first goes to zero, occurs at $\omega' t = \pi/2$ for a jet and at $\omega' t = \pi$ for a buoyant plume. In the general case, maximum rise occurs at $\omega' t = \tan^{-1}(-\omega' F_m/F)$. After this time the plume starts to descend with a dip occurring at a time $\pi/\omega'$ after the maximum.

When s' is constant, we can reverse the procedure used to obtain Eq. (53) to get

$$d^2 F_z/dt^2 = - s' F_z$$

$$F_z = F \cos(\omega' t) - \omega' F_m \sin(\omega' t) \quad . \qquad (55)$$

We see that the buoyancy flux also oscillates, and it is 90° out of phase with the momentum flux. A jet developes negative buoyancy immediately, and a buoyant plume becomes negatively buoyant after $\omega' t = \pi/2$, one-half the maximum rise time.

Common observation shows that plume oscillations damp very rapidly; indeed, there are times when very little "overshoot" of the final rise occurs. In spite of Eq. (55), we hardly expect that the buoyancy flux of a buoyant plume will bounce back and forth between F and -F indefinitely. The rapid damping out of plume motions after the maximum rise is obtained may be due to "wave drag" (Warren, 1960), which occurs as the energy of an oscillating object in stable fluid is propagated outward by waves. This effect is not accounted for in any plume rise model at present, but the models given here do seem adequate for predicting the final rise height.

For vertical, buoyant plumes from a point source, the MTT equations (Eqs. 38) were first solved for constant s by a finite difference technique by Morton, Taylor, and Turner (1956). If we use their suggested (top hat) value of the entrainment coefficient, $\alpha = 0.132$, the maximum rise is predicted to be

$$z_{max} = 5.0\, F^{1/4}\, s^{-3/8} \quad . \qquad (56)$$

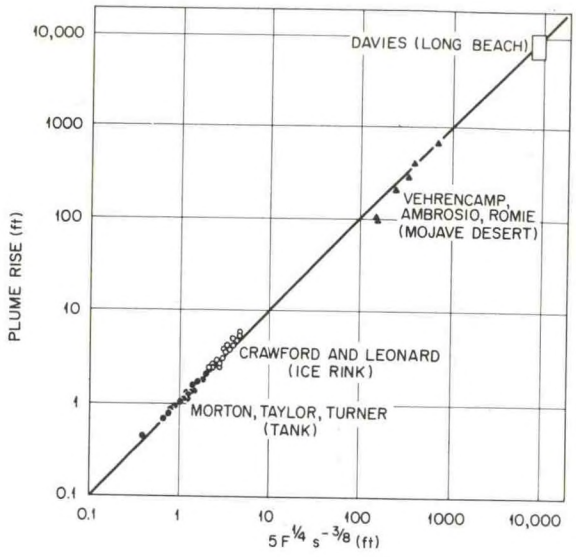


Figure 5. Plume rise vs. $5.0\, F^{1/4}\, s^{-3/8}$

Figure 5 shows that this formula gives a good prediction of the rise of the plume top over 4 orders of magnitude. Many of the data shown are from modeling experiments. Not many observations on vertical plumes in the atmosphere are available, probably because the wind blows most of the time. For ordinary sources, transition to the "bent-over" condition occurs at a very low wind speed, 1 m/sec or less. Briggs (1969) showed that Eq. (56) gives a good estimate of the rise of the plume from the Surtsey volcano, which ranged from 3 to 8 km high. This source had about 1000 times the heat emission rate of a large power plant stack, and Eq. (32) implies vertical velocities exceeding 50 m/sec in the lowest 2 km of rise; on this scale, plumes are almost always vertical or just slightly inclined. Bacci et al. (1974) report one case of a lidar observed vertical plume from a power station. The measured wind was 0.5 m/sec, and the "maximum rise" was $5.1\, F^{1/4}\, s^{-3/8}$ (this is probably the centerline rise).

There is some ambiguity in definitions of the plume geometry here. In the laboratory experiments, the maximum rises of fluid over the center of the plume were measured, but there is some settling back as this material spreads horizontally. In all of the atmospheric observations, while the plume columns are substantially vertical during most of the rise, they do finally shear over aand drift off in the direction of whatever wind is present (true "zero wind" situations, where the plumes spread out axismmetrically from a vertical axis, do occur in the atmosphere, but they are extremely rare). For these observations, the rise measured was the top of the sheared-over plume. In the laboratory, Morton, Taylor, and Turner (1956) observed the bottom of the spreading-out fluid to be at about 0.6 times the maximum rise, but this was in a narrow (0.3 m diameter) tank. Until more definitive measurements are made on the geometry of axisymmetrically

spreading plumes and sheared-over plumes, I would recommend $z \div F^{1/4} s^{-3/8} \simeq 5.0$ for the top of the plume, 3.0 for the bottom, and 4.0 for the centerline.

While the MTT model cannot be solved analytically, there is an analytical approximation to it that gives very similar results, and that is the "unaltered volume flux" approach. It is noted that the numerical results of the MTT model for constant s gives a V that very closely approximates Eq. (33) for s = 0 throughout most of the rise, and drops to 16% less than this value only as the final rise is approached. If we assume the prediction of V as given by Eq. (33), which corresponds to $\alpha = 0.124$, and substitute it into Eq. (54) with $F_m = 0$ and $\bar{w} = dz/dt$, the predicted maximum rise is exactly the same as is given by Eq. (56). Furthermore, the "equilibrium height," where $F_z = 0$, is $(1/2)^{3/8} = 0.77$ times the maximum rise, as compared to 0.76 with the exact MTT solution. We define a "falling back height" as the height where the plume at maximum rise would be in equilibrium if no further mixing takes place (remember that the plume has to acquire negative buoyancy before the rise is brought to a halt). For a buoyant plume, this height is just $z_{max} - F/(s\, V_{max})$. The unaltered volume flux model gives a falling back height equal to 13/16 = 0.81 times the maximum rise, as compared to 0.79 with the exact MTT model. Both of these predictions appear to be good approximations of the final "centerline" height. The real usefulness of the "unaltered volume flux" technique will be in dealing with arbitrary density profiles, to be discussed in Section 4.3.

For vertical jets from a point source with s = 0, the unaltered volume flux model predicts a maximum rise at $(2/\alpha)^{1/2} (F_m/s)^{1/4}$, and $(2/\alpha)^{1/2} = 5.0$ for $\alpha = 0.08$. The "falling back height" would be exactly 1/2 this; since $\partial V/\partial z$ is constant in a jet, with constant s the jet's average potential density would always be equal to the ambient value at 1/2 z. Experimental information on jet rise in stable surroundings is very sparse. Briggs (1969) suggested

$$z_{max} \simeq 4 (F_m/s)^{1/4} \qquad (57)$$

on the basis of only three experimental runs by Fan (1967). The actual coefficients were 4.5, 4.4, and 4.2, but these were not pure jets. They were just marginally momentum-dominated, with $\omega F_m/F = 1.8$, 4.2, and 5.3, respectively. The rises could have been approximated just as well with the buoyant rise equation, with $z_{max}/(F^{1/4} s^{-3/8}) = 5.2$, 6.3, and 6.3 for three runs, respectively. For this reason, Eq. (57) must be taken as tentative. A photograph of the least momentum-dominated plume indicates the centerline of the spreading-out portion of the plume at about $z = 2.5(F_m/s)^{1/4}$.

Morton (1959) investigated the consequences of the MTT model for such mixed cases, and found that moderate amounts of initial momentum flux decrease the rise of a buoyant plume in stable surroundings. This is due to increased entrainment in the lower parts of the plume. Morton's solution indicates rise increased by additional momentum only when $\omega F_m/F$ exceeds about 10, which for most hot effluents would mean that $w_o$ should exceed 100 m/sec! However, Fan's experiment suggests that $\omega F_m/F$ needs to exceed only about 2 for enhanced rise. The lower threshold is consistent with the fact that $\alpha$ appears to be smaller for jets than for buoyant plumes.

Detailed solutions of the MTT equations for finite radius sources and both positive and negative buoyancy are given by Hino (1962) and by Morton and Middleton (1973).

For a bent-over plume, we have $V \simeq U(\beta z)^2$ up to the point of maximum rise regardless of whether the plume is buoyancy or momentum dominated (except that $\beta$ might differ slightly for the two cases). Substituting this into Eq. (54) and integrating, we predict

$$z = \left(\frac{3}{\beta^2 U s'}\right)^{1/3} [\omega' F_m \sin(\omega' t) + F(1 - \cos(\omega' t))]^{1/3}$$

$$z_{max} = \left(\frac{3F}{\beta^2 U s'}\right)^{1/3} (1 + [1 + (\omega' F_m/F)^2]^{1/2})^{1/3} \quad . \qquad (58)$$

For a buoyant plume ($\omega' F_m \ll F$), this also predicts an equilibrium height at $(1/2)^{1/3} = 0.79$ times $z_{max}$ and a "falling back height" at (5/6) = 0.83 times $z_{max}$. This can be compared to the asymptotic height calculated for $\omega t \to \infty$ by Fay et al. (1969a) with the assumption $dr/dt = \beta|w|$, which turns out to be 0.84 times $z_{max}$. For a jet, the "falling back height" is 2/3 of $z_{max}$. Unfortunately, there is no experimental information available on the final rise of bent-over jets in stable conditions.

For the rise of buoyant bent-over plumes in stable air, Briggs (1972) summarized a number of observational studies that found correlations with

$$\Delta h = C_2 \left(\frac{F}{Us}\right)^{1/3} , \qquad (59)$$

where $\Delta h$ refers to the final height of the plume centerline above its source. This summary is extended further in Table 4. The values of $C_2$ range from 1.8 to 3.1, but most cluster in the range 2.3 to 2.9.

The Briggs (1970) and the Fay et al. analyses involve substantially the same data, but the reported best fit values of $C_2$ are disturbingly different. The methods of analysis were quite different, but the main difference is that Briggs used the average rise at x = 5 x' for each trajectory, which is generally beyond the point of maximum rise, while Fay et al. included all data beyond x = 1.55 x' ($x' = U\omega^{-1} = Us^{-1/2}$, the scale distance of leveling-off). Thus, Briggs used many fewer data, since there is a large amount of data "dropout" in the intervening distance, but a substantial portion of the Fay et al. data occurs before the final rise has been achieved (see Figures 6 and 7). This is probably why their value of $C_2$ is lower.

Table 4. Experimental Vaues of $C_2 = \Delta h \div (F/Us)^{1/3}$

| Investigator | Data Source | $C_2$ |
|---|---|---|
| Briggs (1970) | 2 TVA plants - Carpenter et al. (1967)<br>6 industrial stacks - Bringfelt (1968) | 3.1 |
| Briggs (1969) | 2 TVA plants, Van Vleck and Boone (1964) - rocket motors, Frizzola et al. (1966) - ignited fuel | 2.9 |
| Hewett et al. (1971) | Wind tunnel plumes | 2.8*a |
| Bacci et al. (1974) | Ostiglia P. S. | 2.6 |
| Fay et al. (1969b) | TVA and Bringfelt | 2.6*a |
| Briggs (1965) | Gartrell et al. (1964)- One plant with 3 stacks<br>Moses and Strom (1961)- pilot stack | 2.6 |
| Bringfelt (1969) | 8 chimneys - very stable, $R \geq 1.2$ | 2.5[b] |
| Johnson and Uthe (1971) | Keystone plant, lidar | 2.4*b |
| Proudfit (1970) | Keystone plant, $SO_2$ | 2.3[b] |
| Bringfelt (1969) | 4 chimneys - slightly stable, $R \simeq 1.0$ | 1.8[b] |

* - Indicates $F^*$ was used in original analysis (see end of Section 2.2 and Briggs (1972)) - an adjustment for the average $F/F^*$ has been made here

a - With an assumed $\rho_a'/\rho_a = 0.3$.

b - Calculated from information given in table of reference.

The Johnson and Uthe (JU) (1971) and the Proudfit (1970) studies were at the same plant during the same period, and there were four cases in which the rise was almost measured simultaneously by both research teams. The ratios of the measured centerline rises, $\Delta h$ (Proudfit) $\div$ $\Delta h$(JU) were about 1.2, 1.3, 1.4, and 0.7 for these four cases, which should illustrate the difficulty of defining "plume rise" even from the observational standpoint. The JU plume rises were taken from the top and the bottom of the plume as seen by lidar; the cross sections were made at 8 km for the first three cases and at 21 km in the last case. In contrast,the Proudfit observations were all made between 3 and 4 km downwind, taking the top and the bottom of the plume as detected by an $SO_2$ analyzer on slanting helicopter traverses through the plume. Many of the $SO_2$ profiles showed the $SO_2$ maximum skewed toward the top of the plume, which is what we should expect since the less dilute part of the rising plume is also warmer, and will tend to end up on top.

The bottoms of these plumes were rather low compared to those of the TVA plumes shown in Figure 6. The rise of the bottoms divided by the rise of the tops averaged about 0.2, versus 0.4 for TVA. The values of $C_2$ for the plume top are in better agreement, $C_2 \simeq 3.7$ for the Proudfit data and $C_2 \simeq 4.0$ for the TVA data.

The value of $C_2$ determined from plumes in a wind tunnel, about 2.8, corresponds closely to the "falling back height" given by the present model with $\beta = 0.6$ and $M_{eff}/M = s/s' = 2.25$. Since these are the only data for which s really was substantially constant, I am inclined to accept this as the best present value for the "constant density gradient" case. However, $C_2 = 2.6$ appears to be a more typical value for the plumes in the "real" atmosphere. Such observations rarely occur with a linear temperature (density) profile. In all the studies so far, s has been defined by $\Delta\theta/\Delta z$, where $\Delta\theta$ and $\Delta z$ are the potential temperature and the height differences between the top of the stack and the top of the plume. Note that the value $C_2 = 2.6$ corresponds closely to the equilibrium height given by the present model, $C_2 = (3(2.25) / (0.6)^2)^{1/3} = 2.66$.

Weil and Hoult (1973) presented an unusual test of Eq. (59) in that the plume rise was not measured. Instead, they correlated the maximum ground concentration measured at the time of inversion breakup fumigation with Eq. (59) assuming $C_2 = 2.5$. The $SO_2$ concentrations were measured at the Keystone plant by a helicopter flying under the axis of the plume at tree top level (Schiermeier and Niemeyer, 1970).

They assumed the conventional (constant $\sigma_z/\sigma_y$) approach to predicting the maximum ground concentration (MGC). For a Gaussian plume with vertical and lateral standard deviations of concentration distribution $\sigma_z$ and $\sigma_y$, respectively, the MGC is given by

$$\chi = \frac{\sigma_z}{\sigma_y} \frac{2}{\pi e} \frac{Q}{U h_e^2} \quad , \tag{60}$$

where Q is the rate of emission and $h_e = h_s + \Delta h$. With the assumed plume rise equation, Weil and Hoult found the best correlation with Eq. (60) with $\sigma_z/\sigma_y \simeq 0.5$, which is reasonable for the inversion breakup situation. However, the way these $SO_2$ measurements were tabulated more resembles "peak" values than the usual 15 minute to 1 hour average concentration. The geometric standard deviation of the ratio of measured to predicted MGC was about a factor of 2.

The present theory predicts that the maximum rise of a bent-over plume will occur at

$$x = (U/\omega') \tan^{-1} (-\omega' F_m/F)$$
$$= x' (M_{eff}/M)^{1/2} \tan^{-1} (-(M/M_{eff})^{1/2} \omega F_m/F). \tag{61}$$

For most buoyant plumes, $F_m/F$ is about 5 seconds, so $M_{eff}/M = 2.25$ implies a maximum rise at $x/x' \simeq 4.5$. This prediction can be checked by plotting $z \div (F/Us)^{1/3}$ vs. $x/x'$. This is done for the plume trajectories measured by TVA and by Bringfelt in Figures 6 and 7. Five of the six centerline trajectories of TVA reach a very flat maximum somewhere between 3 and 6 x'. The four trajectories of Bringfelt which do exhibit settling back peak somewhere between 3 and 6.5 x'. The wind tunnel plume trajectories of Hewett et al. (1971) are less ambiguous, and display a rather flat peak in rise at just over x = 4 x'.

The idea of different values of the effective momentum flux $M_{eff}$ and internal momentum flux M is presented here for the first time. It arose quite naturally from the derivation of the mementum and buoyancy conservation equations, which attempted to improve upon the rigor of these fundamental plume equations. Past models, in effect, assumed $M_{eff}/M$ to be unity. While the value of 2.25 suggested here, primarily on the basis of Richards' streamlines, is a tentative value, I believe that the concept that $M_{eff}/M > 1$ is a useful refinement of the theory of bent-over plume rise in stable conditions.

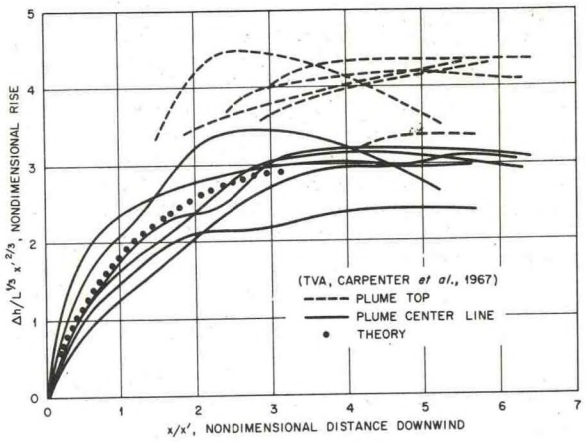


Figure 6. $\Delta h \div (F/Us)^{1/3}$ versus $x \div Us^{-1/2}$ in stable conditions, TVA measurements.

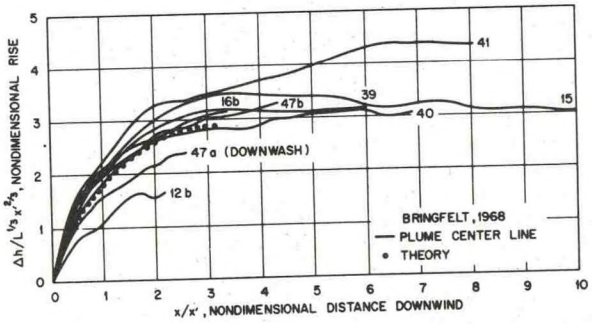


Figure 7. $\Delta h \div (F/Us)^{1/3}$ versus $x \div Us^{-1/2}$ in stable conditions, Bringfelt measurements.

## 4.2 Rise Through a Density Jump

Occasionally the atmosphere is near-neutral except for one or more thin layers of sharp temperature rise (see, e. g., Simon and Proudfit, 1967). We may approximate this situation by assuming $\partial \theta_a/\partial z = 0$ except for a rise of potential temperature $\Delta\theta_i$ at a height above the source $z_i$. For convenience, we define $b_i = (g/\theta_a)\Delta\theta_i = \int s\,dz$ through the inversion layer.

For vertical, buoyant plumes, prediction of whether the inversion can be penetrated is quite straightforward - the plume should penetrate if the temperature excess of the plume when it gets to height $z_i$ exceeds $\Delta\theta_i$. This criterion is met if $F_z/V_i > b_i$, where $V_i$ is the plume volume flux at height $z_i$. If the plume does penetrate, the buoyancy flux is reduced by $V_i b_i$, a direct consequence of the loss of $\Delta\theta_i$ in temperature excess as the

the inversion is penetrated. Using the experimental determination of V as given by Eq. (33), we predict penetration if

$$F > 0.019\ b_i^{3/2}\ z_i^{5/2} \quad . \tag{62}$$

The analysis of Vadot's (1965) laboratory data in Briggs (1969) shows that the above is on the conservative side for very buoyant plumes, but that a slightly larger value of F is needed if the plume is momentum-dominated, i.e. if $F_m\ b_i^{0.8}\ F^{-1.2} > 4$. Typical buoyant sources are well into the buoyancy-dominated regime by the time they reach any inversion where there is a question of penetration ability. Note from Eq. (62) that inversion penetration ability is very sensitive to the height of the inversion.

High momentum vertical plumes lose penetration power due to greater dilution of the plume buoyancy in the lower part of the rise. Using the volume flux for a jet instead of Eq. (33), we find that when $F_m\ b_i^{0.8}\ F^{-1/2} > 1.6$, we require

$$F > 0.16\ F_m^{1/2}\ b_i\ z_i \tag{63}$$

for the plume to retain positive buoyancy after penetration.

If a vertical plume has little or no buoyancy, it is still possible for it to "punch" through an inversion if it has enough momentum. However, since it entrained some fluid from below the inversion, it remains more dense than the fluid above the inversion and must settle back eventually, "sandwiching" itself somewhere in the inversion layer. It will have some inbetween value of potential density, depending on how far it penetrates before settling back. Using the unaltered volume flux assumption and $F_z = -\ b_i\ V_i$ (above the inversion) in the momentum equation, we can estimate the penetration height where $w \to 0$. We can also calculate the potential temperature of the plume at this point, which is $\Delta\theta_p$ above the ambient value below the inversion. The result is

$$z_{max}/z_i = (1 + (2\alpha)^{-2}\ (F_m/b_i)/z_i^{3})^{1/2}$$

$$\Delta\theta_p/\Delta\theta_i = 1 - z_i/z_{max} \quad . \tag{64}$$

Vadot's experimental results, as reported by Briggs (1969), show substantial (subjective) penetration for highly momentum-dominated plumes if $F_m > 0.25\ b_i\ z_i^3$, for which Eq. (64) implies $z_{max} > 3\ z_i$.

For a bent-over jet, using $V = U(\beta z)^2$ and the buoyancy and momentum equations for the bent over plume, we find substantial penetration ($z_{max} > 2\ z_i$) if

$$F_m > 2.2\ \beta^2\ U\ b_i^{1/2}\ z_i^{5/2} \quad . \tag{65}$$

Again, we expect the penetrated jet to settle back and "sandwich" itself in the inversion layer. There are no data at hand for testing Eq. (65).

Briggs (1969) suggested and tested an expression similar to Eq. (62) for the penetration of sharp inversions by bent-over, buoyant plumes. It was assumed that the plume "penetrated" ($\Delta h > z_i$) if the characteristic buoyant acceleration of the plume, $F_z/V$, exceeded $b_i$ when the centerline of the plume arrived at $z_i$. Since $\beta$ was taken to be 0.5 in this study, penetration was predicted if $F > 0.25\ U\ b_i\ z_i^2$; this tested well against the data of Simon and Proudfit (1967), appearing to slightly underpredict the penetration ability of the power plant plumes.

However, this approach neglects the finite depth of the plume and assumes that penetration is total or not at all. In reality, partial penetration of elevated inversions probably occurs more often than does total penetration. Partial penetration could still account for a significant reduction in immediate ground concentration, since inversion layers act as a shield against vertical diffusion. With the more detailed view of the dynamics of bent-over plumes that we have here, it is fairly easy to develope model for partial penetration. To do this, we must abandon the approximation that the whole plume experiences the same ambient stability that happens to be present at the centerline height. We go back to Eq. (8) with the idea in mind that $\partial\theta_a/\partial z$ and s are not constant over the whole depth of the plume, then integrate using our usual bent-over plume approximation $u \ll U$. The resulting buoyancy flux equation is

$$dF_z/dz = -\ U\ {}_p\!\int\ (s\ {}_p\!\int\ (w/\bar{w})dy)\ dz \div \pi \quad , \tag{66}$$

instead of the -s'V we get when s is constant through the plume depth. We see now that s must be weighted by the total upward flow within the plume at any given level, ${}_p\!\int\ w\ dy$. Fortunately, this is easy to determine; since $w = -\ \partial\psi/\partial y$, where $\psi$ is the stream function, s is just weighted by the difference between $\psi$ at the right and the left sides of the thermal. Once again, we can learn something from streamlines measured in and around a two-dimensional thermals (Richards, 1961). On inspecting these streamlines, we find that a strong upflow begins immediately at the bottom of the thermal. As we move up in the thermal, the total upflow increases by only 15%, then gradually decreases back to the value it had at the bottom of the thermal at a height about six-tenths of the way up toward the top of the thermal. Above this height, the decrease is more and more rapid, until there is zero upflow at the very top of the thermal (there is a finite w, of course, but the thermal width is zero at the top; it was not zero at the bottom because of the kidney shape - see Figure 2).

This means that the weighting function of s with height looks rather like a cylinder with a hemispherical cap. It can be approximated by a simple rectangle in the bottom six-tenths of the thermal. A simple rectangular approximation also ought to work fairly well for the top of the

thermal, at least for levels that are traversed by the plume, because for a bent-over plume $d F_z/dz$ is also weighted by cross-sectional area of the plume, which is proportional to $z^2$. Relative to a reference height, $z_s$, the top of the plume arrives when plume centerline height $z \simeq (2/3)\ z_s$, and the bottom of the plume leaves when $z \simeq 2\ z_s$, so the top of the plume only gets $(1/3)^2 = 1/9$ the weighting that the bottom of the plume does in figuring the effect of s at height $z_s$ on $F_z$. Thus the shape of the weighting function is not so critical at the top of the plume. We chose a rectangle because it is simple and should give a conservative estimate of how much the "nose" of a thermal can penetrate an inversion.

The rectangular weighting function is equivalent to the assumption that the plume itself is rectangular, with a constant upward velocity inside. Adopting this assumption and setting $w = \bar{w}$, the total cross-sectional area of the plume must be

$$(2\ \beta_y\ z)\ (2\ \beta_z\ z) = \pi (M/M_{eff})\ (\beta z)^2 \qquad (67)$$

to be consistent with our model for constant s, where $\beta_y\ z$ is the half-width and $\beta_z\ z$ is the half-depth of the rectangular plume. Using the reported plume depths from photographs (Briggs, 1969; Bringfelt, 1969), we set $\beta_z \simeq 0.5$, so the plume extends vertically from 0.5 z to 1.5 z. Assuming $\beta = 0.6$ and $M_{eff}/M = 2.25$, we find that $\beta_y = 0.25 = 1/2\ \beta_z$ (this shape is only an "effective" shape, and is not supposed to approximate the actual plume shape).

Applying this model to the penetration of a sharp inversion, during the traverse of height $z_i$ by the plume ($0.5\ z < z_i < 1.5\ z$) Eq. (66) becomes

$$-d F_z/dz = U\ b_i\ (2\ \beta_y\ z) \div \pi \quad . \qquad (68)$$

Assuming that the plume arrives at the inversion with buoyancy $F_z = F$, we can easily integrate Eq. (68) to find the equilibrium height where $F_z = 0$:

$$z_{eq}/z_i = 2/3\ [1 + (3/2)^2\ (\pi/\beta_y)\ F/(U\ b_i\ z_i^2)]^{1/2} \qquad (69)$$

If $F > 7\ (2/3)^2\ (\beta_y/\pi)\ U\ b_i\ z_i^2$ (which equals $0.28\ U\ b_i\ z_i^2$ in this case), the plume completely penetrates the inversion, but retains reduced buoyancy flux $F_z$ that is equal to the difference implied by this inequality. If complete penetration does not occur, Eq. (69) should give a good approximation of the final rise; in Section 4.1, it can be noted that predicted "equilibrium" heights give very good estimates of final centerline heights.

Finally, let us define a "penetration factor."

$$P = (\text{depth of plume above } z_i) \div (\text{total plume depth})$$
$$= (1.5\ z - z_i) \div (1.5\ z - 0.5\ z)$$
$$= 1.5 - z_i/z \quad . \qquad (70)$$

We can assume that P approximates the percentage of plume material that does get through the inversion, so that only (1 - P) of the material gets reflected and diffused downward. An important implication of this assumption is that 50% penetration requires only about 1/6 the buoyancy that total penetration requires; basically, this results because the plume at $z = z_i$ has only 1/4 the cross-sectional area it has at $z = 2\ z_i$.

The Simon and Proudfit (1967) data can be used to test the penetration prediction of Eqs. (69) and (70) by defining an "observed" value of $P_{obs} = 1.5 - z_i/\Delta h_{obs}$. The inversion layers were of finite thickness, but the average thickness was only 15% of $z_i$. A few were as thick as 37% of $z_i$, but this is still "thin" compared to the thickness of a plume, which is about 100% of z. I calculated $z_i$ as the height of the center of inversion above the stack, and used the windspeed at the height of the plume. Only the July and September runs were usable, since for the spring runs either the data are incomplete or the inversions are thick compared to $z_i$. The resultant comparisons for the lower inversions divide most conveniently into the three groups shown below in Table 5.

Table 5. Observed vs. Calculated Inversion Penetration

| Calculated P | No. | $P_{obs} - P_{calc}$ | |
|---|---|---|---|
| 75 - 100 % | 5 | + 9 % | (± 14 %) |
| 35 - 65 % | 13 | - 5 % | (± 20 %) |
| 0 - 25 % | 8 | + 1 % | (± 11 %) |

On the whole, the method shows no tendency to underpredict or to overpredict the observed rises. Half of the cases fell into the "50% penetration" prediction category, but the observed values of P tended to be more widely scattered in that category; the average correspondence is quite respectable, however. Of the four cases where 75 to 85 % penetration was predicted, total penetration was observed for three of the cases. It was also observed in the one case it was predicted, and the plume continued to rise into a higher inversion layer, where it stopped with $P_{obs} = 85\%$; the method predicts P = 60% for the upper inversion, after a loss of 50% of the initial buoyancy during passage through the lower inversion.

### 4.3 Rise Into an Elevated Stable Layer

A frequently encountered stability situation is near-neutral stability up to some height $z_b$ above the source and stable stratification through a thick layer above $z_b$. Examples are the marine inversion layer in some coastal areas and the ordinary mixing layer with stable air above it. Again, one would like to know the penetration ability of a buoyant plume.

Let us suppose that we can approximate the stability profile with s = 0 below $z = z_b$ and s = constant above this. As before, we will approximate the final centerline rise with the equilibrium height, which works just as well as much more elaborate calculations.

For a vertical plume, we use $d F_z/dz = - s V$ with the unaltered volume flux assumption, using Eq. (33). If $F_z = F$ initially, integration shows that $F_z = 0$ at

$$z_{eq} = z_b = ( 1 + 37 F^{2/3}/(s z_b^{8/3}))^{3/8} . \quad (71)$$

For 100% penetration into the stable layer, $z_{eq}/z_b$ should be approximately 4/3 or greater, based on the shape of buoyant vertical plumes in a constant density gradient.

For a buoyant, bent-over plume, we again make use of the "rectangular plume" approximation and Eq. (66), both discussed in the last section. For partial penetration the result is

$$\frac{3F}{\beta'^2 \, Us \, z_b^3} = \frac{3}{2}\left(\frac{z_{eq}}{z_b}\right)^2 \left(\frac{z_{eq}}{z_b} - 1\right) + \frac{2}{9} , \quad (72)$$

where $\beta' = (M/M_{eff})^{1/2} \beta \simeq 0.4$. Total penetration ($z_{eq} > 2 z_b$) occurs if $3 F / (\beta'^2 Us z_b^3) > 6.2$, in which case

$$z_{eq}/z_b = [1.8 + 3F / (\beta'^2 Us z_b^3)]^{1/3} . \quad (73)$$

A surprising feature of the model is that 50% penetration ($z_{eq} = z_b$) requires only 1/28 the buoyancy required for 100% penetration. However, Weil (1974) reports that observed ground level concentrations at the Dickerson power plant were reduced by about one-half for this same situation when $[1+3F/(\beta'^2 Us z_b^3)]^{1/3} \simeq 1.09$ or somewhat greater. This corresponds to a predicted $P = 1.5 - z_b/z_{eq} = 54\%$ with the present model.

### 4.4 Rise Through an Arbitrary Density Profile

Much more complex temperature profiles than any described so far do occur sometimes in the atmosphere. However complex, such profiles can be approximated with a series of straight lines (end-to-end), i.e., by a series of layers with $s \simeq$ constant in each layer. For the purpose of calculating plume rise, the fit to the actual profile can be quite approximate, since in general the rise height only depends on the -1/3 or the -3/8 power of s. We then can approximate the plume rise as the equilibrium height and calculate this immediately by integrating $d F_z/dz = -s'V$ through each successive layer. Let us designate that $F_z = F_j$ when the plume reaches the bottom of the j th layer at a height above the source $z = z_j$, and $s = s_j$ within this layer.

For a vertical plume, we use the unaltered volume flux assumption with V given by Eq. (33). Within the j th layer, we find

$$F_z = F_j - 0.027 \, s_j \, F^{1/3}(z^{8/3} - z_j^{8/3}) . \quad (74)$$

We can use this to calculate $F_{j+1}$ at $z = z_{j+1}$, until $F_z$ goes negative. In that layer we apply Eq. (74) to calculate $\Delta h = z_{eq}$, by setting $F_z = 0$.

For a bent-over plume we use $V = U(\beta z)^2$, which gives for the j th layer

$$F_z = F_j - (1/3)\beta'^2 \, s_j \, U_j (z^3 - z_j^3) , \quad (75)$$

where $\beta' \simeq 0.4$. The same procedure is used.

If there is a question of whether to use the vertical plume or the bent-over plume assumption in a given layer, choose the assumption that gives the greatest decrease of $F_z$ in that layer. In general, transition from the vertical model to the bent-over model occurs at height $z \simeq 0.1 F/U^3 = 0.1L$, which is usually quite small.

While this model should be able to predict the approximate centerline rise, it is not expected to predict the degree of penetration into an elevated inversion. Some adaptation of the "rectangular plume" model used in the last two sections might be able to do this. However, this is getting into an area where experimental checks are very hard to find.

An example of the actual time history of a plume rising into stable air that demonstrates several different situations is shown in Figure 8. The overall situation is complex, yet is not at all atypical of the early morning hours when a mixing layer is building up (the mixing layer is identified by nearly vertical isopleths of potential temperature). We see, at first, rise into an arbitrary, stable density profile, followed by partial penetration into an elevated stable layer. The degree of penetration diminishes as the mixing layer gets higher, "lifting" the base of the inversion layer.

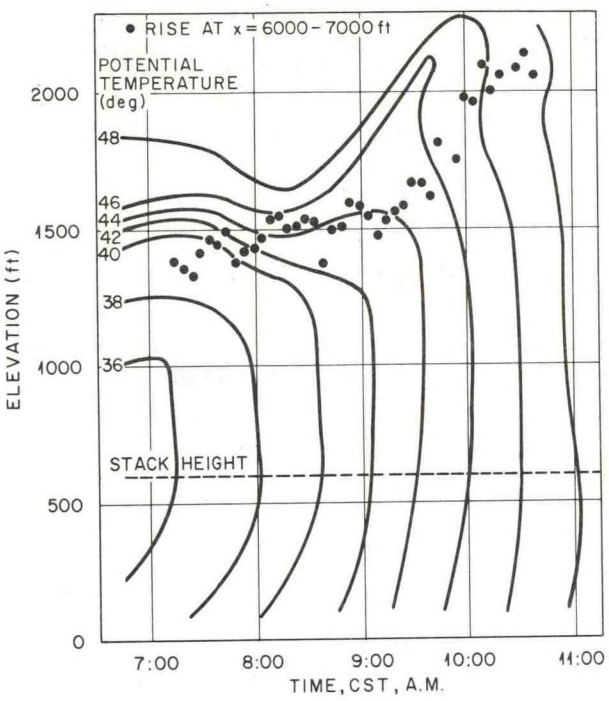


Figure 8. Plume rise (dots) versus time at the Paradise steam plant, TVA.

## 5. RISE LIMITED BY MECHANICAL TURBULENCE

When the atmosphere is not stably stratified it is almost bound to be turbulent. Ambient turbulence is capable of limiting the effective stack height (ESH) of a plume either by causing greatly accelerated mixing, which makes the plume level, or by causing it to contact the ground through the action of large scale eddies. These have no effect on the average plume rise, but do determine the point of maximum ground concentration. In this sense the large eddies affect the ESH if the plume has not yet leveled at that point.

Atmospheric turbulence is of two kinds, convective and mechanical. Convective turbulence is due to heating of the air near the ground, which makes it hydrostatically unstable. This kind of turbulence is normally dominant throughout the mixing layer in the daytime, except on cloudy or windy days or very near the ground. Mechanical turbulence is always present near the ground when $U > 0$, due to mechanical instability caused by the strong wind shear there ($U = 0$ at the ground).

Shear production of turbulence dominates convective production as long as $h < |L''|$, where h is the height above the ground, $L'' = -u^{*3}/(kH)$ is the Monin-Obukhov scaling length, $u^*$ is the friction velocity, k is the von Karmen constant ( = 0.35 to 0.4), and H is the production rate of turbulence due to convection. H is directly proportional to the upward sensible heat flux near the ground. Near the ground, $u^*$ is proportional to the wind speed; it normally ranges between 0.2 and 2 m/sec. H normally ranges from $-0.001$ $m^2/sec^3$ on clear nights to $+0.01$ $m^2/sec^3$ on sunny, summer days, and can be close to zero near sunrise or sunset or on completely overcast days.

Inspection of experimental data on profiles and the turbulence energy budget in the surface layer (Businger et al.,1971; Wyngaard and Cote, 1971) suggests that the upper limit of what might be considered the mechanical turbulence regime is at roughly $h \simeq |L''|$ when H is positive (daytime) and at $h \simeq 0.1\ L''$ when H is negative (night). In clear conditions, this is roughly $250\ u^{*3}$ $sec^3/m^2$ high, and in overcast conditions this can go as high as $1000\ u^{*3}$. Thus, the height of the mechanical turbulence layer is extremely variable. Normally, this layer is 10 to 100 m high. During low winds, it is extremely shallow. During high winds on overcast days mechanical turbulence can dominate the whole planetary boundary layer to 1 km or more.

As a rough rule of thumb, at 100 m above the ground mechanical turbulence dominates only when $U > 10$ m/sec, plus or minus about 30% depending on cloudiness. At greater or lesser heights, adjust this criterion by $h^{1/3}$. The point here is that plume rise formulas based on the assumption of mechanical turbulence are valid only for relatively high wind speeds.

### 5.1 Effect of Plume Breakup

We assumed in Section 2.6 that plume rise effectively terminates due to ambient turbulence when $\eta\ \overline{w^3}/z = \varepsilon$, the ambient turbulent dissipation rate. Whether the plume then "breaks up," "breaks down," or merely gradually levels is mostly a matter of semantics and subjective speculation at this point, but we will call it "plume breakup" for now as a matter of convenience. Hopefully, it will approximate the ESH, which is all we are after.

In general, this rise termination assumption implies that

$$\Delta h = \left(\frac{2}{3\beta^2}\,\frac{F}{U}\right)^{3/5} (\eta/\varepsilon)^{2/5} \qquad (76)$$

for a buoyant plume with a first stage rise given by the "2/3 law" (Eq. 48). For a jet with a first stage rise given by the "1/3 law" (Eq. 45), termination is at

$$\Delta h = \left(\frac{1}{\beta^2}\,\frac{F_m}{U}\right)^{3/7} (\eta/\varepsilon)^{1/7} \qquad (77)$$

For mechanical turbulence, it is convenient to assume the well-known expression for $\varepsilon$ in the neutral surface layer:

$$\varepsilon = u^{*3}/(k\ h) \quad . \qquad (78)$$

For the purpose of calculating the friction velocity from the wind speed, we may also assume the logarithmic law

$$U = (u^*/k)\ \ln(h/z_o) \quad , \qquad (79)$$

where $z_o$ is called the "roughness length" and is found experimentally to be about 1/10 the height of "roughness elements" on the ground, such as trees, crops, and buildings. We may use the following table, based on k = 0.4, for estimates of U/u* in neutral conditions. For elevated sources, it is sufficient to evaluate the ratio at $h = h_s$.

Table 6. Typical Ratios of U/u* in Neutral Conditions

| Site type | $z_o$ | h=30m | 100m | 300m |
|---|---|---|---|---|
| Urban, forest | 1.0 m | 9 | 12 | 14 |
| Mixed countryside | 0.3 m | 12 | 15 | 17 |
| Tall grass, crops | 0.1 m | 14 | 17 | 20 |

Equations (78) and (79) are strictly valid only for the neutral surface layer, which is limited in height by L", as already mentioned, and by the effect of wind turning with height due to Coriolis force. At mid-latitudes, the latter limits the "surface layer" to a height roughly equal to u* times 200 seconds. This is more limiting than the criterion for mechanical turbulence only at high wind speeds, of the order of 10 m/sec or greater. However, regardless of the turning of the wind with height, in neutral conditions the log profile for mean wind speed appears to be approximately valid to several times the height of the surface layer. Furthermore, several studies in recent years have shown that in near-neutral conditions $\varepsilon \sim h^{-1}$ holds to considerable heights. For instance, Herbert (1971) made airplane measurements of $\varepsilon$ in eastern Oregon. For the four days classified as "near neutral" (overcast and U > 7 m/sec), $\varepsilon \propto h^{-1}$ provides a reasonable fit to the mean from h = 150 m to h = 1200 m. This fit, along with Eq. (78), implies that u* was about 0.6 m/sec, so 1200 m is u* times 2000 seconds. This is not to imply that the surface layer relationships usually apply this high; however, Eqs. (78) and (79) do appear to be valid approximations at typical plume heights in "neutral" conditions.

To calculate the terminal rise, apply Eq. (78) at the breakup height by substituting it into Eqs. (76) and (77) with $h = h_e = h_s + \Delta h$. For a buoyant plume, the predicted rise is

$$\Delta h = \left(\frac{2}{3\beta^2}\,\frac{F}{Uu^{*2}}\right)^{3/5} (\eta k\, h_e)^{2/5} =$$

$$= 1.2\,(F/Uu^{*2})^{3/5}\,(h_s + \Delta h)^{2/5}$$

$$= 1.3\,(F/Uu^{*2})\,(1 + h_s/\Delta h)^{2/3}\ , \qquad (80)$$

where the vaues $\beta = 0.6$, $\eta = 1.5$, and k = 0.4 have been assumed. For $\Delta h \gg h_s$, this reduces to $\Delta h = 1.3\ F/(Uu^{*2})$; for a typical ratio of U to u*, say U/u* = 15, this gives $\Delta h \simeq 300\ F/U^3 = 300$ L. The prediction that plume rise is proportional to $F/U^3$ in neutral conditions has been made many times in the literature. However, in spite of individual reports of plume "breakup" at some value of $\Delta h/L$, available observations show no departure from the "2/3 law" when they are plotted together, as in Figure 9. This may be due to the limitations of the data, due to the $(1 + h_s/\Delta h)$ factor, or due to overestimation of the effect of ambient turbulence by the models. Briggs (1965) proposed the largest value of the coefficient, with $\Delta h = 400$ L. This height is reached or exceeded by plumes from over half the sources shown in Figure 9.

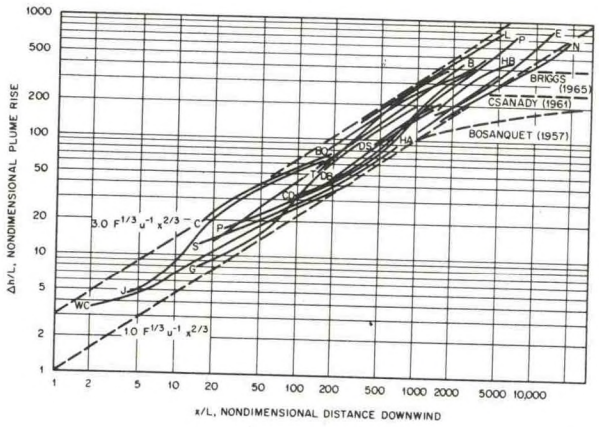


Figure 9. Plots of $\Delta h/L$ vs. x/L for 16 different sources in neutral conditions. Dashed lines are theoretical predictions.

For a jet, the predicted rise is

$$\Delta h = \left(\frac{1}{\beta^2}\,\frac{F_m}{Uu^*}\right)^{3/7} (\eta k\, h_e)^{1/7}$$

$$= \beta^{-1}(F_m/Uu^*)^{1/2}\,(\eta k)^{1/6}\,(1 + h_s/\Delta h)^{1/6}$$

$$\simeq 0.9\ \beta^{-1}(U/u^*)^{1/2}\,F_m^{1/2}\,/\,U\ . \qquad (81)$$

For simplicity, we neglect the term $(1 + h_s/\Delta h)^{1/6}$, which is small whenever the rise is significant. Also, there is no data available for jet rise limited by ambient turbulence, so it seems premature to seek a refined prediction formula. For $\rho_o = \rho_a$, $F_m^{1/2} = w_o D/2$. For typical values $\beta = 0.6$ and $u/u^* = 15$, Eq. (81) predicts $\Delta h \simeq 3$ RD, which is similar to past estimates of final jet rise (Briggs, 1969).

## 5.2 Effect of Vertical Meander

It was mentioned already that large scale eddies can play a role in determining the ESH if they cause the maximum ground concentration (MGC) to occur at distances closer in than where the plume rise terminates (plume rise can continue in the mean, in spite of large up and down fluctuations in height caused by large scale eddies). This effect turns out to be very important in convective conditions.

In neutral conditions, the plume rise probably terminates before ground contact occurs. I base this statement on the presupposition, valid only for the surface layer, that the time-average plume envelope descends at a rate proportional to u*. Above the surface layer, the diffusion rate is slower, so this estimate of the meander effect on rise will be conservative. On the basis of Smith's (1972) elaborated scheme for predicting $\sigma_z$, I estimate the effective downward diffusion rate for the neutral stability category to be 0.9u* (this requires the assumptions that material diffuses downward from height $h_e$ as fast as it diffuses upward to height $h_e$, that the effective plume boundary is at $(h_e - 2^{1/2} \sigma_z)$ since the MGC occurs at $\sigma_z = h_e / 2^{1/2}$, and that x = Ut with U evaluated from the log profile at $h = \sqrt{2}\ \sigma_z$). Consistent estimates for this diffusion rate were found for both $z_o$ = 1 m and $z_o$ = 0.1 m for $h_e$ (= $\sqrt{2}\ \sigma_z$) less than 100 m. For $h_e$ = 300 m, the effective downward diffusion rate would be about 40% less than 0.9 u*.

Using 0.9 u* for the descent rate, it turns out that for a high-rise ($\Delta h >> h_s$) buoyant plume at the rise termination distance the descent is $(2/3)\ (\eta k)^{1/3}\ 0.9 \simeq 0.5$ times the rise at that point. Since the visible plume bottom is also about 0.5 times the rise below the plume axis, this means that the bottom of the plume may just touch ground at the point. In other words, rise termination and the MGC may occur at about the same distance. For all the other cases (jet rise and $\Delta h$ not >> $h_s$), the descent turns out to be a smaller fraction of the rise at the termination distance, so plume rise termination occurs first.

## 5.3 Critical Wind Speed and the MGC

Equation (60) is a useful approximation for the maximum ground concentration (MGC), although it is recognized that the ratio of plume standard deviations $\sigma_z/\sigma_y$ usually does change with distance and therefore Eq. (60) can only be an approximation. The ratio $\sigma_z/\sigma_y$ is not very well established at typical plume heights, however, much less its' variation with x, which is slow, so it seems reasonable at the present to assume it constant for the purpose of estimating MGC.

This equation says that the MGC is inversely proportional to $U\ h_e^2 = U(h_s + \Delta h)^2$, which can be thought of as the effective volume flux of air diluting the plume by the time it reaches the ground. Since $\Delta h$ is predicted to be very large at small values of U by most plume rise formulas, there is usually some wind speed for which the predicted $U\ h_e^2$ is minimum. Consequently, the MGC reaches a maximum at this value of U, which is known as the critical wind speed, $U_c$. It is easily found by differentiating $U(h_s + \Delta h)^2$ and setting this equal to zero: $(h_s + \Delta h)\ dU + 2\ U\ d\ \Delta h = 0$ at the critical wind speed.

For a jet, Eq. (81) gives the minimum value of $u\ h_e^2$ when $\Delta h = h_s$, which means that $U_c \simeq w_o\ (3\ D/h_s)$. For most sources this is a very low wind speed, and "neutral" conditions do not apply.

For a buoyant plume, Eq. (80) gives the minimum value of $u\ h_e^2$ when $\Delta h = 1/3\ h_s$. With the values used previously for the constants, there results

$$U_c = 2.15\ (U/u^*)^{2/3}\ (F/h_s)^{1/3}$$

$$U_c\ h_e^2 = 3.8\ (U/u^*)^{2/3}\ F^{1/3}\ h_s^{5/3} \quad . \qquad (82)$$

Similar equations for $U_c$ and the minimum $U_c\ h_e^2$ are given by many other formulations, among them being $\Delta h = F/Uu^{*2}$ and the "2/3 law" "terminated at either $x \propto (U/u^*)\ h_e$ or $x \propto (U/u^*)\ h_s$. These formulations predict a minimum at $\Delta h/h_s$ = (1/5), (3/5), and 1, respectively, so they must give different coefficients for at least one of the equations in (82). A simple approximation to Eq. (80) that results in $U_c$ at $\Delta h/h_s = 1/3$ and the same coefficients as in Eq. (82) is

$$\Delta h = 1.54\ (F/U\ u^{*2})^{2/3} h_s^{1/3} \quad . \qquad (83)$$

This turns out to be an excellent approximation to the ESH given by Eq. (80) up to the point that $\Delta h = 2\ h_s$, or $F/U\ u^{*2} = 1.5\ h_s$, where it is 10% on the conservative side. If $h_s$ exceeds $4\ F^{1/2}$ in mks units, we find that Eq. (83) is practically always a good approximation to Eq. (80) if the wind speed is large enough for mechanical turbulence to dominate at $h = h_e$. This criterion is met by all sources except for ground sources and short-stacked, high heat rejection sources like gas turbines.

As Figure 9 showed, it is very difficult to validate any formula for turbulence-limited rise using present plume rise observations, since the observed plumes show little or no tendency to level as far as they have been detected except in stable conditions. Consequently, comparisons of theoretical predictions with the observations, such as those of Briggs (1969) and Moore (1974), have shown only small differences in the degree of best fit among several of the models (the models fit the data far better than any of the empirical formulas, however). Deviations of the average trajectories from the first stage rise law are small, and there is much scatter in the data, some of it due to terrain downwash, lakeshore circulation, and other extraneous effects not dealt with directly in the models.

There is another way to test the validity of plume rise formulas, however, and that is by comparing the predicted vs. observed ground concentrations. This requires one to assume a diffusion model, though, in addition to a plume rise model. A model that is widely accepted and that requires no specific knowledge of the magnitude of the diffusion coefficients is Eq. (60) for maximum ground concentration. The MGC requires a good network of samplers to detect, so sufficient data is hard to find. Also, $\sigma_z/\sigma_y$ is not known very precisely; in neutral conditions, it probably ranges from 0.5 to 1.0, i.e., the plume diffuses slightly more laterally than it does vertically.

Once some value for $\sigma_z/\sigma_y$ is assumed, the attraction of using observed values of the MGC to validate plume rise formulas is that the MGC is the usual goal of a plume rise calculation anyway, so direct observations of rise are not essential.

Table 7 compares predictions of the minimum value of $(U\ h_e^2)$ given by all formulas of the type $U_c \propto (F/h_s)^{1/3}$ with observed maximum values of the MGC. The latter have been interpreted assuming Eq. (60), and so the value chosen for $\sigma_z/\sigma_y$ will affect the value of $(U\ h_e^2)$ that fits the observed concentrations. A value of U/u* had to be assumed to apply Eqs. (80) and (83); U/u* = 15 was chosen, which assumes a roughness length of about 0.3 m. The TVA observations of $SO_2$, made at three different plants, were reported by Briggs (1965). The maximum 30 minute average concentration observed over the sampling system during high winds was used. The Tilbury and Northfleet values of MGC represent the average MGC observed whenever the plume was over the network and the wind was in the 18 m/sec category (Moore, 1973, 1974b). However, this $SO_2$ network was much more dense than the TVA network, so was more likely to pick up the true MGC. There also was a problem of interpreting the TVA values since all three plants had multiple stacks (2, 4, and 8 stacks). An empirical function for the ground concentration versus the number of stacks in operation (Thomas et al., 1963) was assumed. More suitable data is now available, but not in a form that could readily be used in this comparison.

Table 7. Observed and Predicted Values of Maximum MGC in Windy, Neutral Conditions

| Plume rise equation | $U_c \div (F/h_s)^{1/3}$ | $(U_c\ h_e^2) \div F^{1/3}\ h_s^{5/3}$ |
|---|---|---|
| $\Delta h = 400\ F/U^3$ | 13 | 18 |
| 2/3 law, cutoff at $x = 10\ h_s$ | 7 | 30 |
| 2/3 law, cutoff at $x = 4.5\ h_e$ | 10 | 26 |
| Eq. (80) or Eq. (83) | 13 | 23 |
| Observations | $U \div (F/h_s)^{1/3}$ | |
| TVA (three plants) | 6-8 | $39\ \sigma_z/\sigma_y$ |
| Tilbury | 12 | $34\ \sigma_z/\sigma_y$ |
| Northfleet | 11 | $27\ \sigma_z/\sigma_y$ |

The observed nondimensionalized values of $(U\ h_e^2)$ are in reasonable agreement. The TVA value might well be higher because the wind speeds were relatively low, 8 to 12 m/sec, and the true critical wind speed may not have been obtained. Indeed, at Northfleet the MGC was still increasing with each higher wind speed category (18 m/sec was the highest category), and at Tilbury the MGC showed some indication of reaching its maximum, although not definitely. At any rate, these observations indicate that the critical wind speed is in the neighborhood of 11 to 12 $(F/h_s)^{1/3}$ or slightly higher. The Northfleet concentrations may be somewhat higher than the others because of a terrain situation that has been observed to adversely affect the plume rise at this plant (Hamilton, 1967). The Tilbury values are probably the most reliable of the three shown in Table 7; with an assumed $\sigma_z/\sigma_y \simeq 0.7$, the minimum $(U\ h_e^2)$ for neutral conditions should be about $24\ F^{1/3}\ h_s^{5/3}$.

Thus, the first formula, even though it is the most optimistic of the $\Delta h \propto F/U^3$ formulas in the literature, probably overestimates the MGC somewhat. The "2/3 law" terminated at $x = 10\ h_s$, as suggested by Briggs (1969) for certain source types, may be slightly too optimistic. At any rate, it predicts too low a value for the critical wind speed. The "2/3 law" cutoff at $x = 0.3\ (U/u^*)\ h_e \simeq 4.5\ h_e$ (Briggs, 1975) looks more promising, as also do Eqs. (80) and (83).

Direct comparison of predicted and observed maximum ground concentrations appears to be a useful tool for checking the validity of plume rise formulas at large distances downwind, where direct observation of plumes becomes tenuous. However, our conclusions somewhat depend on our estimate of $\sigma_z/\sigma_y$. Irregardless of what the appropriate value is, the measurements in Table 7 suggest that the MGC at the critical wind speed for a buoyant plume is

$$(\chi_{max})_c \simeq 0.007\ Q/(F^{1/3}\ h_s^{5/3}) \quad . \tag{84}$$

### 5.4 Neutral-Stable Transition

When it is uncertain just which meteorological situation applies at a particular time, the "safe" thing to do is to compute the plume rise for the various possible situations and then use the lowest predicted rise. When we do this for the transition from neutral to stable plume rise, we find the transition depends most strongly on the wind speed, since $\Delta h \propto U^{-9/5}$ to $U^{-3}$ for neutral conditions and $\Delta h \propto U^{-1/3}$ for stable conditions. Equating Eq. (59) with $C_2 = 2.6$ with Eq. (83), the transition is at

$$u^* = 0.73 \, (F \, h_s \, s \, u^*/U)^{1/5} \quad . \qquad (85)$$

When s is not known, for the stable surface layer the flux-profile relationships given by Businger et al. (1971) imply that $s \simeq - 2.1 \, H/(u^* h)$ below $z = 0.1 \, L"$, where "neutral" turbulence relationships can be assumed. Substituting this with $h = h_s$ in Eq. (85) gives $u^* \simeq 0.9 \, (-F \, H \, u^*/U)^{1/6}$ for transition. Following the same procedure, but with $h = h_e \simeq \Delta h$, the high rise case yields the same criterion except with 0.8 instead of 0.9. We expect for H to vary between -0.0001 $m^2/sec^3$ on a very overcast night to -0.001 on a very clear night. Thus, the surface wind speed at transition ranges roughly from 2 to 6 m/sec. Above this speed, the "neutral" plume rise formulas are preferred.

## 6. RISE LIMITED BY CONVECTIVE TURBULENCE

Convective turbulence has long been recognized as having a very great effect on the diffusion of plumes, but only recently have attempts been made to account for its effect on plume rise (Csanady, 1973; Weil and Hoult, 1973; Weil, 1974). Yet it is obvious from the Monin-Obukov similarity theory (Lumley and Panofsky, 1964), now widely accepted, that convective instability is the dominant producer of turbulence above the height $h \simeq u^{*3}/(kH) = -L"$, where H is the upward sensible heat flux near the ground times $(g/c_p \rho T)$. Perhaps the neglect of this fact in plume rise theories was due to the lack of much experimental information above the surface layer. A considerable collection of information is now available, or is becoming available, for assessing convective turbulence at heights typical of plumes. To summarize:

1. In the daytime, convective turbulence due to heating of the air adjacent to the ground strongly mixes the lower atmosphere. This mixing ends rather abruptly at a height known as the mixing layer height, $z_m$.

2. The air is stable above $z_m$, but as more heat is pumped into the mixing layer, its potential temperature rises and it overturns the lowest part of the stable layer. Thus, $z_m$ starts near the ground near sunrise and continues to build up through the day as long as H is positive.

3. The potential temperature within the mixing layer is approximately constant, due to the vigorous overturning of the air. Actually, the potential temperature gradient is negative (unstable) in the lowest tenth or so, then is very slightly positive above this, with $\overline{s} \propto (H/z_m^2)^{2/3}$.

4. The mixing layer consists of upward thermals carrying heated air from the ground and of compensating downdrafts.

5. The upward and downward velocities scale to $w^* = (H \, z_m)^{1/3}$.

6. The geometry of the updrafts and downdrafts scales to $z_m$. It is also probably influenced by $|z_m/L"|$. (A numerical model by Deardorff (1972) shows convection organized into longitudinal rolls at $|z_m/L"| = 1.5$, suggestive of "cloud streets" sometimes observed in the atmosphere. At $|z_m/L| = 4.5$ there is only slight horizontal elongation of the eddies, and at $|z_m/L"| = 45$ the cells are completely isotropic in the horizontal).

7. The sensible heat flux drops off approximately linearly with height, which is consistent with uniform heating, and becomes slightly negative at the top of the mixing layer due to forced mixing downwards of some of the stable (higher $\theta_a$) air by entrainment.

8. The average eddy dissipation rate is equal to the convective production of turbulent energy which is proportional to the average sensible heat flux. Thus, $\overline{\varepsilon} \simeq 0.4 \, H$, somewhat less than half of the rate of turbulent production at the surface.

9. There is very little change in $\overline{\varepsilon}$ with height. Evidently, the vigorous vertical transport distributes many quantities rather evenly in the vertical.

10. Turbulence is much greater inside the thermals than in the subsiding downdrafts. The thermals are similar to buoyant plumes, with an unstable temperature gradient inside and shear-generated turbulence. The subsiding air is stably stratified, which tends to diminish turbulence.

11. Airplane measurements indicate that $\varepsilon^{1/3}$ is roughly twice as large inside thermals as outside them. Thus, thermals, which comprise a little less than half the total area, have $\varepsilon$ values of the order of H, while in the downdrafts $\varepsilon \simeq 0.1 \, H$.

12. There is very little wind shear above a height of about 5 $|L"|$ in the mixing layer. The ratio of mean windspeed to friction velocity is $U/u^* \simeq (0.35)^{-1} \ln |L"/z_o|$ (Wyngaard et al., 1974).

13. Vertical velocities are nearly constant through most of the mixing layer, except in the lowest and upper tenth.

14. Updraft velocities and downdraft velocities taken separately have a Gaussian distribution, but together display a sharp kink (on probability coordinates) near zero.

This implies that updrafts are different from downdrafts, and so are their statistics, so data on them should not be all thrown into the same basket for averaging. Future diffusion experiments in convective conditions should be conducted with this in mind.

These are only some highlights of current understanding of the convective mixing layer; many are of direct relevance to plume rise. For more detailed discussions on and measurements in the convective boundary layer, see Deardorff (1972), Tennekes (1970, 1972), Wyngaard et al. (1974), Lenschow (1970, 1974).

### 6.1 Effect of Plume Breakup

Since $\varepsilon \propto H$ and is nearly constant with height in the convective mixing layer, determining the termination height of plume rise due to breakup by plume-scale eddies is just a matter of substituting $\varepsilon$ into Eqs. (76) and (77).

The only question is, should we use the mean $\varepsilon$, $\varepsilon$ for updrafts, or $\varepsilon$ for downdrafts? Plume material that gets caught in an updraft generally gets carried all the way up to $z_m$ and then subsides with the surrounding downdrafts. By the time it reaches the ground, the effective volume flux diluting the material is of the order $(U\ z_m^2)$, so the ESH of this material is some fraction of the mixing layer height. In contrast to this, plume material that gets caught in a downdraft has much less time to diffuse before it contacts the ground. It seems likely that downdraft material is responsible for producing the MGC, and so we should be calculating (relative) plume rise for plumes embedded in the subsiding air. On this basis, $\varepsilon \simeq 0.1\ H$ is most appropriate. With $\beta = 0.6$ and $\eta = 1.5$, termination rise is

$$\Delta h = 4.3\ (F/U)^{3/5}\ H^{-2/5} \qquad \text{(buoyant plume)} \qquad (86)$$

$$\Delta h = 2.3\ (F_m/U)^{3/7}\ H^{-1/7} \qquad \text{(jet)} \qquad (87)$$

Weil (1974) has suggested an equation similar to Eq. (86).

Rough ranges of the heat flux parameter H have already been given, but perhaps somewhat less rough estimates would be appreciated. H depends mostly on the incoming solar radiation and the surface conditions, and the solar radiation R depends mostly on the solar elevation angle $\theta_{el}$ and the fractional cloudiness, C. A relation that gives a good fit to values of R proposed by Smith (1972) is

$$R = (2/3)\ \sin\theta_{el}\ (1 - 0.8\ C)\ S\ , \qquad (88)$$

where S is the solar constant. In a dry, dustless atmosphere R may be slightly larger, but there are greater uncertainties at the ground. Some of the radiation is absorbed by the ground and by plants, some is reflected and radiated back, and some is carried as latent heat due to evaporation. Values of H/R reported by Weil (1974) and by Hoult and Weil (1973) range from 0.25 over a crop canopy with high evaporation to 0.55 with no evaporation taken into account. There are possibly better estimates available, but for the present purpose one may assume $H/R = 0.4 \pm 0.15$, depending on the degree of vegetation and dryness of the air, etc. The solar constant times $(g/c_p\rho T)$ is 0.039 $m^2/sec^3$ times $p_s/p_a$.

### 6.2 Effect of Vertical Meander

In convective conditions, the effect of vertical meander can be striking. It is commonly observed that plumes from small sources "loop", frequently being brought right to the ground very close in. Even plumes from large sources have been observed to descend to the ground relatively close in. In a discussion in Atmospheric Environment in which a number of participants reported problems with thermal looping at power plants, Halliday (1967) reports that at two sites in South Africa plumes have been observed to rise over 200 m and then descend to the ground at no more than 450 m from the stack. This situation sometimes lasts for 15 minutes. In the same discussion, Moore (1967) states that thermal looping is seldom observed (in Great Britain) at plants with stacks higher than 150 m. Besides source height and buoyancy being factors, it should be evident that geography plays a strong role here. Convective velocities are proportional to $(H\ z_m)^{1/3}$ and, while maximum values of H do not vary so much during summer months below arctic latitudes, $z_m$ varies from about 1 km near coasts to an average of 4 km over the Southwest plateau of the U.S.A. Climatological information on mixing heights is readily available for the U.S.A. (Holzworth , 1972, 1974a, 1974b).

Weil and Hoult (1973) suggested a simple way to account for the effect of vertical downdrafts on plume rise. They assumed that the first stage rise is, in effect, terminated when the calculated plume vertical velocity is of the order of the convective downdraft velocities, which are proportional to $w^* = (H\ z_m)^{1/3}$. The result for a buoyant plume is $\Delta h \propto F/Uw^{*2}$, which is just like the high rise formula for neutral conditions with $u^*$ replaced by $w^*$. Interestingly, the plume rise termination distance is proportional to $F/w^{*3} \propto F/(H\ z_m)$; $\pi F/H$ is just the area of ground which has a heat (buoyancy) flux equal to that of the stack, which gives us another natural geometric scale relevant to this problem.

I would like to extend the above idea somewhat by assuming that the plume maintains its first stage rise relative to the air in a descending downdraft with a constant downward velocity $w_d \propto w^*$. The rise is terminated when the plume "touches down" at $t = t_d$. Following the photographic evidence for buoyant plumes, we assume that the bottom of the plume rises only half as much as the centerline. The "touchdown equation" is then

$$h_s + 0.5\ \Delta h - w_d t_d = 0\ . \qquad (89)$$

The first stage rise is used in this equation, and the resultant $t_d$ is substituted back into the first stage rise to get the effective stack height. The assumption here is that the average touchdown distance $Ut_d$ also approximates the distance of maximum ground concentration,

therefore is an appropriate place to terminate the rise. It does not matter that the plume happens to be on the ground at the time of touchdown; the concept of ESH is based on the average height of the plume at the chosen distance. The higher the average plume height, the more opportunity the plume will have to swing this way and that before it does touch down, therefore the more dilute the time average concentration. Equation (89) just calculates the time it takes an actively rising plume to be diffused to the ground by large scale vertical meanders; indeed, $w_d$ itself may be estimated from conventional diffusion coefficients, which will be done shortly.

Incidentally, this model can also be used to predict "peak" concentrations in looping conditions, by assuming the material within the plume to be evenly distributed over a radius $\simeq 0.5\ \Delta h$. Then the peak concentration is

$$\chi_p \simeq \frac{Q}{U\ (0.5\ \Delta h)^2} \qquad (90)$$

with $\Delta h$ evaluated at the touchdown distance.

The plume rise might terminate due to "breakup" before touchdown occurs. We can take care of this possibility by using the lowest of the predicted rises.

For a buoyant plume with initial rise given by the "2/3 law", the touchdown model gives

$$\Delta h = \left( \frac{3}{2\beta^2} \frac{F}{U} \right)^{1/3} \left( \frac{h_s + 0.5\ \Delta h}{w_d} \right)^{2/3} \qquad (91)$$

$$= 1.6\ (F/U\ w_d^2)^{1/3}\ h_s^{2/3}\ (1 + 0.5\ \Delta h/h_s)^{2/3}$$

$$= 1.0\ (F/U\ w_d^2)\ (1 + 2\ h_s/\Delta h)^2$$

For $\Delta h \gg h_s$, this is similar to Hoult and Weil's model, but stack height is important even when $\Delta h = 5h_s$ in the present model.

For a jet with initial rise given by the "1/3 law", after substituting $w_d = 0.4\ w^*$, which will be the tentative estimate, we find that the touchdown model gives a rise that is higher than that given by the breakup model (Eq. 87) by a factor larger than $(1600\ h_s/z_m)^{1/7}$, which makes this model irrelevant for a jet. "Breakup" occurs before "touchdown", and Eq. (87) should be used for jet rise in convective conditions.

To apply this model we must estimate $w_d$. One way is to interpret $w_d$ as $(2)^{1/2}\ d\sigma_z/dt$, using $\sigma_z$ for unstable conditions, for in the Gaussian plume model the MGC occurs when $(2)^{1/2}\ \sigma_z = h_e$. Unlike earlier curves of $\sigma_z$ vs. x for the unstable categories, which had a strong upsweep with x (ESSA , 1968), more recent determinations have $\sigma_z$ approximately linear in x in the most unstable categories (ASME, 1973; Smith, 1972). This strongly suggests that, except very close to the ground, $\sigma_z \propto w^*\ x/U$ in these conditions, which is really implied by the downdraft model anyway. Furthermore, the ratio of $\sigma_z/x$, which corresponds closely to the "stability category," is related to the parameter characterizing the whole mixing layer, $|z_m/L''|$. This relationship can be most simply stated by using the following proposed approximation to the model and data for U/u* in the convective mixing layer given by Wyngaard et al. (1974):

$$U/u^* \simeq 6\ |L''/z_o|^{1/6} . \qquad (92)$$

With this, we predict that $\sigma_z/x \propto |z_m/L''|^{1/2}\ (z_o/z_m)^{1/6}$ in very unstable conditions. We note that this is qualitatively in agreement with Golder's (1972) empirical correlation of Pasquill stability category with L" and $z_o$, although his scheme does not take variations in $z_m$ into account.

It was assumed that $w_d = U\ (2)^{1/2}\ \sigma_z/x$, and values were derived from Smith's (1972) method of determining $\sigma_z$. A strong convection case was assumed, with $H = 0.008\ m^2/sec^3$. Smith's method gives stability category as a function of H and U (at 10 m). We can estimate L" for unstable conditions on the basis of Eq. (92), finding that

$$-L'' \simeq 0.056\ z_o^{1/3}\ H^{-2/3}\ U^2. \qquad (93)$$

Using this formula for L", rather consistent estimates for $w_d$ are found at x = 100 m and x = 1000 m when $\sigma_z > |L''|$, which it must if convective diffusion dominates. Specifically, $w_d = 0.53$ m/sec, with an average deviation of less than 10%. One problem remains, and that is that the mean mixing depth is unknown. I assumed $z_m \simeq 1$ km on the basis of annual averages near coasts in the U.S.A. (Smith's data base was developed in the U.K.). This gives $w_d \simeq 0.3w^*$.

A different kind of estimate of $w_d$ can be made from Lenschow's (1970) airplane measurements of vertical velocities. This is only one day's measurements, but $z_m$ was known to be 1.1 km from soundings and H was measured at h = 100 m by the velocity-temperature correlation method. The day was quite convective, with $|z_m/L| \simeq 100$. The variance of vertical velocity was about 0.5 w*. The downdraft velocities were somewhat less than the updraft velocities, but they operated more than half the time, which is consistent with the expectation that thermals take up less than half the area.

On the basis of these two estimates, a tentative recommendation for the mean effective downdraft velocity is $w_d/w^* = 0.4 \pm 0.1$. Better estimates are needed.

### 6.3 Critical Wind Speed and the MGC

We may first note that for jets in convective conditions, there is no critical wind speed. Since $\Delta h \propto U^{-3/7}$, $U(h_s + \Delta h)^2$ gets smaller and smaller as $U \to 0$. There is a limiting factor though, and that is that the atmosphere never holds still in the presence of convection. There is some minimum effective U that is due to convective motion, so it is proportional to w*. From extreme values of $\sigma_z/x$, I would guess that $U \geq 2\ w_d$, i.e., the touchdown distance is at least twice the ESH.

For the buoyant plume in convective conditions, with the convective downdraft model (Eq. 91) we find that at the critical wind speed $\Delta h/h_s = 4.4$, as compared with 0.33 for neutral conditions. This results in

$$U_c = 0.50\ F/h_s\ w_d^2$$
$$U_c\ h_e^2 = 14.4\ Fh_s/w_d^2 \quad . \tag{94}$$

At this point it is noted that Eq. (91) can be approximated over a wide range of U by

$$h = 2.9\ (F/U\ w_d^2)^{3/5}\ h_s^{2/5}, \tag{95}$$

which gives the same value for the minimum $Uh_e^2$ and $U_c$ just 20% lower. This underestimates the value of $h_e$ given by Eq. (91) by no more than 15% in the range $U = 0.2\ U_c$ to $U = \infty$. Eq. (95) is useful as a simplification and to facilitate comparison with Eq. (86) for the terminal rise due to breakup of the plume by convective turbulence. With $w_d = 0.4\ w^*$, we find that Eq. (95) is more conservative, and therefore is more appropriate, whenever $h_s < 0.17 z_m$. This is the case most of the time.

For high stacks with low mixing layers ($h_s/z_m > 0.17$), one should use Eq. (86) for buoyant rise in convective conditions. In this case, as with Eq. (95), $\Delta h = 5\ h_s$ at the critical wind speed; since $h_s > 0.17\ z_m$, the plume then bumps the top of the mixing layer before the critical wind speed is reached. This invalidates the plume rise formula, i.e., we cannot allow $(\Delta h + h_s)$ to exceed $z_m$ without accounting for the stable stratification above $z_m$. If a plume is not capable of penetrating the stable air above the mixing layer, at low wind speeds its effective stack height is limited. At the maximum, $h_e \simeq 0.7\ z_m$ if the top of the plume is at $z_m$. This is called "capping," and has to be allowed for in the case of high buoyancy sources at low wind speeds, should both Eqs. (86) and (91) predict $h_e > 0.7\ z_m$.

Eq. (94) predicts a smaller $U_c h_e^2$, and therefore a larger MGC, than in the neutral case if $w_d > 2.0\ (u^*/U)^{1/3}\ (F/h_s)^{1/3} \simeq 0.8\ (F/h_s)^{1/3}$, especially since $\sigma_z/\sigma_y$ is somewhat larger in the convective case. The range of $w_d$ on sunny, summer afternoons is about 0.5 to 1.5 m/sec, depending on locality. For power plants, $(F/h_s)^{1/3}$ ranges from 1.5 to 2.0 m/sec, so the convective case normally gives lower concentrations than the high wind, neutral case. The convective case should be of no concern for gas turbines with low stacks and ground sources - high winds are most likely to case trouble for them. For small heat emission industrial sources, the low speed convective case may give the highest concentration (unless downwash occurs at high wind speeds). For most of the sources Bringfelt (1968) reported, $(F/h_s)^{1/3}$ ranged from 0.5 to 1.2 m/sec.

There are not many data suitable for testing these formulas. Plumes are notoriously elusive in convective conditions, and it is difficult to trace them very far downwind. We can look for suitable measurements of the MGC, but usually $z_m$ and H are not known. Weil and Hoult (1973) used observations of $SO_2$ from the Keystone plant and found good correlation with the MGC predicted by a more conservative formula than Eq. (91) (since it lacked the $h_s/\Delta h$ factor, the ratio of the two formulas vary and this comparison can not be used to directly test the approach here). However, the best correlation was with $\sigma_z/\sigma_y \simeq 0.6$, a rather low value for convective conditions, and the concentrations measured were more "peak" than average concentrations. A less conservative plume rise formula would be in order for predicting average concentrations.

The $SO_2$ concentrations at the Northfleet and Tilbury plants in the U.K. (Moore 1973, 1974b) are average values obtained by dense networks of ground samplers. They are averaged by stability and wind speed categories. By assuming $\sigma_z/\sigma_y = 1$ for unstable conditions and using Eq. (60) to calculate the ESH from the observed values of $\chi/Q$ vs. U, in the unstable category we do find an approximate $U^{-3/5}$ law for $(h_e - h_s)$ at low wind speeds and a greater dependence on U at high wind speeds. Actually, at the lowest speeds there is even less dependence of $(h_e - h_s)$ on U then the minus 3/5 power. However, a "capping" layer may have had some influence at the lowest wind speeds, especially at Northfleet, where $h_e \simeq 800$ m. The values of $w_d$ required for a best fit to Eq. (91) are 0.7 m/sec at Tilbury and 1.0 m/sec at Northfleet. For moderate instability ($H = 0.005\ m^2/sec^3$) and $z_m = 1$ km, we expect that $w_d \simeq 0.4\ w^* = 0.7$ m/sec. The model does seem to give the right magnitudes, at least for the Tilbury measurements, but obviously more complete measurements are required to properly test it.

## 6.4 Neutral - Convective Transition

Transition from the neutral to the convective case for $\varepsilon$-limited rise, which applies for jets and for buoyant plumes also if $h_s > z_m/6$, depends only on whether the mechanical or the convective values of $\varepsilon$ dominates at height $h_e$. Thus, transition is at $u^{*2}/(k\ h_e) \simeq 0.1\ H$, or $h_e = 10\ L''$. In the buoyant case, for the plume rise calculation to be relevant the plume would have to be in the neighborhood of $0.5\ z_m$, so the convective case applies when $|z_m/L''| > 20$ or so.

For buoyant plumes with $h_s < z_m/6$, it will be helpful to use a different approximation to Eq. (91), namely $\Delta h \simeq 2.8\ (F/U\ w_d^2)^{2/3} h_s^{1/3}$. The purpose is to make a simple comparison with the neutral rise approximation, Eq. (83). We find then that the convective rise formula gives the lowest rise when $w_d > 1.6\ u^*$, which is equivalent to $|z_m/L''| > 25$. For the high rise case ($\Delta h \gg h_s$), we find by equating Eq. (91) and Eq. (80) that convective turbulence cuts off the $\Delta h \propto U^{-3}$ type of rise at $w_d > 0.9\ u^*$, which is equivalent to $|z_m/L''| > 5$. This is only a slightly unstable mixing layer. For the other cases, assuming L'' as given by Eq. (93) and $z_m = 1$ km, we find that transition occurs somewhere in the "C" stability class as determined by the method of Smith (1972), assuming $z_o = 0.1$ to 1m. During "A" and "B" conditions, it appears that convective turbulence limits plume rise, and models that do not account for convective turbulence are inadequate.

## 7. SUMMARY


Methods for predicting plume rise covering a very wide variety of situations have been suggested. All of the predictions are based on a relatively simple, yet versatile, theoretical model.

This model is similar to some past models, but they are extended somewhat and the conservation equations are more carefully derived. One consequence is that for bent-over plumes, conservation of vertical momentum involves an effective momentum flux which includes the acceleration of fluid outside the plume, while the buoyancy decay rate in stable fluid is proportional to only the internal momentum flux. The ratio of these two momentum fluxes is estimated to be 2.25. Another consequence for bent-over plumes is that there is no "drag force" acting on the plume. Adding such a term to the momentum equation leads to results that are inconsistent with observations. To obtain closure, in the self-structured stage of rise the classical assumption that the entrainment velocity is proportional to the shear velocity is employed. The effect of ambient turbulence on plume trajectories is accounted for more simply than in entrainment models, by assuming "breakup" of the plume and rapid termination of the rise when the internal turbulent energy dissipation rate is matched by the ambient value. The basic plume rise model used is summarized in Section 2.7.

Rise near the source is simply and adequately predicted using the momentum conservation equations and $r \propto z$, which follows from the entrainment assumptions. The "1/3 law," $z \propto x^{1/3}$, is predicted for bent-over jets and is supported by wind tunnel experiments. The "2/3 law" is predicted for bent-over, buoyant plumes:

$$z = 1.6\ F^{1/3}\ U^{-1}\ x^{2/3} \quad . \qquad (48)$$

This formula is widely supported by field observations and by some modeling experiments. Perhaps over 90% of field observations of buoyant plumes are approximated by Eq. (48), so it seems a logical standard against which to judge the importance of other effects, such as initial momentum, downwash, terrain and site peculiarities, and limiting of rise due to ambient stability or turbulence.

Rise that is limited due to stable ambient stratification is predicted with the same entrainment assumptions by including the buoyancy conservation equation. Computation of the rise of vertical plumes is simplified greatly by using an "unaltered volume flux" approximation, especially for more complex stability profiles. When the ambient temperature does not strongly depart from a linear change with height, field observations on bent-over, buoyant plumes support

$$\Delta h = 2.6 \left(\frac{F}{Us}\right)^{1/3} \quad . \qquad (59)$$

The degree of penetration of bent-over, buoyant plumes into elevated, thin inversion layers is predicted rather well and rather simply by a "rectangular plume" concept that accounts for the change in plume buoyancy when $\partial\theta_a/\partial z$ is not constant over the whole depth occupied by the plume. This concept also promises to be useful in predicting partial penetration of a plume into an elevated stable layer, but more experimental information is needed. Finally, a simple method for computing the plume rise into ambients with complex density profiles is given.

Rise that is limited due to mechanical ambient turbulence is predicted in a straightforward manner by assuming the well-known relationship for dissipation rate in the neutral surface layer. It is believed that this relationship is valid well above the surface layer in conditions for which mechanical turbulence would be the most limiting factor for plume rise, so the relationship can be applied at plume heights. For buoyant plumes, the predicted rise is

$$\Delta h = 1.2\ (F/Uu^{*2})^{3/5}\ (h_s + \Delta h)^{2/5}$$

$$= 1.3\ (F/Uu^{*2})\ (1 + h_s/\Delta h)^{2/3} \quad . \qquad (80)$$

When mechanical turbulence dominates, for most sources $\Delta h < 2\ h_s$ and Eq. (80) can be approximated more simply with Eq. (83); this is satisfactory if $h_s$ exceeds $4\ F^{1/2}$, in mks units. Available plume rise observations do not provide any definitive value of the "final" rise in neutral conditions, as they do not depart much from the "2/3 law" as far as they have been carried out. Alternatively, the rise can be inferred from observed maximum ground concentrations (MGC) in conjunction with a diffusion model. Eq. (80) does provide good estimates of the "critical wind speed" and the MGC at this speed, compared with the few suitable observations. Taken with the observations, for common values of the roughness parameter ($z_o$ = 0.1 to 1 m) it predicts

$$(\chi_{max})_c \approx 0.007\ Q/(F^{1/3}\ h_s^{5/3}) \quad . \qquad (84)$$

Mechanical turbulence is the limiting factor for plume rise only at relatively high wind speeds.

The structure of the atmospheric boundary layer during convective conditions is in some ways complex, but needs to be considered carefully to determine the plume rise during daytime. Plume "breakup" is easily determined from the model because in the convective mixing layer the dissipation rate is nearly constant with height. However, only the average value for downdrafts should be used for predicting the MGC, since portions of the plume caught in upward thermals are greatly diffused by the time they finally subside to the ground. Plume rise is most limited by "breakup" only for jets, or for buoyant sources if $h_s > z_m/6$. For most buoyant sources, the effective stack height for the MGC is limited by downdraft velocities, which bring the plume to the ground while it is still in the self-structured stage of rise. These velocities scale to $(Hz_m)^{1/3}$, which varies considerably according to the season and the locality. When downdraft velocities exceed

$0.8\ (F/h_s)^{1/3}$, this model predicts higher ground concentrations in low wind, convective conditions than in high wind, neutral conditions.

The model for convective conditions is, to a fair degree, speculative at this time because of the lack of measurements of the appropriate parameters. However, it does predict that convective turbulence is the factor limiting plume rise for most buoyant plumes even if the atmosphere is only moderately unstable. It furthermore implies that, in the very unstable stability categories, vertical diffusion is approximately proportional to $x\ (Hz_m)^{1/3}\ /U$. The numerical model of Deardorff (1972) also predicts this, with a diminished expansion rate as the top of the convective layer is approached. This prediction can be approximated by $\sigma_z/x \propto |z_m/L|^{1/2}\ (z_o/z_m)^{1/6}$, which ought to correlate well with the "stability category."

Acknowledgement

This research was performed under an agreement between the National Oceanic and Atmospheric Administration and the U. S. Energy Research and Development Administration.

REFERENCES

Abraham, G., 1963: Jet diffusion in stagnant ambient fluid. Delft Hydraulics Lab., Publ. No. 29.

Abraham, G., 1971: The flow of round buoyant jets issuing vertically into ambient fluid flowing in a horizontal direction. Delft Hydraulics Lab., Publ. No. 81.

Abramovich, G. N., 1963: The Theory of Turbulent Jets. Cambridge, Mass., The MIT Press.

Anwar, H. O., 1969: Behavior of buoyant jet in calm fluid. Proc. ASCE, 95 (HY4), 1289-1303.

ASME, 1973: Recommended Guide for the Dispersion of Airborne Effluents, ed. M. E. Smith. New York, American Soc. of Mechanical Eng.

Ayoub, G. M., 1973: Test results on buoyant jets injected horizontally in a cross flowing stream. Water, Air, and Soil Pollution, 2, 409-426.

Bacci, P., G. Elisei, and A. Longhetto,1974: Lidar measurement of plume rise and dispersion at Ostiglia power station. Atmos. Environ., 8, 1177-1186.

Ball, F. K., 1958: Some observations of bent plumes. Quart. J. Roy. Meteor. Soc., 84, 61-65.

Barilla, P. A., 1968: Dependence of entrainment coefficients upon oriface conditions in model studies of a smoke plume in a laminar cross wind. S.M. Thesis, Mass. Inst. of Tech.

Batchelor, G. K., 1954: Heat convection and buoyant effects in fluids. Quart. J. Roy. Meteor. Soc., 80, 339-358.

Berlyand, M. Ye., Ye. L. Genikhovich, and R. I. Onikul, 1964: On computing atmospheric pollution by discharge from the stacks of power plants, in Problems of Atmospheric Diffusion and Air Pollution, JPRS-28, 343, 1-27; translated from Tr. Gl. Geofiz. Obser., No. 158.

Berlyand, M. E., 1972: Investigations of atmospheric diffusion providing a meteorological basis for air pollution control. Atmos. Environ., 6, 379-388.

Bodurtha, F. T., Jr., 1961: The behavior of dense stack gases. J. Air Pollut. Contr. Ass., 11, 431-437.

Bosanquet, C. H., 1957: The rise of a hot waste gas plume. J. Inst. Fuel, 30, 322-328.

Bosanquet, C. H., W. F. Carey, and E. M. Halton, 1950: Dust deposition from chimney stacks. Proc. Inst. Mech. Engrs. (London), 162, 355-368.

Bosanquet, C. H., and J. L. Pearson, 1936: The spread of smoke and gases from chimneys. Trans. Faraday Soc., 32, 1249-1264.

Briggs, G. A., 1964: A smoke plume rise theory. Preliminary. Atmospheric Turbulence and Diffusion Laboratory, Oak Ridge, Tn.

Briggs, G. A., 1965: A plume rise model compared with observations. J. Air Pollut. Contr. Ass., 15, 433-438.

Briggs, G. A., 1968: CONCAWE meeting: Discussion of the comparative consequences of different plume rise formulas. Atmos. Environ., 2, 228-232.

Briggs, G. A., 1969: Plume Rise. USAEC Critical Review Series, TID-25075, Clearinghouse for Federal Scientific and Technical Information.

Briggs, G. A., 1970a: Some recent analyses of plume rise observations. International Air Poll. Confer., Wash., D. C., Dec. 1970.

Briggs, G. A., 1970b: A simple model for bent-over plume rise. Ph.D. thesis, Pennsylvania State University.

Briggs, G. A., 1972: Discussion of chimney plumes in neutral and stable surroundings. Atmos. Environ., 6, 507-510.

Briggs, G. A., 1974: Plume rise from multiple sources. Proceedings of Cooling Tower Environment - 1974, symposium held March 4-6, 1974, at University of Maryland Adult Education Center, ERDA Sym. Series, 161-179.

Briggs, G. A., 1975: Discussion of a comparison of the trajectories of rising buoyant plumes with theoretical empirical models. Atmos. Environ., 9, 455-462.

Bringfelt, B., 1968: Plume rise measurements at industrial chimneys. Atmos. Environ., 2, 575-598.

Bringfelt, B., 1969a: A study of buoyant chimney plumes in neutral and stable atmospheres. Atmos. Environ., 3, 609-623.

Bringfelt, B., 1969b: Author's reply to discussion of plume rise measurements at industrial chimneys (see above). Atmos. Environ., 3, 317-319.

Brummage, K. G., 1968: The calculation of atmospheric dispersion from a stack. Atmos. Environ., 2, 197-224.

Bryant, L. W., 1949: The effects of velocity and temperature of discharge on the shape of smoke plumes from a funnel or chimney in a wind tunnel. National Physical Lab., Great Britain, 1-14.

Bryant, L. W., and C. F. Cowdrey, 1955: The effects of velocity and temperature of discharge on the shape of smoke plumes from a tunnel or chimney: Experiments in a wind tunnel. Proc. Inst. Mech. Engrs. (London), 169, 371-400.

Businger, J. A., J. C. Wyngaard, Y. Izumi, and E. F. Bradley, 1971: Flux-profile relationships in the atmospheric surface layer. J. Atmos. Sci., 28, 181-189.

Callaghan, E. E., and R. S. Ruggeri, 1948: Investigation of the penetration of an air jet directed perpendicularly to an air stream. Report NACA-TN-1615, Nat. Advisory Committee for Aeronautics.

Campbell, J. F., and J. A. Schetz, 1973: Analysis of the injection of a heated turbulent jet into a cross flow. NASA Tech. Report. No. R-413.

Carpenter, S. B., et al., 1967: Report on a full scale study of plume rise at large electric generating stations. Paper 67-82, 60th Annual Meeting of the Air Poll. Control Ass., Cleveland, Ohio, 1967.

Carpenter, S. B., T. L. Montgomery, J. M. Leavitt, W. C. Colbaugh, and F. W. Thomas, 1971: Principal plume dispersion models: TVA power plants. J. Air Pollut. Control Ass., 21, 491-495.

CONCAWE, 1966: The Calculation of Dispersion from a Stack. The Hague, The Netherlands, Stichting CONCAWE.

Crawford, T. V., and A. S. Leonard, 1962: Observations of buoyant plumes in calm stably stratified air. J. Appl. Meteor., 1, 251-256.

Csanady, G. T., 1956: The rise of a hot smoke plume. Aust. J. Appl. Sci., 7, 23-28.

Csanady, G. T., 1961: Some observations on smoke plumes. Int. J. Air Water Pollut., 4, 47-51.

Csanady, G. T., 1965: The buoyant motion within a hot gas plume in a horizontal wind. J. Fluid Mech., 22, 225-239.

Csanady, G. T., 1973: Effect of plume rise on ground level pollution. Atmos. Environ., 7, 1-16.

Davies, R. W., 1959: Large-scale diffusion from an oil fire. Advances in Geophy., 6, 413-415, F. N. Frenkiel and P. A. Sheppard (eds.). New York, Academic Press, Inc.

Deardorff, J. W., 1972: Numerical investigation of neutral and unstable planetary boundary layers. J. Atmos. Sci., 29, 91-115.

ESSA (Environmental Science Services Adm.),1968: Meteorology and Atomic Energy - 1968. USAEC Report TID-24190.

Fan, L., 1967: Turbulent buoyant jets into stratified or flowing ambient fluids. Cal. Inst. of Tech., Report KH-R-15.

Fay, J. A., M. Escudier, and D. P. Hoult, 1969a: A correlation of field observations of plume rise. Fluid Mechanics Lab. Pub. No. 69-4, Mass. Inst. of Tech.

Fay, J. A., M. Escudier, and D. P. Hoult, 1969b: Discussion of plume rise measurements at industrial chimneys. Atmos. Environ., 3, 311-315.

Fischer, R. D., L. J. Flanigan, and A. A. Putnam, 1970: Prediction of the rise of a gaseous plume in a calm atmosphere with any lapse-rate profile. Proc. Second International Clean Air Congress, pp. 1007-1013.

Fox, D. G., 1970: Forced plume in a stratified fluid. J. Geophys. Res., 75, 6818-6835.

Frenkiel, F. N., and I. Katz, 1956: Studies of small-scale turbulent diffusion in the atmosphere. J. Meteor., 13, 388-394.

Frizzola, J. A., I. A. Singer, and M. E. Smith, 1966: Measurements of the rise of buoyant clouds. USAEC Report BNL-10524, Brookhaven Nat. Lab., April 1966.

Gartrell, F. E., F. W. Thomas, and S. B. Carpenter, 1961: An interim report on full scale study of dispersion of stack gases. J. Air Pollut. Contr. Ass., 11, 60-65.

Gartrell, F. E., F. W., Thomas, and S. B. Carpenter, 1964: Full scale dispersion of stack gases: A summary report. Tennessee Valley Authority, Chattanooga, Tn.

Gifford, F. A., 1967: The rise of strongly radioactive plumes. J. Appl. Meteor., 6, 644-649.

Golder, D., 1972: Relations among stability parameters in the surface layer. Boundary Layer Meteor., 3, 47-58.

Gordier, R. L., 1959: Saint Anthony Falls Hydraulics Laboratory, U. of Minnesota Technical Paper 28 (Series B).

Halitsky, J., 1966: A method for estimating concentration in transverse jet plumes. Int. J. Air Water Pollut., 10, 821-843.

Halliday, E. C., 1968: Measurements of the rise of hot plumes. Atmos. Environ.,2, 509-516.

Hamilton, P. M., 1966: The use of lidar in air pollution studies. Int. J. Air Water Pollut., 10, 427-434.

Hamilton, P. M., 1967: Plume height measurements at two power stations. Atmos. Environ., 1, 379-387.

Hanna, S. R., B. A. Hutchison, and F. A. Gifford, 1969: Spread of small smoke plumes. ESSA Tech. Memo. ERLTM-ARL 15.

Herbert, G. A., 1971: Energy profiles of small-scale wind fluctuations. Atmospheric Transport and Diffusion in the Planetary Boundary Layer, ed. I. Van der Hoven, NOAA Tech. Memo. ERL ARL-32, 10-17.

Hewett, T. A., J. A. Fay, and D. P. Hoult, 1971: Laboratory experiments of smokestack plumes in a stable atmosphere. Atmos. Environ., 5, 767-789.

Hill, B. J., 1972: Measurement of local entrainment rate in the initial region of axisymmetric turbulent air jets. J. Fluid Mech., 51(4), 773-779.

Hino, M., 1962: Ascent of smoke in a calm inversion layer of atmosphere: Effects of discharge velocity and temperature of stack gases. Tech. Lab., Cent. Res. Inst. Elec. Power Ind. (Japan), Report TH-6201, May 1962.

Hirst, E. A., 1971: Analysis of round, turbulent, buoyant jets discharged to flowing stratified ambients. Oak Ridge National Lab., ORNL-4685.

Holzworth, G. C., 1972: Mixing heights, wind speeds, and potential for urban air pollution throughout the contiguous United States. Environmental Protection Agency, Office of Air Programs Publ. AP-101, Research Triangle Park, N. C., 118 pp.

Holzworth, G. C., 1974a: Climatological data on atmospheric stability in the United States. Paper presented at AMS Sym. on Atmospheric Diffusion and Air Pollution, Sept. 9-13, 1974, Santa Barbara, Cal.

Holzworth, G. C., 1974b: Summaries of the lower few kilometers of rawinsonde and radiosonde observations in the United States. Paper presented at the Climatology Confer. and Workshop of the AMS, Oct. 8-11, 1974, Asheville, N. C.

Hosler, C. R., 1963: Climatological estimates of diffusion conditions in the U.S. Nucl. Safety, 5(2), 184-192.

Hoult, D. P., J. A. Fay, and L. J. Forney, 1969: A theory of plume rise compared with field observations. J. Air Pollut. Contr. Ass., 19, 585-590.

Hoult, D. P., and J. C. Weil, 1972: Turbulent plume in a laminar cross flow. Atmos. Environ., 6, 513-531.

Humphreys,J. F., 1973: The rise of plumes on the South African highveld. Atmos. Environ., 7, 1071-1077.

Johnson, W. B., and E. E. Uthe, 1971: Lidar study of the Keystone stack plume. Atmos. Environ., 5, 703-724.

Jordinson, R., 1956: Aeronautical Research Council Report and Memorandum 3074/1958.

Kamotani, Y., and I. Greber, 1972: Experiments on a turbulent jet in a cross flow. American Inst. of Aeronautics and Astronautics, AIAA 10th Aerospace Sciences Meeting, Jan. 17-19, 1972, San Diego, Cal.

Keffer, J. F., and W. D. Baines, 1963: The round turbulent jet in a cross-wind. J. Fluid Mech., 15, 481-497.

Lamb, Sir Horace, 1932: Hydrodynamics. New York, Dover Publcations, 1945, 738 pp.

Lenschow, D. H., 1970: Airplane measurements of planetary boundary layer structure. J. Appl. Meteor. 9, 874-884.

Lenschow, D. H., 1974: Model of the height variation of the turbulence kinetic energy budget in the unstable planetary boundary layer. J. Atmos. Sci., 31, 465-474.

Lilly, D. K., 1964: Numerical solutions for the shape-preserving two-dimensional thermal convection element. J. Atmos. Sci., 21, 83-98.

Lucas, D. H., 1967: Application and evaluation of results of the Tilbury plume rise and dispersion experiment. Atmos. Environ., 1, 421-424.

Lucas, D. H., K.W. James, and I. Davies, 1967: The measurement of plume rise and dispersion at Tilbury Power Station. Atmos. Environ., 1,353-365.

Lucas, D. H., D. J. Moore, and G. Spurr, 1963: The rise of hot plumes from chimneys. Int. J. Air Water Pollut., 7, 473-500.

Lumley, J. L., and H. A. Panofsky, 1964: The Structure of Atmospheric Turbulence. New York, John Wiley & Sons, Inc. 239 pp.

Moore, D. J., 1965: On the rise of hot plumes in the atmosphere. Int. J. Air Water Pollut., 9, 233-237.

Moore, D. J., 1967: Meteorological measurements on a 187 m tower. Atmos. Environ., 1, 367-377.

Moore, D. J., 1968: Contribution to the round table discussion on plume rise and dispersion. Atmos. Environ., 2, 247-250.

Moore, D. J., 1973: Observed and calculated magnitudes and distances of maximum ground level concentration of gases effluent material downwind of a tall stack. CERL.

Moore, D. J., 1974a: A comparison of the trajectories of rising buoyant plumes with theoretical/empirical models. Atmos. Environ., 8, 441-457.

Moore, D. J., 1974b: The prediction of the mean hourly average maximum ground level concentration of sulphur dioxide at Tilbury. Atmos. Environ., 8, 543-554.

Morton, B. R., 1957: Buoyant plumes in a moist atmosphere. J. Fluid Mech., 2, 127-144.

Morton, B. R., 1959: The ascent of turbulent forced plumes in a calm atmosphere. Int. J. Air. Pollut., 1, 184-197.

Morton, B. R., 1968: On Telford's model for clear air convection (with reply). J. Atmos. Sci., 25, 135-139.

Morton, B. R., 1971: The choice of conservation equations for plume models. J. Geophys. Res., 76, 7409-7416.

Morton, B. R., and J. Middleton, 1973: Scale diagrams for forced plumes. J. Fluid Mech., 58(1), 165-176.

Morton, B. R., G. I. Taylor, and J. S. Turner, 1956: Turbulent gravitational convection from maintained and instantaneous sources. Proc. Roy. Soc. (London), Ser. A, 234, 1-23.

Moses, H., and M. R. Kraimer, 1972a: Plume rise determination - a new technique without equations. JAPCA, 22(8), 621-630.

Moses, H., M. R. Kraimer, 1972b: Tabular data offer easy way to predict stack plume rise. Heating/Piping/Air Conditioning, Sept. 1972, 90-96.

Moses, H., and G. H. Strom, 1961: A comparison of observed plume rises with values obtained from well-known formulas. J. Air Pollut. Contr.Ass., 11, 455-466.

Murthy, C. R., 1970: On the mean path of a buoyant chimney plume in non-uniform wind. J. Appl. Meteor., 9, 603-611.

Narain, J. P., 1973: An isolated buoyant thermal in a stratified medium. Atmos. Environ., 7, 979-989.

Narain, J. P., 1974: Comments on an isolated buoyant thermal in a stratified medium. Atmos. Environ., 8, 863-865.

Ooms, G., 1972: A new method for the calculation of the plume path of gases emitted by a stack. Atmos. Environ., 6, 899-909.

Pai, S. I., 1954: Fluid Dynamics of Jets. New York, D. Van Nostrand Co., Inc.

Pasquill, F., 1974: Atmospheric Diffusion. 2nd Ed., New York, Halsted Press.

Patrick, M. A., 1967: Experimental investigation of the mixing and penetration of a round turbulent jet injected perpendicularly into a traverse stream. Trans. Inst. Chem. Engrs. (London), 45, 16-31.

Priestley, C. H. B., 1956: A working theory of the bent-over plume of hot gas. Quart. J. Roy. Meteor. Soc., 82, 165-176.

Priestley, C. H. B., and F. K. Ball, 1955: Continuous convection from an isolated source of heat. Quart. J. Roy. Met. Soc., 81, 144-157.

Proudfit, B. W., 1970: Final report on plume rise from Keystone plant. Sign X Labs., Inc., Essex, Conn. 06426, No. 203, 767-1700.

Rauch, H., 1964: Zur Schornstein-Uberhohung. Beitr. Phys. Atmos., 37, 132-158; translated in USAEC Report ORNL-tr-1209, Oak Ridge National Lab.

Richards, J. M., 1961: Ph.D. thesis, University of London.

Richards, J. M., 1963: Experiments on the motions of isolated cylindrical thermals through unstratified surroundings. Int. J. Air Water Pollut., 7, 17-34.

Richards, J. M., 1968: Inclined buoyant puffs. J. Fluid Mech., 32,(4), 681-692.

Ricou, F. P., and D. B. Spalding, 1961: Measurements of entrainments by axisymmetrical turbulent jets. J. Fluid Mech., 11, 21-32.

Rouse, H., C. S. Yih, and H. W. Humphreys, 1952: Gravitational convection from a boundary source. Tellus, 4, 201-210.

Schiermeier, F. A., and L. E. Niemeyer, 1970: Large power plant effluent study. Vol. 1 U. S. Dept. of Health, Ed., and Welfare, Public Health Service, Environmental Health Service.

Schlichting, H., 1960: Boundary Layer Theory. McGraw-Hill Book Co., New York, pp 607-613.

Schmidt, F. H., 1965: On the rise of hot plumes in the atmosphere. Int. J. Air Water Pollut., 9, 175-198.

Schmidt, W., 1941: Turbulente Ausbreitung eines Stromes erhitzter Luft. Z. Angew. Math. Mech., 21, 265-278 and 351-363.

Scorer, R. S., 1958: Natural Aerodynamics., Pergamon Press, Inc., New York, 143-217.

Scorer, R. S., 1959: The behavior of chimney plumes. Int. J. Air Pollut., 1, 198-220.

Scorer, R. S., 1968: Air Pollution. Pergamon Press, Oxford, 47-50.

Scorer, R. S., and C. F. Barrett, 1962: Gaseous pollution from chimneys. Int. J. Air Water Pollut., 6, 49-63.

Scriven, R. A., 1966: On the breakdown of chimney plumes into discrete puffs. Int. J. Air Water Pollut., 10, 419-425.

Sherlock, R. H., and E. A. Stalker, 1941: A study of flow phenomena in the wake of smoke stacks. Engineering Research Bulletin 29, University Michigan, Ann Arbor, Mich.

Shwartz, J., M. P. Tulin, 1971: Chimney plumes in neutral and stable surroundings. Atmos. Environ., 6, 19-35.

Simon, C., and W. Proudfit, 1967: Some observations of plume rise and plume concentration distributed over N.Y.C. Paper 67-83, 60th Annual Meeting of the Air Pollution Cont. Ass., Cleveland, Ohio, June 11-16, 1967.

Singer, I. A., J. A. Frizzola, and M. E. Smith, 1964: The prediction of the rise of a hot cloud from field experiments. J. Air Pollut. Cont. Ass., 14, 455-458.

Slawson, P. R., and G. T. Csanady, 1967: On the mean path of buoyant, bent-over chimney plumes. J. Fluid Mech., 28, 311-322.

Slawson, P. R., and G. T. Csanady, 1971: The effect of atmospheric conditions on plume rise. J. Fluid Mech., 47(1), 33-40.

Smith, F. B., 1972: A scheme for estimating the vertical dispersion of a plumes from a source near ground level. Proceedings of the 3rd Meeting of the Expert Panel on Air Pollution Modeling, Oct. 2-3, 1972, Paris, France, XVII-1-14.

Smith, F. B., and J. S. Hay, 1961: The expansion of clusters of particles in the atmosphere. Quart. J. Roy. Met. Soc., 87, 82-101.

Steiner, J. T., 1975: Thermal power station plumes. New Zealand Meteorological Service, Tech. Note 225.

Stewart, N. G., H. J. Gale, and R. N. Crooks, 1954: The atmospheric diffusion of gases discharged from the chimney of the Harwell Pile (BEPO) British Report AERE HP/R-1452.

Stewart, N. G., H. J. Gale, and R. N. Crooks, 1958: The atmospheric diffusion of gases discharged from the chimney of the Harwell reactor BEPO. Int. J. Air Pollut., 1, 87-102.

Sutton, O. G., 1950: The dispersion of hot gases in the atmosphere. J. Met., 7, 307-312.

Taylor, G. I., 1945: Dynamics of a mass of hot gas rising in the air. USAEC Report MDDC-919 (LADC-276), Los Alamos Scientific Lab.

Telford, J. W., 1966: The convective mechanism in clear air. J. Atmos. Sci., 23, 652-665.

Telford, J. W., 1968: Reply to B. R. Morton, on Telford's model for Clear Air Convection. J. Atmos. Sci., 25, 138-139.

Tennekes, H., 1970: Free convection in the turbulent Ekman layer of the atmosphere. J. Atmos. Sci., 27, 1027-1034.

Tennekes, H., 1973: A model for the dynamics of the inversion above a convective boundary layer. J. Atmos. Sci., 30, 558-567.

Tennekes, H., and J. L. Lumley, 1972: A First Course in Turbulence. Cambridge, Mass., The MIT Press, 300 pp.

Thomas, F. W., S. B. Carpenter, and F. E. Gartrell, 1963: Stacks - How High? J. Air Pollut. Contr. Ass., 13, 198-204.

Thomas, F. W., S. B. Carpenter, and W. C. Colbaugh, 1970: Plume rise estimates for electric generating station. J. Air Pollut. Control Ass., 20, 170-177.

Tsang, G., 1970: Laboratory study of two-dimensional starting plumes. Atmos. Environ., 4 519-544.

Tsang, G., 1971: Laboratory study of line thermals. Atmos. Environ., 5, 445-471.

Tsang, G., 1972a: Entrainment of ambient fluid by two-dimensional starting plumes and thermals. Atmos. Environ., 6, 123-132.

Tsang, G., 1972b: Stack exit velocity distribution for higher effective stack height. Atmos. Environ., 6, 815-828.

Tsang, G., 1973: Further laboratory experiments on a stack of optimal exit velocity distribution. Atmos. Environ., 7, 755-762.

Tulin, M. P., and J. Shwartz, 1970: Hydrodynamic aspects of waste discharge. American Inst. of Aeronautics and Astronautics. AIAA 3rd Fluid and Plasma Dynamics Conference, June 29-July 1, 1970, Los Angeles, Cal.

Turner, J. S., 1962: The 'starting plume' in neutral surroundings. J. Fluid Mech., 13, 356-368.

Turner, J. S., 1963: Model experiments relating to thermals with increasing buoyancy. Quart. J. Roy. Meteor. Soc., 89, 62-74.

Turner, J. S., 1969: Buoyant plumes and thermals. Ann. Rev. Fluid Mech., 1, 29-44.

Vadot, L., 1965: Study of Diffusion of Smoke Plumes into the Atmosphere (in French). Centre Interprofessionnel Technique d'Etudes de la Pollution Atmospherique, Paris.

Van Vleck, L. D., and F. W. Boone, 1964: Rocket exhaust cloud rise and size studies, hot volume sources. Paper presented at 225th National Meeting of the Amer. Meteor. Soc., Jan. 29-31, 1964, Los Angeles, Cal.

Vehrencamp, J. E., A. Ambrosio, and F. E. Romie, 1955: Convection from heated sources in an inversion layer. Report 55-27, Univ. of Cal., Los Angeles, Dept. of Engineering.

Wang, C. P., 1973: Motion of a turbulent buoyant thermal in a calm stably stratified atmosphere. Physics of Fluids, 16(6), 744-749.

Warren, F. W. G., 1960: Wave resistance to vertical motion in a stratified fluid. J. Fluid Mech., 7, 209-229.

Weil, J. C., 1968: Model experiments of high stack plumes. S.M. Thesis, Mass. Inst. of Technology.

Weil, J. C., 1974: Comparison between measured and model-estimated ground-level $SO_2$ concentrations downwind from the Dickerson power plant. Maryland Power Plant Siting Program, Report PPSP-MP-11.

Weil, J. C., and D. P. Hoult, 1973: A correlation of ground-level concentrations of sulfur dioxide downwind of the Keystone stacks. Atmos. Environ., 7, 707-721.

Woodward, B., 1959: The motion and around isolated thermals. Quart. J. Roy. Meteor. Soc., 85, 144-151.

Wyngaard, J. C., and O. R. Coté, 1971: The budgets of turbulent kinetic energy and temperature variance in the atmospheric surface layer. J. Atmos. Sci., 28, 190-201.

Wyngaard, J. C., S. P. S. Arya, and O. R. Coté, 1974: Some aspects of the structure of convective planetary boundary layers. J. Atmos. Sci., 31, 747-754.

Yih, C. S., 1951: Convection due to a point source of heat. In Proceedings of 1st U.S. National Congress of Applied Mechanics, 941-947, American Soc. of Mech. Eng.

## APPENDIX A - SYMBOLS

Subscript a - Ambient value

Subscript o - Source value

$b_i$ - Acceleration of air displaced through an inversion = $(g/\theta_a)\Delta\theta_i$ [$\ell/t^2$]

$c_p$ - Specific heat capacity at constant pressure of air

$C_D$ - Drag coefficient, dimensionless

$C_d$ - Dissipation coefficient, dimensionless

$C_1$ - Best fit dimensionless constant for Eq. (48), the "2/3 law"

$C_2$ - Best fit dimensionless constant for Eq. (59), stable rise

D - Source diameter [$\ell$]

ESH - "Effective stack height"

F - Buoyancy flux of source, given by Eqs. 10-12 [$\ell^4/T^3$]

$F_m$ - Momentum flux of source, given by Eq. 28 [$\ell^4/t^2$]

Fr - Local Froude number, defined in Table 1

$F_z$ - Buoyancy flux as a function of plume height [$\ell^4/t^3$]

g - Acceleration due to gravity [$\ell/t^2$]

h - Height above the ground [$\ell$]

$h_e$ - Effective stack height [$\ell$]

$h_s$ - Source height [$\ell$]

$\Delta h$ - Plume rise = $h_e - h_s$ [$\ell$]

H - Sensible upward heat flux times $g/(c_p \rho T)$ [$\ell^2/t^3$]

$\vec{i}$ - Unit vector oriented with mean wind

$\vec{k}$ - Unit vector oriented upwards

k - Von Kármán constant = 0.35 to 0.40

K - Kinetic energy [$\ell^2/t^2$] or eddy diffusivity [$\ell^2/t$]

L - Buoyancy length scale = $F/U^3$ [$\ell$]

$L_m$ - Momentum length scale = $L_m^{1/2}/U$ [$\ell$]

L" - Monin-Obukov length = $-u^{*3}/(k\ H)$ [$\ell$]

$\ell$ - Dominant scale of ambient turbulence [$\ell$]

m - Mean molecular weight

M - Flux of vertical momentum within a bent-over plume; see Eq. (36) [$\ell^4/t^2$]

$M_{eff}$ - Effective flux of vertical momentum of a bent-over plume; see Eq. (36) [$\ell^4/t^2$]

MGC - "Maximum ground concentration"

n - Space coordinate normal to plane of integration [$\ell$]

p - Perturbation pressure due to plume, non-hydrostatic

$p_a$ - Ambient pressure

$p_s$ - Sea level pressure

q - Variance of turbulent velocities in plume [$\ell/t$]

Q - Rate of emission of pollutant or tracer [m/t]

$Q_H$ - Rate of sensible heat emission

r - Effective radius of a plume; see Eqs. (35) and (36) [$\ell$]

$r_o$ - Internal radius of source = D/2 [$\ell$]

R - Ratio of efflux velocity to wind speed = $w_o/U$

$R_e$ - Reynold's number

s - Distance along axis of a plume [$\ell$]

s - Stability parameter = $(g/\theta_a)\ \partial\theta_a/\partial z = \omega^2$ [$t^{-2}$]

s' - $(M/M_{eff})^{1/2} s$ for bent-over plume, s for vertical plumes

$d\vec{s}$ - Element of periphery around area of integration, directed inwards [$\ell$]

$d\vec{S}$ - Element of area of integration [$\ell^2$]

$S_1$ - Dimensionless shape factor for buoyant, vertical plumes; see Eq. (35)

T - Absolute temperature

t - Time after exit, defined in Eqs. (35) and (36) [t]

$t_d$ - Touchdown time, given by Eq. (89) [t]

u - $\vec{i}$ component of perturbation velocity due to plume [$\ell/t$]

$\bar{u}$ - Mean horizontal speed of plume relative to ambient flow [$\ell/t$]

u' - Variance of ambient turbulent velocities [$\ell/t$]

u* - Friction velocity; see Eqs. (78) and (79) [$\ell/t$]

$\vec{U}$ - Mean ambient wind velocity [$\ell/t$]

U - Mean ambient wind speed [$\ell/t$]

$U_c$ - "Critical wind speed," at which $(U\ h_e^2)$ is minimized [$\ell/t$]

$\vec{v}$ - Perturbation velocity due to plume [$\ell/t$]

$v_e$ - Entrainment velocity = $(dV/ds)/(2r)$ [$\ell/t$]

V - Volume flux ÷ π; see Eqs. (35) and (36) [$\ell^3/t$]

$V_o$ - Source volume flux ÷ π [$\ell^3/t$]

w - $\vec{k}$ component of perturbation velocity due to plume [$\ell/t$]

$\bar{w}$ - Mean vertical velocity of vertical plume; see Eq. (35) [$\ell/t$] (centerline vertical velocity = $dz/dt = U\ dz/dx$ of a bent-over plume [$\ell/t$])

w* - Scaling velocity of a convective mixing layer = $(Hz_m)^{1/3}$ [$\ell/t$]

$w_d$ - Effective average downdraft velocity in a convective mixing layer ∝ w* [$\ell/t$]

$w_o$ - Efflux velocity of effluent [$\ell/t$]

x - Downwind space coordinate, originating at the source [$\ell$]

X - Vector cross-product

y - Lateral space coordinate or radial distance from axis [$\ell$]

z - For vertical plume, height above the source [$\ell$]. For bent-over plume, height of plume centerline above the source [$\ell$]

$z_b$ - Height of base of stable layer above the source [$\ell$]

$z_{eq}$ - Equilibrium height, at which $F_z = 0$ [ℓ]

$z_i$ - Height of thin inversion above the source [ℓ]

$z_m$ - Mixing layer height (above the ground) [ℓ]

$z_o$ - Roughness length of surface; see Eq. (79) [ℓ]

$\alpha$ - Entrainment coefficient for shear parallel to plume axis

$\beta$ - Entrainment coefficient for effective plume mass for shear perpendicular to plume axis

$\beta'$ - $(M/M_{eff})^{1/2}\ \beta$

$\gamma$ - Entrainment coefficient of ambient turbulence-induced mixing; $dr/dt = \gamma\ (\varepsilon r)^{1/3}$

$\varepsilon$ - Turbulence energy dissipation rate [$\ell^2/t^3$]

$\eta$ - Coefficient relating plume dissipation rate to $\bar{w}^3/z$; see Eq. (34)

$\theta$ - Potential temperature

$\theta'$ - Potential temperature elevation over ambient = $\theta - \theta_a$

$\Delta\theta_i$ - Change in potential temperature through an inversion layer

$\theta_{el}$ - Slope of plume axis or solar elevation angle

$\nu$ - Kinematic viscosity [$\ell^2/t$]

$\rho$ - Density [$m/\ell^3$]

$\rho'$ - Density deficit relative to the ambient = $\rho_a - \rho$ [$m/\ell^3$]

$\sigma_y$ - Lateral variance of diffused material [ℓ]

$\sigma_y$ - Vertical variance of diffused material [ℓ]

$\tau$ - Characteristic Reynolds stress in plume [$\ell^2/t^2$]

$\vec{\tau}_z$ - Vertical part of Reynolds stress tensor [$\ell^2/t$]

$\phi$ - Velocity potential [$\ell^2/t$]

$\chi_{max}$ - Maximum ground concentration [$m/\ell^3$]

$(\chi_{max})_c$ - Maximum ground cencentration at the critical wind speed [$m/\ell$]

$\chi_p$ - Concentration in the plume [$m/\ell^3$]

$\psi$ - Velocity stream function [$\ell^2/t$]

$\omega$ - Brunt-Väissälä frequency = $s^{1/2}$

$m'$ - Molecular weight deficit = $m_a - m_o$

$v_n$ - Perturbation velocity normal to an intersecting plane

$x'$ - Characteristic distance for stability to be effective = $Us^{-1/2}$

Suggestion - In future papers on plume rise, the buoyancy length scale $F/U^3$ should be designated with $L_b$ instead of L, which has been used in the past, since it now appears that the Monin-Obukov length is also a relevant length to the problem; this length has also been traditionally designated with L.

## APPENDIX B - COOLING TOWER CALCULATIONS

The main body of this paper was addressed to the problem of predicting the rise of dry plumes. The same approach can serve as a starting point for models of moist plume behavior. The main difference is that the water vapor in moist plumes will condense if it is cooled sufficiently. The consequent release of latent heat may or may not add significantly to the plume buoyancy.

This appendix does not attempt to develop a general model for moist plumes; instead, it draws some general conclusions based on models already available, points out some relevant considerations, and compares some simple models with actual observations of condensed plume length. As for general models, for bent-over plumes either the one summarized by Weil (1974) or by Wigley (1975) ought to serve well. These models neglect rainout and supersaturation, but still should be basically valid for cooling tower plumes both near the source and up to the point of leveling in stable surroundings. These models do need to be compared with real data; some adjustments may be required, such as the inclusion of a "peak factor" (to be discussed later).

Adequate data are just beginning to become available. Examples are the mechanical draft cooling tower data of Meyer et. al. (1974), to be used in this appendix, and the recently released natural draft tower data from the Amos plant (Kramer et. al., 1975). Further measurement programs are currently underway in Maryland and in Pennsylvania.

There are any number of "state-of-the-art" reviews of this problem, in spite of the limited work on advancing the state-of-the-art. The recent review of McVehil and Heikes (1975) is so far unique in that it shows plume length predictions made by a number of models compared with real field data (not computer-generated "data"), namely that of Meyer et. al. Hopefully, a lot more comparisons will be made in the next several years, so that more substantial modeling recommendations can be made. Besides this review, the collections of papers on cooling towers in the April 1974 issue of Atmospheric Environment and in "Cooling Tower Environment - 1974" (Hanna and Pell) contain much useful information.

### B.1 Occurrence of Downwash

Many cooling tower effluents have a rather low exit velocity, so the plumes may be subject to downwash in high winds. According to early wind tunnel experiments on straight-sided stacks, slight downwash occurs if $R = w_o/U < 1.5$ and substantial downwash occurs if $R < 1.0$ (Sherlock and Stalker, 1941). However, buoyancy was not a significant factor in these experiments since the stack Froude numbers were quite high. Buoyancy can be important for natural draft plumes.

Overcamp and Hoult (1971) did a towing tank experiment on a hyperbolic-shaped source over a range of Froude numbers and velocity ratios. These experiments showed "strong interaction" with the wake of the tower, defined by ground contact occurring at 2 to 4 $h_s$ downwind, when

$$R \lesssim 0.45 Fr_o^{2/3}, \text{ where } Fr_o = w_o/(r_o g \Delta\rho_o/\rho_a)^{1/2}, \quad (B.1)$$

provided that the source Froude number, $Fr_o$, is less than 3. For a natural draft tower, typically $w_o \approx (0.5 h_s g \Delta\rho_o/\rho_a)^{1/2}$ and $h_s/r_o \approx 4$ to 5, so $Fr_o \approx 1.5$ and the critical velocity ratio $\simeq 0.6$.

### B.2 Supersaturation

It is almost a universal assumption in moist plume models that all water vapor in excess of the saturation humidity condenses. Yet it is well known from cloud physics studies that water droplets develop only on suitable solid particles in the air, known as "condensation nuclei," and that the water droplets grow at a finite rate. In absolutely "clean" air, any degree of supersaturation is possible, with no condensation. Of course this does not happen in the real atmosphere, especially in the vicinity of industrial emissions.

Wigley (1975a) explores the question of how much supersaturation is likely to occur in a rising, moist plume, on the basis of existing cloud physics. The solution depends on many variables, so he shows results for three representative sources. The small jet is predicted to develop a high degree of supersaturation (170% relative humidity), but this diminishes rapidly and the plume becomes undersaturated in only a fraction of a second (just as it takes a water droplet a finite time to grow, it takes it a finite time to evaporate again when conditions become undersaturated). The hypothetical scrubbed plume becomes quite supersaturated also, 150% RH at $T_a = -10°C$. It undersaturates in a little more than one second, however. The natural-draft cooling tower plume supersaturates by only a few per cent, and undersaturates in about 6 seconds. The length of the plume is extended a little more than 5% over that predicted assuming instant droplet formation and dissipation. However, one has to assume a certain concentration of condensation nuclei in order to make such calculations, and this is an extremely variable quantity in the atmosphere. The average count at any one site runs from about $10^3$ particles/cm$^3$ over oceans and in high mountains to about $10^5$ in cities, and at any one site the count may range over several orders of magnitude (Mason, 1957, p42). The value chosen by Wigley is on the conservative side: 2000 particles/cm$^3$ of mean radius = 0.5μm. In an industrial area,

and certainly in a scrubbed plume, much higher particle concentrations, and much lower supersaturations, would be the rule. At least for cooling tower plumes, it appears that neglect of supersaturation is justified.

Another important result of Wigley's calculations is that in his examples the water droplets do not grow to more than 20μm in diameter, which is too small to result in rain-out.

Salt water cooling towers would present a slightly different problem in that salt is hygroscopic, and droplets will grow on it even in undersaturated conditions. This involves a different droplet growth mechanism than was considered by Wigley.

B.3 Effect of Effluent Latent Heat on Rise

Cooling tower plumes sometimes carry five times or more latent heat than sensible heat, especially during warm weather. If the plume's water vapor were to condense completely, the plume's buoyancy would increase severalfold, providing a significant boost in the plume rise. However, complete condensation cannot occur, and the maximum rise enhancement due to latent heat release is rather modest. At best it is 10 to 20% over the rise due to sensible heat and molecular weight difference alone. This much enhancement occurs only when a saturated plume mixes with a just saturated environment, or has carried entrained air up just to its natural condensation height (the "lifting condensation level"). Carried up much higher than this, the latent heat released from the entrained air is much greater than that released from the effluent moisture.

Latent heat release can be simply estimated by using a psychrometric chart method, such as that described by Overcamp and Hoult (1971). For the maximum latent heat boost, assume a mixture of saturated plume at temperature $T_o$ with a saturated ambient at temperature $T_a$. The absolute humidity $\rho_w$ at saturation (subscript "s") is a function only of temperature, as is given by the Clausius-Clapeyron relation:

$$d\rho_{ws}/dT = \rho_{ws}\, L/(R_v T^2), \qquad \text{(B-2)}$$

where $R_v$ is the gas constant for water vapor and L is the latent heat of vaporization, which is weakly a function of temperature. Thus, over a small range of absolute temperature $\rho_{ws}$ is roughly exponential in T, and any mixture of initially saturated gases is supersaturated. (Neglecting any differences in density, the state of any mixture of gases ($\rho_{wa}$, $T_a$) and ($\rho_{wo}$, $T_o$) falls on a straight line between these two points on a plot of $\rho_w$ versus T.)

Let $q \simeq \rho_w/\rho$ be the specific humidity, and let $\Delta$ signify the difference between any quantity and the ambient value of that same quantity, e.g., $\Delta q_o = q_o - q_a$. For any uncondensed mixture of the efluent and the ambient, whose state is represented by ($q_m$, $T_m$), the ratio of total mass to effluent mass is equal to $\Delta T_o/\Delta T_m = \Delta q_o/\Delta q_m$. As this ratio becomes large, $\Delta T_m$ becomes small and the segment of the curve $q_s(T)$ between $T_a$ and $T_m$ can be considered linear. The excess humidity of the mixture over 100% saturation is then $(\Delta q_o/\Delta T_o - (\partial q_s/\partial T)_a)\Delta T_m$.

Not all of this excess can be converted to latent heat, however, since as latent heat is released the mixture warms up. This raises its moisture-holding capacity by $\partial q_s/\partial T$ times the rise in temperature, while its vapor content decreases by $(c_p/L)$ times the same, until $q = q_s$. The fraction of the original humidity excess that can condense is then $(c_p/L) \div [(c_p/L)+(\partial q_s/\partial T)_a] = 1/(1+Q_s)$, where we define $Q_s = (L/c_p)(\partial q_s/\partial T)_a$. (as a rough rule-of-thumb, $Q_s = 1$ at $T_a = 5°C$ and doubles every 10°C; thus, at warm temperatures only a small fraction of the humidity excess condenses). Similarly, we define $\Delta Q_o = (L/c_p)\,\Delta q_o/\Delta T_o$, which is simply the ratio of latent to sensible heat in the effluent. The ratio of latent heat released to the sensible heat $\Delta T_m$ can now be written

$$R_q = (\Delta Q_o - Q_s)/(1+Q_s). \qquad \text{(B-3)}$$

The ratio of buoyancy released by condensation to initial buoyancy is even less, by a factor of $(1+0.61(c_pT/L)\Delta Q_o)$, due to the low molecular weight of water vapor. In moist plume calculations, this factor is usually taken into account by using "virtual temperature," defined by $T_v = T(1+0.61q)$.

For most sources, $\Delta Q_o$ runs higher in warm weather, just when $Q_s$ is high. This is because the volume flux and the total load (sensible plus latent heat) run relatively constant, while $\partial q_s/\partial T$ is much larger than in cool weather. Integrating Eq (B-2) with the approximation $R_v T^2/L = T_s$ = constant, we find that

$$\Delta Q_o \simeq Q_s (T_s/\Delta T_o)[\exp(\Delta T_o/T_s) - 1] \qquad \text{(B-4)}$$

(this expression neglects the terms $(1+T_s/T_a)$ in the denominator and $(1+\Delta T_o/T_a)$ in front of the exponential, which originate due to density differences). Remember that we are assuming $q_a = q_s(T_a)$ and $q_o = q_s(T_o)$. The scaling temperature $T_s$ is of the order of 14°C.

For convenience, since the total load does not vary so much as $\Delta Q_o$ and $\Delta T_o$, we define an equivalent temperature excess that would occur if the entire load were carried by sensible heat alone,

$$\Delta T_e = (1+\Delta Q_o)\Delta T_o \qquad \text{(B-5)}$$

Typically, for cooling towers $\Delta T_e/T_s$ = 4 to 5, with higher values being unacceptable due to loss of plant efficiency. Now $R_q$ can be solved as a function of $Q_s(T_a)$ and $\Delta T_e/T_s$, but not explicitly.

For a constant value of $\Delta T_e$, we find that there is a particular value of $Q_s$ at which the ratio $R_q$ is a maximum, and that $R_q$ drops off very slowly to either side of this maximum. For the value $\Delta T_e/T_s$ = 5, we find the maximum $R_q$ = 0.7 at $Q_s$ = 0.5, or at $T_a \simeq -5°C$. In general, over the whole practical range of $\Delta T_e$ we find that the maximum $R_q \simeq (1/7)\Delta T_e/T_s$.

Since $\Delta T_e/T_s$ seldom exceeds 5 for cooling towers, the rise enhancement due to latent heat carried by the effluent cannot exceed about $(1+0.7)^{1/3}$, about 20% greater than the rise due to sensible heat alone. Since this occurs only in rather special circumstances, normally the boost due to effluent latent heat is much less. Thus, one does not need to include this effect in first order calculations of plume rise; it would require some very excellent data to verify this effect considering the large about of scatter inherent in plume rise observations.

## B.4 Effect of Saturated Ambient on Rise

When both the plume and the ambient are saturated and supersaturation in the plume is negligible, the plume equations simplify considerably. Weil (1974) gives an explicit solution for the case where $\partial T_a/\partial z$ and the ambient liquid water mixing ratio $\sigma_a$ are constant. However, it is valid only when the change of $T_a$ through the layer of rise is small compared to $T_s$, since a constant value of $\partial q_s/\partial T$ is assumed. The result is similar to the one given in Section 4.1 for dry plumes, except that the stability parameter is somewhat modified:

$$s = (1+0.6laQ_s/b)(g/\theta_a)(\partial T_a/\partial z+\Gamma_m), \qquad (B-6)$$

where $a = c_pT_a/L \simeq 0.11$ at 0°C and $b = 1+T_s/T_a \simeq 1.05$. $\Gamma_m$ is a modified wet adiabatic lapse rate. The ordinary wet adiabatic lapse rate, which is the temperature drop with height of just saturated air lifted adiabatically, is $\Gamma_s = \Gamma_d\,(1+1.61aQ_s/b) \div (1+Q_s/b)$, where $\Gamma_d = g/c_p$, the dry adiabatic lapse rate.

$$\Gamma_m/\Gamma_s \simeq 1+(aQ_s/b)(1-1.6a) \div (1+2.2aQ_s)$$

$$\simeq 1+0.09Q_s \div (1+Q_s/4) \qquad (B-7)$$

Thus, $\Gamma_m$ is no more than 20% larger than $\Gamma_s$. The reason that this critical lapse rate is not the same as the wet adiabatic lapse rate is that $\sigma_a$ is assumed constant. Although the plume cools as it is lifted at the rate $\Gamma_s$, condensation occurs and the increasing weight of water droplets works against the buoyancy, so $dF_z/dz<0$ even if $\partial T_a/\partial z = -\Gamma_s$.

The main difference from dry plume rise is that the rise is unlimited when $\partial T_a/\partial z = -\Gamma_m$, instead of $-\Gamma_d$. When $(\partial T_a/\partial z+\Gamma_m) >> (\Gamma_d-\Gamma_m)$, there is no practical difference at all. The only time the difference is really significant is when a plume is rising through cloud or fog with $\partial T_a/\partial z \simeq -\Gamma_s$, as is the case when the saturated layer is well-mixed. Buoyancy still decays with rise, but $(\Gamma_w-\Gamma_s)$ is less than 1/15 of $\partial\theta_a/\partial z \simeq \Gamma_d-\Gamma_s$. This means that the levelling-off time is very large, of the order of 20 minutes or so. Thus, a plume of any respectable size which enters such a layer is likely to reach the top of it. Except for non-aqueous constituents of the plume, it would be hardly distinguishable from the cloud layer.

In the Amos cooling tower study (Kramer et. al., 1975), there are 9 tests during which the plumes reach an elevated cloud layer. In all of these cases, the plumes rise into or among the clouds, but do not get substantially above them (the cloud layers tended to be either very deep, or else thin with very dry, stable air immediately above them). Since a dry plume model would do no worse than a wet one at predicting the essential outcome in these cases, it is becoming questionable to me whether moist plume models, which are complicated, offer any substantial improvement over "dry plume" models in predicting the rise of moist plumes.

## B.5 Prediction of Condensation

There has been some concern about the frequency of shadowing due to condensation of water vapor in cooling tower plumes, as well as about the possibilities of fogging and rain-out. The first step towards predicting these phenomena is to predict the length of the condensed portion of a plume, based on its water vapor content, the ambient temperature and humidity profiles, and some model describing the mixing of the plume with the ambient.

Mixing models are already available, since mixing is a vital consideration in any plume rise model also. For most cases, mixing is strongly a function of plume rise, which is strongly a function of the initial momentum and plume buoyancy. Previous discussion suggests that latent heat release, which feeds back into the mixing process in a complicated way, is not an important factor.

Entrainment assumptions for predicting the near-field rise have been adjusted to include the effective mass outside the plume, as well as the plume mass. Only the latter dilutes the mean temperature and specific humidity of the plume. Section 2.3 indicates that the ratio of effective mass to plume mass is about 2.3 for a buoyant, bent-over plume. Accounting for this difference is straightforward, e.g., by using $V=U(\beta' z)^2$ instead of $U(\beta z)^2$.

A more ellusive effect is the non-uniformity of moisture and temperature within the plume. Mixing involves a cascade process which gradually mixes large blobs of entrained fluid down to smaller and smaller scales, until mixing due to molecular motion is effective and the process is complete. In the meantime, new ambient is being drawn into a plume at the larger scales. Little is known about this process in an actively rising plume. The overall effect must be that saturation persists in some parts of a plume longer than it does in the mean. At present, this effect can be included by introducing some sort of crude assumption, without knowing the details of the process. For instance, Meyer et. al. (1974) employ a "peak factor," which represents additional mixing (beyond 100% saturation in the mean) required to unsaturate lumps of higher-than-average humidity plume material.

The case of a rising, bent-over plume near the source is especially attractive for testing purposes, since in this case the volume of entrained air is a function only of the rise and the crosswind velocity, according to a number of current plume rise models. In the following, comparisons of such models are made with the observations published by Meyer et. al. (1974).

I tried three different expressions for the total volume flux (divided by $\pi$) of the rising plume: $V_1 = U(\beta' z)^2$, as is used in Section 3, $V_2 = (V_o^{1/2}+U^{1/2}\beta' z)^2$, as is used by Hanna (1972), and $V_3 = V_o+U(\beta' z)^2$. The first expression has the advantage of simplicity, while the latter are correct at $z = 0$. If $V/V_o$ is large, it does not matter which expression is used.

As for the dilution $V/V_o$ required to unsaturate the plume, again I tried three different methods. The first, and by far the simplest, is one suggested by Hanna (1974): $V/V_o = q_o/\Delta q_s$, where $\Delta q_s$ is the saturation deficit of the ambient air. This method neglects the increased moisture carrying capacity of the plume due to its elevated temperature. This is strictly valid only when $(\partial q_s/\partial T)_a$ is small compared to $\Delta q_o/\Delta T_o$, i.e., $Q_s \ll \Delta Q_o$. For a typical cooling tower ($\Delta T_e/T_s \simeq 5$), this is a fair approximation, especially during cold temperatures. The second method uses the psychrometric chart, a plot of $q_s$ (or $\rho_{ws}$) versus T. It is described by Overcamp and Hoult (1971), McVehil and Heikes (1975), and others. A straight line is drawn between the points $(q_a, T_a)$ and $(q_o, T_o)$, which represents all possible states of mixtures of ambient and source gases. The point where this line intersects $q_s(T)$, at $(q_i, T_i)$, is the mixture that is just saturated, and $V/V_o = \Delta q_o/\Delta q_i = \Delta T_o/\Delta T_i$. If the effluent is undersaturated or the ambient is warm and dry, there may be no intersection at all with the $q_s(T)$ curve, which means that no condensation is predicted.

The third method is similar to the chart method, but accounts for adiabatic cooling. The procedure is the same, except that the straight line is drawn from $(q_a, T_a-\Gamma_d z)$ to $(q_o, T_o-\Gamma_d z)$. This method has validity in a well-mixed, undersaturated layer, since then $\partial q_a/\partial z \simeq 0$ and $\partial T_a/\partial z \simeq -\Gamma_d$. It would not be appropriate in a stable atmosphere; instead, the ambient point should be replaced by $(\overline{q_a}, T_a-\Gamma_d z+\overline{\theta}_a-\theta_a)$, where $\overline{q}_a$ and $\overline{\theta}_a$ are weighted averages through the plume rise layer. Only a few of the Meyer et. al. runs appear to be in stable air, and then the stability is not large. It is possible with the adiabatic method for no intersection to occur because of sustained supersaturation. This occurred with 8 of the Meyer et. al. runs, but in 6 of these the condensed plume rose into a cloud layer, which is consistent with the "supersaturation" prediction. We denote this method as the chart method with adiabatic correction, or as "chart $-\Gamma_d$."

It is logical to first test the observed versus predicted maximum rise of the condensed portion of plume, z(max), since this quantity is predicted most directly. For this data, correlation of the models was poor when observed rises less than 120m were included (about 40% of the runs). This may be due to the fact that the source was not a single tower, but was a line of 6 to 8 contiguous, operating towers (the diameter of each tower was 9.5m). At smaller values of z, plume merger is taking place, the geometry of which is sensitive to wind direction and other factors. In effect, merger causes the effective $V_o$ to increase at the same time that V is increasing, so that $V/V_o$ may grow in an erratic fashion. To minimize this effect, the following comparison is made only with observed values of z larger than 120m, with complete merger assumed. In addition, the two runs of lowest wind speed (U=1.0m/sec) are omitted, since $z_{max}$ was greatly overpredicted by all of the methods for these runs. Either the measurements were too low, or the bent-over model is not valid at such a low wind, since the predicted z exceeds x.

Table B-1 - Geometric Standard Deviations of Predicted z(max)÷Observed z(max)

| Method | $V_1$ | $V_2$ | $V_3$ |
|---|---|---|---|
| Hanna | 1.33 | 1.43 | 1.34 |
| Chart | 1.39 | 1.67 | 1.46 |
| Chart $-\Gamma_d$ | 1.25 | 1.34 | 1.31 |

In Table B-1 we see that, regardless of method, the least amount of scatter is obtained using $V=V_1$ (perfect correlation of predicted to observed values corresponds to a geometric standard deviation=G=1.00; percentage standard deviation=$(G^2-1)/(G^2+1)\simeq(G-1)$ for small values of (G-1), but never exceeds 100%). This result is encouraging, since use of $V_1$ keeps the equations relatively simple. We can expect it to be inadequate only for the case of very short plumes (small $V/V_o$), which are usually not of much concern.

Of the methods compared in Table B.1, we see that the one using the psychrometric chart with adiabatic correction works best (here it must be admitted that, in order to save time, I used the observed z to calculate $-\Gamma_d z$ instead of the predicted z; nevertheless, the comparison illustrates the importance of the adiabatic cooling effect). Without the adiabatic cooling correction, the psychrometric chart method works relatively poorly, the simple Hanna method giving less scatter. In six of the runs, the plume entered a cloud layer. The "chart $-\Gamma_d$" method predicts supersaturation for these runs. When these runs are omitted, the geometric scatter for the other methods with either $V_1$ or $V_3$ reduces to 1.31 ± 0.01, leaving only the adiabatic method with $V_1$ slightly superior. Since the adiabatic cooling effect gets larger with larger z, and z ranged from 147 to 360m here, I would conclude that this effect must be included in any model for large sources, say if z>200m. For smaller sources, the Hanna method probably works as well as any.

The best fit for rises > 120m was $z(max)=9.8\ (V_o/U)^{1/2}(\Delta q_o/\Delta q_i)^{1/2}$. If we assume that the required dilution is $V/V_o = P\Delta q_o/\Delta q_i$, where P is a "peak factor," and that plumes are merged so that the initial effluent volume is N times that of a single source (N is the average number of towers in operation, 7.3), substituting $V=V_1$ gives $9.8 = (PN)^{1/2}/\beta'$. For the value of $\beta'$ suggested earlier, 0.4, this data implies that P = 2.1. Here we should note that the Meyer et.al. x(max), and corresponding z(max), were the maximum visible plume lengths.

In order to transform the predicted z(max) to predicted plume length, x(max), we need to invert the relationship for z versus x and substitute. I checked this data against the "2/3 law" for a single source, finding a fair correlation but the median observed rise was 1.85 times that predicted by Eq. (48). There are two effects that tend to cause a higher rise. At smaller distances, the initial momentum effect is significant. To account for it, we rewrite Eq. (47):

$$\Delta h = 1.6F^{1/3}U^{-1}x^{2/3}(1+2F_m U/Fx)^{1/3} \qquad (B\text{-}8)$$

The momentum boost ranged from 4% to 170% in this data, averaging about 20%. The second effect, which is greater at large values of z, is the plume merger effect. For this effect, a very simple model will suffice. We suppose that the plumes rise separately until they abruptly merge when z = Δs, where Δs is the distance between the centers of adjacent sources. Then we multiply all fluxes by the number of sources, N, and replace $V = U\beta^2 z^2$ with $V = U\beta^2 z(z+(N-1)\Delta s)$. Thereafter we find the plume rise larger than that for a single source by the enhancement factor

$$E = \left\{\frac{N+(1/2)(N-1)Z^{-3}}{1+(3/2)(N-1)Z^{-1}}\right\}^{1/3}, \qquad (B\text{-}9)$$

where $Z = \Delta h_1/\Delta s$ and $\Delta h_1$ is the rise calculated for a single source. This formulation is just slightly conservative, by 0 to 6%, compared to the semi-empirical formulation given in Briggs (1974). The combined approach of Eqs. (B-8) and (B-9) are compared to the Meyer et. al. data in Table B.2, omitting the 6 cloud runs and the 2 low wind runs.

Table B.2 - Observed z(max) versus Eq. (B-8) times E

| Number of runs | Median $\Delta h_1/\Delta s$ | E (calculated) | z(calc)÷z(obs) (upper 50%/ lower 50%) |
|---|---|---|---|
| 2 | 3.2 | 1.24 | 1.28 |
| 24 | 8.4 | 1.52 | 0.99(1.35/0.70) |
| 14 | 15.4 | 1.70 | 1.05(1.35/0.86) |

The first two runs are shown separately because they are at x(max) = 25m and the momentum enhancement factor was very large (2.7). The bulk of the observations showed a bimodal distribution in the ratio of calculated to observed rises; the upper and lower modes are shown in parenthesis (7 of the 8 runs with the wind parallel to the towers (within 10°) fall into the lower modes, suggesting that merger is more rapid in such cases). Considering, however, that

the momentum term and the plume merger enhancement effect have never been tested together before and that neither has been tested for cooling tower plumes before, the agreement with data shown in Table B.2 is fairly remarkable.

Overall, the momentum boost and merger effects tend to balance each other in this data. It will simplify calculations of x(max) considerably to use the "2/3 law" times an appropriate mean enhancement factor. The median enhancement due to initial momentum predicted by Eq. (B-8) is 1.17, and the median factor due to merger predicted by Eq. (B-9) is 1.54. Together the predicted rise enhancement would be 1.80, just 3% less than the median observed. Using this and $V = U(\beta' z)^2$, the predicted plume length is

$$x(max) = [N_{eff}^{3/4}/1.8^{3/2}](2/3\beta')^{1/2}(\beta/\beta') (PUV_o)^{3/4} F^{-1/2} (V/V_o)^{3/4}, \qquad (B\text{-}10)$$

where $N_{eff}$ is the effective number of merged plumes. For complete merger and negligible momentum effect, $N_{eff} \to N$, $1.8 \to N^{1/3}$, and $[N_{eff}^{3/4}/1.8^{3/2}] \to N^{1/4}$. For the "chart $-\Gamma_d$" method with the previously estimated P=2.1, the best fit with the present data is obtained with $N_{eff}$=5.5, suggesting less than total merger for many of the runs. Using this same method, the best fit to all z(max), incuding those less than 120m, is obtained with $N_{eff}$=5.7.

Finally, let us compare the scatter of ratios of calculated to observed plume lengths given by a number of different methods. We might start with the comparisons made with the Meyer et. al. data by McVehil and Heikes (1975). They test six different models, showing observed versus predicted x(max)'s in scatter diagrams. They have used Hanna's expression for volume flux, $V_2$, while my calculations are based on $V_1$. When $V_1$ is used, the geometric standard deviation of predicted ÷ calculated x(max) is not affected by the choice of $\beta$, $\beta'$, or P. Table B.3 shows these geometric standard deviations, as well as the median ratio for x(max)>300m÷the median ratio for x(max)<300m. A value of unity is desirable, as this would indicate no systematic error with increasing length.

Table B.3 - Ratios of Calculated to Observed Plume Lengths

| Method | V | Geometric Std. Dev. | Ratio for 1>300m ÷ Ratio for 1<300m |
|---|---|---|---|
| Gaussian + chart | -- | 2.62 | 1.12 |
| Jet + Gaussian | -- | 1.65 | 0.92 |
| Hanna + 2/3 law | $V_2$ | 1.49 | 0.67 |
| Chart + 2/3 law: | | | |
| $\beta$=0.6,$\beta'$=0.5,P=1 | $V_2$ | 1.76 | 1.00 |
| $\beta$=0.9,$\beta'$=0.3,P=1 | $V_2$ | 1.44 | 1.30 |
| $\beta$=$\beta'$=0.55,P=1.86 | $V_2$ | 1.91 | 1.20 |
| Hanna + 2/3 law | $V_1$ | 1.59 | 0.56 |
| Chart + 2/3 law | $V_1$ | 1.56 | 0.64 |
| Chart $-\Gamma_d$ +2/3 law | $V_1$ | 1.42 | 0.93 |

Of those models tried by McVehil and Heikes, obviously the "Gaussian" model, which assumes passive diffusion ($V \propto U\sigma_y\sigma_z$), "bombs out." The one involving P=1.86 does relatively poorly, but the others are more or less competitive with each other; those with higher scatter have less systematic drift. My own calculations, using $V=V_1$ instead of $V_2$, shows a little larger scatter with Hanna's method than do the M&H calculations. The uncorrected chart method with $V_1$ shows just the opposite sense of drift of what it showed using $V_2$. This drift is largely corrected by the adiabatic cooling correction, and the scatter is reduced also.

Meyer et. al. (1974) developed a numerical model based on a more complete plume theory and tested it against the first 6 days of their data. The scatter is small compared with the comparisons (for 16 days) shown in Table B.3. In order to make a comparison on equal footing, we compare this model, the Hanna model with $V=V_1$, and the "chart $-\Gamma_d$" model with $V=V_1$ with the first 6 days' data only. To make it more equal, we must leave out the first and second days, since the "chart $-\Gamma_d$" method gives total undersaturation and total supersaturation, respectively (the first day the plume was extremely short, and the second day it entered a cloud deck). Inclusion of these two days would more than double the scatter of the other two methods. The geometric standard deviation of the 4 remaining days (13 runs) was 1.15, 1.17, and 1.16, respectively. For this limited sample, there appears to be no significant difference in the predictive ability of these three models.

## References


Hanna, S. R. (1972): Rise and condensation of cooling tower plumes, J. Appl. Meteor. 11, 793-799.

Hanna, S. R. (1974): Meteorological effects of the mechanical draft cooling towers of the Oak Ridge Gaseous Diffusion Plant, Cooling Tower Environment-1974 (see under Hanna and Pell, coordinators).

Hanna, S. R. and J. Pell, coordinators (1974): Cooling Tower Environment-1974, CONF-74032, National Technical Information Service, Springfield, Va. 22161.

Kramer, M. L. et. al. (1975): John E. Amos Cooling Tower Flight Program Data: December 1974-March 1975, prepared for American Electric Power Service Corp., P.O. 487, Canton, Ohio 44701 by Smith-Singer Meteorologists, Inc.

Mason, B. J. (1957): The Physics of Clouds, Oxford University Press, London.

McVehil, G. E. and K. E. Heikes (1975): Cooling Tower Plume Modeling and Drift Deposition Measurement, prepared for the ASME by Ball Brother Research Corp., Boulder, Colo.

Meyer, J. H., T. W. Eagles, L. C. Kohlenstein, J. A. Kagan, and W. D. Stanbro (1974): Mechanical draft cooling tower visible plume behavior: measurements, models, predictions. Cooling Tower Environment-1974 (see under Hanna and Pell, coordinators).

Overcamp, T. J. and D. P. Hoult (1971): Precipitation in the wake of cooling towers. Atmos. Environ. 5, 751-765.

Sherlock, R. H. and E. A. Stalker (1941): A study of flow phenomena in the wake of smoke stacks. Engineering Research Bulletin 29, University of Michigan, Ann Arbor.

Weil, J. (1974): The rise of moist, buoyant plumes. J. Appl. Meteor. 13, 435-443.

Wigley, T. M. L. (1975a): Condensation in jets, industrial plumes and cooling tower plumes. J. Appl. Meteor. 14, 78-86.

Wigley, T. M. L. (1975b): A numerical analysis of the effect of condensation on plume rise. J. Appl. Meteor. 14, 1105-1109.

# ASYMPTOTIC SOLUTIONS OF A SIMPLE URBAN DISPERSION MODEL FOR CHEMICAL POLLUTANTS

by

Jose´ J. D'Arruda
Department of Physics
Pembroke State University
Pembroke, N.C. 28372

and

Steven R. Hanna
Air Resources
Atmospheric Turbulence and Diffusion Laboratory
National Oceanic and Atmospheric Administration
Oak Ridge, Tennessee 37830

ATDL Contribution File No. 75/16 .

Abstract

An analytical solution is developed for the set of partial differential equations describing the time rate of change of pollutant concentrations over an urban area, knowing the emissions source strengths, the wind speed, the height of the pollutant cloud, the length of the region, and the chemical kinetics equations. The urban dispersion model described by Hanna (1973) and the chemical kinetics system proposed by Friedlander and Seinfeld (1969) are used as the basis for analysis. The resulting asymptotic solutions are shown to agree to three significant figures with solutions obtained by numerical integration using a high speed digital computer.

## I. Introduction

The object of this paper is to show that one can obtain analytic solutions to the equations generated by a simple urban dispersion model for chemical pollutants. This dispersion model (Hanna, 1973) is an extension of a simple model for chemically inert pollutants (Gifford and Hanna, 1970 and 1971). The model starts out by assuming that the time rate of change of the amount of pollutants within a given volume or box is proportional to the net flux of the pollutant into the volume across its boundaries plus the rate of production or destruction of the pollutant within the volume. It is assumed that the concentration [C] of the pollutants within the volume is uniform, and that the internal production or destruction is due only to chemical reactions. Furthermore, it is assumed in accordance with the basic model that cross-wind variations in any of the parameters are unimportant due to the distributed nature of the source.

If there are n chemical substances in the volume, then the general equations describing the time rate of change of concentration in the volume of height Z and width $\Delta X$ are the following:

$$(Z\Delta X)\partial[c_p]/\partial t = Q_{c_p}\Delta X - ZU[c_p] - {}_m\Sigma\alpha_{pm}[c_p]^{a_{pm}}\left(\prod_{Rpm}[c_j]^{a_{jpm}}\right)Z\Delta X. \qquad (1)$$

when $p = 1, 2, \ldots n$

In equation (1), $Q_c$ ($gm^{-2}s^{-1}$ or $cm^3m^{-2}s^{-1}$) is the source strength, U is the wind speed, and $\alpha_{pm}$ is the rate constant for the chemical

reaction pm. The number Rpm indicates the number of substances other than $c_i$ that are involved in reaction m, and $a_{pm}$ and $a_{jpm}$ are the stoichiometric coefficients for substances $c_p$ and $a_j$ in reaction pm. The first and second terms on the right hand side of these equations represents the flux of pollutants due to the source emissions through the bottom of the box and flux of the pollutants due to advection through the downwind side of the volume, respectively. For simplicity, it is assumed that the wind speed U is constant and there is no flux of pollutant into the box through the upwind side or out of the volume through the top. The symbols Z and $\Delta X$ represent the height and length of the box respectively. The validity of these assumptions was discussed by Hanna [1973].

Equation (1) may be transformed into a simple form by introducing the dimensionless concentrations

$$[c]^* = [c]UZ/(Q_c \Delta X) \tag{2}$$

and the dimensionless time

$$t^* = tU/\Delta X \tag{3}$$

Inserting equations (2) and (3) into (1) we find

$$\partial(\ln[c_p]^*)/\partial t^* = 1/[c_p]^* - 1 - \left[\sum_m \prod_{Rpm} [c_j]^{*a_{jpm}}\right] \left[\alpha_{pm}(\Delta X/U) \prod_{Rpm} \left[Q_{cj}\Delta X/(UZ)\right]^{a_{jpm}} \cdot [c_p]^{*a_{pm}-1} \left[Q_{cp}\Delta X/(UZ)\right]^{a_{pm}-1}\right] \quad (4)$$

Using the set of chemical kinetic equations developed by Friedlander and Seinfeld (1969) to represent the photochemical smog reactions for the pollutants [NO], [$NO_2$] and hydrocarbons of relatively high chemical reactivity [RH], equation (4) becomes

$$\partial(\ln[NO]^*)/\partial t^* = 1/[NO]^* - 1 - [NO_2]^*[RH]^* a_1 \quad (5a)$$

$$\partial(\ln[NO_2]^*)/\partial t^* = 1/[NO_2]^* - 1 + [NO]^*[RH]^* a_2 - [NO_2]^*[RH]^* a_3 \quad (5b)$$

$$\partial(\ln[RH]^*)/\partial t^* = 1/[RH]^* - 1 - [NO_2]^* a_4 - [NO_2]^* a_5/[NO]^* \quad (5b)$$

The five dimensionless parameters, $a_i$, in equations (5) are given by

$$a_1=\alpha Q_{NO_2} Q_{RH} (\Delta X)^3 U^{-3} Z^{-2} \tag{6a}$$

$$a_2=\alpha Q_{NO} Q_{RH} (\Delta X)^3 U^{-3} Z^{-2} \tag{6b}$$

$$a_3=\lambda Q_{NO_2} Q_{RH} (\Delta X)^3 U^{-3} Z^{-2} \tag{6c}$$

$$a_4=\theta Q_{NO_2} (\Delta X)^2 U^{-2} Z^{-1} \tag{6d}$$

$$a_5=\mu Q_{NO_2} \Delta X U^{-1} Q_{NO}^{-1} \tag{6e}$$

where $\alpha$, $\theta$, $\mu$, and $\lambda$ are the rate constants, which for the Friedlander and Seinfeld (1969) reactions are

$\alpha=1.7\times10^{-3}$ ppm$^{-2}$ s$^{-1}$ $\quad$ $\theta=3.3\times10^{-5}$ ppm$^{-1}$ s$^{-1}$

$\mu=4.2\times10^{-6}$ s$^{-1}$ $\quad$ $\lambda=3.3\times10^{-4}$ ppm$^{-2}$ s$^{-1}$

2. Analytical technique

Equations (5) represent a set of 3 coupled non-linear first order differential conditions for the concentrations $[NO_2]^*$, $[NO]^*$ and $[RH]^*$. Numerically, one can solve this system for various $a_i$ values. However, up to now, the only analytic solutions have been for the steady state case. Asymptotic solutions of equations (5) may be obtained for values of $a_i$ which satisfy the condition

$$a_i < 1. \qquad i = 1,2,3,4,5 \tag{7}$$

But since $a_2 \geq a_i$, we may restate condition (7) as

$$a_2 < 1. \tag{8}$$

Physically, this condition means that the time scale for the fastest chemical reaction is greater than the time necessary for advection of air across the box.

When condition (8) is satisfied, we may introduce an ordering parameter $\varepsilon$ into equations (5). The parameter $\varepsilon$ will be set equal to unity at the conclusion of our calculations. Equations (5) then become

$$\partial[NO]^*/\partial t^* = (1-[NO]^*)-\varepsilon[NO]^*[NO_2]^*[RH]^* a_1 \qquad (9a)$$

$$\partial[NO_2]^*/\partial t^* = (1-[NO_2]^*)+\varepsilon[NO]^*[NO_2]^*[RH]^* a_2-\varepsilon([NO_2]^*)^2[RH]^* a_3 \qquad (9b)$$

$$\partial[RH]^*/\partial t^* = (1-[RH]^*)-\varepsilon[NO_2]^*[RH]^* a_4-\varepsilon[NO_2]^*[RH]^* a_5/[NO]^* \qquad (9c)$$

We now assume that equations (9) possess asymptotic solutions of the form

$$[NO]^* = \sum_n \varepsilon^n \psi_n \qquad (10a)$$

$$[NO_2]^* = \sum_m \varepsilon^n \phi_n \qquad (10b)$$

$$[RH]^* = \sum_j \varepsilon^j \eta_j \qquad (10c)$$

Introducing the above set of solutions into equations (9), grouping and setting to zero each coefficient of $\varepsilon$ independently in the usual way, we find

$$\partial\psi_n/\partial t^* + \psi_n = \delta_{n,0}+Q_{n-1}a_1 \qquad (11)$$

where $n = 0,1,2,\ldots$ and $Q_{-1} = 0$.

In equation (11), $\delta_{n,0} = \begin{cases} 1, n=0 \\ 0, n\neq 0 \end{cases}$ and

$$Q_R = \sum_{n+p=R} \psi_n d_p \tag{12}$$

where

$$d_p = \sum_{m+j=p} \phi_m \eta_j . \tag{13}$$

For equation (9b) we find

$$\partial\phi_n/\partial t^* + \phi_n = \delta_{n,0} + a_2 R_{n-1} - a_3 P_{n-1} \tag{14}$$

where $n = 0,1,2 \ldots$ and $R_{-1} = P_{-1} = 0$.

In equation (14)

$$R_R = \sum_{m+p=R} \phi_m b_p \tag{15}$$

$$b_p = \sum_{n+j=p} \psi_n \eta_j \tag{16}$$

$$P_R = \sum_{m+p=R} \phi_n \ell_p \tag{17}$$

$$l_p = \sum_{n+j=p} \phi_n \eta_j . \tag{18}$$

Finally, equation (9c) becomes

$$\partial \eta_n / \partial t^* + \eta_n = \delta_{n,0} - a_4 M_{n-1} - a_5 N_{n-1} \tag{19}$$

for n=0,1,2... and $M_{-1}=N_{-1}=0$.

In equation (19),

$$M_R = \sum_{m+j=R} \phi_m \eta_j \tag{20}$$

and the N's are obtained implicitly from the equation

$$y_m = N_0 \psi_m + N_1 \psi_{m-1} \cdots N_{m-1} \psi_1 + N_m \psi_0 \tag{21}$$

where

$$y_R = \sum_{m+j=R} \phi_m \eta_j \tag{22}$$

The first order solutions to equations (9) are now obtained by setting n=0 in equations (11), (14), and (19). There are

$$\partial\left(\psi_o e^{t^*}\right)/\partial t^* = e^{t^*} \tag{23}$$

$$\partial\left(\phi_o e^{t^*}\right)/\partial t^* = e^{t^*} \tag{24}$$

$$\partial\left(\eta_o e^{t^*}\right)/\partial t^* = e^{t^*} \tag{25}$$

which have the solutions

$$\psi_o = 1 + k_1 e^{-t^*} \tag{26}$$

$$\phi_o = 1 + k_2 e^{-t^*} \tag{27}$$

$$\eta_o = 1 + k_3 e^{-t^*} \tag{28}$$

where $k_1$, $k_2$, and $k_3$ are constants to be determined by the initial condition.

We shall choose the initial dimensionless concentration of all pollutants equal to unity, i.e.

$$[NO]_o^* = [NO_2]_o^* = [RH]_o^* = 1 \quad \text{for } t=0. \tag{29}$$

One way of satisfying these initial conditions is to choose

$$(\psi_o)_o = (\phi_o)_o = (\eta_o)_o = 1 \quad \text{at } t=0 \tag{30}$$

and

$$(\psi_n)_o = (\phi_n)_o = (\eta_n)_o = 0 \quad \text{for } t=0 \text{ and } n>0. \tag{31}$$

Using condition (30), equation (26), (27) and (28) become

$$\psi_o=1 \tag{32a}$$

$$\phi_o=1 \tag{32b}$$

$$\eta_o=1 \tag{32c}$$

Setting n=1 in equations (11), (14), and (19) gives the contribution of terms of $0(\varepsilon)$ to the solutions of equations (9)

$$\partial\left(\psi_1 e^{t^*}\right)/\partial t^* = (a_1\psi_o\phi_o\eta_o)e^{t^*} \tag{33}$$

$$\partial\left(\phi_1 e^{t^*}\right)/\partial t^* = (a_2\phi_o\psi_o\eta_o - a_3\phi_o^2\eta_o)e^{t^*} \tag{34}$$

$$\partial\left(\eta_1 e^{t^*}\right)/\partial t^* = -(a_4\psi_o\eta_o + a_5\phi_o\eta_o\psi_o^{-1})e^{t^*} \tag{35}$$

Using the zero order result as given in equation (32) and imposing the initial condition (31), the solutions of equation (33), (34), and (35) are

$$\psi_1 = R[1-e^{-t^*}] \tag{36a}$$

$$\phi_1 = S[1-e^{-t^*}] \tag{36b}$$

$$\eta_1 = T[1-e^{-t^*}] \tag{36c}$$

where

$$R = -a_1$$

$$S = a_2 - a_3$$

$$T = -a_4 - a_5$$

In a similar fashion for the n=2 term we find

$$\psi_2 = P[1-e^{-t^*}(1+t^*)] \tag{37a}$$

$$\phi_2 = L[1-e^{-t^*}(1+t^*)] \tag{37b}$$

$$\eta_2 = M[1-e^{-t^*}(1+t^*)] \tag{37c}$$

where

$$P = R(R + S + T)$$

$$L = a_2(R + S + T) - a_3(2S + T)$$

$$M = (S + T)T + a_5 R.$$

for the n=3 term, we have

$$\psi_3 = Z'[1-e^{-t^*}(1 + t^* + \frac{t^{*2}}{2})] + Y[1-e^{-t^*}(2t^* + e^{-t^*})] \quad (38a)$$

$$\phi_3 = U'[1-e^{-t^*}(1 + t^* + \frac{t^{*2}}{2})] + V[1-e^{-t^*}(2t^* + e^{-t^*})] \quad (38b)$$

$$\eta_3 = G[1-e^{-t^*}(1 + t^* + \frac{t^{*2}}{2})] + H[1-e^{-t^*}(2t^* + e^{-t^*})] \quad (38c)$$

where

$$Z' = -a_1(P + L + M)$$

$$Y = -a_1(RS + ST + RT)$$

$$U' = a_2[L + P + M] - a_3[2L - M]$$

$$V = a_2[RS + ST + RT] - a_3[2TS + S^2]$$

$$G = T[L + M] + a_5 P$$

$$H = ST^2 - a_5 R(R - S - T).$$

As it can be seen, one may continue in this manner computing the contribution of terms of higher order in $\varepsilon$ to the solution.

Introducing equations (32), (36), (37), and (38) into equation (10), we obtain the asymptotic solutions.

$$[NO]^* = 1 - \varepsilon a_1(1-e^{-t^*}) + \varepsilon^2 P(1-e^{-t^*}[1 + t^*]) + \varepsilon^3 Z'[1-e^{-t^*}(1 + t^* + t^{*2}/2)] + \varepsilon^3 Y[1-e^{-t^*}(2t^* + e^{-t^*})] + \theta(\varepsilon^4) \quad (39)$$

$$[NO_2]^* = 1 + \varepsilon S[1-e^{-t^*}] + \varepsilon^2 L[1-e^{-t^*}(1 + t^*)] + \varepsilon^3 U'[1-e^{-t^*}(1 + t^* + t^{*2}/2)] + \varepsilon^3 V[1-e^{-t^*}(2t^* + e^{-t^*})] + \theta(\varepsilon^4) \quad (40)$$

$$[RH]^* = 1 + \varepsilon T(1-e^{-t^*}) + \varepsilon^2 M(1-e^{-t^*}[1 + t^*]) + \varepsilon^3 G[1-e^{-t^*}( 1 + t^* + t^{*2}/2)] + \varepsilon^3 H[1-e^{-t^*}(2t^* + e^{-t^*})] + \theta(\varepsilon^4) \quad (41)$$

Equations (39), (40) and (41) represent asymptotic solutions to the set of equations (9) which satisfy initial conditions (30), (31) and are valid for $a_2 < 1$.

3. Application of Analytical Techniques

In this section we compare the results of equation (39), (40), and (41) for $\varepsilon = 1$ with those obtained through numerical solutions of equation (5), using observations of emissions and wind speed in Los Angeles. The results of equations (39), (40) and (41) were obtained using a hand calculator for various values of $a_i$. The values of $a_i$ are related to the wind speed, source strength and dimensions of the box as given by equation (6). Assuming the following relations for the source strength, as given by Hanna (1973),

$$Q_{NO} = 0.3Q_{RH} \tag{42}$$

$$Q_{NO_2} = 0.2Q_{RH} \tag{43}$$

it is possible to write the parameters in equation (6) in the simple forms

$$a_1 = 3.3X10^{-4}Q_{RH}^2 A^3 Z/U^{-3} \tag{44a}$$

$$a_2 = 1.5\, a_1 \tag{44b}$$

$$a_3 = 0.2\, a_1 \tag{44c}$$

$$a_4 = 0.02\ a_1 UA^{-1} Q_{RH}^{-1} \tag{44d}$$

$$a_5 = 2.8 \times 10^{-6} AZU^{-1} \tag{44e}$$

where the parameter A is defined by

$$A = \Delta X/Z \tag{45}$$

For our comparisons, we chose the following three cases:

CASE 1:
A = 200
Z = 150
U = 3.0
$a_2$ = .55

CASE 2:
A = 50
Z = 150
U = 1.0
$a_2$ = .23

CASE 3:
A = 200
Z = 200
U = 3.0
$a_2$ = .74

TABLE 1

Values of the dimesionless concentrations $[NO]^*$, $[NO_2]^*$, and $[RH]^*$ as a function of dimensionless time, as determined from the analytical solution. $[NO]^* = [NO]U/(AQ_{NO})$; $t^* = tU/\Delta X$.

| Dimensionless Time $t^*$ | $[NO]^*$ | $[NO_2]^*$ | $[RH]^*$ |
|---|---|---|---|
| | CASE 1 | | |
| 0.1 | .965 | 1.045 | .995 |
| 0.2 | .933 | 1.086 | .990 |
| 0.3 | .904 | 1.122 | .986 |
| 0.4 | .878 | 1.154 | .981 |
| 0.5 | .855 | 1.182 | .977 |
| 0.6 | .834 | 1.207 | .973 |
| 0.7 | .816 | 1.228 | .969 |
| 0.8 | .799 | 1.247 | .966 |
| 0.9 | .785 | 1.263 | .962 |
| 1.0 | .772 | 1.276 | .959 |
| | CASE 2 | | |
| 0.1 | .985 | 1.019 | .997 |
| 0.2 | .972 | 1.037 | .994 |
| 0.3 | .960 | 1.052 | .991 |
| 0.4 | .949 | 1.066 | .988 |
| 0.5 | .939 | 1.079 | .986 |
| 0.6 | .930 | 1.090 | .984 |
| 0.7 | .922 | 1.100 | .982 |
| 0.8 | .914 | 1.109 | .980 |
| 0.9 | .908 | 1.117 | .978 |
| 1.0 | .902 | 1.124 | .976 |
| | CASE 3 | | |
| 0.1 | .953 | 1.060 | .993 |
| 0.2 | .911 | 1.114 | .987 |
| 0.3 | .872 | 1.161 | .980 |
| 0.4 | .838 | 1.202 | .974 |
| 0.5 | .808 | 1.238 | .968 |
| 0.6 | .781 | 1.268 | .962 |
| 0.7 | .758 | 1.293 | .957 |
| 0.8 | .738 | 1.315 | .951 |
| 0.9 | .720 | 1.332 | .946 |
| 1.0 | .705 | 1.346 | .941 |

The results are given in Table 1 below. The results of the numerical calculations made using an IBM 360/91 computer are not listed in Table 1, because in all cases the numerical results are within .002 of the analytical results. In most cases the numerical and analytical results agree to three significant figures.

## 4. Conclusions

We have presented an analytic technique which enables us to generate asymptotic solutions to equation (5). Evaluation of the resulting expressions, which requires only a hand calculator, gives excellent agreement with the numerical solutions.

Although we have demonstrated this method using a very specific set of reactions, namely the Friedlander and Seinfeld kinetic equations, the theory is general and is valid for other reaction schemes as well. It can be easily extended to more complex reaction systems.

ACKNOWLEDGMENTS:

The senior author would like to thank both the Oak Ridge Associated University and the Atmospheric Turbulence and Diffusion Laboratory for making this work possible. This work was performed under an agreement between the National Atmospheric and Oceanic Administration and the Energy Research and Development Administration.

## REFERENCES


Friedlander, S. K. and Seinfeld, J. H. (1969): A Dynamic Model of Photochemical Smog. Envir. Sci. Technol. 3, 1175-1181.

Gifford, F. A., Jr. and Hanna, S. R. (1970): Urban Air Pollution Modeling. Proceedings of the Second International Clean Air Congress, (H. England and W. Beery, eds.), 1146-1151.

Hanna, S. R. (1971): A simple Method of Calculating Dispersion from Urban Area Sources. J. Air Poll. Control Ass. 21, 774-777.

Hanna, S. R. (1973): A Simple Dispersion Model for the Analysis of Chemically Reactive Pollutants. Atmospheric Environment, 7, 803-817.

ATDL-75/17

# Environmental Research Laboratories

Air Resources
Atmospheric Turbulence and Diffusion Laboratory

Oak Ridge, Tennessee

September 1975

# 1974 ANNUAL REPORT

U. S. DEPARTMENT OF COMMERCE
NATIONAL OCEANIC AND ATMOSPHERIC ADMINISTRATION

# THE DISTRIBUTION OF SOLAR RADIATION WITHIN A DECIDUOUS FOREST [1,2]

Boyd A. Hutchison and Detlef R. Matt
Atmospheric Turbulence and Diffusion Laboratory
NOAA, P. O. Box E, Oak Ridge, Tennessee 37830



[1]Research supported in part by the Eastern Deciduous Forest Biome, US-IBP, funded by the National Science Foundation under Interagency Agreement AG-199, BMS69-01147 A09 with the U. S. Energy Research and Development Administration, Oak Ridge National Laboratory, and in part by the Division of Biomedical and Environmental Research, U. S. Energy Research and Development Administration.

[2]Contribution No. ___, Eastern Deciduous Forest Biome, US-IBP. ATDL Contribution File No. 75/18.

(WITHDRAWN)

Published in ORNL Chemistry Division Annual Report
October 1, 1975

# CHEMISTRY OF SULFUR IN THE ATMOSPHERE[1]

C. F. Baes, Jr. J. T. Holdeman[2]
W. M. Culkowski[3]

Industrially produced sulfur enters the atmosphere in reactive forms, primarily $SO_2$ and $SO_3$, that should not be treated as inert pollutants for purposes of modeling. Since June of 1974 an effort has been under way to describe the equilibrium and kinetic aspects of sulfur chemistry in a form suitable for inclusion in the atmospheric transport model (ATM) being developed at ORNL.[4]

At the usual low concentrations of $SO_2$ in the atmosphere (typically $10^{-8}$ atm), it reacts with water only if condensed water already is present, producing the dissolved species $H^+$, $SO_2(aq)$, $HSO_3^-$, and $SO_3^{2-}$. In contrast, $SO_3$ reacts vigorously and completely with either gaseous or liquid water to produce acid droplets containing the additional species $HSO_4^-$ and $SO_4^{2-}$. These droplets can be partially or completely neutralized by atmospheric $NH_3$, the end product being solid particles of $(NH_4)_2SO_4$ or, if the relative humidity exceeds ~80%, droplets of ammonium sulfate.

A computer program has been written which--given the total concentrations of S(IV), S(VI), $NH_3$, and $CO_2$, along with the relative humidity and the temperature--calculates the amount and composition of aerosol and the equilibrium partial pressure of the gases. Such a detailed calculation is made possible by the availability of accurate thermodynamic data[5] for all the species involved. The calculation also includes estimates of the activity coefficients of the aqueous ions[6] needed to correct for the non-ideal behavior of the solutions involved and to estimate the aqueous vapor pressure.

The program next calculates the rate of oxidation of S(IV) to S(VI) in the atmosphere, which can occur by several mechanisms. Recently, Castleman *et al*[7]



ATDL Contribution File No. 75/19

and Davis and Klauber[8] have concluded that the most rapid reaction involving a gaseous oxidant is that with the OH radical.

$$SO_2(g) + OH \rightarrow \text{products}$$

With concentrations of OH radical (an intermediate in other reactions) in the range 0.1 to $6 \times 10^7$ molecules/cm$^3$ (0.4 to $24 \cdot 10^{-13}$ atm)[9], the half time of reaction of $SO_2$ should be in the range 16 days to 7 hrs. Of the reactions that occur in solution, the oxidation of $HSO_3^-$ by ozone may be the fastest,[10]

$$HSO_3^- + O_3(aq) \rightarrow SO_4^{2-} + H^+ + O_2(aq) \quad .$$

With an atmospheric concentration of ozone of $10^{-7}$ atm, we estimate a half time of 2 min for the reaction of $HSO_3^-$ in solution. With the composition of a specified atmospheric system known in detail at a given instant from the equilibrium calculation, it is a simple matter to calculate and sum the instantaneous rates of S(IV) oxidation by these kinetic pathways, as well as others which have been proposed.

A set of time-dependent differential equations that relate the atmospheric concentration of the various components to the instantaneous rate is then integrated by the Runga-Kutta method. The program in its present form (SULCAL) calculates the composition of the aerosol and the partial pressure of $SO_2$ in a power-plant plume as a function of the distance downwind from the source.

References


1. Work performed for the Ecology and Analysis of Trace Contaminants (EATC) Program supported by the National Science Foundation. This work was previously described in ORNL-NSF-EATC-11, Dec. 1974, pp. 22-24.
2. Member of Computer Sciences Division.
3. Atmospheric Turbulence and Diffusion Laboratory (ATDL), Oak Ridge, TN.
4. M. T. Mills and M. Reeves, "A Multi-Source Atmospheric Transport Model for Deposition of Trace Contaminants," ORNL-NSF-EATC-2 (1973).
5. Selected Values of Chemical Thermodynamic Properties, NBS Technical Note 270-3, 1968.
6. Activity coefficients of ions and the osmotic coefficient in mixtures principally of $H_2SO_4$ and $(NH_4)_2SO_4$ were estimated from: (1) known solubilities of $(NH_4)_2SO_4$ in $H_2O$-$H_2SO_4$, (2) known osmotic coefficients of $H_2SO_4$ and of $(NH_4)_2SO_4$ solutions, and (3) known dissociation quotients of $HSO_4^-$ in $H_2SO_4$ solutions.
7. A. W. Castleman, Jr., R. E. Davis, H. R. Munkelwitz, I. N. Tang, and William P. Wood, "Kinetics of Association Reactions Pertaining to $H_2SO_4$ Aerosol Formation," in Intnational J. of Chemical Kinetics, Chem. Kinetics Symposium No. 1, S. W. Benson, D. N.Golden, and J. R. Baker, Eds., Interscience, New York, 1975, p. 543.
8. D. D. Davis and G. Klauber, "Atmospheric Gas-Phase Oxidation Mechanism for the Molecule $SO_2$," in Intnational J. of Chemical Kinetics, Chem. Kinetics Symposium No. 1, S. W. Benson, D. N. Golden and J. R. Baker, Eds., Interscience, New York, 1975, p. 629.


(continued)

References (Cont'd)

9. C. C. Wang, L. I. Davis, Jr., C. H. Wu, S. Japar, H. Niki, and B. Weinstock, Science, 189, 797 (1975).

10. S. A. Penkett, Nature-Physical Science 240, 105 (1972).

*Atmospheric Environment* Vol. 10, pp. 563–569. Pergamon Press 1976. Printed in Great Britain.

# DISCUSSIONS

## A SIMPLE MODEL TO CALCULATE THE $SO_2$-CONCENTRATIONS IN URBAN REGIONS*

The study by Goumans and Clarenburg (1975) is an excellent example of the results that can be got by using a simple urban pollution model, as we have proposed; see for example Gifford and Hanna (1970), and Hanna (1971). In fact their model and ours are identical apart from minor notational differences; their $Q/ab$ equals our $Q$, their $n_z$ equals $(1 - b)$, and their $C_z$ is $\sqrt{2}a$ in our notation. It is encouraging to see that these new data from Amsterdam and Hague support our conclusion, that simple models are adequate for many urban pollution problems.

*NOAA/ATDL*
*Oak Ridge,*
*Tennessee, TN U.S.A.*

F. A. GIFFORD
S. R. HANNA

REFERENCES

Gifford F. A. and Hanna S. R. (1970) Urban air pollution modeling. *Proc. 2nd Int. Clean Air Congress*, pp. 1146–1151.

Hanna S. R. (1971) Simple methods of calculating dispersion from urban area sources. *J. Air Pollut. Control Ass.* **21,** 774–777.

---

* GOUMANS H. H. J. M. and CLARENBERG L. A. (1975) *Atmospheric Environment* **9,** 1071–1077.

## AUTHOR'S REPLY

We certainly agree with the comment of Gifford and Hanna that the model we derived to calculate pollution concentrations in urban regions (equation 6 in our paper) is apart from some notational differences identical to the model they used.

However, we would like to point out that by using equation (2) in our paper one cannot only calculate the pollution concentrations in urban regions, but also the concentration patterns in larger regions with very great changes in source strength.

As can be easily shown it is not permissible to neglect the effect of the error function and gamma function in these cases.

*Rijnmond Authority,*
*Vasteland* 96,
*Rotterdam,*
*The Netherlands*

H. H. J. M. GOUMANS

# PREDICTED AND OBSERVED COOLING TOWER PLUME RISE AND VISIBLE PLUME LENGTH AT THE JOHN E. AMOS POWER PLANT

by

Steven R. Hanna

Air Resources
Atmospheric Turbulence and Diffusion Laboratory
National Oceanic and Atmospheric Administration
Oak Ridge, Tennessee 37830

June, 1976

ATDL Contribution File No. 75/21.

(Accepted for publication in Atmospheric Environment.)

## ABSTRACT

A one-dimensional numerical cloud growth model and several empirical models for plume rise and cloud growth are compared with twenty seven sets of observations of cooling tower plumes from the 2900 MW John E. Amos power plant in West Virginia. The three natural draft cooling towers are 200m apart. In a cross wind, the plumes begin to merge at a distance of about 500m downwind. In calm conditions, with reduced entrainment, the plumes often do not merge until heights of 1000m. The average plume rise, 750m, is predicted well by the models, but day-to-day variations are simulated with a correlation coefficient of about .5. Model predictions of visible plume length agree, on the average, with observations for visible plumes of short to moderate length (less than about 1km). The prediction of longer plumes is hampered by our lack of knowledge of plume spreading after the plumes level off. Cloud water concentrations predicted by the numerical model agree with those measured in natural cumulus clouds (about .1g/kg to 1g/kg).

## 1. Introduction

In the assessment of atmospheric effects of energy centers, a crucial problem is the calculation of visible plume and cloud growth caused by emissions from cooling towers. At a power plant, for example, cooling towers emit as much as twice the energy generated for electricity. Typically, more than half of this "waste" energy is in the form of latent heat. Many current power plants use from one to four large natural draft cooling towers, which have the following physical characteristics:

| | |
|---|---|
| top diameter: | ~70m |
| height: | ~150m |
| vertical plume speed: | ~5m/sec |
| difference between plume and ambient T; | ~20°C |

Some power plants use mechanical draft cooling towers, which rely on fans to force the air flow and are not as tall (a typical height is 20 or 30m). Arrays of mechanical draft towers have historically been built in lines, but recent construction includes disc and doughnut shaped systems.

Proposed energy centers, if constructed, will dissipate about 100,000MW of waste heat from a surface area of about $100km^2$. Energy fluxes of this magnitude put energy centers on the same scale as large geophysical phenomena such as bushfires, volcanoes, and thunderstorms (Hanna and Gifford, 1975). Clearly it is very important that we study the possible environmental effects of energy centers before they are built, in order to determine the spacing, tower type, and so on, that will minimize environmental impact.

Unfortunately, the models and observations necessary for these assessments do not exist. The state of art of this area of research is summarized in the conference proceedings entitled Cooling Tower Environment - 1974 and in the critical review by McVehil and Heikes (1975). A few models for estimating visible plume are presented in these publications, but there is very little discussion of cloud growth models. The only published attempts at modeling the cloud physics processes in cooling tower plumes are so-called "one-dimensional models", where plume parameters are a function only of height, as reported by EG&G (1971) and Hanna (1971). In both of these models, Weinstein's (1970) cloud growth model is used as a basis.

In determining the atmospheric effects of energy centers, it is reasonable to begin with simple one dimensional models. Then, after the capabilities of these models are assessed, the research can proceed to two or three dimensional models. The model by Hanna (1971) was revived, encouraged by recent developments in the area of aircraft measurements of cooling tower plumes. For example, M. Wolf (1976), of Battelle Pacific Northwest Laboratory, is using an aircraft-mounted cloud droplet spectrometer to measure water drop characteristics in cooling tower plumes

at the Rancho Seco Plant in California. Norman et al. (1975) of Penn State University are making a nearly complete series of cloud physics and turbulence measurements from their aircraft at the Keystone, Pa., cooling towers. Similar measurements are being made by Woffinden et al. (1976) of Meteorology Research, Inc. as part of the Chalk Point Project.

The observations that are used to test our model were obtained by Kramer et al. (1975) at the John E. Amos, West Virginia, power plant of the American Electric Power Service Corporation. Observations were made on 54 separate occasions during the winter of 1974-1975, aiming for periods when the plume would be as long as possible. Ambient profiles of temperature, dew point, and wind speed were obtained by aircraft; and many photographs of the plume were taken. These measurements are particularly valuable, since in many cases the visible plume obviously extended beyond the point of maximum plume rise, and therefore final plume rise could be obtained. Unfortunately, no in-plume observations were made.

The Amos measurements were analyzed statistically by Brennan et al. (1976), who found very little relationship between plume rise and wind speed, but a good relationship between plume rise and haze layer or inversion height. It is expected that the relationship with haze layer height will deteriorate for measurements made during the warmer seasons of the year, when the haze layer is much deeper.

## 2. Numerical Model Description

The numerical model has been constructed so that it agrees with known relationships for the rise of buoyant stack plumes at small heights and the growth of natural continental cumulus clouds at large heights. It is based on theories of plume rise developed by Briggs (1969), cloud growth developed by Weinstein (1970), and cloud microphysics developed by Kessler (1969). Since the model is one-dimensional (i.e., plume parameters are a function of height only), it cannot be expected to portray cloud growth as well as two or three dimensional models which account for cross-plume gradients. But one-dimensional models have been shown to work quite well for stack plumes and for many cumulus clouds, and are a necessary first step in the analysis of atmospheric effects of energy centers.

The framework of this model was first reported by Hanna (1971), but testing of the model had to wait until sufficient observations of cooling tower plumes were made. A few modifications to the 1971 model were made, based on recent developments in plume rise theory. The first change reflects a suggestion by Briggs (1975) which resolves the paradox that, for a given entrainment rate for bent over plumes, the final plume rise and the rate of change of plume radius with height cannot simultaneously agree with observations. This problem is solved using the knowledge that the rate of

change of the momentum flux with height depends partly on the fact that ambient air above the rising plume must also be accelerated. The effective radius of the "momentum plume" is therefore larger than the radius as determined from temperature differences. Briggs finds that agreement with observations is reached when the following relations are used:

$$\text{For bent over plumes:} \begin{cases} \partial R_m/\partial z = .6 \text{ (momentum plume)} & (1) \\ \partial R_t/\partial z = .4 \text{ (temperature plume)} & (2) \end{cases}$$

where $R_m$ is the radius of the momentum plume and $R_t$ is the radius of the temperature plume. Consequently the ratio, $E_m$, of the effective momentum flux to the momentum flux within the temperature plume approaches $(.6/.4)^2$, or 2.25.

The second modification to the model reflects observations by Slawson et al. (1974) and Meyer et al (1974), that visible plume lengths are consistently underpredicted by basic plume models, due to the fact that inhomogeneities in the plume can result in locally saturated spots, even though the plume is unsaturated on the average. Meyer et al (1974) resolve this problem through the use of a peak factor, explaining that: "it was simply assumed that the excess water-vapor content at the plume center is higher than the average excess water-vapor content predicted in the plume by an empirically

determined constant that is referred to as the peak factor." They suggest that the peak factor equals 1.86. Briggs (1975) has reanalyzed their data and other data, and finds that the peak factor equals 2.0. This factor is incorporated into the present model by assuming that the ratio, $E_w$, of the cross-sectional area of the moisture plume to the temperature plume approaches 1/2. In terms of the rate of change of the radius with height, this assumption can be written:

$$\partial R_w/\partial z = .71\ \partial R_t/\partial z, \tag{3}$$

where $R_w$ is the radius of the moisture plume. Note that the constant .71 is the inverse of the square root of the peak factor. Equation (3) applies to both vertical and bent over plumes.

The third modification to the model accounts for the stretching of the plume as it rises through layers of wind shear. In order to maintain continuity in the volume flux, the term $(R_t/2U)\ \partial U/\partial z$ is subtracted from the right hand side of equation (1). Since the wind shear is usually positive in the boundary layer, the rate of growth of the plume radius is not as great as it would be in a region of constant wind speed. Murthy (1970) gives solutions to the plume rise equations for a wind profile which satisfies a power law.

The final basic modification to the model is made to account for merging of multiple cooling tower plumes. This states simply that, when the radius of the plume equals one half of the distance between the centers of the towers, the plumes merge and the cross-sectional area of the single merged plume equals the cross-sectional areas of the two or more individual plumes at the time of the merger.

Photographs of the Amos plumes in the report by Kramer et al. (1975) suggest that for bent-over plumes, merger begins at a distance of 300 to 500m downwind. For vertical plumes, where entrainment is less, merger does not begin until heights of 500 to 1000m are reached. It is also interesting that the observed plumes in calm conditions do not constrict, as predicted by plume rise theory, but in all cases steadily increase their radius as height increases. From the plume photographs, it appears that the plume diameter doubles or triples after it rises one tower height (150m).

The following equations are used in the model:

Equation of Motion:

$$\partial(w^2/2)/\partial z=(g/E_m)[(T_p(1 + .61E_wQ_p)-T_e(1 + Q_e))/(T_p(1 + .61E_wQ_p)) -E_w(Q_c + Q_h)]-(O_m w^2/R_m) \quad (4)$$

where w(m/s) is the vertical speed, g($m/s^2$) is the acceleration of gravity, T(°K) is temperature, and the Q's (g/g) are specific water densities. The entrainment coefficient for the momentum plume, $O_m$, is defined by $(1/V)dV/dz = O_m/R_m$, where the volume flux, V, equals $UR_m^2$ for a bent over plume and $wR_m^2$ for a vertical plume. Subscripts p, e, c, and h refer to plume variables, environmental variables, cloud water content, and hydrometeor water content, respectively. The term on the left is the vertical acceleration of the plume. The terms on the right are the buoyancy force and the drag or entrainment force.

Equation for Temperature Change:

$$\partial T_p/\partial z = \{-(LE_w/c_p)\partial Q_{ps}/\partial z\} - g/c_p - O(T_p - T_e)/R + \{(L_i E_w/c_p)(Q_h + Q_c)/\Delta z\}$$
$$- \{(LE_w/c_p)O_w(Q_p - Q_e)/R_w\} \qquad (5)$$

The terms in curly brackets apply only when the plume is saturated. The subscript s refers to a saturated variable. The parameters L(j/g), $L_i$(j/g), and $c_p$(j/g°K) are the latent heats for vapor-water and water-ice transitions, and the specific heat of air at constant pressure. The entrainment rates O and $O_w$ refer to the temperature and water plumes, respectively. $\Delta z$ is the height increment of the numerical integration. The terms on the right are the heat gained due to condensation, the heat lost due to dry adiabatic expansion, the entrainment rate or heat required to warm entrained air, the heat gained due to freezing of liquid water, and the heat lost as liquid water is evaporated in order to saturate the entrained air. A term suggested by Weinstein (1970) which accounts for the evaporation of liquid water at the plume's edge, was originally included in equation (5). Since the contribution of this term was found to be insignificant, it was removed from the equation.

Equation for Water Vapor Change:

Unsaturated $\partial Q_p/\partial z = -O_w(Q_p - Q_e)/R_w$ (6)

Saturated $\partial Q_p/\partial z = \partial Q_{ps}/\partial z$ (7)

In equation (6), for an unsaturated plume, $Q_p$ changes only because of entrainment. In equation (7), for a saturated plume, the loss is due to condensation of liquid water in the rising plume.

Equation for Cloudwater Change:

$$\partial Q_c/\partial z = -\partial Q_{ps}/\partial z - 10^{-3}(Q_c - .0005)/w - .00522 Q_c (1000 Q_h)^{.875}/w - O_w(Q_p + Q_c - Q_e)/R_w \quad (8)$$

The first term on the right hand side is the gain due to condensation in the rising plume. The second and third terms are losses due to conversion and coalescence of cloudwater into hydrometeor water (after Kessler, 1969). The last term is a decrease due to entrainment. Note that cloud water is used first to saturate the entrained air.

Equation for Hydrometeor Water Change:

$$\partial Q_h/\partial z = 10^{-3}(Q_c-.0005)/w + .00522Q_c(1000Q_h)^{.875}/w-4.5Q_h(1000Q_h)^{.125}/(w R_w \cdot \cos(\arctan(w/U)))-O_w Q_h/R_w + K_2/\Delta z \quad (9)$$

Terms one and two are the gains due to conversion and coalescence of cloudwater into hydrometeor water. Term three is the loss due to rainout. Term four is the decrease due to entrainment. The last term ($K_2$), required because of the finite height steps taken by the computer, is the saturation deficit of the plume if all of the cloud water has been evaporated into the entrained air after a given height increment, $\Delta z$, but the entrained air after a given height increment, $\Delta z$, but the entrained air is still not saturated. Then if all of the hydrometeor water is evaporated after a given height increment and the entrained air is still not saturated, the whole plume must become unsaturated.

Entrainment:

Vertical Plume:

$$O_m = O = .15 \qquad O_w = .107$$

$$\partial R_m/\partial z = \partial R/\partial z = .15-R(g/T_p)(T_p-T_e)/2w^2$$

$$\partial R_w/\partial z = .71\partial R/\partial z \quad (10)$$

Bent Over Plume:

$$O_w = .57 \qquad O = .8 \qquad O_m = 1.2$$

$$\partial R/\partial z = .4-(R/2U)\partial U/\partial z \quad (11)$$

$$\partial R_w/\partial z = .71\partial R/\partial z$$

$$\partial R_m/\partial z = 1.5\partial R/\partial z$$

The entrainment relations are based on Briggs (1975) latest guidelines. They are in rough agreement with Cotton's (1975) review of entrainment rates used in cumulus cloud models. He finds that various investigators use entrainment coefficients, 0, ranging from zero to unity, depending on which value gives predicted cloud heights in agreement with a particular set of observations.

The entrainment formulas for bent over plumes are used when the local wind speed, U, exceeds 1 m/s. Consequently, the entrainment constants may switch from those appropriate for bent over plumes to those appropriate for vertical plumes at different heights in the same run.

Saturation Specific Humidity:

a) $T_1 = 273.16°K<T<373°K$

$$\ln Q_{ps} = 2.303(10.79574(1-T_1/T) + 1.50475\times10^{-4}(1-10^{-8.2969(T/T_1-1)}) + .42873\times10^{-3}(10^{4.76955(1-T_1/T)}-1)) - 5.028 \ln T/T_1 - \ln p + 1.335 \quad (12)$$

b) $T<T_1 = 273.16°K$

$$\ln Q_{ps} = 2.303(-9.09685(T_1/T-1) + .87682(1-T/T_1)) - 3.56654 \ln T_1/T - \ln p + 1.335 \quad (13)$$

where p is pressure in millibars, calculated by means of the hydrostatic equation. These two empirical equations are the "Goff-Gratch" formulas, as given by the World Meteorological Organization (1966). Any equation relating T and $Q_{ps}$, such as the Clausius-Clapeyron equation, could be used in place of equations (12) and (13).

Equations (12) and (13) are plotted in Figure 1, for p = 1000mb, forming the psychrometric curve which is the basis of several published methods for determining the vapor content and temperature of plumes (e.g., Wigley and Slawson, 1971). The technique is illustrated by plotting the initial saturated plume position ($T_{po}$,$Q_{po}$) and the unsaturated environment position ($T_e$,$Q_e$). Depending on the relative amounts of plume air and environment air in the resulting mixture, the rising plume can be predicted to be somewhere along the line between these two points. However, if the resulting mixing ratio, $Q_{pl}$, is greater than the saturation mixing ratio, $Q_{pls}(T_{pl})$, then some of the water vapor must condense, and the actual position ($T'_{pl}$,$Q'_{pl}$) is approached. The slope of the dotted line, $\Delta Q/\Delta T$, or $c_p/L$ equals -.8 on this figure. If there were no initial liquid water, then the concentration of liquid water at position ($T'_{pl}$,$Q'_{pl}$) would be ($Q_{pl}-Q'_{pl}$). The end of the visible plume is the point at which the straight line crosses the curved line near the bottom of figure 1.

Unfortunately, the psychrometric technique is not so handy for plumes from natural draft cooling towers, which rise several hundred meters. The saturation curve shifts as height (i.e., pressure) changes. Furthermore, the environmental position ($T_e$, $Q_e$) may vary considerably over the depth of the plume. It is still possible to use the psychrometric chart for a well-mixed adiabatic environment (see Briggs, 1975) where the straight line in Figure 1 can be shifted uniformly to the left by the amount $zg/c_p$ in order to account for temperature changes with height. The psychrometric chart technique has been applied most successfully to short plumes from mechanical draft cooling towers (see McVehil and Heikes, 1975).

Equations (1) through (13) are a complete set, and are solved on a high-speed digital computer using height steps of .01m, .1m, and 1m for heights less than 10m, between 10 and 100m, and above 100m, respectively. As may be expected, the possibility of a phase change requires detailed logical steps in the computer program. For example, if the calculated vapor content $Q_p$ happens to be greater than the saturated vapor content $Q_{ps}$ after a single height step is taken, it is necessary to condense some of the excess vapor. The condensation takes place in such a way that the energy released by condensation just balances the heat gained due to a temperature increase.

Several of the parameterizations in this model are based on measurements in natural clouds rather than cooling tower clouds. For example, rainout is included in the program (eq. 9, term 3), using a mechanism suggested by Simpson and Wiggert (1969). This mechanism is based on the assumption that the relative rate of loss of hydrometeor water in a given time interval is proportional to the distance that the water drops would fall in that interval, divided by the vertical component of the plume radius. Because this relation was first developed for large cumulus clouds, it is questionable whether the rainfall rates that it yields in our application are realistic. Unfortunately, there are not yet sufficient observations in cooling tower plumes to derive empirical relationships for cloud physics processes. Some of this information is beginning to come from the Penn State program (Norman et al, 1975), but much more needs to be done.

3. Input Data

All of the observation periods were during the winter of 1974-1975, and were deliberately chosen by Kramer et al (1975) so that a long visible plume would be present. Low temperatures, high relative humidities, low wind speeds and stable conditions all increase the chances of a long visible plume. The first two conditions lower the saturation deficit (saturated water vapor content minus actual water vapor content, or $(Q_{es}-Q_e)$) of the ambient air, while the last two conditions increase the concentration of excess water in the plume. During a run, the aircraft would obtain vertical profiles of dry bulb temperature, dew point, and wind speed in the lowest 2000m. Several photographs of the plume were taken, and the visible plume height and length were noted. At the same time, power plant personnel provided information on the net load of the three cooling towers. These data have been summarized in a very complete fashion, including drawings of the visible plume, by Kramer et al (1975). About half of the runs could not be used in this study, because of problems such as the disappearence of the plume in a cloud deck or insufficient ambient profile data. Of the 27 runs which are analyzed, seven have bent over plumes in which the visible plume does not extend to the point

of maximum plume rise, seven have vertical plumes, and 13 have bent over plumes in which the visible plume does extend to the point of maximum plume rise.

The three cooling towers at the Amos plant have the characteristics listed in Table 1.

Table 1

Specifications for Amos Cooling Towers (from Kramer et al (1975)

| | height | top radius | $w_o$ | Capacity |
|---|---|---|---|---|
| Towers 1 & 2 | 132m | 29m | 4.6m/s | 800MW(each) |
| Tower 3 | 150m | 40m | 4.2m/s | 1300MW |

The towers are in a line, spaced 200m apart. During the observation periods, the plant ran close to its generating capacity of 2900MW. The initial heat flux used in the model is modified based on the actual energy output for each observation period. Also, prior to plume merger (which is assumed to occur when plume radius equals ½ tower spacing, or 100m), only the plume from tower 3 is modeled. The initial plume radius, $R_o$, is taken as 40m, and the initial plume vertical speed, $w_o$, is assumed to be 4.4m/s (the average over the towers).

The initial plume temperature is estimated by an empirical relation derived from the specifications in Kramer et al. (1975):

$$T_{po} = (297.4 + .635(T_d - 273))(1 + .01(1-RH)), \qquad (14)$$

where $T_d$ and RH are the ambient dew point and relative humidity. Since the Amos plant does not always operate at full capacity, the ratio of actual to full power is also input for each run. This ratio is used to revise the plume temperature calculated by equation (14) by assuming that the actual difference between the plume and environment temperatures equals the power ratio times the temperature difference calculated using equation (14). These assumptions were not tested, since no measurements of initial plume temperature were made at the Amos plant.

To insure continuity of the momentum flux, the effective initial plume radius for bent over plumes is calculated from the equation (Hanna, 1972):

$$R_{eff} = R_o(w_o/U)^{1/2} \qquad (15)$$

The mixing ratio of the initial cloud water, $Q_c$, and hydrometeor water, $Q_h$, are also required as input to the model. Both have arbitrarily been set equal to .001, on the basis that fog or cloud is obviously present at the tower mouth; and the sum of the two, .002g/g, is typical for vigorous natural cumulus clouds (Fletcher, 1962). If the plume evaporates, however, buoyancy will be reduced slightly due to the energy that must be taken from the air to evaporate the liquid drops. For example, if the initial liquid water content, .002g/g, were to evaporate at the tower mouth, plume temperature would be reduced by $(L/c_p)(.002g/g)$, or 5°C.

Because of the possibility that errors would be introduced by the arbitrary specification of $Q_c$ and $Q_h$, a sensitivity test was run in which $Q_c$ (which equals $Q_h$) was set equal to .00001, .0001, .001, and .01 g/g. It was found that, when the visible plume is large and a cloud forms in its upper reaches, the initial values of $Q_c$ and $Q_h$ have little effect on final plume rise and cloud water concentration. But for dry ambient conditions when the plume evaporates at a height of about 50m, the initial values of $Q_c$ and $Q_h$ can have a significant effect on plume length and plume rise. The results of running the model for an isothermal ambient atmosphere (10°C) with 50% relative humidity are given in Table 2.

Table 2

Model Output for Isothermal Atmosphere (10°C)

with 50% RH and U = 10m/s.

| Initial $Q_h$ and $Q_c$ (g/g) | Plume Rise (m) | Visible Plume Height (m) | Visible Plume Length (m) | $Q_c$ at max | z(m) |
|---|---|---|---|---|---|
| .00001 | 249 | 52 | 165 | .00057 | 15 |
| .0001 | 248 | 52 | 165 | .00063 | 15 |
| .001 | 232 | 67 | 230 | .00129 | 10 |
| .01 | 138 | 138 | 610 | .01000 | 0 |

It is seen from this table that when the initial $Q_c$ equals $10^{-5}$ or $10^{-4}$, plume parameters are not significantly affected. But when $Q_c$ equals $10^{-3}$, the value used in analyzing the Amos data, plume rise decreases by 7% and visible plume height increases by 29% above that for plumes which begin with essentially no liquid water. When $Q_c$ equals $10^{-2}$, which is a concentration at least an order of magnitude greater than that observed in natural clouds, plume rise is nearly halved and the plume is visible through its point of maximum rise. It can be concluded that the possibility of errors in our choice of initial $Q_h$ and $Q_c$ introduces an uncertainty of about 10 to 20% in calculations of visible plume length for plumes on dry days, but has little effect for plumes on humid or cold days, when the initial liquid water never has a chance to evaporate.

There is not room here to include all of the 27 sets of Amos data used in this analysis. But as an example of the input data, the observations by Kramer et al. (1975) during run 6 are listed in Table 3. These data were used to generate the output in Figure 2, which is discussed in a later section.

Table 3

Observations at John E. Amos power plant (Kramer et al., 1975), for 18 Dec. 1974 (Run 6).

| Height Above Tower (m) | Ambient Dry Bulb °K | Ambient Dew Point °K | Wind Speed m/s |
|---|---|---|---|
| 0 | 268.0 | 266.9 | |
| 122 | 266.9 | 266.9 | 9 |
| 243 | 265.2 | 265.2 | |
| 365 | 264.1 | 264.1 | |
| 426 | 263.6 | 263.6 | |
| 578 | 263.0 | 263.0 | |
| 700 | 262.4 | 262.4 | |
| 821 | 261.9 | 261.9 | |
| 942 | 260.8 | 260.8 | |
| 1064 | 259.7 | 259.7 | |
| 1186 | 259.1 | 259.1 | 12 |

Ratio of actual power to maximum power = .83
Initial plume temperature (from equation 14) = 290°K
Observed plume rise = 850m
Observed visible plume length = 9.6km

## 4. Results

The computer model was run for each of the 27 test cases, and values of total plume rise and visible plume height and length were noted. Also, some simple formulas for estimating plume rise and visible plume parameters were tested.

### 4.1 Final plume rise

In nineteen of the observation periods analyzed, the visible plume extends through the point of maximum plume rise. The average wind speed and vertical potential temperature gradient through the layer in which plume rise took place are given in Table 4. In addition, the saturation deficit in the ambient air at the tower top is given. The observed plume rise listed in the table refers to the final equilibrium height of the plume centerline. All heights are in meters above the tower top.

In column five of the table, the height of the base of the lowest significant inversion in the temperature sounding is given. This height might also be called the mixing height. For the observations when an inversion is present, the average inversion height is 820m and the average observed plume height is 790m. The correlation coefficient between inversion height and observed plume height is .90. This good agreement has led Brennan et al. (1976),

Table 4

Observed and Calculated Plume Rise

| Run | $\bar{U}$ (m/s) | Ambient tower top saturation deficit (g/kg) | $\Delta\theta/\Delta Z$ over depth of plume (°C/mx10$^3$) | Inversion height above tower (m) | Observed plume rise (m) | Model plume rise (m) | Analytical Plume rise sensible one unit (m) | Analytical Plume rise sensible + latent all units (m) | $E_N$ applied to sensible one unit (m) |
|---|---|---|---|---|---|---|---|---|---|
| 1 | 14 | .43 | 13.5 | | 560 | 260 | 250 | 450 | 270 |
| 6 | 11 | .13 | 3.0 | | 850 | 820 | 430 | 770 | 490 |
| 8a | 9 | 0 | 9.8 | | 370 | 350 | 250 | 450 | 270 |
| 10a | 5 | .60 | 2.1 | 720 | 820 | 820 | 590 | 1060 | 700 |
| 11 | 0 | 1.34 | 6.1 | 660 | 880 | 900 | 980 | 1500 | |
| 12 | 6 | 1.25 | 1.2 | 1140 | 1060 | 1200 | 720 | 1280 | 870 |
| 15 | 3 | .28 | 10.7 | | 1120 | 790 | 780 | 1200 | |
| 16 | 6 | .41 | 7.2 | 1200 | 1160 | 700 | 380 | 680 | 430 |
| 17a | 8 | .29 | 6.7 | 360 | 360 | 430 | 410 | 730 | 460 |
| 18 | 6 | .78 | 5.6 | | 910 | 720 | 410 | 730 | 460 |
| 19 | 0 | 1.07 | 6.9 | 840 | 800 | 970 | 910 | 1400 | |
| 24 | 6 | .60 | 4.0 | 750 | 760 | 630 | 500 | 900 | 580 |
| 28a | 5 | .52 | 21.8 | | 360 | 400 | 310 | 570 | 340 |
| 31 | 0 | 1.02 | 11.6 | | 500 | 900 | 780 | 1200 | |
| 35a | 3 | .87 | 9.8 | 390 | 360 | 590 | 480 | 880 | 550 |
| 44 | 8 | 1.16 | 1.9 | 960 | 910 | 420 | 510 | 910 | 590 |
| 45 | 7 | 1.16 | 5.6 | 1200 | 910 | 370 | 390 | 700 | 440 |
| 47 | 0 | 1.44 | 3.8 | 900 | 800 | 1020 | 910 | 1400 | |
| 48a | 7 | 1.46 | 7.6 | 750 | 670 | 360 | 340 | 610 | 380 |
| Avg. | 5.6 | .76 | 7.4 | 820 | 750 | 670 | 540 | 920 | |

in an independent assessment of these observations, to conclude that, when an inversion lid is present, the plume will rise to this lid and stop. The inversion lids are formed by the natural buoyant and mechanical mixing actions in the boundary layer. Apparently the energy fluxes in the cooling tower plumes are similar to those in natural convective elements during the winter in West Virginia, and the plumes, like the natural convective elements, rise to the base of the inversion lid. But since these inversion layers are often shallow and weak, it is difficult to measure them accurately with the aircraft probe. Consequently, the detailed structure of the inversion lid cannot be included in the numerical plume and cloud growth model. During the summer, when the height of the inversion layer is greatly increased due to the increased surface heat fluxes, the cooling tower plume is less likely to reach the top of the mixed layer.

The output of a typical computer run is given in Figure 2, based on the input data in Table 3. A slight change in curvature of the predicted $\Delta T$, w, and $Q_c$ profiles is evident at a height of about 200m. This is the height at which the three plumes merge in this run, and the buoyancy flux increases by

a factor of about 2.3. Since the ambient atmosphere in this run is nearly saturated pseudoadiabatic, the plume rises quite high and contains a moderate amount of cloud water through its entire trajectory.

The estimates of plume rise from the numerical model for each run are in column 7 of Table 4. The difference between average observed (750m) and estimated (670m) plume rise is about 12%. The correlation coefficient is .49, which can be considered fair. The observed and predicted plume rises are plotted in Figure 3.

Maximum cloud water concentration, $Q_c$, predicted by the numerical model ranges from .0010 to .0016 g/g, in agreement with typical values reported by Fletcher (1962) for natural cumulus clouds. Unfortunately, the aircraft did not obtain any measurements of liquid water concentrations for comparison with these predictions.

The last three columns in Table 4 contain analytical estimates of plume rise. The formulas suggested by Briggs (1969)

for plume rise, H, are used:

$$H = 5.0F^{1/4}s^{-3/8} \qquad \text{Vertical} \qquad (16)$$

$$H = 2.9(F/Us)^{1/3} \qquad \text{Bent-over} \qquad (17)$$

where the buoyancy flux, F, and stability parameter, s, are defined by the relations:

$$F = w_o R_o^2 (g/T_{vpo})(T_{vpo} - T_{veo}) \qquad (18)$$

$$s = (g/T_{eo})(\partial\theta_e/\partial z) \qquad (19)$$

In these relations the subscript v refers to virtual temperature. If the sensible heat from a single tower unit is used in estimating the buoyancy flux, F, then the estimated plume rises in column 8 of Table 4 are obtained. The average estimated plume rise is 540m, or 28% lower than observed. The correlation coefficient between estimated and observed plume rise is .37. One reason for this low correlation is that average temperature gradients are used in calculating the stability parameter, s. The effects of small inversion layers are smoothed out by the analytic technique, but have a great influence on the observed plumes.

Note that the correlation between estimates of the analytical and numerical models is .82. In otherwords, the numerical model is not much different from or better than the simple analytical model for estimating plume rise.

Another estimate of plume rise can be obtained by redefining the buoyancy parameter to include the latent heat (Hanna, 1972):

$$F = w_o R_o^2 g[(T_{vpo}-T_{veo})/T_{vpo} + (L/c_p T_{vp})(Q_{po}-Q_{eo})] \qquad (20)$$

If the sensible plus latent fluxes from the three cooling towers are added together to form F, the predictions are obtained which are listed in column 9 of Table 4. The average plume rise using the maximum F is 920m, or 23% greater than observed. Clearly the actual effective buoyancy flux is somewhere between the sensible flux from a single tower and the total heat fluxes from all towers.

The empirical technique suggested by Briggs (1974) for estimating the plume rise from multiple sources was also applied, and the results are in the last column of Table 4. He derived his formula from observations of plume rise from multiple stacks at TVA power plants. The plume rise from N stacks equals the plume rise from a single stack, H, multiplied by an enhancement factor, $E_N$, defined by:

$$E_N = ((N + S)/(1 + S))^{1/3}$$

where $$S = ((N-1)\,\Delta x/N^{1/3}H)^{3/2}$$

The distance $\Delta x$ is the spacing between towers, which equals 200m at Amos. It is seen from the last column of Table 4 that the enhancement factor for these data, assuming that H is the plume rise due to sensible heat only from a single tower, ranges from 1.08 to 1.21. This additional rise brings the magnitudes of the plume rise estimates closer to the observations, but does not increase the correlation coefficient.

4.2 Visible plume dimensions

In addition to the runs analyzed above, there were also seven runs in which the visible plume was moderately long but did not extend through the point of maximum plume rise. Since visible plume length is not well defined for plumes occurring in calm conditions, analysis will be limited to the bent over cases. Observed visible plume lengths are obtained using the photographs published by Kramer et al. (1975) for the short plumes in Table 5, and from aircraft observers' notes supplied by Conte (private letter, 1975) for the longer plumes in Table 6. The aircraft observers' notes were not used for the shorter plumes because the accuracy of the visible plume length listed by the aircraft observers is ±¼ mile.

Table 5

Visible Plume Dimensions for Plumes whose Visible Portion

does not Reach the Point of Maximum Rise

| Run | $\bar{U}$ (m/s) | ambient saturation deficit (g/Kg) | | observed | | numerical model | | analytical model | | ambient RH at plume level |
|---|---|---|---|---|---|---|---|---|---|---|
| | | tower top | plume level | visible plume height (m) | visible plume length (m) | visible plume height (m) | visible plume length (m) | visible plume height (m) | visible plume length (m) | |
| 2 | 13 | 3.0 | 3.9 | 100 | 200 | 75 | 290 | 100 | 370 | .4 |
| 3 | 10 | 2.6 | 2.7 | 150 | 500 | 120 | 350 | 140 | 400 | .65 |
| 13 | 10 | .86 | 1.8 | 100 | 300 | 150 | 480 | 210 | 730 | .6 |
| 20 | 10 | 2.8 | 3.9 | 200 | 400 | 70 | 250 | 120 | 290 | .45 |
| 27 | 20 | 1.5 | 2.0 | 390 | 600 | 120 | 450 | 110 | 800 | .55 |
| 39 | 15 | 2.9 | 3.6 | 240 | 450 | 140 | 240 | 100 | 430 | .45 |
| 41 | 16 | 3.5 | 3.2 | 50 | 300 | 55 | 290 | 80 | 360 | .35 |
| Avg. | 13 | 2.5 | 3.0 | 180 | 390 | 100 | 340 | 120 | 450 | .50 |

Table 6

Visible Plume Dimensions for Plumes where the Visible Plume Extends through the Point of Maximum Rise

| Run | $\bar{U}$ (m/s) | ambient tower top saturation deficit g/kg | saturation deficit at plume elev. g/kg | observed visible plume length (m) | ambient RH at plume level |
|---|---|---|---|---|---|
| 1 | 14 | .43 | 2.2 | 1600 | .4 |
| 6 | 11 | .13 | 0 | 9600 | 1. |
| 8a | 9 | 0 | .65 | 4800 | .9 |
| 10a | 5 | .60 | 0 | 25600 | 1. |
| 12 | 6 | 1.2 | 0 | 4800+ | 1. |
| 16 | 6 | .41 | 1.3 | 2400 | .8 |
| 17a | 8 | .29 | .29 | 8000 | .9 |
| 18 | 6 | .78 | 1.1 | 1600 | .7 |
| 21 | 9 | .43 | 1.8 | 1600 | .6 |
| 24 | 6 | .60 | .55 | 16000+ | .85 |
| 44 | 8 | 1.2 | .29 | 9000 | .9 |
| 45 | 7 | 1.2 | 1.5 | 1600 | .6 |
| 48a | 7 | 1.5 | 1.2 | 32000+ | .8 |
| Avg. | 8 | .67 | .84 | 4800m (median) | .80 |

In Table 5 the observed relative humidity, wind speed, visible plume height and length, and ambient saturation deficits at tower top and plume height are given for the set of plumes of moderate length. The average visible plume height and length predicted by the numerical model are seen to agree with the average of the observations fairly well. But the correlation between variations in observed and predicted lengths is poor. This poor correlation can be explained by the fact that weather conditions (U, T, $\Delta Q$, RH) are quite similar for each of the runs in Table 5, and consequently we are dealing with comparatively small differences among fairly large numbers. It can be concluded that, for wind speeds of about 13 m/s and saturation deficits of about 3g/kg, visible plume length at the Amos Plant is about 400m.

The results of a simple analytical model suggested by Hanna (1974) are given in columns nine and ten of Table 5. Formulas for visible plume height, h, and length, $\ell$, of bent over plumes are based in this model on the hypothesis that the tip of the visible plume occurs when the initial flux of excess water, $V_o Q_{po}$, in the plume just balances the saturation deficit flux, $V(Q_{eos}-Q_{eo})$:

$$h = 2R_o(w_o/U)^{1/2}[(2Q_{po}/(Q_{eos}-Q_{eo}))^{1/2}-1] \qquad (23)$$

$$\ell = 1.4(R_o^{3/2}U^{3/4}w_o^{3/4}/F^{1/2})[(2Q_{po}/Q_{eos}-Q_{eo}))^{1/2}-1]^{3/2} \qquad (24)$$

Note the occurrence of the peak factor, set equal to 2, inside the brackets of these equations. As expected, the analytical predictions of h and $\ell$ agree fairly well with the predictions of the numerical model, but offer no significant improvement in accounting for the variability of the observed parameters.

Observations and predictions for the longer plumes are in Table 6. Note that for these longer plumes, extending beyond the point of maximum plume rise, average saturation deficit has dropped to .7 g/kg, average wind speed has dropped to 8 m/s, and average relative humidity increased to 80%, when compared with the shorter plumes in Table 5. The plus sign after three of the observed visible plume lengths indicates that the plume merged with existing clouds at that distance.

In Figure 4, observed plume length is plotted versus (1-RH) for all the observations in Tables 5 and 6. The ambient relative humidity at plume height is used for RH. The correlation coefficient is -.58 for these data. The line on the figure is given by the formula

$$\ell = (2.15 \times 10^4 \text{m}) e^{-7.6(1-RH)} \qquad (25)$$

and is valid only for the Amos location during the winter. During the summer, when a given relative humidity implies a much larger saturation deficit, the line in Figure 4 can be expected to shift downwards considerable.

It is expected that the chances for a long plume would increase as wind speed, U, decreases and as saturation deficit, $Q_{es}-Q_e$, decreases. This relationship is tested in Figure 5, where observed plume length is plotted versus $U(Q_{es}-Q_e)$. The saturation deficit is measured at plume level. If the data followed by a + are not included, then the correlation coefficient is -.51.

The analytical model, equation (24), was not applied to the data in Table 6 because there is no information available on the increase in radius of cooling tower plumes after they have leveled off. Gifford (1975) reports TVA data on the observed spread of stack plumes, but they have a much smaller initial size and less plume rise than cooling tower plumes. Since most of the Amos plumes analyzed here terminate in stable layers, the passive diffusion should be very slight. This question cannot be satisfactorily resolved until further measurements are made.

## 6. Acknowledgements

This work was performed under an agreement between the National Oceanic and Atmospheric Administration and the Energy Research and Development Administration. Discussions with G. A. Briggs were very helpful. I would not have been able to obtain the observations so quickly without the assistance of M. E. Smith, P. T. Brennan, M. L. Kramer, and J. J. Conte of Smith-Singer Meteorologists, Inc. and D. L. Mazzitti of the American Electric Power Service Corporation. V. Quinn of the Air Resources Laboratory in Las Vegas contributed many valuable suggestions in his review of this manuscript.

## REFERENCES


Brennan P. T., Seymour D.E., Butler M.J., Kramer M. L., Smith M.E., and Frankenburg T. T. (1976) The observed rise of visible plumes from hyperbolic natural draft cooling towers. Atmos. Environ., in press.

Briggs G. A. (1969) Plume Rise. AEC Critical Review Series, TID-25075 from Clearinghouse for Fed. Scient. and Tech. Inf., U.S. Dept. of Comm., Springfield, Va., 82 pp.

Briggs G. A. (1974) Plume rise from multiple sources, in Cooling Tower Environment-1974, National Technical Information Service, U. S. Department of Commerce, Springfield, VA., 22161, 161-179.

Briggs G. A. (1975) Plume rise predictions. Lectures on Air Pollution and Environmental Impact Analyses. American Meteorol. Soc., 45 Beacon St., Boston, Mass., 59-111.

Cooling Tower Environment-1974, ERDA Symposium Series, CONF-740302, Nat. Tech. Information Service, U. S. Dept. of Commerce, Springfield, Va., 22161, ($13.60), 638 pp.

Cotton W. R. (1975) Theoretical cumulus dynamics. Reviews of Geophysics and Space Physics, 13, 419-447.

E. G. & G., Inc. (1971) Potential environmental modifications produced by large evaporative cooling towers, prepared for Water Quality Office, EPA, Cont. no. 14-12-542 by E. G. & G. Environmental Services Operation, Boulder, Colo., 75 pp.

Fletcher N. H. (1962) The Physics of Rainclouds. Cambridge Univ. Press, London, 386 pp.

Gifford F. A. (1975) Turbulent diffusion typing schemes: a review. Nuclear Safety, 17, 68-86.

Hanna S. R. (1971) Meteorological effects of cooling tower plumes. presented at Cooling Tower Inst. Meeting, Houston, 25 Jan., 17 pp., available as report no. 48 from ATDL, P.O. Box E, Oak Ridge, Tenn., 37830.

Hanna S. R. (1972) Rise and condensation of large cooling tower plumes. J. Appl. Meteorol., 11, 793-799.

Hanna S. R. (1974) Meteorological effects of the mechanical draft cooling towers of the Oak Ridge Gaseous Diffusion Plant, in Cooling Tower Environment-1974, ERDA Symposium Series, CONF-740302, Nat. Tech. Information Service, U.S. Dept. of Commerce, Springfield, Va., 22161, ($13.60), pp 291-306.

Hanna S. R. and Gifford F. A. (1975) Meteorological Effects of Energy Dissipation at Large Power Parks, Bull. Am. Meteorol. Soc., 56, 1069-1076.

Kessler E. (1969) On the Distribution and Continuity of Water Substance in Atmospheric Circulations Meteorol. Monographs, 10, 84 + ixpp, published by the Am. Meteorol. Soc, 45 Beacon St., Boston.

Kramer M.L., Seymour D. E., Butler M. J., Kempton R. N., Brennan P. J., Conte J. J. and Thomson R. G. (1975) John E. Amos Cooling Tower Flight Program Data, December 1974-March 1975, by Smith-Singer Meteorologists, Inc., 134 Broadway, Amityville, N.Y., 11701 for American Electric Power Service Corp., P.O. Box 487, Canton, Ohio, 44701.

McVehil G. E. and Heikes K. E. (1975) Cooling Tower Plume Modeling and Drift Measurement. A Review of the State-of-the-Art, prepared for ASME (Contract G-131-1) by Aerospace Division, Ball Brothers Research Corporation, Boulder, Colorado, 80302.

Meyer J. H., Eagles T. W., Kohlenstein L. C., Kagan J. A., and Stanbro W. D. (1974) Mechanical draft cooling tower visible plume behavior: measurements, models, predictions, in Cooling Tower Environment-1974, ERDA Symposium Series, CONF-740302 Nat. Tech. Information Service, U. S. Dept. of Commerce, Springfield, Va., 22161, ($13.60), 307-352.

Murthy C. R. (1970) On the mean path of a buoyant chimney plume in non-uniform wind. J. Appl. Meteorol., 9, 603-611.

Norman J. M., Thomson D. W., Pena J., and Miller R. (1975) Aircraft turbulence and drift water measurements in evaporative cooling tower plumes. Dept. of Meteorol., Penn. State Univ., University Park, PA., 16802.

Simpson J. and Wiggert V. (1970) Models of precipitating cumulus towers. Mon. Wea. Rev., 97, 471-489.

Slawson P. R., Coleman J. H., and Frey J. W. (1974) Some observations on cooling-tower plume behavior at the Paradise Steam Plant, in Cooling Tower Environment-1974, ERDA Symposium Series, CONF-740302, Nat. Tech. Information Service, U.S. Dept. of Commerce, Springfield, Va., 22161, ($13.60), 147-160.

Wigley T.M.L. and Slawson P. R. (1971) On the condensation of buoyant, moist, bent-over plumes. J. Appl. Meteorol., 10, 259-263.

Weinstein A. I. (1970) A numerical model of cumulus dynamics and microphysics. J. Atmos. Sci., 27, 246-255.

Woffinden, G. J., Anderson, J. A., and Harrison, P. R. (1976) Aircraft Survey, Chalk Point Cooling Tower Plume, Dec. 1975, Rept. no. 76R-1910 by MRI, Altadena, Calif. 91001 for the Md. Power Plant Siting Program. 32 pp + appendices.

Wolf, M. A., (1976) Natural draft cooling tower plume characteristics determined with airborne instrumentation. Pac. Northwest Lab. Annual Rep. for 1975 to the USERDA DBER. Part 3 Atmospheric Sciences, BNWL-2000 PT3, 281-288.

World Meteorol. Org., 1966: International Meteorological Tables, WMO-188-TP-94, introd. to tables 4.6 and 4.7.

Figure 1: Psychrometric chart, from eqs. (12) and (13). As an example, the initial plume ($T_{po}$, $Q_{po}$) is mixed with a uniform environment ($T_e$, $Q_e$). If $Q_{pl}$ is greater than $Q_{pls}(T_{pl})$, condensation must occur.

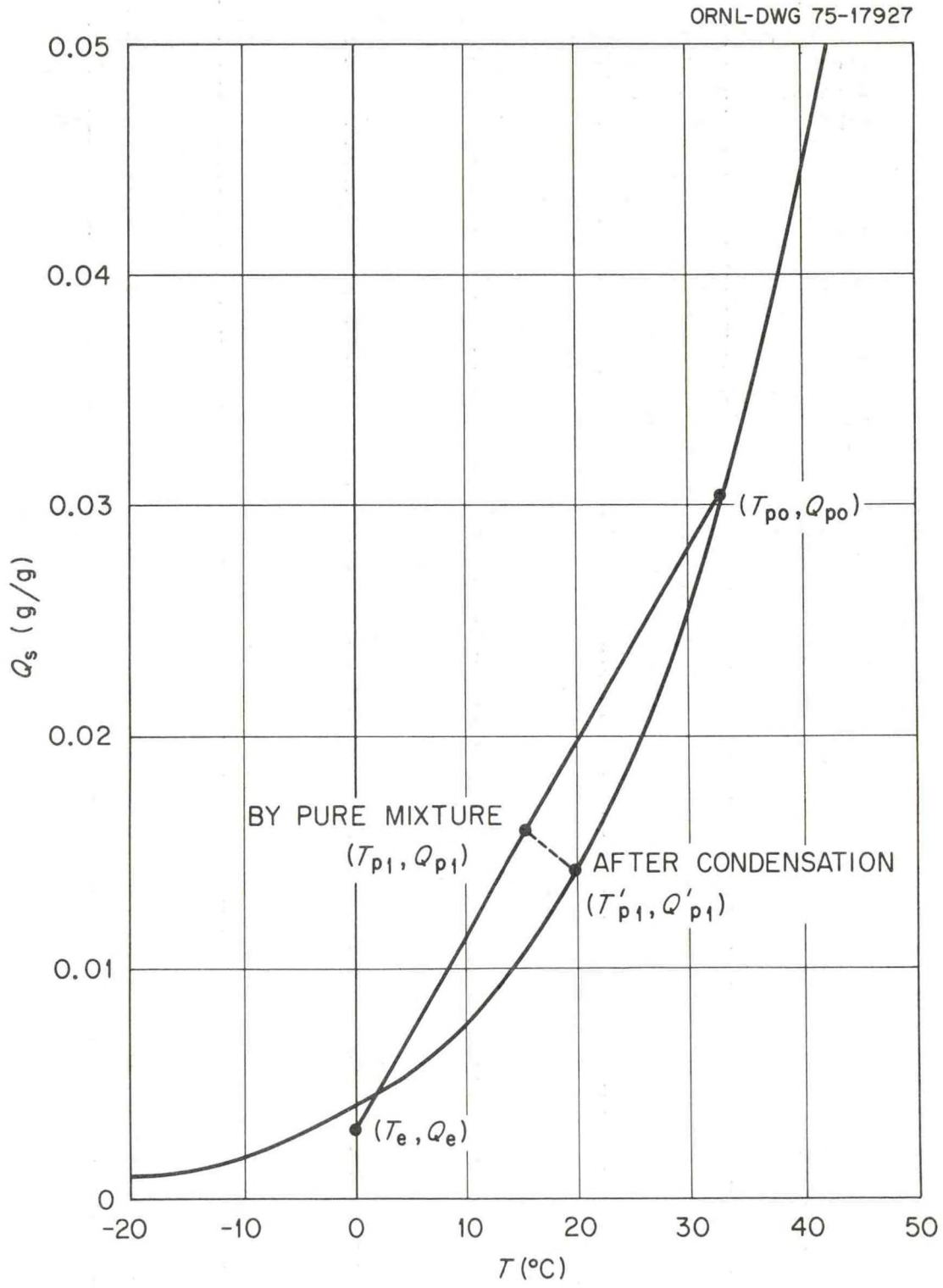

Figure 2: Numerical model output for run 6. Ambient conditions: $\bar{U}$ = 11m/s, $T_{eo}$ = 268°K, $\partial\theta_e/\partial z$ = 3°C/1000m, RH∿100%. The complete sounding is given in Table 3.

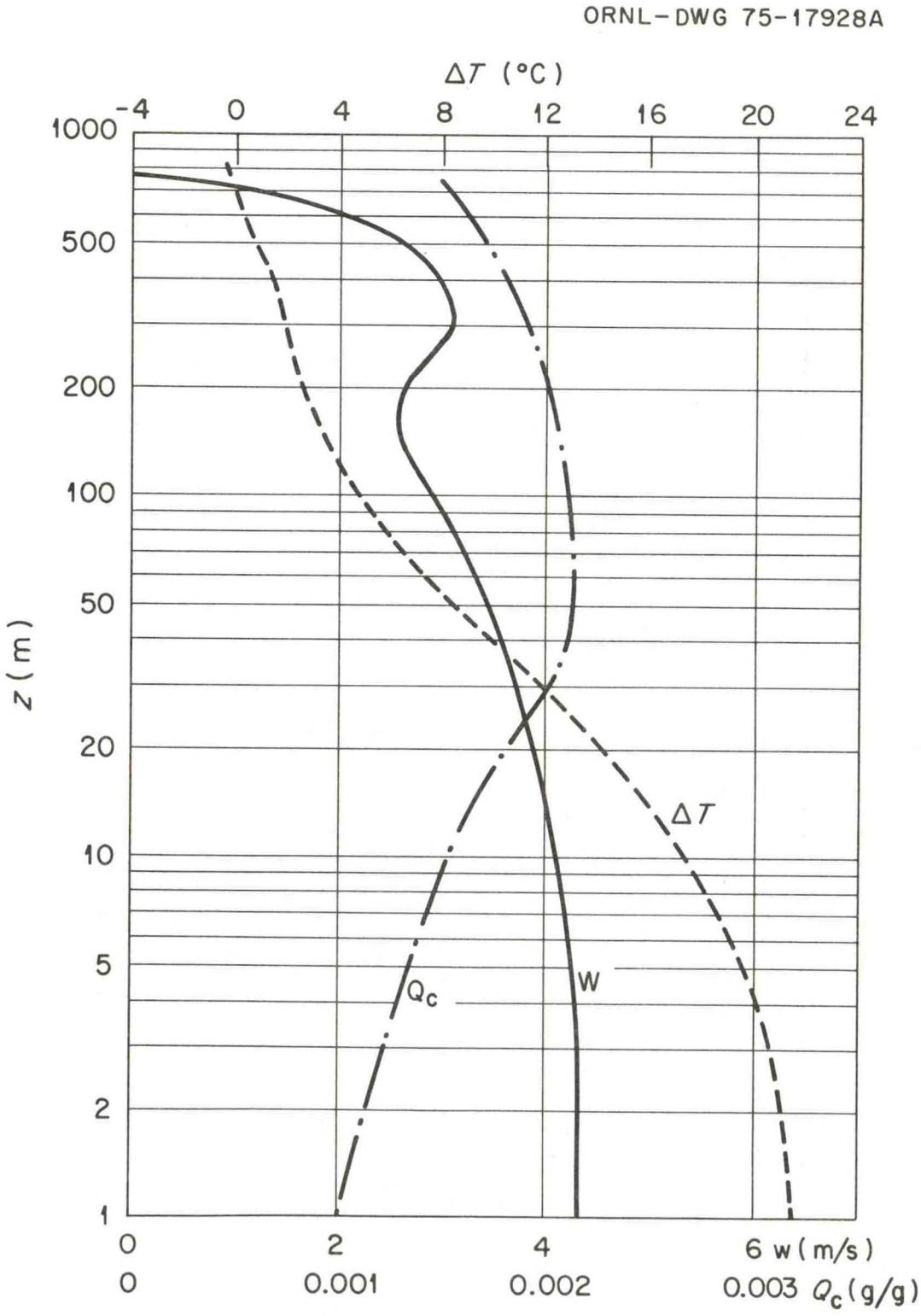

Figure 3: Observed plume rise compared with predictions of numerical model.

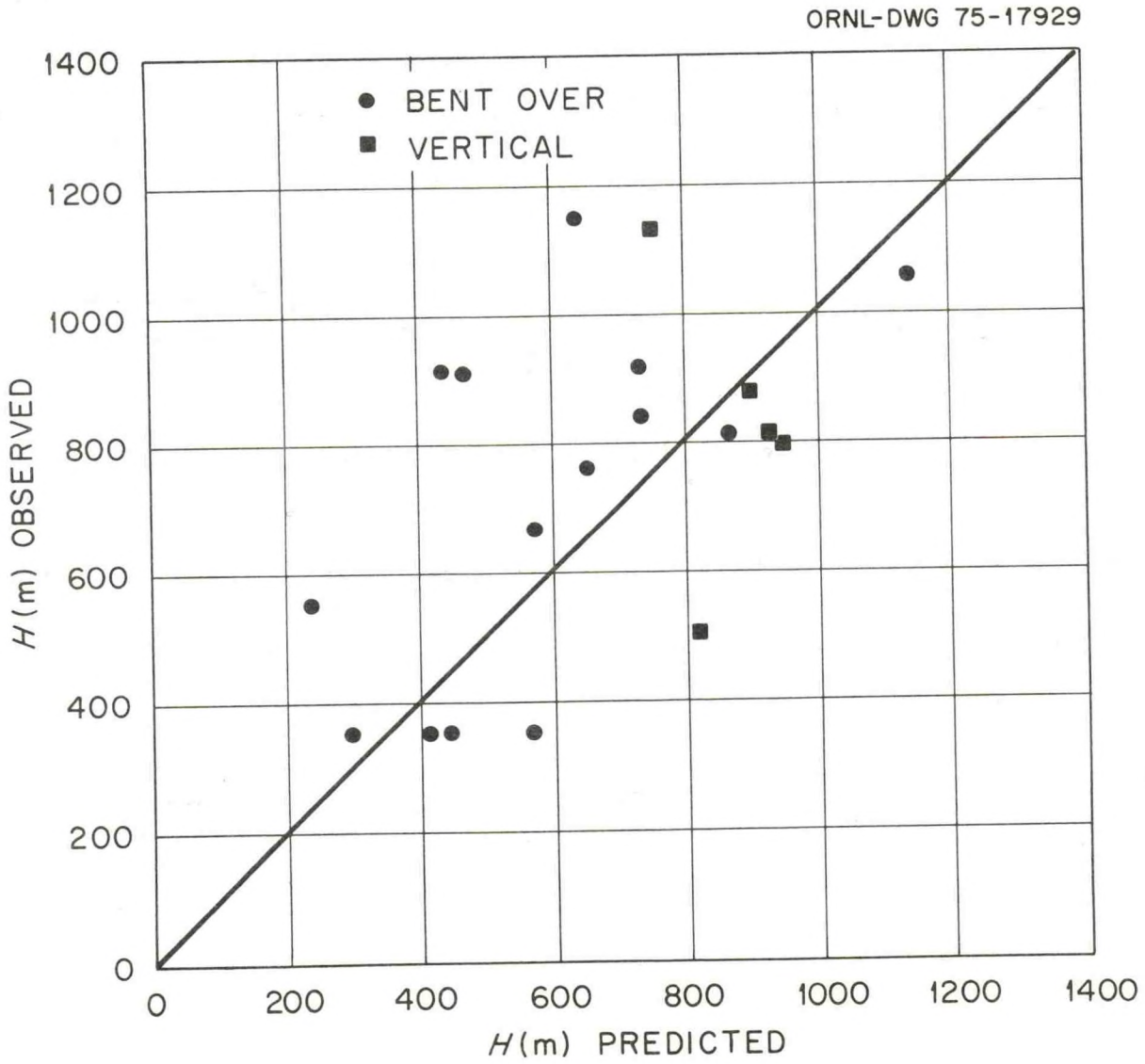

Figure 4: Observed visible plume length compared with (1.-ambient relative humidity at level of plume).

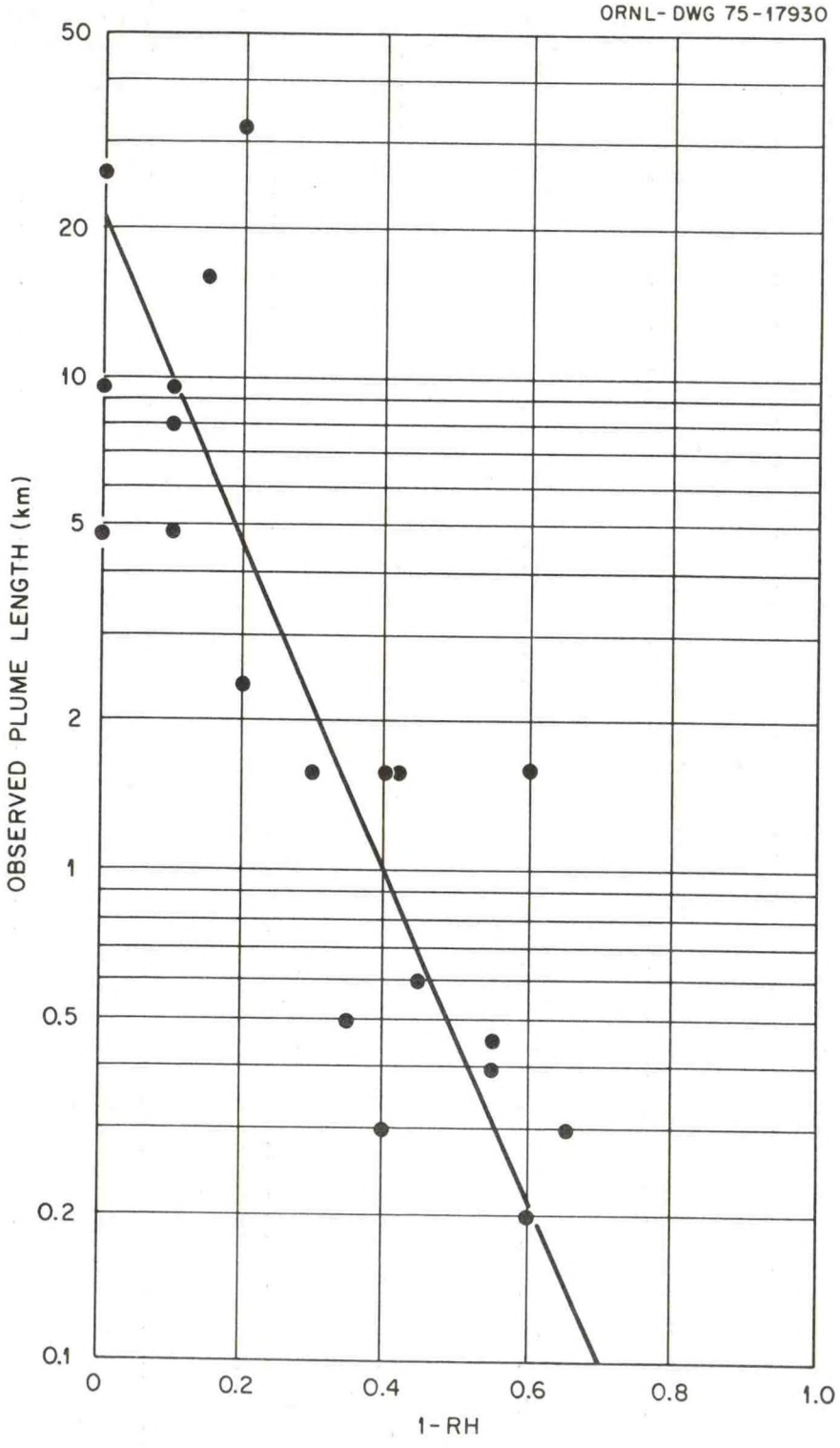

Figure 5: Observed visible plume length compared with $U(Q_{es}-Q_e)$; i.e., wind speed times saturation deficit at plume level.

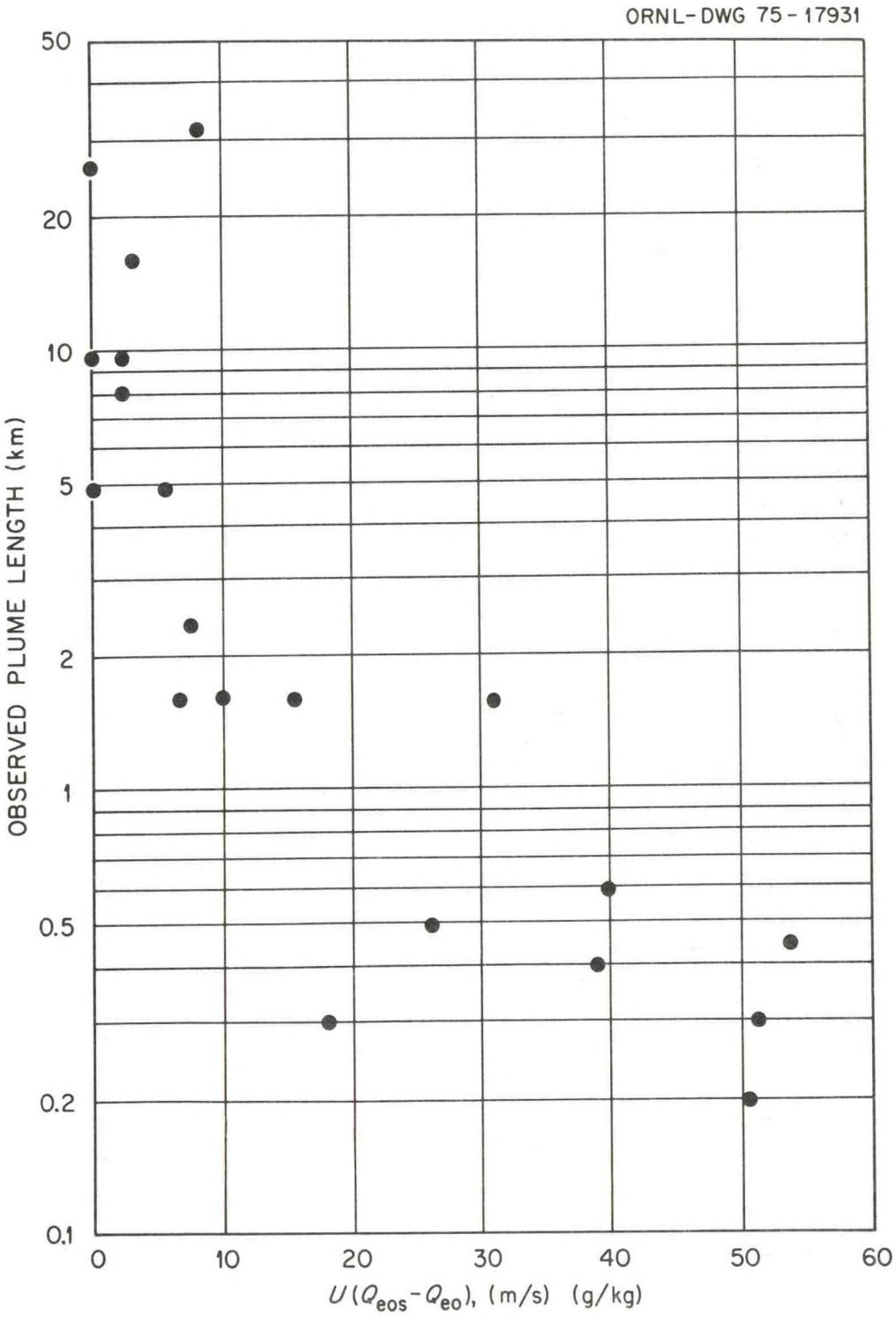

# A Note on Diffusion from Some Simple Extended Sources Treated as a Collection of Gaussian Point Sources

Pablo Ulriksen *

March 1975

## 1. Introduction

The common use of the Gaussian diffusion formula for estimating concentrations of a contaminant emitted from a point source has led to extension of the method to line and area sources. In practical applications, highways are treated usually as infinite line sources, while domestic and small industrial emissions become area sources, divided into small squares, each one represented by a point source. The approximations of finite line sources by infinite lines, or of area sources by point sources, are valid only within a certain distance range, a fact not always taken into account. Some models in use are described in Stern (1970) and in Pasquill (1974).

This note examines the behavior of several simple extended sources, treated as summations of point sources, each having a Gaussian diffusion pattern. Line sources, vertical area sources, and horizontal area sources are included. Line and horizontal area sources are common in air pollution problems. Vertical area sources are not usual in atmospheric diffusion, but can be found in some problems of fluid mechanics or oceanic applications.

*International Atomic Energy Association Fellow.
Presently with the University of Chile.

ATDL Contribution File No. 75/22

Diffusion from extended sources is found by summing contributions from an infinite number of point sources. The integration process assumes linear superposition, without interaction between the point sources or their effluents. Diffusion from point sources is presented in Section 2. Line sources and vertical area sources are treated in Sections 3 and 4, respectively. Integration in these cases is straightforward, giving diffusion formulas which include the error function. To integrate the expressions for horizontal area sources, treated in Section 5, the distance dependence of the vertical diffusion coefficient $\sigma_z$ must be specified. Results are obtained using both a simple linear expression and a power law expression for $\sigma_z$. This latter case leads to results inconsistent with the starting assumptions, so its use is not recommended. A simple formula for $\sigma_z$ proposed by Briggs (1973) is used also in a particular solution.

Results show that extended sources can be treated as simple sources (point, line, or infinite area sources), when distances fall in appropriate ranges. The asymptotic behavior of extended sources provides a working tool for concentration estimates. Nevertheless, it must be kept in mind that the starting assumption of Gaussian distribution follows from the K-theory diffusion equation only for the special condition K = constant (Pasquill, 1970), so for complex problems an attempt to solve the diffusion differential equation with appropriate boundary conditions may be worthwhile, rather than incorporating additional approximations into the Gaussian format.

Instantaneous releases from volume sources for various initial distributions were found by Frenkiel (1952) and Gifford (1955), using a similar integration process.

## 2. Point Sources

In all this work, it is assumed that effluent is emitted into a constant velocity field u parallel to the x-axis.

An instantaneous release of a quantity Q (in grams, say) of contaminant by a point source leads to a concentration field given by

$$\chi(x,y,z,t) = \frac{Q}{(2\pi)^{3/2}\sigma_x\sigma_y\sigma_z} \exp\left\{ -\frac{(x-ut)^2}{2\sigma_x^2} - \frac{y^2}{2\sigma_y^2} - \frac{z^2}{2\sigma_z^2} \right\} \qquad (1)$$

The cloud translates with velocity u. Its spread is a function of time, depending on the instantaneous value of the diffusion coefficients $\sigma_x$, $\sigma_y$, and $\sigma_z$.

To obtain the concentration field created by a continuous source, the above expression is integrated over time, assuming that successively emitted puffs can be superposed linearly, and setting $Q = Q'dt$, where $Q'$ is the rate of continuously emitted contaminant (g/sec, assumed constant). Explicit forms for the dispersion coefficients are needed. Following Csanady (1973) or Frenkiel (1953) we obtain

$$\chi(x,y,z) \simeq \frac{Q}{2\pi u \sigma_y \sigma_z} \exp\left[-\frac{y^2}{2\sigma_y^2} - \frac{z^2}{2\sigma_z^2}\right] \quad (2)$$

The assumptions are that the plume is elongated in x, the turbulence intensity is small, and that $x \simeq ut \gg y,z$. Frenkiel (1953) demonstrated that this expression is valid for small distances, where the diffusion coefficients are proportional to $x (x \ll L_n$, the Lagrangian macroscale) and for large distances ( $x \gg L_n$), where the proportionality is to $x^{1/2}$.

In the presence of a physical boundary like the earth's surface, the solution is obtained by assuming a perfect reflection and using an appropriate image source. When the surface is located in the plane x-y (z=o), and the real and image sources are at $z = \pm h$, respectively, the concentration field, for $z \geq 0$ is given by

$$\chi(x,y,z) = \frac{Q'}{2\pi\, u\, \sigma_y \sigma_z} \exp\left[-\frac{y^2}{2\sigma_y^2}\right] \left\{ \exp\left[-\frac{(z-h)^2}{2\sigma_z^2}\right] + \exp\left[-\frac{(z+h)^2}{2\sigma_z^2}\right] \right\} \quad (3)$$

This formula is extensively used in practical applications (see, e.g., Slade, 1968; Smith, 1968; Turner, 1969).

## 3. Line Sources

Extended sources will be represented as a collection of point sources, each one independent of the others. Line sources treated here are oriented perpendicular to the wind direction and include two cases: infinite line and finite line. It is assumed in this section and in the remaining sections of this note that no boundary surface is present.

### 3.1 Infinite line source

The solution is found using equation 2 for the continuously emitting point source, setting $Q' = q(y)\,dy$ and integrating along the line source (which coincides with the y-axis). The concentration is given by

$$\chi = \int_{-\infty}^{\infty} \frac{q(y')}{2\pi\, u\, \sigma_y \sigma_z} \exp\left(\frac{-(y-y')^2}{2\sigma_y^2}\right) \exp\left(\frac{-z^2}{2\sigma_z^2}\right) dy', \qquad (4)$$

where $q(y')$ is the emission rate per unit length (g $\sec^{-1}$ $cm^{-1}$). When q = constant, the integration gives

$$\chi(x,z) = \frac{q}{\sqrt{2\pi}\, u\, \sigma_z} \exp\left(\frac{-z^2}{2\sigma_z^2}\right) \qquad (5)$$

an expression which also describes 2-dimensional diffusion from a point source.

3.2 Finite line source

A line source of finite length b (Figure 1a) produces a concentration field given by the previous integral, where the limits are changed to $y' = \pm b/2$. Assuming q = constant, the integration leads to

$$\chi(x,y,z) = \frac{q}{2\sqrt{2\pi}\, u\sigma_z} \exp\left(\frac{-z^2}{2\sigma_z^2}\right) \left\{ \operatorname{erf}\left(\frac{b/2 + y}{\sqrt{2}\sigma_y}\right) + \operatorname{erf}\left(\frac{b/2 - y}{\sqrt{2}\sigma_y}\right) \right\}, \quad (6)$$

where $\operatorname{erf}(p) \equiv \frac{2}{\sqrt{\pi}} \int_0^p e^{-g^2}\, dg$ is the error function.

The total emission rate from this source is

$$Q' = \int_{-b/2}^{b/2} q(y')dy' = qb. \quad (7)$$

Thus when distance is large compared to the source dimension ($x \gg b$), the continuous point source expression (eqn. 2) can be used, with emission rate $Q' = qb$. For small distances ($x \ll b$) near the x-axis ($y,z \ll b$), the source can be treated as an infinite line source (eqn. 5). Figure 2 illustrates the asymptotic behavior of the finite line source.

4. Vertical Area Sources

Vertical area sources are not common in atmospheric diffusion problems; their major application can be found in some fluid mechanics experiments performed in channels or wind tunnels. They are included

here as an illustrative example of asymptotic behaviour. Three different vertical sources are treated: an infinite vertical area source, a strip source, and a finite rectangular area source.

## 4.1 Infinite vertical area source

The concentration field from a source extended infinitely along the y-z plane (x = o) is given by

$$\chi = \int_{-\infty}^{\infty} \int_{-\infty}^{\infty} \frac{q'(y',z')}{2\pi\, u\, \sigma_y \sigma_z} \exp\left[-\frac{(y-y')^2}{2\sigma_y^2}\right] \exp\left[-\frac{(z-z')^2}{2\,\sigma_z^2}\right] dy'dz'. \quad (8a)$$

Here q' represents the emission rate per unit area (g $sec^{-1}cm^{-2}$). If q' = constant, the expression reduces to

$$\chi = q'/u, \quad (8b)$$

which corresponds to a constant flux of material out of the y-z plane in the direction of the positive x-axis.

## 4.2 Vertical strip source

An infinite strip source extended along the y-axis with a finite dimension in z (=h), shown in Figure 1b, has a concentration field given by

$$\chi(x,z) = \frac{q'}{2u} \left\{ \operatorname{erf}\left[\frac{h/2 + z}{\sqrt{2}\,\sigma_z}\right] + \operatorname{erf}\left[\frac{h/2-z}{\sqrt{2}\,\sigma_z}\right] \right\}, \quad (9)$$

when q' = constant. For large distances downwind (x>>h), the source can be treated as an infinite line (eqn. 5) with strenth q=q'h (g $sec^{-1}cm^{-1}$). For small distances (x<<h), and near the x - y plane (z<<h), the concentration field tends to the solution for the infinite vertical area source (eqn. 8b). Figure 3 shows this behaviour.

### 4.3 Finite vertical area source

A rectangular vertical area source of size b x h (Figure 1c) and constant emission rate q' (g $sec^{-1}cm^{-2}$) produces a concentration field given by

$$\chi(x,y,z) = \frac{q'}{4u} \left\{ \operatorname{erf}\left(\frac{b/2+y}{\sqrt{2}\,\sigma_y}\right) + \operatorname{erf}\left(\frac{b/2-y}{\sqrt{2}\,\sigma_y}\right) \right\} \left\{ \operatorname{erf}\left(\frac{h/2+z}{\sqrt{2}\,\sigma_z}\right) + \operatorname{erf}\left(\frac{h/2-z}{\sqrt{2}\,\sigma_z}\right) \right\} . \quad (10)$$

If x is large compared to b and h, the source can be treated as a point source (eqn. 2) with emission rate Q' = q'bh (g $sec^{-1}$). When x<<b,h and y<<b, z<<h, the source acts as an infinite vertical area source (eqn. 8b). Figure 3 indicates this behavior.

## 5. Horizontal Area Sources

These kinds of extended sources are common in atmospheric diffusion problems, such as representing emissions from large conglomerates of small individual sources which are not treated separately, vehicle emissions from an urban street complex, and others.

The horizontal area sources extend over the x-y plane. A double integration over x and y is performed to sum the infinite point source contributions. The functional dependence of the dispersion coefficients $\sigma_y$ and $\sigma_z$ with distance must be known in order to evaluate the integral over x. The horizontal area sources treated below are an infinite source, and a strip source, for which the problem is reduced to specifying only $\sigma_z$ as a function of x. Two forms are used for $\sigma_z$:

(a) a linear expression

$$\sigma_z = c_z x, \tag{11a}$$

which is a good approximation for distances up to $x \simeq 3000$ m, according to the values proposed by Briggs (1973), and

(b) a power law expression

$$\sigma_z = c_z x^r, \tag{11b}$$

used by some authors (e.g., Smith, 1968) as an approximation to mid-distance values of the vertical diffusion coefficient.

(c) Briggs' (1973) expressions of the form

$$\sigma_z = \frac{c_z x}{\sqrt{1 + d_z x}} \tag{11c}$$

are in agreement with the theoretical variation of $\sigma_z$ as mentioned in Section 2, but proved intractable for an analytic solution of the integral that gives concentration values. This expression is

used in a particular solution, when z = 0, in order to compare it with the other two solutions for $\chi$ using the linear expression and the power law expression for $\sigma_z$.

5.1 Infinite horizontal area source

Concentration at the point (x,y,z) will be given by

$$\chi(x,y,z) = \int_{-\infty}^{x}\int_{-\infty}^{\infty} \frac{q'(x',y')}{2\pi u \sigma_y(x-x')\sigma_z(x-x')} \exp\left[-\frac{(y-y')^2}{2\sigma_y^2(x-x')}\right] \exp\left[-\frac{z^2}{2\sigma_z^2(x-x')}\right] dy'dx', \quad (12)$$

since source points located at distances greater than x give no contribution to $\chi(x,y,z)$ when the ambient fluid is in motion and the turbulence intensity is not large ($\overline{u'^2} \ll u^2$).

Assuming q' = constant, the problem reduces to the 2-dimensional expression:

$$\chi(x,z) = \frac{q'}{\sqrt{2\pi}\, u} \int_{-\infty}^{x} \frac{\exp\left[-\frac{z^2}{2\sigma_z^2(x-x')}\right]}{\sigma_z(x-x')} dx' \quad (13)$$

where $\sigma_z(x)$ must be known in order to evaluate the integral.

Using the linear expression (11a) for $\sigma_z$, the integral can be converted to

$$\chi(x,z) = \frac{q'}{2\sqrt{2\pi}\, u\, c_z} \int_o^\infty \frac{\exp\left(\frac{-z^2 t}{2c_z^2}\right)}{t}\, dt \qquad (14)$$

which gives $\chi = \infty$, and a similar result holds for the power law expression (11b) for $\sigma_z$. Thus an infinite horizontal source produces infinite concentrations, due to the transport of material by the wind flow along the x-axis.

5.2 Infinite horizontal strip source

The source extends from x = 0 to x = a in the x-y plane, as shown in Figure 1d. The concentration field will be given by the integral

$$\chi(x,z) = \frac{q'}{\sqrt{2\pi}\, u} \int_o^{x_o} \frac{\exp\left[-\frac{z^2}{2\sigma_z^2 (x-x')}\right]}{\sigma_z (x-x')}\, dx', \qquad (15)$$

assuming q' = constant. The upper limit of the integral will be $x_o = x$ when $x < a$ and $x_o = a$ when $x > a$.

5.2.a

Using the linear expression (11a) for $\sigma_z$, the integral (15) can be transformed to

$$\chi(x,z) = \frac{q'}{2\sqrt{2\pi}\, uc_z} \int_{x^{-2}}^{(x-x_o)^{-2}} \frac{\exp\left(-\frac{z^2}{2c_z^2}\, t\right)}{t}\, dt \qquad (16)$$

This integrates to

$$\chi(x,z) = \frac{q'}{2\sqrt{2\pi}\, uc_z}\, E_1\left(\frac{z^2}{2c_z^2 x^2}\right), \quad \text{for } x \leq a, \qquad (17a)$$

$$\text{and } \chi(x,z) = \frac{q'}{2\sqrt{2\pi}\, uc_z}\left\{E_1\left(\frac{z^2}{2c_z^2 x^2}\right) - E_1\left(\frac{z^2}{2c_z^2 (x-a)^2}\right)\right\} \qquad (17b)$$

for $x > a$. $E_1$ is the exponential integral function, defined by

$$E_1(\mu) \equiv \int_1^{\infty} \frac{e^{-\mu t}}{t}\, dt. \qquad (18)$$

$E_1(\mu) \to \infty$ when $\mu \to 0$; i.e., if $z \to 0$ in the expression for $x \leq a$, $\chi \to \infty$ (which corresponds to points on the source). When the argument of $E_1$ is very small it can be approximated by $E_1(\mu) \simeq -\gamma - \ell n(\mu)$, where $\gamma \equiv$ Euler's constant, so the expression (17b) for $x > a$ takes the form

$$\chi(x,0) = \frac{q'}{\sqrt{2\pi}\, uc_z} \ln\left(\frac{x}{x-a}\right), \text{ for } x > z, \tag{19}$$

which gives the concentrations over the x-y plane. The same result can be obtained directly setting z = 0 before integrating (16).

For large x, this expression can be reduced to

$$\chi(x,0) \simeq \frac{q'a}{\sqrt{2\pi}\, uc_z x}, \tag{20}$$

the result obtained (eqn. 5) for an infinite line source with strength $q = q'a$ ($g\ sec^{-1} cm^{-1}$). Figure 4 shows the asymptotic behaviour of this case, which can be treated as a line source for large distances.

5.2.b

Using the power law expression (11b) for $\sigma_z$, the formula for concentrations can be reduced to

$$\chi(x,z) = \frac{q'}{2\sqrt{2\pi}\, urc_z} \int_{x^{-2r}}^{(x-x_o)^{-2r}} \frac{\exp\left(-\frac{z^2}{2c_t^2} t\right)}{(t)^{\frac{r+1}{2r}}}\, dt, \tag{21}$$

which leads to

$$\chi(x,z) = \frac{q'}{2\sqrt{2\pi}\, uc_z r} \left(\frac{z^2}{2c_z^2}\right)^{-\nu} \Gamma\left(\frac{z^2}{2c_z^2 x^2}\right), \text{ for } x \le a, \qquad (22a)$$

and

$$\chi(x,z) = \frac{q'}{2\sqrt{2\pi}\, uc_z r} \left(\frac{z^2}{2c_z^2}\right)^{-\nu} \left\{ \Gamma\left(\nu, \frac{z^2}{2c_z^2 x^2}\right) - \Gamma\left(\nu, \frac{z^2}{2c_z^2 (z-a)^2}\right) \right\}, \qquad (22b)$$

for $x > a$.

Here

$$\Gamma(\nu,s) \equiv \int_s^\infty t^{\nu-1} e^{-t} dt \qquad (23)$$

is the incomplete gamma function, which exists for all $\nu$, and $\nu \equiv \frac{r-1}{2r}$ is negative for typical r values. When $\nu = 0$, $\Gamma(0,s) = E_1(s)$, the result obtained using the linear expression for $\sigma_z$. When $s \to 0$, $\Gamma(\nu,s) \to \Gamma(\nu) \cdot \left(1 - \frac{s^\nu}{\nu\Gamma(\nu)}\right)$ for $\nu < 0$ (derived from Abramowitz and Stegun, 1966), so

$$\chi(x,0) \simeq \frac{q'}{\sqrt{2\pi}\, uc_z (1-r)} x^{1-r}, \text{for } x < a. \qquad (24a)$$

This gives finite concentration values at points on the source ($z = 0$), a result not consistent with the starting assumption of a source represented by a collection of point sources, each of whose concentration $\chi \to \infty$ as the distance to it decreases. (This result is attributed to a failure of the power law expression to accord with the principle of linear superposition). The same result can be obtained by setting $z = 0$ in equation 21 for $\chi$ before integrating, as was done, e.g., in Pasquill (1974). For $x > a$, when $z \to 0$ the expression reduces to

$$\chi(x,0) = \frac{q'}{\sqrt{2\pi}\, uc_z(1-r)} \left[x^{1-r} - (x-a)^{1-r}\right]. \qquad (24b)$$

when $x >> a$, this expression can be approximated by

$$\chi(x,0) \simeq \frac{q'a}{\sqrt{2\pi}\, uc_z x^r} , \qquad (24c)$$

which corresponds to diffusion from an infinite line source (eqn. 5) with emission rate $q = q'\, a(g\ sec^{-1} cm^{-1})$.

The behavior of this case is illustrated in Figure 5.

5.2.c

The linear expression for $\sigma_z$ and the power law expression approximate experimental results in different distance ranges.

The formulas (11c) proposed by Briggs (1973) are perhaps the best adjustment available to $\sigma_z$ values, but they lead to complicated integrands in the expression for $\chi$. However, for air pollution studies, the most interesting solution is the surface concentration, for which the integrands are much simpler. Setting z = 0 in the integral which gives the concentration field from the horizontal strip source, and using eqn. (11c) for $\sigma_z$, we obtain

$$\chi(x,0) = \frac{q'}{\sqrt{2\pi}\, uc_z} \left\{ 2[R(x) - R(x-a)] + \ell n \frac{R(x)-1}{R(x-a)-1} - \ell n \frac{R(x)+1}{R(x-a)+1} \right\} , \quad (25)$$

for $x > a$, where $R(x') \equiv \sqrt{1 + d_z x'}$ . This expression is asymptotic (Figure 6) to the linear $\sigma_z$ solution (eqn. 19) of $\chi$ for small x, and to an infinite line source solution (eqn. 5) of the form

$$\chi(x,0) \simeq \frac{q'a}{\sqrt{2\pi}\, u\sigma_z} \quad , \text{ with } \sigma_z = \frac{c_z x}{\sqrt{1 + d_z x}} \quad ,$$

for large distances. As seen in Figure 6, the linear $\sigma_z$ expression gives the same results as Briggs' formula when the source dimension a equals a few meters, and $x < 100$ a. However, the more common source sizes are of the order of thousands of meters; in that case, the departure from the linear $\sigma_z$ solution is large, and the expression for $\chi$ which uses Briggs' $\sigma_z$ is probably preferable.

## 6. Conclusions

The following conclusions can be stated:

(a) Extended sources (line and area sources) can be represented quite well by their asymptotic simple sources at the appropriate distance ranges. However, at middle-distances the error made by using asymptotic approximations can exceed 100%. Transition from one asymptotic solution to the other usually takes place in the distance range from d to 10d, d being the characteristic size of the source. Finite line sources behave as infinite lines at short distances from the source and as point sources at large distances. Infinite strip sources (vertical and horizontal) behave as infinite line sources at large distances from the source. Finite size sources behave as point sources at large distances.

(b) As long as the distances involved do not exceed 3000m, a linear expression for $\sigma_z$ can be used. For larger distances, Briggs' formulas are preferable.

## 7. Acknowledgements

I am grateful to Dr. R. P. Hosker, who has reviewed the manuscript and made many suggestions. This note is an offshoot developed from a main subject proposed by him. The work is being done under a fellowship awarded by the International Atomic Energy Agency.

## 8. References


Abramowitz, M. and Stegun, I. A., eds., 1966, Handbook of Mathematical Functions with Formulas, Graphs, and Mathematical Tables, U.S. National Bureau of Standards, Applied Mathematics Series No. 55.

Briggs, G. A., 1973, Diffusion Estimation for Small Emissions, NOAA, Atmospheric Turbulence and Diffusion Laboratory, Contribution File No. (Draft) 79.

Csanady, G. T., 1973, Turbulent Diffusion in the Environment, Reidel Pub. Co., Boston.

Frenkiel, F. N., 1952, Turbulent diffusion from a nonpunctual source, Proc. First Natl. Cong. Appl. Mech., 837-841.

Frenkiel, F. N., 1953, Turbulent Diffusion: Mean Concentration Distribution in a Flow Field of Homogeneous Turbulence, Advances in Applied Mechanics, Vol. III, p. 61-107.

Gifford, F. A., 1955, Atmospheric Diffusion from Volume Sources, Journal of Meteorology, V. 12, p. 245-251.

Pasquill, F., 1970, General Discussion, in Proceedings of Symposium on Multiple-Source Urban Diffusion Models, A. C. Stern, ed., U. S. Environmental Protection Agency, Air Pollution Control Office Publication No. AP-86, p. 14-10.

Pasquill, F., 1974, Atmospheric Diffusion 2nd ed., John Wiley.

Slade, D., ed., 1968, Meteorology and Atomic Energy, U. S. Atomic Energy Commission, Division of Technical Information.

Smith, M., ed., 1968, Recommended Guide for the Prediction of the Dispersion of Airborne Effluents, The American Society of Mechanical Engineers.

Stern, A. C., ed., 1970, Proceedings of Symposium on Multiple-Source Urban Diffusion Models, U. S. Environmental Protection Agency, Air Pollution Control Office, Publication No. AP-86.

Turner, D. B., 1969, Workbook of Atmospheric Dispersion Estimates, U. S. Department of Health, Education, and Welfare, Public Health Service Publication No. 999-AP-26.

ORNL-DWG 75-9733

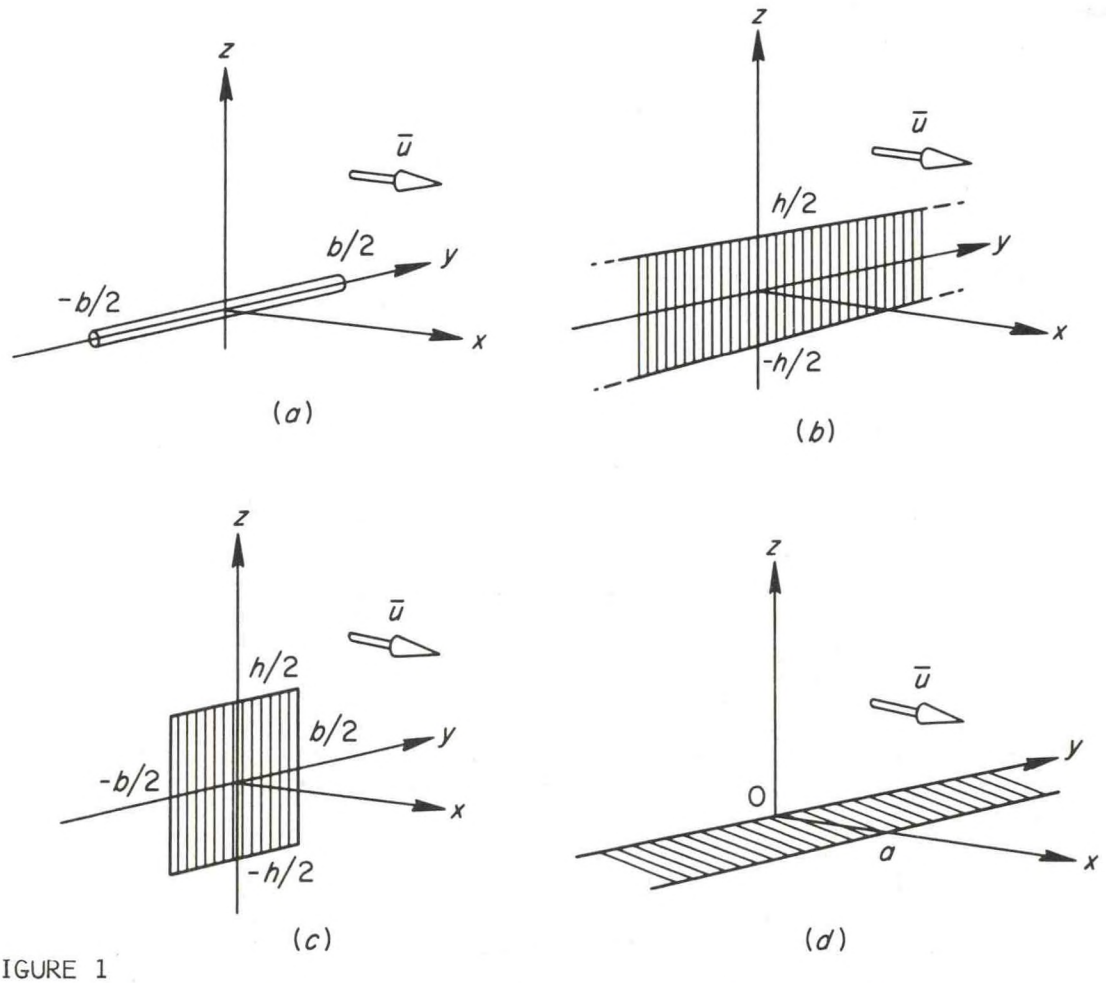


FIGURE 1

Some Extended Sources: (*a*) Finite Line Source, (*b*) Vertical Strip Source, (*c*) Finite Vertical Area Source, (*d*) Horizontal Strip Source. Wind is Along the *x*-Axis for all Cases.

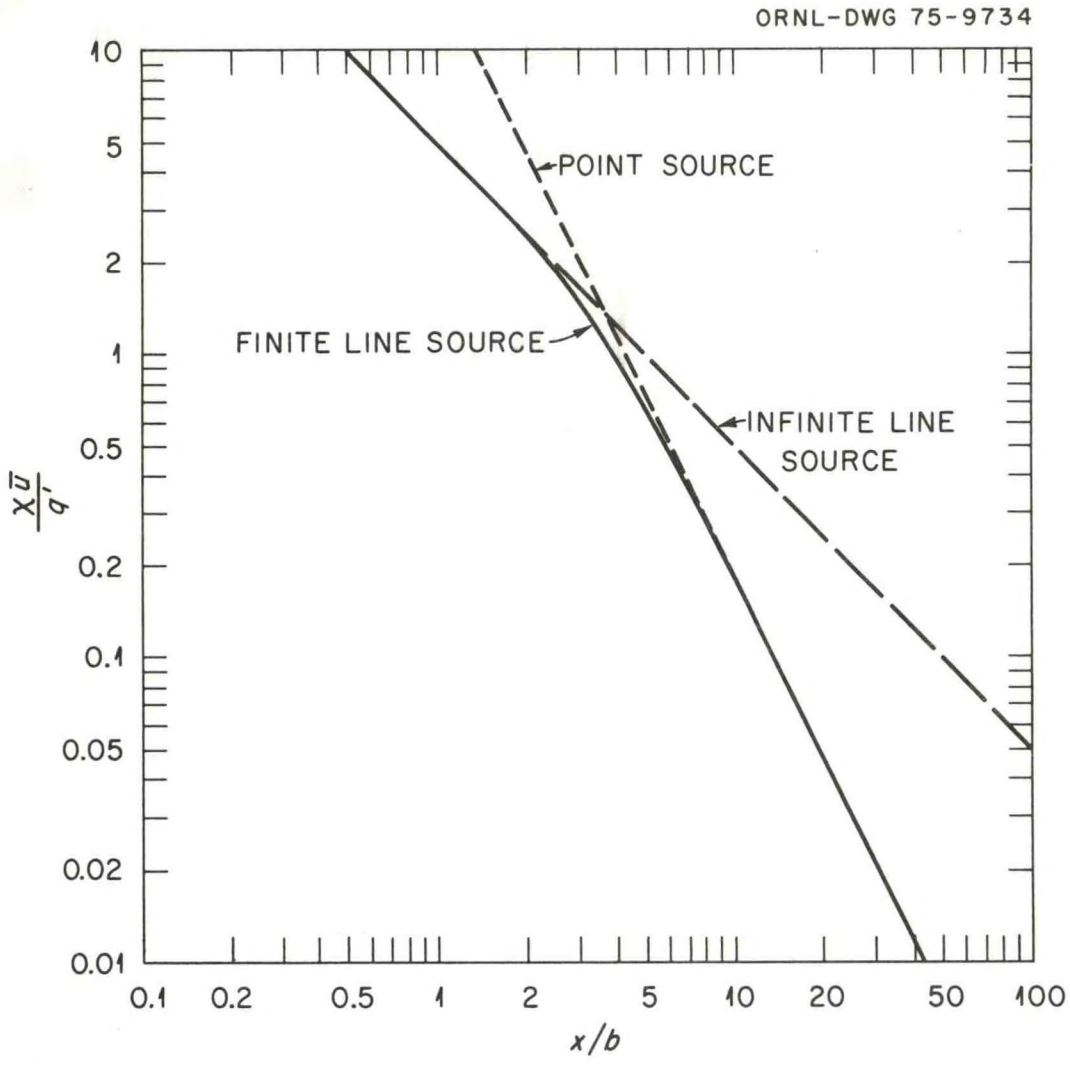


FIGURE 2

Asymptotic Behavior of Finite Line Source (Length $b$), for $\sigma_y = 0.112x$, $\sigma_z = 0.08x$ (Pasquill Class C), at $z = 0$. Point Source Strength $Q' = q'b^2$ (g sec$^{-1}$); Line Source Strength $q = q'b$ (g cm$^{-1}$ sec$^{-1}$).

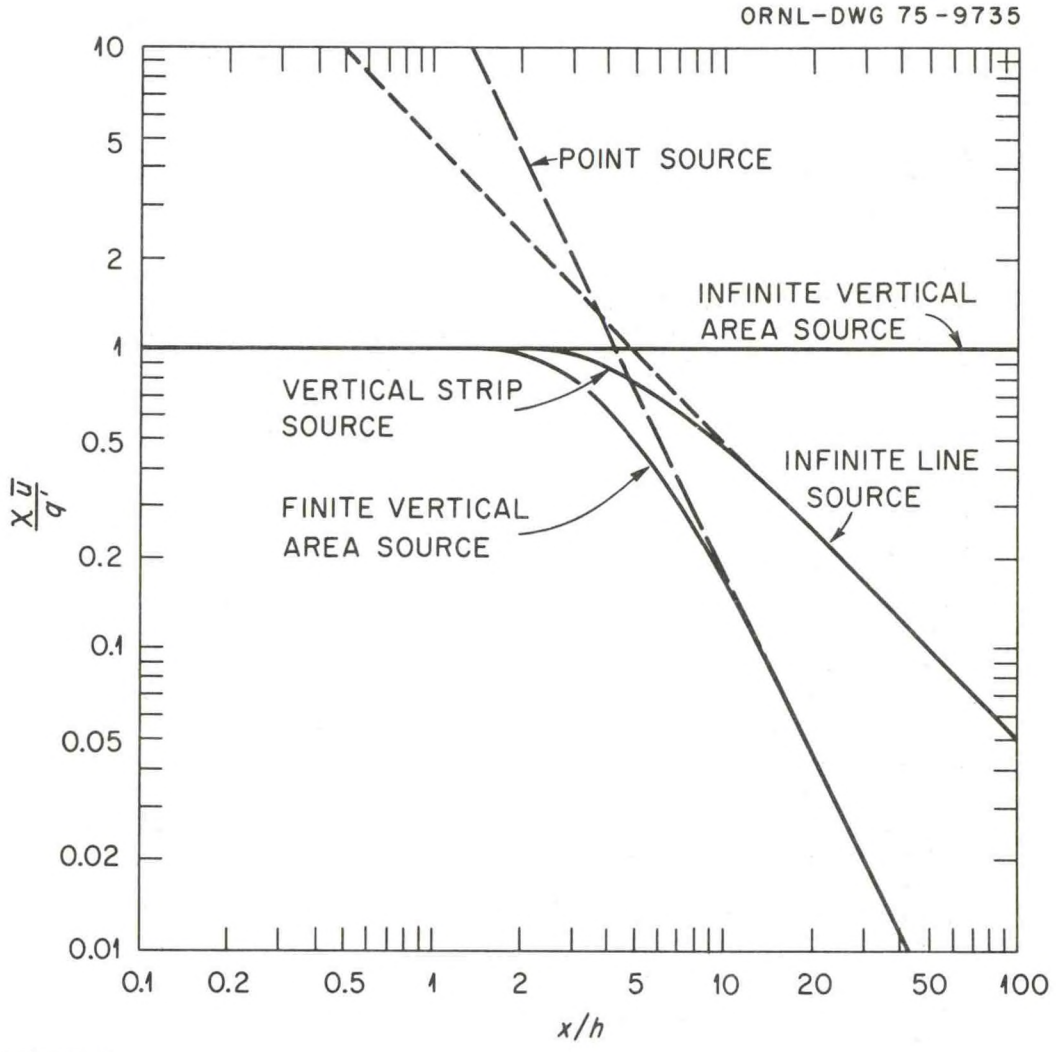


FIGURE 3

Asymptotic Behavior of Vertical Area Sources for $\sigma_y = 0.112x$, $\sigma_z = 0.08x$ (Pasquill Class C), at $z = 0$. Point Source Strength $Q' = q'bh$ (g $sec^{-1}$); Line Source Strength $q = q'h$ (g $cm^{-1}$ $sec^{-1}$). Width $b$ = Height $h$ for Finite Area Source in This Example.

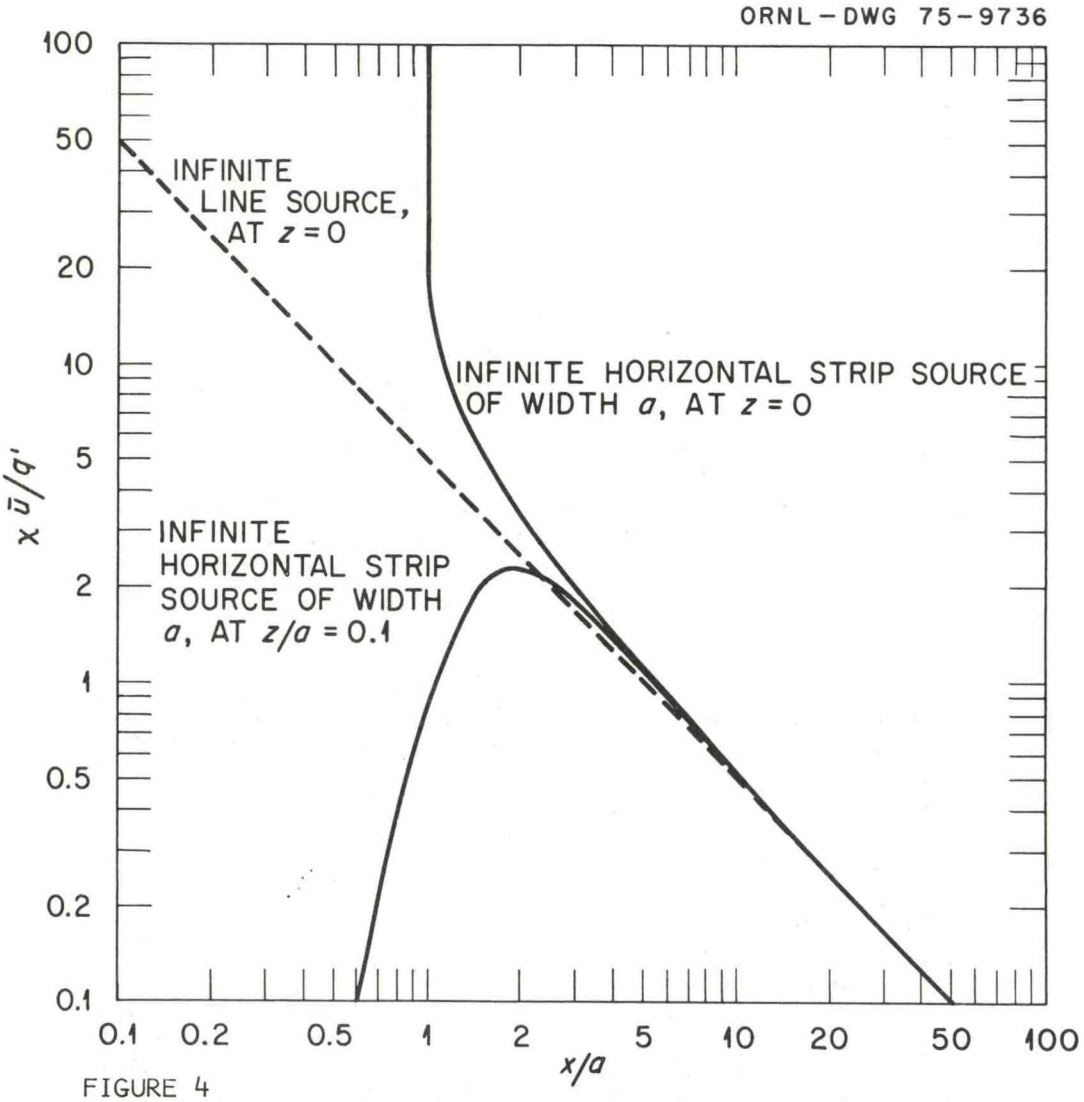


FIGURE 4

Asymptotic Behavior of Horizontal Strip Source of Width $a$, for linear $\sigma_z$ ($\sigma_z = 0.08x$; Pasquill Class C), at $z = 0$ and at $z/a = 0.1$.

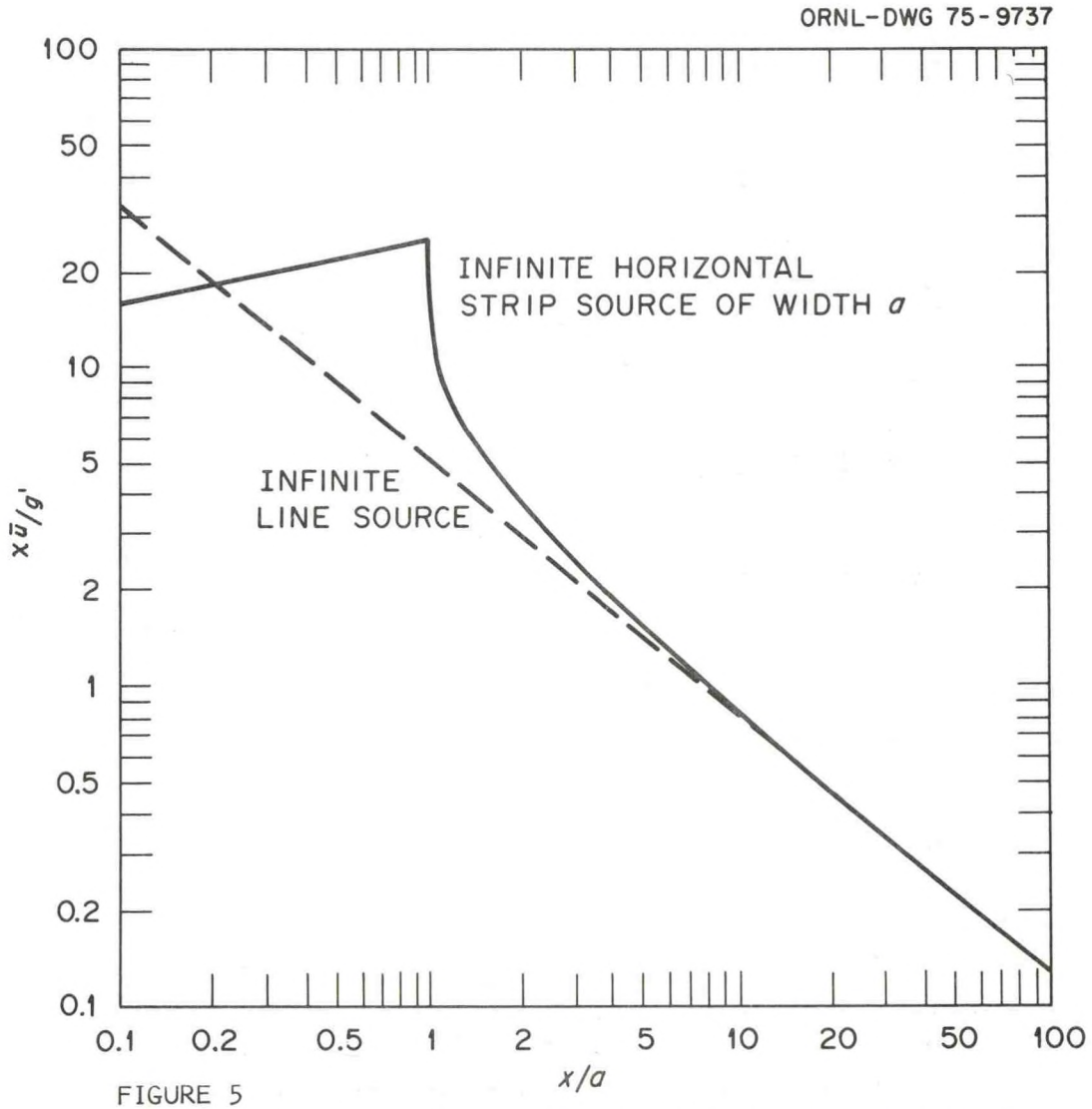


FIGURE 5

Asymptotic Behavior of Horizontal Strip Source of Width $a$, for Power-Law $\sigma_z$ ($\sigma_z = 0.08\, x^{0.8}$), at $z = 0$.

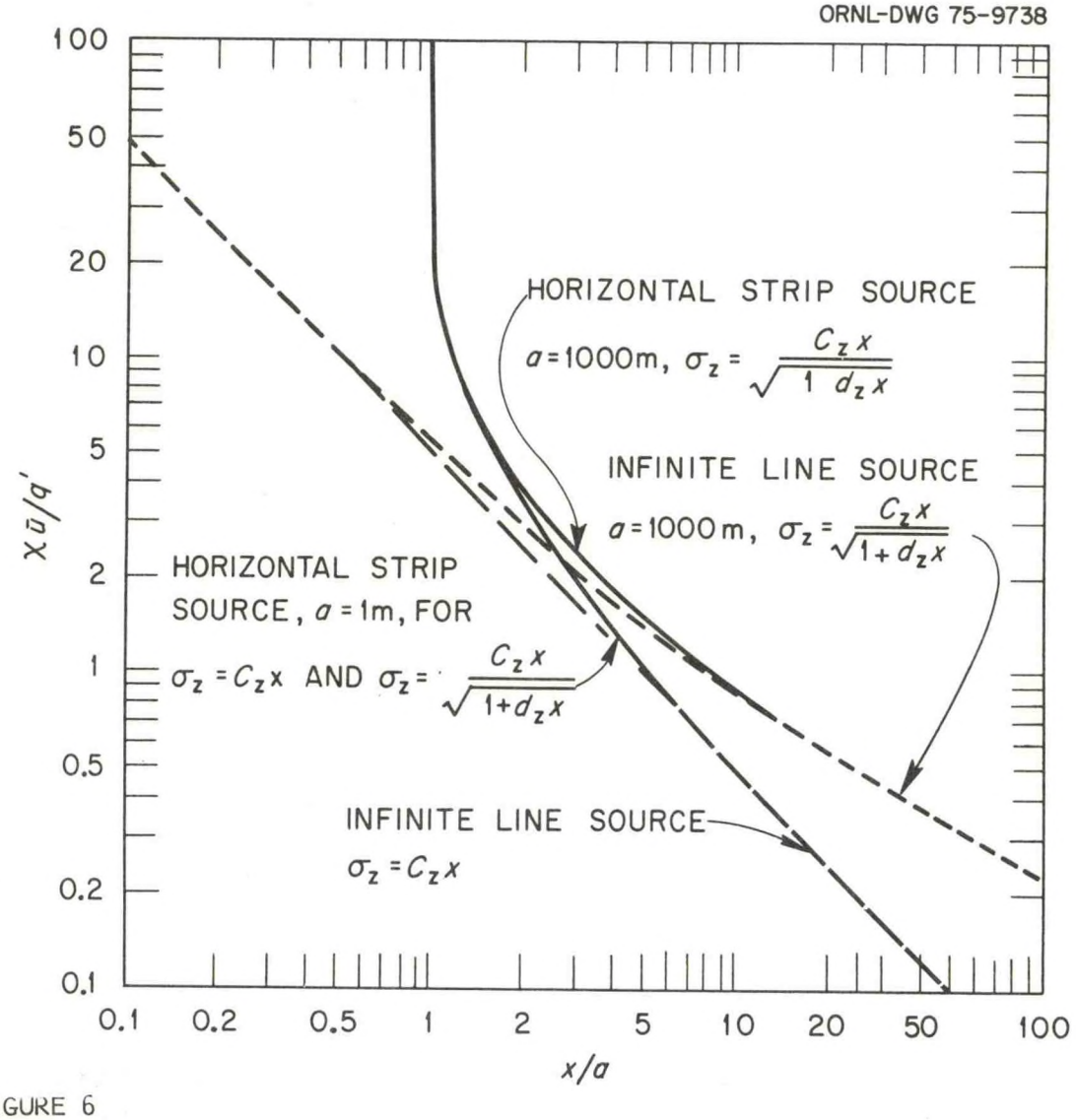


FIGURE 6

Asymptotic Behavior of Horizontal Strip Source of Width $a$, for $\sigma_z = C_z x$ and for $\sigma_z = \frac{C_z x}{\sqrt{1+d_z x}}$ ($C_z = 0.08$, $d_z = 0.0002\,m^{-1}$) at $z = 0$.

# ESTIMATION OF DOWNWASH EFFECTS

Gary A. Briggs

Air Resources
Atmospheric Turbulence and Diffusion Laboratory
National Oceanic and Atmospheric Administration
Oak Ridge, Tennessee

Published as Chapter 6 of Section II in Power Generation: Air Pollution Monitoring and Control, Ann Arbor Science Publishers Inc., P. O. Box 1425, Ann Arbor, Mich. 48106, pp. 65-71.

ATDL Contribution File No. 75/23

# POWER GENERATION:

## Air Pollution Monitoring and Control

edited by

Kenneth E. Noll
Professor, Environmental Engineering
Illinois Institute of Technology, Chicago

Wayne T. Davis
Assistant Professor, Environmental Engineering
University of Tennessee, Knoxville

**6**

# Estimation of Downwash Effects

**Gary A. Briggs**
Air Resources Atmospheric Turbulence and Diffusion Laboratory,
NOAA, Oak Ridge, Tennessee

## INTRODUCTION

This is a simplified approach to the calculation of ground-level concentrations of effluents from small industrial and fuel-burning installations. It is intended to serve as a first approximation to a very complex process. Because each stack, building, and terrain configuration is different, actual ground concentration may frequently differ from the values calculated here by a factor of two.[1]

The procedures given here were designed especially for source heights of less than 100 m; some of the simplifications made are not valid for large emissions. It is important to note that all *lengths are in meters* (m) and *velocities are in meters per second* (m/sec) in these formulas; this avoids needless reiteration of the formulas for different units. Table 6.1 provides all necessary conversion factors.

This chapter gives a method for predicting the occurrence of downwash. This is a common occurrence with small emissions, and greatly increases ground concentrations in the immediate vicinity downwind of the source.

## ELEVATED SOURCE OR GROUND SOURCE?

The answer to this question can mean either a zero concentration or a very high concentration of effluent at the ground in the neighborhood of an emission. Does the plume keep its distance from the ground, and if so, what is its effective height, or is the plume brought to the ground very near the source? The latter can happen if the

**Table 6.1.** Conversion Factors.

| | |
|---|---|
| 1 m = 3.28 ft | 1 cal/sec = 4.185 watt |
| $10^3$m = 0.621 mi | 1 cal/g-°C = 1.00 Btu/lb-°F |
| 1 sec = min/60 = hr/3600 = day/86,400 = 30 days/259 $10^7$ = yr/3.14 • $10^7$ | 1 watt = 1 joule/sec = 1 kg-m$^2$/sec$^3$ |
| | 1 ft = 0.305 m |
| | 1 mi = 1.61 • $10^3$m |
| 1 kg = $10^3$ g = $10^6$ mg = $10^9\mu$g | 1 lb = 0.454 kg |
| 1 kg = 2.2 lb | 1°R = 0.555 °K |
| 1 °K = 1.8°R | °R = °F + 460 |
| °K = °C + 273 | 1 Btu = 252 cal |
| 1 cal = 1 g-cal = $10^{-3}$ kg-cal | 1 ft/sec = 0.305 m/sec |
| 1 cal = 0.00397 Btu | 1 mph = 0.447 m/sec |
| 1 m/sec = 3.28 ft/sec | 1 ton/hr = 0.252 kg/sec |
| 1 m/sec = 2.24 mph | 1 ppm = $10^{-6}$($m_o$/24)kg/m$^3$ = ($m_o$/24)mg/m$^3$ |
| 1 kg/sec = 3.96 ton/hr | 1 lb/hr = 0.126 g/sec |
| 1 kg/m$^3$ = $10^6$(24/$m_o$)ppm | 1 ton/mi$^2$ = 0.35 g/m$^2$ |
| 1 g/sec = 7.93 lb/hr | 1 watt = 0.239 cal/sec |
| 1 g/m$^2$= 2.85 ton/mi$^2$ | 1 Btu/lb-°F = 1.00 cal/g-°C |

efflux velocity is too low, the stack is too short, or the emission is denser than air. Downwash of the plume due to terrain is also possible, particularly if there is an escarpment upwind of the source, but this case is relatively rare.

The answer to the above question can depend on the wind speed. It also can depend on the location of the stack relative to buildings and the wind direction. The great variety of possible building geometries gives ample reason for not expecting great accuracy from the following "rules-of-thumb."

### Stack Aerodynamic Effect

An effluent emitted vertically from a stack can rise due to its momentum or can be brought downward by the low pressure in the wake of the stack. Which occurs depends on the ratio of the efflux velocity, $v_s$, to the crosswind velocity, u. Make the following computation, where D is the inside stack diameter and $h_s$ is the source height above the ground:

$$h' = h_s + 2(v_s/u - 1.5)D \qquad (1)$$

It is suggested that this be done for the following values of u: 1, 2.5, 4.5, 7, and 10 m/sec. The efflux velocity can be determined from direct measurement, from the amount of forced draft, from the rate of the process and relative proportions of its gaseous product (thermal expansion should be taken into account), or from visual or cine-

matographic estimates (if there are visible tracers in the effluent.) Building and stack measurements can be made directly, taken from drawings, or scaled from photographs.

If the effluent is emitted from a nonvertical stack or vent, set $h' = h_s$.

Equation (1) is based partly on wind tunnel observations of Sherlock and Stalker[2] who showed that downwash (negative rise) occurs when $v_s/u$ is less than about 1.5 and that the plume downwashes about one stack diameter at $v_s/u = 1$. For high values of $v_s/u$, it is a conservative form of Equation (5.2) recommended by Briggs[3] for momentum rise; $2(v_s/u)D$ approximates the plume rise at the point where it is equal to 1.7 times the downwind distance, so essentially represents the very close-in plume rise. Buoyancy is neglected in this stage, since it does not cause a doubling of the plume rise until a distance $x = 10\ u\ v_s/(-g\ \Delta)$.

**Building Effect**

If the effluent is emitted from a stack or vent on or near a building, it may be brought downward by the flow of air over and around the building. Let $l_b$ equal the lesser of the building height, $h_b$, or the building width perpendicular to the wind direction, $w_b$. If $h'$ is less than $(h_b + 1.5\ l_b)$ and the point of emission is on the roof, anywhere within $l_b/4$ of the building, or within $3l_b$ directly downwind of the building, the plume can be considered to be within the regional of building influence. If the plume is within the region of building influence, there are several possibilities:

A. If $h'$ in Equation (1) is less than $(h_b + 0.5l_b)$, part or all of the effluent is likely to circulate within the aerodynamic "cavity" that forms in the lee of the building. This cavity usually begins at the upwind edge of a flat roof or at the crest of a pitched roof (unless the crest is parallel to the wind). It grows to a height of about $(h_b + 0.5\ l_b)$ and a width a little greater than $w_b$, and extends over all lee sides of the building and downwind 2 to 3.5 $l_b$. Thus, effluents in the cavity region may affect persons on the ground and in the building. One must especially consider the placement of intake vents providing ventilation within the building. Following are some rough guidelines for estimating the concentration ($\chi$) experienced in the cavity region. Let $\chi = KQ/(u\ l_b^2)$, where Q is source strength. If $H' > 0.35$, K is generally 1 or less throughout the cavity. If $H' < 0.35$, K is typically 1.5 and at most is 3.0, except on the side of the building where the effluent is emitted (for instance, the roof). Here, K can range up to 100 ($H' = (h' - b_b)/l_b$), The concentration along the axis of the plume can be roughly approximated by $\chi = 4Q/(us^2)$, where s is the distance from the source measured along the axis. The airflow near

buildings is complicated, and it is difficult to predict the trajectory of the plume axis. For example, in the cavity within $l_b/4$ of the roof, the flow is usually upwind.

B. If $h' > h_b$, compute $h'' = 2\,h' - (h_b + 1.5\,l_b)$ (2)
If $h' < h_b$, compute $h'' = h' - 1.5\,l_b$ (3)

C. If $h''$ is greater than $l_b/2$, the plume remains an elevated source. If $h''$ is less than $l_b/2$, treat the plume as a ground source with an initial cross-sectional area $A = l_b^2$.

The above rules reduce to a simpler form in the case of a squat building, *i.e.*, when $h_b < w_b$: If $h' \geqslant 2.5\,h_b$, the plume escapes the region of building influence and $h'' = h'$; if $h' \leqslant 1.5\,h_b$, the plume downwashes into the building cavity [see (1) above] and also becomes a ground source with $A = h_b^2$ [see (3) above]; for in-between values of $h'$, the plume remains elevated and $h'' = 2\,h' - 2.5h_b$ [see (2) above].

The method suggested here for accounting for the building effect is an interpolation of several rules-of-thumb respecting air flow around buildings. It is generally accepted that a building has very little effect on the airflow at 2½ building heights above the ground and above. On the other hand, the aerodynamic cavity downwind of a sharp-edged building develops to roughly 1½ building heights. It develops higher over a very wide (*i.e.*, squat) building, but the plume also has more distance in which to rise out of the cavity in this case. This method does allow some close-in plume rise to be considered with respect to escaping the cavity; however, it should be conservative since it does not allow for the lower wind speed near the building, which promotes greater rise. The cavity height may be less than 1½ building heights in the case of pitched or rounded roofs.

For a squat building, this method assumes that if $h' < 1.5\,h_b$, the plume behaves as if it were a ground source of initial area $A = h_b^2$. This gives concentrations in approximate agreement with those measured by Yang and Meroney[4] near the end of the cavity. The values of $\chi$ within the cavity adjacent to the building were estimated from measurements around cubes and rectangles by Halitsky.[5] Equation (2) is a linear interpolation formula giving $h'' = h'$ when $h' = 2.5\,h_b$ and $h'' = 0.5\,h_b$ when $h' = 1.5\,h_b$, thus giving a $\chi$ of the same order as that given for a ground source ($h' < 1.5\,h_b$, $A = h_b^2$).

For tall buildings, $w_b$ replaces $h_b$ as the characteristic cavity width and height above $h_b$. It is assumed that a roof level plume is not pulled all the way down to the ground within the cavity if $h_b > 2\,w_b$; hence, $h''$ is no more than $1.5\,w_b$ below $h'$.

Yang and Meroney[4] found that atmospheric stability had only a slight effect on concentrations immediately downwind of a building, so this effect is neglected here.

## SUMMARY OF EQUATIONS AND WORKED EXAMPLE

### Summary of Equations

Stack aerodynamic effect:

$$h' = h_s + 2D(v_s/u - 1.5). \quad (1)$$

Building effect: applies only if stack is on or near building or is within 3 $l_b$ downwind and $h' < h_b = 1.5\ l_b$, where $l_b$ = lesser of $h_b$ or $w_b$; if not, $h'' = h'$.

If $h' < h_b + 0.5\ l_b$, high concentrations may occur in building "cavity."

If $h' > h_b$, compute $h'' = 2h' - (h_b + 1.5\ l_b)$ (2)

If $h' < h_b$, compute $h'' = h' - 1.5\ l_b$ (3)

If $h'' < l_b/2$, treat plume as ground source with $A = l_b^2$

### Worked Example

Suppose we have a plant with a stack located on the roof of a long, flat building with the following specifications:

$h_b = l_b = 66$ ft $= 20$ m
$h_s = 99$ ft $= 30$ m
$r = 1.64$ ft $= 0.5$ m
$V_s = 16$ ft/sec $= 5$ m/sec
Q ($SO_2$) $= 0.035$ lb/sec $= 0.016$ kg/sec
Effluent temperature $= 290$ °F $= 416$ °K
Ambient temperature $= 70$ °F $= 294$ °K
Distance to nearest property line $= 330$ ft $= 100$ m

*Solution*

Stack aerodynamic effect: $h' = h_s + 4\ (V_s/u - 1.5)\ r$
$u = 1$ m/sec: $h' = 30 + 4\ (5/1 - 1.5)\ (0.5) = 37$ m
$u = 2.5$ m/sec: $h' = 30 + 4\ (5/2.5 - 1.5)\ (0.5) = 31$ m
$u = 5$ m/sec: $h' = 30 + 4\ (5/5 - 1.5)\ (0.5) = 29$ m
$u = 10$ m/sec: $h' = 30 + 4\ (5/10 - 1.5)\ (0.5) = 28$ m

Building effect: $h'' = 2h' - (h_b + 1.5\ l_b)$ if $30\text{ m} < h' < 50$ m
$h'' = h_b - l_b = 0$ if $h' < 30$ m (downwash)
$u = 1$ m/sec: $h'' = 2\ (37) - 50 = 24$ m
$u = 2.5$ m/sec: $h'' = 2\ (31) - 50 = 12$ m
$u = 5$ m/sec: $h'' = 0$
$u = 10$ m/sec: $h'' = 0$
(plume becomes ground source when $h' = 30$ m, $h' = h_s + 4\ (V_s/u - 1.5)r$
Solving for u, $30 = 30 + 4\ (5/u - 1.5)\ (0.5)$, $u = 3.33$ m/sec

## SYMBOLS AND DEFINITIONS

| *Symbol* | *Definition* | *Units* |
|---|---|---|
| A | Initial cross-sectional area of a ground plume | $m^2$ |
| D | Inside stack diameter | m |
| h | Effective source height (after stack aerodynamic, building, and buoyancy effects have been accounted for) | m |
| h′ | Plume height after stack aerodynamic effect is accounted for | m |
| h″ | Plume height after building effect is accounted for | m |
| $h_b$ | Building height | m |
| $h_s$ | Source height above the ground | m |
| K | Dimensionless concentration coefficient in cavity region | — |
| $l_b$ | The lesser of $h_b$ or $w_b$ | m |
| Q | Source strength of a component of the effluent | kg/sec |
| u | Wind speed at source height or at an open location | m/sec |
| $v_s$ | Average efflux velocity (volume flow rate ÷ area) | m/sec |
| $w_b$ | Building width perpendicular to the wind direction | m |
| x | Distance downwind of the source | m |
| $\chi$ | Concentration of a component of the effluent | $kg/m^3$ |

## REFERENCES

1. Smith, Maynard (Ed.) *Recommended Guide for the Prediction of the Dispersion of Airborne Effluents.* (New York: American Society of Mechanical Engineers, 1968).
2. Sherlock, R. H. and E. A. Stalker. "A Study of Flow Phenomena in the Wake of Smoke Stacks," *Engineering Research Bulletin No. 29* (Ann Arbor, Michigan: University of Michigan, 1941).
3. Briggs, G. A. *Plume Rise,* AEC Critical Review Series TID-25075 (1969).
4. Yang, B. T. and R. N. Meroney. "Gaseous Dispersion into Stratified Building Wakes," Fluid Dynamics and Diffusion Laboratory, Colorado State University, Fort Collins, CER70-71BTY-RNM-8 (1970).
5. Halitsky, J. "Gas Diffusion near Buildings," In *Meteorology and Atomic Energy,* USAEC Report TID-24190 (1968), pp. 221-255.

*U.S. GOVERNMENT PRINTING OFFICE: 1976-641-358/26